frontiers | Research Topics

Sharing technical knowledge to understand the distribution patterns and migration history of marine organisms

Edited by
Tomihiko Higuchi, Ming-Tsung Chung,
Chisato Yoshikawa and Yuki Minegishi

Published in
Frontiers in Marine Science

ISSN 1664-8714
ISBN 978-2-8325-4739-7
DOI 10.3389/978-2-8325-4739-7

About Frontiers

Frontiers is more than just an open access publisher of scholarly articles: it is a pioneering approach to the world of academia, radically improving the way scholarly research is managed. The grand vision of Frontiers is a world where all people have an equal opportunity to seek, share and generate knowledge. Frontiers provides immediate and permanent online open access to all its publications, but this alone is not enough to realize our grand goals.

Frontiers journal series

The Frontiers journal series is a multi-tier and interdisciplinary set of open-access, online journals, promising a paradigm shift from the current review, selection and dissemination processes in academic publishing. All Frontiers journals are driven by researchers for researchers; therefore, they constitute a service to the scholarly community. At the same time, the *Frontiers journal series* operates on a revolutionary invention, the tiered publishing system, initially addressing specific communities of scholars, and gradually climbing up to broader public understanding, thus serving the interests of the lay society, too.

Dedication to quality

Each Frontiers article is a landmark of the highest quality, thanks to genuinely collaborative interactions between authors and review editors, who include some of the world's best academicians. Research must be certified by peers before entering a stream of knowledge that may eventually reach the public - and shape society; therefore, Frontiers only applies the most rigorous and unbiased reviews. Frontiers revolutionizes research publishing by freely delivering the most outstanding research, evaluated with no bias from both the academic and social point of view. By applying the most advanced information technologies, Frontiers is catapulting scholarly publishing into a new generation.

What are Frontiers Research Topics?

Frontiers Research Topics are very popular trademarks of the *Frontiers journals series*: they are collections of at least ten articles, all centered on a particular subject. With their unique mix of varied contributions from Original Research to Review Articles, Frontiers Research Topics unify the most influential researchers, the latest key findings and historical advances in a hot research area.

Find out more on how to host your own Frontiers Research Topic or contribute to one as an author by contacting the Frontiers editorial office: frontiersin.org/about/contact

Sharing technical knowledge to understand the distribution patterns and migration history of marine organisms

Topic editors

Tomihiko Higuchi — The University of Tokyo, Japan

Ming-Tsung Chung — National Taiwan University, Taiwan

Chisato Yoshikawa — Japan Agency for Marine-Earth Science and Technology (JAMSTEC), Japan

Yuki Minegishi — The University of Tokyo, Japan

Citation

Higuchi, T., Chung, M.-T., Yoshikawa, C., Minegishi, Y., eds. (2024). *Sharing technical knowledge to understand the distribution patterns and migration history of marine organisms*. Lausanne: Frontiers Media SA. doi: 10.3389/978-2-8325-4739-7

Table of contents

frontiers | Frontiers in Marine Science

TYPE Editorial
PUBLISHED 27 March 2024
DOI 10.3389/fmars.2024.1392102

OPEN ACCESS

EDITED AND REVIEWED BY
Rui Rosa,
University of Lisbon, Portugal

*CORRESPONDENCE
Tomihiko Higuchi
thiguchi@aori.u-tokyo.ac.jp

RECEIVED 26 February 2024
ACCEPTED 18 March 2024
PUBLISHED 27 March 2024

CITATION
Higuchi T, Chung M-T, Yoshikawa C and Minegishi Y (2024) Editorial: Sharing technical knowledge to understand the distribution patterns and migration history of marine organisms.
Front. Mar. Sci. 11:1392102.
doi: 10.3389/fmars.2024.1392102

Editorial: Sharing technical knowledge to understand the distribution patterns and migration history of marine organisms

Tomihiko Higuchi[1]*, Ming-Tsung Chung[2], Chisato Yoshikawa[3] and Yuki Minegishi[4]

[1]Department of Living Marine Resources, Atmosphere and Ocean Research Institute, The University of Tokyo, Kashiwa, Chiba, Japan, [2]Institute of Oceanography, National Taiwan University, Taipei, Taiwan, [3]Biogeochemistry Research Center, Research Institute for Marine Resources Utilization, Japan Agency of Marine-Earth Science and Technology (JAMSTEC), Yokosuka, Japan, [4]Otsuchi Coastal Research Center, Atmosphere and Ocean Research Institute, The University of Tokyo, Otsuchi, Iwate, Japan

KEYWORDS

migration history, otoliths, distributions patterns, isoscapes, environmental DNA, field surveys

Editorial on the Research Topic
Sharing technical knowledge to understand the distribution patterns and migration history of marine organisms

1 Introduction

Marine organisms contribute to many important biogeochemical processes while their ecological functions provide resources for human activity not only as food sources but also through natural products, and tourism. Despite their importance, the distribution patterns and migration history of many marine organisms are still unknown. Often even fish that are well-known for their importance to aquaculture and fisheries have unclear distribution patterns due to the difficulty of accessing their marine habitat. This Research Topic was aimed at collecting related research on the distribution patterns and migration history of marine organisms with recent technical advances and their combinations.

2 Fish otolith analysis

Recently, the reproduced migration history of the sardine has been reported by combining high-resolution otolith stable oxygen isotope ratio ($\delta^{18}O$) analysis and numerical simulation (Sakamoto et al., 2019). This kind of method can be expected to apply to other species.

Hanson et al. suggested a comprehensive approach involving precise stable isotope sampling of otoliths, genetic identification, analysis of growth increments, and the use of a basic movement model. This integrated method aims to determine the whereabouts of individual wild Atlantic salmon. The research establishes an analytical framework for

predicting the ocean migratory paths by leveraging a natural data storage structure inherent to each salmon. This methodology proves particularly effective in uncovering the historical movements of species that are highly migratory or anadromous.

Gou et al. newly provide temperature-dependent fractionation in otolith $\delta^{18}O$ of chum salmon based on a rearing experiment. Also, carbon isotope ($\delta^{13}C$) in otolith was measured to examine the potential kinetic and metabolic effect of isotopic fractionations. $\delta^{13}C$ in otolith can be a tool to estimate metabolic rate in the field (Chung et al., 2019).

3 Isotopes and iso-logging

The use of isotope analysis (iso-logging) for tracking highly migratory marine fish has gained prominence as a promising tool in recent years (e.g. Matsubayashi et al., 2020). However, the effectiveness of this method is frequently impeded by the absence of crucial information, such as spatial variations in isotope ratios across different habitats, commonly referred to as "isoscapes."

Matsubayashi et al. conducted a study to assess the effectiveness of geostatistical analysis in creating isoscapes for $\delta^{13}C$ and $\delta^{15}N$ in the western Pacific. They aimed to estimate ontogenetic shifts in δ13C and $\delta^{15}N$ values of skipjack tuna (*Katsuwonus pelamis*). The geostatistical model successfully generated isoscapes and accurately predicted ontogenetic shifts based on skipjack isotope ratios. The resulting isoscapes revealed that $\delta^{13}C$ and $\delta^{15}N$ could distinctly differentiate the latitudinal migration patterns of skipjack tuna in the Western Pacific.Yoshikawa et al. documented the development of nitrogen isoscapes for phytoplankton in the western North Pacific using a marine nitrogen isotope model. The simulated distributions of $\delta^{15}N$ for nitrate, phytoplankton, and particulate organic nitrogen aligned well with observed $\delta^{15}N$ values in the same region. The seamless nitrogen isoscapes can enhance the comprehension of the habitats of marine organisms and aid in the study of fish migration in the Western North Pacific.

Ohno et al. investigated the inter-annual variations in the feeding habits and food sources of Japanese sardine and mackerel captured in the Kuroshio-Oyashio transition zone of the Western North Pacific by analyzing bulk stable isotopes ($\delta^{13}C$ and $\delta^{15}N$) and amino acid nitrogen isotopes ($\delta^{15}N_{AA}$). These analytical methods supplied insights into distinctions in the structure of the food web, revealing that the variability in food sources stems from variations in migration area, depth, and feeding behaviors.

Jackel et al. indicated that the ecological significance of deep-sea squids in the Great Australian Bight, comparing them with other cephalopod species found in global, southern temperate, and polar squid distributions by using $\delta^{13}C$ and $\delta^{15}N$ stable isotopes, fatty acids, and energy content. This study underscored that, aside from enhancing our comprehension of the trophic ecology of deep-sea squids, the use of partial specimens highlighted the valuable ecological information that can be derived from a few samples.

4 Field survey and environmental DNA

Recent advancements in environmental DNA (eDNA) techniques have significantly enhanced the capacity to carry out ecological monitoring across diverse locations. (e.g. Minegishi et al., 2019). Also, genetic analysis can be a powerful tool connectivity of organisms.

Kawakami et al. developed a novel species-specific qPCR assay targeting the eDNA of polar cod and collected the samples from various latitudinal points across their study area. The results align with existing information regarding the distribution and habitat of polar cod, indicating that eDNA can be considered a dependable tool, either as a substitute for or in conjunction with traditional methods.

Yu et al. investigated the distribution patterns of economically significant small pelagic fishes within the Kuroshio Current system (offshore of Japan) through the monitoring of eDNA. Utilizing generalized additive models (GAM), they examined the impact of environmental factors, including sea water temperature, salinity, and the presence of prey fish, on the occurrence and quantity of target fish eDNA. This study successfully unveiled intricate spatial distribution patterns of small pelagic fishes in the Kuroshio Current system, and hypothesized that predator–prey relationships play a role in influencing the distribution within small pelagic fish communities.

Marino et al. used a multidisciplinary approach to examine the connectivity of the marbled crab in the Adriatic and Ionian basins. Their investigation incorporated genetic analyses, Lagrangian simulations, and individual-based forward-time simulations to reveal both realized and potential connectivity among various locations. This study suggested that, when combined with representative sampling and the application of genome-wide approaches, this approach enables a more comprehensive understanding of the factors influencing oceanographic, demographic, and genetic connectivity.

As another survey, Henderson et al. utilized a dataset of tourist vessel locations in the southwest Atlantic sector of the Southern Ocean to ascertain the necessary number of tourist vessel voyages for reliable abundance estimates of baleen whales. Their findings demonstrated that surveys conducted from tourist vessels surpassed the performance of standardized line transect surveys in accurately reproducing simulated baleen whale abundances and distribution. These analyses indicate that tourist vessel-based surveys represent a viable method for estimating baleen whale abundance in remote regions.

5 Conclusions

A combination of several methods, such as isotope and/or genetic analysis, along with simulation and/or modeling, can bring new insights into the distribution patterns and migration history of marine organisms. Additionally, utilizing commercial ship voyages, such as cargo or tourist vessels, for survey can be expected to capture spatiotemporal trends. We believe that the research techniques proposed in this Research Topic can improve the ecological study of marine organisms in the near future.

Author contributions

TH: Writing – original draft, Writing – review & editing. M-TC: Writing – original draft, Writing – review & editing. CY: Writing –

original draft, Writing – review & editing. YM: Writing – original draft, Writing – review & editing.

Conflict of interest

The authors declare that the research was conducted in the absence of any commercial or financial relationships that could be construed as a potential conflict of interest.

Publisher's note

References

Chung, M. T., Trueman, C. N., Godiksen, J. A., Holmstrup, M. E., and Grønkjær, P. (2019). Field metabolic rates of teleost fishes are recorded in otolith carbonate. *Commun. Biol.* 2, 1–10. doi: 10.1038/s42003-018-0266-5

Matsubayashi, J., Osada, Y., Tadokoro, K., Abe, Y., Yamaguchi, A., Shirai, K., et al. (2020). Tracking long-distance migration of marine fishes using compound-specific stable isotope analysis of amino acids. *Ecol. Lett.* 23, 881–890. doi: 10.1111/ele.13496

Minegishi, Y., Wong, M. K.-S., Kanbe, T., Araki, H., Kashiwabara, T., Ijichi, M., et al. (2019). Spatiotemporal distribution of juvenile chum salmon in Otsuchi Bay, Iwate, Japan, inferred from environmental DNA. *PloS One* 14, e0222052. doi: 10.1371/journal.pone.0222052

Sakamoto, T., Komatsu, K., Shirai, K., Higuchi, T., Ishimura, T., Setou, T., et al. (2019). Combining microvolume isotope analysis and numerical simulation to reproduce fish migration history. *Methods Ecol. Evol.* 10, 59–69. doi: 10.1111/2041-210X.13098

frontiers | Frontiers in Marine Science

TYPE Original Research
PUBLISHED 29 September 2022
DOI 10.3389/fmars.2022.944851

OPEN ACCESS

EDITED BY
Alberto Basset,
University of Salento, Italy

REVIEWED BY
Temim Deli,
University of Regensburg, Germany
Khaled Said,
University of Monastir, Tunisia
Sara Fratini,
University of Florence, Italy

*CORRESPONDENCE
Lorenzo Zane
lorenzo.zane@unipd.it

†These authors have contributed equally to this work

SPECIALTY SECTION
This article was submitted to Marine Ecosystem Ecology, a section of the journal Frontiers in Marine Science

RECEIVED 15 May 2022
ACCEPTED 01 September 2022
PUBLISHED 29 September 2022

CITATION
Marino IAM, Schiavina M, Aglieri G, Bevilacqua S, Boscari E, Congiu L, Faggion S, Kruschel C, Papetti C, Patarnello T, Paterno M, Voutsinas E, Zane L and Melià P (2022) Assessment of connectivity patterns of the marbled crab *Pachygrapsus marmoratus* in the Adriatic and Ionian seas through combination of genetic data and Lagrangian simulations. *Front. Mar. Sci.* 9:944851. doi: 10.3389/fmars.2022.944851

Assessment of connectivity patterns of the marbled crab *Pachygrapsus marmoratus* in the Adriatic and Ionian seas through combination of genetic data and Lagrangian simulations

Ilaria Anna Maria Marino[1,2†], Marcello Schiavina[2,3†], Giorgio Aglieri[2,4], Stanislao Bevilacqua[2,5], Elisa Boscari[1,2], Leonardo Congiu[1,2], Sara Faggion[1,6], Claudia Kruschel[7], Chiara Papetti[1,2], Tomaso Patarnello[2,6], Marta Paterno[1,2], Emanuela Voutsinas[8], Lorenzo Zane[1,2*] and Paco Melià[2,3]

[1]Dipartimento di Biologia, Università di Padova, Padova, Italy, [2]Consorzio Nazionale Interuniversitario per le Scienze del Mare, Roma, Italy, [3]Dipartimento di Elettronica, Informazione e Bioingegneria, Politecnico di Milano, Milano, Italy, [4]Department of Integrative Marine Ecology, Sicily, Stazione Zoologica Anton Dohrn, Palermo, Italy, [5]Dipartimento di Scienze della Vita (DSV), Università degli Studi di Trieste, Trieste, Italy, [6]Dipartimento di Biomedicina Comparata e Alimentazione, Università di Padova, Padova, Italy, [7]Department of Ecology, Agriculture, and Aquaculture, University of Zadar, Ul. Mihovila Pavlinovića, Zadar, Croatia, [8]Institute of Oceanography, Hellenic Centre for Marine Research, Anavyssos, Greece

Seascape connectivity studies, informing the level of exchange of individuals between populations, can provide extremely valuable data for marine population biology and conservation strategy definition. Here we used a multidisciplinary approach to investigate the connectivity of the marbled crab (*Pachygrapsus marmoratus*), a high dispersal species, in the Adriatic and Ionian basins. A combination of genetic analyses (based on 15 microsatellites screened in 314 specimens), Lagrangian simulations (obtained with a biophysical model of larval dispersal) and individual-based forward-time simulations (incorporating species-specific fecundity and a wide range of population sizes) disclosed the realized and potential connectivity among eight different locations, including existing or planned Marine Protected Areas (MPAs). Overall, data indicated a general genetic homogeneity, after removing a single outlier locus potentially under directional selection. Lagrangian simulations showed that direct connections potentially exist between several sites, but most sites did not exchange larvae. Forward-time simulations indicated that a few generations of drift would produce detectable genetic differentiation in case of complete isolation as well as when considering the direct connections predicted by Lagrangian simulations.Overall, our results suggest that the observed genetic homogeneity reflects a high level of realized connectivity among sites, which might result from a regional metapopulation dynamics, rather than from direct exchange among populations of the existing or planned MPAs. Thus, in the Adriatic and Ionian basins, connectivity might be

critically dependent on unsampled, unprotected, populations, even in species with very high dispersal potential like the marbled crab. Our study pointed out the pitfalls of using wide-dispersing species with broad habitat availability when assessing genetic connectivity among MPAs or areas deserving protection and prompts for the careful consideration of appropriate dispersing features, habitat suitability, reproductive timing and duration in the selection of informative species.

KEYWORDS

Lagrangian simulations, marbled crab, microsatellites, seascape genetics, individual-based simulations

Introduction

Seascape connectivity, i.e. connectivity among habitats in seascapes, informs about population interdependency and resilience, key to marine population biology and conservation strategy definition (Palumbi, 2003; Selkoe and Toonen, 2011; Olds et al., 2016). For most marine species, connectivity involves primarily dispersal of early developmental stages, planktonic larvae or propagules (Ward et al., 1994), which typically reach the open sea and are carried by currents to suitable habitats where they settle and develop into adults (Levin, 2006). As direct tracking of larvae is technically demanding (Cowen and Sponaugle, 2009), genetic data can be conveniently used to infer connectivity based on patterns of population differentiation (Palumbi, 2003). This approach, however, is particularly challenging when genetic differentiation is weak, as it occurs in many marine species, making it difficult to disentangle true genetic differentiation from background noise due to chance, experimental artefacts, and genetic patchiness (Hauser and Carvalho, 2008; Knutsen et al., 2011).

In this context, Lagrangian biophysical models have become increasingly popular, as they allow the modelling of larval dispersal, incorporating specific vital traits, and considering temporal variation in ocean currents (Gilg and Hilbish, 2003; Hohenlohe, 2004). The comparison of biophysical model outputs with genetic data can be effective to gain a better understanding of broad-scale genetic structure (Galindo et al., 2006; Galindo et al., 2010), to quantify the influence of dispersal on genetic differentiation, and to increase confidence in inferences when genetic differentiation is weak (Selkoe et al., 2010; Schiavina et al., 2014).

In the western Mediterranean Sea, Lagrangian simulations and genetic analyses have been first combined to infer directional gene flow in the comber *Serranus cabrilla* across the major oceanographic discontinuities of the Ibiza Channel and the Almeria-Oran front (Schunter et al., 2011). In the central Mediterranean Sea, a similar approach has been used for the white sea bream (*Diplodus sargus*) to demonstrate panmixia between a Marine Protected Area (MPA) of the southwestern Adriatic Sea and the neighbouring non-protected areas (Di Franco et al., 2012; Pujolar et al., 2013).

Coupled biophysical and genetic analyses concordantly showed high levels of connectivity between populations of the sea urchin *Paracentrotus lividus* (a keystone species of Mediterranean infralittoral rocky shores) in the Adriatic basin (Paterno et al., 2017) while, in the same region, both approaches indicated the presence of geographic subdivision and consequent population differentiation in the Mediterranean shore crab (*Carcinus aestuarii*), a global invader native to the Mediterranean Sea and inhabiting estuaries and lagoons (Schiavina et al., 2014). These different patterns of genetic structure in two species characterized by a long pelagic larval duration (about four weeks for the four crab pelagic zoeal stages: deRivera et al., 2007, Schiavina et al., 2014; about 30 days for the pelagic sea urchin larvae: Fenaux et al., 1985; Pedrotti, 1993; Paterno et al., 2017) suggest that other differences in biological and ecological traits or in evolutionary histories can play a key role in determining species-specific population genetic structures (Melià et al., 2016). Thus, further studies on species with long pelagic larval duration in the same area are needed.

The present work investigates the connectivity of the marbled crab *Pachygrapsus marmoratus* (Fabricius, 1787) (Brachyura: Grapsidae) in the Adriatic and Ionian seas, combining Lagrangian biophysical simulations and genetic microsatellite analyses. Considering the lack of habitat mapping information for this species, we assessed the direct connections among the locations sampled for genetics using Lagrangian simulations. In addition, we performed individual-based forward-time simulations to explicitly link the dispersal scenario estimated *via* Lagrangian simulations to the observed population genetics pattern.

The marbled crab is a species with a long larval duration and a high fecundity, thus similar to the Mediterranean shore crab *C. aestuarii* studied by Schiavina et al. (2014). However, it has a

different habitat, being very common in the intertidal zone of rocky shores. *P. marmoratus* is a semiterrestrial crab occurring on upper and middle levels of rocky shores. It is widespread throughout the entire Mediterranean basin, in the Black Sea and along the eastern Atlantic coasts of Europe and Africa, including the Canary and Azores islands (Zariquiey Alvarez, 1968; Ingle, 1980). In the last decade, *P. marmoratus* expanded northward its Atlantic distribution range, as a consequence of the warming of sea surface waters (Dauvin, 2009). This species is also found in artificial habitats such as breakwaters, ports, and marinas, since it is tolerant to anthropogenic disturbance (Fratini et al., 2008; Baratti et al., 2022). Adults are relatively sedentary and faithful to a specific area (whose extent depends on the sex and size of the owner) that they actively defend from conspecific intrusion (Cannicci et al., 1999). Planktonic larval stages last approximately four weeks in the water column (Drake et al., 1998; Cuesta and Rodriguez, 2000) before settlement. *P. marmoratus* breeds from late spring to late summer depending on the geographic area (Vernet-Cornubert, 1958; Zariquiey Alvarez, 1968; Ingle, 1980), thus the settlement of megalopae has a peak between June and October (Cuesta and Rodriguez, 2000; Flores et al., 2002) and seems to follow a semilunar cycle, at least along the open Atlantic coast where tidal excursions are more marked than in the Mediterranean Sea (Flores et al., 2002). On a microgeographic scale, hydrological features operating in coastal areas (i.e., the magnitude of the across-shore wind component and of the onshore currents) are among the main factors affecting settlement, while oceanographic processes are involved on a meso- and macrogeographic scale (Flores et al., 2002).

Previous genetic studies based on microsatellite polymorphisms (Fratini et al., 2008; Silva et al., 2009; Fratini et al., 2011; Fratini et al., 2013; Deli et al., 2016; Iannucci et al., 2020; Çetin et al., 2022) and mtDNA sequencing (Fratini et al., 2011; Kalkan et al., 2013; Deli et al., 2016; Fratini et al., 2016; Çetin et al., 2022) revealed weak but significant genetic heterogeneity among marbled crab populations in different areas including the Atlantic Ocean, the Black Sea and several Mediterranean Sea regions. In addition, former microsatellite studies, based on population samples separated by a few hundred kilometres, indicated that deviation from panmixia might occur at a small geographic scale, albeit the lack of geographically coherent differentiation suggests the existence of genetic patchiness.

This study aims at understanding the genetic structure of *P. marmoratus* among eight different locations spanning the central and the southern Adriatic Sea and the northern Ionian basins and including existing or planned MPAs. The study area has been selected for a Mediterranean Pilot Study in the framework of the CoCoNET FP7 project to identify groups of putatively interconnected MPAs, pointing out the importance of MPA networks instead of local single MPAs for conservation approaches (Boero et al., 2016). The inclusion of sampling sites along both the eastern and western coasts of the Adriatic and Ionian seas is of particular interest because both sides of the two basins include existing or planned MPAs. It is thus important to understand if they can act as an MPA network, using the marbled crab as a proxy for species with high dispersal potential. Using a multidisciplinary approach that combines microsatellite genetic analysis with Lagrangian simulations of dispersal and individual-based forward-time simulations, we: a) assessed nuclear genetic structure among *P. marmoratus* populations; b) estimated potential direct larval connectivity and retention at the sites used for genetics, with a biophysical model incorporating key vital traits affecting larval dispersal; c) investigated the genetic outcomes of different genetic drift-migration scenarios, with models incorporating species-specific fecundity and a wide range of population sizes; d) compared genetics and modelling results to elucidate and interpret the observed patterns of connectivity. In addition to these main goals, in this study we report 11 new microsatellite loci useful for population genetics studies of this widely investigated species.

Materials and methods

Sampling

Three hundred and fourteen samples of *Pachygrapsus marmoratus* were collected in 2013 and 2014 at eight different sites in the Adriatic and Ionian seas (Figure 1 and Table 1). All the locations, except Boka Kotorska (Montenegro) and Ammoudia (Greece), host a MPA or are reference areas for the establishment of a new MPA (Otranto, Italy). At each location, adult crabs were caught by hand from 30 cm above to 30 cm below the average sea level, and a cheliped or a pereiopod was removed from each individual and preserved in absolute ethanol. Genomic DNA was extracted using a standard salting out protocol (Patwary et al., 1994) and stored at −20°C before PCR amplifications.

Microsatellites genotyping

Fifteen polymorphic microsatellite loci specific for *P. marmoratus* were used for genetic analysis. Four of these loci (pm79, pm108, pm183, pm187) were previously isolated by Fratini et al. (2006), whereas eleven additional microsatellite loci (pmar01, pmar08, pmar10, pmar12, pmar13, pmar14, pmar15, pmar16, pmar17, pmar19, pmar20) were obtained *ex novo*, by an external service (http://www.genoscreen.fr), through a 454 GS-FLX Titanium pyrosequencing of enriched DNA libraries as described in Malausa et al. (2011). Forward primers of all 15 loci were labelled with fluorescent dyes for detection with ABI PRISM automatic sequencer and amplified together in two separate multiplex reactions. Table S1

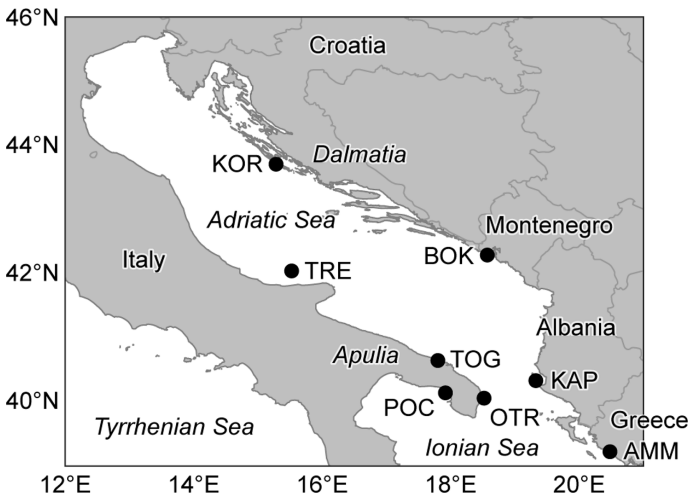

FIGURE 1
Sampling locations of *Pachygrapsus marmoratus*. See Table 1 for location acronyms.

(Supporting Information) reports details on all the microsatellite loci used in this study. PCRs were carried out in 10 µl total volume containing: 1X QIAGEN Multiple PCR Master mix (QIAGEN, HotStarTaq DNA Polymerase, Multiplex PCR Buffer, dNTP Mix), 0.2 µM primer mix and 100 ng of DNA template (diluted from DNA extractions). PCR conditions were as follows: an initial denaturation/activation step (95°C, 15 min) was followed by 35 cycles of denaturation (94°C, 30 s), annealing (61°C, 90 s) and extension (72°C, 60 s), and by a final elongation step (60°C, for 30 min). Fragment analysis was performed by an external service (http://www.bmr-genomics.it) on an ABI 3100 automated sequencer, and PCR products were sized with the internal standard LIZ500 (Applied Biosystems). To ensure reproducibility of results and minimize differences due to capillary electrophoresis, 10–15% of all specimens were re-genotyped and re-scored. Scoring was performed with PEAK SCANNER ver. 1.0 (Applied Biosystems). To minimize the negative consequences of poor allele calling, binning was automated with FLEXIBIN ver. 2 (Amos et al., 2007), which implements a method that does not assume collinearity between expected and measured fragment length. The scoring was manually checked and analysed with MICROCHECKER 2.2.3 (van Oosterhout et al., 2004) that allows detection of null alleles and estimation of their allelic frequency.

Statistical analyses of microsatellite data

Neutrality test

To detect outlier loci putatively under selection, whose inclusion in the analysis might distort genetic connectivity estimates, we applied two neutrality tests relying on the expectation that divergent selection should increase the observed level of genetic differentiation between populations.

TABLE 1 Summary of samples analysed in this study.

Country	Location	Acronym	Geographic coordinates		Sample size
			North	East	
Greece	Ammoudia	AMM	39°14.179’	20°28.721’	51
Albania	Karaburun Peninsula	KAP	40°23.568’	19°19.498’	17
Montenegro	Boka Kotorska Bay	BOK	42°23.252’	18°34.178’	31
Croatia	Kornati National Park	KOR	43°47.535’	15°16.889’	30
Italy	Tremiti Islands	TRE	42°08.315’	15°31.437’	34
Italy	Torre Guaceto	TOG	40°42.999’	17°48.003’	56
Italy	Otranto	OTR	40°06.554’	18°31.153’	42
Italy	Porto Cesareo	POC	40°11.715’	17°55.077’	53

The table reports the area of collection of population samples (countries and location), the sample acronym, the geographic coordinates, and the sample size.

First, the F_{ST}-outlier method implemented in LOSITAN (Antao et al., 2008), was run with the following settings: 1000000 simulations, stepwise mutation model (SMM), neutral F_{ST} and forced mean F_{ST}. Comparisons were performed first among all population samples and then between pairs of population. The second method, implemented in the R package DETSEL (Vitalis et al., 2003; Vitalis, 2012; R Team Core, 2015), relies on a model where a common ancestor population splits up into two populations, which afterward diverge only by random drift after a possible bottleneck event. In this case 500000 coalescent simulations were performed with a SMM mutation rate equal to 5×10^{-4} (Estoup and Angers, 1998) and, for nuisance parameters, ancestral population size varying from 500 to 10000 effective individuals, population size before the split from 0 to 500, number of generations since divergence from 50 to 100 generations, and time since the bottleneck varying from 0 to 200 generations. As suggested by the authors, because of the uncertainty in the nuisance parameter values, it is recommended to perform simulations using different combinations of values for the ancestral population size, divergence time and bottleneck parameters (Vitalis, 2012), that should correspond to the user knowledge of the biological model.

Using both tests, all loci falling outside the resulting 99% probability region under neutral expectations were considered as potentially under selection and excluded from further analysis.

Genetic diversity, Hardy-Weinberg and linkage equilibrium

Number of alleles (N_A), observed (H_O) and unbiased expected (H_E) heterozygosity were estimated, using GENETIX ver. 4.05.2 (Belkir et al., 2005); allelic richness (A_R) was computed with FSTAT 2.9.3.2 (Goudet, 2001) based on the smallest sample size across all population samples. We also tested for deviation from Hardy-Weinberg equilibrium (HWE) at each locus, and for linkage disequilibrium between pairs of loci using GENEPOP ver. online 4.2 (Raymond and Rousset, 1995; Rousset, 2008). Significance levels of HWE and linkage equilibrium were determined *via* the Markov Chain method (dememorizations = 10000, batches = 500, iterations = 10000); significance for tests involving multiple comparisons was obtained using the Benjamini-Hochberg correction (Benjamini and Hochberg, 1995).

Population differentiation

Genetic differentiation was investigated using ARLEQUIN 3.5 (Excoffier and Lischer, 2010) by analysis of molecular variance (AMOVA; Excoffier et al., 1992) and pairwise F_{ST} estimation following Weir and Cockerham (1984). Significance of differentiation was determined using 10000 random permutations of individuals among populations. As in the case of HW and linkage equilibrium tests, the Benjamini-Hochberg correction (Benjamini and Hochberg, 1995) was applied in case of multiple tests.

Since F_{ST} distance has been criticized because it can underestimate genetic differentiation in the case of high mutation rates (Hedrick, 2005; Wang, 2015), we also calculated the unbiased estimator of Jost's D, D_{est} (Jost, 2008), using the DIVERSITY package (Keenan et al., 2013). D_{est} considers the allele distribution among populations, and it is independent from the average within-population heterozygosity (Jost, 2008). In this case, the significance of pairwise comparisons was assessed by 1000 bootstrap replicates.

We also applied the Bayesian clustering approach implemented in STRUCTURE (Pritchard et al., 2000) and the discriminant analysis of principal components (DAPC) implemented in ADEGENET for R 3.2.3. (Jombart, 2008). Since both analyses identified a single population in the area, results are not further reported.

Lagrangian simulations

Potential connectivity of *P. marmoratus* among the eight sampling locations was investigated *via* Lagrangian simulations. Since basin-wide habitat mapping is not currently available for *P. marmoratus*, we conservatively assessed only the direct connections among the limited number of locations used for genetics. Considering that the species is very common in the study area, the inclusion of other release points would allow in the future a thorough and more realistic investigation of connectivity across the whole Adriatic–Ionian basin. At present, considering that sampling sites were representative of the existing MPA in the southern Adriatic and the northern Ionian seas, our results can provide conservative indications about the existence of a potential network of protected sites. The existence of additional unmodelled (and unprotected) *P. marmoratus* populations in suitable rocky shore habitats scattered across the surveyed area is expected to further increase the potential for dispersal among sampled locations through stepwise processes.

Daily average fields of current velocity produced by the Adriatic Forecasting System provided the physical engine of the model. The ocean circulation dataset (produced by the AREG model; Oddo et al., 2006; Guarnieri et al., 2010) covers the whole Adriatic basin and extends into the Ionian Sea down to the 39° N parallel, and it has a regular horizontal grid with a resolution of 1/45° (about 2.2 km) and 31 vertical sigma layers. Bathymetry has a horizontal resolution of 1/60°, and the coastline is set at the 10-m isobath.

Lagrangian particles, representing individual zoeae (larvae), were released from the eight sampling locations. Simulations were run over the period 2006–2013 to cover the temporal range in which sampled individuals were likely born (assuming an age at capture between 0 and 8 years). The release time was set to fit the available information regarding the duration of the zoea stage (1 month: Drake et al., 1998) and the subsequent

settlement of *P. marmoratus* megalopae (which peaks between June and October; Cuesta and Rodriguez, 2000; Flores et al., 2002). Therefore, releases were randomly distributed in time with a Gaussian distribution centred in mid-July and with 95% confidence bounds extending from May to September to match the subsequent settlement in June-October. We described larval release as a continuous random process since different release settings can strongly affect the results of the simulations (Pires et al., 2020), and because larval release patterns recorded for *P. marmoratus*, differently from most brachyurans studied so far, did not show a strong synchronization with lunar phases and were rather continuous over the lunar month (Flores and Paula, 2002a).

At each spawning event, Lagrangian particles (625,000 per site per year) were released according to a 2-D Gaussian distribution within a 1-km radius from each site, with a uniform distribution between 0.5 and 1 m depth along the vertical direction (to mimic the neustonic habit of *P. marmoratus* larvae: Flores et al., 2002; dos Santos et al., 2008). Trajectories were stepped forward at a fixed depth *via* an explicit 4th-order Runge-Kutta integration method with a 6-minute time step. To account for the (unknown) duration of the larval competency period, as well as for the swimming and navigation ability of megalopae (which take advantage of tidal stream transport to reach settlement areas; Flores et al., 2002), larvae were considered to successfully colonize the destination location if their position at the end of the pelagic phase fell within a circular buffer with a 10-km radius from each of the eight sampling sites.

Connectivity intensity (*sensu* Melià et al., 2016) was calculated as the percentage of particles released from a location and successfully reaching another one, averaged over the whole simulation period. Connectivity persistence (measuring the continuity of the flux throughout the years, *sensu* Melià et al., 2016) was defined as the stabilization coefficient, which is the reciprocal of the coefficient of variation of connectivity intensity.

Forward-time individual based genetic simulations with isolation and migration

To establish the number of generations and the amount of gene flow needed to obtain an F_{ST} equal to or greater than that observed with the empirical dataset, we carried out individual-based forward-time simulations with SIMUPOP (Peng and Kimmel, 2005).

For each simulation, we modelled eight populations, one for each sampling site. All the populations were of equal size, reflecting the lack of significant differences at genetic variability statistics (see Results section), with no overlapping generations. This latter assumption was justified by the difficulties associated with aging crabs (Kilada and Driscoll, 2017) and the subsequent limited information about age structure in this species (Arab et al., 2015), though size-frequency distributions of *Pachygrapsus marmoratus* clearly indicates that several cohorts co-occur in the same population (Flores and Paula, 2002b). Due to this assumption, the correlation of allelic frequencies between generations in our simulated populations is smaller than the one expected in age structured populations (Jorde and Ryman, 1995), namely in the real ones. Individual genotypes were generated for 14 loci (after removing an outlier locus, see Results section) from the overall microsatellite allele frequencies of the Adriatic–Ionian samples and sex was assigned randomly according to a 1:1 sex ratio. A SMM with a rate of 5×10^{-4} mutations per generation was assumed (Estoup and Angers, 1998). Individuals mated randomly within each population with the number of matings arbitrarily fixed to half of the population size for computational reasons. Each mating produced a fixed number of 22402 larvae, according to the average fecundity reported for this species (Arab et al., 2015) and assuming no sperm limitation. After reproduction, the larvae of each population were re-allocated according to local recruitment estimates and to specific scenarios of isolation or migration. After allocation, local larval pools were resized to the original local population dimension, assuming a density dependence acting in a constant and homogeneous way at all the sites, to produce the next generation population. The process was repeated for 160 generations, which was estimated from pilot runs to produce well-defined patterns of differentiation, and population genotypes were saved in SIMUPOP format at generations 0, 10, 20, 30, 40, 80, 160. Then, we used a custom python script to randomly subsample individual genotypes from each simulated population, matching the original sample sizes of the empirical dataset, and to generate the appropriate file formats for subsequent analysis. We used ARLEQUIN and the R package DIVERSITY, as for the empirical dataset, to calculate from simulated data the global F_{ST} and the pairwise F_{ST} together with their significance, and the Jost's *D* and its confidence intervals.

We tested two scenarios of population size with isolation and migration. To obtain the range of simulated populations sizes that is relevant for our dataset, an aspect that is often neglected in forward time individual based simulations (and obscure due to the non ideality of simulated populations), we proceeded as follows. We first estimated effective population sizes (N_e) from our empirical genetic data using different approaches including a SMM heterozygosity-based method (Ohta and Kimura, 1973; Papetti et al., 2009), Bayesian inference with MIGRATE (Beerli and Palczewski, 2010), and the LD method in NeEstimator (Do et al., 2014). Details on these methodologies are reported in Table S2. We then defined a reasonable range of N_e to be covered by the simulations, conservatively adding extreme values to take into account the uncertainty associated with N_e estimation by genetic methods, and we finally determined the simulated population sizes (N) needed to cover this range. To this end,

we performed several pilot runs with SIMUPOP, using the "lineage" module of the package, which allows measuring the true N_e of simulated populations of size N, by tracing directly alleles across generations, and we adjusted the simulated population sizes until obtaining the desired true effective population sizes. At the end of this exercise, N_e ranging from 500 to 20000 were tested, corresponding to simulated local population sizes ranging from 125 and 5000 individuals.

For each population size, the simulations were first run under a pure drift model (0 migrants per generation) and the number of generations of divergence needed to reach and exceed the overall F_{ST} observed in the empirical dataset was determined. To this end, as mentioned before, the simulated data were exported at predefined numbers of generations, subsampled, converted to ARLEQUIN format, and used to calculate the overall F_{ST} observed in simulations at generations 0, 10, 20, 30, 40, 80, and 160. For the same number of generations, we calculated pairwise F_{ST} and Jost's D to allow comparison of the simulated and empirical pattern of genetic differentiation. The same procedure was used to investigate the outcome of simulations performed under the scenario of migration outlined by Lagrangian simulations, with larvae allocated to sites according to the estimated connectivity intensity.

Results

Neutrality test

Both LOSITAN and DETSEL simulations identified locus pm108 as the only outlier (Figure S1). In LOSITAN, this locus showed a higher-than-expected F_{ST} both globally and in all pairwise comparisons involving Greece (AMM) and Croatia (KOR) populations. This locus fell outside the upper 99% CI of the F_{ST} versus H_E expected distribution (P-value$_{(Simul\ Fst\ <\ Sample\ Fst)}$ = 1). In the analysis with DETSEL, locus pm108 consistently laid outside the 99% probability region of population-specific parameters F_1 and F_2, whereas loci pm79, pm183 and pm187 were detected as outliers only in few comparisons. Based on these results and considering that the aim of this study is to investigate connectivity among locations, the analyses were performed on the 14 "neutral" loci after removal of pm108.

Genetic diversity, Hardy-Weinberg and linkage equilibrium

The analysis of 14 microsatellite loci on 314 specimens of *P. marmoratus* revealed relatively high molecular variability in the Adriatic and Ionian seas. All microsatellites were polymorphic with a minimum of three alleles per locus (pm79) and a maximum of 28 (pm187). Observed and expected heterozygosity ranged from 0.3706 (locus pmar16) to 0.8646 (locus pmar12) and from 0.4077 (locus pmar16) to 0.8981 (locus pmar12), respectively. In general, an excess of homozygotes was found (Table 2). At the population level, observed and expected heterozygosity ranged from 0.5688 in Torre Guaceto (TOG) to 0.6598 in Croatia (KOR) and from 0.6508 in Tremiti Islands (TRE) to 0.6931 in Montenegro (BOK), respectively (Table 3). The average allelic richness, based on a minimum sample size of $N = 16$, was similar in all populations, ranging from 5.9298 in TRE to 6.5959 in BOK. Probability tests of HWE were conducted for each of the 14 loci and for each of the eight sites. Fourteen out of 112 tests showed a significant departure from HWE, with a nominal significance threshold of 0.05 corrected for multiple tests. Departures were distributed almost evenly across loci, although 11 significant tests involved loci pm183, pmar17 and pmar19. For these loci, MICROCHECKER suggested the presence of null alleles. After correction for null alleles with MICROCHECKER, all tests involving these three loci were still significant; for this reason, all the subsequent analyses were performed considering both uncorrected data and data corrected for the presence of null alleles and the results were cross-checked. However, since the correction did not affect the final results, only results for the original data are reported. Overall, tests for linkage disequilibrium among all loci showed no significant departure from expected values.

Population differentiation

Overall, 99.6% of the total genetic variation was within individuals; correspondingly, an extremely small, yet significant, F_{ST} value was detected (global F_{ST} = 0.0041, $P < 0.01$). Pairwise comparisons based on the analysis of neutral loci showed a general homogeneity among sites with fixation indices ranging from negative values to a maximum of 0.0111, none of them significant after Benjamini-Hochberg correction for multiple tests (Table 4). The few comparisons associated with P-values below the uncorrected 0.05 threshold involved the Greek (AMM) and Porto Cesareo (POC) samples but did not show a spatial genetic pattern (Table 4). Similar results were obtained with Jost's D. The global D_{est} estimate was as small as 0.0017 (95% CI: -0.0092 – 0.0152). D_{est} between sampling locations ranged from –0.0022 to 0.0062 and all pairwise comparisons had a negative lower 95% CI boundary, which indicates lack of significant differentiation among samples (Table 5).

Lagrangian simulations

Figures 2, 3 summarize the results of the biophysical simulations and show the trajectories followed by Lagrangian particles across the study area and the links

TABLE 2 *Pachygrapsus marmoratus* microsatellites genetic variability and Hardy-Weinberg equilibrium.

Locus	N_A	H_O	H_E	HWE
pm79	3	0.4896	0.4994	0.1346
pm183	24	0.5428	0.7770	**P<0.0001**
pm187	28	0.6376	0.6590	0.1936
pmar01	6	0.7342	0.6426	0.5439
pmar08	9	0.6579	0.6984	0.1022
pmar10	16	0.7853	0.8340	0.0175
pmar12	23	0.8646	0.8981	0.0609
pmar13	9	0.7064	0.7288	0.4526
pmar14	6	0.4926	0.4853	0.2690
pmar15	9	0.6259	0.7647	**P<0.0001**
pmar16	5	0.3706	0.4077	0.0833
pmar17	14	0.7145	0.8794	**P<0.0010**
pmar19	9	0.4041	0.5441	**P<0.0001**
pmar20	11	0.5881	0.6589	0.0349

For each locus, we report the overall number of alleles (N_A), the average observed (H_O) and unbiased expected heterozygosity (H_E) and P-values associated with the Hardy-Weinberg test (HWE). Significant departures from Hardy-Weinberg equilibrium are reported in bold, according to the nominal significance threshold corrected for multiple tests (Benjamini and Hochberg, 1995).

between the study sites over the simulation period (2006–2013). Estimates of connectivity intensity among the eight locations and the corresponding connectivity persistence are shown in Tables 6 and 7, respectively. Estimated local retention was maximum in TOG (94%), KAP (40%) and BOK (30%), while it was lower in AMM, KOR and POC (between 10 and 20%) and negligible in TRE and OTR (Table 6). The intensity of estimated connections between sampling sites was, on average, two orders of magnitude lower than that of local retention (Table 6). "Alongshore" potential connections were highest in the western side of the basin (Figure 3A), with connectivity intensity between TRE, TOG and OTR ranging from 0.202 to 1.458% (Table 6), and a directional exchange orientated from north to south in the Adriatic and extending further along the Italian coastline in the Ionian (connectivity intensity range with POC: 0.008 – 0.293%, Table 6). In contrast, potential connections along the eastern shore of the basin were much weaker (connectivity intensity range: <0.001 – 0.022%) and restricted to neighbouring populations (Table 6). On the other hand, East to West connections were found, potentially linking the two sides of the Adriatic Sea (Figure 3A). The most intense connected Montenegro (BOK) with Apulia (especially TOG and OTR; connectivity intensity range: 1.265 – 1.573), as reported in Table 6. The Tremiti Islands (TRE) was one of the most connected sites, exchanging propagules with KOR (along a bidirectional link) and potentially providing a recruitment subsidy to the remaining Adriatic Apulian sites (especially TOG and OTR), with minor connections towards POC and BOK. The Greek site (AMM) was almost isolated from the others, with no incoming connections and only minor outgoing connections with Albania (KAP) and southern Apulia (POC, OTR). In terms of persistence, the most stable connections were those linking KOR and TRE, as well as those driven by the coastal current linking Apulian sites from north to south (Table 7 and Figure 3B).

TABLE 3 Summary of genetic variability estimates across sampling locations averaged over all 14 microsatellite loci.

Sample	A_R	H_O	H_E
AMM	6.3656	0.6255	0.6669
KAP	5.9857	0.6284	0.6787
BOK	6.5959	0.6018	0.6931
KOR	6.3403	0.6598	0.6887
TRE	5.9298	0.6213	0.6508
TOG	6.2074	0.5688	0.6754
OTR	6.3230	0.5854	0.6823
POC	6.3353	0.6312	0.6797

The table reports: average allelic richness among samples (A_R), average observed (H_O) and average unbiased expected heterozygosity (H_E). See Table 1 for sample acronyms.

TABLE 4 *Pachygrapsus marmoratus* pairwise genetic differentiation based on 14 neutral loci.

	AMM	KAP	BOK	KOR	TRE	TOG	OTR	POC
AMM	–	0.0645	0.0543	0.3307	*0.0470*	*0.0168*	0.0977	0.1782
KAP	0.0085	–	0.9167	0.4399	0.3276	0.3527	0.2720	*0.0280*
BOK	0.0062	-0.0047	–	0.1766	0.1179	0.1659	0.0625	0.0791
KOR	0.0016	0.0015	0.0048	–	0.1850	0.2028	0.1552	*0.0187*
TRE	*0.0059*	0.0031	0.0058	0.0038	–	0.9366	0.4645	*0.0385*
TOG	*0.0066*	0.0041	0.0048	0.0039	-0.0026	–	0.9203	0.1530
OTR	0.0043	0.0051	0.0071	0.0046	0.0013	-0.0018	–	0.0685
POC	0.0026	*0.0111*	0.0056	*0.0078*	*0.0061*	0.0033	0.0050	–

Estimates of pairwise F_{ST} among eight population samples are reported below the diagonal; associated P-values are provided above the diagonal. Significant values at the nominal threshold of $\alpha = 0.05$ and corresponding F_{ST} are reported in italic. No values were significant after correction for multiple tests (Benjamini and Hochberg, 1995).

Individual based forward-time genetic simulations

Individual-based forward-time simulations were performed to investigate if the observed patterns of genetic differentiation are compatible with different scenarios of isolation and migration. In order to set up simulations, global effective population size (N_e) was first estimated from our marbled crab empirical dataset using different methods, resulting in values ranging from about 600 to 2700 individuals (Table S2). When performing SIMUPOP simulations and calculating global effective population size by directly tracing alleles across generations in SIMUPOP (see Materials and methods section), these N_e values are obtained when the simulated local population sizes (N) are set to 150 – 675 individuals, considering 8 populations and panmixia (see Nunney, 1999 for the influence of inbreeding and genetic structure). Taking into account the many assumptions behind N_e estimations from genetic data, we included a wider range of local population sizes in SIMUPOP, ranging from 125 to 5000 individuals (Tables S3, S4).

SIMUPOP forward-time simulations revealed that in the case of complete isolation under pure drift, the F_{ST} values observed among Adriatic–Ionian population samples are reached and exceeded in few generations. Even when considering the biggest local population size tested ($N = 5000$), 30 generations of drift were sufficient to produce F_{ST} values higher than the 0.0041 of the empirical dataset (Table S3). Importantly, under this scenario, a large fraction of the pairwise comparisons of genetic differentiation (F_{ST}) becomes quickly significant after correction for multiple tests, thus contrasting the non-significant values observed for the empirical dataset (Table 4). Jost's D exhibited a somewhat lower power to detect differences, but still showed some confidence intervals excluding zero, differently from the original dataset (Table 5), starting from 40 generations of drift. This difference between the dataset simulated in case of isolation and the empirical dataset is even clearer when considering the smallest population sizes (N = 125 – 250), for which 10 generations of drift allow to reach complete significance with all the statistics.

The pattern remains similar when considering simulations incorporating Lagrangian estimates of dispersal (Table S4). A reduction of F_{ST} values in simulated samples is observed with respect to the case of isolation. However, also in this case all the genetic differentiation statistics increased monotonically, quickly exceeding the values observed in the empirical dataset. For instance, with all the local population sizes tested, 30 generations already produced significant pairwise F_{ST}

TABLE 5 *Pachygrapsus marmoratus* pairwise genetic differentiation measured as Jost's *D* based on 14 neutral loci.

	AMM	KAP	BOK	KOR	TRE	TOG	OTR	POC
AMM	–	(-0.0212-0.0456)	(-0.0108-0.0251)	(-0.0130-0.0224)	(-0.0101-0.0203)	(-0.0075-0.0154)	(-0.0068-0.0121)	(-0.0091-0.0149)
KAP	0.0051	–	(-0.0174-0.0293)	(-0.0201-0.0355)	(-0.0204-0.0343)	(-0.0203-0.0345)	(-0.0216-0.0380)	(-0.0196-0.0425)
BOK	0.0040	-0.0007	–	(-0.0161-0.0259)	(-0.0149-0.0250)	(-0.0136-0.0216)	(-0.0164-0.0264)	(-0.0137-0.0214)
KOR	0.0001	0.0000	0.0008	–	(-0.0114-0.0198)	(-0.0110-0.0212)	(-0.0107-0.0215)	(-0.0101-0.0293)
TRE	0.0022	0.0000	0.0008	0.0007	–	(-0.0092-0.0088)	(-0.0125-0.0192)	(-0.0121-0.0217)
TOG	0.0019	0.0004	0.0010	0.0012	-0.0022	–	(-0.0078-0.0129)	(-0.0086-0.0156)
OTR	0.0008	0.0002	0.0008	0.0019	0.0000	0.0000	–	(-0.0084-0.0229)
POC	0.0012	0.0061	0.0005	0.0062	0.002	0.0019	0.0045	–

Estimates of pairwise D_{est} among eight population samples are reported below the diagonal; associated 95% Confidence Interval (CI) are reported above the diagonal. No values were significant as all pairwise comparisons had a negative lower 95% CI limit.

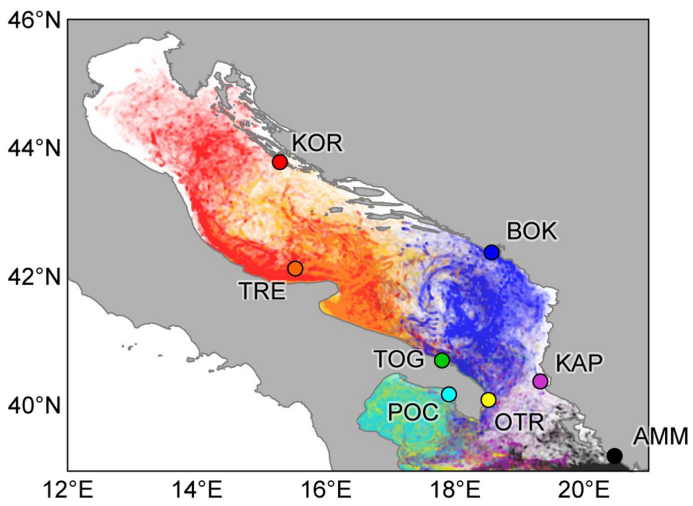

FIGURE 2
Larval dispersal resulting from Lagrangian simulation. Coloured circles indicate the locations of larval release (black: AMM; violet: KAP; blue: BOK; red: KOR; orange: TRE; green: TOG; yellow: OTR; cyan: POC). Each dot represents the arrival location of a particle released from each site over the time horizon of the simulation (2006–2013).

(minimum 6 comparisons when N = 5000), not observed with the original dataset. As before, Jost's *D* were slower to reach significance, but still showed confidence intervals excluding 0 starting from 10 – 80 generations, depending on local population size. In summary, the level of direct migration estimated by Lagrangian simulations was too low to explain the lack of genetic differentiation observed in the original dataset: the observed differentiation statistics were exceeded in few generations in the individual-based simulated dataset.

Discussion

This study, examining eight different locations spanning the central and the southern Adriatic Sea and the northern Ionian basins including existing or planned MPAs, unearthed the seascape connectivity of *P. marmoratus*, furthering our understanding of the impact of ocean currents on larval dispersal and genetic structure of this species and thus providing crucial information for conservation strategy definition.

The study focused on marbled crab, that has been selected as a model species with long larval duration. Nevertheless, the study significance goes beyond this target species, and its outcomes contribute to the general framework of larval dispersion and connectivity modelling key to marine area management. Our results suggest the existence of a genetically homogeneous population of marbled crab in the study area, pointing out a high level of exchange, but the direct connections between several sites highlighted by Lagrangian simulations did not completely explain how genetic homogeneity is maintained, according to the results of individual-based forward-time simulations. Noticeably, we identified a single outlier locus potentially under selection, whose inclusion in the analysis would produce a different picture, largely inflating genetic differentiation estimates. Collectively, our results indicate a high realized connectivity in the study area, which however, even for this species characterized by a relatively long larval duration, is not sustained by direct exchange between the existing and planned MPAs considered in this study.

Genetic homogeneity of marbled crabs' populations in the Adriatic-Ionian basins

When excluding the outlier locus pm108, no significant pairwise F_{ST} nor Jost's *D* comparisons were found. However, an extremely small, though still significant, global F_{ST} was detected, due to five F_{ST} pairwise comparisons with no clear spatial clustering.

Individual-based forward-time simulations clearly showed that this pattern is not expected in the case of isolation, where all the genetic differentiation statistics are expected to increase sharply and to quickly reach significance in few generations under a wide range of simulated population sizes. Importantly, strong genetic differentiation should arise under isolation after less than 10 generations when considering the smallest local population sizes, likely the most appropriate for the marbled crab, whereas a pattern similar to that observed in the empirical dataset is obtained for small population sizes at

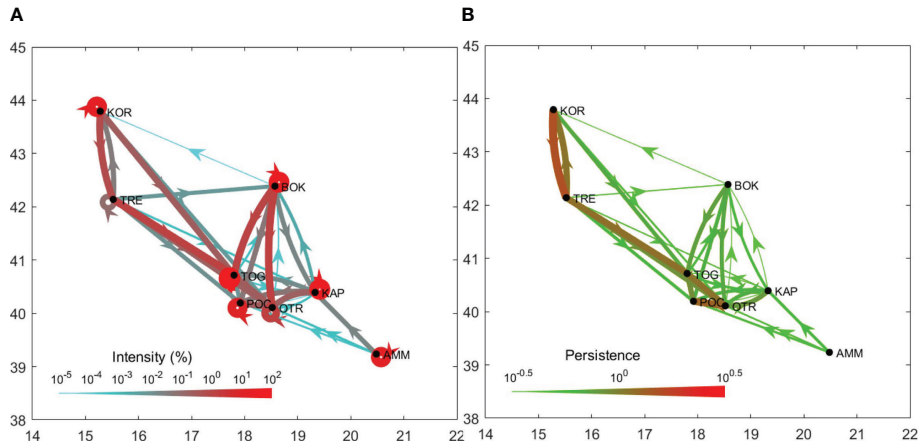

FIGURE 3
(A) Connectivity intensity graph for *Pachygrapsus marmoratus*. Connectivity intensity (estimated *via* Lagrangian simulation) is measured as the percentage (averaged across the simulation period) of larvae successfully moving from a site of origin to the destination sites. Loops (i.e. edges connecting a location with itself) indicate local retention. **(B)** Connectivity persistence graph for *Pachygrapsus marmoratus*. Connectivity persistence is defined as the stabilization coefficient (i.e. the reciprocal of the coefficient of variation) of the average annual flux of larvae successfully moving from a site of origin to the destination sites, calculated over the simulation period.

generation 0, i.e. by instantaneous drift due to sampling from a homogeneous gene pool.

Lagrangian simulations highlighted the existence of potential connections among sites, strongest for a group of sites in the southern Adriatic Sea and in the Italian portion of the Ionian Sea (KAP, BOK, TOG, OTR, POC), which were only partially connected to the Greek Ionian site (AMM) and to the two northernmost Adriatic populations (KOR and TRE). However, individual-based forward-time simulations clearly indicated that direct connections are not strong enough to maintain genetic homogeneity, and that, considering them alone, would produce a very mild effect compared with pure isolation. Importantly, a close inspection of simulation results showed that genetic homogeneity is not achieved even for the strongest potential connections (i.e. TRE to TOG and BOK to OTR, range intensity 1.458 – 1.573%). In fact, the few comparisons not achieving significance at the end of our simulations (1/28 to 4/28 depending on the simulated population size, Table S4) involved consistently only the TRE-KOR pair of sites, which was apparently characterized by a low potential recruitment at TRE (0.104%) rather than a higher exchange of larvae (unidirectional 0.775% from KOR to TRE).

This result has potential conservation implications, suggesting that direct connections among existing and planned MPA are not sufficient to maintain genetic homogeneity, and deserve further consideration.

The results of our Lagrangian simulations might have underestimated potential connectivity due to limits in our model. For instance, the two Ionian sites (AMM and POC) are very close to the border of the model domain, so edge effects may have negatively affected estimates of their connectivity strength. In fact, larvae moving south of 39°N and falling outside the oceanographic

TABLE 6 Connectivity intensity for *Pachygrapsus marmoratus*.

	AMM (%)	KAP (%)	BOK (%)	KOR (%)	TRE (%)	TOG (%)	OTR (%)	POC (%)
AMM	**16.477**	**0.022**	0.000	0.000	0.000	0.000	**<0.001**	**<0.001**
KAP	0.000	**40.159**	**0.002**	0.000	0.000	**0.016**	**0.222**	**0.064**
BOK	0.000	**0.021**	**30.496**	**<0.001**	0.000	**1.265**	**1.573**	**0.055**
KOR	0.000	0.000	0.000	**17.811**	**0.775**	**0.270**	**0.006**	0.000
TRE	0.000	**<0.001**	**0.007**	**0.040**	**0.104**	**1.458**	**0.202**	**0.011**
TOG	0.000	**<0.001**	**<0.001**	0.000	0.000	**93.591**	**0.263**	**0.008**
OTR	0.000	**<0.001**	**<0.001**	0.000	0.000	0.000	**1.631**	**0.293**
POC	0.000	**<0.001**	0.000	0.000	0.000	0.000	0.000	**10.790**

Connectivity intensity (estimated *via* Lagrangian simulation) is measured as the percentage (averaged across the simulation period) of larvae successfully moving from the sites of origin (in rows) to the destination sites (in columns). Values >0 are in bold. Cells on the diagonal indicate retention.

TABLE 7 Connectivity persistence for *Pachygrapsus marmoratus*.

	AMM	KAP	BOK	KOR	TRE	TOG	OTR	POC
AMM	2.175	0.561	–	–	–	–	0.435	0.490
KAP	–	3.468	0.361	–	–	0.361	0.678	0.626
BOK	–	0.539	2.809	0.354	–	0.753	0.706	0.662
KOR	–	–	–	3.047	1.546	0.696	0.463	–
TRE	–	0.402	0.390	1.126	1.079	1.163	0.851	0.594
TOG	–	0.536	0.514	–	–	17.095	1.128	0.895
OTR	–	0.816	0.354	–	–	–	0.884	1.300
POC	–	0.354	–	–	–	–	–	2.592

Connectivity persistence is defined as the stabilization coefficient (i.e. the reciprocal of the coefficient of variation) of the average annual flux of larvae successfully moving from the sites of origin (in rows) to the destination sites (in columns), calculated over the simulation period. Cells on the diagonal indicate retention.

domain considered in our model are indeed lost. In addition, the oceanographic engine is likely unable to describe hydrodynamic processes acting at a very fine scale along the coast. Moreover, disregarding the information on key behavioural features of *P. marmoratus* larvae (e.g., vertical migration and distribution and degree of active swimming) might have contributed to the underestimation of connectivity among sites.

Besides, the modelled potential connectivity could itself not translate into realized dispersal for a variety of reasons. For instance, we modelled arrival to a wide area (circular buffer with 10-km radius from destination) in a precise day corresponding to the end of the specified larval duration. Especially for long distances, such as those separating many of our sites, this assumption excludes the possibility of settlement before the end of the pelagic larval duration or adaptations to limit dispersal when favourable settlement habitats are found. Finally, we did not include mortality and predation, which can still reduce success of individual larvae in reaching distant places.

For all these reasons, we believe that the result of no direct connection should be considered conservative and that a high level of gene flow, much higher than that predicted by our simulations, is needed to maintain genetic homogeneity. This aspect deserves further attention, and, in particular, the inclusion of other aspects in the individual-based forward-time simulations, such as variability in fecundity and recruitment, a more skewed reproductive success, age structure, directionality in migration, is expected to add details and increase the level of connectivity needed to maintain genetic homogeneity.

The marbled crab is very common, typically occurring in habitats including rocks, crevices and cleavages, as well as artificial substrates such as breakwaters, pier piles and other (Edwards, 2005). Thus, considering the prevalence of rocky habitats along the coasts of our study area, many additional intermediate populations exist and could act as steppingstones between the sites at which genetic sampling and modelling was performed, strongly increasing the level of realized connectivity. Thus, the addition of other intermediate sites in the analysis should be considered for further detailed analysis.

Comparison with connectivity patterns of other species in the same study area

Integrating results of population genetics and Lagrangian connectivity, a general mixing in the area of study is evident for the marbled crab. Compared with previous studies on rocky shore species, our findings are in line with those obtained for *Diplodus sargus* in the southwestern Adriatic Sea (Di Franco et al., 2012; Pujolar et al., 2013). For this species, genetic homogeneity was observed at the local scale of Torre Guaceto and surrounding non-protected areas extending 100 km north and south of the MPA (Di Franco et al., 2012), and biophysical models suggested a potential dispersal extending up to the Ionian Sea (Pujolar et al., 2013). Our data confirm the connection of the western portion of South Adriatic and Ionian seas but extend the scale at which mixing occurs to the eastern side of the two basins. In the case of the black scorpionfish (*Scorpaena porcus*), a benthic coastal species inhabiting the same region, and the Mediterranean mussel (*Mytilus galloprovincialis*), a sessile filter-feeder with pelagic larvae very common in the Mediterranean and Black seas, a pattern of genetic differentiation slightly different from that of the marbled crab was observed (Boissin et al., 2016; Paterno, et al., 2019), with a clear break between the eastern and western part of the Adriatic basin indicated by genetic data. This is not in line with the results of Lagrangian simulations produced by Melià et al. (2016) for the black scorpionfish, which suggested that the eastern side of the Adriatic Sea can act as a potential source of propagules directed toward Apulia. On the other hand, genetic homogeneity among black scorpionfish samples from the western Adriatic and Ionian seas (Boissin et al., 2016) is consistent with the view of a strong potential connectivity within this part of the basin (Melià et al., 2016), in agreement with the results obtained for the marbled crab.

A high genetic connectivity along the western Adriatic and Ionian coasts was also observed in the estuarine and lagoon species *Atherina boyeri* (Congiu et al., 2002; Astolfi et al., 2005) and *Flexopecten glaber* (Pujolar et al., 2010). Genetic homogeneity and high potential connectivity between southwestern Adriatic and northern Ionian seas has also been found in the

Mediterranean mussel (Paterno et al., 2019) and in the Mediterranean shore crab *Carcinus aestuarii*, another species inhabiting estuaries and lagoons (Schiavina et al., 2014). In the shore crab, however, a clear subdivision between northern, central, and southern Adriatic Sea was found both with genetic markers and biophysical models. In contrast, genetic homogeneity and potential dispersal in *P. marmoratus* were found to extend also to the two northernmost samples, in the central Adriatic (TRE and KOR). While Schiavina et al. (2014) did not include any sample geographically close to KOR, their sample from the Lesina lagoon is approximately at the same latitude of our western Adriatic sample (TRE). The power to detect differences is also similar in the two studies (statistical power to detect an F_{ST} as low as 0.0025 was 100% and > 95% in *C. aestuarii* and *P. marmoratus*, respectively). However, in *C. aestuarii* the sample from Lesina was genetically differentiated from the closest South Adriatic sample (F_{ST} = 0.0030, P = 0.035; Lagrangian larval connectivity intensity = 0.001; Schiavina et al., 2014), in contrast with the TRE sample of *P. marmoratus*, which was homogeneous with the closest South Adriatic sample (TRE-TOG: F_{ST} = −0.0026, P = 0.937; Lagrangian larval connectivity intensity = 1.458; present study). This difference warns from generalizing results to different species/habitats in the absence of specific population genetic data and Lagrangian simulations suitably tailored to the specific dispersing traits of each species (as pointed out also by Melià et al., 2016 based on their analysis, conducted at the community level, in the same study area). The distinct genetic structures found for *C. aestuarii* and *P. marmoratus* could be related to a slightly different current pattern along and off the shore and can be further explained by the different habitat availability for the two species. In fact, the southwestern Adriatic coast is mostly rocky, with very few lagoons, likely determining a different geographical arrangement of sites acting as possible steppingstones with distinct effects on the connectivity of the two species. Thus, while a steppingstone effect would strongly increase connectivity for a rocky shore species such as the marbled crab, the same effect would be weaker (at least in this area) for a species inhabiting estuaries and lagoons such as the Mediterranean shore crab.

Outlier detection and methodological aspects

Interestingly, our genetic results identified one locus (pm108) as an outlier potentially subject to directional selection. Indeed, this locus revealed a much higher genetic divergence than the remaining 14 loci analysed, despite being a Type II marker, randomly isolated from genomic DNA, and not showing (at the time of the present study) significant BLAST matches with the NCBI nucleotide database.

This pattern contrasts with the results emerging from biophysical simulations and provides an indication about the utility of cross comparing the outcomes of genetic analyses and Lagrangian simulations. This is especially true when genetic differences are very small, and it is difficult to recognise a biologically meaningful signal of differentiation from noise and artefacts due to sampling and laboratory procedures. The advantage of cross comparisons is twofold: while genetic data can potentially validate and improve biophysical simulations (Selkoe et al., 2010), the latter can point out unrealistic genetic results. At present, any interpretation of the significance of the results obtained with the outlier locus would be highly speculative but, considering that the locus pm108 was used in all the microsatellite studies of *P. marmoratus* published so far, it would be useful to understand to what extent its inclusion in the analyses has contributed to determining the weak genetic differentiation reported in the literature. Therefore, this locus clearly deserves further consideration in future studies.

From the methodological point of view, we believe that neutrality tests, or, at least, an examination of how many loci support a given differentiation pattern, should be routinely performed, and reported in studies dealing with weak differentiation results. While this was a very well-established procedure in early times when permutation tests were not available to check for significance, and it has always been considered a good practice in case of weak differentiation (e.g. Wirth and Bernatchez, 2001), this approach has been neglected in many recent microsatellite studies. Now, with an increasing number of microsatellite loci used to perform genetic analyses, the probability to pick up loci putatively under selection is increasing, and we think that neutrality tests should be systematically applied to avoid reporting biased estimates. As a side note, no outliers were indeed detected in the previously cited *C. aestuarii* study (Schiavina et al., 2014; original data at http://dx.doi.org/10.5061/dryad.r0d1q).

In conclusion, our study pointed out the pitfalls of using *P. marmoratus* as a model species to assess the genetic connectivity among MPAs or areas deserving protection at the considered spatial scale. Indeed, the broad availability of rocky shore habitats within the study area likely results in the presence of several unsampled connected populations that operate as steppingstones interposed among the sampled locations. Nevertheless, while this could be true for a wide-dispersing species like the marbled crab, a completely different picture might emerge considering habitat former species with low dispersal such as those found in bioconstructions (Ingrosso et al., 2018) such as the sunset cup coral *Leptopsammia pruvoti* (Boscari et al., 2019). Indeed, connectivity patterns may vary widely among species, due to differences in reproductive phenology, duration of the larval phase and/or habitat range (Boissin et al., 2016; Melià et al., 2016; Carreras et al., 2017). Thus, when using genetic data to assist design and management of MPA networks, it is crucial to carefully choose informative species, with appropriate dispersing features, habitat suitability, and reproductive timing and duration. The explicit incorporation of these aspects, together with a representative sampling and the use of genome-wide approaches, will allow a

better understanding of the factors that shape oceanographic, demographic, and genetic connectivity.

Data availability statement

The datasets presented in this study can be found in online repositories. The names of the repository/repositories and accession number(s) can be found below: https://doi.org/10.5061/dryad.brv15dvc4. Sequences of new microsatellite loci have been deposited in Genbank under accession numbers KX185954-KX185964.

Author contributions

IAMM, PM, MS, and LZ conceived and designed the experiments. SF, IAMM, and MS performed the experiments. SF, IAMM, PM, MS, and LZ analysed the data. PM, TP, and LZ contributed reagents/materials/analysis tools. GA, SB, EB, LC, SF, CK, IAMM, PM, CP, TP, MP, MS, EV, and LZ critically discussed results. IAMM, PM, MS and LZ wrote the paper, which was approved by all the co-authors. All authors contributed to the article and approved the submitted version.

Acknowledgments

This project has received funding from the European Union's Seventh Framework Programme for Research, Technological Development and Demonstration under Grant Agreement No. 287844 (CoCoNET), which also supported IAMM post doc fellowship, and by the Italian Ministry of Research (PRIN 2020, Prot. 2020J3W3WC). We are thankful to the following people for their precious help for logistics and for collecting samples on the field: "Antheus srl (Lecce, Italy)"; G Guarnieri, F Boero, S Fraschetti and A Terlizzi (University of Salento, Italy); V Mačić (Institute of Marine Biology Kotor, Montenegro); D Micu (National Institute of Marine Research and Development, Romania); S Reizopoulou and MA Pancucci-Papadopoulou (Hellenic Centre for Marine Research, Greece); S Beqiraj (University of Tirana, Albania); E Hajdëri (Catholic University "Our Lady of Good Counsel", Albania).

Conflict of interest

The authors declare that the research was conducted in the absence of any commercial or financial relationships that could be construed as a potential conflict of interest.

Publisher's note

All claims expressed in this article are solely those of the authors and do not necessarily represent those of their affiliated organizations, or those of the publisher, the editors and the reviewers. Any product that may be evaluated in this article, or claim that may be made by its manufacturer, is not guaranteed or endorsed by the publisher.

Supplementary material

The Supplementary Material for this article can be found online at: https://www.frontiersin.org/articles/10.3389/fmars.2022.944851/full#supplementary-material

References

Amos, W., Hoffman, J. I., Frodsham, A., Zhang, L., Best, S., and Hill, V. S. (2007). Automated binning of microsatellite alleles: Problems and solutions. *Mol. Ecol. Notes* 7, 10–14. doi: 10.1111/j.1471-8286.2006.01560.x

Antao, T., Lopes, A., Lopes, R. J., Beja-Pereira, A., and Luikart, G. (2008). LOSITAN: A workbench to detect molecular adaptation based on a fst-outlier method. *BMC Bioinf.* 9, 323. doi: 10.1186/1471-2105-9-323

Arab, A., Kazanjian, G., and Bariche, M. (2015). Biological traits suggest a niche overlap between two grapsid crabs sharing the rocky intertidal of the eastern Mediterranean. *J. Mar. Biol. Assoc. UK* 95, 1685–1692. doi: 10.1017/S0025315415001010

Astolfi, L., Dupanloup, I., Rossi, R., Bisol, P. M., Faure, E., and Congiu, L. (2005). Mitochondrial variability of sand smelt *Atherina boyeri* populations from north Mediterranean coastal lagoons. *Mar. Ecol. Prog. Ser.* 297, 233–243. doi: 10.3354/meps297233

Baratti, M., Pinosio, S., Gori, M., Biricolti, S., Chini, G., Fratini, S., et al. (2022). Differential gene expression and chemical patterns of an intertidal crab inhabiting a polluted port and an adjacent marine protected area. *Sci. Tot. Env.* 822, 153463. doi: 10.1016/j.scitotenv.2022.153463

Beerli, P., and Palczewski, M. (2010). Unified framework to evaluate panmixia and migration direction among multiple sampling locations. *Genetics* 185, 313–326. doi: 10.1534/genetics.109.112532

Belkir, K., Borsa, P., Goudet, J., and Bonhomme, F. (2005). *Genetix v. 4.05, logiciel sous windows pour la génétique des populations* (Université Montpellier II: Laboratoire Génome et Populations. CNRS UPR 9060).

Benjamini, Y., and Hochberg, Y. (1995). Controlling the false discovery rate: A practical and powerful approach to multiple testing. *J. R. Stat. Soc B Met.* 57, 289–300. doi: 10.1111/j.2517-6161.1995.tb02031.x

Boero, F., Foglini, F., Fraschetti, S., Goriup, P., Planes, S., Soukissian, T., et al. (2016). CoCoNet: towards coast-to-coast networks of marine protected areas (From the shore to the high and deep sea), coupled with sea-based wind energy potential. *SCIRES IT* 6, 1–95. doi: 10.2423/i22394303v6Sp1

Boissin, E., Micu, D., Janczyszyn-Le Goff, M., Neglia, V., Bat, L., Todorova, V., et al. (2016). Contemporary genetic structure and post-glacial demographic history of the Black scorpionfish, *Scorpaena porcus*, in the Mediterranean and the Black seas. *Mol. Ecol.* 25, 2195–2209. doi: 10.1111/mec.13616

Boscari, E., Abbiati, M., Badalamenti, F., Bavestrello, G., Benedetti-Cecchi, L., Cannas, R., et al. (2019). A population genomics insight by 2b-RAD reveals populations' uniqueness along the Italian coastline in *Leptopsammia pruvoti* (Scleractinia, dendrophylliidae). *Divers. Distrib.* 25, 1101–1117. doi: 10.1111/ddi.12918

Cannicci, S., Paula, J., and Vannini, M. (1999). Activity pattern and spatial strategy in *Pachygrapsus marmoratus* (*Decapoda: grapsidae*) from Mediterranean and Atlantic shores. *Mar. Biol.* 133, 429–435. doi: 10.1007/s002270050481

Carreras, C., Ordóñez, V., Zane, L., Krushel, C., Nasto, I., Macpherson, E., et al. (2017). Population genomics of an endemic Mediterranean fish: Differentiation by fine scale dispersal and adaptation. *Sci. Rep.* 7, 43417. doi: 10.1038/srep43417

Çetin, C., Furman, A., Kalkan, E., and Bilgin, R. (2022). Mitonuclear genetic patterns of divergence in the marbled crab, *Pachygrapsus marmoratus* (Fabriciu) along the Turkish seas. *PloS One* 7, e0266506. doi: 10.1371/journal.pone.0266506

Congiu, L., Rossi, R., and Colombo, G. (2002). Population analysis of the sand smelt *Atherina boyeri* (*Teleostei atherinidae*), from Italian coastal lagoons by random amplified polymorphic DNA. *Mar. Ecol. Prog. Ser.* 229, 279–289. doi: 10.3354/meps229279

Cowen, R. K., and Sponaugle, S. (2009). Larval dispersal and marine population connectivity. *Annu. Rev. Mar. Sci.* 1, 443–466. doi: 10.1146/annurev.marine.010908.163757

Cuesta, J. A., and Rodriguez, A. (2000). Zoeal stages of the intertidal crab *Pachygrapsus marmoratus* (Fabricius) (*Brachyura, grapsidae*) reared in the laboratory. *Hydrobiologia* 436, 119–130. doi: 10.1023/A:1026576614590

Dauvin, J. C. (2009). Record of the marbled crab *Pachygrapsus marmoratus* (*Crustacea: Brachyura: Grapsidea*) on the coast of northern cotentin, Normandy, western English channel. *Mar. Biodivers. Rec.* 2, e92. doi: 10.1017/S1755267209001109

Deli, T., Fratini, S., Ragionieri, L., Said, K., Chatti, N., and Schubart, C. D. (2016). Phylogeography of the marbled crab *Pachygrapsus marmoratus* (*Decapoda, grapsidae*) along part of the African Mediterranean coast reveals genetic homogeneity across the siculo-Tunisian strait versus heterogeneity across the Gibraltar strait. *Mar. Biol. Res.* 12, 471–487. doi: 10.1080/17451000.2016.1154972

deRivera, C. E., Hitchcock, N. G., Teck, S. J., Steves, B. P., Hines, A. H., and Ruiz., G. M. (2007). Larval development rate predicts range expansion of an introduced crab. *Mar. Biol.* 150, 1275–1288. doi: 10.1007/s00227-006-0451-9

Di Franco, A., Coppini, G., Pujolar, J. M., De Leo, G. A., Gatto, M., Lyubartsev, V., et al. (2012). Assessing dispersal patterns of fish propagules from an effective Mediterranean marine protected area. *PloS One* 7, e52108. doi: 10.1371/journal.pone.0052108

dos Santos, A., Santos, A. M. P., Conway, D. V. P., Bartilotti, C., Lourenço, P., and Queiroga, H. (2008). Diel vertical migration of decapod larvae in the Portuguese coastal upwelling ecosystem: Implications for offshore transport. *Mar. Ecol. Prog. Ser.* 359, 171–183. doi: 10.3354/meps07341

Do, C., Waples, R. S., Peel, D., Macbeth, G. M., Tillett, B. J., and Ovenden, J. R. (2014). NeEstimator V2: Re-implementation of software for the estimation of contemporary effective population size (Ne) from genetic data. *Mol. Ecol. Resour.* 14, 209–214. doi: 10.1111/1755-0998.12157

Drake, P., Arias, A. M., and Rodriguez, A. (1998). Seasonal and tidal abundance patterns of decapod crustacean larvae in a shallow inlet (SW Spain). *J. Plankton Res.* 20, 585–601. doi: 10.1093/plankt/20.3.585

Edwards, R. V. (2005). "*Pachygrapsus marmoratus* a marbled rock crab," in *Marine life information network: Biology and sensitivity key information reviews*. Eds. H. Tyler-Walters and K. Hiscock (Plymouth: Marine Biological Association of the United Kingdom). Available at: http://192.171.193.68/species/detail/1978.

Estoup, A., and Angers, B. (1998). "Microsatellites and minisatellites for molecular ecology: theoretical and empirical considerations," in *Advances in molecular ecology*. Ed. G. Carvalho (Amsterdam: IOS Press), 55–86.

Excoffier, L., and Lischer, H. E. L. (2010). Arlequin suite ver 3.5: a new series of programs to perform population genetics analyses under Linux and windows. *Mol. Ecol. Resour.* 10, 564–567. doi: 10.1111/j.1755-0998.2010.02847.x

Excoffier, L., Smouse, P. E., and Quattro, J. M. (1992). Analysis of molecular variance inferred from metric distances among DNA haplotypes: Application to human mitochondrial DNA restriction data. *Genetics* 131, 479–491. doi: 10.1093/genetics/131.2.479

Fenaux, L., Cellario, C., and Etienne, M. (1985). Croissance de la larve de l'Oursin *Paracentrotus lividus*. *Mar. Biol.* 86, 151–157. doi: 10.1007/BF00399021

Flores, A. A. V., Cruz, J., and Paula, J. (2002). Temporal and spatial patterns of settlement of brachyuran crab megalopae at a rocky coast in central Portugal. *Mar. Ecol. Prog. Ser.* 229, 207–220. doi: 10.3354/meps229207

Flores, A. A. V., and Paula, J. (2002a). Sexual maturity, larval release and reproductive output of two brachyuran crabs from a rocky intertidal area in central Portugal. *Invert. Reprod. Dev.* 42, 21–34. doi: 10.1080/07924259.2002.9652506

Flores, A., and Paula, J. (2002b). Population dynamics of the shore crab *Pachygrapsus marmoratus* (Brachyura: Grapsidae) in the central Portuguese coast. *J. Mar. Biol. Ass. UK* 82, 229–241. doi: 10.1017/S0025315402005404

Fratini, S., Ragionieri, L., Cutuli, G., Vannini, M., and Cannicci, S. (2013). Pattern of genetic isolation in the crab *Pachygrapsus marmoratus* within the Tuscan archipelago (Mediterranean Sea). *Mar. Ecol. Prog. Ser.* 478, 173–183. doi: 10.3354/meps10247

Fratini, S., Ragionieri, L., Deli, T., Harrer, A., Marino, I. A. M., Cannicci, S., et al. (2016). Unravelling population genetic structure with mitochondrial DNA in a notional panmictic coastal crab species: Sample size makes the difference. *BMC Evol. Biol.* 16, 150. doi: 10.1186/s12862-016-0720-2

Fratini, S., Ragionieri, L., Papetti, C., Pitruzzella, G., Rorandelli, R., Barbaresi, S., et al. (2006). Isolation and characterization of microsatellites in *Pachygrapsus marmoratus* (Grapsidae; decapoda; brachyura). *Mol. Ecol. Notes* 6, 179–181. doi: 10.1111/j.1471-8286.2005.01184.x

Fratini, S., Schubart, C. D., and Ragionieri, L. (2011). "Population genetics in the rocky shore crab *Pachygrapsus marmoratus* from the western Mediterranean and eastern Atlantic: Complementary results from mtDNA and microsatellites at different geographic scales," in *Phylogeography and population genetic in Crustacea*. Eds. C. Held, S. Koenemann and C. D. Schubart (Boca Raton: Taylor & Francis/CRC Press), 191–213.

Fratini, S., Zane, L., Ragionieri, L., Vannini, M., and Cannicci, S. (2008). Relationship between heavy metal accumulation and genetic variability decrease in the intertidal crab *Pachygrapsus marmoratus* (Decapoda; grapsidae). *Estuar. Coast. Shelf Sci.* 79, 679–686. doi: 10.1016/j.ecss.2008.06.009

Galindo, H. M., Olson, D. B., and Palumbi, S. R. (2006). Seascape genetics: A coupled oceanographic-genetic model predicts population structure of Caribbean corals. *Curr. Biol.* 16, 1622–1626. doi: 10.1016/j.cub.2006.06.052

Galindo, H. M., Pfeiffer-Herbert, A. S., McManus, M. A., Chao, Y. I., Chai, F., and Palumbi, S. R. (2010). Seascape genetics along a steep cline: Using genetic patterns to test predictions of marine larval dispersal. *Mol. Ecol.* 19, 3692–3707. doi: 10.1111/j.1365-294X.2010.04694.x

Gilg, M. R., and Hilbish, T. J. (2003). The geography of marine larval dispersal: coupling genetics with fine-scale physical oceanography. *Ecology* 84, 2989–2998. doi: 10.1890/02-0498

Goudet, J. (2001) *FSTAT, a program to estimate and test gene diversities and fixation indices (version 2.9.3)*. Available at: www.unil.ch/popgen/softwares/fstat.html.

Guarnieri, A., Oddo, P., Pastore, M., Pinardi, N., and Ravaioli, M. (2010). "The Adriatic basin forecasting system: New model and system development," in *Proceeding of the Fifth International Conference on EuroGOOS*, 184–190 (Exeter, UK: EuroGOOS Publication).

Hauser, L., and Carvalho, G. R. (2008). Paradigm shifts in marine fisheries genetics: Ugly hypotheses slain by beautiful facts. *Fish.* 9, 333–362. doi: 10.1111/j.1467-2979.2008.00299.x

Hedrick, P. W. (2005). A standardized genetic differentiation measure. *Evolution* 59, 1633–1638. doi: 10.1111/j.0014-3820.2005.tb01814.x

Hohenlohe, P. A. (2004). Limits to gene flow in marine animals with planktonic larvae: models of *Littorina* species around point conception, California. *Biol. J. Linn. Soc* 82, 169–187. doi: 10.1111/j.1095-8312.2004.00318.x

Iannucci, A., Cannicci, S., Caliani, I., Baratti, M., Pretti, C., and Fratini, S. (2020). Investigation of mechanisms underlying chaotic genetic patchiness in the intertidal marbled crab *Pachygrapsus marmoratus* (Brachyura: Grapsidae) across the Ligurian Sea. *BMC Evol. Biol.* 20, 108. doi: 10.1186/s12862-020-01672-x

Ingle, R. W. (1980). *British Crabs* (London: Oxford University Press).

Ingrosso, G., Abbiati, M., Badalamenti, F., Bavestrello, G., Belmonte, G., Cannas, R., et al. (2018). Mediterranean Bioconstructions along the Italian coast. *Adv. Mar. Biol.* 79, 61–136. doi: 10.1016/bs.amb.2018.05.001

Jombart, T. (2008). Adegenet: A r package for the multivariate analysis of genetic markers. *Bioinformatics* 24, 1403–1405. doi: 10.1093/bioinformatics/btn129

Jorde, P. E., and Ryman, N. (1995). Temporal allele frequency change and estimation of effective size in populations with overlapping generations. *Genetics* 139, 1077–1090. doi: 10.1093/genetics/139.2.1077

Jost, L. (2008). G_{ST} and its relatives do not measure differentiation. *Mol. Ecol.* 17, 4015–4026. doi: 10.1111/j.1365-294X.2008.03887.x

Kalkan, E., Karhan, S.Ü., and Bilgin, R. (2013). Population genetic structure of the marbled crab, *Pachygrapsus marmoratus* from Turkish coasts of the Black Sea and the eastern Mediterranean. *Rapp. Commun. Int. Mer Médit.* 40, 713.

Keenan, K., McGinnity, P., Cross, T. F., Crozier, W. W., and Prodöhl, P. A. (2013). diveRsity: An r package for the estimation of population genetics parameters and their associated errors. *Methods Ecol. Evol.* 4, 782–788. doi: 10.1111/2041-210X.12067

Kilada, R., and Driscoll, J. G. (2017). Age determination in crustaceans: A review. *Hydrobiologia* 799, 21–36. doi: 10.1007/s10750-017-3233-0

Knutsen, H., Olsen, E. M., Jorde, P. E., Espeland, S. H., André, C., and Stenseth., N. C. (2011). Are low but statistically significant levels of genetic differentiation in marine fishes 'biologically meaningful'? A case study of coastal Atlantic cod. *Mol. Ecol.* 20, 768–783. doi: 10.1111/j.1365-294X.2010.04979.x

Levin, L. A. (2006). Recent progress in understanding larval dispersal: New directions and digressions. *Integr. Comp. Biol.* 46, 282–297. doi: 10.1093/icb/icj024

Malausa, T., Gilles, A., Meglécz, E., Blanquart, H., Duthoy, S., Costedoat, C., et al. (2011). High-throughput microsatellite isolation through 454 GS-FLX

titanium pyrosequencing of enriched DNA libraries. *Mol. Ecol. Resour.* 11, 638–644. doi: 10.1111/j.1755-0998.2011.02992.x

Melià, P., Schiavina, M., Rossetto, M., Gatto, M., Fraschetti, S., and Casagrandi, R. (2016). Looking for hotspots of marine metacommunity connectivity: A methodological framework. *Sci. Rep.* 6, 23705. doi: 10.1038/srep23705

Nunney, L. (1999). The effective size of a hierarchically structured population. *Evolution* 53, 1–10. doi: 10.1111/j.1558-5646.1999.tb05328.x

Oddo, P., Pinardi, N., Zavatarelli, M., and Coluccelli, A. (2006). The Adriatic basin forecasting system. *Acta Adriat.* S47, 169–184. Available at: https://hrcak.srce.hr/8550

Ohta, T., and Kimura, M. (1973). A model of mutation appropriate to estimate the number of electrophoretically detectable alleles in a finite population. *Genet. Res.* 22, 201–204. doi: 10.1017/S0016672300012994

Olds, A. D., Connolly, R. M., Pitt, K. A., Pittman, S. J., Maxwell, P. S., Huijbers, C. M., et al. (2016). The conservation value of seascape connectivity. *Glob. Ecol. Biogeogr.* 25, 3–15. doi: 10.1111/geb.12388

Palumbi, S. R. (2003). Population genetics, demographic connectivity, and the design of marine reserves. *Ecol. Appl.* 13, S146–S158. doi: 10.1890/1051-0761(2003)013[0146:PGDCAT]2.0.CO;2

Papetti, C., Susana, E., Patarnello, T., and Zane, L. (2009). Spatial and temporal boundaries to gene flow between *Chaenocephalus aceratus* populations at South Orkney and South Shetlands. *Mar. Ecol. Prog. Ser.* 376, 269–281. doi: 10.3354/meps07831

Paterno, M., Bat, L., Souissi, J. B., Boscari, E., Chassanite, A., Congiu, L., et al. (2019). A genome-wide approach to the phylogeography of the mussel *Mytilus galloprovincialis* in the Adriatic and the Black seas. *Front. Mar. Sci.* 6, 566. doi: 10.3389/fmars.2019.00566

Paterno, M., Schiavina, M., Aglieri, G., Ben Souissi, J., Boscari, E., Casagrandi, R., et al. (2017). Population genomics meet Lagrangian simulations: Oceanographic patterns and long larval duration ensure connectivity among *Paracentrotus lividus* populations in the Adriatic and Ionian seas. *Ecol. Evol.* 7, 2463–2479. doi: 10.1002/ece3.2844

Patwary, M. U., Kenchington, E. L., Bird, C. J., and Zouros, E. (1994). The use of random amplified polymorphic DNA markers in genetic studies of the sea scallop *Placopecten magellanicus* (Gmelin 1791). *J. Shellfish Res.* 13, 547–553.

Pedrotti, M. L. (1993). Spatial and temporal distribution and recruitment of echinoderm larvae in the Ligurian Sea. *J. Mar. Biol. Assoc. UK* 73, 513–530. doi: 10.1017/S0025315400033075

Peng, B., and Kimmel, M. (2005). simuPOP: A forward-time population genetics simulation environment. *Bioinformatics* 21, 3686–3687. doi: 10.1093/bioinformatics/bti584

Pires, R. F.T., Peliz, Á., Pan, M., and dos Santos, A. (2020). "There and Back Again" – How Decapod Megalopae Find the Way Home: A Modelling Exercise for *Pachygrapsus marmoratus*. *Prog. Oceanogr.* 184, 102231. doi: 10.1016/j.pocean.2020.102331

Pritchard, J. K., Stephens, M., and Donnelly, P. (2000). Inference of population structure using multilocus genotype data. *Genetics* 155, 945–959. doi: 10.1093/genetics/155.2.945

Pujolar, J. M., Marčeta, T., Saavedra, C., Bressan, M., and Zane, L. (2010). Inferring the demographic history of the Adriatic *Flexopecten* complex. *Mol. Phylogenet. Evol.* 57, 942–947. doi: 10.1016/j.ympev.2010.08.002

Pujolar, J. M., Schiavina, M., Di Franco, A., Melià, P., Guidetti, P., Gatto., M., et al. (2013). Understanding the effectiveness of marine protected areas using genetic connectivity patterns and Lagrangian simulations. *Divers. Distrib.* 19, 1531–1542. doi: 10.1111/ddi.12114

Raymond, M., and Rousset, F. (1995). GENEPOP (Version 1.2): Population genetics software for exact tests and ecumenicism. *J. Hered.* 86, 248–249. doi: 10.1093/oxfordjournals.jhered.a111573

Rousset, F. (2008). GENEPOP'007: A complete re-implementation of the GENEPOP software for windows and Linux. *Mol. Ecol. Resour.* 8, 103–106. doi: 10.1111/j.1471-8286.2007.01931.x

R Team Core (2015). *R: a language and environment for statistical computing* (Vienna, Austria: R Foundation for Statistical Computing). Available at: http://www.R–project.org.

Schiavina, M., Marino, I. A. M., Zane, L., and Melià, P. (2014). Matching oceanography and genetics at the basin scale. Seascape connectivity of the Mediterranean shore crab in the Adriatic Sea. *Mol. Ecol.* 23, 5496–5507. doi: 10.1111/mec.12956

Schunter, C., Carreras-Carbonell, J., Macpherson, E., Tintoré, J., Vidal-Vijande, E., Pascual, A., et al. (2011). Matching genetics with oceanography: Directional gene flow in a Mediterranean fish species. *Mol. Ecol.* 20, 5167–5181. doi: 10.1111/j.1365-294X.2011.05355.x

Selkoe, K. A., and Toonen, R. J. (2011). Marine connectivity: A new look at pelagic larval duration and genetic metrics of dispersal. *Mar. Ecol. Prog. Ser.* 436, 291–305. doi: 10.3354/meps09238

Selkoe, K. A., Watson, J. R., White, C., Horin, T. B., Iacchei, M., Mitarai, S., et al. (2010). Taking the chaos out of genetic patchiness: Seascape genetics reveals ecological and oceanographic drivers of genetic patterns in three temperate reef species. *Mol. Ecol.* 19, 3708–3726. doi: 10.1111/j.1365-294X.2010.04658.x

Silva, I. C., Mesquita, N., Schubart, C. D., Judite Alves, M., and Paula, J. (2009). Genetic patchiness of the shore crab *Pachygrapsus marmoratus* along the Portuguese coast. *J. Exp. Mar. Biol. Ecol.* 378, 50–57. doi: 10.1016/j.jembe.2009.07.032

van Oosterhout, C., Hutchinson, W. F., Wills, D. P. M., and Shipley, P. (2004). MICRO-CHECKER: software for identifying and correcting genotyping errors in microsatellite data. *Mol. Ecol. Notes* 4, 535–538. doi: 10.1111/j.1471-8286.2004.00684.x

Vernet-Cornubert, G. (1958). Recherches sur la sexualité du crabe *Pachygrapsus marmoratus* (Fabricius). *Arch. Zool. Exp. Gen.* 96, 101–276.

Vitalis, R. (2012). DetSel: an r-package to detect marker loci responding to selection. *Methods Mol. Biol.* 888, 277–293. doi: 10.1007/978-1-61779-870-2_16

Vitalis, R., Dawson, K., Boursot, P., and Belkhir, K. (2003). DetSel 1.0: A computer program to detect markers responding to selection. *J. Hered.* 94, 429–431. doi: 10.1093/jhered/esg083

Wang, J. (2015). Does G_{ST} underestimate genetic differentiation from marker data? *Mol. Ecol.* 24, 3546–3558. doi: 10.1111/mec.13204

Ward, R. D., Woodwark, M., and Skibinski, D. O. F. (1994). A comparison of genetic diversity levels in marine, freshwater, and anadromous fishes. *J. Fish. Biol.* 44, 213–232. doi: 10.1111/j.1095-8649.1994.tb01200.x

Weir, B. S., and Cockerham, C. C. (1984). Estimating f-statistics for the analysis of population structure. *Evolution* 38, 1358–1370. doi: 10.2307/2408641

Wirth, T., and Bernatchez, L. (2001). Genetic evidence against panmixia in the European eel. *Nature* 409, 1037–1040. doi: 10.1038/35059079

Zariquiey Alvarez, R. (1968). *Crustaceos decapodos ibericos* Vol. 32 (Barcelona: Investigación Pesquera), 1–510.

frontiers | Frontiers in Marine Science

TYPE Original Research
PUBLISHED 28 November 2022
DOI 10.3389/fmars.2022.1049056

OPEN ACCESS

EDITED BY
Tomihiko Higuchi,
The University of Tokyo, Japan

REVIEWED BY
Julie Vecchio,
South Carolina Department of Natural Resources, United States
Juliano Coletto,
Federal University of Rio Grande, Brazil

*CORRESPONDENCE
Jun Matsubayashi
matsuj@fra.affrc.go.jp

SPECIALTY SECTION
This article was submitted to Marine Biology, a section of the journal Frontiers in Marine Science

RECEIVED 20 September 2022
ACCEPTED 26 October 2022
PUBLISHED 28 November 2022

CITATION
Matsubayashi J, Kimura K, Ohkouchi N, Ogawa NO, Ishikawa NF, Chikaraishi Y, Tsuda Y and Minami H (2022) Using geostatistical analysis for simultaneous estimation of isoscapes and ontogenetic shifts in isotope ratios of highly migratory marine fish. *Front. Mar. Sci.* 9:1049056. doi: 10.3389/fmars.2022.1049056

Using geostatistical analysis for simultaneous estimation of isoscapes and ontogenetic shifts in isotope ratios of highly migratory marine fish

Jun Matsubayashi[1]*, Katsuya Kimura[1], Naohiko Ohkouchi[2], Nanako O. Ogawa[2], Naoto F. Ishikawa[2], Yoshito Chikaraishi[3], Yuichi Tsuda[1] and Hiroshi Minami[1]

[1]Fisheries Resources Institute, Japan Fisheries Research and Education Agency, Yokohama, Kanagawa, Japan, [2]Biogeochemistry Research Center, Japan Agency for Marine-Earth Science and Technology, Yokosuka, Kanagawa, Japan, [3]Institute of Low Temperature Science, Hokkaido University, Sapporo, Hokkaido, Japan

Tracking migration of highly migratory marine fish using isotope analysis (iso-logging) has become a promising tool in recent years. However, application of this method is often hampered by the lack of essential information such as spatial variations in isotope ratios across habitats (isoscapes) and ontogenetic shifts of isotope ratios of target animals. Here, we test the utility of geostatistical analysis to generate isoscapes of $\delta^{13}C$ and $\delta^{15}N$ in the western Pacific and estimate the ontogenetic shifts in $\delta^{13}C$ and $\delta^{15}N$ values of a target species. We first measured $\delta^{13}C$ and $\delta^{15}N$ in the white muscle of juvenile (n = 210) and adult (n = 884) skipjack tuna *Katsuwonus pelamis* sampled across the northwest Pacific. Next we fitted a geostatistical model to account for the observed spatial variations in $\delta^{13}C$ and $\delta^{15}N$ of skipjack by fork length and other environmental variables with spatial random effects. We then used the best-fit models to predict the isoscapes of $\delta^{13}C$ and $\delta^{15}N$ in 2021. Furthermore, we measured $\delta^{15}N$ of amino acids ($\delta^{15}N_{AAs}$) of skipjack (n = 5) to determine whether the observed spatial variation of isotope ratios resulted from baseline shifts or differences in trophic position. The geostatistical model reasonably estimated both isoscapes and ontogenetic shifts from isotope ratios of skipjack, and the isoscapes showed that $\delta^{13}C$ and $\delta^{15}N$ can clearly distinguish the latitudinal migration of skipjack in the western Pacific. The $\delta^{15}N_{AAs}$ supported the results of the geostatistical model, that is, observed variations in skipjack $\delta^{15}N$ were largely derived from a baseline shift rather than regional differences in trophic position. Thus, we showed that geostatistical analysis can provide essential basic information required for iso-logging without compound-specific isotope analysis.

KEYWORDS

iso-logging, isoscape, ontogenetic shift, skipjack tuna, δ 13 C, δ 15 N, compound-specific isotope analysis

Introduction

Shared fish stocks, namely fish resources with high migration ability that cross exclusive economic zone (EEZ) boundaries, are more prone to overexploitation than other stocks (e.g. McWhinnie, 2009; Kraska et al., 2015; Popova et al., 2019). Therefore, cooperative stock management among stakeholders is a necessary prerequisite for achieving sustainable fisheries of these species (e.g. Caddy, 1997; Miller and Munro, 2004). Appropriate understanding of migration routes and their individual and temporal variation is crucial for better cooperative management of shared fish stocks. Knowledge of a migration route is also essential for determining which countries share fishery resources from the same stock, as well as for assessing the effect of changes in the migration routes on the stock and fishing conditions in each country (Miller and Munro, 2004; Vatsov, 2016). Recently developed models (e.g. Carvalho et al., 2015; Sippel et al., 2015) can make use of migration data for stock assessment, thus demonstrating the benefits of understanding the migration routes of these fish.

In fishery science, one of the main approaches for studying fish migration is dynamic tracking using electronic technologies such as telemetry, radio, and computer networks (e.g. Priede et al., 1988; Thorstad et al., 2013). Although these methods have excellent spatial and temporal resolution, there are several intrinsic drawbacks, such as the high cost of bio-logging equipment (Hebblewhite and Haydon, 2010; Graves and Horodysky, 2015), the large effort required for capturing and tagging the fish, and body-size limitations for tagged fish: conventionally, the recommended tag weight is less than 3% of the fish body mass (e.g. Winter, 1983; Jepsen et al., 2002; Cooke et al., 2011). Stock assessment models are generally based on population-level data, but bio-logging methods only yield individual-level inferences, making them difficult to incorporate into overall stock condition assessments. In addition, equipment attached to a target fish can change its behavior, potentially resulting in biased migration data, although the effect is highly context-dependent and species-specific (Jepsen et al., 2015).

To overcome these drawbacks of bio-logging and make use of migration data for stock assessment of shared fish stocks, other approaches with lower cost and less effort are warranted. Recently, migration tracking techniques using isotope analysis of incremental-growth tissues such as otoliths, eye lenses, and vertebral bones (Matsubayashi et al., 2017; Sakamoto et al., 2019; Matsubayashi et al., 2020; Vecchio and Peebles, 2020) have proven promising for inferring the migration routes of individual fish. The isotopic composition of local environment and an animal's tissue can be used as a natural tag to track its movements through isotopically distinct habitats (Graham et al., 2010), and we call this technique "iso-logging". The major advantages of iso-logging over bio-logging are lower cost and effort, longer period of tracking (Vecchio and Peebles, 2020), and no influence on the behavior of target fish before death, although the temporal resolution and accuracy of estimated ranges are not equal to those from bio-logging.

In the case of marine fish, the ^{18}O:^{16}O ratio ($\delta^{18}O$) in otoliths is the most frequently used isotope ratio for iso-logging (e.g. Trueman et al., 2012; Hsieh et al., 2019; Sakamoto et al., 2019). $\delta^{18}O$ can be retrospectively measured from otoliths and reflects the ambient temperature experienced by the fish. However, $\delta^{18}O$ is not effective for iso-logging of fish that 1) migrate in oceans with similar thermal gradients, 2) have a stable body temperature, like tuna (*Thunnus* spp.; Carey and Teal, 1969), or 3) often dive deep, crossing the thermocline. Skipjack tuna *Katsuwonus pelamis* comprises one of the most commercially important shared fish stocks inhabiting warm and temperate waters. Skipjack in western Pacific populations prefer sea-surface temperatures ranging from 20.5 to 26.0°C (Mugo et al., 2010) and can maintain its body temperature higher than that of ambient water (Barrett and Hester, 1964; Stevens et al., 1974), which hampers the use of otolith $\delta^{18}O$ for migration tracking. For this reason, it is necessary to test the applicability of other isotope ratios for tracking skipjack migration. Recent studies have suggested that stable carbon and nitrogen isotope ratios ($\delta^{13}C$ and $\delta^{15}N$) can be excellent indicators for the migration histories of marine animals in some areas (Trueman et al., 2017; Matsubayashi et al., 2020), and these isotopes may be also applicable for tracking skipjack in the western Pacific (Coletto et al., 2021).

To use $\delta^{13}C$ and $\delta^{15}N$ for iso-logging of marine fish, at least three types of information are required: 1) the isoscapes across the habitat, 2) any ontogenetic shifts of isotope ratios of target fish, and 3) isotopic offsets between isoscapes and target fish. Unfortunately, it is generally difficult to obtain all of this information for $\delta^{13}C$ and $\delta^{15}N$. The generation of isoscapes requires thorough field sampling of proxy organisms with low swimming ability (Trueman et al., 2017; Matsubayashi et al., 2020). Understanding isotopic offsets between isoscape and target animal requires feeding experiments over several months (e.g. Matsubayashi et al., 2019; Canseco et al., 2021). Furthermore, in the case of highly migratory piscivorous species, understanding the ontogenetic shifts of $\delta^{13}C$ and $\delta^{15}N$ is particularly difficult because isoscapes and ontogenetic dietary shifts have mutual interactions. To overcome these difficulties in iso-logging, we conceived of using a geostatistical model to simultaneously estimate isoscapes and ontogenetic shifts of isotope ratios using the fish targeted for migration tracking as a proxy organism for isoscapes. With this approach, isotopic offsets between isoscapes and target fish can be ignored. Although such modeling was technically difficult up until a few years ago, recent advances in geostatistical analysis (e.g. Rue et al., 2009; Thorson, 2019; Anderson et al., 2022) allow us to

account for these factors in a single model with a user-friendly interface.

Here, we test the utility of geostatistical analysis for generating isoscapes using $\delta^{13}C$ and $\delta^{15}N$ of skipjack in the western Pacific, considering ontogenetic shifts in isotope ratios of this species. In this region, skipjack is mainly distributed from 20°S to 40°N and from 110°E to 180°E (Bartoo, 1987; Kiyofuji and Ochi, 2016), and some individuals exhibit dynamic northward migration from the subtropics into waters off the Pacific coast of Japan (Kiyofuji et al., 2019a). The water temperature range preferred by skipjack is from 18.8°C to 28.1°C and the 18.0 isotherm is the lowest thermal limit of skipjack tuna distribution (Kiyofuji et al., 2019a). We sampled the muscle tissue of skipjack of various body sizes and determined the $\delta^{13}C$ and $\delta^{15}N$ values of bulk tissue ($\delta^{13}C_{Bulk}$ and $\delta^{15}N_{Bulk}$). We then applied a geostatistical model to account for variations in the $\delta^{13}C$ and $\delta^{15}N$ of skipjack muscle with fork length, several environmental variables, and a spatial random field. Furthermore, we performed compound-specific nitrogen isotope analysis of amino acids ($\delta^{15}N_{AAs}$) for five samples with different $\delta^{15}N_{Bulk}$ values to evaluate whether the differences in bulk values resulted from a baseline shift in isotope ratios or from trophic differences (see Matsubayashi et al., 2020). On the basis of these data, we discuss the applicability of $\delta^{13}C_{Bulk}$ and $\delta^{15}N_{Bulk}$ for assessing the migration of skipjack in the western Pacific.

Materials and methods

Sample collection and preparation

Samples of juvenile skipjack (n = 210) were collected during 1995–2019 from multiple sampling stations in the western Pacific by mid-water trawl (mesh size: 16mm) during several research cruises of the Fisheries Resources Institute, Japan Fisheries Research and Education Agency. Juvenile fish from the EEZs of countries other than Japan were collected under formal agreement with each country. The 20 cm fork length is the threshold that distinguishes juvenile from adults, and it takes about 3 months for skipjack to reach this length (Kiyofuji et al., 2019b). Dorsal white muscle sampled from juvenile fish was rinsed in distilled water for at least six hours, because the samples were preserved in ethanol, and then the samples were freeze-dried. Most samples of adult skipjack (n = 884) were purchased from commercial fisheries, and some were caught by research vessel surveys. None of them were from the EEZ of countries other than Japan (Figure 1). Dorsal white muscle was sampled from each fish and kept frozen until isotopic analysis. The sampling stations for skipjack ranged from 5.0°S to 40.9°N and from 123.0°E to 164.9°E (Figure 1). The muscle samples were ground into fine powder and defatted using a methanol: chloroform mixture (1:2, v:v) and then used for bulk and compound-specific isotopic analyses.

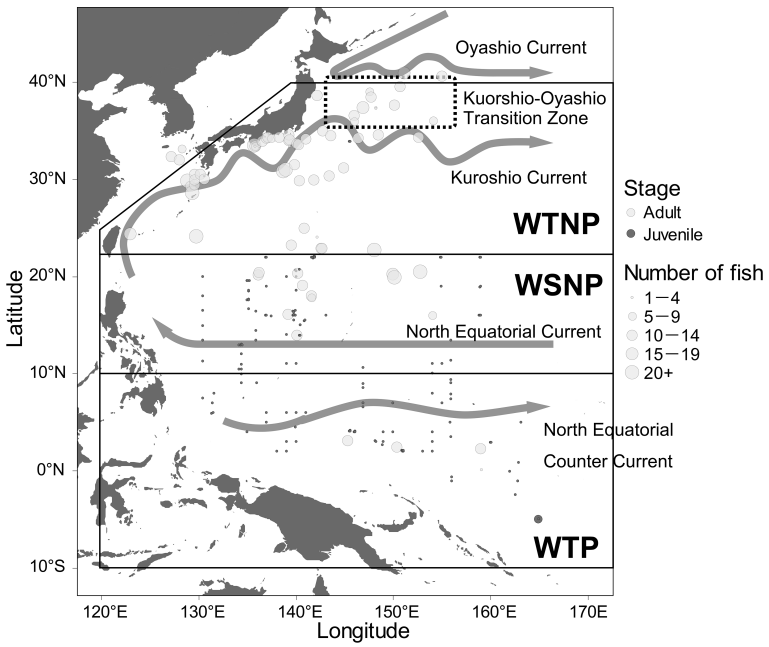

FIGURE 1
Sampling points and sample sizes of juvenile and adult skipjack tuna (*Katsuwonus pelamis*), boundaries of the western tropical Pacific (WTP), western subtropical North Pacific (WSNP), western temperate North Pacific (WTNP), and schematic diagram of the major currents in the western Pacific Ocean. The Kuroshio-Oyashio Transition Zone is known to have high net primary productivity (Nishikawa et al., 2020).

Measurement of $\delta^{13}C_{Bulk}$ and $\delta^{15}N_{Bulk}$

The $\delta^{13}C_{Bulk}$ and $\delta^{15}N_{Bulk}$ values were measured using continuous-flow elemental analyzer (EA)/isotope-ratio mass spectrometry (IRMS) systems. Stable isotope ratios are expressed in conventional δ notation in accordance with the international standard scale, based on the following equation:

$$\delta X(‰) = (R_{sample}/R_{standard} - 1) \times 10^3$$

where X is ^{13}C or ^{15}N, R_{sample} is the ^{13}C:^{12}C or ^{15}N:^{14}N ratio of the sample, and $R_{standard}$ is that of Vienna Pee Dee Belemnite (VPDB) or atmospheric nitrogen (AIR), respectively. Elemental concentrations and isotope ratios of carbon and nitrogen were calibrated against those of alanine, glycine, and histidine laboratory standards, which are traceable back to international standards. The analytical errors (SDs) of $\delta^{13}C$ and $\delta^{15}N$ were smaller than 0.18‰ and 0.16‰, respectively.

Measurement of $\delta^{15}N_{AAs}$

The $\delta^{13}C_{Bulk}$ and $\delta^{15}N_{Bulk}$ values allow the study area to be isotopically divided into at least three regions: the western tropical Pacific (WTP), western subtropical North Pacific (WSNP), and western temperate North Pacific (WTNP). We chose a total of five skipjack samples representing the $\delta^{13}C_{Bulk}$ and $\delta^{15}N_{Bulk}$ values in each region for $\delta^{15}N_{AAs}$ analysis. Samples for $\delta^{15}N_{AAs}$ were prepared using a method based on the amino-acid derivatization procedures described in Chikaraishi et al. (2015) as follows. Samples were initially hydrolyzed with 12 M HCl at 110°C overnight (>12 h) and then washed with *n*-hexane: dichloromethane (3:2, v:v) to remove any hydrophobic constituents. After hydrolysis, samples were derivatized using thionyl chloride:2-propanol (1:4, v:v) at 110°C for 2 h and then pivaloyl chloride:dichloromethane (1:4, v:v) at 110°C for 2 h. The amino-acid derivatives were then extracted with *n*-hexane: dichloromethane (3:2, v:v). The $\delta^{15}N$ value of each amino acid was determined by gas chromatography/combustion/isotope-ratio mass spectrometry (GC/C/IRMS) using a 6890N GC instrument (Agilent Technologies, Palo Alto, CA, USA) coupled to a Delta plus XP IRMS *via* GC-combustion III interface (Thermo Finnigan, Bremen, Germany) at the Japan Agency for Marine-Earth Science and Technology. Reference mixtures of nine amino acids (alanine, glycine, leucine, norleucine, aspartic acid, methionine, glutamic acid, phenylalanine, and hydroxyproline) with known $\delta^{15}N$ values (ranging from −26.4‰ to +45.6‰; Indiana University, Bloomington, IN, USA, and SI Science Co., Sugito-machi, Japan) were analyzed every four to six sample runs. The average SD of the standards was 0.7‰ (n = 16).

Estimation of trophic position

The trophic positions (TPs) of the fish sampled for $\delta^{15}N_{AAs}$ (n = 5) were estimated from differences between the $\delta^{15}N$ values of glutamic acid and phenylalanine as follows (Chikaraishi et al., 2009):

$$TP_{Glu-Phe} = \left(\delta^{15}N_{Glu} - \delta^{15}N_{Phe} - \beta\right)/TDF_{Glu-Phe} + 1$$

where $\delta^{15}N_{Glu}$ is the $\delta^{15}N$ of glutamic acid, $\delta^{15}N_{Phe}$ is the $\delta^{15}N$ of phenylalanine, β is the difference between $\delta^{15}N_{Glu}$ and $\delta^{15}N_{Phe}$ in primary producers, and $TDF_{Glu\text{-}Phe}$ is the trophic discrimination factor for $\delta^{15}N$ of glutamic acid relative to phenylalanine. We used a value of 3.4 for β and 7.6‰ for $TDF_{Glu\text{-}Phe}$ (Chikaraishi et al., 2009).

Environmental variables

Data for the following environmental variables in the euphotic zone (depth < 100 m) of the western Pacific were obtained from Copernicus Marine Environment Monitoring Service (CMEMS, https://marine.copernicus.eu/): potential temperature, salinity, concentrations of chlorophyll *a*, dissolved oxygen, nitrate, phosphate, and iron, and surface partial pressure of carbon dioxide (spCO2). These data have at most four dimensions: latitude, longitude, date (year and month), and depth. Among these, latitude and longitude were set to the same as the skipjack sampling points; however, it was necessary to assume an interval for data aggregation of date and depth prior to allocating the environmental variables for each data point.

To determine the aggregation interval for the environmental information for each data point, we estimated the isotopic turnover rate (i.e., the rate at which the elements comprising a tissue are replaced) of muscle for adult and juvenile skipjack. Although there are no empirical studies estimating species-specific turnover times for skipjack, Coletto et al. (2021) suggested that adult skipjack has a shorter turnover time than *Thunnus* species, considering the faster growth rates of this species, and assumed a turnover time similar to those estimated for juvenile yellowfin tuna (around 2–4 months; Graham et al. 2007). For this reason, we used the average values of the environmental variables at each sampling point over the four months leading up to and including the sampled month for adult fish with fork length greater than 200 mm. Because juvenile fish with fork length<200 mm seem to have shorter turnover times than adult fish, given their higher growth rate (Hoyle et al., 2011), we used monthly mean values of environmental variables at each sampling point for the sampled year and month for juvenile skipjack.

As the representative depth for aggregating the environmental variables, we selected the depth at which the concentration of phytoplankton was highest by using data for phytoplankton concentration from CMEMS, assuming that $\delta^{13}C$ and $\delta^{15}N$ of phytoplankton at that depth were the main influences on the values in skipjack muscle. We then extracted and allocated the environmental variables at the location, period and depth corresponding to each data point (Supplementary Table 1).

Statistical analysis

To estimate spatial distributions of $\delta^{13}C_{Bulk}$ and $\delta^{15}N_{Bulk}$ values in the western Pacific, we used the R package "sdmTMB" ver. 0.0.26.9001 (Anderson et al., 2022), which accounts for independent region-specific noise *via* the stochastic partial differential equations (SPDE) approach. In sdmTMB, the spatial random effect is assumed to form continuous Gaussian Markov random fields (GMRF) and is approximated by creating a Delaunay triangularized mesh over the study area (Lindgren et al., 2011). sdmTMB makes use of the integrated nested Laplace approximation (INLA; Rue et al., 2009) to create the triangularized meshes. We set the number of nodes to 200 and determined the optimal cutoff value for the number of nodes *via* the "cutoff_search" option in sdmTMB (Anderson et al., 2022). Meshes on land were transformed into barrier meshes (meshes with correlation barriers) using the "add_barrier_mesh" function of sdmTMB (Anderson et al., 2022).

To maximize the prediction ability of the model, we implemented thin plate regression splines (Wood, 2003) for all covariates. We used smoothers with specified basis dimensions (k values), which were 3 for fork length and 5 for the other covariates. A smaller basis dimension (k = 3) was assumed for fork length because the relationships between fork length and $\delta^{13}C_{Bulk}$ and $\delta^{15}N_{Bulk}$ are expected to be either positive linear or positive asymptotic relationships (Fry and Sherr, 1984; Minagawa and Wada, 1984). The relationships between $\delta^{13}C_{Bulk}$ or $\delta^{15}N_{Bulk}$ and the other parameters were unknown, hence we assigned these a larger basis dimension (k = 5). We did not implement temporal random effects because there is a large bias in the year the samples were taken. The response variables were modelled using the Gaussian family with identity link function.

From this, the model can be specified as: $y_i = \alpha_0 + X_i\beta + W_i$ where y_i is the $\delta^{13}C_{Bulk}$ or $\delta^{15}N_{Bulk}$ value of skipjack muscle at sampling location i (i = 1, …, n; n = 1094), α_0 is the intercept, $\boldsymbol{\beta}$ is the vector of regression parameters, X_i is the matrix of the explanatory covariates (fork length and environmental variables) at location i, and W_i represents the spatially structured random effect at location i. We searched for the best combinations of the covariates (X_i) for prediction of $\delta^{13}C_{Bulk}$ and $\delta^{15}N_{Bulk}$ values of skipjack muscle by model selection based on the Akaike information criterion (AIC). We tested three options for each covariate—the variable with smoothing, the variable without smoothing, and without the variable at all—and then calculated the AIC for models with all combinations of these three options for nine covariates. Due to computational time limitations for model selection, we could not incorporate additional explanatory variables such as the effect of season. St John Glew et al. (2021) incorporated the effect of season as explanatory variables, which improved the model predictions. However, we believe that seasonal effects are not an important variable in our model, because the CMEMS environmental data are themselves highly seasonally variable, and their effects are incorporated into the model with smoothing splines. Finally, models with the smallest AIC were chosen as best-fit models for the prediction of $\delta^{13}C_{Bulk}$ and $\delta^{15}N_{Bulk}$ values of skipjack muscle.

For the best fit models, sanity checks on the items listed below were performed by the "sanity" function of sdmTMB; the non-linear minimizer suggests successful convergence, the Hessian matrix is positive definite, no extreme or very small eigen values are detected, no gradients with respect to fixed effects are greater than 0.001, no fixed-effect standard errors are not applicable (N/A), no fixed-effect standard errors look unreasonably large, no sigma parameters are less than 0.001, and the range parameter does not look unreasonably large. All statistical analysis was conducted using R (R Core Team, 2021).

Generation of isoscapes

To generate isoscapes of $\delta^{13}C$ and $\delta^{15}N$ in the western Pacific, we obtained monthly mean values of the environmental variables within the triangularized meshes of sdmTMB from January to December 2021 from CMEMS. The environmental variables were then fitted with the best-fit models of $\delta^{13}C$ and $\delta^{15}N$ to generate isoscapes for 2021, while fork length was set to 0. The uncertainties (standard deviations) of spatial prediction were estimated *via* simulation from the fitted model (n = 500). Predictions with uncertainty >2 for $\delta^{15}N$ and >1 for $\delta^{13}C$ were excluded from the isoscapes to avoid excessive extrapolation.

Results

Size and distribution of sampled fish

The fork length of skipjack sampled ranged from 11 to 834 mm (384 ± 186 mm), and that of juveniles and adults were from 11 to 170 mm (36 ± 26 mm) and from 25 to 83 mm (466 ± 85 mm), respectively. Juveniles were distributed from 130.4°E to 164.9°E (mean 146.0°E) and from 5.0°S to 33.9°N (10.0°N) Adults were found from 123.0°E to 159.0°E (140.1°E) and from 2.3°S to 40.9°N (28.8°N) (Figure 1). The sample sizes at each sampling station were generally small for juvenile fish (1.3 ± 0.7) but large for adult fish (11.5 ± 7.7).

$\delta^{13}C_{Bulk}$ and $\delta^{15}N_{Bulk}$ values

The observed $\delta^{13}C_{Bulk}$ and $\delta^{15}N_{Bulk}$ values of skipjack ranged from −20.0‰ to −15.7‰ (mean ± SD, −17.8‰ ± 0.8‰) and from 3.1‰ to 18.9‰ (9.7‰ ± 2.4‰), respectively. Skipjack in the WTP had high $\delta^{15}N_{Bulk}$ values and those in the WSNP and WTNP had low and intermediate values, respectively (Figure 2). The spatial variation in $\delta^{13}C_{Bulk}$ of skipjack muscle is characterized by lower values in the WTNP than in the WSNP and WTP (Figure 2).

Model fit and selection

The best-fit model for $\delta^{15}N$ included salinity, temperature, phosphate, and nitrate concentrations without smoothing, and fork length and iron concentration with smoothing (Supplementary Figures 1 and 2, Table 1). All sanity checks were positive for the best-fit model. The ΔAIC (the difference between the AIC for a model and the best-fit model) of the model with the second lowest AIC ($\Delta AIC_{2nd\ -\ Best}$) was 0.986, and the best-fit model accounted for 86.9% of the variation in observed $\delta^{15}N$ values of skipjack muscle.

The best-fit model for $\delta^{13}C$ included fork length, temperature, phosphate, nitrate, and iron concentrations without smoothing, and salinity, concentrations of chlorophyll *a* and dissolved oxygen, and the surface partial pressure of carbon dioxide with smoothing (Table 1). All sanity checks were positive for the best-fit model. The $\Delta AIC_{2nd\ -\ Best}$ was 0.942, and the best-fit model accounted for 72.1% of the variation in observed $\delta^{13}C$ values of skipjack muscle.

The $\delta^{15}N$ and fork length of skipjack show a positive asymptotic relationship (Figure 3A), with a largely monotonous increase until fork length reaches 400 mm (0.01265‰/mm), approaching an asymptotic value at 600 mm ($\Delta\delta^{15}N_{600mm-0mm}$ = 5.84‰). Fork length with smoothing was included in all models with ΔAIC smaller than 2 for $\delta^{15}N$. The $\delta^{13}C$ and fork length of skipjack showed a positive linear relationship (Supplementary Figure 2) with a small coefficient (0.00077‰/mm). Fork length without smoothing was included in all models with ΔAIC smaller than 2 for $\delta^{13}C$.

Isoscapes in the western Pacific

The western Pacific $\delta^{15}N$ isoscape showed a clear latitudinal trend, with values in the WTP (from 10°S to 10–15°N) higher than in other northern regions (Figure 4). Overall, the uncertainty profile of $\delta^{15}N$ was low around the sampling points, but high in the marginal region of our study area. On the other hand, $\delta^{13}C$ was low in the WTNP (north of 20°N) and around the equator (from 2°S to 4°N) compared with the other regions. The uncertainty of estimated $\delta^{13}C$ was low around the sampling points north of 4°N, but high in the marginal regions of the study area and south of 4°N regardless of the spatial density of sampling points.

Measurement of $\delta^{15}N_{AAs}$

The results of compound-specific $\delta^{15}N$ analysis for five skipjack samples representing the main regions (WTP, WSNP, and WTNP) with typical bulk-tissue isotope ratios are shown in Table 2. In summary, regional mean $\delta^{15}N_{Bulk}$ was highest for WTP, followed by WTNP and WSNP, while $TP_{Glu-Phe}$ was highest for WTNP followed by WSNP and WTP. Thus, the

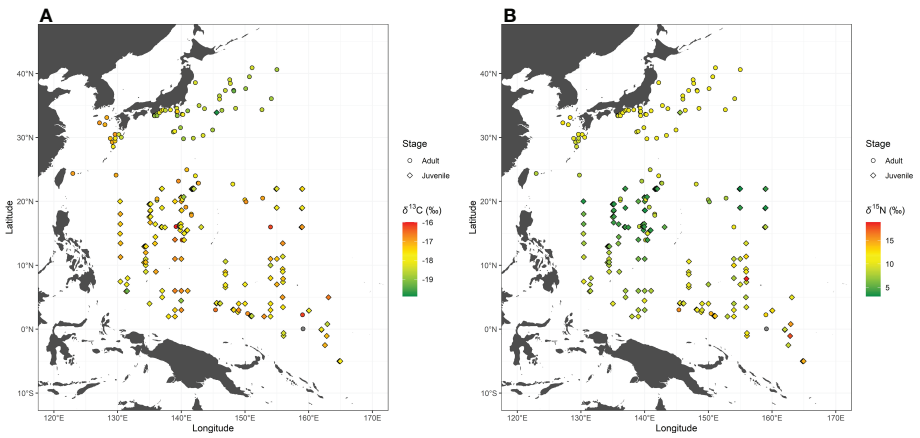

FIGURE 2
Bulk tissue carbon ($\delta^{13}C_{Bulk}$: **A**) and nitrogen ($\delta^{15}N_{Bulk}$: **B**) stable isotope ratios of skipjack tuna (*Katsuwonus pelamis*) in the western Pacific. Isotope ratios of skipjack of the same stage collected at the same location are averaged.

10.3389/fmars.2022.1049056

TABLE 1 Results of model selection based on the Akaike information criterion (AIC). Models with ΔAIC ≤ 2 are shown.

y	x1	x2	x3	x4	x5	x6	x7	x8	x9	AIC	ΔAIC
$\delta^{15}N$	so	Temp	PO_4	NO_3	s (FL)	s (Fe)				3240.2	0.0
	so	Temp	PO_4	NO_3	Chl	s (FL)	s (Fe)			3241.2	1.0
	so	Temp	PO_4	NO_3	Chl	s (FL)	s (O_2)			3241.2	1.0
	so	PO_4	NO_3	Chl	s (FL)	s (Fe)				3241.5	1.3
	so	Temp	PO_4	NO_3	Chl	O_2	s (FL)	s (Fe)		3241.6	1.4
	so	Temp	PO_4	NO_3	O_2	s (FL)	s (Fe)			3242.0	1.8
	so	Temp	PO_4	NO_3	O_2	s (FL)	s (Chl)			3242.0	1.8
	so	Temp	PO_4	NO_3	$spCO_2$	s (FL)	s (Fe)			3242.2	2.0
	so	Temp	PO_4	NO_3	$spCO_2$	s (FL)	s (Chl)			3242.2	2.0
	so	Temp	PO_4	NO_3	$spCO_2$	s (FL)	s (O_2)			3242.2	2.0
	so	PO_4	NO_3	s (FL)	s (Temp)	s (Fe)				3242.2	2.0
	Temp	PO_4	NO_3	s (FL)	s (so)	s (Fe)				3242.2	2.0
$\delta^{13}C$	FL	Temp	Fe	PO_4	NO_3	s (so)	s (Chl)	s (O_2)	s ($spCO_2$)	1670.9	0.0
	FL	Temp	PO_4	NO_3	s (so)	s (Fe)	s (Chl)	s (O_2)		1671.8	0.9
	FL	Temp	PO_4	NO_3	$spCO_2$	s (so)	s (Fe)	s (Chl)	s (O_2)	1672.0	1.1
	FL	Temp	Fe	PO_4	NO_3	s (Chl)	s (O_2)	s ($spCO_2$)		1672.0	1.1
	FL	Temp	PO_4	NO_3	s (so)	s (Fe)	s (Chl)	s (O_2)	s ($spCO_2$)	1672.4	1.5

Temp, water temperature; so, water salinity; FL, fork length of skipjack; PO_4, phosphate concentration; NO_3, nitrate concentration; O_2, dissolved oxygen concentration; Chl, chlorophyll a concentration; Fe, iron concentration; $spCO_2$, surface partial pressure of carbon dioxide in seawater.
s () indicates variables processed with a smoothing function.

trend in the regional variability of $\delta^{15}N_{Bulk}$ was not consistent with that of TPGlu–Phe (Figure 5).

Discussion

For generation of isoscapes, previous studies have used species with lower mobility like jellyfish and copepods as proxy organisms (Trueman et al., 2017; Matsubayashi et al., 2020). The advantage of using other species with low swimming ability to create isoscape is that location-specific isotope ratios can be detected with high representativeness. On the other hand, the ontogenetic shift of isotope ratios in target fish and the offset of isotope ratios between target fish and isoscapes should be estimated separately in this method. This study used a target fish as a proxy organism for isoscapes, and successfully estimated both isoscapes (Figure 4) and the ontogenetic shifts of isotope ratios (Figure 3) of skipjack without compound-specific isotope analysis, through the use of geostatistical models. Furthermore, we can apply iso-logging of skipjack without considering the

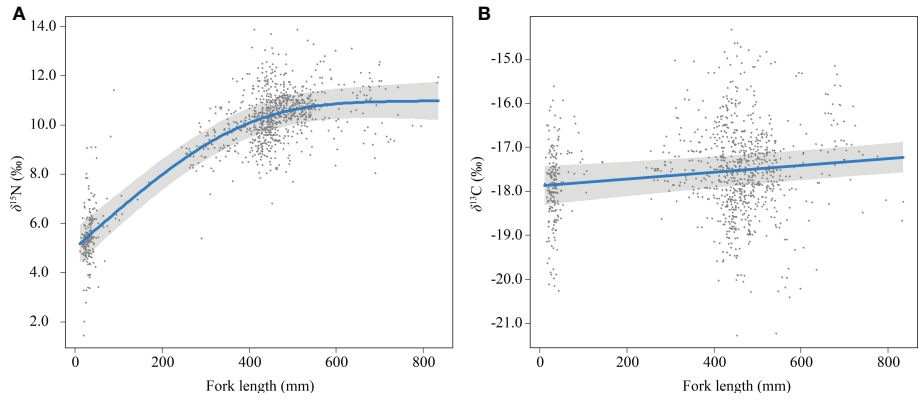

FIGURE 3
Relationship between fork length and $\delta^{15}N_{Bulk}$ **(A)** and $\delta^{13}C_{Bulk}$ **(B)** of skipjack tuna (*Katsuwonus pelamis*) in the western Pacific (blue lines) with randomized quantile partial residuals (gray areas) from the best-fit models. Each data point represents residuals from each data.

10.3389/fmars.2022.1049056

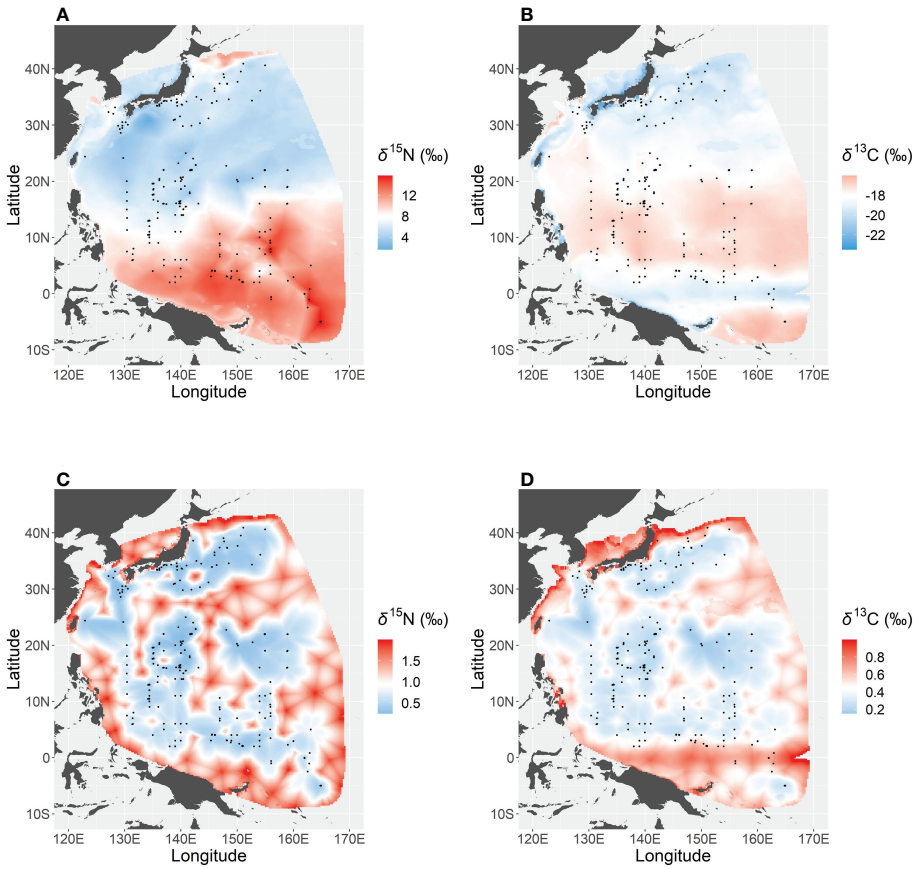

FIGURE 4
Isoscapes of nitrogen **(A)** and carbon **(B)** stable isotope ratios in the western Pacific, and the uncertainty (standard deviation) of predicted nitrogen **(C)** and carbon **(D)** isotope ratios estimated by simulation from the best-fit models (n = 500).

isotopic offset between isoscapes and target organism, because the isoscapes were generated based on the isotope ratios of the skipjack. Thus, our approach can be a useful alternative to the previous method, although our method has one drawback in that the uncertainty of isoscapes will increase with the number of fish captured that had migrated across regions with different isoscapes in the several months before they were caught. We addressed this issue by increasing the number of adult fish at each sampling point and period (Figure 1), and this may have contributed somewhat to decreasing the uncertainty of isoscapes given the high prediction ability of our models. Another solution would be to use juvenile fish only for generating isoscapes and then to construct another model to account for the ontogenetic shift of isotope ratios. However, this is not applicable when the distribution of juvenile and adult fish does not completely overlap, as with skipjack in the western Pacific where juvenile

TABLE 2 Detailed sample information for five skipjack tuna (*Katsuwonus pelamis*) specimens used for compound-specific isotope analysis.

Region[a]	Latitude (°N)	Longitude (°E)	Fork length (mm)	$\delta^{13}C_{Bulk}$ (‰)	$\delta^{15}N_{Bulk}$ (‰)	$\delta^{15}N_{Glu}$ (‰)	$\delta^{15}N_{Phe}$ (‰)	$TP_{Glu-Phe}$
WTP	2.0	160.7	490	−16.8	14.9	29.0	12.7	2.7
WSNP	20.3	150.0	543	−16.9	6.9	21.9	4.2	2.9
WSNP	20.3	150.0	542	−16.7	7.5	19.4	0.2	3.1
WTNP	34.6	148.5	489	−18.7	11.1	27.1	7.6	3.1
WTNP	34.6	148.5	484	−18.7	11.0	26.2	7.1	3.1

[a]WTP, western tropical Pacific; WSNP, western subtropical North Pacific; WTNP, western temperate North Pacific.
Listed are stable isotope ratios (‰) of bulk-tissue carbon ($\delta^{13}C_{Bulk}$), bulk-tissue nitrogen ($\delta^{15}N_{bulk}$), glutamic acid ($\delta^{15}N_{Glu}$), and phenylalanine ($\delta^{15}N_{Phe}$), and trophic position ($TP_{Glu-Phe}$), along with the capture point and fork length (FL) of each specimen.

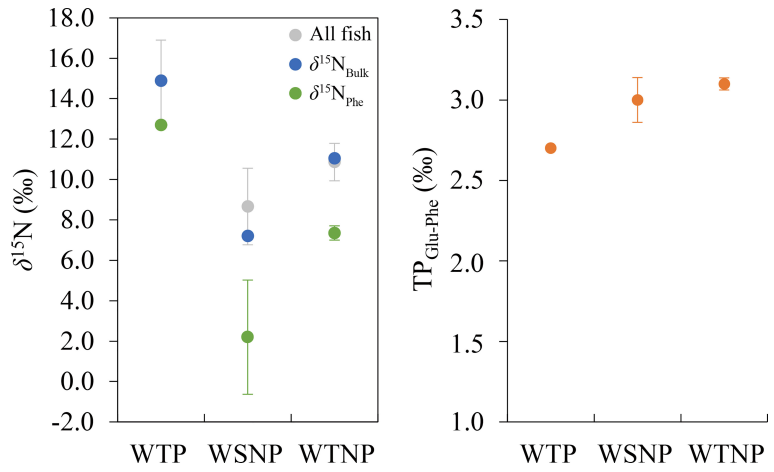

FIGURE 5
Mean $\delta^{15}N_{Bulk}$ and $\delta^{15}N_{Phe}$ (left), and $TP_{Glu-Phe}$ (right) of skipjack tuna (*Katsuwonus pelamis*) in the western tropical Pacific (WTP), western subtropical North Pacific (WSNP), and western temperate North Pacific (WTNP). Gray, blue and green datapoints in the left panel indicate the mean (±SD) $\delta^{15}N_{Bulk}$ of all skipjack samples, $\delta^{15}N_{Bulk}$ and $\delta^{15}N_{Phe}$ of skipjack used for $\delta^{15}N_{AAs}$, respectively. Orange datapoints in the right panel are the $TP_{Glu-Phe}$ of skipjack used for determining $\delta^{15}N_{AAs}$.

fish are scarce in the northern area (Lehodey et al., 2013). To minimize the uncertainty associated with a high migration ability of proxy organisms, it is important to use tissues with a high turnover rate. As of now, the fish tissue with the shortest stable isotope turnover time is epidermal mucus (Winter and Britton, 2021), but this is difficult to sample from juvenile fish smaller than 100 mm. Therefore, it is important to further explore turnover rates in other tissues to discover better ways to sample proxy organisms for generation of isoscapes.

Together with the results of the geostatistical models, our $\delta^{15}N_{AAs}$ data also show that the variation in isotope ratios of skipjack in the western Pacific was generally derived from the baseline shift of the isoscape and not from differences in prey items. Adult skipjack in the western Pacific are mainly piscivorous and occasionally consume cephalopods, with low selectivity for their prey (Iizuka et al., 1989). Therefore, regional shifts in prey abundance can cause regional differences in $\delta^{15}N_{Bulk}$. If the observed fluctuations of $\delta^{13}C_{Bulk}$ and $\delta^{15}N_{Bulk}$ in skipjack muscle resulted from differences in trophic position, the regional trend of $\delta^{15}N_{Bulk}$ should be similar to that of $TP_{Glu-Phe}$ (Figure 5). However, our $\delta^{15}N_{AAs}$ data show that skipjack in the western Pacific have small individual variation in $TP_{Glu-Phe}$ (maximum difference: 0.4). Assuming that $\delta^{15}N_{Bulk}$ increases 3.4‰ with trophic level (Minagawa and Wada, 1984), differences in $TP_{Glu-Phe}$ can only explain 1.4‰ of the observed variation of $\delta^{15}N_{Bulk}$ out of 10.2‰ (Table 2, Figure 5). Given that the $\delta^{15}N_{Phe}$, which generally has a small trophic discrimination factor (about 0.4%; Chikaraishi et al., 2009), was more correlated with $\delta^{15}N_{Bulk}$ of skipjack muscle than $TP_{Glu-Phe}$, individual differences in $\delta^{15}N_{Bulk}$ of adult skipjack largely reflect the variation of $\delta^{15}N$ at the base of the food web.

$TP_{Glu-Phe}$ of skipjack estimated by commonly used $TDF_{Glu-Phe}$ (7.6 ‰) were somewhat lower (2.7–3.1) than the trophic position estimated by stomach-content analysis (TP_{SCA} = 3.8; Bradley et al., 2015). Although the optimal $TDF_{Glu-Phe}$ to use for estimating the trophic position of skipjack remains controversial (e.g., Bradley et al., 2015; McMahon and McCarthy, 2016; Ohkouchi et al., 2017; Coletto et al., 2022), differences in $TP_{Glu-Phe}$ of skipjack do not affect intraspecific variation in $TDF_{Glu-Phe}$, and thus would not affect our conclusion that regional variation in $TDF_{Glu-Phe}$ are unlikely to explain $\delta^{15}N_{Bulk}$ differences among regions.

Regional differences in $\delta^{15}N$ of skipjack in the western Pacific were largely consistent with the $\delta^{15}N$ distribution of nitrate in this region (Rafter et al., 2019). Low $\delta^{15}N$ around 10°N to 35°N (Figure 4) is related to extensive N_2 fixation in this region (Gruber, 2016), because N_2 fixers typically exhibit lower $\delta^{15}N$ values than non-N_2 fixers (McClelland et al., 2003). On the other hand, our isoscape suggests that the low-$\delta^{15}N$ area extends as far as 40°N, which is not consistent with known distributions of N_2 fixers or low nitrate $\delta^{15}N$ (Gruber, 2016; Rafter et al., 2019). Presumably, this inconsistency is attributable to the relatively longer turnover time of skipjack muscle. The area around 35–40°N is the northern limit of skipjack migration and they can stay there at most four months a year (from June to September; Mugo et al., 2011; Kiyofuji et al., 2019a). Given that the turnover time of adult skipjack white muscle is about four months, isotope ratios of the muscle of skipjack captured around 35–40°N are likely to reflect the low $\delta^{15}N$ values south of 35°N, and thus our isoscape shows low $\delta^{15}N$ up to 40°N. On the other hand, the high $\delta^{15}N$ south of 10–15°N can be explained by high nitrate utilization and limited N_2 fixation. In the surface layer of the tropical Pacific Ocean, a strong halocline above the

thermocline generates a barrier layer, which impedes vertical mixing and nutrient supply from subsurface to surface waters (Sprintall & Tomczak, 1992). The limited nutrient influx results in high nitrate utilization (i.e. low nitrate concentration)—the ratio of nitrate assimilation by phytoplankton to nitrate supply in the euphotic layer—and nitrate $\delta^{15}N$ increases with nitrate depletion (Yoshikawa et al., 2018). Furthermore, N_2 fixation is limited in this region (Gruber, 2016; Tanita et al., 2021) mainly due to the depleted dissolved iron concentration (Tanita et al., 2021). Such biogeochemical factors result in a clear latitudinal trend in $\delta^{15}N$, rendering it useful for segregating the habitat use of skipjack in the western Pacific.

Interpretation of spatial variation in $\delta^{13}C$ is much more difficult than that of $\delta^{15}N$. The spatial variations in $\delta^{13}C$ of skipjack muscle should be ultimately determined by that of phytoplankton ($\delta^{13}C_{phy}$), which is strongly influenced by the $\delta^{13}C$ of dissolved inorganic carbon (DIC) and the isotopic fractionation associated with carbon uptake (Tuerena et al., 2019). In the case of the western Pacific, there are no clear latitudinal differences in $\delta^{13}C$ of DIC (Quay et al., 2003), and therefore the spatial variation in the $\delta^{13}C$ isoscape would be driven by the uptake fractionation by phytoplankton. Until the early 1990s, the $\delta^{13}C$ of phytoplankton was thought to be determined by the DIC concentration in the ambient water (Sackett et al., 1965; Rau et al., 1991). Our geostatistical model also predicted an inverse relationship between DIC and $\delta^{13}C$ (Supplementary Figure 2), and the belt-shaped low-$\delta^{13}C$ zone around the equator (Figure 4) may be mainly due to the high $spCO_2$ in this region (Supplementary Figure 3). However, there is a large uncertainty associated with the equatorial low-$\delta^{13}C$ zone and further sampling in this region would provide important clarification (Figure 4). On the other hand, the clear $\delta^{13}C$ gradient around 20°N is not likely explained by spatial variation in $spCO_2$. Recent studies have shown that local differences in phytoplankton species composition can be important controls on $\delta^{13}C_{phy}$ (e.g. Francois et al., 1993; Bidigare et al., 1997; Popp et al., 1998; Tuerena et al., 2019) as well as the DIC concentration, specifically in regions where the DIC is not high and is less variable, as in the western Pacific (Supplementary Figure 3). Thus, we presume that local differences in environmental variables altered the phytoplankton species composition, and ultimately generated spatial variation in $\delta^{13}C$ of skipjack muscle in this region. It is worth noting that anthropogenic CO_2 emission can be another factor influencing the spatial variation in $\delta^{13}C_{phy}$ (Tuerena et al., 2019).

In this study, we demonstrated that $\delta^{13}C$ and $\delta^{15}N$ measurements of skipjack in the western Pacific can help to identify their latitudinal migration. Because the dorsal muscle, which is a major tissue used for isotope analysis of fishes, only represents isotope ratios at a specific point in time, the utility of isoscapes will be maximized when they are used along with the isotopic analysis of incremental growth tissues such as eye lenses and vertebral bone (e.g. Quaeck-Davies et al., 2018; Matsubayashi et al., 2019). Iso-logging using such incremental growth tissue would allow us to understand how skipjack in this region utilize different habitats though their lifetime without using electronic tags. For example, if time series isotopic data for eye lens are available, the migration pattern can be tracked by the following steps: i) calculate the fork length when each layer is formed from the equation relating lens diameter to fork length, ii) using the equation relating fork length to isotopic ratios (Figure 3), correct the isotope ratios of eye lens so that the fork length is at zero; iii) subtract $\Delta\delta^{15}N_{muscle\ -\ eye\ lens}$ from the value obtained in ii), iv) corrected lens isotope ratios can then be compared to the isoscape (Figure 4). We also suggest that the isoscapes generated in this study can be applied to other fish species that migrate in the western Pacific Ocean, such as albacore *Thunnus alalunga* (Nikolic et al., 2017), Pacific bluefin tuna *Thunnus orientalis* (Fujioka et al., 2018), and Japanese eel *Anguilla japonica* (Aoyama et al., 2014). For these other target species, however, it will be necessary to apply an appropriate correction to the trophic discrimination factor for differences between skipjack muscle and specific tissues of these other species. By using this method, we can better understand the immigration/emigration rates and connectivity in each region, which is crucial for cooperative management of shared fish stocks like skipjack. Further studies to generate precise isoscapes of $\delta^{13}C$ and $\delta^{15}N$ based on ocean models hold promise for improving the spatiotemporal resolution of isotope tracking and, together with the results of this study, will facilitate its use.

Data availability statement

The original contributions presented in the study are included in the article/Supplementary Material. Further inquiries can be directed to the corresponding author.

Author contributions

JM and HM conceived this study. HM and YT provided skipjack samples and contextual information. HM, YC, NO, KK, NFI, and NOO performed bulk and compound-specific stable isotope analyses. JM performed statistical analyses and wrote the first draft of the paper. All authors contributed to the article and approved the submitted version.

Funding

This study was partially supported by the Foundation for the Japan Society for the Promotion of Science (JSPS) KAKENHI Grants 19H04247, 21H03579, 21H04784, and 22H05028 to JM, and 20H00208 to NO, and the Research and Assessment Program for Fisheries Resources of the Fisheries Agency of Japan.

Acknowledgments

This study was conducted with the support of the Joint Research Grant for the Environmental Isotope Study of the Research Institute for Humanity and Nature. We thank H. Ashida, S. Ohashi, F. Tanaka, and H. Kiyofuji at the Fisheries Resources Institute, Japan Fisheries Research and Education Agency, for their help with sample collection. We thank C. Yoshikawa at the Japan Agency for Marine-Earth Science and Technology for her helpful comments on a draft of this manuscript. We also thank the reviewers for their prompt and careful review of our draft and for their helpful comments.

Conflict of interest

The authors declare that the research was conducted in the absence of any commercial or financial relationships that could be construed as a potential conflict of interest.

Publisher's note

All claims expressed in this article are solely those of the authors and do not necessarily represent those of their affiliated organizations, or those of the publisher, the editors and the reviewers. Any product that may be evaluated in this article, or claim that may be made by its manufacturer, is not guaranteed or endorsed by the publisher.

Supplementary material

The Supplementary Material for this article can be found online at: https://www.frontiersin.org/articles/10.3389/fmars.2022.1049056/full#supplementary-material

References

Anderson, S. C., Ward, E. J., English, P. A., and Barnett, L. A. K. (2022). sdmTMB: An r package for fast, flexible, and user-friendly generalized linear mixed effects models with spatial and spatiotemporal random fields. *bioRxiv* 2022.03.24.485545. doi: 10.1101/2022.03.24.485545

Aoyama, J., Watanabe, S., Miller, M. J., Mochioka, N., Otake, T., Yoshinaga, T., et al. (2014). Spawning sites of the Japanese eel in relation to oceanographic structure and the West Mariana ridge. *PloS One* 9, e88759. doi: 10.1371/journal.pone.0088759

Barrett, I., and Hester, F. J. (1964). Body temperature of yellowfin and skipjack tunas in relation to sea surface temperature. *Nature* 203, 96–97. doi: 10.1038/203096b0

Bartoo, N. W. (1987). "Tuna and billfish summaries of major stocks," in *Administrative report LJ-87-26* (La Jolla: National Marine Fisheries Service).

Bidigare, R. R., Fluegge, A., Freeman, K. H., Hanson, K. L., Hayes, J. M., Hollander, D., et al. (1997). Consistent fractionation of c-13 in nature and in the laboratory: Growth-rate effects in some haptophyte algae. *Global Biogeochem. Cy.* 11, 279–292. doi: 10.1029/96gb03939

Bradley, C. J., Wallsgrove, N. J., Choy, C. A., Drazen, J. C., Hetherington, E. D., Hoen, D. K., et al. (2015). Trophic position estimates of marine teleosts using amino acid compound specific isotopic analysis. *Limnol. Oceanogr. Meth.* 13, 476–493. doi: 10.1002/lom3.10041

Caddy, J. F. (1997). "Establishing a consultative mechanism or arrangement for managing shared stocks within the jurisdiction of contiguous states," in *Taking stock: Defining and managing shared resources, Australian society for fish biology and aquatic resource management association of Australasia joint workshop proceedings*, vol. 15 . Ed. D. A. Hancock (Sydney: Australian Society for Fish Biology), 81–123.

Canseco, J. A., Niklitschek, E. J., and Harrod, C. (2021). Variability in $\delta^{13}C$ and $\delta^{15}N$ trophic discrimination factors for teleost fishes: A meta-analysis of temperature and dietary effects. *Rev. Fish. Biol. Fish.* 32, 313–329. doi: 10.1007/s11160-021-09689-1

Carey, F. G., and Teal, J. M. (1969). Regulation of body temperature by the bluefin tuna. *Comp. Biochem. Physiol.* 28, 205–213. doi: 10.1016/0010-406X(69)91336-X

Carvalho, F., Ahrens, R., Murie, D., Bigelow, K., Aires-Da-Silva, A., Maunder, M. N., et al. (2015). Using pop-up satellite archival tags to inform selectivity in fisheries stock assessment models: A case study for the blue shark in the south Atlantic ocean. *ICES. J. Mar. Sci.* 72, 1715–1730. doi: 10.1093/icesjms/fsv026

Chikaraishi, Y., Ogawa, N. O., Kashiyama, Y., Takano, Y., Suga, H., Tomitani, A., et al. (2009). Determination of aquatic food-web structure based on compound-specific nitrogen isotopic composition of amino acids. *Limnol. Oceanogr. Meth.* 7, 740–750. doi: 10.4319/lom.2009.7.740

Chikaraishi, Y., Steffan, S. A., Takano, Y., and Ohkouchi, N. (2015). Diet quality influences isotopic discrimination among amino acids in an aquatic vertebrate. *Ecol. Evol.* 5, 2048–2059. doi: 10.1002/ece3.1491

Coletto, J. L., Besser, A. C., Botta, S., Madureira, L. A. S. P., and Newsome, S. D. (2022). Multi-proxy approach for studying the foraging habitat and trophic position of a migratory marine consumer in the southwestern Atlantic ocean. *Mar. Ecol. Prog. Ser.* 690, 147–163. doi: 10.3354/meps14036

Coletto, J. L., Botta, S., Fischer, L. G., Newsome, S. D., and Madureira, L. S. (2021). Isotope-based inferences of skipjack tuna feeding ecology and movement in the southwestern Atlantic ocean. *Mar. Environ. Res.* 165, 105246. doi: 10.1016/j.marenvres.2020.105246

Cooke, S. J., Woodley, C. M., Eppard, M. B., Brown, R. S., and Nielsen, J. L. (2011). Advancing the surgical implantation of electronic tags in fish: A gap analysis and research agenda based on a review of trends in intracoelomic tagging effects studies. *Rev. Fish. Biol. Fish.* 21, 127–151. doi: 10.1007/s11160-010-9193-3

Francois, R., Altabet, M. A., Goericke, R., McCorkle, D. C., Brunet, C., and Poisson, A. (1993). Changes in the delta c-13 of surface water particulate organic matter across the subtropical convergence in the SW Indian ocean. *Global Biogeochem. Cy.* 7, 627–644. doi: 10.1029/93GB01277

Fry, B., and Sherr, E. (1984). $\delta^{13}C$ measurements as indicators of carbon flow in marine and freshwater ecosystems. *Contrib. Mar. Sci.* 27, 49–63. doi: 10.1007/978-1-4612-3498-2_12

Fujioka, K., Fukuda, H., Tei, Y., Okamoto, S., Kiyofuji, H., Furukawa, S., et al. (2018). Spatial and temporal variability in the trans-pacific migration of pacific bluefin tuna (*Thunnus orientalis*) revealed by archival tags. *Prog. Oceanogr.* 162, 52–65. doi: 10.1016/j.pocean.2018.02.010

Graham, B. S., Koch, P. L., Newsome, S. D., McMahon, K. W., and Aurioles, D. (2010). "Using isoscapes to trace the movements and foraging behavior of top predators in oceanic ecosystems," in *Isoscapes*. Eds. J. West, G. Bowen, T. Dawson and K. Tu (Dordrecht: Springer), 299–318.

Graham, B. S., Grubbs, D., Holland, K., and Popp, B. N. (2007). A rapid ontogenetic shift in the diet of juvenile yellowfin tuna from Hawaii. *Mar. Biol.* 150, 647–658. doi: 10.1007/s00227-006-0360-y

Graves, J. E., and Horodysky, A. Z. (2015). Challenges of estimating post-release mortality of istiophorid billfishes caught in the recreational fishery: A review. *Fish. Res.* 166, 163–168. doi: 10.1016/j.fishres.2014.10.014

Gruber, N. (2016). Elusive marine nitrogen fixation. *Proc. Natl. Acad. Sci. U.S.A.* 113, 4246–4248. doi: 10.1073/pnas.1603646113

Hebblewhite, M., and Haydon, D. T. (2010). Distinguishing technology from biology: A critical review of the use of GPS telemetry data in ecology. *Philos. Trans. R. Soc B.* 365, 2303–2312. doi: 10.1098/rstb.2010.0087

Hoyle, S., Kleiber, P., Davies, N., Langley, A., and Hampton, J. (2011). "Stock assessment of skipjack tuna in the Western and central pacific ocean," in *WCPFC-SC7-2011/SA-WP-04* (Pohnpei, Federated States of Micronesia: Western and Central Pacific Fisheries Commission, Seventh Regular Session).

Hsieh, Y., Shiao, J. C., Lin, S. W., and Iizuka, Y. (2019). Quantitative reconstruction of salinity history by otolith oxygen stable isotopes: An example of a euryhaline fish *Lateolabrax japonicus*. *Rapid Commun. Mass. Spectrom.* 33, 1344–1354. doi: 10.1002/rcm.8476

Iizuka, K., Asano, M., and Naganuma, A. (1989). Feeding habits of skipjack tuna (*Katsuwonus pelamis* Linnaeus) caught by pole and line and the state of young skipjack tuna distribution in the tropical seas of the Western pacific ocean. *Bull. Tohoku. Reg. Fish. Res. Lab.* 51, 107–116.

Jepsen, N., Koed, A., Thorstad, E., and Baras, E. (2002). Surgical implantation of transmitters in fish: How much have we learned? *Hydrobiologia* 483, 239–248. doi: 10.1007/978-94-017-0771-8_28

Jepsen, N., Thorstad, E. B., Havn, T., and Lucas, M. C. (2015). The use of external electronic tags on fish: an evaluation of tag retention and tagging effects. *Anim. Biotelem.* 3, 49. doi: 10.1186/s40317-015-0086-z

Kiyofuji, H., Aoki, Y., Kinoshita, J., Ohashi, S., and Fujioka, K. (2019b). "A conceptual model of skipjack tuna in the western and central pacific ocean (WCPO) for the spatial structure configuration," in *WCPFC-SC15-2019/SA-WP-11* (Pohnpei, Federated States of Micronesia: Western and Central Pacific Fisheries Commission), 2019, 23.

Kiyofuji, H., Aoki, Y., Kinoshita, J., Okamoto, S., Masujima, M., Matsumoto, T., et al. (2019a). Northward migration dynamics of skipjack tuna (*Katsuwonus pelamis*) associated with the lower thermal limit in the western pacific ocean. *Prog. Oceanogr.* 175, 55–67. doi: 10.1016/j.pocean.2019.03.006

Kiyofuji, H., and Ochi, D. (2016). Proposal of alternative spatial structure for skipjack stock assessment in the WCPO. *Twelfth. Session. Sci. Committee.*, 3–11.

Kraska, J., Crespo, G. O., and Johnston, D. W. (2015). Bio-logging of marine migratory species in the law of the sea. *Mar. Policy* 51, 394–400. doi: 10.1016/j.marpol.2014.08.016

Lehodey, P., Senina, I., Calmettes, B., Hampton, J., and Nicol, S. (2013). Modelling the impact of climate change on pacific skipjack tuna population and fisheries. *Clim. Change* 119, 95–109. doi: 10.1007/s10584-012-0595-1

Lindgren, F., Rue, H., and Lindström, J. (2011). An explicit link between Gaussian fields and Gaussian Markov random fields: The stochastic partial differential equation approach. *J. R. Stat. Soc Ser. A. Stat. Soc* 73, 423–498. doi: 10.1111/j.1467-9868.2011.00777.x

Matsubayashi, J., Osada, Y., Tadokoro, K., Abe, Y., Yamaguchi, A., Shirai, K., et al. (2020). Tracking long-distance migration of marine fishes using compound-specific stable isotope analysis of amino acids. *Ecol. Lett.* 23, 881–890. doi: 10.1111/ele.13496

Matsubayashi, J., Saitoh, Y., Osada, Y., Uehara, Y., Habu, J., Sasaki, T., et al. (2017). Incremental analysis of vertebral centra can reconstruct the stable isotope chronology of teleost fishes. *Methods Ecol. Evol.* 8, 1755–1763. doi: 10.1111/2041-210X.12834

Matsubayashi, J., Umezawa, Y., Matsuyama, M., Kawabe, R., Mei, W., Wan, X., et al. (2019). Using segmental isotope analysis of teleost fish vertebrae to estimate trophic discrimination factors of bone collagen. *Limnol. Oceanogr. Meth.* 17, 87–96. doi: 10.1002/lom3.10298

McClelland, J. W., Holl, C. M., and Montoya, J. P. (2003). Relating low $\delta^{15}N$ values of zooplankton to N_2-fixation in the tropical north Atlantic: Insights provided by stable isotope ratios of amino acids. *Deep. Sea. Res. Part I. Oceanogr. Res. Papers.* 50, 849–861. doi: 10.1016/S0967-0637(03)00073-6

McMahon, K. W., and McCarthy, M. D. (2016). Embracing variability in amino acid δ15N fractionation: Mechanisms, implications, and applications for trophic ecology. *Ecosphere* 7, e01511. doi: 10.1002/ecs2.1511

McWhinnie, S. F. (2009). The tragedy of the commons in international fisheries: An empirical examination. *J. Environ. Econ. Manage.* 57, 321–333. doi: 10.1016/j.jeem.2008.07.008

Miller, K. A., and Munro, G. R. (2004). Climate and cooperation: A new perspective on the management of shared fish stocks. *Mar. Res. Econ.* 19, 367–393. doi: 10.1086/mre.19.3.42629440

Minagawa, M., and Wada, E. (1984). Stepwise enrichment of ^{15}N along food chains: Further evidence and the relation between $\delta^{15}N$ and animal age. *Geochim. Cosmochim. Acta* 48, 1135–1140. doi: 10.1016/0016-7037(84)90204-7

Mugo, R., Saitoh, S. I., Nihira, A., and Kuroyama, T. (2010). Habitat characteristics of skipjack tuna (*Katsuwonus pelamis*) in the western north pacific: A remote sensing perspective. *Fish. Oceanogr.* 19, 382–396. doi: 10.1111/j.1365-2419.2010.00552.x

Mugo, R., Saitoh, S., Nihira, A., and Kuroyama, T. (2011). "Application of multi-sensor satellite and fishery data, statistical models and marine GIS to detect habitat preferences of skipjack tuna," in *Handbook of satellite remote sensing image interpretation: Applications for marine living resources conservation and management*. Eds. J. Morales, V. Stuart, T. Platt and S. Sathyendranath (Dartmouth, Canada: EU PRESPO and IOCCG), 166–185.

Nikolic, N., Morandeau, G., Hoarau, L., West, W., Arrizabalaga, H., Hoyle, S., et al. (2017). Review of albacore tuna, *Thunnus alalunga*, biology, fisheries and management. *Rev. Fish. Biol. Fish.* 27, 775–810. doi: 10.1007/s11160-016-9453-y

Nishikawa, H., Nishikawa, S., Ishizaki, H., Wakamatsu, T., and Ishikawa, Y. (2020). Detection of the oyashio and kuroshio fronts under the projected climate change in the 21st century. *Prog. Earth Planet. Sci.* 7, 29. doi: 10.1186/s40645-020-00342-2

Ohkouchi, N., Chikaraishi, Y., Close, H. G., Fry, B., Larsen, T., Madigan, D. J., et al. (2017). Advances in the application of amino acid nitrogen isotopic analysis in ecological and biogeochemical studies. *Org. Geochem.* 113, 150–174. doi: 10.1016/j.orggeochem.2017.07.009

Popova, E., Vousden, D., Sauer, W. H., Mohammed, E. Y., Allain, V., Downey-Breedt, N., et al. (2019). Ecological connectivity between the areas beyond national jurisdiction and coastal waters: Safeguarding interests of coastal communities in developing countries. *Mar. Policy* 104, 90–102. doi: 10.1016/j.marpol.2019.02.050

Popp, B. N., Laws, E. A., Bidigare, R. R., Dore, J. E., Hanson, K. L., and Wakeham, S. G. (1998). Effect of phytoplankton cell geometry on carbon isotopic fractionation. *Geochim. Cosmochim. Acta* 62, 69–77. doi: 10.1016/S0016-7037(97)00333-5

Priede, I. G., Solbé, J. D. L., Nott, J. E., O'Grady, K. T., and Cragg-Hine, D. (1988). Behaviour of adult Atlantic salmon, *Salmo salar* l., in the estuary of the river ribble in relation to variations in dissolved oxygen and tidal flow. *J. Fish. Biol.* 33, 133–139. doi: 10.1111/j.1095-8649.1988.tb05567.x

Quaeck-Davies, K., Bendall, V. A., MacKenzie, K. M., Hetherington, S., Newton, J., and Trueman, C. N. (2018). Teleost and elasmobranch eye lenses as a target for life-history stable isotope analyses. *PeerJ* 6, e4883. doi: 10.7717/peerj.4883

Quay, P., Sonnerup, R., Westby, T., Stutsman, J., and McNichol, A. (2003). Changes in the $^{13}C/^{12}C$ of dissolved inorganic carbon in the ocean as a tracer of anthropogenic CO2 uptake. *Global Biogeochem. Cy.* 17, 1004. doi: 10.1029/2001GB001817

Rafter, P. A., Bagnell, A., Marconi, D., and DeVries, T. (2019). Global trends in marine nitrate n isotopes from observations and a neural network-based climatology. *Biogeosciences* 16, 2617–2633. doi: 10.5194/bg-16-2617-2019

Rau, G. H., Froelich, P. N., Takahashi, T., and Des Marais, D. J. (1991). Does sedimentary organic $d^{13}C$ record variations in quaternary ocean $[CO_2(aq)]$? *Paleoceanography* 6, 335–347. doi: 10.1029/91pa00321

R Core Team (2021). *R: A language and environment for statistical computing* (Vienna, Austria: R Foundation for Statistical Computing). Available at: https://www.R-project.org/.

Rue, H., Martino, S., and Chopin, N. (2009). Approximate Bayesian inference for latent Gaussian models by using integrated nested Laplace approximations. *J. R. Stat. Soc Ser. B.* 71, 319–392. doi: 10.1111/j.1467-9868.2008.00700.x

Sackett, W. M., Eckelmann, W. R., Bender, M. L., and Be, A. W. H. (1965). Temperature dependence of carbon isotope composition in marine plankton and sediments. *Science* 148, 235–237. doi: 10.1126/science.148.3667.23

Sakamoto, T., Komatsu, K., Shirai, K., Higuchi, T., Ishimura, T., Setou, T., et al. (2019). Combining microvolume isotope analysis and numerical simulation to reproduce fish migration history. *Methods Ecol. Evol.* 10, 59–69. doi: 10.1111/2041-210X.13098

Sippel, T., Eveson, J. P., Galuardi, B., Lam, C., Hoyle, S., Maunder, M., et al. (2015). Using movement data from electronic tags in fisheries stock assessment: A review of models, technology and experimental design. *Fish. Res.* 163, 152–160. doi: 10.1016/j.fishres.2014.04.006

Sprintall, J., and Tomczak, M. (1992). Evidence of the barrier layer in the surface layer of the tropics. *J. Geophys. Res. Oceans.* 97, 7305–7316. doi: 10.1029/92JC00407

St John Glew, K., Espinasse, B., Hunt, B.P., Pakhomov, E.A., Bury, S.J., Pinkerton, M., et al. (2021). Isoscape models of the Southern Ocean: Predicting spatial and temporal variability in carbon and nitrogen isotope compositions of particulate organic matter. *Glob. Biogeochem. Cycles* 35, e2020GB006901. doi: 10.1029/2020GB006901

Stevens, E. D., Lam, H. M., and Kendall, J. (1974). Vascular anatomy of the counter-current heat exchanger of skipjack tuna. *J. Exp. Biol.* 61, 145–153. doi: 10.1242/jeb.61.1.145

Tanita, I., Shiozaki, T., Kodama, T., Hashihama, F., Sato, M., Takahashi, K., et al. (2021). Regionally variable responses of nitrogen fixation to iron and phosphorus enrichment in the pacific ocean. *J. Geophys. Res. Biogeosci.* 126, e2021JG006542. doi: 10.1029/2021JG006542

Thorson, J. T. (2019). Guidance for decisions using the vector autoregressive spatio-temporal (VAST) package in stock, ecosystem, habitat and climate assessments. *Fish. Res.* 210, 143–161. doi: 10.1016/j.fishres.2018.10.013

Thorstad, E. B., Rikardsen, A. H., Alp, A., and Økland, F. (2013). The use of electronic tags in fish research–an overview of fish telemetry methods. *Turk. J. Fish. Aquat. Sci.* 13, 881–896. doi: 10.4194/1303-2712-v13_5_13

Trueman, C. N., MacKenzie, K. M., and Palmer, M. R. (2012). Identifying migrations in marine fishes through stable-isotope analysis. *J. Fish. Biol.* 81, 826–847. doi: 10.1111/j.1095-8649.2012.03361.x

Trueman, C. N., MacKenzie, K. M., and St. John Glew, K. (2017). Stable isotope-based location in a shelf sea setting: Accuracy and precision are comparable to light-based location methods. *Methods Ecol. Evol.* 8, 232–240. doi: 10.1111/2041-210X.12651

Tuerena, R. E., Ganeshram, R. S., Humphreys, M. P., Browning, T. J., Bouman, H., and Piotrowski, A. P. (2019). Isotopic fractionation of carbon during uptake by phytoplankton across the south Atlantic subtropical convergence. *Biogeosciences* 16, 3621–3635. doi: 10.5194/bg-16-3621-2019

Vatsov, M. (2016). Changes in the geographical distribution of shared fish stocks and the mackerel war: Confronting the cooperation maze. *Scottish. Centre. Int. Law. Working. Paper. Ser.* 13. doi: 10.2139/ssrn.2863853

Vecchio, J. L., and Peebles, E. B. (2020). Spawning origins and ontogenetic movements for demersal fishes: An approach using eye-lens stable isotopes. *Estuar. Coast. Shelf. Sci.* 246, 107047. doi: 10.1016/j.ecss.2020.107047

Winter, J. D. (1983). "Underwater biotelemetry," in *Fisheries techniques*. Eds. L. A. Nielsen and D. L. Johnson (Bethesda, Maryland: American Fisheries Society), 371–395.

Winter, E. R., and Britton, J. R. (2021). Individual variability in stable isotope turnover rates of epidermal mucus according to body size in an omnivorous fish. *Hydrobiologia* 848, 363–370. doi: 10.1007/s10750-020-04444-2

Wood, S. N. (2003). Thin plate regression splines. *J. R. Stat. Soc Ser. B. Stat. Meth.* 65, 95–114. doi: 10.1111/1467-9868.00374

Yoshikawa, C., Makabe, A., Matsui, Y., Nunoura, T., and Ohkouchi, N. (2018). Nitrate isotope distribution in the subarctic and subtropical north pacific. geochem. *Geophys. Geosyst.* 19, 2212–2224. doi: 10.1029/2018GC007528

frontiers | Frontiers in Marine Science

TYPE Original Research
PUBLISHED 14 December 2022
DOI 10.3389/fmars.2022.1071081

OPEN ACCESS

EDITED BY
Tomihiko Higuchi,
The University of Tokyo, Japan

REVIEWED BY
Gotje von Leesen,
Aarhus University, Denmark
Juan Andrés López,
University of Alaska Fairbanks,
United States

*CORRESPONDENCE
Nora Hanson
nora.hanson@gov.scot

SPECIALTY SECTION
This article was submitted to Marine Biology, a section of the journal Frontiers in Marine Science

RECEIVED 15 October 2022
ACCEPTED 28 November 2022
PUBLISHED 14 December 2022

CITATION
Hanson N, Ounsley J, Middlemas SJ, Gilbey J and Todd CD (2022) Inferring individual marine migration from otolith ecogeochemical signatures of a wide-ranging fish.
Front. Mar. Sci. 9:1071081.
doi: 10.3389/fmars.2022.1071081

Inferring individual marine migration from otolith ecogeochemical signatures of a wide-ranging fish

Nora Hanson[1]*, James Ounsley[1], Stuart J. Middlemas[1], John Gilbey[1] and Christopher D. Todd[2]

[1]Freshwater Fisheries Laboratory, Marine Scotland, Pitlochry, United Kingdom, [2]Scottish Oceans Institute, School of Biology, University of St Andrews, St Andrews, United Kingdom

Despite technical advances in archival tag attachment and functional longevity, long-term tracking of individuals of some fish species remains prohibitively difficult. Here we combined high resolution stable isotope sampling of otoliths, genetic assignment, growth increment analyses and a simple movement model to inform a hidden Markov model of the location of individual wild Atlantic salmon (*Salmo salar* L.) at sea. The model provided a reconstruction of North Atlantic migration for a species which is extremely difficult to track throughout its marine life-stage. We show that plausible emigration and return migration patterns can be achieved from wild fish. Simulations of simplified northward and westward movement patterns in the North Atlantic were used to quantify precision and accuracy of the model which differed between these two directional scenarios. Because otolith-derived migratory information does not rely on capture, release and subsequent recapture of the individual, this can be retrieved from any fish. Thus these techniques offer a powerful tool for improving our understanding of the processes that govern movement and survival of individual fish during a protracted and largely unobservable life-stage in the oceanic environment.

KEYWORDS

otolith, isotope, hidden Markov model, salmon, migration, sea surface temperature

1 Introduction

Migratory species are subject to diverse anthropogenic and ecological pressures because of their movement across broad spatial scales. Full characterization of the factors affecting different life-stages therefore is contingent on knowledge of their migratory behavior and space-use (Tamario et al., 2019). Such information is particularly difficult to derive for highly mobile species such as anadromous salmon, which emigrate from

freshwater as juvenile smolts and can migrate over large distances in the marine environment prior to their coastal return as mature adults after one or more years at sea (Thorstad et al., 2010).

An understanding of the distribution, migration and behavior of wild Atlantic salmon, *Salmo salar* L., at sea is of particular importance due to recent multi-decadal and geographically broad-scale declines in survival and growth during the marine phase, often linked to a changing ocean environment (Todd et al., 2008; Chaput, 2012; Friedland and Todd, 2012; Todd et al., 2012; Olmos et al., 2020). Spatial and temporal analyses of the impact of changing ocean conditions are hampered by our limited knowledge of the migratory routes and destinations of Atlantic salmon stocks in the open ocean, how they get there, and the extent to which individuals or populations vary in their movement trajectories. These questions need to be addressed as a priority in disentangling the multiple factors affecting survival and growth of salmon at sea.

Historically, the marine migration routes and destinations of salmon have been elucidated using conventional tagging data, based on known release and recapture points (Drenner et al., 2012; Ó Maoiléidigh et al., 2018). More recently, technological advances in how electronic tag data are stored and/or transmitted have allowed anadromous species to be fitted with environment-sensing archival data storage tags (DST) commonly recording temperature and depth. Concurrent with increased use of archival tags to recover detailed information about the abiotic environment experienced by fish, has been the development and proliferation of statistical approaches to infer movement, and especially those utilizing hidden Markov models (HMMs) (Pedersen et al., 2008; Thygesen et al., 2009; Guðjónsson et al., 2015; Strøm et al., 2018).

Whilst archival tag development is providing valuable insights into the behavior of individual fish at particular life-stages, there remain some significant challenges to their application across the whole life history of wide-ranging species exploiting both freshwater and marine environments. For some species successful retrieval of archival DST is extremely difficult and/or unlikely due to low numbers of tagged individuals and/or the difficulty in targeting sufficient sampling effort to have a high probability of successful recapture. The tags often are costly, especially when only a small proportion of those deployed may be retrieved. Pop-off satellite tag data are retrievable from satellite transmissions but typical tag durations are approximately months rather than years. Finally, internally fitted tags capable of long-term (e.g. >12 months) battery life may be prohibitively large for use on smaller fish, including juvenile wild salmon. In cases where tracking of small fish, or mapping of complete life history stages, is required traditional bio-telemetry may not be an effective way of addressing broad-scale environmental questions. Advances in our understanding of stock-specific spatial exploitation and migration patterns have also recently been made using genetic stock identification. This is reliant upon commercial trawls and/or research surveys to obtain the empirical samples but does provide invaluable information on stock locations at specific times (Beacham et al., 2006; Jeffery et al., 2018; Bradbury et al., 2021; Gilbey et al., 2021).

An alternative, and often complimentary, approach to the deployment of animal-borne tags or sensors in the study of fish movement is the use of natural ecogeochemical markers (McMahon et al., 2013). Such elemental or isotopic marks are created by environmental properties and recorded within biological tissues or structures of the individual; animals residing within a particular environment are thus "tagged" with some indication of its properties, and changes therein over time. As noted by McMahon et al. (2013), the ecogeochemical approach has proven particularly useful in interrogating diadromous species which move through distinct geochemical environments. These species often are difficult to access during large portions of their life history, making natural tags a useful source of information during those times. Furthermore, the continuous accretion of calcium carbonate by skeletal components such as the sagittal otoliths ('ear bones') of teleost fish throughout the lifetime of the individual yields a structure which can be sequentially sub-sampled to reveal chronological change (Campana and Thorrold, 2001; Hanson et al., 2013; Sakamoto et al., 2019; Matsubayashi et al., 2020). Provided that the environmental parameters recorded by the natural tag can be related spatially and temporally to those available within the species' habitat, ecogeochemical markers can be utilized as natural DST to infer likely movement paths (e.g. Sakamoto et al., 2019; Matsubayashi et al., 2020).

Otoliths are biomineralized structures of the inner ear that function in hearing and balance which record various ecogeochemical markers of water chemistry encountered by the fish (Reis-Santos et al., 2022). One such marker is the stable oxygen isotope value ($\delta^{18}O$), which relates to water temperature (Campana, 1999). Water temperatures can be estimated from otolith oxygen stable isotope values because the partitioning of the stable isotopes ^{16}O and ^{18}O between otolith aragonite and ambient water is temperature-dependent (Degens et al., 1969; Kalish, 1991; Thorrold et al., 1997). Otolith growth is continuous, often displaying annual (macroscopic) or even daily (microscopic) banding; for this reason, they are commonly used in fish ageing. However, in Atlantic salmon, growth rings formed on the scale are commonly used to derive freshwater and sea ages through the demarcation of annular growth patterns (Shearer, 1992), and also to provide detailed growth histories through measurement of ring spacing (e.g. Todd et al., 2021).

Here we present a new method to infer two-dimensional movement of individual fish at sea based upon limited one-dimensional ecogeochemical data. The method was applied to two wild Atlantic salmon as a case study to examine the feasibility of using otolith oxygen stable isotope ratios as a

natural migratory tag. Specifically, we inferred ambient sea surface temperature (SST) time series for individual salmon by using, as a proxy, oxygen stable isotope ratios retrieved from otoliths by means of high resolution secondary ion mass spectrometry (SIMS). We inferred time series of likely North Atlantic locations using a body length-related model of salmon swim speed and movement applied to high resolution gridded SST data within a discrete-time, discrete-space HMM accounting for individual growth patterns. To explore the sensitivity of this approach, we simulated simplified marine migration trajectories with known thermal profiles and compared the estimated paths to true locations.

2 Materials and methods

Two adult wild Atlantic salmon were obtained in June-July 2009 from commercial coastal nets located on the north coast of Scotland (58.56°N 03.92°W). Fish body fork length (rounded down to the nearest 0.5 cm) was recorded, scales were sampled and 1 cm^3 of white muscle was excised and stored at -20°C. Sagittal otoliths were removed, cleaned of organic material and rinsed thoroughly in deionized water. Observations of the scale growth confirmed that one of the fish had spent just one winter at sea (one sea-winter; 1SW adult), and the other had spent two winters at sea (2SW adult).

To model individual salmon movement throughout the marine migration, it was necessary to define a start and end location for the marine phase. The end location was defined as the netting station site where fish were sampled; but, because coastal net fisheries may exploit multiple river stocks (Downie et al., 2018), natal origin was determined for each fish from genetic analyses of scale samples (Table 1; see Gilbey et al., 2016 for details of methods).

2.1 Thermal profile estimation

To extract time-resolved otolith oxygen stable isotope values ($\delta^{18}O$) for use as a proxy for seawater temperature, otoliths were prepared for SIMS analyses as reported in Hanson et al. (2013). Oxygen isotope ratios were measured with a Cameca IMS-1270 ion microprobe (#309) (Edinburgh Ion Microprobe Facility) using a ~ 5 nA primary $133Cs^+$ beam focused to 15 μm diameter. Step sizes between sample spots averaged 63 μm and spot depth was 2 - 3 μm. Secondary ions were extracted at -10 kV, and ^{16}O and ^{18}O were monitored simultaneously on dual Faraday cups (L'2 and H'2) at intensities of 3 x 10^9 and 4 x 10^6 cps, respectively. Mass resolution was 2600 for oxygen to remove $^{16}O^2H$ and $^{17}O^1H$ on ^{18}O. Each analysis involved a pre-sputtering period of 40 s, followed by automatic secondary beam and entrance slit centering, and finally data collection in two blocks of ten cycles. Mean external precision based on daily analysis of an inorganic carbonate standard (University of Wisconsin Calcite, UWC) was ± 0.19SD. Otolith oxygen isotope values are reported in per mil (‰) notation relative to Vienna Pee Dee Belemnite (VPDB) (Coplen, 1996), according to the equation $\delta^{18}O_{sample} = [(R_{sample}/R_{standard)} - 1] \times 1000$, where R is equal to $\frac{^{18}O}{^{16}O}$. Each sampling transect originated at the outer margin of the otolith and was terminated once a freshwater isotope signal was recorded (when values dropped to< -4 ‰). To compare isotope profiles between individual salmon, and to estimate a chronology for the sample spots, the transect was re-scaled to relative distance from the transition between freshwater and marine residency of the juvenile fish (i.e. smolt emigration from the river).

The isotope fractionation equation, $1000ln\alpha = a + b(10^3T^{-1})$ (Kim et al., 2007) was used to estimate seawater temperature values at each SIMS sample spot, where $\alpha = \frac{\delta^{18}O_{otolith}+1000}{\delta^{18}O_{water}+1000}$ and temperature T is in Kelvin. For the present analysis, the value of a was estimated from similar data from 1SW Atlantic salmon (-33.43, Hanson et al., 2013), and assuming a slope b = 17.88 ± 0.13 derived using synthetic aragonite (Kim et al., 2007). $\delta^{18}O_{water}$ was set to 0, which is a reasonable average across the North Atlantic (LeGrande and Schmidt, 2006). VPDB values were converted to the Vienna standard mean ocean water (VSMOW) scale using the Coplen et al. (1983) equation for temperature calculations. Estimated temperatures were converted to degrees Celsius (°C) by subtracting 273.15.

2.2 Marine growth and body length estimation

Detailed investigation of scale growth was necessary for the present analysis for two reasons; first, in the absence of an otolith growth model for adult Atlantic salmon, scale growth was used

TABLE 1 Capture details and genetic assignment of river or region of origin for individual wild Atlantic salmon used in the analysis.

ID	Capture site	Capture date	Capture length (cm)	Sea age	River origin assignment	Assignment probability [1]
1SW	Melvich (58.56°N 03.92° W)	2009-07-07	56.0	1SW	Oykel/Cassley/Shin (57.86 N 03.98 W)	1
2SW	Melvich (58.56°N 03.92° W)	2009-08-05	72.2	2SW	Oykel/Cassley/Shin (57.86 N 03.98 W)	1

[1]ONCOR (Kalinowski et al., 2007) probability of assignment to river using reference baseline of Gilbey et al., 2016.

as a proxy with which to anchor $\delta^{18}O$ values in time (Hanson et al., 2013). As salmon grow their scales increase in size, but not number, and growth of the scale radius is directly linked to growth in body length of the fish. It is unlikely that the relative distances along the otolith and scale growth axes would be exactly equivalent but we considered this assumption to be justified given that growth of both structures is linked to somatic growth (Degens et al., 1969; Campana and Thorrold, 2001) and is correlated in this species (Wells et al., 2003). Our second objective here was to include, as observational data in the movement model, the body length of the individual (and thence an estimate of swim speed) at each $\delta^{18}O$ spot back-calculated using the incremental measurements of the scale circuli (see below).

Details of Atlantic salmon scale increment analysis, and the method for assigning calendar dates to each growth ring for an individual fish, are reported by Todd et al. (2013). This method requires information on three recognizable scale features. Emigration of the juvenile smolt from freshwater was assumed to be April 27 2007, or May 7 2008 based on median smolt emigration dates for those calendar years taken from the only available Scottish monitoring archive (for River North Esk, E Scotland; Marine Scotland Science, unpublished data). The midpoint growth circulus of the winter annulus (1SW adult), or both winter annuli (2SW adult) was assumed to be set at the winter solstice (December 21), and the final capture date (= scale edge) was known. This method allowed the date of each growth ring to be expressed as the relative distance from smolt emigration.

We back-calculated body length increment throughout the marine phase from scale circuli measurements. Smolt length at emigration was back-calculated using a modification of the Dahl-Lea method (see Hanson et al., 2019 for details), and all subsequent growth in body length during the marine phase was assuming to be isometric with scale radius increment. Finally, back-calculated body lengths at each observed $\delta^{18}O$ otolith value were assigned by matching to the nearest calendar date.

2.3 Estimation of marine migration

Given the series of otolith-derived water temperature time series (T^O), we used a state space model to estimate progressive changes in the geographic location of the sampled salmon throughout their marine phase. Our modelling of Atlantic salmon movement assumed otolith T^O are predominantly reflective of ocean surface temperature which is justified by archival DST data having confirmed that these fish forage predominantly within the top 10m of the water column, whilst also undertaking occasional intermittent deep dives (Guðjónsson et al., 2015; Hedger et al., 2017).

We adapted the methodology of Thygesen et al. (2009) who present an HMM for the geolocation of fish, in discrete space, using DST data. In this approach, the true location of the fish at a given time-step was modelled as an unobserved state in a Markov process. The state transition probabilities were determined by a movement model, with the DST data providing observations on the hidden states.

We used a 0.25° regular grid between -75.125 and 25.125° longitude and 45.125 and 80.125° latitude to define the state space, Z, of the HMM. The resolution of the state space was aligned to available SST data (NOAA OISST v2; https://www.esrl.noaa.gov/psd/data/gridded/data.noaa.oisst.v2.highres.html), with an associated land-sea mask. States that were designated as land in the NOAA SST data had a likelihood of zero for all time-steps. Transitions between states occurred at weekly time intervals (modelled as the first day in each 7-day period since the date of river emigration).

Following Thygesen et al. (2009), let $p(\tau|\tau)$ denote the discrete probability distribution of the location of the fish, i.e. over Z, given all observations taken at, or before, time τ and $p(\tau + 1|\tau)$ be the predicted distribution at time $\tau + 1$ given all observations strictly before time $\tau + 1$. Applying the movement model then corresponds to the update:

$$p(\tau + 1|\tau) = H * p(\tau|\tau), \quad (1)$$

where H defines the transition probabilities between states as determined by the movement model, and $*$ denotes convolution over the state space (i.e. all locations), such that for state $s \in Z$ we have:

$$(H * p(\tau|\tau))_s = \sum_{t \in Z} H_{s,t} p(\tau|\tau)_t,$$

where $H_{s,t}$ is the probability of moving to state s from state t and p_t is the value of $p(\tau|\tau)$ at t.

Previous HMMs of fish behavior have modelled movement as a diffusion process resulting from an assumed unbiased random walk at a finer temporal resolution than that of the HMM (Thygesen et al., 2009; Guðjónsson et al., 2015; Strøm et al., 2017; Strøm et al., 2018). Unbiased random walk models do not appropriately capture persistence (i.e. directional correlation) in animal movement and therefore may not always be suitable for application to migratory data such as those of the present study (Codling et al., 2008); this is particularly relevant when the data are sparse and have high uncertainty. Random walk models, usually modelled with a Gaussian distribution, also have the disadvantage of allowing for a non-zero probability at large distances in finite time. As a simple alternative we used a uniform circular movement model, with radius dependent on the swim speed estimated from back-calculated body length of the fish in meters, l (Andersen et al., 2007). Thus the probability of moving to location s given starting location t and body length l_τ at time-step τ is

$$H_{s,t} = H_{s,t}(l_\tau) = \frac{\alpha_{s,t}(l_\tau)}{\sum_t \alpha_{s,t}(l_\tau)},$$

$$\alpha_{s,t}(l_\tau) = \begin{cases} 1 \text{ if } (\Delta x_{s,t})^2 + (\Delta y_{s,t})^2 \leq (Vl_\tau)^2 \\ 0 \text{ if } (\Delta x_{s,t})^2 + (\Delta y_{s,t})^2 > (Vl_\tau)^2 \\ 0 \text{ if } t \text{ is on land,} \end{cases}$$

where $\Delta x_{s,t}$, $\Delta y_{s,t}$ are the x and y components of the horizontal distance in meters between the two locations s and t, calculated as:

$$\Delta x_{s,t} = 111,320 \times (\lambda_t - \lambda_s)\cos\phi_s,$$

$$\Delta y_{s,t} = 110,574 \times (\phi_t - \phi_s),$$

where λ_z, ϕ_z are the longitude and latitude of state z in radians, and an equirectangular projection is used to approximate distance. Given that our state space was defined over a regular longitudinal and latitudinal grid, the movement model results in an ellipse with its extent dependent on the latitude of the location at which it was applied. V is the progression rate in a time interval of one week,

$$V = b \times 60 \times 60 \times 24 \times 7$$

assuming a migration speed, b, of 1.25 body lengths per second (BLs^{-1}; Drenner et al., 2012; Thorstad et al., 2012). As a consequence of using a body length-dependent progression rate, the number of non-zero values in H increases as l increases over time.

Next, the predicted distribution at time $\tau + 1$, $p(\tau + 1|\tau)$ is updated to the estimate $p(\tau + 1|\tau + 1)$ by taking into account the data at time $\tau + 1$. For the present application, in the absence of DST data, we treat the series of otolith-derived SST values (T^O) as observations of the sea surface temperature (T^{SST}) at the unobserved location.

Given an observation of otolith-derived SST, $T^O_{\tau+1}$, the likelihood of the fish being at location, s, at time $\tau + 1$ is

$$L_s(\tau + 1) \begin{cases} \frac{1}{\sigma\sqrt{2\pi}} \exp\left(-\frac{1}{2}\left(\frac{T^O_{\tau+1} - T^{SST}_{s,\tau+1}}{\sigma}\right)^2\right) & \text{if } s \text{ is at sea} \\ 0 & \text{if } s \text{ is on land,} \end{cases}$$

where $T^{SST}_{s,\tau+1}$ is the OISST at location s at time $\tau + 1$. The error in the observations, σ, was set to 1°C to account for variability in T^O - T^{SST} from various sources such as the precision of the SIMS analyses (Hanson et al., 2013), spatial variability in $\delta^{18}O$ seawater (LeGrande and Schmidt, 2006), and the accuracy and precision of the applied thermometry equation.

The above defines a discrete likelihood function $L(\tau + 1)$ over all states, and the updated estimate of the location conditional on the new observation is given by:

$$p(\tau + 1|\tau + 1) = \frac{L(\tau + 1) \times p(\tau + 1|\tau)}{|L(\tau + 1) \times p(\tau + 1|\tau)|} \quad (2)$$

By iterating through all time-steps, $\tau = 1 \ldots N - 1$, applying Equations 1 and 2, a series of probability distributions over the state space for the location of the fish was generated, with the distribution at each step conditional on all prior observations. The initial and final locations were known, so L (1) and L (N) were set to 1 at the location of the assigned river of origin (northeast Scotland) and north Scotland capture point respectively, and 0 at all other locations.

Weekly time-steps were used in the model, but time assignments of the available otolith sample spots did not result in a data point for each time-step for each fish. Accordingly, there were numerous time-steps for which there were no data with which to apply Equation 2. In this case no observation update was performed, or equivalently:

$$p(\tau + 1|\tau + 1) = p(\tau + 1|\tau).$$

In the absence of conditionality on observations, the resulting distributions were more diffuse than time-steps with associated observation data (Figure S1).

Finally, a backward smoothing recursion was performed such that the probability distributions at each time-step were conditional not only on all prior observations but also all subsequent observations. Specifically, the smoothed probability distribution over the state space at time-step τ, given all observations, was calculated by iterating from $\tau = N \ldots 1$ applying the calculation:

$$p(\tau|\infty) = \begin{cases} p(\tau|\tau), & \text{if } \tau = N \\ p(\tau|\tau) \times [H(l_{\tau+1}) * (p(\tau + 1|\infty)/p(\tau + 1|\tau))], & \text{otherwise} \end{cases}$$

resulting in the final series of smoothed probability distributions, $p(\tau|\infty)$ defined over Z.

For visualization, we also derived the mean latitude and longitude at each time-step as follows:

$$\overline{\lambda} = \sum_\lambda \lambda(\sum_\phi p(\tau|\infty)_{\lambda,\phi}),$$

$$\overline{\phi} = \sum_\phi \phi(\sum_\lambda p(\tau|\infty)_{\lambda,\phi}),$$

where $p(\tau|\infty)_{\lambda,\phi}$ is the value of $p(\tau|\infty)$ at the state with latitude and longitude λ,ϕ.

2.4 Simulation

We simulated simplified migration trajectories, and associated SST observations, to better understand the limitations of the HMM. Body length, otolith sampling frequency and origin locations were all taken from the 1SW salmon used in the study to mimic the data obtained by means of SIMS sampling. Trajectories were constructed by simulating movement from the genetically assigned origin (NE Scotland) with fixed orientation, but with distance travelled between time-steps drawn from a uniform distribution between 0 and Vl_τ. Two orientation profiles were used, either northward to the Norwegian Sea or westward toward the mid-Atlantic ridge then moving longitudinally or latitudinally, respectively, before returning

to the origin travelling backward along the same vector as the outward migration. These orientation profiles represented simplified migration trajectories which were not strictly biologically plausible (e.g. fish would not travel in a straight line) but which captured the major axes of movement for this species emigrating from southern Europe within the North Atlantic (e.g. Rikardsen et al., 2021) in a way that allowed some isolation of model performance with respect to movement trajectory. $T_{s,\tau}^{SST}$ was extracted from simulated locations and uncertainty added by sampling from a normal distribution with $\mu = T_{s,\tau}^{SST}$ and $\sigma = 1$°C. Sampled $T_{s,\tau}^{SST}$ was then thinned to reflect the sampling frequency achieved by means of SIMS.

The HMM was applied to the simulated $T_{s,\tau}^{SST}$ values allowing a direct comparison of the inferred location of the HMM against true values. The performance of the HMM was qualitatively evaluated by visualizing the true and mean inferred locations and quantitatively evaluated by calculating the absolute error (in km) between true and inferred locations over the time series, using the equirectangular projection approximation. For the latter, values were weighted by the likelihood of each inferred location. Specifically, at time-step τ the error in the location estimate, e_τ was calculated by

$$e_\tau = \sum_z \frac{d_z p(\tau|\infty)_z}{\sum_w p(\tau|\infty)_{w,}}$$

where

$$d_z = R \sqrt{\Delta x_z^2 + \Delta y_{z,}^2}$$

and

$$\Delta x_z = \left(\lambda_z - \lambda_\tau{}'\right) \cos\phi_z,$$
$$\Delta y_z = \left(\phi_z - \phi_\tau'\right),$$

where $\lambda_\tau', \phi_\tau'$ are the true latitude and longitude of the simulated migration at time τ and R is an approximation of the Earth's radius set to 6378.1 km.

As an additional comparison, we visualise the inferred locations from the HMM against SST thermal bands encompassed by $T_{s,\tau}^{SST} \pm 1$°C. This provides an indication of the impact of the movement model in reducing the uncertainty of the location estimates relative to a naïve estimate using only $T_{s,\tau}^{SST}$ to infer location (e.g. Hanson et al., 2010).

All data analyses and plotting was performed in the statistical package R (R Core Team, 2022).

3 Results

3.1 Simulation

In both simulation scenarios, the thermal profiles retrieved from the mean path closely mirrored the pattern of SST along the true simulated path (Figure 1A). However, the mean migratory path inferred from the northward simulation more closely represented the true path than that fitted to the westward migratory scenario (Figure 1B), indicating the paucity of information within thermal gradients in the westward (longitudinal) direction with which to inform the movement model.

A subset of individual time-steps of the posterior likelihood of locations for the two migratory scenarios are illustrated in Figure 2 together with locations within $\sigma = 1$°C of that measured along the true simulated path. Using the HMM to infer location, conditional both on irregular observations of SST and a movement model constrained by fish size, improved the precision of inferred locations relative to estimates based on SST alone – and most especially on the longitudinal axis. The true simulated location was contained within the 90% confidence intervals of the posterior distribution of inferred locations in 76% of the time-steps for the northward simulation and in 56% of time-steps for the westward simulation (Figure 2; Figures S2 & S3).

The absolute error (in km) between the true location and all inferred locations (including those time-steps with no associated data), weighted by their probability, varied between 0 and 2070 km. The HMM was more accurate and precise in reconstructing predominantly northward movement than predominantly westward movement. Median error was 519 km [IQR = 326] for the northward simulation and 1321 km [IQR = 871] for the westward simulation.

3.2 Otolith $\delta^{18}O$ profiles and estimation of marine migration

Figure 3A shows the $\delta^{18}O$ profiles from the two salmon examined in the present study. The SIMS sampling transects yielded 34 and 38 $\delta^{18}O$ values over 59 (1SW fish) to 112 (2SW fish) sea weeks. Profiles indicated a pattern of peaks and troughs in $\delta^{18}O$ values, associated with colder months (Figure 3B). SST values extracted from the mean inferred location were consistent with, but less variable than, the otolith-derived estimates.

Both fish were genetically allocated with high confidence ($p = 1$) to an assignment unit comprising the rivers Oykel/Cassley/Shin in north Scotland. Within the Scottish baseline, this assignment unit has high assignment accuracy ($p > 0.89$; Gilbey et al., 2016). These three rivers share a common catchment, and are confluent at the Kyle of Sutherland which itself drains to the northern North Sea (57.86 N 03.98 W). Metadata for each fish can be found in Table 1. Length profiles and emigration/capture locations are shown in Supplementary Material Figures S4 & S5.

The long-distance out-and-back migration patterns estimated by the HMM were broadly consistent with available information on the migration routes for this species (Figure 3C) (Gilbey et al., 2021; Maoiléidigh et al., 2018; Rikardsen et al., 2021).

Individual time-steps of the posterior likelihood of migratory locations for the two wild Atlantic salmon are

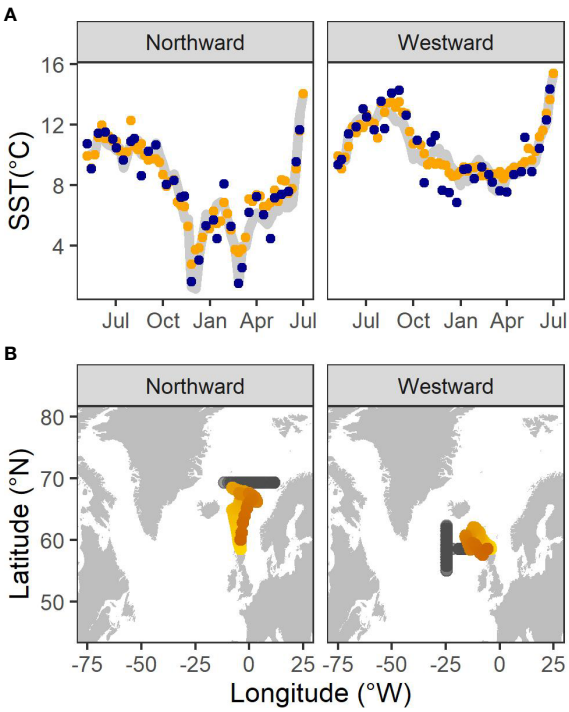

FIGURE 1
(A) SST values sampled from a normal distribution centered on SST values extracted from the true simulated location (grey line) with σ = 1°C (blue points), thinned to the SIMS sampling frequency of a 1SW fish and used as data in the hidden Markov Model to infer locations. SST values extracted from the mean inferred location (orange points) also are presented. **(B)** The mean locations (orange points) inferred from the hidden Markov model together with the true simulated locations (grey points) for each simulation. Lighter colour indicates the beginning of the migration.

illustrated in Figure 4, together with locations within $\sigma = 1$°C of that measured in the otolith. The inferred migratory locations of the 1SW individual (Figure 4A) were characterized by northward travel past the Faroe Islands into the Norwegian Sea, over-wintering around the Iceland-Faroes Ridge and the Vøring Plateau (67°N, 04°E), before return migration to the Scottish coast. The inferred migratory locations for the 2SW salmon (Figure 4B) also were characterized by northward travel to the northeast of Iceland, with seasonal transitions between the polar front zone and the Norwegian Sea. By spring of its second year at the sea the positions were located near the Faroe Islands prior to return migration to the Scottish coast. Full outputs can be seen in Figures S6, S7.

4 Discussion

We present a method for inferring the full oceanic migration of a wide-ranging anadromous fish species, using data from high resolution stable isotope sampling of individual otoliths analyzed within a hidden Markov model framework. High resolution SIMS sampling of each otolith provided a time series of individual $\delta^{18}O$ values from which we could reconstruct estimates of the experienced sea surface thermal profiles for the individual fish. The model was constrained using potential migration distance steps based upon body length estimates (and thence swim speeds) derived from scale increment analysis. We explored the precision and accuracy of the HMM using simulations of simple migratory paths within the North Atlantic and originating from NE Scotland. The model was most accurate when reconstructing primarily northward movement and less accurate when reconstructing a westward trajectory. We interpret these results to suggest that the present method of inferring movement from temperature histories may be most accurate when applied to species or demographic groups with primarily north - south migration trajectories in the North Atlantic.

4.1 Development of otolith $\delta^{18}O$ for tracking marine migration

In the present analysis, we explore an approach to inferring movement of individual fish within the marine environment from stable isotope data, which can be applied to basin-scale marine migration. Sequential sampling of ecogeochemical markers derived from biogenic structures, coupled with movement modelling techniques, provides a potentially powerful new method to track migratory animals through time and space. This general approach has been successfully applied to, among others, sub-stock movement of plaice (Darnaude and Hunter, 2018), point-to-point movement of Japanese sardine (Sakamoto et al., 2019) and chum salmon (Matsubayashi et al., 2020). Importantly, our approach allows inference on complex out-and-back migratory patterns over the time period encapsulated in the otolith (in this case, a period of one to two years from juvenile emigrant to return adult stages).

At a basic level, the temperatures estimated from Atlantic salmon otolith $\delta^{18}O$ can be used to infer broadscale movement patterns on the basis of seasonal temperature variation within the North Atlantic (Figure 4). Darnaude et al. (2014) demonstrated strong concordance between otolith $\delta^{18}O$ values and environmental conditions (temperature and salinity) for wild free-ranging plaice, while von Leesen et al. (2021) showed that SIMS-measured mean otolith $\delta^{18}O$ values were well correlated with predicted otolith $\delta^{18}O$ values based on temperature and salinity derived from DST-tagged free-swimming cod. However, such inferences would necessarily be poorly defined in the longitudinal direction because thermal gradients are predominantly latitudinal within the migratory range of this species in the eastern North Atlantic (see Reynolds et al., 2007); they would also be restricted to specific time points measured on the otolith. By using a state-space hidden Markov model we found it possible to account for the unobserved fish movement between

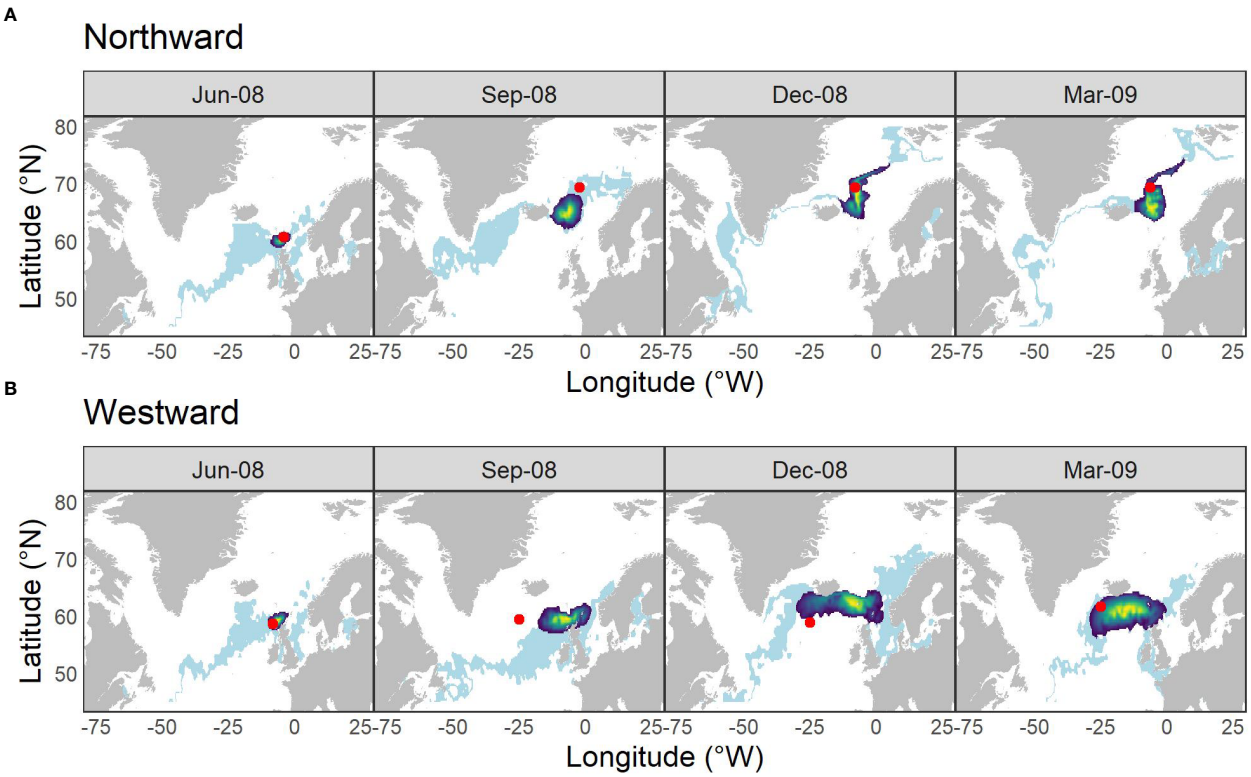

FIGURE 2
Locations inferred from SST at various time points along the **(A)** northward and **(B)** westward simulated simplified migration paths. Light blue banding illustrates the distribution of all locations within σ = 1°C of the SST at the true location (red spot); heatmap area indicates 90% C.I. of the density distribution of locations derived from the hidden Markov movement model. Time-steps were restricted to those with T^{O} values.

otolith $\delta^{18}O$ observations, and to constrain progression between observation steps using *a priori* assumptions about salmon movement thereby markedly increasing precision of location estimates in the longitudinal direction and providing inferences of location at all time-steps (Figures 2, 4).

The available information regarding at-sea distribution of wild Atlantic salmon with which to evaluate the plausibility of our modelled migration distributions is limited both in time and space. Recent analyses of available research and fisheries cruise data found Atlantic salmon postsmolt aggregations concentrated within the North Atlantic Current (April-June), around the Vøring Plateau (June-July), further north off the Barents Sea Plateau (August) and along the Iceland-Faroes Ridge (October) (Gilbey et al., 2021). From tag recaptures and, more recently, genetic screening of fisheries samples, it is apparent that Scottish salmon returning as 1SW and 2SW adults are present around the Faroe Islands at least during November – May. Some 2SW salmon of Scottish origin do latterly migrate westwards to spend their second summer in the western North Atlantic and have been captured in Greenlandic fisheries during August – October prior to their return migration (Bradbury et al., 2016; Ó Gilbey et al., 2017; Maoiléidigh et al., 2018). Our modelled locations in the eastern North Atlantic (Figures 4, S6, S7 & S8) therefore broadly conform with available fishery and survey-derived capture data. Marine migratory tracks of individual salmon tagged with archival DST are not available for Scottish salmon but such information is available for adult salmon originating from other European countries which had previously spawned, been tagged, and returned to sea. Whilst those data for spawned kelts are not directly comparable to the paths we infer here for maiden salmon undertaking marine migration for the first time, there are remarkable similarities between the tracks inferred here and those derived for salmon migrating especially from Denmark and southern Norway (Figure S8; Rikardsen et al., 2021).

Notwithstanding the fact that migratory inferences derived from our HMM were broadly plausible, it was important to test the limitations of the underlying model and to be mindful of its assumptions. While Darnaude et al. (2014) were able to validate movement inferences from otolith $\delta^{18}O$ for plaice using DST, such data are not available for many fish species due to size and/or recapture probability limitations. In the absence of such

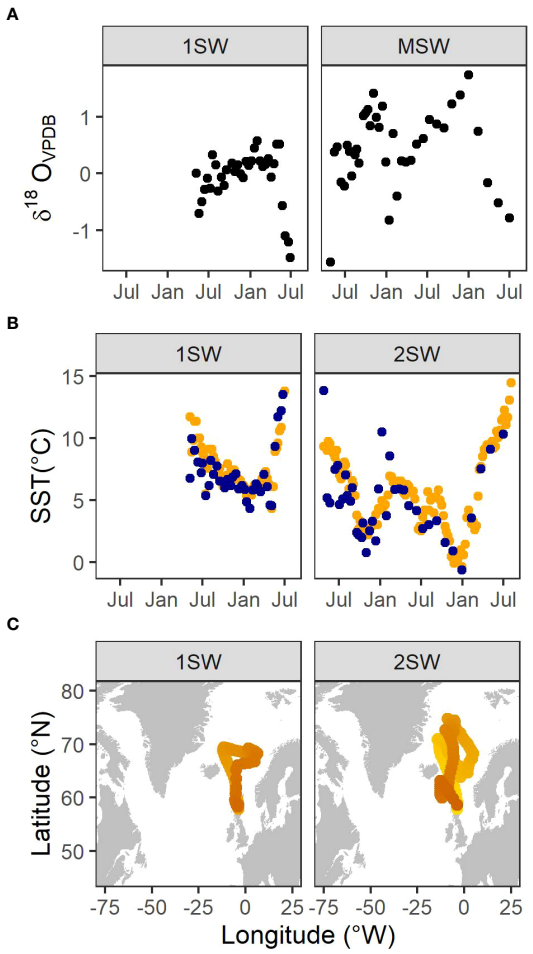

FIGURE 3
(A) Otolith $\delta^{18}O$ values along transects of wild Atlantic salmon (Salmo salar, L.) returning to Scotland. Profiles start at the transition to the marine phase and end at capture one or two sea-winters (1SW, 2SW, respectively) later. **(B)** SST values estimated from otolith $\delta^{18}O$ values (blue points) together with SST values extracted from the mean inferred location (orange points). **(C)** Mean locations inferred from the hidden Markov model. Lighter colour indicates the beginning of the migration.

validation data, we explored simple simulations of movements to test the limitations of our approach.

The performance of the HMM on simulated data highlighted some of the difficulties in recovering location from SST observations alone. In general the inferred temperature profiles were close to the true simulated values (Figure 1A); however the HMM had high error when predicting the most extreme longitudinal locations visited by the simulation. Temperature gradients are primarily north-south rather than east-west in the eastern North Atlantic (Reynolds et al., 2007), and consequently, in the presence of the uncertainty in the observation step, there is a lower signal-to-noise ratio contained within a thermal profile extracted from east-west movement. This resulted in the HMM over-smoothing the location estimates, and remaining close to the center of mass during the extremes of the migration.

For simplicity, and to test extreme scenarios, the simulated trajectories included persistent straight line migration over multiple time-steps. However, the uniform circular movement assumption gives equal probability to continue in the same direction as to move in any other direction, making it a sub-optimal movement model for the simulated scenarios. This also impacts the ability of the HMM to infer extreme locations.

Overall, the precision of our method was comparable to other studies using temperature or stable isotope data to infer marine animal distribution (MacKenzie et al., 2011; Chittenden et al., 2013; Guðjónsson et al., 2015; Trueman et al., 2017; Sakamoto et al., 2019; Matsubayashi et al., 2020). We are not aware of other attempts to quantify accuracy of movement inferences based on indirect observations using simulated data. Methods that are GPS or DST-based will be more accurate given the amount and accuracy of data that can now be stored in tags (e.g. Rikardsen et al., 2021). However, it is important to recognize that inferring movement from these data sources also requires assumptions about fish behavior and physiology that are not frequently explored. Whilst a stable isotope-based method of geolocating aquatic animals may be less accurate than more traditional telemetry approaches, it does allow lower resolution data to be readily obtained from a larger number of individuals (Table 2). In the specific case of otolith-derived information, a major advantage is that the method may be applied retrospectively to any fish.

4.2 Potential improvements

The accuracy and precision of our modelled movement inferences for individual fish appear limited by the predominant direction of travel within the North Atlantic, with constraints on inference regarding longitudinal (east-west) movement. However, there are several avenues which have the potential to improve the accuracy of inferences. A ‘center of attraction’ within the migratory domain could be included as a prior within the model if there is good information on the likely distribution of animals at a particular time (e.g. McClintock et al., 2012). Information derived from, for example, capture-mark-release-recapture studies (Ó Maoiléidigh et al., 2018), research trawls (Gilbey et al., 2021), or even isoscape-based foraging location assignments from scale stable isotope analyses (MacKenzie et al., 2011) may help to parameterize a center of attraction. The failure of the HMM to recover extreme longitudinal locations during simulated migrations suggests that a more sophisticated movement model may improve performance. Specifically, directional persistence and/or variable migration speed in combination with assumptions about stage of migration (e.g. ‘traveling’, ‘searching’, or ‘foraging’) might provide better results (e.g. Michelot et al., 2017). However, parameterizing such

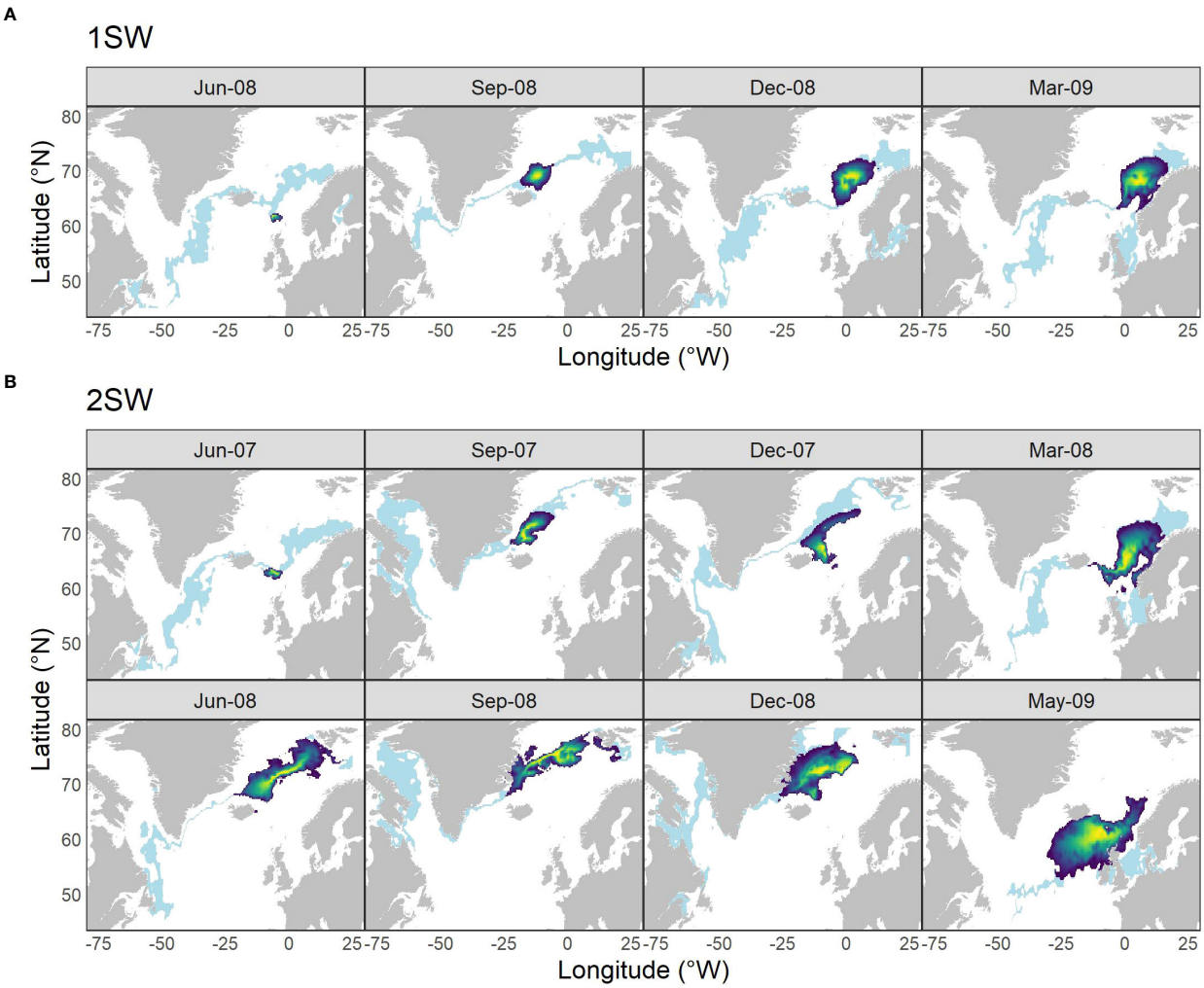

FIGURE 4
Locations of two wild Atlantic salmon at various time points during the marine migration inferred from otolith $\delta^{18}O$ derived water temperatures. The model was applied to one **(A)** 1SW and one **(B)** 2SW adult salmon for illustrative purposes. Light blue banding illustrates the distribution of all locations within σ = 1°C of the SST measured within the otolith; heatmap area indicates 90% C.I. of the density distribution of locations derived from the hidden Markov movement model. Time-steps were restricted to those with T^{O} values.

behaviors in the HMM would require additional data or strong prior information; we purposefully did not take that approach here due to the datasets being sparse and a lack of robust priors. For some species analysis of otoliths retrieved from individuals fitted with archival DST for the duration of their migration would permit cross-validation of different model formulations, including sensitivity to error in smolt emigration timing. However, for Atlantic salmon, this validation step is not readily available

TABLE 2 Comparison of various aspects of common methods used for tracking wild Atlantic salmon in the North Atlantic.

Factor	Scales SIA	Otolith SIA	Trawling	DST
Spatial resolution	Low	Low	High	Moderate
Temporal resolution	Low (unclear)	Moderate	Low (point)	High
Coverage of N. Atlantic	High	High	Low (restricted)	Moderate
Sample availability	High	High	Low	Low

SIA, Stable Isotope Analysis.

because of the present lack of sufficiently small DST for most juvenile smolts at river emigration. None the less, the use of downstream-migrating smolts that had been uniquely tagged (or recorded telemetrically) near the head of tide would offer the model advantage of confidence in the individual's date of river emigration.

Some assumptions implicit within our approach may warrant closer consideration. Perhaps the foremost of these is that the error in SST values derived from otolith $\delta^{18}O$ values is spatially random. Spatial variation in seawater $\delta^{18}O$ values (LeGrande and Schmidt, 2006) must be incorporated into future iterations of the approach, and experimental determination of an Atlantic salmon-specific $\delta^{18}O$ fractionation equation may also improve predictions for this species.

5 Conclusions

With respect to wild anadromous salmonids, the stable isotopic approach presented here has the potential to provide insight into large-scale movements of individual salmon to complement the fine-scale movements derivable for a restricted number of individuals bearing DST, and the snapshots of distribution at a given time and location provided by capture-tag-recapture and genetic stock identification data (Strøm et al., 2018; Maoiléidigh et al., 2018; Rikardsen et al., 2021; Gilbey et al., 2021).

The present combined application of ecogeochemical markers and fish movement modelling provides an analytical framework for the estimation of ocean migratory trajectories based upon a natural data storage morphological structure intrinsic to each individual. The power of this approach is especially apparent in revealing the movement history of highly migratory or anadromous species, for which traditional capture-tag-recapture techniques are difficult to implement due to the small size of the emigrant juvenile fish and their low survival to adulthood and probability of recapture. Because otolith-derived migratory information does not rely on recapturing known individual fish, and can be retrieved from any salmon, the technique represents a powerful tool for improving our understanding of the processes that govern survival during this extensive and largely unobservable lifestage.

Data availability statement

The datasets presented in this study can be found in online repositories. The names of the repository/repositories and accession number(s) can be found below: https://github.com/MarineScotlandScience/salmon-otolith-hmm.

Author contributions

NH, conceptualization. NH and JO, formal analysis and writing – original draft. NH and CT, funding acquisition for isotope analysis. NH, JO, SM, and JG, investigation. NH, JO, SM, JG, and CT, writing – review and editing. All authors contributed to the article and approved the submitted version.

Funding

This study was supported by funding from the Scottish Government. Access to the EIMF instruments was supported by grant numbers 383/1109 and 415/1010 from the Natural Environment Research Council.

Acknowledgments

The authors thank the staff at the Edinburgh Ion Microprobe Facility. Proprietors and staff of various commercial netting operations were instrumental in providing access to samples for this study (John Salkeld and the Strath Halladale Partnership; James Mackay, Armadale Salmon Fishing). The authors are grateful to J. Sampayo for genotyping of scale samples and to previous reviewers for their constructive comments on how the manuscript could be improved, including the use of a simulation study.

Conflict of interest

The authors declare that the research was conducted in the absence of any commercial or financial relationships that could be construed as a potential conflict of interest.

Publisher's note

Supplementary material

The Supplementary Material for this article can be found online at: https://www.frontiersin.org/articles/10.3389/fmars.2022.1071081/full#supplementary-material

References

Andersen, K. H., Nielsen, A., Thygesen, U. H., Hinrichsen, H.-H., and Neuenfeldt, S. (2007). Using the particle filter to geolocate Atlantic cod (*Gadus morhua*) in the Baltic sea, with special emphasis on determining uncertainty. *Can. J. Fish. Aquat. Sci.* 64, 618–627. doi: 10.1139/f07-037

Beacham, T. D., McIntosh, B., MacConnachie, C., Miller, K. M., Withler, R. E., and Varnavskaya, N. (2006). Pacific rim population structure of sockeye salmon as determined from microsatellite analysis. *Trans. Am. Fish. Soc.* 135, 174–187. doi: 10.1577/T05-149.1

Bradbury, I. R., Hamilton, L. C., Sheehan, T. F., Chaput, G., Robertson, M. J., Dempson, J. B., et al. (2016). Genetic mixed-stock analysis disentangles spatial and temporal variation in composition of the West Greenland Atlantic salmon fishery. *ICES J. Mar. Sci.* 73, 2311–2321. doi: 10.1093/icesjms/fsw072

Bradbury, I. R., Lehnert, S. J., Messmer, A., Duffy, S. J., Verspoor, E., Kess, T., et al. (2021). Range-wide genetic assignment confirms long-distance oceanic migration in atlantic salmon over half a century. *ICES J. Mar. Sci.* 78, 1434–1443. doi: 10.1093/icesjms/fsaa152

Campana, S. E. (1999). Chemistry and composition of fish otoliths: pathways, mechanisms and applications. *Mar. Ecol. Prog. Ser.* 188, 263–297. doi: 10.3354/meps188263

Campana, S. E., and Thorrold, S. R. (2001). Otoliths, increments, and elements: keys to a comprehensive understanding of fish populations? *Can. J. Fish. Aquat. Sci.* 58, 30–38. doi: 10.1139/f00-177

Chaput, G. (2012). Overview of the status of Atlantic salmon (*Salmo salar*) in the north Atlantic and trends in marine mortality. *ICES J. Mar. Sci.* 69, 1538–1548. doi: 10.1093/icesjms/fss013

Chittenden, C. M., Fauchald, P., and Rikardsen, A. H. (2013). Important open-ocean areas for northern Atlantic salmon (*Salmo salar*) — as estimated using a simple ambient-temperature approach. *Can. J. Fish. Aquat. Sci.* 70, 101–104. doi: 10.1139/cjfas-2012-0215

Codling, E. A., Plank, M. J., and Benhamou, S. (2008). Random walk models in biology. *J. R. Soc. Interface* 5, 813–834. doi: 10.1098/rsif.2008.0014

Coplen, T. B. (1996). New guidelines for reporting stable hydrogen, carbon, and oxygen isotope-ratio data. *Geochim. Cosmochim. Acta* 60, 3359–3360. doi: 10.1016/0016-7037(96)00263-3

Coplen, T. B., Kendall, C., and Hopple, J. (1983). Comparison of stable isotope reference samples. *Nature* 302, 236–238. doi: 10.1038/302236a0

Darnaude, A. M., and Hunter, E. (2018). Validation of otolith $\delta^{18}O$ values as effective natural tags for shelf-scale geolocation of migrating fish. *Mar. Ecol. Prog. Ser.* 598, 167–185. doi: 10.3354/meps12302

Darnaude, A. M., Sturrock, A., Trueman, C. N., Mouillot, D.EIMF, , Campana, S. E., et al. (2014). Listening in on the past: what can otolith $\delta^{18}O$ values really tell us about the environmental history of fishes? *PloS One* 9, e108539. doi: 10.1371/journal.pone.0108539

Degens, E. T., Deuser, W. G., and Haedrich, R. L. (1969). Molecular structure and composition of fish otoliths. *Mar. Biol.* 2, 105–113. doi: 10.1007/BF00347005

Downie, H., Hanson, N., Smith, G. W., Middlemas, S. J., Anderson, J., Tulett, D., et al. (2018). Using historic tag data to infer the geographic range of salmon river stocks likely to be taken by a coastal fishery. *Scottish Mar. Freshw. Sci. Rep.* 9, 23 doi: 10.7489/12905-1.

Drenner, S. M., Clark, T. D., Whitney, C. K., Martins, E. G., Cooke, S. J., and Hinch, S. G. (2012). A synthesis of tagging studies examining the behaviour and survival of anadromous salmonids in marine environments. *PloS One* 7, e31311. doi: 10.1371/journal.pone.0031311

Friedland, K. D., and Todd, C. D. (2012). Changes in Northwest Atlantic Arctic and subarctic conditions and the growth response of Atlantic salmon. *Polar Biol.* 35, 593–609. doi: 10.1007/s00300-011-1105-z

Gilbey, J., Cauwelier, E., Coulson, M. W., Stradmeyer, L., Sampayo, J. N., Armstrong, A., et al. (2016). Accuracy of assignment of Atlantic salmon (*Salmo salar*, l.) to rivers and regions in Scotland and northeast England based on single nucleotide polymorphism (SNP) markers. *PloS One* 11, e0164327. doi: 10.1371/journal.pone.0164327

Gilbey, J., Utne, K. R., Wennevik, V., Beck, A. C., Kausrud, K., Hindar, K., et al. (2021). The early marine distribution of Atlantic salmon in the north-east Atlantic: A genetically informed stock-specific synthesis. *Fish. Fish.*, 1-33. doi: 10.1111/faf.12587

Gilbey, J., Wennevik, V., Bradbury, I. R., Fiske, P., Hansen, L. P., Jacobsen, J. A., et al. (2017). Genetic stock identification of Atlantic salmon caught in the faroese fishery. *Fish. Res.* 187, 110–119. doi: 10.1016/j.fishres.2016.11.020

Guðjónsson, S., Einarsson, S. M., Jónsson, I. R., and Guðbrandsson, J. (2015). Marine feeding areas and vertical movements of Atlantic salmon (*Salmo salar*) as inferred from recoveries of data storage tags. *Can. J. Fish. Aquat. Sci.* 72, 1087–1098. doi: 10.1139/cjfas-2014-0562

Hanson, N. N., Smith, G. W., Middlemas, S. J., and Todd, C. D. (2019). Precision and accuracy of Dahl-lea back-calculated smolt lengths from adult scales of Atlantic salmon *Salmo salar*. *J. Fish. Biol.* 94, 183–186. doi: 10.1111/jfb.13863

Hanson, N. N., Wurster, C. M.EIMF, , Todd, C. D. (2013). Reconstructing marine life-history strategies of wild Atlantic salmon from the stable isotope composition of otoliths. *Mar. Ecol. Prog. Ser.* 475, 249–266. doi: 10.3354/meps10066

Hanson, N. N., Wurster, C. M., and Todd, C. D. (2010). Comparison of secondary ion mass spectrometry and micromilling/continuous flow isotope ratio mass spectrometry techniques used to acquire intra-otolith $\delta^{18}O$ values of wild atlantic salmon (salmo salar). *Rapid Commun. Mass Spectrom.* 24, 2491–2498. doi: 10.1002/rcm.4646

Hedger, R. D., Rikardsen, A. H., Strøm, J. F., Righton, D. A., Thorstad, E. B., and Næsje, T. F. (2017). Diving behaviour of Atlantic salmon at sea: effects of light regimes and temperature stratification. *Mar. Ecol. Prog. Ser.* 574, 127–140. doi: 10.3354/meps12180

Jeffery, N. W., Wringe, B. F., McBride, M. C., Hamilton, L. C., Stanley, R. R. E., Bernatchez, L., et al. (2018). Range-wide regional assignment of atlantic salmon (salmo salar) using genome wide single-nucleotide polymorphisms. *Fish. Res.* 206, 163–175. doi: 10.1016/j.fishres.2018.05.017

Kalinowski, S. T., Manlove, K. R., and Taper, M. L. (2007). *ONCOR: A computer program for genetic stock identification* (Montana State University: Department of Ecology). Available at: http://www.montana.edu/kalinowski/Software/ONCOR.htm.

Kalish, J. M. (1991). Oxygen and carbon stable isotopes in the otoliths of wild and laboratory-reared Australian salmon (*Arripis trutta*). *Mar. Biol.* 110, 37–47. doi: 10.1007/BF01313090

Kim, S.-T., O'Neil, J. R., Hillaire-Marcel, C., and Mucci, A. (2007). Oxygen isotope fractionation between synthetic aragonite and water: influence of temperature and Mg2+ concentration. *Geochim. Cosmochim. Acta* 71, 4704–4715. doi: 10.1016/j.gca.2007.04.019

Leesen, G., Bardarson, H., Halldórsson, S. A., Whitehouse, M. J., and Campana, S. E. (2021). Accuracy of otolith oxygen isotope records analyzed by SIMS as an index of temperature exposure of wild icelandic cod (Gadus morhua). *Front. Mar. Sci.* 8. doi: 10.3389/fmars.2021.698908

LeGrande, A. N., and Schmidt, G. A. (2006). Global gridded data set of the oxygen isotopic composition in seawater. *Geophys. Res. Lett.* 33, L12604. doi: 10.1029/2006GL026011

MacKenzie, K. M., Palmer, M. R., Moore, A., Ibbotson, A. T., Beaumont, W. R. C., Poulter, D. J. S., et al. (2011). Locations of marine animals revealed by carbon isotopes. *Sci. Rep.* 1, 21. doi: 10.1038/srep00021

Maoiléidigh, N. Ó, White, J., Hansen, L. P., Jacobsen, J. A., Potter, T., Russell, I., et al. (2018). Fifty years of marine tag recoveries from atlantic salmon. *ICES Cooperative Res. Rep.* 343, 121. doi: 10.17895/ices.pub.4542

Matsubayashi, J., Osada, Y., Tadokoro, K., Abe, Y., Yamaguchi, A., Shirai, K., et al. (2020). Tracking long-distance migration of marine fishes using compound-specific stable isotope analysis of amino acids. *Ecol. Lett.* 23, 881–890. doi: 10.1111/ele.13496

McClintock, B. T., King, R., Thomas, L., Matthiopoulos, J., McConnell, B. J., and Morales, J. M. (2012). A general discrete-time modeling framework for animal movement using multistate random walks. *Ecol. Monogr.* 82, 335–349. doi: 10.1890/11-0326.1

McMahon, K. W., Hamady, L. L., and Thorrold, S. R. (2013). A review of ecogeochemistry approaches to estimating movements of marine animals. *Limnol. Oceanogr.* 58, 697–714. doi: 10.4319/lo.2013.58.2.0697

Michelot, T., Langrock, R., Bestley, S., Jonsen, I. D., Photopoulou, T., and Patterson, T. A. (2017). Estimation and simulation of foraging trips in land-based marine predators. *Ecology* 98, 1932–1944. doi: 10.1002/ecy.1880

Olmos, M., Payne, M. R., Nevoux, M., Prévost, E., Chaput, G., Du Pontavice, H., et al. (2020). Spatial synchrony in the response of a long range migratory species (*Salmo salar*) to climate change in the north Atlantic ocean. *Glob. Change Biol.*, 26 1319–1337. doi: 10.1111/gcb.14913

Pedersen, M. W., Righton, D., Thygesen, U. H., Andersen, K. H., and Madsen, H. (2008). Geolocation of north Sea cod (*Gadus morhua*) using hidden Markov models and behavioural switching. *Can. J. Fish. Aquat. Sci.* 65, 2367–2377. doi: 10.1139/F08-144

R Core Team (2022). *R: A language and environment for statistical computing* (Vienna, Austria: R Foundation for Statistical Computing). Available at: https://www.R-project.org/.

Reis-Santos, P., Gillanders, B. M., Sturrock, A. M., Izzo, C., Oxman, D. S., Lueders-Dumont, J. A., et al (2022). Reading the biomineralized book of life: expanding otolith biogeochemical research and applications for fisheries and ecosystem-based management *Rev. Fish. Biol. Fish.* doi: 10.1007/s11160-022-09720-z

Reynolds, R. W., Smith, T. M., Liu, C., Chelton, D. B., Casey, K. S., and Schlax, M. G. (2007). Daily high-Resolution-Blended analyses for Sea surface temperature. *J. Climate* 20, 5473–5496. doi: 10.1175/2007JCLI1824.1

Rikardsen, A. H., Righton, D., Strøm, J. F., Thorstad, E. B., Gargan, P., Sheehan, T., et al. (2021). Redefining the oceanic distribution of Atlantic salmon. *Sci. Rep.* 11, 12266. doi: 10.1038/s41598-021-91137-y

Sakamoto, T., Komatsu, K., Shirai, K., Higuchi, T., Ishimura, T., Setou, T., et al. (2019). Combining microvolume isotope analysis and numerical simulation to reproduce fish migration history. *Methods Ecol. Evol.* 10, 59–69. doi: 10.1111/2041-210X.13098

Shearer, W. M. (1992). *Atlantic Salmon scale reading guidelines* (Copenhagen: International Council for the Exploration of the Seas). Available at: http://www.nefsc.noaa.gov/sos/spsyn/af/salmon/ICES_AtlanticSalmonScaleReadingGuidlines.pdf.

Strøm, J. F., Thorstad, E. B., Chafe, G., Sørbye, S. H., Righton, D., Rikardsen, A. H., et al. (2017). Ocean migration of pop-up satellite archival tagged Atlantic salmon from the miramichi river in Canada. *ICES J. Mar. Sci.* 74, 1356–1370. doi: 10.1093/icesjms/fsw220

Strøm, J. F., Thorstad, E. B., Hedger, R. D., and Rikardsen, A. H. (2018). Revealing the full ocean migration of individual Atlantic salmon. *Anim. Biotelemetry* 6, 2. doi: 10.1186/s40317-018-0146-2

Tamario, C., Sunde, J., Petersson, E., Tibblin, P., and Forsman, A. (2019). Ecological and evolutionary consequences of environmental change and management actions for migrating fish. *Front. Ecol. Evol.* 7. doi: 10.3389/fevo.2019.00271

Thorrold, S. R., Campana, S. E., Jones, C. M., and Swart, P. K. (1997). Factors determining δ^{13} and δ^{18} fractionation in aragonitic otoliths of marine fish. *Geochim. Cosmochim. Acta* 61, 2909–2919. doi: 10.1016/S0016-7037(97)00141-5

Thorstad, E. B., Whoriskey, F., Rikardsen, A. H., and Aarestrup, K. (2010). "Aquatic nomads: The life and migrations of the Atlantic salmon," in *Atlantic Salmon ecology* (Wiley-Blackwell, U.K.), 1–32. doi: 10.1002/9781444327755.ch1

Thorstad, E. B., Whoriskey, F., Uglem, I., Moore, A., Rikardsen, A. H., and Finstad, B. (2012). A critical life stage of the Atlantic salmon *Salmo salar*: behaviour and survival during the smolt and initial post-smolt migration. *J. Fish. Biol.* 81, 500–542. doi: 10.1111/j.1095-8649.2012.03370.x

Thygesen, U. H., Pedersen, M. W., and Madsen, H. (2009). "Geolocating fish using hidden Markov models and data storage tags," in *Tagging and tracking of marine animals with electronic devices reviews: Methods and technologies in fish biology and fisheries*. Eds. J. L. Nielsen, H. Arrizabalaga, N. Fragoso, A. Hobday, M. Lutcavage and J. Sibert (Dordrecht: Springer Netherlands), 277–293. doi: 10.1007/978-1-4020-9640-2_17

Todd, C. D., Friedland, K. D., MacLean, J. C., Whyte, B. D., Russell, I. C., Lonergan, M. E., et al. (2012). Phenological and phenotypic changes in Atlantic salmon populations in response to a changing climate. *ICES J. Mar. Sci.* 69, 1686–1698. doi: 10.1093/icesjms/fss151

Todd, C. D., Hanson, N. N., Boehme, L., Revie, C. W., and Marques, A. R. (2021). Variation in the post-smolt growth pattern of wild one sea-winter salmon (Salmo salar l.), and its linkage to surface warming in the eastern north Atlantic ocean. *J. Fish. Biol.* 98, 6–16. doi: 10.1111/jfb.14552

Todd, C. D., Hughes, S. L., Marshall, C. T., MacLean, J. C., Lonergan, M. E., and Biuw, E. M. (2008). Detrimental effects of recent ocean surface warming on growth condition of Atlantic salmon. *Global Change Biol.* 14, 958–970. doi: 10.1111/j.1365-2486.2007.01522.x

Todd, C. D., Whyte, B. D. M., MacLean, J. C., Revie, C. W., Lonergan, M. E., and Hanson, N. N. (2013). A simple method of dating marine growth circuli on scales of wild one sea-winter and two sea-winter Atlantic salmon (*Salmo salar*). *Can. J. Fish. Aquat. Sci.* 71, 645–655. doi: 10.1139/cjfas-2013-0359

Trueman, C. N., MacKenzie, K. M., and Glew, K. S. J. (2017). Stable isotope-based location in a shelf sea setting: Accuracy and precision are comparable to light-based location methods. *Methods Ecol. Evol.* 8, 232–240. doi: 10.1111/2041-210X.12651

Wells, B., Friedland, K., and Clarke, L. (2003). Increment patterns in otoliths and scales from mature Atlantic salmon *Salmo salar*. *Mar. Ecol. Prog. Ser.* 262, 293–298. doi: 10.3354/meps262293

frontiers | Frontiers in Marine Science

TYPE Original Research
PUBLISHED 22 December 2022
DOI 10.3389/fmars.2022.1072068

OPEN ACCESS

EDITED BY
Pedro Morais,
Florida International University,
United States

REVIEWED BY
Patricia Lastra Luque,
Technological Center Expert in Marine and Food Innovation (AZTI), Spain
Gotje von Leesen,
Aarhus University, Denmark

*CORRESPONDENCE
Yuxiao Gou
gouyuxiao@aori.u-tokyo.ac.jp

SPECIALTY SECTION
This article was submitted to Marine Biology, a section of the journal Frontiers in Marine Science

RECEIVED 17 October 2022
ACCEPTED 05 December 2022
PUBLISHED 22 December 2022

CITATION
Gou Y, Higuchi T, Iino Y, Nagasaka T, Shimizu Y, Shirai K and Kitagawa T (2022) Determination of temperature-dependent otolith oxygen stable isotope fractionation on chum salmon *Oncorhynchus keta* based on rearing experiment.
Front. Mar. Sci. 9:1072068.
doi: 10.3389/fmars.2022.1072068

Determination of temperature-dependent otolith oxygen stable isotope fractionation on chum salmon *Oncorhynchus keta* based on rearing experiment

Yuxiao Gou[1]*, Tomihiko Higuchi[2], Yuki Iino[1], Tsuyoshi Nagasaka[3], Yuichi Shimizu[3], Kotaro Shirai[2] and Takashi Kitagawa[1]

[1]Otsuchi Coastal Research Center, The Atmosphere and Ocean Research Institute, The University of Tokyo, Iwate, Japan, [2]Atmosphere and Ocean Research Institute, The University of Tokyo, Chiba, Japan, [3]Iwate Fisheries Technology Center, Iwate, Japan

Reconstruction of water temperatures experienced by marine fishes using otolith oxygen stable isotopes ($\delta^{18}O$) as natural thermometers has been proven to be a useful approach for estimating migration routes or movement patterns. This method is based on the mechanism that the equilibrium fractionation of $\delta^{18}O_{otolith}$ against ambient water exhibits a species-specific thermal sensitivity during the process of otolith aragonitic $CaCO_3$ precipitation. In this study, a laboratory-controlled rearing experiment was conducted to determine the temperature dependency of $\delta^{18}O$ fractionation on the anadromous fish species, chum salmon (*Oncorhynchus keta*), of which the detailed migration routes have not been elucidated yet. To test that temperature was the only factor affecting $\delta^{18}O_{otolith}$ fractionation, this study ensured a relatively stable rearing condition, evaluated the isotope composition of the rearing water, and analyzed carbon isotope ($\delta^{13}C_{otolith}$) to examine the potential effect of kinetic and metabolic isotopic fractionations. The $\delta^{18}O_{otolith}$ fractionation equation on chum salmon was thereby determined within a temperature range of 9–20°C and was indistinguishable from the equation of synthetic aragonite; The $\delta^{13}C_{otolith}$ was affected by both physiological processes and $\delta^{13}C_{DIC}$; In lower temperatures settings, both oxygen and carbon isotopes depleted simultaneously. This study suggests that the chum salmon species-specific oxygen isotope fractionation equation could be used on reconstruction of temperature history and also throw insights into understanding the incorporation of oxygen and carbon sources during calcification process for otoliths.

KEYWORDS

chum salmon, otolith, stable oxygen isotope, oxygen isotope fractionation, temperature-dependence

1 Introduction

Chum salmon *Oncorhynchus keta* is one of the most abundant species in the North Pacific, and its overall population has increased dramatically due to the success of hatchery programs (Ruggerone and Irvine, 2018). However, in many areas, especially in the southern stocks, the population of chum salmon has decreased sharply over the last few decades, though the continuance of hatchery enhancement programs (Irvine et al., 2009; Abdul-Aziz et al., 2011; Healey, 2011; Irvine and Fukuwaka, 2011; Ruggerone and Irvine, 2018). The productivity of chum salmon is correlated with the capacity of the North Pacific (Sanger, 1972), which can be affected by climate change and high-density hatchery enhancement (Beamish and Mahnken, 2001; Ruggerone and Nielsen, 2004; Beamish, 2017; Schoen et al., 2017; Connors et al., 2020). Furthermore, the mortality rates of juvenile chum salmon are the highest after release (Fukuwaka and Suzuki, 2002), which may be caused by the sharp decrease in available feed mass evolved with the residence with high density of juvenile chum salmon in the coastal area, modified by the limited utilization of migration routes (Sanger, 1962). Thus, studies on chum salmon's early life migration ecology are required for the management of artificial hatchery enhancement (Iino et al., 2022).

As an anadromous fish species, chum salmon migrate to the sea after their emergence from gravel beds in spawning rivers and spend most of their life in the ocean (Perry et al., 1996). This suggests that growth and survival depend more on the littoral zone in estuaries than on the freshwater habitat (Seki, 1978; Johnson et al., 1997). In Honshu, Japan, there are many small coastal rivers that produce chum salmon, and the juveniles enter the estuary within 24 h after release (Iwata, 1995). Generally, Japanese juvenile chum salmon species migrate toward the Okhotsk Sea after leaving coastal areas (Irie, 1990; Urawa et al., 2004; Shubin and Akinicheva, 2016; Urawa et al., 2018), and were expected to habitat at Sanriku coastal areas in Japan within sea surface temperature (SST) of 9–13°C (Irie, 1990), although detailed migration routes and actual temperature histories have not yet been identified.

Electronic tagging technology is commonly used in fish behavioral ecology studies (e.g. Tanaka et al., 2000; Kitagawa et al., 2000; Kitagawa et al., 2004; Kitagawa et al., 2009). The method has also been applied to adult chum salmon by using an acoustic transmitter system to investigate natal homing behavior on the Sanriku coast in North Japan (e.g. Tanaka et al., 2000; Nobata et al., 2019). However, the methodology described above is not suitable for juvenile chum salmon because the tagging devices are too heavy for small juveniles to carry. Recently, the implementation of methods to estimate fish movement in oceans from biogeochemical information stored in fish otoliths (such as water temperature and seawater stable oxygen isotope values, Patterson, 1999; Høie et al., 2004a; Walther and Thorrold, 2009) has proven to be a useful indirect approach for describing the thermal and geochemical conditions experienced by fish (Campana, 1999; Campana and Thorrold, 2001; Høie et al., 2004b; Tanner et al., 2013). It has been over half a century since the precursory works of Urey (1947) and Epstein et al. (1951) suggested that accurate determination of the oxygen stable isotope ($\delta^{18}O$) composition in mineral carbonates is a powerful indicator of the ambient temperature at which the carbonates formed, since the thermodynamic mechanisms of the isotopic composition of minerals is reflected by both mineralization temperature and ambient water isotopic composition. A temperature dependence response also occurs in carbonates, as they discriminate relatively lighter ^{16}O from ambient water at higher temperatures during the mineralization process (Kim and O'Neil, 1997). Similarly, fish otoliths which are metabolically inert acellular aragonite compounds in the inner ear (Campana, 1999; Grønkjær, 2016), have proven to be effective for reconstructing temperatures experienced by fish (Jones and Campana, 2009; West et al., 2012; Willmes et al., 2019; Hane et al., 2020). Using the daily deposition pattern of otoliths, the temperature and water-$\delta^{18}O$-isoscape allows otoliths to be applied to fish migration and behavioral studies (e.g., Sakamoto et al., 2019). Furthermore, since the dissolved carbon in fish blood is physiologically controlled to regulate the fluid pH, which fluctuate with diet digestion and metabolic activities (Solomon et al., 2006), the carbon isotope composition in fish otoliths can therefore be applied to estimate individual field metabolic rate (Chung et al., 2019).

To utilize the otolith $\delta^{18}O$ composition as a thermometer, the species-specific temperature dependent equation representing the negative relationship of otolith isotopic fractionation against ambient water temperature should be initially identified (Darnaude et al., 2014). Previous studies with several fish species used laboratory-controlled rearing experiments under gradient temperatures to ensure that temperature was the only factor influencing the deposition of otolith $\delta^{18}O$ ($\delta^{18}O_{otolith}$, e.g. Kitagawa et al., 2013; Sakamoto et al., 2017). The relationships between fractionation of $\delta^{18}O_{otolith}$ against water and temperature could then be quantified based on well-established thermodynamic equations (Kim and O'Neil, 1997) under the assumption that $\delta^{18}O$ in mineral aragonite is precipitated in, or near, equilibrium; however, it is still controversial that the temperature dependency is species-specific or purely under thermodynamic control (Patterson et al., 1993; Radtke et al., 1996; Thorrold et al., 1997; Høie et al., 2004b; Walther and Thorrold, 2009; Kitagawa et al., 2013; Sakamoto et al., 2017; Shirai et al., 2018b).

Several methods have been employed to reduce systematic errors and evaluate the results in previous studies with otoliths, including isotopic distinction of intra-fish paired sagittal otoliths (Thorrold et al., 1997), high-precision otolith extraction procedures (Sakamoto et al., 2017), isotope mass spectrometry instrument calibration (von Leesen et al., 2021) and back-

calculated temperature and *in situ* temperature correlation (Willmes et al., 2019). The chum salmon *Oncorhynchus keta*, as an anadromous fish, shift the habitat from freshwater to seawater in early life stages (Salo, 1991; Johnson et al., 1997; Beamish, 2017), indicating the shift between isotopically distinct environments (LeGrande and Schmidt, 2006; Oppo et al., 2007). Thus, to accurately determine the relationship between otolith isotopic fractionation and seawater, otolith portions reflecting the freshwater life stages should be restricted from the extraction. This study aims to determine the temperature dependence of otolith oxygen isotopic fractionation against seawater on anadromous chum salmon by adopting a laboratory-controlled gradient-temperature rearing experiment. The accuracy of the results will be promoted by the high precision extraction of otolith portions, excluding the low $\delta^{18}O_{otolith}$ values during the freshwater period induced by the uneven morphological structures, as well as by testing for the attribution of the isotopic composition in seawater on $\delta^{18}O_{otolith}$.

2 Materials and methods

2.1 Laboratory-rearing experiment

Juvenile chum salmon were obtained and reared at the Touni Salmon Masu Hatchery Enhancement Station, Iwate Fishery Technology Center, Kamaishi, Japan. Individuals (300; 40–50 mm FL) hatched between March 1 and April 1, 2020 were selected and transported into two 100 L tanks filled with freshwater. On May 20, the otoliths of the juveniles were marked with 10 ppm Alizarin Complexone solution (ALC) at 10.1–10.7°C for 1 d to record the start of the experiment (Saito et al., 2007; Kasugai et al., 2013). After 1 week of temporary rearing in freshwater, juveniles were transported to the International Coastal Research Center (Current name: Otsuchi Coastal Research Center), Atmosphere and Ocean Research Institute, The University of Tokyo, Otsuchi Bay, Japan, and reared for another 3 d at 12°C in a 500 L freshwater tank to ensure recovery from transportation stress. The procedure above produced a mortality rate of 8.3% with the cost of 15 individuals during ALC dyeing and 10 individuals during transportation.

After acclimation, another 500 L tank at 12°C was filled with filtered seawater (salinity = 33.5) pumped from Otsuchi Bay for 1d seawater domestication. While the experienced temperatures for wild individuals were 9–13°C (Irie, 1990) and the significant lethality from constant exposure to 22°C (Hicks, 2000), the following gradient-temperature acclimation was conducted within a temperature range of 9–20°C (uppermost temperature treatment was 2°C below upper incipient lethal temperature to permit a high survival rate), and the temperature treatments were arranged as 9, 12, 15, 18 and 20°C, implemented in five tanks (2 in 150L and 3 in 80L because tanks in the same size were unavailable). On June 1, 50 individuals each were randomly selected and transferred into two 150 L (9 and 12°C) and three 80 L (15, 18, and 20°C) temperature gradient rearing tanks, respectively (Figure 1). Water temperatures were elevated or depressed by automatic heater-cooler units (AQUA Co., Ltd, Tokyo, Japan, ARK802-301A-5) within 3.5 h after the juveniles were transferred. The juvenile were then acclimated in 5 temperature groups for three months, a timescale represents the approximate migration period from coastal zones to Okhotsk Sea for wild juvenile chum salmon spawned in Iwate prefecture (Urawa et al., 2018). Juvenile chum salmon were fed twice a day with 4% body weight of formula pellets (Marubeni Nissin Feed Co., Ltd, Tokyo, Japan; EPC4: water 12.7%, protein 42.6%, fat 6.9%, fiber 1.0%, ash 12.6%, nitrogen-free extract 24.2%, particle size 1.5 mm) and maintained under artificial light with a 12:12 h light/dark regime. The seawater was aerated and refreshed daily with an exchange rate of 10% tank volume of fresh seawater during the 90 d experimental period (except for the 18°C group that ended on the 83rd day evolved by instrumental trouble of pump, and the fish were then sacrificed, somatically measured and frozen at –20°C). Tanks were capped with transparent covers to prevent evaporation of seawater (80L tanks with original packing covers while 150L tanks with hand-made PVC plate caps) and were sanitized at the end of the 3rd, 7th, and 11th weeks with 100% seawater exchange to reduce the isotopic effect of background

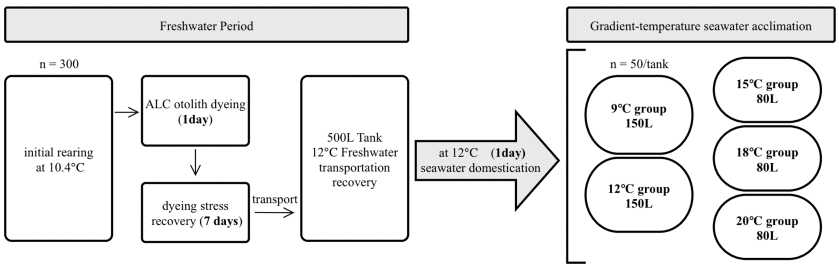

FIGURE 1
Flowchart of the rearing experiment in respective freshwater and seawater period. n: juvenile chum salmon individual number; ALC, alizarin complexone.

respiration (e.g., bacterial oxygen consumption and algal photosynthesis). The rearing experiment ended on August 30, and the sampling strategies for seawater and fish were followed.

2.2 Sample strategy and otolith sample preparation

Rearing seawater samples for isotopic analysis were collected weekly from the first day of the gradient-temperature rearing experiment. After recording the salinity and instant water temperature, the seawater from each temperature group was filtered with a 0.45 μm syringe filter and transferred into separate 50 mL plastic vials. The water samples were then stored at 4°C until oxygen isotopic analysis. Filtered seawater for carbon isotopic analysis of dissolved inorganic carbon (DIC) in each group was injected into 20 mL septum-sealed glass vials to prevent air contamination. After samplings, the seawater samples were sent by refrigerated courier to Atmosphere Ocean Research Institute, The University of Tokyo, and the oxygen and carbon isotopic analysis were conducted soon after.

Juveniles at the end of the rearing were used for determination of $\delta^{18}O_{otolith}$ fractionation equation, but 6 individuals were randomly sampled from each tank every two weeks (once a week at the beginning and the end of the experiment) to record the somatic and otolith growth. The fork length and body weight of individuals were measured to calculate the feed pellet mass. Juveniles sampled at the end of the rearing experiment were frozen at −20°C and defrosted for sagittal otolith extraction using a lateral extraction method (Wakefield et al., 2016) and nylon brushes were used to remove any adhered material, whereby 42 otoliths in total: 11 at 9°C, 8 at 12°C, 9 at 15°C, 8 at 18°C, 6 at 20°C and one random otolith, either left or right, from one individual were selected. The otoliths were then maintained in an ultrasonic Milli-Q water bath and dried at room temperature (23°C). Cleaned otoliths were attached to glass slides with epoxy resin (Burnham Petrographics LLC) and ground with 15 μm sandpaper followed by a polishing procedure with 10 μm diamond films until the otolith cores were observed clearly under a microscope (10×). The ALC marks of the polished otoliths were identified under a fluorescence microscope (30×, Olympus BX63 coupled with a U-RFL-T fluorescence light source, Olympus, Tokyo, Japan). Based on the fluorescence results, daily rings corresponding to ALC marks were identified on the light microscopic results using an otolith measurement system (Ratoc System Engineering Co. Ltd., Tokyo, Japan) (Figures 2A, B). To extract the newly deposited portion on the otolith that reflected the seawater rearing period at respective temperature group for isotope analysis, the growth ring representing the day on which the temperature gradient introduced was also identified on the light microscopic results by counting 11 daily rings from the ALC mark to the otolith margin (7 d assimilating rearing after ALC treatment in freshwater, 3 d stabilization rearing after transportation, and 1 d domestication rearing before seawater temperature gradients were introduced, Figure 2C).

Otolith powder for isotope analysis was sampled using a high-precision micro-drilling system (QuickPro, MicroSupport, Shizuoka, Japan) coupled with video monitoring and analysis software. Considering the variance of $\delta^{18}O_{seawater}$ values during 3 months rearing and the mix of the otolith powder representing the freshwater rearing period, the newly deposited proportion on the otolith was divided into three equivalent samples (hereafter inner, middle, and edge) to improve the accuracy of the estimation on $\delta^{18}O$ fractionation (Figures 2D–F). Another sample was examined for alternatively selected otoliths from each temperature group by drilling from the ALC mark to the core (freshwater period), and the $\delta^{18}O_{otolith}$ values were compared with those of the three samples collected from the same otolith, to evaluate the effect of contamination from freshwater period. To satisfy the instrumental detection limit of the following isotope analysis, > 8 μg powder for each otolith portion was collected into cleaned glass vials. This approach allows for a reduction of the operation error by adjusting the ALC mark, and the influence of freshwater can also be excluded based on the three equivalent extractions method. Otolith powder samples were then used for isotope analysis. The carbon isotope values were also analyzed to examine the potential effect of kinetic and metabolic isotopic fractionations.

2.3 Stable oxygen and carbon isotope analysis

The $\delta^{18}O$ and $\delta^{13}C$ values of otolith powder samples and $\delta^{13}C$ values of DIC ($\delta^{13}C_{DIC}$) in rearing seawater were measured using an isotope ratio mass spectrometer (Delta V plus, Thermo Fisher Scientific, Waltham, Massachusetts) equipped with an automated carbonate reaction device (GasBench II, Thermo Fisher Scientific) installed at the Atmosphere and Ocean Research Institute, University of Tokyo. The traditional CO_2 conversion technique was used, whereby the otolith powder and DIC in seawater were extracted to CO_2 by reacting with 100% phosphoric acid at 72°C for carbonate and 25°C for DIC, after flushing with pure helium. Equilibrated gaseous CO_2 was then transported with the helium flow to the mass spectrometer for $\delta^{18}O$-CO_2 and $\delta^{13}C$-CO_2 determination. The detailed analytical conditions for otoliths and DIC in seawater samples have been reported previously (e.g., Shirai et al., 2018b; Zhao et al., 2019), with modifications for small quantity of samples (see Breitenbach and Bernasconi, 2011). The isotopic results used delta notation standardized to the Vienna Pee Dee Belemnite (V-PDB) scale based on NBS-19 values of −2.20‰ and 1.95‰ for $\delta^{18}O$ and $\delta^{13}C$, respectively. No correction was applied for the acid fractionation factor between calcite and aragonite at the

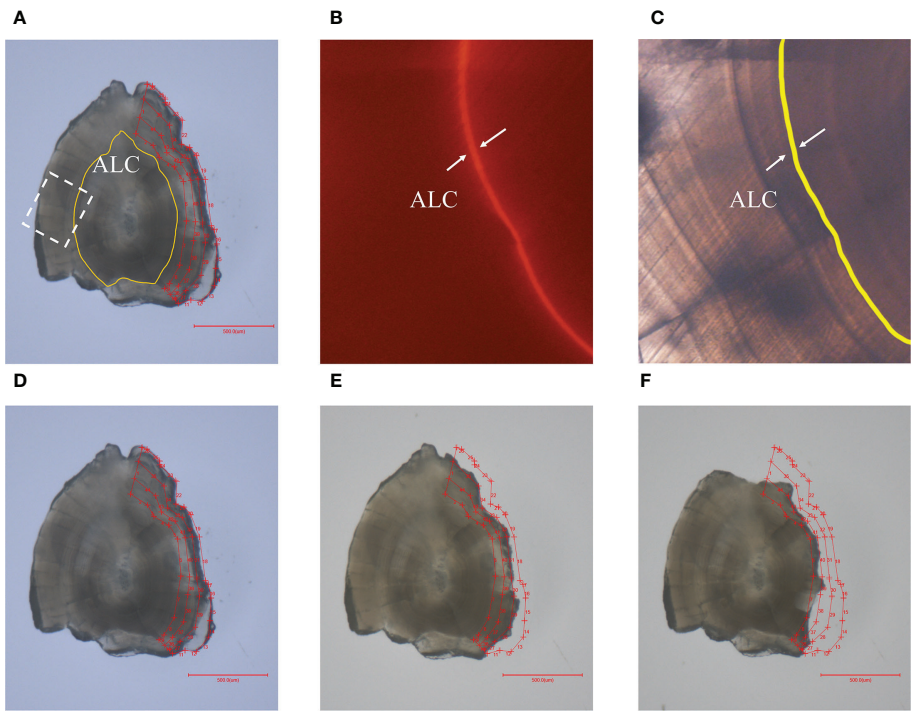

FIGURE 2
(A) Extraction portions surrounded by several red line segments out of the yellow ALC mark to the edge, and labeled as inner, middle, and edge from the core to the edge of an alternative otolith used in this study. The white dotted square shows the images of the ALC mark correlated to **(B)** and **(C)**; **(B)** Orange ALC mark was observed under fluorescence microscope (× 20); **(C)** ALC mark was identified by a yellow line using light microscopy at the same field of **(B)**; **(D–F)** show the otoliths after the extraction procedure for edge, middle and inner portions, respectively, for isotope analysis.

phosphoric acid-calcium carbonate reaction temperature of 72° C (Kim et al., 2007; Shirai et al., 2018a). The standard deviation of the external reproducibility of $\delta^{18}O$ and $\delta^{13}C$ analysis for otoliths and $\delta^{13}C$ of DIC were better than 0.15‰, 0.12‰ and 0.14‰, respectively, based on the reproducibility of NBS-19.

The $\delta^{18}O$ values of the rearing seawater samples were determined using a Picarro L2120-i analyzer at the Atmosphere and Ocean Research Institute, University of Tokyo. Before introduction into the analyzer, samples were filtered using a membrane filter (φ = 0.45μm) to reduce suspended particles and prevent blocking of the sampling line. Data are reported in delta notation and standardized against Vienna Standard Mean Ocean Water (VSMOW). The long-term instrument reproducibility was ±0.08‰.

2.4 Statistical analysis

Two-factor permutational univariate analysis of variance (ANOVA) was used to determine the differences in $\delta^{18}O_{otolith}$or $\delta^{13}C_{otolith}$ values among otolith portions and temperature treatments. Two-sample *t*-test was used to evaluate the means differences of otolith radius, somatic and otolith growth rate, body mass among temperature treatments. Linear regression analysis were used to assess the relationship between otolith isotopes and temperatures, and non-linear regression analysis was used to describe the best-fitted curve for somatic growth. Analysis of covariance (ANCOVA) was used to compare the slopes and intercepts calculated in this study against synthetic aragonite. Partial correlation analysis was used to determine whether the correlation between carbon and oxygen fractionation remained after removing the effect of temperature. All the statistical analysis and graphical plotting were performed in OriginPro (ver. 2022, OriginLab Corporation, USA).

3 Results

3.1 Rearing condition and somatic growth

Variations in $\delta^{18}O_{seawater}$, $\delta^{13}C_{seawater}$, water temperature, and seawater salinity during the rearing experiment are shown in Figure 3. Covariation among the parameters was not evident. Average salinity among 5 groups was 33.20 ± 0.17, and the large

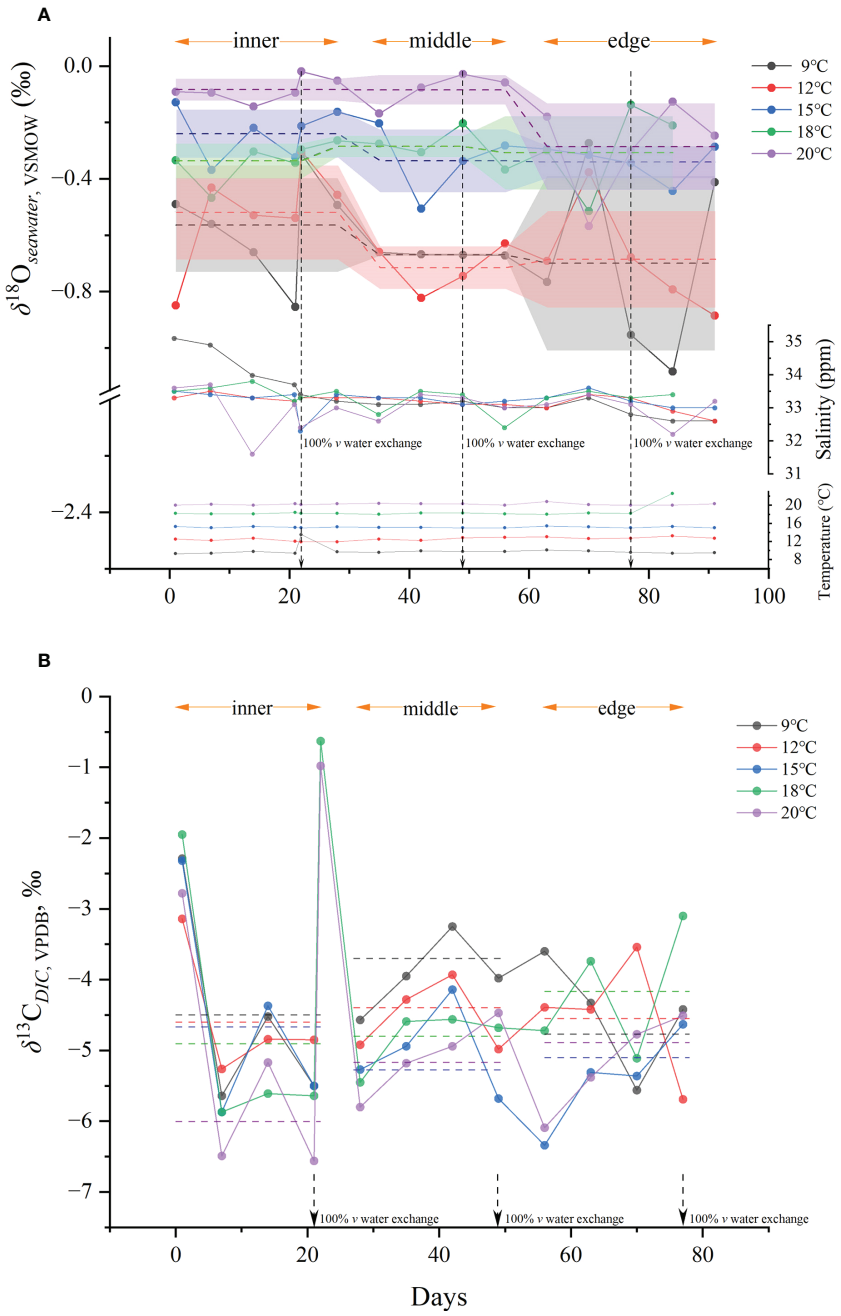

FIGURE 3
(A) Variation of $\delta^{18}O_{seawater}$ values, salinity and temperatures of rearing water of five temperature groups during rearing experiment; **(B)** variation of $\delta^{13}C_{seawater}$ values during rearing experiment. The dashed lines represent the average isotope values used in fractionation calculation.

fluctuation occurred in the inner otolith deposition period for 9 and 20°C groups, with standard deviations of 1.10 and 0.79, respectively. In general, the rearing water of the 9 and 12°C groups showed greater $\delta^{18}O$ depletion compared to the other three groups. The 9°C group presented $\delta^{18}O_{seawater}$ fluctuations fueled by standard deviations during the period at which the inner and edge otolith portions deposited were larger than the middle portion, with values of −0.56 ± 0.17‰ for the inner and −0.70 ± 0.31‰ for the edge regions, compared with −0.67 ± 0.004‰ for the middle portion. Therefore, the middle portion of otoliths reflected the most stable rearing period.

Juvenile chum salmon had an average primary weight of 1.69 g and the general somatic growth patterns for individuals in the five temperature groups are shown in Figure 4. The final

10.3389/fmars.2022.1072068

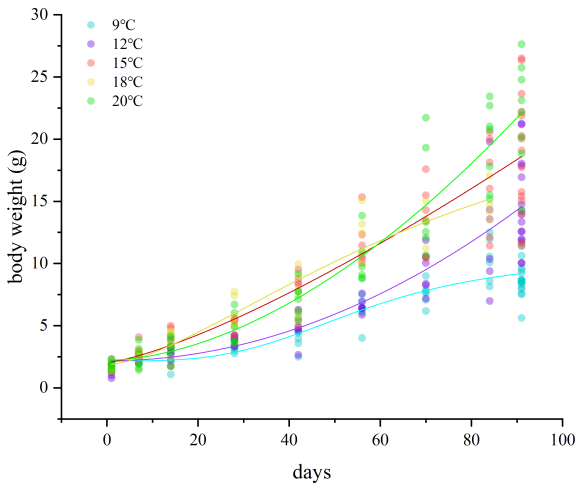

FIGURE 4
Potential variation of body mass of juvenile chum salmon during rearing experiment of five temperature groups. An alternate solid point represents the body weight (g) of an individual sampled randomly at the specified date.

weights at the end of the rearing experiment for juveniles at 9°C were significantly lower than those for the other four groups (two-sample *t*-test, $p< 0.001$). The average otolith radius was 539.81 ± 38.47, 658.66 ± 54.45, 630.8 ± 55.34, 617.34 ± 62.52, and 741.11 ± 56.76 µm, and otolith growth rate was 1.02 ± 0.42, 2.32 ± 0.60, 2.02 ± 0.61, 1.87 ± 0.69, and 3.23 ± 0.62 µm/d for the 9, 12, 15, 18 and 20°C groups, respectively. The average otolith radius and precipitation rate for individuals in the 9°C group were less than those of the other 4 groups (significant at 0.001 level for the 12, 15, and 20°C groups, two-sample *t*-test, $p< 0.001$; significant at 0.05 level for the 18°C group, two-sample *t*-test, $0.05< p< 0.01$).

3.2 Isotope composition of otoliths

The mean oxygen isotope value of otoliths ($\delta^{18}O_{otolith}$) from each temperature treatment varied from −0.91 ± 0.30 to 0.57 ± 0.46‰ (Table 1), and there was a significant difference among the five temperature groups (one-way ANOVA, $p< 0.001$). The $\delta^{18}O_{otolith}$ values of the inner otolith portions differed from those of the middle portions (one-way ANOVA, $p = 0.0012$), and differed significantly from those of the edge portions (one-way ANOVA, $p = 0.0009$). There was no difference between the $\delta^{18}O$ values of the middle and edge otolith portions (one-way ANOVA, $p = 0.919$), indicating a mix of otolith portions deposited in the freshwater period in the inner otolith samples. The $\delta^{18}O_{otolith}$ and $\delta^{13}C_{otolith}$ values for extra otolith represented the freshwater period was −3.65 ± 0.49 and −11.00 ± 0.35‰. By comparing the isotope values of inner portions with middle, it was indicated that only 4 out of 42 otolith samples were not mixed with otolith portions formed during freshwater period. The mix proportions ranged from 0.3% to 47.7% with an average value of 15.1% for all the samples. The proportions calculated by respective $\delta^{18}O$ and $\delta^{13}C$ were not statistically different (one-way ANOVA, $p = 0.73$). Thus, the mix of otolith portions deposited at freshwater period was assignable and the data of the inner portion were excluded from the following analysis. The $\delta^{18}O$ values of the middle and edge portions of the otoliths among the five temperatures remained significantly different after the exclusion (one-way ANOVA, $p< 0.001$). Detailed otolith isotope values of individuals can be found in Table S1. The $\delta^{18}O_{otolith}$ values of the edge and middle otolith portions are shown in Figure 5. In the 9°C group, $\delta^{18}O_{otolith}$ values ranged from −0.64 to 1.23‰, with the $\delta^{18}O_{otolith}$ edge values generally lower than those of the middle portions (one-way ANOVA, $p< 0.05$). The linear relationship between $\delta^{18}O_{otolith}$ values of the five groups and water temperature can be generally described as:

$$\delta^{18}O_{otolith,\,VPDB} = \mathbf{-0.109\ (\pm 0.010)} \times T\ (°C) + \mathbf{1.593\ (\pm 0.159)} \quad \text{(Equation 1)}$$

The mean $\delta^{13}C_{otolith}$ values of each temperature group ranged from −9.77 ± 0.25 to −8.18 ± 0.55‰, with significant differences among the five groups (one-way ANOVA, $p< 0.001$). Similarly, the $\delta^{13}C_{otolith}$ values of the inner portions were significantly lower than those of the middle (paired-sample t-test, $p< 0.001$), while the difference with the $\delta^{13}C_{otolith}$ values of the edge portions was not significant (paired-sample t-test, $p = 0.06$). Paired $\delta^{13}C_{otolith}$ and $\delta^{18}O_{otolith}$values were used in the following analysis; therefore, the $\delta^{13}C_{otolith}$ values of the inner portions were not included.

The $\delta^{13}C_{otolith}$ values of the middle and edge regions were significantly different among the five temperature groups (one-way ANOVA, $p< 0.001$). A plot of carbon isotopes versus temperature showed a decrease in $\delta^{13}C$ with increasing temperature (Figure 6), indicating a negative weak correlation (Pearson's $r = -0.692$, $r^2 = 0.472$, $p< 0.001$). The deviations of $\delta^{13}C_{otolith}$ from the DIC of seawater were also plotted against temperature and little correlation identified ($r^2 = 0.05$, Figure S1).

3.3 Otolith oxygen isotope fractionation

The mean $\delta^{18}O_{seawater}$ values during each deposition period were used to calculate the otolith oxygen isotope fractionation for the middle and edge otolith portions. To achieve the difference between otolith and seawater isotope values as accurately as possible, the deviations of the $\delta^{18}O_{seawater}$ mean values should be restrained within a relatively small range to narrow the impact of seawater isotopic fluctuation. As described

TABLE 1 Summary of oxygen and carbon isotope analysis results, including the numbers of otoliths used for isotopic analysis, mean $\delta^{18}O$ and $\delta^{13}C$ values of each extracted portion of otoliths, mean $\delta^{18}O_{seawater}$ and $\delta^{13}C_{DIC}$ values of rearing water and DIC corresponding to the period of otolith precipitation, the oxygen isotope fractionation of otolith against rearing seawater and the carbon isotope fractionation of otolith against DIC.

Water temperature (°C)	Number of otoliths	Extracted portions of otoliths	$\delta^{18}O_{otolith}$ (‰, VPDB)	$\delta^{18}O_{seawater}$ (‰, VSMOW)	$\delta^{13}C_{otolith}$ (‰, VPDB)	$\delta^{13}C_{DIC}$ (‰, VPDB)	$\delta^{18}O_{otolith}$ minus $\delta^{18}O_{seawater}$ (‰, VPDB)	$\delta^{13}C_{otolith}$ minus $\delta^{13}C_{DIC}$ (‰, VPDB)
9	**11**	Inner	−0.25 ± 0.46	−0.56 ± 0.17	−8.64 ± 0.46	−3.86 ± 1.81	0.32 ± 0.46	−4.78 ± 0.46
		Middle	0.57 ± 0.46	−0.67 ± 0.01	−8.18 ± 0.55	−3.70 ± 0.30	1.24 ± 0.46	−4.49 ± 0.55
		Edge	0.22 ± 0.54	−0.70 ± 0.31	−8.60 ± 0.56	−4.77 ± 0.56	0.92 ± 0.54	−3.82 ± 0.56
12	**8**	Inner	−0.04 ± 0.48	−0.52 ± 0.17	−8.69 ± 0.40	−3.96 ± 1.58	0.47 ± 0.47	−4.72 ± 0.40
		Middle	0.48 ± 0.20	−0.71 ± 0.08	−8.42 ± 0.29	−4.40 ± 0.38	1.19 ± 0.20	−4.02 ± 0.29
		Edge	0.47 ± 0.10	−0.68 ± 0.17	−8.42 ± 0.28	−4.55 ± 0.88	1.15 ± 0.09	−3.87 ± 0.28
15	**9**	Inner	0.03 ± 0.22	−0.24 ± 0.08	−8.63 ± 0.27	−3.97 ± 1.94	0.27 ± 0.22	−4.66 ± 0.27
		Middle	0.17 ± 0.13	−0.33 ± 0.11	−8.59 ± 0.20	−5.28 ± 0.82	0.50 ± 0.13	−3.31 ± 0.20
		Edge	0.38 ± 0.12	−0.34 ± 0.06	−8.69 ± 0.19	−5.10 ± 0.33	0.72 ± 0.12	−3.59 ± 0.19
18	**8**	Inner	−0.91 ± 0.30	−0.33 ± 0.06	−9.45 ± 0.35	−4.19 ± 2.09	−0.58 ± 0.30	−5.26 ± 0.35
		Middle	−0.51 ± 0.18	−0.28 ± 0.05	−9.29 ± 0.20	−4.80 ± 0.33	−0.23 ± 0.18	−4.49 ± 0.20
		Edge	−0.43 ± 0.28	−0.31 ± 0.13	−9.19 ± 0.45	−4.17 ± 0.79	−0.12 ± 0.28	−5.02 ± 0.45
20	**6**	Inner	−0.87 ± 0.07	−0.08 ± 0.04	−9.77 ± 0.25	−4.63 ± 2.07	−0.79 ± 0.07	−5.14 ± 0.25
		Middle	−0.87 ± 0.14	−0.08 ± 0.05	−9.54 ± 0.23	−5.17 ± 0.59	−0.79 ± 0.14	−4.37 ± 0.23
		Edge	−0.79 ± 0.09	−0.28 ± 0.15	−9.22 ± 0.29	−4.89 ± 0.36	−0.50 ± 0.09	−4.34 ± 0.29

All the parameters are expressed as means ± SD.

above, the $\delta^{18}O_{seawater}$ mean value during the edge otolith portion deposited in the 9°C group fluctuated with a large standard deviation, which may impact the accuracy of the calculation. Therefore, the fractionation values of the edge portions were treated separately for the equation determination. Detailed $\delta^{18}O_{seawater}$ and $\delta^{13}C_{DIC}$ values can be found in Table S2.

The oxygen isotope fractionation between otolith and rearing seawater was expressed as approximately $\delta^{18}O_{otolith,\ VPDB} - \delta^{18}O_{seawater,\ VSMOW}$ (‰), or as $10^3 \ln \alpha$ converted by

$$\alpha = \frac{1000 + \delta^{18}O_{otolith,\ VPDB}}{1000 + \delta^{18}O_{seawater,\ VSMOW}}$$

The conversion of $\delta^{18}O_{seawater}$ from V-SMOW to V-PDB according to Coplen et al. (1983) was

$$\delta^{18}O(V\text{−}SMOW) = 1.03091 \times \delta^{18}O(V - PDB) + 30.91 \quad \text{(Equation 2)}$$

The oxygen isotope fractionation was calculated based on the $\delta^{18}O_{otolith}$ values of middle otolith portions in the 9°C group and both the middle and edge portions in the 12, 15, 18, and 20°C groups, and the mean $\delta^{18}O_{seawater}$ values during the period in which the otolith portions precipitated (Figure 7). The relationship between oxygen isotope fractionation of otoliths and water temperature was fitted with the linear regression model, resulting in a slope of −0.186 ± 0.010 and an intercept of 3.219 ± 0.155 (Pearson's r = −0.846, r^2 = 0.713). Although the slope did not differ (ANCOVA, $p < 0.01$), the intercept was significantly different from that of the synthetic aragonite determined by Kim et al. (2007) (ANCOVA, $p > 0.05$). However, within the temperature scale of this study (1000/T (K) = 3.41–3.544), the difference in the reflected $10^3 \ln\alpha$ value calculated by these two equations was not more than 0.292.

Overall, the relationship between oxygen isotope fractionation and water temperature at the 9–20°C scale for the middle otoliths portion of juvenile chum salmon *Oncorhynchus keta*, can be described as a linear regression equation:

$$\delta^{18}O_{otolith,VPDB} - \delta^{18}O_{seawater,VSMOW} = -0.186\ (\pm 0.010) \times T\ (°C) + 3.219\ (\pm 0.155)\ (n = 72)\ (\text{Pearson's } r = -0.910,\ r^2 = 0.827, p < 0.001) \quad \text{(Equation 3)}$$

or expressed as a fractionation factor:

$$10^3 \ln \alpha = 15.314\ (\pm 0.850) \times 10^3\ T^{-1}(K) - 22.2788\ (\pm 2.952)(n = 72)\ (\text{Pearson's } r = -0.907,\ r^2 = 0.823, p < 0.001) \quad \text{(Equation 4)}$$

Based on the $\delta^{18}O_{otolith}$ values including middle and edge otolith portions but only from the 12, 15, 18, and 20°C groups, the fractionation equation was also calculated as

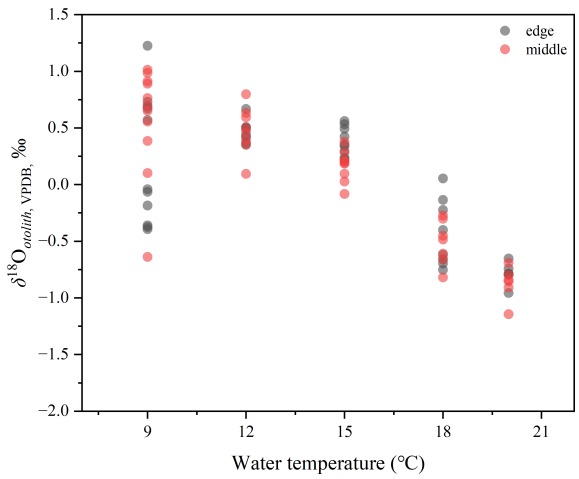

FIGURE 5
Distribution of middle and edge portions of five temperature groups. Solid circle represents one isotope value of otolith powder sample.

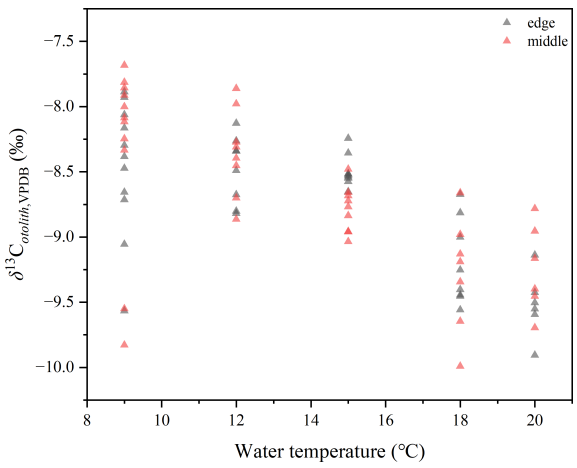

FIGURE 6
Distribution of $\delta^{13}C_{otolith}$ values of middle and edge portions of five temperature groups. Each isotopic value of otolith powder sample is represented by a triangle.

$$\delta^{18}O_{otolith,\ VPDB} - \delta^{18}O_{seawater,\ VSMOW} = -0.246\ (\pm 0.011) \times T\ (°C) + 4.165\ (\pm 0.172)\ (n = 61)\ (Pearson's\ r = -0.975,\ r^2 = 0.950, p < 0.001) \quad \text{(Equation 5)}$$

or

$$10^3 \ln \alpha = 19.211\ (\pm 0.733) \times 10^3\ T^{-1}(K) - 35.703\ (\pm 2.538)(n = 61)\ (Pearson's\ r = -0.960,\ r^2 = 0.921, p < 0.001) \quad \text{(Equation 6)}$$

There were no significant differences between these two equations.

3.4 Relationship between carbon and oxygen fractionation

To determine the involvement of kinetic and metabolic fractionation, the fractionation of oxygen and carbon calculated by middle and edge otolith portions for each group was bi-plotted, as shown in Figure 8. No correlation was found in 15, 18 and 20°C group ($r^2 < 0.06$), while weak correlation was found in 9 and 12°C group (r^2 = 0.25 and 0.43). And the fractionation values variated in a wide range among the 5 groups.

The analytical result between the partial correlation of oxygen isotope fractionation and carbon isotopes ($t_{xy,z}$ = −25.600) indicated that the carbon isotopes in the otoliths were not strongly controlled by temperature. However, the depleted values of $\delta^{13}C$ in the edge otolith portions of the 9°C group showed co-variation with $\delta^{18}O$, indicating that the carbon isotopes could be used as indicators of the appearance of outliers.

4 Discussion

In this study, to evaluate the accuracy of the relationship between otolith oxygen isotope fractionation and water temperature using a rearing method, three parameters potentially responsible were considered: operation error during otolith sample extraction, invasion into freshwater deposition period for inner extraction portions, and correlation with the carbon isotopes. The mix of otolith proportions deposited during the freshwater period was responsible for the depleted $\delta^{18}O_{otolith}$ values in the inner otolith portions. In contrast to the period during which middle otolith portions were deposited, the $\delta^{18}O_{seawater}$results indicated that the edge otolith portions were deposited under a relatively unstable rearing environment; thus, the middle otolith $\delta^{18}O_{otolith}$ values showed a strong correlation with temperature within a narrow $\delta^{18}O$ range, except for the data from the 9°C group.

There were no significant differences between the temperature-dependent oxygen isotope fractionation equations calculated from the middle and edge otolith $\delta^{18}O_{otolith}$ values of the 9–20°C groups (Equation 3, 4) and 12–20°C groups (Equation 5, 6). The calculated slopes were not significantly different from those of the synthetic aragonite determined by Kim et al. (2007), and there was a low deviation in the intercepts. The difference between middle and edge otolith fractionation values was not significant in the 9°C group, and the general

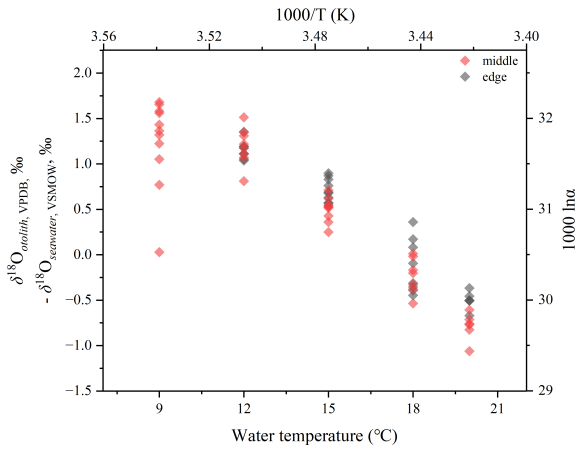

FIGURE 7
Plot of otolith oxygen isotope fractionation values versus water temperature. Open diamonds represent the fractionation values, expressed in both δ-T and lnα-Kelvin T scales.

variation range within the group (1.652‰) was below or near the index of other fish species (Godiksen et al., 2010; Kitagawa et al., 2013; Sakamoto et al., 2017). Overall, the fractionation equation for chum salmon was identified based on the $\delta^{18}O_{otolith}$ values of the 9–20°C groups. The regression line of chum salmon and inorganic aragonite intersects at the temperature of 16.7°C. At temperature range of 16.7–20°C, for the same isotope fractionation value, the difference of deduced temperatures by these two equations would differ not more than 0.5°C. Similarly, at temperature range of 9–16.7°C, the deduced temperatures differs within 1°C. The calculated slope was lower than that of Atlantic cod *Gadus morhua* (18.70 and 16.75, Radtke et al., 1996; Høie et al., 2004b) and Atlantic croaker *Micropogonias undulatus* (18.56, Thorrold et al., 1997), and considerably lower than that of bluefin tuna *Thunnus orientalis* (24.28, Kitagawa et al., 2013) (Figure 9). The difference in slopes between the other salmonoids species Arctic char *Salvelinus alpinus* (20.43, Godiksen et al., 2010) indicated the importance to determine the otolith oxygen isotope fractionation equation species-specifically.

For $\delta^{18}O_{seawater}$ in the 9 and 12°C groups in this study, the values were significantly lower than the other three groups, which is considered to be attributed to the effect of condensation. Although 10% of the volume of the rearing seawater was exchanged every day, set seawater temperatures that were considerably lower than the set room temperature (23°C), were susceptible to condensation (the 9 and 12°C groups). In addition, the bigger tanks (150L) with larger water surface had a higher risk of exposure to condensation, facilitating the mix of condensation from the room atmosphere with low $\delta^{18}O$ values. And cooler temperature of 9°C was considered to be influenced by heavier condensation than 12°C group. Therefore, otolith isotopic composition is susceptible to produce lower and unstable values resulting in an underestimation of the isotopic fractionation for these two groups. However, though the potential fluctuation of $\delta^{18}O_{seawater}$ could be determined (Figure 3), the depletion of $\delta^{18}O_{otolith}$ values for edge otolith portions in 9°C group (Figure 5) may be contributed by the occasional condensation with lower $\delta^{18}O_{seawater}$ values, which was not captured by weekly seawater sampling.

Extremely low isotope fractionation values in some individuals from the 9°C group were observed. Given that the condensation

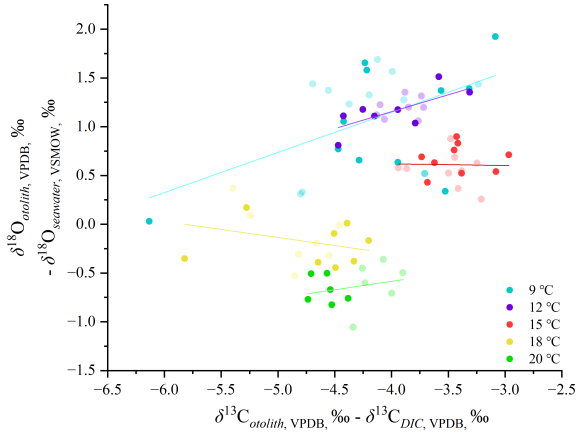

FIGURE 8
Plot of otolith isotope fractionation of $\delta^{18}O$ and $\delta^{13}C$ versus seawater and DIC of five temperature groups, respectively. Shallow spots represent the middle otolith portions.

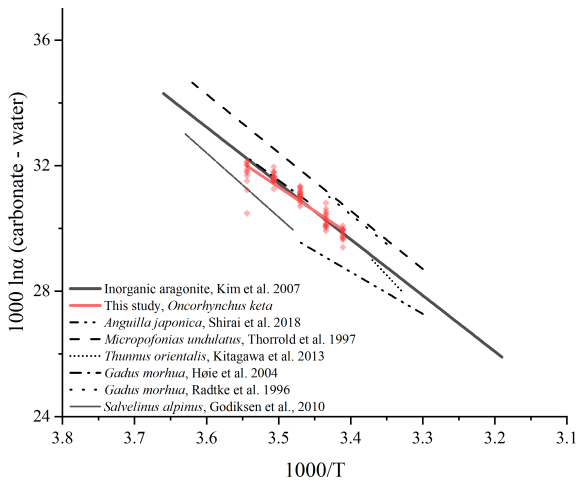

FIGURE 9
Comparison of temperature-dependent oxygen stable isotope fractionation equation calculated in this study with the published equations for several fish otoliths and inorganic aragonite. The length of each regression line represents the range of applicable temperature.

likely affects all individuals in the same tank, in the same manner, the variability at an individual level should be attributed to other controlling factors. The microscopic observation indicated that there were no irregular morphological characteristics, for example, the prevalence of vaterite on the otolith, discolorations, or wrinkled structures (Figure S2). It should be noted that a weak correlation between the oxygen and carbon fractionation was observed for the 9°C group (see Figure 8), with a wide fluctuation of the oxygen isotopes. In biogenetic carbonates, isotopic disequilibrium is mainly attributed to metabolic and kinetic isotope effects (McConnaughey, 1989a; Cohen and McConnaughey, 2003; Daëron et al., 2019; Prada et al., 2019; Huyghe et al., 2020), and it is difficult to discriminate between them. Kinetic effects are more significant, resulting in the depletion of heavier ^{13}C and ^{18}O simultaneously, rather than the incorporation of metabolic CO_2 alone. The lower $\delta^{18}O$ data in the 9°C group was largely associated with lower $\delta^{13}C$ values, of which pattern is similar to the typical fractionation pattern of kinetic isotope fractionation (Kalish, 1991b; McConnaughey, 1989b), namely a positive correlation between $\delta^{18}O$ and $\delta^{13}C$ (Figure S3). Regardless of the fractionation mechanism, the simultaneous depletion remained in both oxygen and carbon isotope fractionation in lower temperature settings indicated that incorporating carbon and oxygen compounds originated from other alternative sources that were isotopically different from seawater, e.g. metabolically derived carbon (Kalish, 1991a; Chung et al., 2019). Unfortunately, the data obtained in this study was not enough to identify the ultimate mechanism of isotopic heterogeneity between individuals from the same tank.

It is reported that when ambient water was colder than preferred temperatures, endothermic fish species may conserve heat by thermal inertia to maintain their body and brain temperatures above the ambient temperature (Carey et al., 1984), e.g. Pacific bluefin tuna (Kitagawa et al., 2001; Kitagawa et al., 2006; Kitagawa et al., 2022). Then, the $\delta^{18}O_{otolith}$ may therefore reflect the temperature of brain rather than the ambient water (Radtke et al., 1996). Whereas chum salmon is an ectothermic fish species, of which the somatic temperatures vary with ambient temperatures, and the thermoregulation for wild individuals depends on behavioral locomotion but physiological processes (Tanaka et al., 2000; Azumaya and Ishida, 2005). Furthermore, 9 and 12°C treatments in this study were located within the preferred temperature scale of chum salmon (7–14.8°C, Hicks, 2000; Nagata et al., 2007). Hence, the $\delta^{18}O_{otolith}$ values of chum salmon reflect temperatures of ambient water, and physiological thermoregulation processes were not susceptible for depleting the $\delta^{18}O_{otolith}$ in the cold water treatments in this study. To discriminate the relevant mechanisms, further studies under chemical scopes are needed, as for physiological scopes, the preferred temperatures are expected to be context-dependent (Clark et al., 2013; Norin et al., 2014).

Irrespective of the vital effects might be evolved, by discriminating the factors in spite of temperature that affect the isotope precipitation on otolith, the determined equation in this study was applicable for thermal history reconstruction on chum salmon.

5 Conclusion

The temperature dependency of otolith oxygen isotope fractionation in chum salmon was assessed based on a temperature gradient rearing experiment. The isotopic analysis results of the three equivalent otolith samples and rearing seawater suggested that the inner otolith portions were mixed with proportions deposited during the freshwater life stages; the edge otolith portions were deposited from an isotopically unstable environment and middle otolith portions were deposited from relatively stable seawater, thus providing more convincing data. The $\delta^{18}O_{otolith}$ values of middle otolith portions showed a strong correlation with temperature within a narrow value scale, except that the $\delta^{18}O_{otolith}$ values from 9°C group were distributed over a wide range. The otolith oxygen isotope fractionation equations based on the 9–20°C and 12–20°C groups were not statistically different from each other, and there was no significant difference with synthetic inorganic aragonite determined by Kim et al. (2007). The correlation between the oxygen and carbon isotope fractionation and the widely distributed $\delta^{18}O_{otolith}$ values in the 9°C group were speculated to be the effect of humid condensation (lower $\delta^{18}O_{seawater}$values) or the kinetic isotope effect (lower $\delta^{18}O_{otolith}$ values) alone or combined. The $\delta^{18}O_{otolith}$ values in the 9°C group had a relatively wide range compared with the other four groups, but the variation range was near or below the indexes in the studies on other species. Therefore, it was concluded that the chum salmon otoliths in this study were deposited under an isotopic quasi-equilibrium and the chum salmon species-specific otolith oxygen isotope fractionation equation could be used on reconstruction of temperature history.

Data availability statement

The original contributions presented in the study are included in the article/Supplementary Material. Further inquiries can be directed to the corresponding author.

Ethics statement

The animal study was reviewed and approved by the Animal Ethics Committee of the University of Tokyo, Japan.

Author contributions

Conceptualization: KS and TK. Rearing experiment: YG, YI, TN, and YS. Sample analysis: TH and KS. Writing (original

draft): YG. All the authors read article critically and gave approval for publication.

Funding

This work was supported by the Research Fund KAKENHI Grants from the Japan Society for the Promotion of Science (JSPS), Grant Number JP22H05026, JP22H05028 (KS), 20H00428, 22H05027 (TK), and JST SPRING JAPAN, Grant Number JPMJSP2018 (YG).

Acknowledgments

We owe thanks to the Iwate Fisheries Technology Center for providing the juvenile chum salmon and feed pellets. Special thanks to Noriko Izumoto (Atmosphere and Ocean Research Institute, The University of Tokyo) for her support with the IRMS measurements and initial statistical analysis.

Conflict of interest

The authors declare that the research was conducted in the absence of any commercial or financial relationships that could be construed as a potential conflict of interest.

Publisher's note

Supplementary material

The Supplementary Material for this article can be found online at: https://www.frontiersin.org/articles/10.3389/fmars.2022.1072068/full#supplementary-material

References

Abdul-Aziz, O. I., Mantua, N. J., and Myers, K. W. (2011). Potential climate change impacts on thermal habitats of pacific salmon (Oncorhynchus spp.) in the north pacific ocean and adjacent seas. *Can. J. Fisheries Aquat. Sci.* 68 (9), 1660–1680. doi: 10.1139/F2011-079

Azumaya, T., and Ishida, Y. (2005). Mechanism of body cavity temperature regulation of chum salmon (*Oncorhynchus keta*) during homing migration in the north pacific ocean. *Fisheries Oceanogr.* 14 (2), 81–96. doi: 10.1111/j.1365-2419.2004.00323.x

Beamish, R. J. (2017). What the past tells us about the future of pacific salmon research. *Fish Fisheries* 18 (6), 1161–1175. doi: 10.1111/faf.12231

Beamish, R. J., and Mahnken, C. (2001). A critical size and period hypothesis to explain natural regulation of salmon abundance and the linkage to climate and climate change. *Prog. Oceanogr.* 49 (1-4), 423–437. doi: 10.1016/S0079-6611(01)00034-9

Breitenbach, S. F., and Bernasconi, S. M. (2011). Carbon and oxygen isotope analysis of small carbonate samples (20 to 100 Âµg) with a GasBench II preparation device. *Rapid Commun. Mass Spectrometry* 25 (13), 1910–1914. doi: 10.1002/rcm.5052

Campana, S. E. (1999). Chemistry and composition of fish otoliths: pathways, mechanisms and applications. *Mar. Ecol. Prog. Ser.* 188, 263–297. doi: 10.3354/meps188263

Campana, S. E., and Thorrold, S. R. (2001). Otoliths, increments, and elements: keys to a comprehensive understanding of fish populations? *Can. J. Fisheries Aquat. Sci.* 58 (1), 30–38. doi: 10.1139/f00-177

Carey, F. G., Kanwisher, J. W., and Stevens, E. D. (1984). Bluefin tuna warm their viscera during digestion. *J. Exp. Biol.* 109 (1), 1–20. doi: 10.1242/jeb.109.1.1

Chung, M. T., Trueman, C. N., Godiksen, J. A., Holmstrup, M. E., and Grønkjær, P. (2019). Field metabolic rates of teleost fishes are recorded in otolith carbonate. *Commun. Biol.* 2 (1), 1–10. doi: 10.1038/s42003-018-0266-5

Clark, T. D., Sandblom, E., and Jutfelt, F. (2013). Aerobic scope measurements of fishes in an era of climate change: respirometry, relevance and recommendations. *J. Exp. Biol.* 216 (15), 2771–2782. doi: 10.1242/jeb.084251

Cohen, A. L., and McConnaughey, T. A. (2003). Geochemical perspectives on coral mineralization. *Rev. mineral. geochem.* 54 (1), 151–187. doi: 10.2113/0540151

Connors, B., Malick, M. J., Ruggerone, G. T., Rand, P., Adkison, M., Irvine, J. R., et al. (2020). Climate and competition influence sockeye salmon population dynamics across the northeast pacific ocean. *Can. J. Fisheries Aquat. Sci.* 77 (6), 943–949. doi: 10.1139/cjfas-2019-0422

Coplen, T. B., Kendall, C., and Hopple, J. (1983). Comparison of stable isotope reference samples. *Nature* 302 (5905), 236–238. doi: 10.1038/302236a0

Daëron, M., Drysdale, R. N., Peral, M., Huyghe, D., Blamart, D., Coplen, T. B., et al. (2019). Most earth-surface calcites precipitate out of isotopic equilibrium. *Nat. Commun.* 10 (1), 1–7. doi: 10.1038/s41467-019-08336-5

Darnaude, A. M., Sturrock, A., Trueman, C. N., Mouillot, D., Campana, S. E., and Hunter, E. (2014). Listening in on the past: what can otolith δ18O values really tell us about the environmental history of fishes? *PloS One* 9 (10), e108539. doi: 10.1371/journal.pone.0108539

Epstein, S., Buchsbaum, R., Lowenstam, H., and Urey, H. C. (1951). Carbonate-water isotopic temperature scale. *Geol. Soc. America Bull.* 62 (4), 417–426. doi: 10.1130/0016-7606(1951)62[417:CITS]2.0.CO;2

Fukuwaka, M., and Suzuki, T. (2002). Early sea mortality of mark-recaptured juvenile chum salmon in open coastal waters. *J. Fish Biol.* 60 (1), 3–12. doi: 10.1111/j.1095-8649.2002.tb02384.x

Godiksen, J. A., Svenning, M. A., Dempson, J. B., Marttila, M., Storm-Suke, A., and Power, M. (2010). Development of a species-specific fractionation equation for Arctic charr (*Salvelinus alpinus* (L.)): an experimental approach. *Hydrobiologia* 650 (1), 67–77. doi: 10.1007/s10750-009-0056-7

Grønkjær, P. (2016). Otoliths as individual indicators: a reappraisal of the link between fish physiology and otolith characteristics. *Mar. Freshw. Res.* 67 (7), 881–888. doi: 10.1071/MF15155

Høie, H., Andersson, C., Folkvord, A., and Karlsen, Ø. (2004a). Precision and accuracy of stable isotope signals in otoliths of pen-reared cod (*Gadus morhua*) when sampled with a high-resolution micromill. *Mar. Biol.* 144 (6), 1039–1049. doi: 10.1007/s00227-003-1275-5

Høie, H., Otterlei, E., and Folkvord, A. (2004b). Temperature-dependent fractionation of stable oxygen isotopes in otoliths of juvenile cod (*Gadus morhua* l.). *ICES J. Mar. Sci.* 61 (2), 243–251. doi: 10.1016/j.icesjms.2003.11.006

Hane, Y., Kimura, S., Yokoyama, Y., Miyairi, Y., Ushikubo, T., Ishimura, T., et al. (2020). Reconstruction of temperature experienced by pacific bluefin tuna *Thunnus orientalis* larvae using SIMS and microvolume CF-IRMS otolith oxygen isotope analyses. *Mar. Ecol. Prog. Ser.* 649, 175–188. doi: 10.3354/meps13451

Healey, M. (2011). The cumulative impacts of climate change on Fraser river sockeye salmon (*Oncorhynchus nerka*) and implications for management. *Can. J. Fisheries Aquat. Sci.* 68 (4), 718–737. doi: 10.1139/F2011-010

Hicks, M. (2000). "Evaluating standards for protecting aquatic life in washington's surface water quality standards," in *Draft discussion paper and literature summary. revised 2002*, vol. 1. (Olympia, WA: Washington State Department of Ecology), 97. Available at: https://apps.ecology.wa.gov/publications/documents/0010070.pdf.

Huyghe, D., Emmanuel, L., de Rafélis, M., Renard, M., Ropert, M., Labourdette, N., et al. (2020). Oxygen isotope disequilibrium in the juvenile portion of oyster shells biases seawater temperature reconstructions. *Estuarine Coast. Shelf Sci.* 240, 106777. doi: 10.1016/j.ecss.2020.106777

Iino, Y., Kitagawa, T., Abe, T. K., Nagasaka, T., Shimizu, Y., Ota, K., et al. (2022). Effect of food amount and temperature on growth rate and aerobic scope of juvenile chum salmon. *Fisheries Sci.* 88 (3), 397–409. doi: 10.1007/s12562-022-01599-w

Irie, T. (1990). Ecological studies on the migration of juvenile chum salmon, *Oncorhynchus keta*, during early ocean life. *Bull. Seikai Natl. Fish. Res. Inst.* 68, 1–142.

Irvine, J. R., and Fukuwaka, M. A. (2011). Pacific salmon abundance trends and climate change. *ICES J. Mar. Sci.* 68 (6), 1122–1130. doi: 10.1093/icesjms/fsq199

Irvine, J. R., Macdonald, R. W., Brown, R. J., Godbout, L., Reist, J. D., and Carmack, E. C. (2009). Salmon in the Arctic and how they avoid lethal low temperatures. *N. Pac. Anadr. Fish Commun. Bull.* 5, 39–50. doi: 10.1002/mcf2.10023

Iwata, M. (1995). Downstream migratory behavior of salmonids and its relationship with cortisol and thyroid hormones: a review. *Aquaculture* 135 (1-3), 131–139. doi: 10.1016/0044-8486(95)01000-9

Johnson, O. W., Grant, W. S., Kope, R. G., Neely, K. G., Waknitz, F. W., and Waples, R. S. (1997) *Status review of chum salmon from Washington, Oregon, and California*. Available at: https://repository.library.noaa.gov/view/noaa/3029.

Jones, J. B., and Campana, S. E. (2009).). stable oxygen isotope reconstruction of ambient temperature during the collapse of a cod (*Gadus morhua*) fishery. *Ecol. Appl.* 19 (6), 1500–1514. doi: 10.1890/07-2002.1

Kalish, J. M. (1991a). 13C and 18O isotopic disequilibria in fish otoliths: metabolic and kinetic effects. *Mar. Ecol. Prog. Ser.* 75 (2-3), 191–203. doi: 10.3354/meps075191

Kalish, J. M. (1991b). Oxygen and carbon stable isotopes in the otoliths of wild and laboratory-reared Australian salmon (*Arripis trutta*). *Mar. Biol.* 110 (1), 37–47. doi: 10.1007/BF01313090

Kasugai, K., Torao, M., Nagata, M., and Irvine, J. R. (2013). The relationship between migration speed and release date for chum salmon *Oncorhynchus keta* fry exiting a 110-km northern Japanese river. *Fisheries Sci.* 79 (4), 569–577. doi: 10.1007/s12562-013-0615-8

Kim, S. T., and O'Neil, J. R. (1997). Equilibrium and nonequilibrium oxygen isotope effects in synthetic carbonates. *Geochim. cosmochim. Acta* 61 (16), 3461–3475. doi: 10.1016/S0016-7037(97)00169-5

Kim, S. T., O'Neil, J. R., Hillaire-Marcel, C., and Mucci, A. (2007). Oxygen isotope fractionation between synthetic aragonite and water: Influence of temperature and Mg2+ concentration. *Geochim. Cosmochim. Acta* 71 (19), 4704–4715. doi: 10.1016/j.gca.2007.04.019

Kitagawa, T., Abe, T. K., Kubo, K., Fujioka, K., Fukuda, H., and Tanaka, Y. (2022). Rapid endothermal development of juvenile pacific bluefin tuna. *Front. Physiol.* 13, 968468. doi: 10.3389/fphys.2022.968468

Kitagawa, T., Ishimura, T., Uozato, R., Shirai, K., Amano, Y., Shinoda, A., et al. (2013). Otolith δ18O of pacific bluefin tuna *Thunnus orientalis* as an indicator of ambient water temperature. *Mar. Ecol. Prog. Ser.* 481, 199–209. doi: 10.3354/meps10202

Kitagawa, T., Kimura, S., Nakata, H., and Yamada, H. (2004). Diving behavior of immature, feeding pacific bluefin tuna (*Thunnus thynnus orientalis*) in relation to season and area: the East China Sea and the kuroshio–oyashio transition region. *Fisheries Oceanogr.* 13 (3), 161–180. doi: 10.1111/j.1365-2419.2004.00282.x

Kitagawa, T., Kimura, S., Nakata, H., and Yamada, H. (2006). Thermal adaptation of pacific bluefin tuna *Thunnus orientalis* to temperate waters. *Fisheries Sci.* 72 (1), 149–156. doi: 10.1111/j.1444-2906.2006.01129.x

Kitagawa, T., Kimura, S., Nakata, H., Yamada, H., Nitta, A., Sasai, Y., et al. (2009). Immature pacific bluefin tuna, *Thunnus orientalis*, utilizes cold waters in the subarctic frontal zone for trans-pacific migration. *Environ. Biol. fishes* 84 (2), 193–196. doi: 10.1007/s10641-008-9409-8

Kitagawa, T., Nakata, H., Kimura, S., Itoh, T., Tsuji, S., and Nitta, A. (2000). Effect of ambient temperature on the vertical distribution and movement of pacific bluefin tuna *Thunnus thynnus orientalis*. *Mar. Ecol. Prog. Ser.* 206, 251–260. doi: 10.3354/meps206251

Kitagawa, T., Nakata, H., Kimura, S., and Tsuji, S. (2001). Thermoconservation mechanisms inferred from peritoneal cavity temperature in free-swimming pacific bluefin tuna *Thunnus thynnus orientalis*. *Mar. Ecol. Prog. Ser.* 220, 253–263. doi: 10.3354/meps220253

LeGrande, A. N., and Schmidt, G. A. (2006). Global gridded data set of the oxygen isotopic composition in seawater. *Geophys. Res. Lett.* 33 (12). doi: 10.1029/2006GL026011

McConnaughey, T. (1989a). 13C and 18O isotopic disequilibrium in biological carbonates: I. patterns. *Geochim. Cosmochim. Acta* 53 (1), 151–162. doi: 10.1016/0016-7037(89)90282-2

McConnaughey, T. (1989b). 13C and 18O isotopic disequilibrium in biological carbonates: II. *In vitro* simulation of kinetic isotope effects. *Geochim. Cosmochim. Acta* 53 (1), 163–171. doi: 10.1016/0016-7037(89)90283-4

Nagata, M., Miyakoshi, Y., Ando, D., Fujiwara, M., Sawada, M., Shimada, H., et al. (2007). Influence of coastal seawater temperature on the distribution and growth of juvenile chum salmon, with recommendations for altered release strategies. *N. Pac. Anadr. Fish Commun. Bull.* 4, 223–235.

Nobata, S., Kitagawa, T., Tanaka, K., Komatsu, K., Aoki, Y., Sato, K., et al. (2019). Spreading of river water guides migratory behavior of homing chum salmon *Oncorhynchus keta* in otsuchi bay, a narrow inlet with multiple river flows. *Zool. Sci.* 36 (6), 449–457. doi: 10.2108/zs190026

Norin, T., Malte, H., and Clark, T. D. (2014). Aerobic scope does not predict the performance of a tropical eurythermal fish at elevated temperatures. *J. Exp. Biol.* 217 (2), 244–251. doi: 10.1242/jeb.089755

Oppo, D. W., Schmidt, G. A., and LeGrande, A. N. (2007). Seawater isotope constraints on tropical hydrology during the Holocene. *Geophys. Res. Lett.* 34 (13). doi: 10.1029/2007GL030017

Patterson, W. P. (1999). Oldest isotopically characterized fish otoliths provide insight to Jurassic continental climate of Europe. *Geology* 27 (3), 199–202. doi: 10.1130/0091-7613(1999)027<0199:OICFOP>2.3.CO;2

Patterson, W. P., Smith, G. R., and Lohmann, K. C. (1993). Continental paleothermometry and seasonality using the isotopic composition of aragonitic otoliths of freshwater fishes. *Washington DC Am. Geophys. Union Geophys. Monograph Ser.* 78, 191–202. doi: 10.1029/GM078p0191

Perry, R. I., Hargreaves, N. B., Waddell, B. J., and Mackas, D. L. (1996). Spatial variations in feeding and condition of juvenile pink and chum salmon off Vancouver island, British Columbia. *Fisheries Oceanogr.* 5 (2), 73–88. doi: 10.1111/j.1365-2419.1996.tb00107.x

Prada, F., Yam, R., Levy, O., Caroselli, E., Falini, G., Dubinsky, Z., et al. (2019). Kinetic and metabolic isotope effects in zooxanthellate and non-zooxanthellate Mediterranean corals along a wide latitudinal gradient. *Front. Mar. Sci.* 6. doi: 10.3389/fmars.2019.00522

Radtke, R. L., Lenz, P., Showers, W., and Moksness, E. (1996). Environmental information stored in otoliths: insights from stable isotopes. *Mar. Biol.* 127 (1), 161–170. doi: 10.1007/BF00993656

Ruggerone, G. T., and Irvine, J. R. (2018). Numbers and biomass of natural-and hatchery-origin pink salmon, chum salmon, and sockeye salmon in the north pacific ocean 1925–2015. *Mar. Coast. Fisheries* 10 (2), 152–168. doi: 10.1002/mcf2.10023152

Ruggerone, G. T., and Nielsen, J. L. (2004). Evidence for competitive dominance of pink salmon (*Oncorhynchus gorbuscha*) over other salmonids in the north pacific ocean. *Rev. Fish Biol. Fisheries* 14 (3), 371–390. doi: 10.1007/s11160-004-6927-0

Saito, T., Kaga, T., Seki, J., and Otake, T. (2007). Otolith microstructure of chum salmon *Oncorhynchus keta*: formation of sea entry check and daily deposition of otolith increments in seawater conditions. *Fisheries Sci.* 73 (1), 27–37. doi: 10.1111/j.1444-2906.2007.01298.x

Sakamoto, T., Komatsu, K., Shirai, K., Higuchi, T., Ishimura, T., Setou, T., et al. (2019). Combining microvolume isotope analysis and numerical simulation to reproduce fish migration history. *Methods Ecol. Evol.* 10 (1), 59–69. doi: 10.1111/2041-210X.13098

Sakamoto, T., Komatsu, K., Yoneda, M., Ishimura, T., Higuchi, T., Shirai, K., et al. (2017). Temperature dependence of δ18O in otolith of juvenile Japanese sardine: Laboratory rearing experiment with micro-scale analysis. *Fisheries Res.* 194, 55–59. doi: 10.1016/j.fishres.2017.05.004

Salo, E. O. (1991). "Life history of chum salmon (Oncorhynchus keta)," in *Pacific salmon life histories*. (Vancouver: UBC press) G. Groot and L. Margolis (eds.) p. 231–310. Available at: http://jeffersonco-treis.info/PDF%20Files/3.04%20Water%20References/Healey,%20M.C.%201991%20Life%20History%20of%20Chinook%20Salmon.pdf.

Sanger, D. (1962). *The archaeology of EeQw: 1: a burial site near chase, British Columbia*. (Vancouver: University of British Columbia Library). doi: 10.14288/1.0105730

Sanger, G. A. (1972). "Fishery potentials and estimated biological productivity of the subarctic pacific region," in *Biological oceanography of the northern pacific ocean*. (Tokyo: Idemitsu Shoten: A.Y. Takenouti (ed)) 561–574. Available at: https://cir.nii.ac.jp/crid/1570291225693426432.

Schoen, E. R., Wipfli, M. S., Trammell, E. J., Rinella, D. J., Floyd, A. L., Grunblatt, J., et al. (2017). Future of pacific salmon in the face of environmental change: Lessons from one of the world's remaining productive salmon regions. *Fisheries* 42 (10), 538–553. doi: 10.1080/03632415.2017.1374251

Seki, J. (1978). An ecological study on the chum salmon juveniles in kesennuma–i. prey animals and growth of juvenile chum salmon in the estuarine waters. *Sci. Rep. Kesennuma Fisheries Exp. Station* 4, 10–18.

Shirai, K., Koyama, F., Murakami-Sugihara, N., Nanjo, K., Higuchi, T., Kohno, H., et al. (2018a). Reconstruction of the salinity history associated with movements of mangrove fishes using otolith oxygen isotopic analysis. *Mar. Ecol. Prog. Ser.* 593, 127–139. doi: 10.3354/meps12514

Shirai, K., Otake, T., Amano, Y., Kuroki, M., Ushikubo, T., Kita, N. T., et al. (2018b). Temperature and depth distribution of Japanese eel eggs estimated using otolith oxygen stable isotopes. *Geochim. Cosmochim. Acta* 236, 373–383. doi: 10.1016/j.gca.2018.03.006

Shubin, A. O., and Akinicheva, E. G. (2016). Origin of juvenile chum salmon *Oncorhynchus keta* (Salmonidae) in the Sea of Okhotsk coastal waters off south Sakhalin. *J. ichthyol.* 56 (5), 728–737. doi: 10.1134/S0032945216050131

Solomon, C. T., Weber, P. K., Ingram, B. L., Conrad, M. E., Machavaram, M. V., Franklin, R. L., et al. (2006). Experimental determination of the sources of otolith carbon and associated isotopic fractionation. *Can. J. Fisheries Aquat. Sci.* 63 (1), 79–89. doi: 10.1139/f05-20

Tanaka, H., Takagi, Y., and Naito, Y. (2000). Behavioural thermoregulation of chum salmon during homing migration in coastal waters. *J. Exp. Biol.* 203 (12), 1825–1833. doi: 10.1242/jeb.203.12.1825

Tanner, S. E., Reis-Santos, P., Vasconcelos, R. P., Fonseca, V. F., França, S., Cabral, H. N., et al. (2013). Does otolith geochemistry record ambient environmental conditions in a temperate tidal estuary? *J. Exp. Mar. Biol. Ecol.* 441, 7–15. doi: 10.1016/j.jembe.2013.01.009

Thorrold, S. R., Campana, S. E., Jones, C. M., and Swart, P. K. (1997). Factors determining δ13C and δ18O fractionation in aragonitic otoliths of marine fish. *Geochim. Cosmochim. Acta* 61 (14), 2909–2919. doi: 10.1016/S0016-7037(97)00141-5

Urawa, S., Beacham, T. D., Fukuwaka, M. A., and Kaeriyama, M. (2018). "Ocean ecology of chum salmon," in *The ocean ecology of pacific salmon and trout* (Bethesda: American Fisheries Society), 161–318. Available at: https://www.researchgate.net/publication/326381529.

Urawa, S., Seki, J., Kawana, M., Saito, T., Crane, P. A., Seeb, L., et al. (2004). Juvenile chum salmon in the Okhotsk Sea: their origins estimated by genetic and otolith marks. *N. Pac. Anadr. Fish Commun. Tech. Rep.* 5, 87–88.

Urey, H. C. (1947). The thermodynamic properties of isotopic substances. *J. Chem. Soc. (Resumed)*, 562–581. doi: 10.1039/JR9470000562

von Leesen, G., Bardarson, H., Halldorsson, S. A., Whitehouse, M. J., and Campana, S. E. (2021). Accuracy of otolith oxygen isotope records analyzed by SIMS as an index of temperature exposure of wild icelandic cod (*Gadus morhua*). *Front. Mar. Sci.* 8, 698908. doi: 10.3389/fmars.2021.698908

Wakefield, C. B., Boddington, D. K., and Newman, S. J. (2016). Rapid lateral extraction of otoliths that maintains the integrity of fish product to improve access to catches and reduce potential sampling biases. *Open Fish Sci. J.* 9 (1), 26–28. doi: 10.2174/1874401X01609010026

Walther, B. D., and Thorrold, S. R. (2009). Inter-annual variability in isotope and elemental ratios recorded in otoliths of an anadromous fish. *J. Geochem. Explor.* 102 (3), 181–186. doi: 10.1016/j.gexplo.2008.10.001

West, C. F., Wischniowski, S., and Johnston, C. (2012). Pacific cod (*Gadus macrocephalus*) as a paleothermometer: otolith oxygen isotope reconstruction. *J. Archaeol. Sci.* 39 (10), 3277–3283. doi: 10.1016/j.jas.2012.05.009

Willmes, M., Lewis, L. S., Davis, B. E., Loiselle, L., James, H. F., Denny, C., et al. (2019). Calibrating temperature reconstructions from fish otolith oxygen isotope analysis for california's critically endangered delta smelt. *Rapid Commun. Mass Spectrometry* 33 (14), 1207–1220. doi: 10.1002/rcm.8464

Zhao, L., Zuykov, M., Tanaka, K., Shirai, K., Anderson, J., McKindsey, C. W., et al. (2019). New insight into light-enhanced calcification in mytilid mussels, mytilus sp., infected with photosynthetic algae coccomyxa sp.: δ13C value and metabolic carbon record in shells. *J. Exp. Mar. Biol. Ecol.* 520, 151211. doi: 10.1016/j.jembe.2019.151211

frontiers | Frontiers in Marine Science

TYPE Original Research
PUBLISHED 01 March 2023
DOI 10.3389/fmars.2023.1048869

OPEN ACCESS

EDITED BY
Chisato Yoshikawa,
Japan Agency for Marine-Earth Science and Technology (JAMSTEC), Japan

REVIEWED BY
Heloise Pavanato,
Cawthron Institute, New Zealand
Russell Leaper,
International Fund for Animal Welfare, United States

*CORRESPONDENCE
Angus Fleetwood Henderson
angus.henderson@utas.edu.au

SPECIALTY SECTION
This article was submitted to Marine Biology, a section of the journal Frontiers in Marine Science

RECEIVED 20 September 2022
ACCEPTED 01 February 2023
PUBLISHED 01 March 2023

CITATION
Henderson AF, Hindell MA, Wotherspoon S, Biuw M, Lea M-A, Kelly N and Lowther AD (2023) Assessing the viability of estimating baleen whale abundance from tourist vessels.
Front. Mar. Sci. 10:1048869.
doi: 10.3389/fmars.2023.1048869

Assessing the viability of estimating baleen whale abundance from tourist vessels

Angus Fleetwood Henderson[1,2]*, Mark Andrew Hindell[1], Simon Wotherspoon[3], Martin Biuw[4], Mary-Anne Lea[1,2], Nat Kelly[3] and Andrew Damon Lowther[1,5]

[1]Institute of Marine and Antarctic Studies, College of Science and Engineering, University of Tasmania, Hobart, TAS, Australia, [2]Centre for Marine Socioecology, University of Tasmania, Hobart, TAS, Australia, [3]Australian Antarctic Division, Hobart, TAS, Australia, [4]Norwegian Institute of Marine Research, Bergen, Norway, [5]Biodiversity Section, Norwegian Polar Institute, Tromø, Norway

Many populations of southern hemisphere baleen whales are recovering and are again becoming dominant consumers in the Southern Ocean. Key to understanding the present and future role of baleen whales in Southern Ocean ecosystems is determining their abundance on foraging grounds. Distance sampling is the standard method for estimating baleen whale abundance but requires specific logistic requirements which are rarely achieved in the remote Southern Ocean. We explore the potential use of tourist vessel-based sampling as a cost-effective solution for conducting distance sampling surveys for baleen whales in the Southern Ocean. We used a dataset of tourist vessel locations from the southwest Atlantic sector of the Southern Ocean and published knowledge from Southern Ocean sighting surveys to determine the number of tourist vessel voyages required for robust abundance estimates. Second, we simulated the abundance and distributions of four baleen whale species for the study area and sampled them with both standardized line transect surveys and non-standardized tourist vessel-based surveys, then compared modeled abundance and distributions from each survey to the original simulation. For the southwest Atlantic, we show that 12-22 tourist vessel voyages are likely required to estimate abundance for humpback and fin whales, with relative estimates for blue, sei, Antarctic minke, and southern right whales. Second, we show tourist vessel-based surveys outperformed standardized line transect surveys at reproducing simulated baleen whale abundances and distribution. These analyses suggest tourist vessel-based surveys are a viable method for estimating baleen whale abundance in remote regions. For the southwest Atlantic, the relatively cost-effective nature of tourist vessel-based survey and regularity of tourist vessel voyages could allow for annual and intra-annual estimates of abundance, a fundamental improvement on current methods, which may capture spatiotemporal trends in baleen whale movements on forging grounds. Comparative modeling of sampling methods provided insights into the behavior of general additive model-based abundance modeling, contributing to the development of detailed guidelines of best practices for these approaches.

Through successful engagement with tourist company partners, this method has the potential to characterize abundance across a variety of marine species and spaces globally, and deliver high-quality scientific outcomes relevant to management organizations.

KEYWORDS

Southern Ocean (Atlantic sector), distance sampling, density surface modeling (DSM), West Antarctic peninsula (WAP), CCAMLR, GAM (generalized additive model), Krill fishery, platforms of opportunity

Introduction

Baleen whales are an important consumer in polar regions, migrating from winter breeding grounds in low latitudes to high latitudes to acquire most of their annual energy budget (Horton et al., 2022). Most populations of baleen whales are recovering from industrialized whaling during the mid-part of the 20th century (Baker and Clapham, 2004; Leaper and Miller, 2011; Tulloch et al., 2019) and are again dominating polar food webs (Ratnarajah et al., 2014; Ratnarajah et al., 2016; Savoca et al., 2021). However, we have a limited understanding of current population trends for many baleen whale species, particularly those which do not winter and/or migrate coastally, e.g., blue (*Balaenoptera musculus*), fin (Balaenoptera physalus), Antarctic minke (*Balaenoptera bonaerensis*, *herein*, minke) and sei (*Balaenoptera borealis*) whales for the southern hemisphere, for which the Southern Ocean foraging grounds may represent a single geographic location where the entire population can be surveyed simultaneously.

This study focuses on the southwest Atlantic sector of the Southern Ocean which is a hotspot for human and biological activity in the Southern Ocean (Tin et al., 2009; Tin et al., 2014; Bender et al., 2016; Erbe et al., 2019; Palmowski, 2020). It is also one of the fastest-warming regions in the Southern Ocean experiencing significant changes to sea-ice conditions (Carrasco et al., 2021; Lin et al., 2021) and the focus of the majority of the current krill fishing effort (Kawaguchi and Nicol, 2020). The current trigger limit for the catch of Antarctic krill (*Euphausia superba*) is based on a precautionary fishery approach managed by the Convention for the Conservation of Marine and Antarctic Living Resources (CCAMLR), to avoid potentially negative effects on krill populations and krill-dependent predators. The status of the recovering baleen whale populations foraging in the southwest Atlantic sector is unclear (Erbe et al., 2019). This is despite baleen whales being potentially the greatest consumers of Antarctic krill in the Southern Ocean (Baines et al., 2021; Warwick-Evans et al., 2021) and that the competitive relationships between baleen whales and other krill predators are likely to be as influential on the demographic signals monitored for krill fishing management as climate change and krill fishing itself (Ainley et al., 2006; Trivelpiece et al., 2011; McMahon et al., 2019). Annual monitoring of baleen whale abundance on foraging grounds, from which to estimate aggregate krill consumption by krill predators, will enhance CCAMLR's Ecosystem-based Management (EBM) of the krill fishery.

While there is a need for surveys of baleen whale populations on Southern Ocean foraging grounds, ship-based surveys have been restricted spatially (e.g., Santora et al., 2014; Johannessen et al., 2022), temporally (e.g., Headly et al., 2001; Baines et al., 2021), or spatiotemporally (e.g., Herr et al., 2016; Herr et al., 2019; Bassoi et al., 2020). As illustrated by the 19-year gap between broad-scale surveys of the southwest Atlantic sector of the Southern Ocean by CCAMLR (Hedley et al., 2001; Baines et al., 2021) and the cessation of International Whaling Commission (IWC), IDCR/SOWER circumpolar surveys in the early 2000s (Branch and Butterworth, 2001a; Branch and Butterworth, 2001b). Determining ocean basin-scale abundance of baleen whales foraging in the Southern Ocean and inferring environmental, and/or prey-mediated drivers of baleen whale densities in both time and space has therefore proved elusive (El-Gabbas et al., 2020).

Increased collaborations between the tourist industry and scientific endeavors in recent years (e.g., the polar collective) have provided the opportunity to better estimate baleen whale abundance (Johannessen et al., 2022). Before the COVID-19 pandemic, Antarctic tourism was undergoing year-on-year growth (Lynch et al., 2010; Bender et al., 2016; Palmowski, 2020), a trend that after the pandemic-driven hiatus is expected to continue (IAATO Report, 2020). Antarctic tourist ships thus represent platforms of opportunity for repeated and ongoing surveys of baleen whales in the Southern Ocean, though several challenges exist.

Ship-based line transect distance sampling is the common method for surveying air-breathing predators at sea (Buckland et al., 2001; Thomas et al., 2010). For baleen whales, this method involves a vessel passing through a study area, typically along an *a priori*-designed survey track with trained observers logging animal sightings and recording their perpendicular distance to the transect line during defined periods of effort. Detection functions describe the relationship between the number of sightings and their perpendicular distance to the transect line, which generally decreases as the perpendicular distance from the transect line increases (Thomas et al., 2010). The ability to detect animals along a transect is influenced by several factors in addition to distance, such as sighting conditions, the height of the platform, whale species and behavior, and observer experience, and as such, covariates can be added to account for this variation, termed Multi-Covariate Distance Sampling (MCDS) (Marques and Buckland, 2003). Buckland et al. (2001) recommend 60 – 80 sightings per species to fit robust detection functions which are then used for subsequent density estimation. Recent tourist vessel-

based surveys of the Bransfield straight suggest minimum sighting requirements are achievable for humpback whales (*Megaptera novaeangliae*) (Johannessen et al., 2022). Whether this is the case for other species across a wider study area is unclear.

Generally, scientific surveys follow a strict set of survey design principles when considering the placement of proposed transects, that ensure even spatial coverage and allow for both design and model-based analysis (Strindberg and Buckland, 2004; Thomas et al., 2007; Williams and Thomas, 2009). However, in the case of tourist vessel-based surveys, transects are not randomly placed evenly across the study area, rather, track locations are dictated by factors such as tourist landing sites, wildlife hotspots, weather, anchorages, and other ship traffic (Bender et al., 2016). Model-based approaches, such as Generalized Additive Model (GAM) based density surface modeling (DSM), are reasonably robust to such non-randomly placed surveys for the purposes of estimating abundance or distributions (Hedley and Buckland, 2004; Miller et al., 2013). DSM is a two-stage approach, modeling the incomplete detection of animals on the transect, as described by the detection function/s, combined with segment level (portions of the transect) survey effort information (e.g., sightings conditions) and environmental covariates (e.g., sea surface temperature and water depth, or even space) using a GAM, or alternative methods (Miller et al., 2013). DSM are most likely to accurately represent the underlying animal distribution when transects sample the range of explanatory covariates used in the model (Hedley et al., 1999; Cañadas and Hammond, 2008; Williams et al., 2006) and are spatially spread reasonably evenly within the study area (Strindberg and Buckland, 2004; Thomas et al., 2007; Williams and Thomas, 2009). For tourist vessel-based surveys, it is unclear if the assumed bias in sampling will allow for good spatial coverage and/or adequate sampling of explanatory co-variates to achieve robust results.

Herein, we aim to determine whether tourist ship-based surveys can yield data to support reliable estimates of baleen whale abundance on foraging grounds in the southwest Atlantic sector of the Southern Ocean. We used a dataset of tourist vessel locations collected before the Covid-19 pandemic to respond to the following four aims. First, we aimed to determine the amount of survey effort that is achievable per tourist vessel voyage, and second, use these results to determine the number of tourist vessel voyages needed to return enough sightings to support fitting MCDS detection functions for each baleen whale species. Our third aim was to test the validity of sampling with tourist vessel-based surveys by comparatively sampling simulated whale fields with non-standardized tourist vessel-based surveys against a previously completed standardized line transect survey. Finally, we determined at which point increasing the number of additional voyages no longer returns significant improvements in the accuracy and precision of abundance estimates.

Methods

The study region

The study area (~1.4 million km^2) was a region of the southwest Atlantic sector of the Southern Ocean between (70˚W and 40˚W south of 55˚S), including the waters surrounding the west Antarctic Peninsula and South Shetland and South Orkney Islands. The region contains CCAMLR management regions, including the entirety of Subarea 48.1, the western third of Subarea 48.2, and the region north of Subarea 48.1 between 57˚S and 55˚S, and is exclusive of the Weddell Sea (Subarea 48.5), which is rarely traversed by any vessels due to the dense ice conditions (Figure 1).

Estimating the survey effort (km) per tourist vessel-based survey

Automatic identification system (AIS) locations from tourist vessel voyages within the study area from November to March during the 2019/20 austral summer were used to analyze the potential for tourist vessels to make baleen whale observations. This dataset was a subset of the total voyages that the fleet of tourist vessels completed in the western Antarctic Peninsula region in the 2019/20 austral summer season (29 of the 45 tourist vessels and 209 of the total 318 voyages). As vessels report AIS locations at different time frequencies (typically ≈ 500 times/day), the dataset was regularized to hourly locations. To include only locations with appropriate sighting conditions for whale survey, locations with low light conditions (zenith angle of greater than 85°) and average hourly speeds slower than 6 knots or faster than 16 knots were removed (Figure 1). There were two basic voyage plans; (i) voyages that transit from southern Patagonia *via* South Georgia (and sometimes the South Orkney Islands) before reaching the west Antarctic Peninsula (*Type A*), and (ii) those that transit directly to the west Antarctic Peninsula, occasionally *via* the Falkland Islands/Islas Malvinas (*Type B*). Most vessels complete a variety of voyage plans across a single season.

Additional potential survey effort is lost due to poor weather. The resultant survey effort achieved is termed, *realized survey effort* (*i.e.*, the survey design minus the sections of track missed due to weather, poor light, *etc.*). Here, we estimated *realized survey effort* by correcting the potential survey effort (our 'survey design') for expected weather conditions. We then multiplied the estimated *realized survey effort* by the expected baleen whale sighting rates for the region to estimate the expected number of sightings achieved per voyage.

To estimate the hours of survey effort potentially lost to poor weather we used weather data collected during IWC's IDCR/SOWER surveys (Branch and Butterworth, 2001b). This dataset was used as it contained a routine hourly collection of weather observations between 0600 and 2000 local time. The proportion of time deemed good weather during IWC's IDCR/SOWER survey was binned spatially (10˚ Longitude* 2.5˚ Latitude). Good weather was defined as when the sightability score (a measure of sighting conditions on a scale from 1 (poor) – 5 (excellent)) ranged from 3 to 5. Potential survey effort was split to a maximum of 25km lengths, (as is typical for surveys covering ocean basins) and binned spatially (10˚ Longitude* 2.5˚ Latitude). To simulate a dataset of *realized survey effort*, a random sample was drawn from this split potential survey effort of equivalent size to the proportion of good weather days in that spatial bin (Supplementary Material 1). This was used to estimate the number of kilometers of *realized survey effort* per voyage (Supplementary Material 2), creating a dataset of *realized survey effort* segments to sample the simulated whale fields (described below). Note for spatial bins where <10 IWC's IDCR/SOWER survey-derived hourly weather observations were recorded (colored dark grey in Supplementary Material 2), the mean proportion of good weather hours was used.

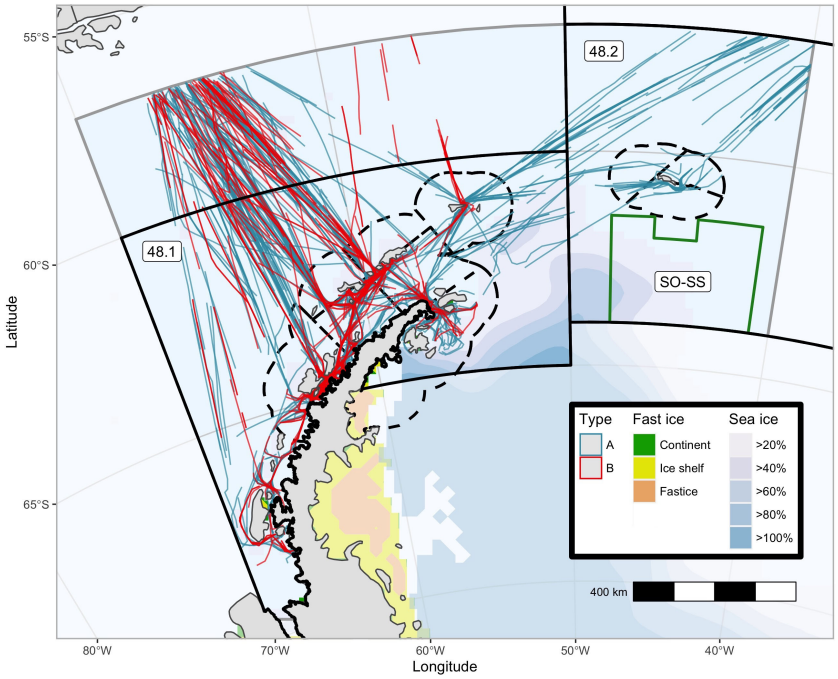

FIGURE 1
Potential survey effort from a portion of the tourist vessels that tour the southwest Atlantic Ocean (November-March). Modified tourist vessel tracks from 29 of the 45 vessels which toured the southwest Atlantic Ocean in the 2019/20 Antarctic summer tourist season. CCAMLR Management regions Subarea 48.1 and.2 (solid black lines), Small Scale Management Units (dash black lines), and the south Orkney Island Southern Shelf MPA (green line) are plotted. The two basic tourist vessel itineraries are plotted, type (A, B) Sea Ice (extracted from the National Snow and Ice Data Centre *via* R Package 'raadtools') and Fast Ice (Fraser et al., 2020) are as of March 2020.

Estimating the number of sightings per tourist vessel-based survey

Many Southern Ocean whale species are recovering (Leaper and Miller, 2011; Tulloch et al., 2019), and as such sighting rates of equivalent surveys will also be expected to change commensurately. We define a sighting as an observation of a group of whales from 1 to n individuals (moving together, less than 5 body lengths apart, and only separating temporarily), and a sighting rate as the average number of sightings per distance covered (in this case, per km). We divided the number of sightings of each species by the total distance surveyed for each study. To estimate sighting rates for future summer sampling seasons (i.e., 2022/23), a compound interest rate formula was applied:

$$Sighting\ \ rate = \left(\frac{Recent\ \ sighting\ \ rate}{Past\ \ sighting\ \ rate}\right) \hat{} \left(\left(\frac{1}{time\ \ period}\right) - 1\right)$$

to estimate the annual rate of change in sighting rates for the period between past (2000) and recent studies (2019) and project into the future (2022/23 season). Past sighting rates were taken from surveys in the year 2000 (The IWC SOWER/CCAMLR krill survey of the year 2000 (Hedley et al., 2001), *herein*, CCAMLR 2000) and in 2001/02 austral summer (tourist vessel-based survey (Williams, 2003; Williams et al., 2006)). Recent sighting rates were taken from surveys early in the year 2019 (a repeat of the CCAMLR 2000 Survey (Baines et al., 2021), *herein*, CCAMLR 2019) and the 2018/19 and 2021/22 tourist vessel-based surveys (Johannessen et al., 2022). The spatial range of these studies vary, but all covered the study area at least partially. Sighting rates were calculated separately for the six most common baleen whale species (humpback, fin, Antarctic minke, southern right, sei, and blue) and large unidentified baleen whales (unids). The time period between past and recent surveys was 19 years. The error was not propagated across these estimates due to inconsistent calculation and reporting across the four studies included.

It is reasonable to assume that only small observation teams will be accommodated on tourist vessels, so we assumed a team of two observers per vessel. To maintain consistent observer effort and manage fatigue for a team of this size, the field of observation was restricted to a single observer focused from 0 to 90° on one side of the vessel. The second observer would be required to log information on the observational effort, environmental conditions, and animal sightings. Alternative use of two observers was considered, but a 90° field of view was considered the best use of a small team of observers. This is because of the limited space allocated on the bridge, the distraction of bridge crew and radio interference due to the high volume of radio chatter between observers on both bridge wings, and occasional super high densities of whales potentially overwhelming observers (Herr et al., 2022). Scientific surveys generally have larger teams on dedicated platforms and can survey the full 180° in front of the vessel. To account for this difference in survey design, the final estimated sighting rates for the 2022/23 season were divided by two (where appropriate). Finally, this sighting rate was multiplied by our estimated *realized survey effort* per voyage to predict the number of sightings per voyage and therefore the voyages required to reach the 60-80 sightings per species for fitting detection functions (Buckland et al., 2001).

Creating simulated whale fields

To understand the extent to which the spatial distribution of the tourist vessel-based survey may bias subsequent model-based abundance estimates, we simulated four whale fields (rasters of whale densities with paired abundances) and sampled them with our dataset of *realized survey effort*. The four simulated whale fields were created to represent four Southern Ocean foraging baleen whale species: humpback, fin, minke, and blue. Each was generated using rasters of a suite of satellite-derived environmental variables for January 2020 extracted using the R package 'raadtools' (Sumner, 2015). For each of the simulated whale fields, a series of environmental variable rasters (n = 3-4) were selected, with paired mean and standard deviation; chosen to reflect previously reported predictors of high densities of the respective baleen whale species in the Southern Ocean (Table 1). Values from a normal distribution (created from the above paired mean and standard deviation) replaced the values in the selected environmental variable rasters. For example, peak humpback whale densities are thought to occur around the 1˚ isotherm (Kasamatsu et al., 2000; Branch, 2011; Johannessen et al., 2022), so all values of 1˚ had the highest density of humpback whales, with decreasing densities towards higher or lower temperatures (SD:1, range: 0-2, Table 1). In this example, sea surface temperature values outside this range (0-2) were assigned a value of 0. A random field was also created for the study area, using the R function 'sim.rf()' in package 'fields' (Furrer et al., 2009) to incorporate "noise" into the relationship between environmental variables and whale densities by "simulating a stationary Gaussian random field on a regular grid with unit marginal variance" (Furrer et al., 2009). Each of these environmental variable-derived whale fields and the random field were scaled to values of between 0 and 1 (to ensure equal influence), and summed, before being rescaled to reflect probable study area-wide abundance. Simulated whale fields were plotted in Figures 2A–D(i) with tourist vessel-based sampling overlaid, and in Figures 3A–D(i) with scientific vessel-based sampling overlaid.

Sampling simulated whale fields

A total of 6346 sampling segments with a maximum of 25 km transect lengths were derived from 209 voyages. As it is practically unfeasible to sample from 209 voyages in a single summer season, we reduced this dataset to 30 randomly selected voyages, resulting in 974 sampling segments. We used the midpoints of these 974 sampling segments to directly sample our simulated whale density (the observation process was not simulated/recreated). The response variable density was modeled as a function of environmental covariates used to create the simulated whale field, a spatial correlation term (a smooth function of easting and northing) and a Gaussian distribution with a log link using GAMs (i.e., whale.density ~ s(x,y) + s(Enviro 1) + s (Enviro n)+…, Table 1) (using R package '*mgcv*' (Wood, 2015)). No spatial autocorrelation was introduced into simulated whale fields other than that inherently presented in environmental variables (where values of similar magnitude often occur in adjacent cells). R functions,

TABLE 1 Literature sort to determine satellite-derived environmental variables used in creating simulated whale fields.

Simulated species	Environmental covariates	Mean	SD	Reference	Study area wide abundance
Humpback ~ s (bathy) + s(sst) + s(clam)	Bathymetry in meters (bathy)	-700	600	(Santora and Reiss, 2011; Santora and Veit, 2013; Herr et al., 2016)	~50,000 whales (Baines et al., 2021)
	Sea Surface Temperature (˚C) (sst)	1	1	(Kasamatsu et al., 2000; Branch, 2011; Johannessen et al., 2022)	
	Log of Chlorophyl A (Johnson Improved) (clam)	0.5	0.5	(Baines et al., 2021; Meynecke et al., 2021)	
Fin ~ s(sst) + s (dice) + s(bathy) + s(eke)	sst	2	1	(Kasamatsu et al., 2000; Santora et al., 2014)	~17,000 whales (Herr et al., 2016; Baines et al., 2021)
	Distance (kilometers) from the sea ice edge (AMSR2-3.125kms, 15% concentration) (dice)	300	75	(Kasamatsu et al., 2000)	
	bathy	-3000	1000	(Kasamatsu et al., 2000; Herr et al., 2016)	
	Eddy Kinetic Energy (eke)	0.2	0.1	(Santora et al., 2014)	
Minke ~ s (bathy) + s(ice) + s(dice)	bathy	500	200	(Kasamatsu et al., 2000; Herr et al., 2016; Herr et al., 2019)	~7,000 whales, using densities estimates from Herr et al. (2019)
	Sea ice (AMSR2-3.125kms) concentration percentage (ice)	35	20	Kasamatsu et al., 2000; Herr et al., 2019; El-Gabbas et al., 2020)	
	dice	30	60	(Kasamatsu et al., 2000; Murase et al., 2013; Bombosch et al., 2014; Herr et al., 2019; El-Gabbas et al., 2020)	
Blue ~ s(sst) + s (bathy) + s(dice)	sst	-1	1	(Kasamatsu et al., 2000; Branch, 2007)	~700 whales, assuming an increase since 2001 (Hedley et al., 2001; Branch, 2007; Baines et al., 2021)
	bathy	-2000	-1000	(Kasamatsu et al., 2000; Branch, 2007)	
	dice	30	45	(Kasamatsu et al., 2000; Branch, 2007)	

All data was extracted via the R package 'raadtools' (Sumner et al., 2015), details can be found here https://github.com/AustralianAntarcticDivision/blueant#data-source-summary.

FIGURE 2
Tourist vessel-based sampling of the humpback **(A)**, fin **(B)**, minke **(C)**, and blue **(D)** simulated whale fields. Plotted left to right are; (i) the simulated whale field (lighter blues are the higher density of whales) and tourist vessel-based sampling (red lines), (ii) the equivalent modeled whale densities on the same color scale (noting dark grey regions are those where predictions are far greater than the original simulated whale field, *see* Table 4 for the value ranges), (iii) grid-scale coefficient variations (CV) and, (iv) the true spatiality explicit differences between simulated (i) and modeled (ii) whale fields (scale from greens (underestimate) to white (approximately equal) to browns (overestimated)) with tourist vessel-based sampling (grey lines). These plots show the model generally predicted the spatial patterns in the original simulated whale fields well but performed poorly in some regions (iv). Compare grid-scale CV (iii) with true differences (iv) for inconsistencies between model output and the actual differences between the simulated and modeled grid-scale whale densities.

predict.gam() and dsm_var_gam() (R package 'dsm' (Miller et al., 2021)) were used to estimate grid-scale densities and coefficient of variation (CV), and summed to represent modeled abundance. The coefficient of variation associated with the modeled abundance estimate was calculated using the delta method (Ver Hoef, 2012). To provide a comparison to the results achieved with tourist vessel-based sampling, this process was repeated with the true set of realized survey effort achieved during a systematically designed scientific survey, CCAMLR 2019 (Baines et al., 2021) (*herein*, scientific vessel based-survey). Again, using a maximum segment length of 25km, resulting in 370 sampling segments.

Tourist vessel-based resampling of simulated whale fields

To further our understanding of the relationship between an increasing number of tourist vessel-based surveys (voyages) and the performance of the model (i.e., modeled abundance and associated CV), we compared abundance estimates obtained by six through 30 voyages, each drawn randomly from the dataset. Each of these 25 samples (six-30 voyages) was redrawn randomly from the dataset 40 times, for a total of 1,000 samples. The GAM was fit (relevant to the simulated whale field, Table 1), and modeled abundance and associated CV were calculated. This process was repeated for each of the four simulated whale fields.

All data analysis was conducted in the scientific programming language R (R Core Team, 2021). R packages 'tidyverse' (Wickham et al., 2019), 'sf' (Pebesma, 2018), 'raster' (Hijmans et al., 2013), and 'ggplot2' (Wickham, 2011) were used for data manipulation, plotting and analysis.

Results

Estimated length of survey effort per tourist vessel-based survey

After filtering out night and low light locations the 29 vessels covered 279,473 km of potential survey effort with a mean vessel speed of 9.5 knots (range: 0-16, SD: 2.93, SE: ± 0.05) and a mean of 1,293 km per voyage (range: 583-3908, SD: 499, SE: ± 32.9). After allowing for potential weather effects on the sighting conditions, the 29 vessels provided 119,133 km of *realized survey effort*, or a mean of

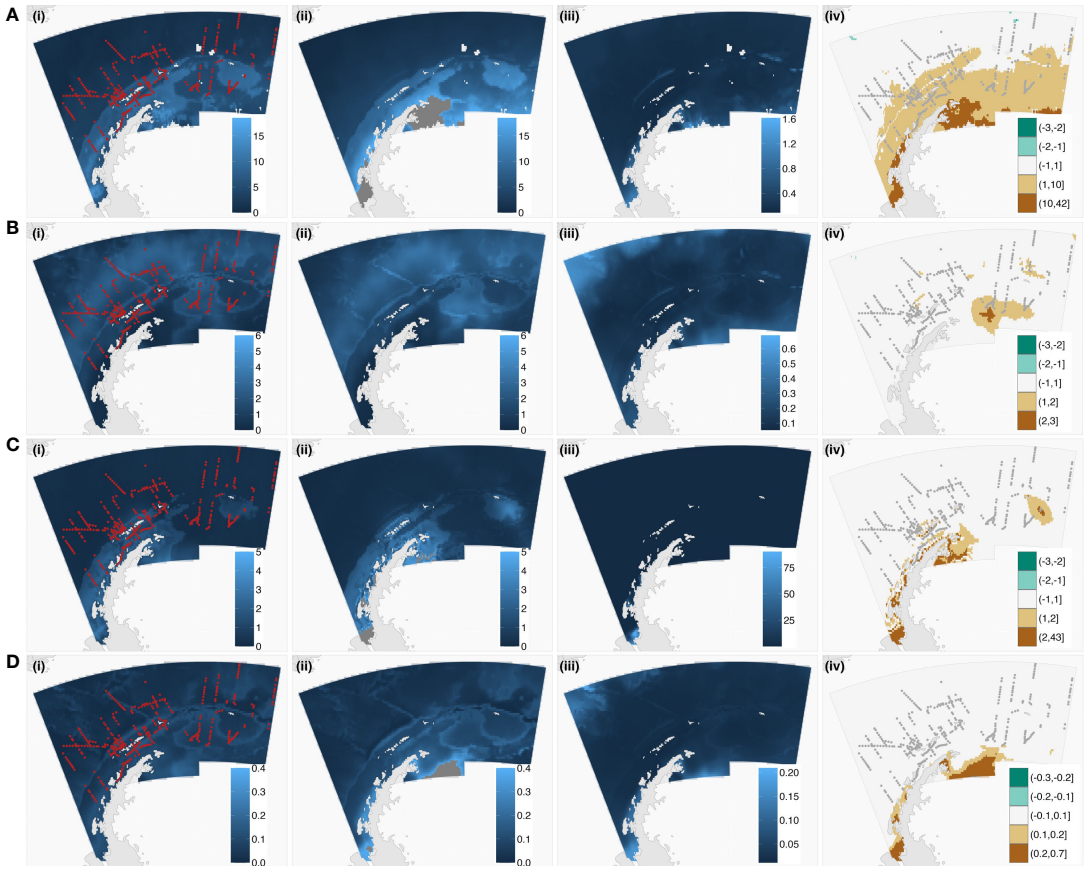

FIGURE 3
Scientific vessel-based sampling of the humpback **(A)**, fin **(B)**, minke **(C)**, and blue **(D)** simulated whale fields. Plotted left to right are; (i) the simulated whale field (lighter blues are the higher density of whales) and scientific vessel-based sampling (red lines), (ii) the equivalent modeled whale densities on the same color scale (noting dark grey regions are those where predictions are far greater than the original simulated whale field, *see* Table 4 for the value ranges), (iii) grid-scale coefficient variations (CV) and, (iv) the true spatiality explicit differences between simulated (i) and modeled (ii) whale fields (scale from greens (underestimate) to white (approximately equal) to browns (overestimated)) with science vessel-based sampling (grey lines). These plots show the model generally predicted the spatial patterns in the original simulated whale fields well but performed poorly in some regions (iv). Compare grid-scale CV (iii) with true differences (iv) for inconsistencies between model output and the actual differences between the simulated and modeled grid-scale whale densities.

551 km per voyage (range: 211-1515, SD: 201, SE: ± 13.7) (Supplementary Material 2). Assuming a strip width of 2 km from a 0 to 90˚ observation field the 29 vessels included in this study could have surveyed a maximum of 15% of the 1.4 million km^2 study area. On average each voyage would sample 0.078% of the study area (1102 km^2), with 18 voyages required for a similar percentage to broad-scale scientific surveys CCAMLR 2000 and 2019 surveys (Table 2).

Estimated sighting rates per tourist vessel-based survey

Expected sighting rates differed by three orders of magnitude among species (range: 0.0002-0.0974 whale sightings/km of survey effort) (Table 3). The annual rate of change in sighting rates over the 19 years was a ~10% increase for humpback, fin, sei, and blue (range:

TABLE 2 Comparisons of the searched area between scientific vessel-based surveys and tourist platform-based surveys.

Study	Study area size	Strip width	Coverage	Reference
Current study (18 voyage estimate)	1.4 million km2	2 km	1.42%	Current study
CCAMLR 2019 survey	2.8 million km2 CCAMLR sub-Areas 48.1,.2 and.3	5 km	1.29%	(Baines et al., 2021)
CCAMLR-IWC 2000 survey	3.4 million km2 CCAMLR sub-Areas 48.1,.2,.3 and.4	5 km	1.43%	(Hedley et al., 2001)

CCAMLR 2000 – 9740 km of realized survey effort (Hedley et al., 2001; Reilly et al., 2004).
CCAMLR 2019 – 7219 km of realized survey effort (Baines et al., 2021).
Similar spatial coverage (as a percentage of the study area) to previous broadscale baleen whale surveys is achieved with ≈18 tourist vessel-based surveys.

TABLE 3 Predicted baleen whale sighting rates (whale sightings/kilometer of *realized survey effort*) for the 2022/23 season calculated from past and recent sighting surveys.

	Past recorded sightings			Recently recorded sightings			Recorded Change	Future			
Species	CCAMLR 2000	Tourist vessel-based study 2001/02	Mean of previous studies	CCAMLR 2019	Tourist vessel-based study 2018/19 and 2021/22	Mean of recent studies	Annual change in sighting rates	Expected sightings (2022/23)	Sightings per voyage (551kms)	No. voyages for 60 sightings	No. voyages for 80 sightings
Humpback	0.0186 (181)	0.0129 (129)	0.0158	0.0237 (171)	0.1262 (701)	0.0750	0.081	0.0947	26	2	3
Fin	0.0068 (66)	0.0080 (80)	0.0074	0.0047 (34)	0.0348 (189)	0.0197	0.050	0.0229	6	10	13
Minke	0.0122 (119)	0.0075 (75)	0.0099	0.0003 (2)	0.0151 (90)	0.0077	-0.012	0.0074	2	30	40
Right	0.0025 (24)	0.0004 (4)	0.0014	0.0004 (3)	0.0000 (0)	0.0002	-0.092	0.0002	0	1421	1894
Sei	0.0008 (8)	0.0004 (4)	0.0006	0.0001 (1)	0.0079 (43)	0.0040	0.099	0.0054	1	41	55
Blue	0.0001 (1)	0.0000 (0)	0.0001	0.0007 (5)	0.0012 (7)	0.0009	0.156	0.0014	0	155	207
Unid	0.0093 (91)	NA	0.0093	0.0111 (80	0.0150 (88)	0.0130	0.017	0.0137	4	16	22
Total whale sightings per voyage								39			

This table details baleen whale sighting rates from past (2000-01) and recent (2019-20) baleen whale surveys of the southwest Atlantic Ocean, and estimates sightings rates for the 2022/23 season. The number of baleen whale sightings is noted in parenthesis, and the *realized survey effort is* listed below. Using the compound interest rate formula described above, estimates of the annual change in sighting rates between the past and recent surveys are calculated. This estimate of annual change is then projected forward to the 2022/23 season (assuming a constant change in abundance and therefore sighting rates) and multiplied by our estimate of predicted *realized survey effort* per tourist vessel voyage (551kms) and halved due to a 90° observation quadrant, to estimate a predicted number of sightings per tourist vessel voyage (sightings per voyage). This estimate was then used to estimate the number of voyages needed for minimum data requirements (60-80 sightings) for multi-covariate distance sampling functions (Buckland et al., 2001) of each species. For humpback and fin whales this was between two and three, and 10 and 13 voyages respectively.

Unid: large unidentified baleen whales.

Previous studies

CCAMLR 2000 – 9740 km of realized survey effort (Hedley et al., 2001; Reilly et al., 2004).

Tourist vessel-based study – 9981kms of realized survey effort (Williams, 2003; Williams et al., 2006).

Recent studies

CCAMLR 2019 – 7219 km of realized survey effort (Baines et al., 2021)

Tourist vessel-based study – combined 5375 km of realized survey effort (2018/19 – 5 voyages) (Johannessen et al., 2022) and 6375 km of realized survey effort (2021/22 – 4 voyages) (Henderson et al., unpublished).

10.3389/fmars.2023.1048869

0.050 - 0.156 whale sightings/km of survey effort) while for Antarctic minke and southern right whales, rates declined by ~5% (range: -0.092 - -0.012 whale sightings/km of survey effort) (Table 3). Sighting rates for large unidentified baleen whales (*unids*) remained relatively stable (Table 3). Humpback and fin whales are likely to dominate sightings with approximately 26 and 6 sightings predicted per voyage respectively, with a total of 39 baleen whale sightings on average (Table 3). Two-three voyages were needed to estimate detection functions for humpback whales, and 10-13 for fin whales (Table 3). Greater than 30 voyages per season were required for the four other species (Table 3).

Comparative sampling of simulated whale fields

When using tourist vessel-based sampling, the spatial patterns in the simulated whale fields (Figures 2A–D(i), (ii), (iii), and (iv)) were well reflected in modeled whale abundance (Figures 2A–D(i), (ii), (iii), and (iv)). However, these four models overestimated the simulated whale abundance by approximately 30% (overestimation range: 23-36%, Table 4). Regions where the 'true' simulated whale density differed from the modeled whale density (Figures 2A–D(i), (ii), (iii), and (iv)), were generally well highlighted by high grid-scale CV values (Figures 2A–D(i), (ii), (iii), and (iv)), with the possible exception of minke whales (compare Figure 2C(iii) with Figure 2C (iv)), which also had the greatest overestimation in total abundance (36%, Table 4). It appears that when high densities were close to the southern edges of the study region, which was the case for humpback, minke, and blue simulated whale fields, this caused problems for the model, particularly in the western Weddell Sea region (60°W, Figure 2).

Scientific vessel-based sampling performed worse at recreating each of the four simulated whale fields, with a higher overestimation of modeled abundance and associated variance (Table 4). Again, models had difficulty in the southern reaches of the study area. Regions where the 'true' simulated whale density differed from the modeled whale density (Figures 3A–D(i), (ii), (iii), and (iv)), were generally well highlighted by higher grid-scale CV values (compare Figures 3A–D(iii) with Figure 3A–D(iv))). Note the scales in these plots, dark grey regions in Figures 2 and 3A–D(ii) depict where values were overestimated outside the plotted scale (consistent scales were used across Figures 2 and 3 to accurately depict values).

In both cases, sampling of the simulated fin whale field (Figure 2D and Figure 3D) fared better than the simulated humpback and minke whale fields (Figure 2A and C and Figure 3A and C) perhaps due to the greater relative densities of simulated whales in the north portion of the study area for fin whales. Full model outputs for each GAM were presented in the supplementary material (Supplementary Material 3). Although this has not been tested here, an exploration into soap film smoothing (Wood et al., 2008), particularly along the convoluted southern edge of the study area may reduce some overestimation of models.

Resampling improved precision and accuracy with increased sample size

The resampling analysis showed model precision (CV) and accuracy (abundance) improved with each additional sample added to the dataset, which is depicted in the reduced spread of values and median of each sample group (six-30 voyages) for both abundance and CV (Figure 4). The median CV within each sample was below 0.25 for all samples but tapered differently between samples. Based on the progressive improvement of precision (CV) and accuracy (abundance), we suggest a sample size of 18-22, 12-16, 17-22, and 13-18 for the humpback, fin, minke, and blue simulated whale fields respectively (grey boxes, Figure 4). For smaller sample sizes there remained substantial improvement in the CV, while for larger sample sizes the improvement was negligible, suggesting an overall sample size of 12-22 voyages. Almost all samples have CVs below 0.25 after ≈18 voyages (except for the humpback whale simulation). Compared to the CV

TABLE 4 Simulated abundance estimates for the four simulated whale fields and their respective modeled abundance estimates (see Table 1 for formulas) from tourist vessel-based and scientific vessel-based sampling.

	Simulated whale fields		Tourist vessel-based sampling		Scientific vessel-based sampling	
Whale species	Simulated abundance	Simulated density range (Figures 2 and 3A-D(i), (ii), (iii), and (iv))	Modeled abundance	Modeled density range (Figures 2A-D(i), (ii), (iii), and (iv)	Modeled abundance	Modeled density range (Figures 3A-D(i), (ii), (iii), and (iv)
Humpback	56,285	0-15	71,443 (CV=0.039, 29%)	0-27	91,440 (CV=0.060, 62%)	0-42
Fin	20,841	0-3.5	25,665 (CV=0.024, 23%)	0-5	27,828 (CV=0.050, 34%)	0-6
Minke	7,442	0-3	10,153 (CV=0.052, 36%)	0-6	13,329 (CV=3.238, 56%)	0-42
Blue	850	0-0.2	1,101 (CV=0.038, 30%)	0-0.4	1,337 (CV=0.077, 64%)	0-0.6

The coefficient of variation (CV) associated with the abundance estimate and the true percentage difference between simulated and modeled abundances are listed in parentheses. All models overestimated abundance, with scientific vessel-based sampling performing notably worse than tourist vessel-based sampling.

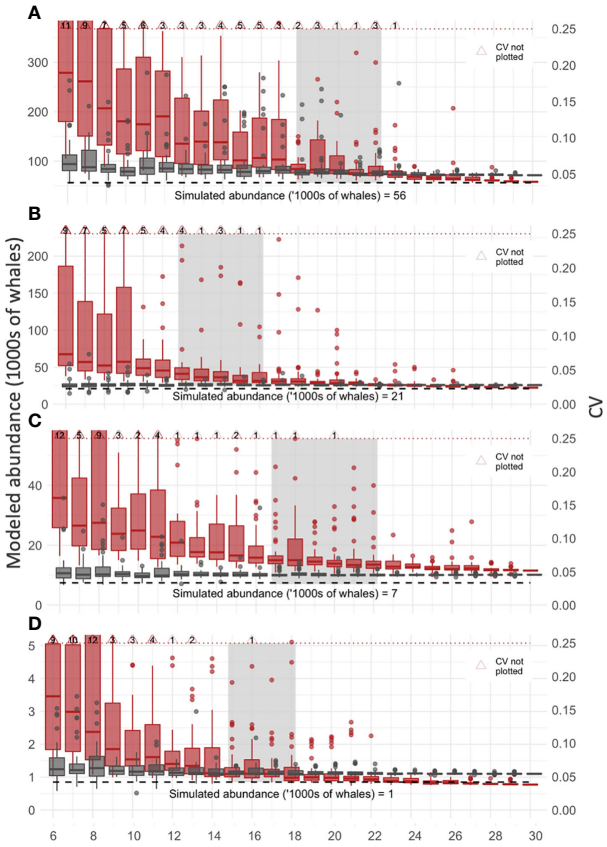

FIGURE 4
Resampling to detect improvement in precision and accuracy of abundance estimates. The relationship between sample size (number of voyages, x-axis) and improvements in accuracy (modeled abundance, grey boxplots, left y-axis) and precision (CV, red boxplots, right y-axis) are plotted for each of the four simulated whale fields (**A-D**, humpback, fin, minke, blue respectively). Median values are horizontal lines on boxplots. The upper bound on a useful CV value (0.25, dashed red line) and true simulated whale abundance (dashed black line) are plotted. Light grey boxes mark the sample size, before which CV improves substantially with increased sample size and after which there is negligible improvement in CV. Note these plots are zoomed to exclude some CV values (large red triangles), and the number of values not plotted is noted (black text inside large red triangles).

values, abundance values were less variable, with improvements mimicking that of CV values.

Discussion

We demonstrate that tourist vessel-based distance sampling surveys have the potential to provide accurate abundance estimates for baleen whales in remote regions. We show that for the southwest Atlantic, 12-22 tourist voyages are likely required to provide an adequate number of sightings to estimate abundance for humpback and fin whales and enable relative approximations of abundance for several other species (as per Reilly et al. (2004); Baines et al. (2021)). We found on average, for each tourist vessel-based baleen whale survey (one voyage) 551km of *realized survey effort* would be achieved, resulting in 39 baleen whale sightings. Surveys would be dominated by fin and humpback whale sightings. Two-three voyages for humpback whales and 10-13 voyages for fin whales were needed to meet model requirements for abundance estimates. Each tourist vessel-based survey would result in 1102 km^2 of ocean surveyed, or 0.078% of the study area, suggesting 18 voyages are required to provide similar spatial coverage to earlier science vessel-based baleen whale surveys in the region (1.42%, Table 2, Reilly et al., 2004; Baines et al., 2021). Tourist vessel-based sampling also performed better than scientific vessel-based sampling in estimating whale abundance of simulated whale fields, but still overestimated abundance by approximately 30%. Consequently, the resampling analysis suggested an appropriate sample size of between 12 and 22 voyages.

Potential for inter- and intra-seasonal abundance estimates

The relatively cost-effective nature of tourist vessel-based surveys will allow researchers to repeatedly survey vast regions of the ocean and provide, at minimum, annual estimates of regional abundance for several species of baleen whale. However, given tourist vessels are now operating in the Southern Ocean for more than five months each

year, tourist vessel-based survey should also allow intra-annual characterization of abundance, that may capture the spatiotemporal trends in baleen whale movement on foraging grounds (e.g., Johannessen et al., 2022); a fundamental improvement in the data that is currently collected. Currently, most Southern Ocean cetacean surveys aim to detect inter-decadal differences and provide a single abundance estimate from surveys conducted between late December and February (Reilly et al., 2004; Baines et al., 2021) when numbers of baleen whales are thought to be at their maximum (Laws, 1977). This will influence the species composition detected because species arrival on foraging grounds is staggered. Based on whaling records (noting the potential inaccuracies of these data, and the potential changes to baleen whale movement and clustering behavior since whaling) the largest (blue and fin) arrived first followed by humpbacks, then sei and southern right whales much later in the season (February/March) (Mackintosh, 1972). There is also thought to be an inshore and southerly shift of species later in the foraging season around the Antarctic Peninsula, following the contraction of the sea ice (February – June) (Thiele et al., 2004; Johnston et al., 2012; Santora et al., 2014). Neither staggered arrival times nor within-season movement is well captured by current survey efforts, with a recent tourist vessel-based survey illustrating the potential for detecting these trends (Johannessen et al., 2022).

Reliability of modeled abundance estimates derived from tourist ship-based surveys

Tourist vessel-based surveys outperformed the tested scientific vessel-based surveys when sampling our simulated whale fields. When compared to the tourist vessel-based sampling, the relatively worse overestimation of modeled abundance of scientific vessel-based sampling might be because these surveys sample relativity little of the putative high whale density regions in the southern reaches of the survey area. This resulted in an exaggerated spatial smooth (compare contour plots of spatial smooths, Supplementary Material 3). Additionally, scientific vessel-based sampling had a narrower spread of sampled covariate values (compare smoothed covariate plots, noting the x-axis scales vary, Supplementary Material 3). These two constraints (limited sampling of the southern reaches and narrower spread of sampled covariates) likely contributed to the poorer performance of scientific vessel-based sampling and highlight the potential utility of tourist vessel-based sampling.

These simulated examples do not depict real-world whale distributions nor the observation process but do provide real-world examples of sets of circumstances under which models can fail to accurately predict whale densities. Whale densities tend to peak close to the ice edge (Herr et al., 2019) and/or coastal regions for many species (Nowacek et al., 2011; Johnston et al., 2012) which is often the edge of the surveyable study area and potentially punctuated with complex coastal features, characteristics that were all present in the simulated whale fields presented here. Miller and Bravington (2017) describe similar potential real-world examples which can have an almost pathological series of characteristics, causing modeled estimates to deviate substantially from the underlying simulated whale fields. Those presented here contribute to the development of detailed guidelines of best practices for these approaches [as the IWC developed for designed-based surveys (IWC, 2013; Hedley and Bravington, 2014)].

Practical challenges

There are several practical challenges in the use of tourist vessel-based sampling to estimate baleen whale abundance. The most significant of these is ensuring standardization of the data collection process across vessels and observers. The most consistent and replicable observation platform on tourist vessels is likely the bridge; although the field of view will be obstructed by the ship's superstructure, windows frames, glass, etc. Outside areas on vessels are more problematic as they have uncontrolled tourist interactions with the observer (*i.e.*, alerting observers to sightings) and are inconsistent across vessels. To ensure observers are conducting the observation process in as consistent a manner as possible, the development and implementation of pre-departure training, in-field training, and detailed field protocols in consultation with vessel crews will be required.

These will be passing mode surveys, with no consistent ability to close in on sightings to confirm species identification, group size, etc. Whale approach guidelines for Antarctic tour operators can be found at iaato.org.

Relevance to other regions

This study describes an opportunity for successful engagement with the tourism industry on broad-scale multiday voyages to deliver high-quality scientific outcomes that could benefit the management of living resources in the Southern Ocean. For example, many of the krill-dependent predator groups in the Southern Ocean are monitored as part of the CCAMLR Environmental Monitoring Program (CEMP). However, there remains a large gap in our understanding of baleen whales in this context, with broad-scale monitoring currently occurring only every two decades and no mechanism to include the impact of recovering baleen whale populations on krill stock. The method outlined here appears to be a possible solution for producing annual abundance estimates of baleen whales in the southwest Atlantic Ocean.

There is also potential for the use of tourist ships for surveys of cetaceans and other species (e.g., seals, penguins, and Pelecaniformes seabirds) in other parts of the world, particularly into the Arctic, as many of the same companies operate in both poles. Tourist vessel-based surveys are suited to regions with a relatively high volume of tourist traffic, multiple voyage plans, and low volumes of survey effort from dedicated scientific voyages (Kaschner et al., 2012). In the Arctic, the north Pacific and north Atlantic Ocean sectors appear to be suited (Compton et al., 2007), however further site-specific investigation is needed to determine the viability of achieving robust abundance estimates. Here, the southwest Atlantic region of the Southern Ocean appears to be a viable location for tourist vessel-based surveys, while other regions, such as the Ross Sea and east Antarctica may not be as suitable, due to limited tourist vessel traffic.

There are many examples of coastal vessels being used as 'platforms of opportunity' (e.g., tourist, fishing, and cargo vessels and ferries) for collecting scientific data, e.g., marine mammal surveys (Williams et al., 2006; Kiszka et al., 2007; Hupman et al., 2015; Vinding et al., 2015; Viquerat and Herr, 2017) and we now have the statistical tools and

computational power to model data from larger spatial areas, across large-scale oceanic regions from multiple tourist vessel platforms. There is potential for a conflict of interests between scientific investigation and vessel operators (e.g., violation of approach distances by tourist vessel operators for enhanced tourist experience (Bearzi, 2017)). However, the success of science and management in resolving complex issues and potential conflicts of interest relies on a holistic approach, such as using social science as a tool for reducing negative wildlife interactions described in Filby et al. (2015); and scientific innovation for reducing seabird bycatch outlined in Avery et al. (2017). Thus, engaging the tourist industry to collect scientific data relevant to management has the potential to result in positive outcomes for all stakeholders; in addition to fostering and incorporating local talent and engaging tourists in the process of science.

Data availability statement

The original contributions presented in the study are included in the article/Supplementary Material, further inquiries can be directed to the corresponding author/s.

Author contributions

This work was conceived by AH, MH, SW, M-AL, NK, and AL. Data provided and curated by MB and AL. Data analysis by AH with support of MH, SW and NK. Drafting of the manuscript by AH, with review from MH, SW, M-AL, MB, NK and AL. All authors contributed to the article and approved the submitted version.

Funding

This work was funded by the Australian Government, Antarctic Science Foundation, and Antarctic Wildlife Research Foundation. In-kind support from University of Tasmania, Australian Antarctic Division, Norwegin Polar Institue, and Insitute of Marine Science.

Conflict of interest

The authors declare that the research was conducted in the absence of any commercial or financial relationships that could be construed as a potential conflict of interest.

The reviewer RL declared a past co-authorship with the author NK to the handling editor.

Publisher's note

Supplementary material

The Supplementary Material for this article can be found online at: https://www.frontiersin.org/articles/10.3389/fmars.2023.1048869/full#supplementary-material

SUPPLEMENTARY MATERIAL 1
Spatial binned weather data. The proportion of good weather hours is plotted in spatial bins (10° Longitude* 2.5° Latitude) on a continuous gradient scale (lighter blues have a greater proportion of good weather survey conditions). Hourly locations from IWC SOWER surveys from which this weather data was derived are plotted in red. Spatial bins with 0 and<10 weather observations were colored white and grey respectively.

SUPPLEMENTARY MATERIAL 2
Histogram of the length of potential survey effort (km, blue) and estimated *realized survey effort* (red) per voyage each month (November **(A)** to March **(E)** and overall **(F)**. The median for each group is plotted as a vertical line.

SUPPLEMENTARY MATERIAL 3
Model outputs of R package 'mgcv' function plot.gam(), and vis.gam() from GAMs in and . These plots are presented in pairs to compare tourist vessel-based sampling with scientific vessel-based sampling.

References

Ainley, D. G., Ballard, G., and Dugger, K. M. (2006). Competition among penguins and cetaceans reveals trophic cascades in the Western Ross Sea, Antarctica. *Ecology* 87, 2080–2093. doi: 10.1890/0012-9658

Avery, J. D., Aagaard, K., Burkhalter, J. C., and Robinson, O. J. (2017). Seabird longline bycatch reduction devices increase target catch while reducing bycatch: A meta-analysis. *J. Nat. Conserv.* 38, 37–45. doi: 10.1016/j.jnc.2017.05.004

Baines, M., Kelly, N., Reichelt, M., Lacey, C., Pinder, S., Fielding, S., et al. (2021). Population abundance of recovering humpback whales megaptera novaeangliae and other baleen whales in the Scotia arc, south Atlantic. *Mar. Ecol. Prog. Ser.* 676, 77–94. doi: 10.3354/meps13849

Baker, C. S., and Clapham, P. J. (2004). Modelling the past and future of whales and whaling. *Trends Ecol. Evol.* 19, 365–371. doi: 10.1016/j.tree.2004.05.005

Bassoi, M., Acevedo, J., Secchi, E. R., Aguayo-Lobo, A., Dalla Rosa, L., Torres, D., et al. (2020). Cetacean distribution in relation to environmental parameters between drake passage and northern Antarctic peninsula. *Polar Biol.* 43, 1–15. doi: 10.1007/s00300-019-02607-z

Bearzi, M. (2017). *Impacts of marine mammal tourism* (Cham: Ecotourism's promise and peril Springer), 73–96. doi: 10.1007/978-3-319-58331-0_6

Bender, N. A., Crosbie, K., and Lynch, H. J. (2016). Patterns of tourism in the Antarctic peninsula region: A 20-year analysis. *Antarct. Sci.* 28, 194–203. doi: 10.1017/S0954102016000031

Bombosch, A., Zitterbart, D. P., Van Opzeeland, I., Frickenhaus, S., Burkhardt, E., Wisz, M. S., et al. (2014). Predictive habitat modelling of humpback (*Megaptera novaeangliae*) and Antarctic minke (*Balaenoptera bonaerensis*) whales in the southern ocean as a planning tool for seismic surveys. *Deep Sea Res. Part Oceanogr. Res. Pap.* 91, 101–114. doi: 10.1016/j.dsr.2014.05.017

Branch, T. A. (2007). Abundance of Antarctic blue whales south of 60 s from three complete circumpolar sets of surveys. *J. Cetacean. Res. Manage* 9, 253–262.

Branch, T. (2011). Humpback whale abundance south of 60°S from three complete circumpolar sets of surveys. *J. Cetacean Res. Manage. Spec.* 3, 53–69. doi: 10.47536/jcrm.vi.305

Branch, T. A., and Butterworth, D. S. (2001a). Estimates of abundance south of 60°S for cetacean species sighted frequently on the 1978/79 to 1997/98 IWC/IDCR-SOWER sighting surveys. *J. Cetacean Res. Manage.* 3 (3), 251–270.

Branch, T. A., and Butterworth, D. S. (2001b). Southern hemisphere minke whales: Standardised abundance estimates from the 1978/79 to 1997/98 IDCR-SOWER surveys. *Cetacean Res. Manage.* 3 (2), 143–174.

Buckland, S. T., Anderson, D. R., Burnham, K. P., Laake, J. L., Borchers, D. L., and Thomas, L. (2001). *Introduction to distance sampling: Estimating abundance of biological populations*. Oxford, United Kingdom): Oxford Univ. Press.

Cañadas, A., and Hammond, P. S. (2008). Abundance and habitat preferences of the short-beaked common dolphin Delphinus delphis in the southwestern Mediterranean: Implications for conservation. *Endanger. Species Res.* 4 (3), 309–331.

Carrasco, J. F., Bozkurt, D., and Cordero, R. R. (2021). A review of the observed air temperature in the Antarctic peninsula. did the warming trend come back after the early 21st hiatus? *Polar Sci.* 28, 100653. doi: 10.1016/j.polar.2021.100653

Compton, R., Banks, A., Goodwin, L., and Hooker, S. K. (2007). Pilot cetacean survey of the sub-Arctic north Atlantic utilizing a cruise-ship platform. *J. Mar. Biol. Assoc. U. K.* 87, 321–325. doi: 10.1017/S0025315407054781

El-Gabbas, A., Opzeeland, I. V., Burkhardt, E., and Boebel, O. (2020). Static species distribution models in the marine realm: The case of baleen whales in the southern ocean. *Divers. Distrib* 27 (8), 1536–1552. doi: 10.1111/ddi.13300

Erbe, C., Dähne, M., Gordon, J., Herata, H., Houser, D. S., Koschinski, S., et al. (2019). Managing the effects of noise from ship traffic, seismic surveying and construction on marine mammals in Antarctica. *Front. Mar. Sci.* 0. doi: 10.3389/fmars.2019.00647

Filby, N. E., Stockin, K. A., and Scarpaci, C. (2015). Social science as a vehicle to improve dolphin-swim tour operation compliance? *Mar. Policy* 51, 40–47. doi: 10.1016/j.marpol.2014.07.010

Fraser, A. D., Massom, R. A., Ohshima, K. I., Willmes, S., Kappes, P. J., Cartwright, J., et al. (2020). High-resolution mapping of circum-Antarctic landfast sea ice distribution 2000–2018. *Earth Syst. Sci. Data* 12, 2987–2999. doi: 10.5194/essd-12-2987-2020

Furrer, R., Nychka, D., Sain, S., and Nychka, M. D. (2009). *Package 'fields.' r found. stat. comput* (Vienna Austria).

Hedley, S., and Bravington, M. (2014). "Comments on design-based and model-based abundance estimates for the RMP and other contexts," in *Paper SC/65b/RMP11 presented to the 65b IWC Scientific Committee*, , May 2014. 9.

Hedley, S., Reilly, S., Borberg, J., Holland, R., Hewitt, R., Watkins, J., et al. (2001). "Modelling whale distribution: A preliminary analysis of data collected on the CCAMLR-IWC krill synoptic surve," in *Paper SC/53/E9 presented to the 54th Meeting of the International Whaling Commission*, , July 2001.

Herr, H., Viquerat, S., Devas, F., Lees, A., Wells, L., Gregory, B., et al. (2022). Return of large fin whale feeding aggregations to historical whaling grounds in the Southern Ocean. *Sci. Rep.* 12, 9458. doi: 10.1038/s41598-022-13798-7

Herr, H., Kelly, N., Dorschel, B., Huntemann, M., Kock, K.-H., Lehnert, L. S., et al. (2019). Aerial surveys for Antarctic minke whales (*Balaenoptera bonaerensis*) reveal sea ice dependent distribution patterns. *Ecol. Evol.* 9, 5664–5682. doi: 10.1002/ece3.5149

Herr, H., Viquerat, S., Siegel, V., Kock, K.-H., Dorschel, B., Huneke, W. G. C., et al. (2016). Horizontal niche partitioning of humpback and fin whales around the West Antarctic peninsula: evidence from a concurrent whale and krill survey. *Polar Biol.* 39, 799–818. doi: 10.1007/s00300-016-1927-9

Hijmans, R. J., van Etten, J., Mattiuzzi, M., Sumner, M., Greenberg, J. A., Lamigueiro, O. P., et al. (2013). *Raster package in r. version*.

Horton, T. W., Palacios, D. M., Stafford, K. M., and Zerbini, A. N. (2022). "Baleen whale migration," in *Ethology and behavioral ecology of mysticetes. ethology and behavioral ecology of marine mammals*. Eds. C. W. Clark and E. C. Garland (Cham: Springer). doi: 10.1007/978-3-030-98449-6_4

Hupman, K., Visser, I., Martinez, E., and Stockin, K. (2015). Using platforms of opportunity to determine the occurrence and group characteristics of orca (*Orcinus orca*) in the hauraki gulf, new Zealand. *N. Z. J. Mar. Freshw. Res.* 49, 132–149. doi: 10.1080/00288330.2014.980278

International Association of Antarctic Tour Operators *Overview of Antarctic tourism: A historical review of growth, the 2020-21 season, and preliminary estimates for 2021-22*. Available at: https://iaato.org/wp-content/uploads/2021/07/ATCM43_ip110_e.docx (Accessed 14-May-2021).

International Whaling Commission (2013). Reports of the subcommittee on in-depth assessments. *J. Cetacean Res. Manage.* 14 (Suppl.), 195–213.

Johannessen, J. E. D., Biuw, M., Lindstrøm, U., Ollus, V. M. S., Martín López, L. M., Gkikopoulou, K. C., et al. (2022). Intra-season variations in distribution and abundance of humpback whales in the West Antarctic peninsula using cruise vessels as opportunistic platforms. *Ecol. Evol.* 12, e8571. doi: 10.1002/ece3.8571

Johnston, D., Friedlaender, A., Read, A., and Nowacek, D. (2012). Initial density estimates of humpback whales megaptera novaeangliae in the inshore waters of the western Antarctic peninsula during the late autumn. *Endanger. Species Res.* 18, 63–71. doi: 10.3354/esr00395

Kasamatsu, F., Matsuoka, K., and Hakamada, T. (2000). Interspecific relationships in density among the whale community in the Antarctic. *Polar Biol.* 23, 466–473. doi: 10.1007/s003009900107

Kaschner, K., Quick, N. J., Jewell, R., Williams, R., and Harris, C. M. (2012). Global coverage of cetacean line-transect surveys: Status quo, data gaps and future challenges. *PloS One* 7, e44075. doi: 10.1371/journal.pone.0044075

Kawaguchi, S., and Nicol, S. (2020). Krill fishery. *Fish Aquac* 9, 137. doi: 10.1093/oso/9780190865627.003.0006

Kiszka, J., Macleod, K., Van Canneyt, O., Walker, D., and Ridoux, V. (2007). Distribution, encounter rates, and habitat characteristics of toothed cetaceans in the bay of Biscay and adjacent waters from platform-of-opportunity data. *ICES J. Mar. Sci.* 64, 1033–1043. doi: 10.1093/icesjms/fsm067

Laws, R. M. (1977). Seals and whales of the southern ocean. *Philos. Trans. R. Soc Lond. B Biol. Sci.* 279, 81–96.

Leaper, R., and Miller, C. (2011). Management of Antarctic baleen whales amid past exploitation, current threats and complex marine ecosystems. *Antarct. Sci.* 23, 503–529. doi: 10.1017/S0954102011000708

Lin, Y., Moreno, C., Marchetti, A., Ducklow, H., Schofield, O., Delage, E., et al. (2021). Decline in plankton diversity and carbon flux with reduced sea ice extent along the Western Antarctic peninsula. *Nat. Commun.* 12, 4948. doi: 10.1038/s41467-021-25235-w

Lynch, H. J., Crosbie, K., Fagan, W. F., and Naveen, R. (2010). Spatial patterns of tour ship traffic in the Antarctic peninsula region. *Antarct. Sci.* 22, 123–130. doi: 10.1017/S0954102009990654

Mackintosh, N. A. (1972). Biology of the populations of large whales. *Sci. Prog. 1933-60*, 449–464.

Marques, F. F. C., and Buckland, S. T. (2003). Incorporating covariates into standard line transect analyses. *Biometrics* 59, 924–935. doi: 10.1111/j.0006-341X.2003.00107.x

McMahon, K. W., Michelson, C. I., Hart, T., McCarthy, M. D., Patterson, W. P., and Polito, M. J. (2019). Divergent trophic responses of sympatric penguin species to historic anthropogenic exploitation and recent climate change. *Proc. Natl. Acad. Sci.* 116, 25721–25727. doi: 10.1073/pnas.1913093116

Meynecke, J.-O., de Bie, J., Barraqueta, J.-L. M., Seyboth, E., Dey, S. P., Lee, S. B., et al. (2021). The role of environmental drivers in humpback whale distribution, movement and behavior: A review. *Front. Mar. Sci.* 8. doi: 10.3389/fmars.2021.720774

Miller, D. L., and Bravington, M. V. (2017). "When can abundance surveys be analysed with "design-based" methods?," in *Paper SC/67B/NH/04 presented to the 67th Meeting of the International Whaling Commission*, , September 2018.

Miller, D. L., Burt, M. L., Rexstad, E. A., and Thomas, L. (2013). Spatial models for distance sampling data: Recent developments and future directions. *Methods Ecol. Evol.* 4, 1001–1010. doi: 10.1111/2041-210X.12105

Miller, D. L., Rexstad, E., Burt, L., Bravington, M. V., Hedley, S., and Model, A. (2021). *Package 'dsm.'*.

Murase, H., Kitakado, T., Hakamada, T., Matsuoka, K., Nishiwaki, S., and Naganobu, M. (2013). Spatial distribution of Antarctic minke whales (*Balaenoptera bonaerensis*) in relation to spatial distributions of krill in the Ross Sea, Antarctica. *Fish. Oceanogr.* 22, 154–173. doi: 10.1111/fog.12011

Nowacek, D. P., Friedlaender, A. S., Halpin, P. N., Hazen, E. L., Johnston, D. W., Read, A. J., et al. (2011). Super-aggregations of krill and humpback whales in Wilhelmina bay, Antarctic peninsula. *PloS One* 6, e19173. doi: 10.1371/journal.pone.0019173

Palmowski, T. (2020). Development of Antarctic tourism. *Geoj Tour Geosites* 33, 1520–1526. doi: 10.30892/gtg.334spl11-602

Pebesma, E. J. (2018). Simple features for r: Standardized support for spatial vector data. *R J.* 10 (1), pp.439–pp.446. doi: 10.32614/RJ-2018-009

Ratnarajah, L., Bowie, A. R., Lannuzel, D., Meiners, K. M., and Nicol, S. (2014). The biogeochemical role of baleen whales and krill in southern ocean nutrient cycling. *PloS One* 9, e114067. doi: 10.1371/journal.pone.0114067

Ratnarajah, L., Melbourne-Thomas, J., Marzloff, M. P., Lannuzel, D., Meiners, K. M., Chever, F., et al. (2016). A preliminary model of iron fertilisation by baleen whales and Antarctic krill in the southern ocean: Sensitivity of primary productivity estimates to parameter uncertainty. *Ecol. Model.* 320, 203–212. doi: 10.1016/j.ecolmodel.2015.10.007

R Core Team (2021). *R: A language and environment for statistical computing*. R Foundation for Statistical Computing, Vienna, Austria. Available at: https://www.Rproject.org/.

Reilly, S., Hedley, S., Borberg, J., Hewitt, R., Thiele, D., Watkins, J., et al. (2004). Biomass and energy transfer to baleen whales in the south Atlantic sector of the southern ocean. *Deep Sea Res. Part II Top. Stud. Oceanogr.* 51, 1397–1409. doi: 10.1016/j.dsr2.2004.06.008

Santora, J. A., and Reiss, C. S. (2011). Geospatial variability of krill and top predators within an Antarctic submarine canyon system. *Mar. Biol.* 158, 2527–2540. doi: 10.1007/s00227-011-1753-0

Santora, J. A., Schroeder, I. D., and Loeb, V. J. (2014). Spatial assessment of fin whale hotspots and their association with krill within an important Antarctic feeding and fishing ground. *Mar. Biol.* 161, 2293–2305. doi: 10.1007/s00227-014-2506-7

Santora, J., and Veit, R. (2013). Spatiotemporal persistence of top predator hotspots near the Antarctic Peninsula. *Mar. Ecol. Prog. Ser* 487, 287–304. doi: 10.3354/meps10350

Savoca, M. S., Czapanskiy, M. F., Kahane-Rapport, S. R., Gough, W. T., Fahlbusch, J. A., Bierlich, K. C., et al. (2021). Baleen whale prey consumption based on high-resolution foraging measurements. *Nature* 599, 85–90. doi: 10.1038/s41586-021-03991-5

Strindberg, S., and Buckland, S. T. (2004). Zigzag survey designs in line transect sampling. *J. Agricultural Biol. Environ. Stat* 9, 443–461. doi: 10.1198/108571104X15601

Sumner, M. D. (2015). *Raadtools: Tools for synoptic environmental spatial data. r package version 0.5*, Vol. 3. 9001, (2020).

Thiele, D., Chester, E. T., Moore, S. E., Širovic, A., Hildebrand, J. A., and Friedlaender, A. S. (2004). Seasonal variability in whale encounters in the Western Antarctic peninsula. *Deep Sea Res. Part II Top. Stud. Oceanogr.* 51, 2311–2325. doi: 10.1016/j.dsr2.2004.07.007

Thomas, L., Buckland, S. T., Rexstad, E. A., Laake, J. L., Strindberg, S., Hedley, S. L., et al. (2010). Distance software: design and analysis of distance sampling surveys for

estimating population size. *J. Appl. Ecol.* 47, 5–14. doi: 10.1111/j.1365-2664.2009.01737.x

Thomas, L., Williams, R., and Sandilands, D. (2007). Designing line transect surveys for complex survey regions. *J. Cetacean Res. Manage.* 9, 1–13.

Tin, T., Fleming, Z. L., Hughes, K. A., Ainley, D. G., Convey, P., Moreno, C. A., et al. (2009). Impacts of local human activities on the Antarctic environment. *Antarct. Sci.* 21, 3–33. doi: 10.1017/S0954102009001722

Tin, T., Lamers, M., Liggett, D., Maher, P. T., and Hughes, K. A. (2014). "Setting the scene: Human activities, environmental impacts and governance arrangements in Antarctica," in *Antarctic Futures*. Eds. T. Tin, D. Liggett, P. T. Maher and M. Lamers (Dordrecht: Springer Netherlands), 1–24. doi: 10.1007/978-94-007-6582-5_1

Trivelpiece, W. Z., Hinke, J. T., Miller, A. K., Reiss, C. S., Trivelpiece, S. G., and Watters, G. M. (2011). Variability in krill biomass links harvesting and climate warming to penguin population changes in Antarctica. *Proc. Natl. Acad. Sci.* 108, 7625–7628. doi: 10.1073/pnas.1016560108

Tulloch, V. J. D., Plagányi, É.E., Brown, C., Richardson, A. J., and Matear, R. (2019). Future recovery of baleen whales is imperiled by climate change. *Glob. Change Biol.* 25, 1263–1281. doi: 10.1111/gcb.14573

Ver Hoef, J. M. (2012). Who invented the delta method? *Am. Statistician* 66, 124–127. doi: 10.1080/00031305.2012.687494

Vinding, K., Bester, M., Kirkman, S. P., Chivell, W., and Elwen, S. H. (2015). The use of data from a platform of opportunity (whale watching) to study coastal cetaceans on the southwest coast of south Africa. *Tour. Mar. Environ.* 11, 33–54. doi: 10.3727/154427315X14398263718439

Viquerat, S., and Herr, H. (2017). Mid-summer abundance estimates of fin whales (*Balaenoptera physalus*) around the south Orkney islands and elephant island. *Endanger. Species Res.* 32, 515–524. doi: 10.3354/esr00832

Warwick-Evans, V., A Santora, J., Waggitt, J. J., and Trathan, P. N. (2021). Multi-scale assessment of distribution and density of procellariiform seabirds within the northern Antarctic peninsula marine ecosystem. *ICES J. Mar. Sci.* 78 (4), 1324–1339. doi: 10.1093/icesjms/fsab020

Wickham, H. (2011). ggplot2. *Wiley Interdiscip. Rev. Comput. Stat.* 3, 180–185.

Wickham, H., Averick, M., Bryan, J., Chang, W., McGowan, L. D., François, R., et al. (2019). Welcome to the tidyverse. *J. Open Source Software* 4, 1686. doi: 10.21105/joss.01686

Williams, R. (2003). Cetacean studies using platforms of opportunity. unpublished PhD thesis in biology. *Univ. St Andrews St Andrews Scotl. UK* 238.

Williams, R., Hedley, S. L., and Hammond, P. S. (2006). Modeling distribution and abundance of Antarctic baleen whales using ships of opportunity. *Ecol. Soc.* 11 (1). doi: 10.5751/ES-01534-110101

Williams, R., and Thomas, L. (2009). Cost-effective abundance estimation of rare marine animals: Small-boat surveys for killer whales in British Columbia, Canada. *Biol. Conserv.* 142, 1542–1547. doi: 10.1016/j.biocon.2008.12.028

Wood, S. (2015). *Package 'mgcv.' r package version*, 1. 729.

Wood, S. N., Bravington, M. V., and Hedley, S. L. (2008). Soap film smoothing. *J. R. Stat. Soc Ser. B Stat. Methodol.* 70, 931–955. doi: 10.1111/j.1467-9868.2008.00665.x

frontiers | Frontiers in Marine Science

TYPE Original Research
PUBLISHED 01 June 2023
DOI 10.3389/fmars.2023.1121088

OPEN ACCESS

EDITED BY
Muniyandi Nagarajan,
Central University of Kerala, India

REVIEWED BY
Eva Garcia-Vazquez,
Universidad de Oviedo Mieres, Spain
Ana Verissimo,
Centro de Investigacao em Biodiversidade e Recursos Geneticos (CIBIO-InBIO), Portugal
Jan McDowell,
College of William & Mary, United States

*CORRESPONDENCE
Shin-ichi Ito
goito@aori.u-tokyo.ac.jp

RECEIVED 11 December 2022
ACCEPTED 03 May 2023
PUBLISHED 01 June 2023

CITATION
Yu Z, Wong MK-S, Inoue J, Ahmed SI, Higuchi T, Hyodo S, Itoh S, Komatsu K, Saito H and Ito S (2023) Environmental DNA in the Kuroshio reveals environment-dependent distribution of economically important small pelagic fish.
Front. Mar. Sci. 10:1121088.
doi: 10.3389/fmars.2023.1121088

Environmental DNA in the Kuroshio reveals environment-dependent distribution of economically important small pelagic fish

Zeshu Yu[1,2], Marty Kwok-Shing Wong[1,3], Jun Inoue[1], Sk Istiaque Ahmed[1], Tomihiko Higuchi[1], Susumu Hyodo[1], Sachihiko Itoh[1], Kosei Komatsu[1], Hiroaki Saito[1] and Shin-ichi Ito[1]*

[1]Atmosphere and Ocean Research Institute, The University of Tokyo, Kashiwa, Japan, [2]Graduate School of Agricultural and Life Sciences, The University of Tokyo, Tokyo, Japan, [3]Faculty of Sciences, Toho University, Funabashi, Japan

Introduction: Small pelagic fishes constitute large proportions of fisheries and are important components linking lower and higher trophic levels in marine ecosystems. Many small pelagic fishes in the Northwest Pacific spawn upstream in the Kuroshio and spend their juvenile stage in the Kuroshio Front area, indicating that the Kuroshio Current system impacts their stock fluctuations. However, the distribution of these fish relative to the Kuroshio has not been determined due to dynamic spatio-temporal fluctuations of the system. Here, the recent development of environmental DNA (eDNA) monitoring enabled us to investigate the distribution patterns of four economically important small pelagic fishes (Japanese sardine *Sardinops melanostictus*, Japanese anchovy *Engraulis japonicus*, chub mackerel Scomber japonicus, and blue mackerel *Scomber australasicus*) in the Kuroshio Current system.

Methods: The influence of environmental factors, such as sea water temperature, salinity, oxygen concentration, chlorophyll-a concentration, and prey fish on the occurrence and quantity of target fish eDNA was analyzed using generalized additive models. In addition, the detection (presence) of target fish eDNA were compared between the offshore and inshore side areas of the Kuroshio axis.

Results: Sea water temperature showed important effect, especially on the distribution of Japanese sardine and Japanese anchovy, whereas the distribution pattern of chub mackerel and blue mackerel was greatly influenced by the eDNA quantity of Japanese sardine and Japanese anchovy (especially potential prey fish: Japanese anchovy). In addition, we found that the four target fish species could be observed in areas on the inshore side or around the Kuroshio axis, while they were hardly found on the offshore side.

Conclusion: Based on eDNA data, we succeeded in revealing detailed spatial distribution patterns of small pelagic fishes in the Kuroshio Current system and

hypothesized predator–prey relationships influence their distribution in small pelagic fish communities.

KEYWORDS

environmental DNA, qPCR, small pelagic fish, distribution pattern, prey fish effect, temperature, Kuroshio

1 Introduction

Fish production is critical for people's livelihoods worldwide (Food and Agriculture Organization of the United Nations, 2020). Although aquaculture production has developed greatly, capture fishery production remains important, especially in marine fishery production where the percentage of capture contributed around 54% in 2016 (Food and Agriculture Organization of the United Nations, 2020). Small pelagic fish species, such as anchovy, sardine, and chub mackerel, have been major contributors to the total marine capture fishery production (Food and Agriculture Organization of the United Nations, 2020) especially in Japan, one of the most important fishery countries in the world (Ichinokawa et al., 2017). For example, the chub mackerel (*Scomber japonicus*) catch constituted around 2% of the world's total catch in 2018 (Food and Agriculture Organization of the United Nations, 2020). Large-scale production of small pelagic fishes is based on prey zooplankton production. Small pelagic fishes also play critical roles in marine ecosystems as important prey of large predatory fishes, sea birds, as well as mammals, and connect lower and higher trophic levels (Cury et al., 2000; Duarte and Garcíia, 2004; Navarro et al., 2009; Cury et al., 2011; Navarro et al., 2017; Saraux et al., 2019). Thus, it is important to understand the distribution, migration, and response to climate variability of small pelagic fishes.

The resource (such as landings and body condition) of small pelagic fishes is influenced by many environmental factors, such as sea water temperature and chlorophyll-a concentration (Sumaila et al., 2011; Brosset et al., 2017; Quattrocchi and Maynou, 2017) as well as climate fluctuations or changes (Mantua et al., 1997; Brochier et al., 2013; Alheit et al., 2014; Pennino et al., 2020). For the Northwest Pacific area, rich in small pelagic fishes, the Kuroshio was found to influence climate, ecosystems, and fisheries (Yatsu et al., 2013). The Kuroshio is the western boundary current of the subtropical gyre in the North Pacific and a warm ocean current that flows from the northern Philippines and east of Taiwan, along the south coast of the Japanese Archipelago (Figure 1A). The section of the Kuroshio that flows eastward toward the open Pacific is called the Kuroshio Extension. The Kuroshio contains important spawning and nursery grounds, thought to be associated with many small pelagic fish species (Nakata et al., 2001; Sassa et al., 2006; Yatsu et al., 2013; Kaneko et al., 2018). Aggregation in the frontal eddies in the western boundary currents (Nakata et al., 2000; Okazaki et al., 2002; Mullaney and Suthers, 2013) as well as enhanced growth of small pelagic fish larvae in the frontal eddies (Okazaki et al, 2003) has been observed. Besides, the Kuroshio is thought to restrict the upstream movement of fishes on its inshore side (Kai and Motomura, 2022), which is hereinafter referred to as the "barrier effect", these results indicate the importance of the frontal structure of the western boundary currents and their possible relationship to the distribution of small pelagic fishes.

One of the possible effects of frontal structure on fish distribution is the thermal effect and oxygen demands (Pörtner and Knust, 2007). The relationship between environmental factors and the distribution of small pelagic fish in the ocean has been studied. Sabatés et al. (2006) found the distribution of round

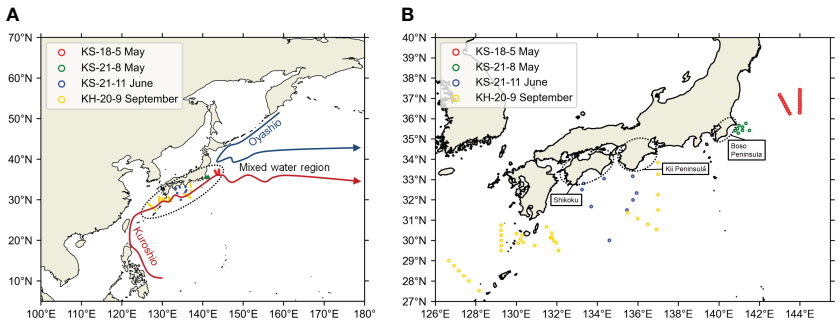

FIGURE 1
Location of the survey area of this study to the Northwest Pacific **(A)** and the zooming of the survey area **(B)**. Maps were made in Spyder (Python 3.7) using Natural Earth data. Free vector and raster map data was obtained from @ naturalearthdata.com. The hollow circles represent the sampling stations. The stations from different cruises were distinguished by the colors of the hollow circles.

sardinella (*Sardinella aurita*) in the western Mediterranean was affected by the sea surface temperature (SST). Furthermore, Georgakarakos and Kitsiou (2008) analyzed the acoustic data of small pelagic fish and found SST and bathymetric depth are the environmental variables that provide the best spatial distribution model to predict the abundance. Similar studies have also been performed in the small-pelagic-fish-rich Northwest Pacific. Moreover, the winter catch per unit effort (CPUE) distribution of Japanese anchovy (*Engraulis japonicus*) in the Yellow and East China Seas demonstrated strong relationships with the salinity front and SST (Liu et al., 2020). The spatio-temporal variation of Japanese sardine (*Sardinops melanostictus*) population in the Sea of Japan was found to be influenced by SST, primary production, and ocean currents during 1970–1999 (Muko et al., 2018). Furthermore, Sassa et al. (2010) collected fish larvae in the southern East China Sea and discovered *Scomber australasicus* was distributed in the more southern and warmer (20 to 23°C versus 15 to 22°C) area than *S. japonicus*. Occurrence and density of Pacific saury *Cololabis saira* larvae and juveniles was found to be highly related to SST with an optimal temperature of 19–20°C (Takasuka et al., 2014). Therefore, these previous studies support an idea the SST is one of the main controlling factors which determine the distribution of small pelagic fish. This is not surprising because small pelagic fishes are ectothermic and have a small body size.

However, the SST dependency of small pelagic fish distribution is impacted by competition between fish species (Fuji et al., 2023). In the pelagic waters of the Northwest Pacific, the Pacific saury shifted to a cooler temperature range when the biomass of Japanese sardine expanded and the potential competition between the two species increased (Fuji et al., 2023). Small pelagic fish aggregate in the Kuroshio Front, and therefore, the competition between species might be enhanced and the effect of SST on distribution might be modified. This may especially be true for chub and blue mackerel, which are piscivorous fishes (Robert et al., 2010) whose main prey are anchovy (Nakatsuka et al., 2010; Robert et al., 2010). Currently there is no study showing a direct link between the distribution of chub and blue mackerel and that of Japanese anchovy. However, the distribution of Spanish mackerel, a predator of Japanese anchovy, highly depends on the distribution of Japanese anchovy (Liu et al., 2023). Consequently, in the aggregated frontal region, prey-predator interaction might alter the distribution characteristics of small pelagic fish.

Indeed, much is still unknown about the relationship between frontal structures, such as the Kuroshio Front, and small pelagic fish distribution. The frontal structures have complex and variable horizontal and vertical environmental conditions (Kasai et al., 2002; Nagai et al., 2012). Therefore, high horizontal and vertical resolution fish distribution data is needed to investigate the environmental effects and inter-specific effects on fish distribution in the frontal area. For larvae, it is possible to conduct high spatio-temporal resolution observations using small larval nets. However, for juveniles and adult fish, this is difficult because their swimming ability is high and large sampling nets are required. In addition, there is a limitation on obtaining information on vertical distribution differences of fish using fishing net sampling although there are multi-depth-sampling net systems. Acoustic sonar is another method for observing fish distribution but currently there are still problems with species identification (Wei et al., 2022). The local fishing catch data is usually needed as a reference in the species identification during acoustic sonar fish detection, which can be unfeasible if the fish species composition is expected to be complex (Georgakarakos and Kitsiou, 2008). Due to these limitations, it has been difficult until now to clarify the environmental and inter-specific effects on the distribution of small pelagic fish in the frontal structures.

The environmental DNA (eDNA) method is a novel technology used in organism surveys which has been developed in recent years. Organisms contain DNA that provides species identification information (Wolf et al., 1999; Ali et al., 2014). When DNA is released into the surrounding environment such as water, sediment, and soil (Thomsen and Willerslev, 2015; Barnes and Turner, 2016; Nevers et al., 2020) through feces, skin, scales, and other means (Poinar et al., 1998; Bunce et al., 2005; Lydolph et al., 2005), it is called eDNA. The sampling of fish eDNA is made possible by collecting and filtering water, enabling high-resolution observations of fish distribution in frontal regions. The procedure of collecting water can be simply performed and be combined with a conductivity temperature depth (CTD) system carried by a research vessel measuring the environmental factors at different depths (Yu et al., 2022). Therefore, the sampling of fish eDNA can be performed with a relatively high horizontal and vertical resolution together with the environmental measurements.

The eDNA method has been widely used for fish distribution surveys in inland and coastal waters worldwide (Minamoto et al., 2011; Kalchhauser and Burkhardt-Holm, 2016; Plough et al., 2018; Minegishi et al., 2019; Stat et al., 2019). Using eDNA analysis methods such as quantitative polymerase chain reaction (qPCR) and metabarcoding, information, including species and quantity, can be revealed. Recently, an optimized protocol for eDNA extraction in fish and robust qPCR conditions have been developed (Wong et al., 2020). A multiplex qPCR system was developed for the quantitative analysis of six small pelagic fishes' eDNA (Wong et al., 2022): the Japanese sardine (hereafter sardine, *S. melanostictus*), Japanese anchovy (anchovy) *E. japonicus*, chub mackerel, blue mackerel (*S. australasicus*), Japanese jack mackerel (jack mackerel, *Trachurus japonicus*), and Pacific saury (saury, *C. saira*). The effectiveness of the multiplex qPCR system was confirmed by the detection of small pelagic fishes in the Kuroshio Extension (Yu et al., 2022). Here, as a new attempt, we used the validated multiplex qPCR system to analyze open ocean water samples from the Kuroshio Current system to explore the environment-dependent distribution patterns of several economically important small pelagic fishes. This study aimed to help improve the understanding of environmental and inter-specific effects on small pelagic fish distribution in the frontal region. The Kuroshio Current system was used as a testbed because it is one of the most productive areas of small pelagic fish. The improved understanding can be extended to other frontal regions including the Gulf Stream, as well as the Brazil, East Australian and the Agulhas Currents.

In this study, 488 sea water samples were collected during four Kuroshio cruises and used to detect the eDNA of six small pelagic

fishes using qPCR. These fish species were chosen for their importance in fisheries. Subsequently, qPCR data were integrated with environmental data to estimate the influence of environmental parameters on the distribution of the target fishes. Among the six small pelagic fish we detected, the eDNA detection of saury and jack mackerel was very limited (details were shown in the Section 3.1), so the target fishes in this study were sardine, anchovy, chub mackerel, and blue mackerel.

Our study successfully revealed the environment-dependent spatial distribution characteristics of these target fishes in the Kuroshio Current system based on eDNA data. The success of this study supports the effectiveness of eDNA methods in revealing the relationship between fish and the environment. We expect a wider usage of its in other areas and on other species. In addition, we believe that our findings on the influence of predator–prey relationships will improve further studies and the understanding of small pelagic fish distribution patterns.

2 Materials and methods

2.1 Water sampling

Sea water samples were collected at 72 different stations during four cruises in the Kuroshio Current system (Figures 1, 2, Table S1). The research cruises KS-18-5 (May 2018), KS-21-8 (May 2021), and KS-21-11 (June 2021) were performed by the research vessel Shinsei-Maru, and the KH-20-9 (September–October 2020) research cruise was performed by the research vessel Hakuho-Maru. Shinsei-Maru and Hakuho-Maru are cooperative research vessels. Their cruise plan is based on open application systems (https://www.aori.u-tokyo.ac.jp/english/coop/index.html). The cruise period is limited to two weeks at the maximum for Shinsei-Maru. The cruise period of Hakuho-Maru is longer, but the open application is called every three years. Since it is not easy to conduct research cruises in a specific region for a sufficient period, we decided to cover the Kuroshio Current system by pooling data from different cruises.

Samples collected from three cruises, KS-18-5, KS-21-8, and KS-21-11, were pooled to analyze the effect of environmental factors (sea water temperature, temperature gradient, salinity, salinity gradient, dissolved oxygen concentration, chlorophyll-a concentration; see Section 2.5) on the small pelagic fishes in a wide area of the Kuroshio (Figures 1, 2). These cruises were all undertaken during the same season (May or June). Consequently, the effects of the seasonal environmental variability as well as seasonal distribution changes, such as seasonal migration of the target fishes, (Li et al., 2014; Sarr et al., 2021) was minimized. All four target species have long spawning periods lasting from winter to early summer, May–June overlapped with their spawning season. Furthermore, the target fishes in this study have wide spawning grounds in the southern coast of Japan (Hattori, 1964; Takasuka et al., 2008a; Nishikawa, 2018; Kanamori et al., 2021; Kume et al., 2021). Therefore, pooling samples from the three cruises are thought to be able to cover the distribution areas including the wide spawning grounds. The samples are expected to include the

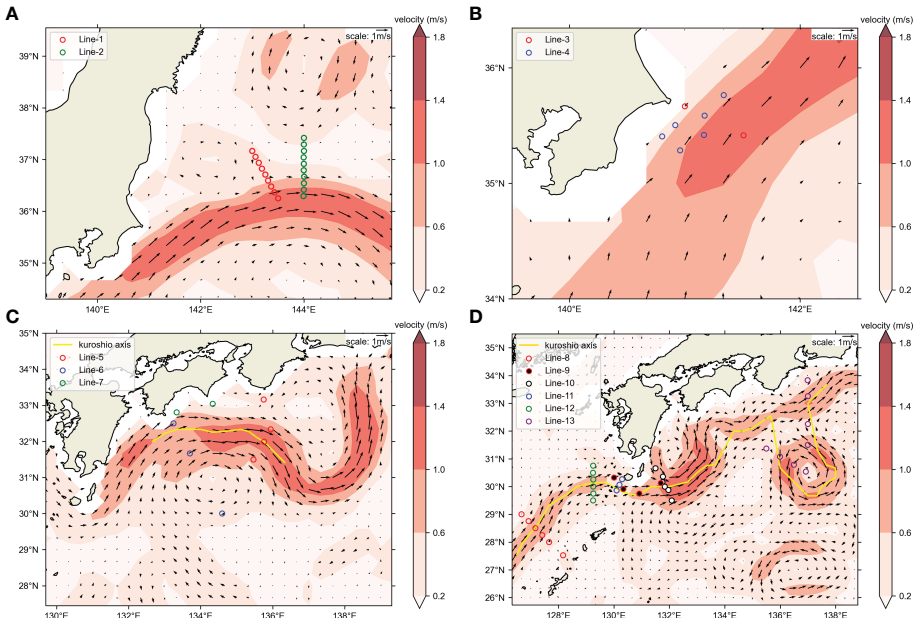

FIGURE 2
Positions of OceanDNA sampling stations in this study. Sampling area maps of **(A)** KS-18-5, **(B)** KS-21-8, **(C)** KS-21-11, **(D)** KH-20-9. Maps were made in Spyder (Python 3.7) using Natural Earth data. Free vector and raster map data was obtained from @ naturalearthdata.com. The hollow circles represent the sampling stations. Please note that the colors of hollow circles here were not used to distinguish the cruises. Colors of the background represent current speeds and arrows represent current velocity vectors on the sea surface (5-day mean of **(A)** May 10–14, 2018; **(B)** May 17–21, 2021; **(C)** June 17–21, 2021; **(D)** September 20–24, 2020) from Ocean Surface Current Analysis Real-time (OSCAR) data (ESR, 2009; https://podaac.jpl.nasa.gov/Data hosted and openly shared by the PO.DAAC, without restriction, in accordance with NASA's Earth Science program Data and Information Policy). The position of Kuroshio axes was also estimated from OSCAR data, based on the method in Ambe et al. (2004).

information from the mature stages and reproductive early life stages of the target fishes.

To further test the "barrier effect" of the Kuroshio, this study analyzed the differences in small pelagic fish distribution between the inshore and the offshore side of the Kuroshio using the samples of KS-21-11 and KH-20-9 because those cruises crossed the Kuroshio at the southern coast of Japan (the detailed method is shown in Section 2.7). Because these two cruises took place at different places and in different seasons, they were not pooled but analyzed separately.

The detailed water sampling methods of all cruises were as follows. In the KS-18-5 (19 stations, Figure 2A), water samples were collected from 13 depths (0, 5, 10, 15, 25, 30, 50, 80, 100, 125, 150, 200, and 300 m). In the KS-21-8 (eight stations, Figure 2B) and KS-21-11 (nine stations, Figure 2C), water samples were collected from seven depths (0, 10, 30, 50, 100, 150, and 200 m). At the KH-20-9 (32 stations, Figure 2D), water samples were collected at 10, 50, 100, and 150 m. Surface water samples (0 m depth) were collected using a clean bucket. Deeper water samples were collected using Niskin bottles combined with a CTD system that accurately determined the sampling depth and recorded environmental data. Sea water samples from each depth at each station were transferred to a clean plastic bag (Rontainer, Sekisui Chemical Co., Ltd., Tokyo, Japan) that had been rinsed three times with the sampled water. Each sample (~7 L in the KS-18-5 and ~10 L in the KS-21-8, KS-21-11, and KH-20-9) was weighed and then immediately filtered according to a previously described method (Yu et al., 2022). Sterivex-GP pressure filter units (0.22 µm pore size in the KS-18-5 and 0.45 µm pore size in the other cruises; Merck Millipore, Burlington, MA, USA) were used. Each filter unit has an inlet and an outlet (Wong et al., 2020). When the water filtration was finished, the interior of each filter unit was immediately filled with RNAlater (Thermo Fisher Scientific, Waltham, MA, USA) using a disposable syringe from the inlet and kept in a -30°C freezer before the next step to avoid DNA degradation. In addition to sea water samples, we also filtered negative controls on board (two 1.5 L Milli-Q water samples and two 10 L freshwater samples).

2.2 The eDNA extraction and purification

For the KS-18-5 samples, eDNA extraction and purification were performed by the Bioengineering Lab. Co., Ltd. (Kanagawa, Japan) using the procedure based on a previously described protocol (Miya et al., 2015), details of which have been previously described (Yu et al., 2022). For samples collected in the KS-21-8, KS-21-11, and KH-20-9, eDNA extraction and purification were performed using an in-house protocol described by Wong et al. (2020). Prior to extraction and purification, the equipment (silicon tubes, connectors, etc.) was treated with 1% bleach and rinsed with Milli-Q water to prevent contamination. Before each extraction, the Sterivex filter units were removed from the freezer and kept on ice to thaw the RNAlater which was then removed from the outlet by aspiration. A 2 mL lysis buffer mix (PBS 990 µL, Buffer AL 910 µL, Proteinase K 100 µL) was introduced through the outlet using a 2.5 mL syringe (Terumo Corporation, Tokyo, Japan). The outlet and inlet of each Sterivex filter unit were sealed, and all Sterivex filter units were incubated at 56°C for 30 min. After incubation, each Sterivex filter unit was centrifuged to collect the lysate, and the DNA in the lysate was extracted using the DNeasy Blood and Tissue Kit. For each column, we twice eluted the DNA with 75 µL of AE buffer to obtain a 150 µL DNA sample from each Sterivex filter unit.

2.3 The qPCR assays

Real-time qPCR assays were performed to measure the eDNA of six small pelagic fishes: sardine, anchovy, chub mackerel, blue mackerel, jack mackerel, and saury (Wong et al., 2022). Detailed sequence information for the primers and probes is listed in Table S2. In short, each multiplex real-time PCR reaction system (10 µL) included 1x Takara probe qPCR mix (Takara), 1x ROX reference Dye, 1 µg/µL BSA (A4161, Sigma-Aldrich), 0.8 µM forward and reverse primers for two species, 0.25 µM fluorescent probes for two species, and 2.5 µl of eDNA template. qPCR reactions were performed using an ABI 7900HT real-time PCR system (Thermo Fisher Scientific). The reactions entailed activation at 50°C for 2 min, denaturation at 95°C for 10 min, and then 50 cycles of denaturation at 95°C for 15 s and annealing and extension at 65°C for 1 min. All samples were assayed in duplicate.

We used qPCR assays to quantify the eDNA of the six small pelagic fishes in all sea water samples and negative controls (Wong et al., 2022). The plasmids of the six small pelagic fishes were used as the standard samples for the qPCR assays. Plasmids were diluted to a series of standard samples that contained 10^1–10^7 copies of DNA molecules per 2.5 µl. During each qPCR assay, the Sequence Detection System Software v2.4.1 (SDS2.4) in the ABI 7900HT real-time PCR system recorded the Ct value in each eDNA sample (sea water sample or negative control) as well as the standard sample. The standard curve for each qPCR assay was determined using SDS 2.4, based on the Ct values and DNA copy numbers of standard samples. Then, the eDNA quantity (copy number per microliter) of each fish species in each eDNA sample was calculated using SDS 2.4, based on the Ct value in each eDNA sample and the standard curve. The quantity of eDNA was normalized against the volume of each filtered water sample. As shown in the Results (Section 3.1), no eDNA was detected from any negative control, therefore we assumed that there was no eDNA signal noise caused by contamination in this study. Consequently, when the eDNA quantity of one fish species in a sample was greater than 0, this species was judged to be present. In contrast, we used a normalized eDNA quantity (copy number per microliter) to represent the fish quantity at each sampling position (Takahara et al., 2012; Rourke et al., 2021; Everts et al., 2022). As the detection of saury and jack mackerel was very limited among our samples (Table S3), we chose sardine, anchovy, chub and blue mackerel as our target fishes for the following analyses.

2.4 Environmental data collection

Sea water temperature, salinity, dissolved oxygen concentration, and chlorophyll-a concentration were collected at every 1 m depth

using a CTD system during sea water sampling (Table S4). Before the analysis, the chlorophyll-a concentration data were naturally log-transformed (as listed in Table S4, the lowest chlorophyll-a concentration value we recorded was 0.007 mg/m^3 with no data for which the chlorophyll-a concentration value was zero).

The sea water temperature and salinity data were treated with a Gaussian filter (Gaussian sigma = 2.5, width = 11; performed by scipy.ndimage.gaussian_filter1d in Python 3.7) to eliminate instrument noise. Then, the temperature and salinity gradients were calculated from temperature data after Gaussian filtering (T) and salinity after Gaussian filtering (S) within a 10 m depth range. For example, the temperature and salinity gradients at a depth of 5 m were calculated as follows:

$$Temperature\ gradient_{5\,m}=(T_{10\,m}-T_{0\,m})/10\ m$$

$$Salinity\ gradient_{5\,m}=(S_{10\,m}-S_{0\,m})/10\ m$$

2.5 Generalized additive model

We used the Generalized additive model (GAM) to study the influence of environmental factors on the spatial distribution of the target fishes (presence/absence or quantity of eDNA). As explained in Section 2.1, for the GAM analyses in this study, data collected during the May–June cruises (KS-18-5, KS-21-8, and KS-21-11) were selected to prevent the effects of seasonal variability. At station D01 of the KS-21-11 cruise, the measurement of environmental factors failed because of sensor malfunction in the CTD. Thus, the D01 samples were not included in the analysis, and the data of the remaining 351 samples (from KS-18-5, KS-21-8, and KS-21-11) were included in the GAM analyses.

First, we used the GAM to investigate the influence of the six CTD-measured environmental factors (sea water temperature, temperature gradient, salinity, salinity gradient, dissolved oxygen concentration, and chlorophyll-a concentration) on the spatial distribution of the target fishes, which we referred to as the first GAM. Before the first GAM, we confirmed that collinearity did not occur among the six environmental factors using the Variance Inflation Factor method (VIF), calculated by the calculate_vif tool in Python 3.7. The depth (pressure) data were also measured by the CTD. However, many characteristics of sea water in the ocean, such as temperature, salinity, and dissolved oxygen concentration, change greatly with the depth (Webb, 2019). We also tested the collinearity when including depth in the environmental factors, and the results showed depth has the highest VIF value (~4.64) which suggested the collinearity between depth and other factors. Therefore, depth was not included in the list of environmental factors for GAM analysis.

Considering that mackerel (chub and blue) are piscivorous fishes (Robert et al., 2010) whose main prey are anchovy (Nakatsuka et al., 2010; Robert et al., 2010), we performed the second GAM to investigate their spatial distribution. Thus, the second GAM included anchovy and sardine quantities (both eDNA quantities) rather than the chlorophyll-a concentration as the food factor (i.e., the explanatory variable list included sea water temperature, salinity, temperature gradient, salinity gradient, dissolved oxygen concentration, and sardine and anchovy quantities). Using the VIF method, we also confirmed that collinearity did not occur among these environmental factors.

To perform the GAM analyses, we used pyGAM tools in Python 3.7 which use models to relate the predictor variables to the expected value of the dependent variable in the form shown below.

$$g(E[y|X]) = \beta_0 + f_1(X_1) + f_2(X_2) + \ldots + f_n(X_n)$$

$X.T = [X_1, X_2,\ldots,X_n]$ are the independent variables, y is the dependent variable, and $g()$ is the link function that relates our predictor variables to the expected value of the dependent variable. The $f_i()$ and feature functions were built using several penalized B-splines (six in this study). The pyGAM tools also judged the significance of each feature function, which suggested the significance of the effect of independent variables on dependent variable. In the first GAM, independent variables were sea water temperature (°C), salinity (PSU), temperature gradient (°C/m), salinity gradient (PSU/m), dissolved oxygen concentration (mL/L), and natural logarithmic transformed chlorophyll-a concentration (mg/m^3). In the second GAM, independent variables were sea water temperature, salinity, temperature gradient, salinity gradient, dissolved oxygen concentration, and natural logarithmic transformed sardine and anchovy eDNA quantities. The predictor variable was the presence/absence or eDNA quantity of the target fishes. When examining the influence of environmental factors on the presence/absence of the four target fishes, we used PyGAM.LogisticGAM (n_splines = 6) in which the link function $g()$ is a logit link and binomial error distribution was assumed. Therefore, the model was structured as follows.

$$log(\frac{P(y=1|X)}{P(y=0|X)}) = \beta_0 + f_1(X_1) + f_2(X_2) + \cdots + f_n(X_n)$$

When examining the influence of environmental factors on the eDNA quantity of the four target fishes, we used PyGAM.LinearGAM (n_splines = 6) in which the link function $g()$ is an identity link, normal error distribution was assumed, and only samples where the target fish eDNA quantity was >0 were included. The model was structured as shown below.

$$E[y|X] = \beta_0 + f_1(X_1) + f_2(X_2) + \cdots + f_n(X_n)$$

The fish eDNA quantity was logarithmically transformed before the GAM analyses. The GAM model with the lowest AICc (small-sample corrected Akaike Information Criterion) value was selected as the optimal model in the GAM analyses.

2.6 Temperature preference index analysis

The temperature preference index (TPI; Lluch-Belda et al., 1991) was used to evaluate how the spatial distribution of the target fishes (based on the presence/absence or eDNA quantity) actually varied among places with different sea water temperatures.

If the effects of temperature are dominant, the TPI and temperature effects derived from the GAM are expected to show similar trends. To calculate the TPI, we divided the eDNA samples in this study into different temperature range groups (according to the CTD-measured temperature, groups were set every 2°C to ensure at least two samples per group). Then, for each target fish, the TPI of fish presence/absence ($TPI_{(0/1)}$) and fish eDNA quantity ($TPI_{(q)}$) in a specified temperature range was calculated as shown below.

$$TPI_{(0/1)}=\frac{N_1(T_{lower}\sim T_{upper})/\sum N_1}{\{N_0(T_{lower}\sim T_{upper})+N_1(T_{lower}\sim T_{upper})\}/(\sum N_0+\sum N_1)}$$

$$TPI_{(q)}=\frac{\sum_{T_{lower}}^{T_{upper}} q_{DNA}/\sum q_{DNA}}{\{N_0(T_{lower}\sim T_{upper})+N_1(T_{lower}\sim T_{upper})\}/(\sum N_0+\sum N_1)}$$

where N_1 (N_0) means the number of samples with presence (absence) (of the given target species) within a temperature range between T_{lower} and T_{upper}. q_{DNA} means the DNA quantity (of the given target species). The numerator represents relative frequency of presence or DNA quantity within the specific temperature range and the denominator represents relative sampling effort. Therefore, a TPI >1 indicated the possibility that the target fish preferred that temperature range, while a TPI<1 indicated the opposite.

2.7 Analyses for the influence of the Kuroshio

The KS-21-11 and KH-20-9 cruises transected the Kuroshio Current (Figures 2C, D), and we investigated the influence of this current on the distribution of target fishes using samples collected from the above cruises. We compared the presence percentage of each target fish between samples collected on the offshore and inshore sides (the inshore side included the Kuroshio axis in this study). This axis represents the locally strongest part of the sea surface velocity field which was estimated based on the method introduced in Ambe et al. (2004). The percentage of samples present was calculated for either inshore side or offshore of KS-21-11 or KH-20-9, as well as for each station.

The percentage of samples at, for example, sardine on inshore side samples in the KS-21-11 cruise ($R_{KS-21-11-IN-sardine}$) was calculated as shown below.

$$R_{KS-21-11-IN-sardine}=\frac{number\ of\ samples\ in\ which\ sardine\ presented}{number\ of\ inshore\ side\ samples\ in\ KS-21-11}*100\%$$

The percentage of samples at, for example, station A02 of the sardine ($R_{A02-sardine}$) was calculated as shown below.

$$R_{A02-sardine}=\frac{number\ of\ samples\ in\ which\ sardine\ presented}{samples\ number\ in\ A02\ station}*100\%$$

2.8 Ethics approval statement

This study did not involve any live animal experiments.

3 Results

3.1 qPCR assay results for six small pelagic fishes

Our qPCR assays did not detect any small pelagic fish eDNA in the negative controls (Milli-Q water and fresh water). Among the 488 sea water samples, chub mackerel eDNA was detected in 118 samples (24.18% of all samples), blue mackerel in 53 samples (10.86%), anchovy in 115 samples (23.57%), saury in 2 samples (0.41%), sardine in 184 samples (37.70%), and jack mackerel eDNA was detected in 15 water samples (3.07%). Detailed results of the qPCR assays are listed in Tables S3 and S5. As saury and jack mackerel showed limited distribution (<5%, Table S3), we excluded them from the analysis. The eDNA quantity vertical distributions of each species are shown in Figures 3 and S1–S9. DNA from the four target fishes was detected from water samples taken at various depths (Figures 3, 4) and horizontal locations (Figures 5, S10–13), but samples containing high eDNA quantities were mostly located above 50 m depth (Figure 4). As for the horizontal distribution in different depth layers, the eDNA of all target fishes were more abundant in the ocean area around the Boso Peninsula, especially in the water layer above 50 m depth (Figures S10, 11). A large number of chub mackerel eDNA was also located close to the Kii Peninsula and Shikoku (Figures S10–13). Generally, the eDNA of target fishes are more common in the inshore (northern) side than the offshore (southern) side of the Kuroshio axis (the Kuroshio Extension) (Figures S3–S9 and 3).

3.2 Environmental effects on target fish distribution revealed by the first GAM

For the first GAM, which included six CTD-measured environmental factors as explanatory variables, the optimal models for the presence/absence and quantity of the four target fishes (fish quantity was represented by the eDNA quantity) are summarized in Table 1. The partial dependence functions of the explanatory variables that had a significant effect ($p<0.05$, judged by pyGAM tools, same in the following) in the optimal models are listed in Figures S14–S21.

Each optimal model included different environmental factors, but only sea water temperature (ranging from 4.5 to 26.5°C here) was included in the optimal models for the presence/absence and quantity of all target fishes (Table 1). Moreover, the effects of temperature were significant in most optimal models except for presence/absence of blue mackerel. Temperature gradient was included in the optimal models for the presence/absence of blue mackerel, and the quantity of anchovy and chub mackerel. Salinity was included in all optimal models except those for the quantity of anchovy and blue mackerel. Salinity gradient was only significant for the quantity of blue mackerel. Chlorophyll-a concentration was included in all optimal models except those for the presence/absence of chub mackerel or the quantity of blue mackerel. Dissolved oxygen concentration was included in all optimal

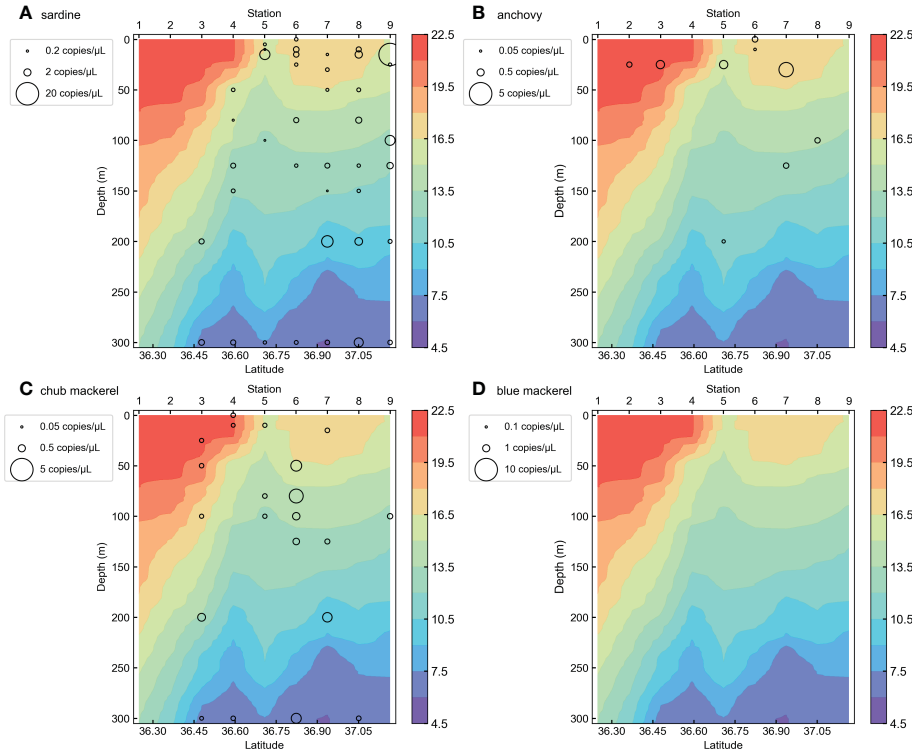

FIGURE 3
The vertical distribution section of target fish eDNA quantities in KS-18-5 Line-1 for **(A)** sardine, **(B)** anchovy, **(C)** chub mackerel, and **(D)** blue mackerel. The colors of the background represent sea water temperature recorded during the sampling.

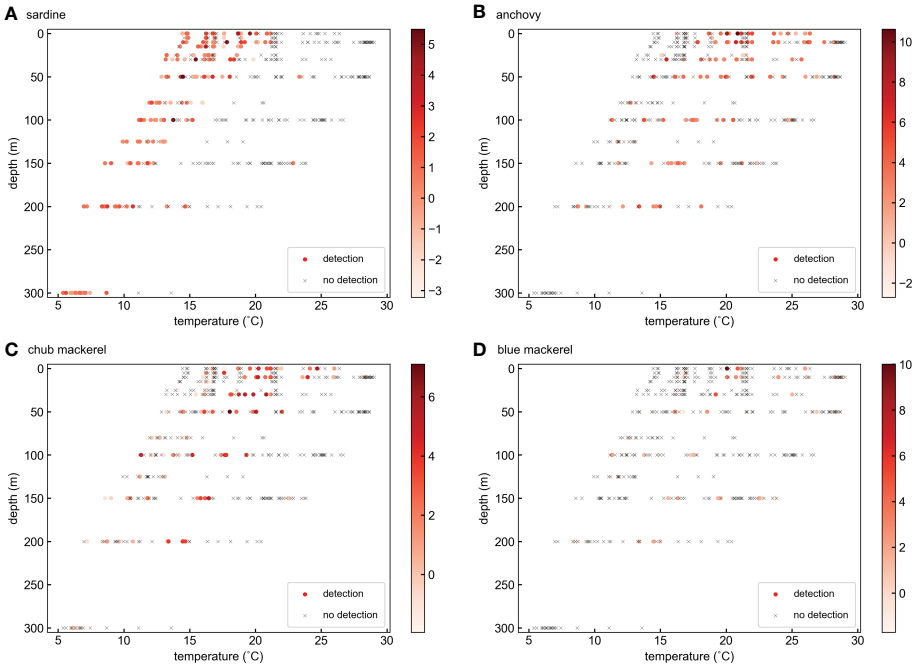

FIGURE 4
Distribution of target fish DNA at different water temperatures and depths for **(A)** sardine, **(B)** anchovy, **(C)** chub mackerel, and **(D)** blue mackerel. The colors of 'O' markers represent the ln(x) transformed target fish eDNA quantity. The 'x' marks represent the samples in which target fish eDNA was not detected.

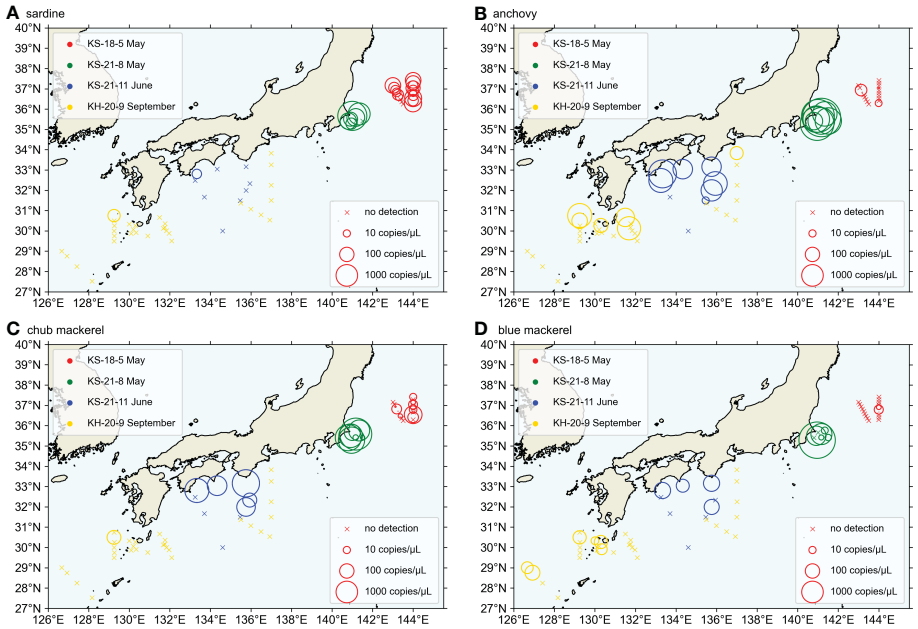

FIGURE 5
The horizontal distribution of target fish abundance above 60 m depth, represented by eDNA quantity for **(A)** sardine, **(B)** anchovy, **(C)** chub mackerel, and **(D)** blue mackerel. The abundance above 60 m depth was calculated as the depth-weighted sum of eDNA quantity, like $quantity_{0m}$*5 +$quantity_{10m}$*15 + $quantity_{30m}$*20 + $quantity_{50m}$*20. The sizes of 'O' markers represent the target fish eDNA quantity. The 'x' marks represent the locations where target fish eDNA was not detected. The stations from different cruises were distinguished by the colors of the 'O' and 'x' marks.

models except those for the presence/absence of sardine and blue mackerel.

Sea temperature showed the most prevalent and significant effect compared to other environmental factors analyzed here. A temperature of 5–12°C had a positive effect on the presence of sardine, whose quantity reached a maximum at 12–21°C (Figures 6A, B). For anchovy, the presence possibility increased as the temperature increased, and the maximum quantity was observed at 21°C (Figures 6C, D). For chub mackerel, the maximum was reached at 19°C, regardless of its presence or quantity (Figures 6E, F). For blue mackerel, both the presence possibility and quantity always increased as temperature increased (Figures 6G, H).

Lower salinity generally correlated with an increase of presence or quantity of fishes (Figures S14-S16, S18, S20). Higher chlorophyll-a concentration also correlated with the increase of the presence and quantity of sardine and the quantity of anchovy (Figures S14, S18, S19), whereas it did not show any systematic tendency for the presence of anchovy and blue mackerel and quantity of chub mackerel. Lower dissolved oxygen concentration showed the increase of the presence or quantity of fishes (Figures S15, S16, S18, S20). Stronger salinity gradient showed the quantity increase of blue mackerel (Figure S21).

3.3 Temperature preference indexes of target fish distribution

Given the broad and significant effects of temperature found by the GAM analyses, we further calculated the temperature preference

TABLE 1 The optimal GAM models (derived from the first GAM) showing how environmental factors influence the distribution of each target fish.

	temperature	temperature gradient	salinity	salinity gradient	ln(chl)	oxygen	pseudo R^2
sardine-0/1	***	–	**	O	***	-	0.4401
anchovy-0/1	***	–	**	–	*	***	0.3756
chub mackerel-0/1	**	–	***	O	–	***	0.1204
blue mackerel-0/1	O	**	O	O	***	-	0.1901
ln(sardine)	*	–	**	–	*	**	0.1211
ln(anchovy)	*	O	–	–	***	O	0.3831
ln(chub mackerel)	***	***	**	–	**	*	0.6314
ln(blue mackerel)	*	-	-	***	-	O	0.6273

'*fish name*-0/1' refers to the absence (value = 0) or presence (value = 1) of this fish. 'ln(*fish name*)' refers to the ln(x) transformed OceanDNA quantity of this fish. '*' marks and 'O' represent the significance of the influence from each factor; '***' means p< 0.001, '**' means p< 0.01, '*' means p< 0.05, 'O' means p ≥ 0.05. '-' means this factor was not included in the optimal GAM model.

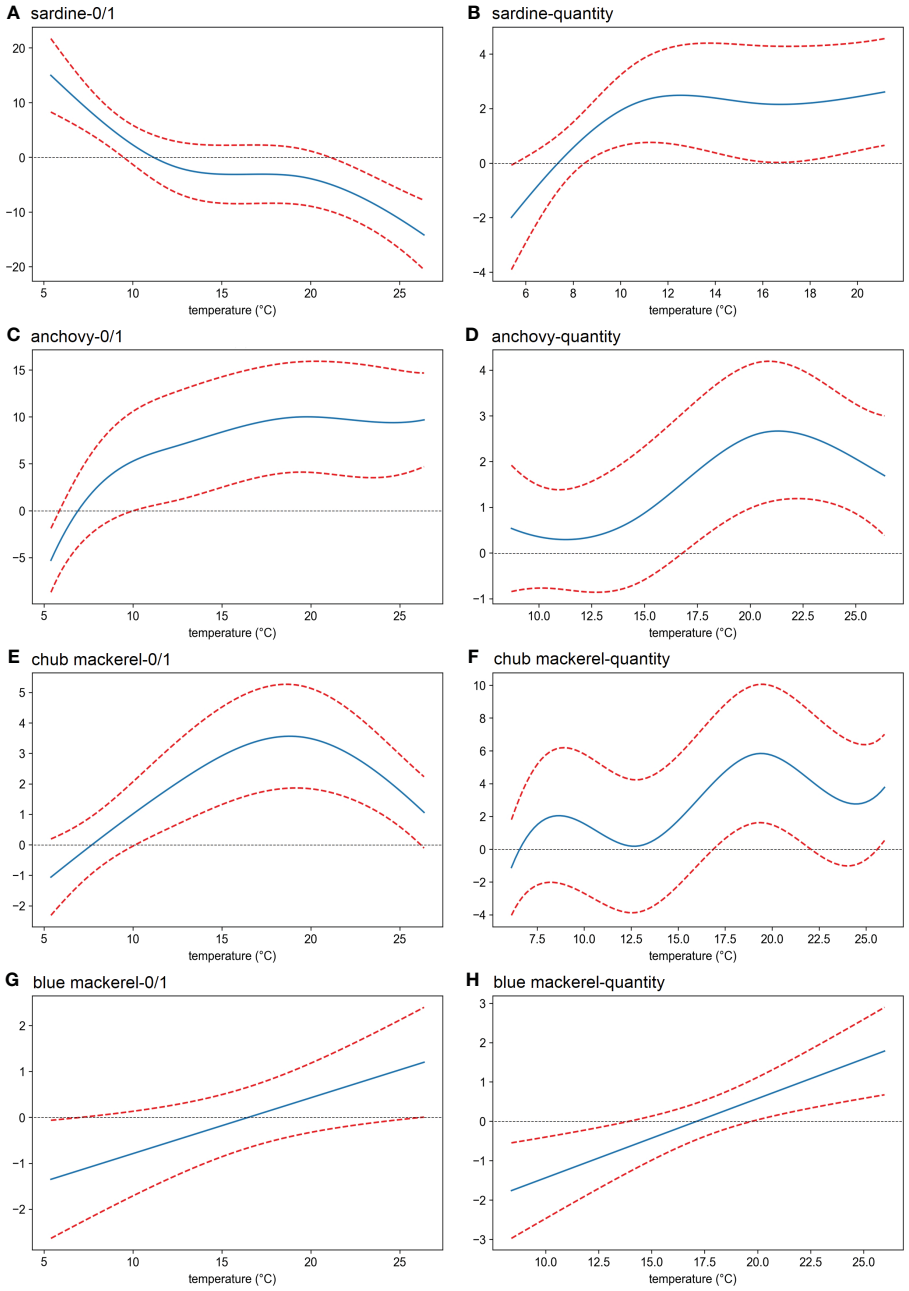

FIGURE 6
Effects (derived from the first GAM) of sea water temperature on the presence/absence **(A, C, E, G)** and the eDNA quantity **(B, D, F, H)** of four target fish. The x-axis shows the value of the explanatory variable (temperature), and the y-axis shows the contribution of the explanatory variable to the fitted values: presence/absence and eDNA quantity of **(A, B)** sardine (*Sardinops melanostictus*), **(C, D)** anchovy (*Engraulis japonicus*), **(E, F)** chub mackerel (*Scomber japonicus*), **(G, H)** blue mackerel (*Scomber australasicus*). The area between the two red dotted lines represents the 95% confidence intervals.

indices of the presence/absence and quantity of each target fish (Figures S27, S28). In the presence of sardine, the TPI was >1 at 4.5–18.5°C, decreasing as the temperature decreased (Figure S27A). In contrast, the preference index increased as the temperature increased in the presence of anchovy (>1 at 18.5–26.5°C, Figure S27B) and blue mackerel (>1 at 16.5–26.5°C, Figure S27D). For the presence of chub mackerel, the TPI had no obvious regularity with temperature change (Figure S27C).

For the quantity of sardine and anchovy the TPI was >1 at 12.5–20.5°C and 18.5–22.5°C, respectively (Figures S28A, B). For the

quantity of chub mackerel, the TPI was >1 at 16.5–20.5°C and 22.5–26.5°C (Figure S28C). For the quantity of blue mackerel, the TPI was >1 at 18.5–20.5°C (Figure S28D).

3.4 Environmental effects on the distribution of mackerel revealed by the second GAM

For the second GAM, where we replaced chlorophyll-a concentrations in the explanatory variable list with sardine and anchovy quantities, the optimal models for the presence/absence and quantity of mackerel are summarized in Table 2. The partial dependence functions of the explanatory variables that had significant effects in the optimal models are listed in Figures S22–S25.

Compared with the first GAM, the optimal models of the second GAM showed a higher fitting (higher pseudo R^2). The quantity of anchovy and sardine was included in most of the optimal models (Table 2), where the former had significant effects in all optimal models for both chub and blue mackerel (Table 2). Sardine quantity also had significant effects in the optimal models of the presence/absence of the two mackerel (Table 2) but was excluded from the optimal models of blue mackerel quantity, and its effect on chub mackerel quantity was not significant.

For chub mackerel, the presence possibility increased with an increase in either sardine or anchovy quantities (Figures 7A, C). In the case of chub mackerel quantity, the effect of the quantity of sardine and anchovy was more complex (Figures 7B, D). The chub mackerel quantity appeared to increase with an increase in sardine quantity, but the dependency on anchovy quantity had the maximum when anchovy quantity was around 20 copies/μL. In the case of the combined effect of sardine and anchovy quantities, the chub mackerel quantity maximum appeared when the anchovy and sardine eDNA quantity was 20 and 150 copies/μL, respectively (Figure S26). The possibility and quantity of blue mackerel increased with anchovy quantity (Figures 7F, G).

3.5 Distribution difference of target fishes between the inshore and offshore sides of the Kuroshio

In both KS-21-11 and KH-20-9, the average presence percentages of each target fish were higher at the inshore stations (including those on the Kuroshio axis) than the offshore stations (Tables 3, S6). In KS-21-11, the average presence percentage of anchovy was 85.7 and 4.8% among inshore and offshore stations, respectively. In KH-20-9, the average presence percentage of anchovy was 25.0 and 0.0% among inshore and offshore stations, respectively. In the case of blue mackerel, the average presence percentage was 16.7% in KS-21-11 inshore stations, 0.0% in KS-21-11 offshore stations, 21.4% in KH-20-9 offshore stations, and 2.8% in KH-20-9 offshore stations. Moreover, sardine and chub mackerel were only detected at the inshore stations. The Student's *t*-test results confirmed the significant difference between the presence percentage of inshore and offshore stations ($p< 0.0001$, the presence sample percentage data were normally distributed in both KS-21-11 and KH-20-9 samples).

4 Discussion

Here, we analyzed the environment-dependent distribution of four small pelagic fishes in the Kuroshio Current system based on eDNA data, the first study of its kind to our knowledge. By measuring fish eDNA quantity in sea water samples using qPCR, we obtained information on the spatial distribution of the target fishes in this system. We then analyzed the influence of each environmental factor on the target fish distribution, mainly using GAM and preference index analyses. In this section, we discuss our findings and potential limitations of the above analyses.

4.1 The environment-dependent small pelagic fish distribution pattern in the May–June Kuroshio current system

The optimal models produced by the first GAM, revealed how six CTD-measured environmental factors influenced the distribution of four targeted small pelagic fishes (Table 1; Figures S14–21). To simplify the description, we only consider the significant effects on fish occurrence here. The optimal environmental range for sardine to occur included temperature< 12°C, salinity< 34.8 PSU, and chlorophyll-a concentration > 0.14 mg/m^3. The optimal environmental range for sardine quantity included temperature > 8°C, salinity< 33.9 PSU, and chlorophyll-a concentration > 0.37 mg/m^3. As a result, the optimal environmental range for sardine is regarded as temperature

TABLE 2 The optimal GAM models (derived from the second GAM) showing how environmental factors influence the distribution of mackerels.

	temperature	temperature gradient	salinity	salinity gradient	oxygen	ln (sardine)	ln (anchovy)	pseudo R^2
chub mackerel-0/1	-	-	-	○	○	***	***	0.2022
ln(chub mackerel)	*	○	○	–	○	○	***	0.6771
blue mackerel-0/1	-	–	–	–	○	*	***	0.3066
ln(blue mackerel)	○	-	-	***	-	-	**	0.7198

'*fish name*-0/1' refers to the absence (value = 0) or presence (value = 1) of this fish. 'ln(*fish name*)' refers to the ln(x) transformed OceanDNA quantity of this fish. '*' marks and '○' represent the significance of the influence from each factor; '***' means $p< 0.001$, '**' means $p< 0.01$, '*' means $p< 0.05$, '○' means $p \geq 0.05$. '-' means this factor was not included in the optimal GAM model.

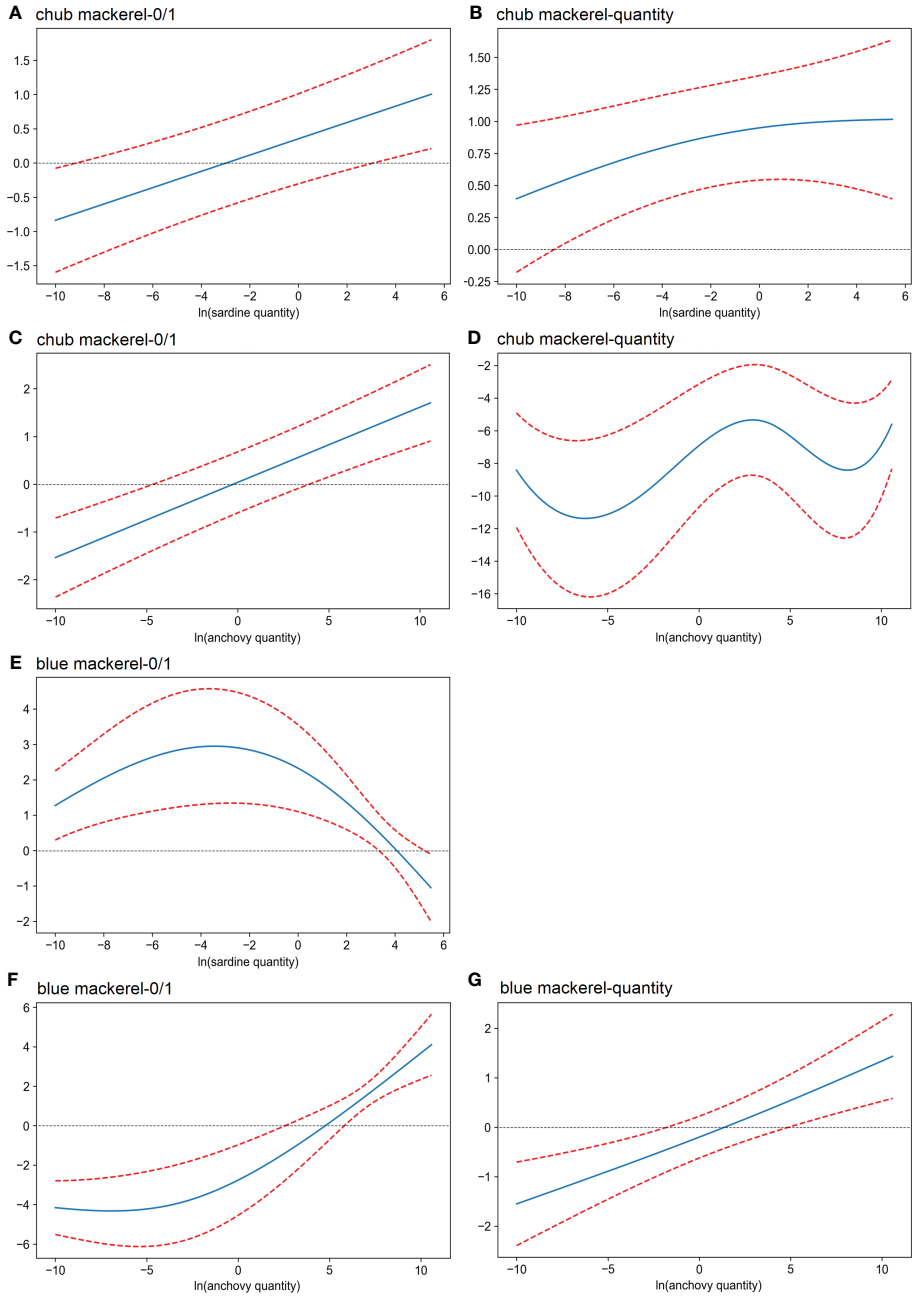

FIGURE 7
Effects (derived from the second GAM) of the quantity of sardine and anchovy on the presence/absence **(A, C, E, F)** and the eDNA quantity **(B, D, G)** of mackerel. The x-axis shows the value of the explanatory variables: **(A, B, E)** ln(x) transformed sardine quantity; **(C, D, F, G)** ln(x) transformed anchovy quantity. The y-axis shows the contribution of the explanatory variable to the fitted values: **(A, C)** presence/absence of chub mackerel; **(E, F)** presence/absence of blue mackerel; **(B, D)** ln(x) transformed chub mackerel quantity; **(G)** ln(x) transformed blue mackerel quantity. The area between the two red dotted lines represents the 95% confidence intervals.

between 8 and 12°C, salinity< 33.9 PSU, and chlorophyll-a concentration > 0.37mg/m^3. The optimal environmental range for anchovy to occur included temperature > 6.5°C, salinity< 33.9 PSU, and oxygen concentration< 4.2mL/L. The optimal environmental range for anchovy quantity included temperature > 15.0°C and chlorophyll-a concentration > 1.9 mg/m^3. As a result, the optimal environmental range for anchovy is regarded as temperature > 15°C, salinity< 33.9 PSU, and chlorophyll-a concentration > 1.9 mg/m^3.

Catch data in the Sea of Japan also indicated the influence of SST and primary production on sardines (Muko et al., 2018). The CPUE distribution in the Yellow and East China Seas was found to be influenced by SST and sea surface salinity (SSS; Liu et al., 2020). A comparison of larval and juvenile growth in the Northwest Pacific showed clear dependency on prey availability for sardine growth but not for that of anchovy, whereas growth of both sardine and anchovy also depended on temperature (Takahashi et al., 2009). Those results are consistent with eDNA derived information on

TABLE 3 The presence sample percentages at inshore (including the Kuroshio axis) and offshore sides of the Kuroshio.

		sardine	anchovy	chub mackerel	blue mackerel
KS-21-11	inshore side	4.8% (0.0~28.6%)	85.7% (57.1~100.0%)	64.3% (0.0~100.0%)	16.7% (0.0~42.9%)
	offshore side	0.0% (0.0%)	4.8% (0~14.3%)	0.0% (0.0%)	0.0% (0.0%)
KH-20-9	inshore side	3.6% (0.0~25.0%)	25.0% (0.0~100.0%)	5.4% (0.0~25.0%)	21.4% (0.0~25.0%)
	offshore side	0.0% (0.0%)	0.0% (0.0%)	0.0% (0.0%)	2.8% (0.0~25.0%)

The table listed ratio of detection in each region (inshore side or offshore side). Ratios in brackets indicate range of the ratio at each station.

environmental dependency. The eDNA sampling is relatively simple and enables high horizontal and vertical resolution fish distribution observation corresponding to the environment. Our results support the possibility of using eDNA to better understand the relationship between fish species distribution and environments.

4.2 The role of sea water temperature in target fish distribution

For sardine and anchovy, significant effects of sea water temperature on the occurrence and quantity of eDNA were revealed (Table 1). Moreover, as temperature-dependent patterns derived from GAM and TPI analyses were always similar (e.g., Figures 6A vs. S27A; 6C vs. S27B), it can be concluded that sea water temperature was a decisive factor influencing the distribution of sardine and anchovy in the Kuroshio Current system. In addition, our results showed the different temperature preferences where anchovies preferred warm water while sardines preferred cooler environments.

Differences in temperature preferences of sardine and anchovy have been noted in previous studies, and a hypothesis on the different temperature responses to explain the alternations between the two species was proposed (Takasuka et al., 2007; Takasuka et al., 2008b; Itoh et al., 2009). For example, otolith analysis by Takasuka et al. (2007) showed that anchovy and sardine larvae had the highest growth rate at 22.0 and 16.2°C, respectively. They also found that the preferred spawning temperatures of the two species (Takasuka et al., 2008b) had the same temperature dependence difference. As GAM analyses decomposed and inspected the contribution of each feature, our study supported this hypothesis by providing clearer evidence for the effects of temperature on the distribution of sardine and anchovy.

For chub and blue mackerel, researchers have also studied the relationship between temperature and their distribution. For example, larval sampling in the southern East China Sea by Sassa and Tsukamoto (2010) showed that the habitat temperature range of blue mackerel larvae was higher and narrower than that of chub mackerel, which was consistent with the distribution pattern revealed when sardine and anchovy quantity information was not considered (Figures 6E vs. 6G; 6F vs. 6H). However, our results suggest that the influence of temperature on the distribution of mackerel is less decisive. Although the GAM and TPI analyses for blue mackerel occurrence showed similar trends (Figure 6G vs. S27D), this temperature effect was not significant (Table 1). Moreover, for blue mackerel quantity as well as chub mackerel occurrence, the GAM and TPI analyses did not find the same temperature-dependent pattern. Thus, we speculated that temperature may not be the most important factor in determining the mackerel distribution—other factors are also involved, such as the anchovy and sardine quantity effects which will be discussed further in the next section (Section 4.3). In fact, the results of our study have revealed that the temperature is less effective in determining mackerel distribution when sardine and anchovy quantity information is considered (see Section 3.4).

Sea water temperature not only changes with horizontal position but also usually decreases with depth. Therefore, it is possible that the effects of temperature deduced from the GAM included the effects of preferred habitat layer differences among species. Sardine and anchovy have different temperature preferences, as shown in the GAM analysis. Indeed, for the occurrence of these fishes, the vertical distribution pattern deduced from eDNA data (Figure S29) partially revealed a mirrored structure. However, in terms of eDNA quantity, all target fishes were concentrated in the water layer at 0–50 m depth (Figure S30), which did not explain the temperature preference of the target fishes (Figure S28). An earlier study also did not support the hypothesis that sardine and anchovy prefer to stay at different depths (Yatsu et al., 2005). Indeed, the distribution of target fish eDNA on the water temperature and depth plane (Figure 4) revealed the significant temperature effects on the distribution of sardine and anchovy. The occurrence of sardine eDNA was obviously concentrated at cooler temperatures regardless of depth.

However, the temperature range shifts to cooler with depth. Because sardine larvae are distributed mainly in the surface layer shallower than 50 m (Hayashi, 1990; Matsuo et al., 1997), the temperature range shift might reflect the different temperature preferences of sardine in different life stages. Because a high eDNA quantity appeared more often in the layers shallower than 50 m, it follows that it appeared between 14 and 20°C. These characteristics are consistent with the GAM results (Figures 6A, B). The occurrence of anchovy eDNA was mainly distributed in the

warmer temperature range compared with that of sardine in all depth layers (Figure 4B). In addition, the samples with high anchovy eDNA quantities mainly appeared when the water temperature was 21°C above 50 m depth (Figure 4B). These characteristics are also partially consistent with the GAM results (Figures 6C, D). Thus, we suggest that the temperature effects deduced from the GAM analyses mostly reflect the temperature preferences of the target fishes. However, because the eDNA methods are unable to distinguish different body sizes or life stages in the same species, the GAM-deduced temperature effect for one species might be evaluating the overall water temperature preferences of a fish group that includes different life stages. Special caution is needed for this issue, as discussed in Section 4.5.

The fishing catch can provide direct information on fish, including species, abundance, size, and life history. However, the use of scientific fishing surveys has been limited, especially in the open ocean. The research vessels included in this study also did not have equipment such as large nets for fishing. Acoustic sonar, another technology used for fish surveys, can measure fish size and abundance (Medwin and Clay, 1998; Boswell and Wilson, 2011) but cannot accurately distinguish fish species. Moreover, with the prior knowledge from fishing, it is possible to judge the life history stage from fish size. Therefore, in the future survey, we suggest combining the use of eDNA with other methods such as acoustic sonar (and fishing, if possible), to provide more accurate data on small pelagic fish distribution patterns.

4.3 Anchovy and sardine quantity effects on mackerel distribution patterns

Abiotic environmental factors, such as temperature, together with chlorophyll-a concentration (or primary production), have long been used to analyze the distribution patterns and estimate the habitat areas of small pelagic fishes, including chub and blue mackerel (Chen et al., 2009; Li et al., 2014; Lee et al., 2018; Yu et al., 2018). Conversely, although researchers have recognized the piscivorous habits of chub and blue mackerel (Yoon et al., 2008; Robert et al., 2010), prey fish have not yet been considered as influencing factors in their distribution patterns.

Mackerel (chub and blue) are piscivorous fishes (Robert et al., 2010) whose main prey is anchovy (Nakatsuka et al., 2010; Robert et al., 2010). Our results suggest an influence of anchovy and sardine quantity on the distribution patterns of chub and blue mackerel in the Kuroshio Current system. Indeed, abiotic environmental factors, including temperature (Table 2), as well as chlorophyll-a concentration (Table 1), appeared less influential when compared with sardine and anchovy eDNA levels, especially anchovy (Table 2). The results revealed anchovy-dependent patterns in chub and blue mackerel distributions in that as the density of anchovy increased, the possibility of the presence and density of mackerel increased (Figures 7, S26). Based on our data, the estimated blue mackerel quantity (derived from the GAM) increased more than seven times when the anchovy quantity increased from the minimum to the maximum (Figure 7). Higher anchovy quantities also had a positive effect on chub mackerel quantity (Figures 7, S26).

However, eDNA method does not detect the fish size or life stage, and capturing larger mackerel which has high swimming speed is difficult. Indeed, the Shinsei-Maru and Hakuho-Maru research vessels are unable to conduct a large size net survey. Thus, we did not collect any fish body samples. Therefore, direct information about predation, such as the stomach content of mackerels, was not available. However, considering anchovy is the main prey of mackerel (Nakatsuka et al., 2010; Robert et al., 2010), it might be hypothesized that the GAM results indicate prey-predator interaction between anchovy and mackerel. In the offshore waters, between the Kuroshio Extension and Oyashio Front (mixed water region), distribution temperature overlapped between anchovy and chub mackerel in early summer (Fuji et al., 2023), which was confirmed by a surface trawl survey. Nakatsuka et al. (2010) confirmed anchovy in the stomach contents of chub mackerel in the mixed water region. Those results support our hypothesis that mackerel distribution depends on anchovy because mackerel prey on anchovy. However, this is still a hypothesis and there are other possible explanations, such as that the mackerel and anchovy came to the same place to predate on the same kind of zooplankton. Therefore, a future study combining the eDNA survey with a net survey is recommended.

Even if we know the prey-predator relationship, it is difficult to investigate the influence of prey fishes on predator fish distribution because of the lack of distribution data for both these fish types. Studies on the effect of prey fishes on fish distribution have been limited to large predators such as tuna (Schick and Lutcavage, 2009; Lezama-Ochoa et al., 2010) and Spanish mackerel (Liu et al., 2023). Most habitat models for fish distribution have used satellite-derived data that can cover wide spatial-temporal scales. Our results indicate the effectiveness of eDNA in investigating predator–prey overlap and interactions and also suggest that there is a great need to analyze the role of prey fish, seldom thought to be an influence in the distribution of piscivorous fishes (Pepin et al., 1987; Cabral and Murta, 2002; Emmett and Krutzikowsky, 2011). The predator–prey overlap shown by eDNA, combined with the data from other methods like stomach content analysis, can improve the understanding of the relationship between prey fish and the distribution of piscivorous fishes. The collaboration of eDNA with other methods can also help with the study of the diet selectivity of the predator. The typical idea to analyze diet selectivity is to compare diet composition in the stomach content with prey availability (Pine et al., 2005). This analysis needs the distribution of prey species around the predator, which could be more easily obtained by the eDNA method.

4.4 Small pelagic fish distribution differences between inshore and offshore sides of the Kuroshio

In addition to the environmental factors discussed above, this study also tested the “barrier effect” of the Kuroshio on the

distribution of our targeted small pelagic fishes. Our results showed that anchovy, chub mackerel, and blue mackerel were significantly more abundant on the inshore side of the Kuroshio (or on the Kuroshio axis) than on the offshore side (Tables 3, S6). The occurrence of these target fishes decreased suddenly or even disappeared in the offshore side (Tables 3, S6). Despite of its low occurrence, sardine was only detected on the inshore side. Our eDNA sampling indicated the "barrier effect" of the Kuroshio on the distribution of the small pelagic fishes.

The distribution characteristics were consistent with those reported in previous studies. Nishikawa et al. (2022) suggested that the environmental condition (temperature and Chl-a concentration) on the inshore side/axis of the Kuroshio is suitable for sardine and anchovy larvae. It was shown that chub mackerel larvae on the northern (inshore) side of the Kuroshio axis have better growth chances (Higuchi et al., 2019; Sogawa et al., 2019; Guo et al., 2022). The first GAM results showed a lower salinity preference in the presence of sardine, anchovy, and chub mackerel (Figures S14-16) as well as the quantity of sardine and chub mackerel (Figures S18, 20). The inshore side of the Kuroshio axis has lower salinity than the offshore side; therefore, this lower salinity preference tendency corresponds to a higher abundance of the small pelagic fishes in the inshore side of the Kuroshio.

Zooplankton are an important food source for small pelagic fishes; therefore, the different distributions of zooplankton (Watanabe et al., 2002; Miyamoto et al., 2017) on the two sides of the Kuroshio axis could be one of the reasons for the different distributions of fish. For example, Miyamoto et al. (2017) found that in zooplankton samples, copepod abundance was highest in the north-frontal area of the Kuroshio. To clarify whether the different distributions of zooplankton caused the different distributions of fish on the two sides of the Kuroshio axis, a simultaneous and co-located distribution information of fish and zooplankton are needed, which can be provided by the eDNA method. For example, Minegishi et al. (2023) simultaneously measured the spatiotemporal distribution of chum salmon (*Oncorhynchus keta*) eDNA as well as the eDNA of its three zooplankton prey (*Pseudocalanus newmani*, *Eucalanus bungii*, and *Themisto japonica*) in the Otsuchi Bay, using the same water samples. Similarly, by simultaneously measuring the distribution of targeted small pelagic fish and their zooplankton prey (e.g., the species found in fish stomach contents) in the Kuroshio, we expect the eDNA method can be helpful in clarifying the reasons of fish distribution difference between the two sides of the Kuroshio axis. However, the reasons for this difference remain unclear and the possible influence of other factors (such as water current velocity) cannot be ignored, necessitating further research for any possible reasons in the future.

4.5 Seasonal difference of small pelagic fish distribution patterns

The sections above have discussed the environment-dependent distribution patterns of the small pelagic fishes that were observed in this study. Those analyses on the effects of six CTD-measured environmental factors and the potential prey fish on the small pelagic fish distribution were all based on samples from three cruises during May–June (KS-18-5, KS-21-8, and KS-21-11). However, the environmental conditions and the fish distribution in the ocean may vary among different seasons. We wanted to compare the distributional characteristic of the small pelagic fishes in September. But, in KH-20-9, the detection of small pelagic fishes was limited to 2, 16, 3, and 13 for sardine, anchovy, chub and blue mackerel, respectively. The presence data was too few to conduct GAM analyses. Therefore, this study could not evaluate seasonal variability of distributional characteristics of the small pelagic fishes. Especially, September is not active spawning season for the target fishes, which may alter the environmental dependency of the fish distribution. Thus, we need to suggest that the dependency of the small pelagic fish distribution on environments and potential prey fish, we revealed in this study, may only be representative in certain seasons or for fish in certain ontogenetic stages. The comprehensive understanding of the distribution pattern of these fishes requires more study in the future.

4.6 Limitations and challenges of eDNA on fish distribution surveys

Being non-invasive and having low energy consumption (compared with traditional trawling sampling), eDNA methods have been actively used in fish surveys. Even so, as eDNA methods cannot directly observe individual fish, there are several limitations and challenges in eDNA observation for detecting fish distribution.

The first concerns the adequacy of using eDNA quantity to represent fish quantity. Many previous studies have shown notable positive correlations between eDNA concentration and fish biomass or number of individuals in aquarium experiments (Takahara et al., 2012; Doi et al., 2015; Horiuchi et al., 2019). In addition, by comparing eDNA data with data from other survey methods, similar relationships have also been recorded in field surveys in large natural waters (Yamamoto et al., 2016; Minegishi et al., 2019; Salter et al., 2019). For example, Salter et al. (2019) found significantly positive correlations ($p = 0.003$) between the trawl-biomass and eDNA quantity of Atlantic cod (*Gadus morhua*) in oceanic waters around the Faroe Islands. Therefore, the idea to represent fish quantity by eDNA quantity has its rationale. However, because the proportionality coefficient between eDNA concentration and abundance is species-specific, it is not possible to compare the relative abundance of fish species by eDNA concentration. Additional laboratory experiments and field data comparisons are essential for developing methods for estimating fish abundance using eDNA.

The second is the spatio-temporal representativeness of eDNA data. After being released into water, eDNA remains detectable for a while during which time it may move to other places. In one field experiment by Murakami et al. (2019) using caged fish at the sea surface in Maizuru Bay (Kyoto, Japan), it was found that eDNA was only detectable<2 h after release and mostly found within 30 m horizontally and 4 m vertically from the fish cage (Murakami et al., 2019). Other studies also suggested that the spread of eDNA was

limited from the release point both horizontally (O'Donnell et al., 2017; Yamamoto et al., 2016) within 100–150 m and vertically (Yamamoto et al., 2016; Jeunen et al., 2019; Littlefair et al., 2020) within 5–30 m. These studies support the idea that eDNA is swiftly degraded and not advected far from the fish; therefore, we considered that eDNA distributions represent fish distributions. However, since degradation time depends on temperature and species, and the advected distance depends on the current speed, more studies on the degradation and transportation of eDNA are necessary, like those by Tsuji et al. (2017); Saito and Doi (2021), and Murakami et al. (2019). In addition, knowledge regarding eDNA sedimentation is limited. Although the modeling performed by Allan et al. (2021) suggested that settling, as well as other physical processes such as mixing and advection, only caused a 10–20m vertical displacement, more fieldwork data is needed to truly understand the vertical space accuracy of eDNA signals.

Another problem with eDNA methods is the inability to determine whether the DNA originates from a living individual. Thus, carcasses, or even DNA left in predator feces (Parsons et al., 2006; Deagle et al., 2009), may become unexpected eDNA sources and result in false-positive detections. For example, the sardine DNA signals we found in several 300 m water samples (Table S5 and Figure 3A) may have come from the eDNA source that sank from the upper layer. Because of gravity, large carcass pieces or feces sink quickly rather than remaining in a certain water layer, so they are likely to gather at the sea bottom. However, the sea bottom is much deeper than where we collected our samples at most of the stations (e.g., the sea bottom depth of stations in Line 1 is deeper than 5000 m; Table S1), so the large pieces of eDNA on the sea bottom are not likely to contribute to the eDNA of our samples, except for KS-21-8 Lines 3 and 4 and KH-20-9 Line 8. The effect of the sea bottom was not obvious in KS-18-5 Lines 1 and 2. The smaller particles from carcasses or predator feces are also likely to suspend and aggregate in the pycnocline, where the vertical water density gradient is high. However, neither temperature nor salinity gradients were included as significant influencing factors in the optimal GAM models for the eDNA distribution of either sardine or anchovy (Table 1, Figures S14, 15, 18, 19). Indeed, an extremely high eDNA quantity was not detected in the thermocline layer in all the vertical sections. In KS-18-5 Lines 1 and 2, where water samples were collected at 300 m, sardine were detected even at that depth. Because the temperature gradient was not high in the layer (Figures 3, S1), it was difficult to consider the eDNA aggregates there. As mentioned above, sardine larvae are concentrated above 50 m, but there is also a sardine egg record at a depth of 300 m (Hayashi, 1990). Therefore, we could not conclude that the eDNA at 300 m originated from this layer. Prior knowledge of this problem is limited and inconsistent. For example, Kamoroff and Goldberg (2018) found that goldfish (*Carassius auratus*) carcasses in tanks produced detectable eDNA, but less than that from live goldfish. In contrast, Curtis and Larson (2020) found that crayfish (*Procambarus clarkii*) carcasses in streams did not produce any detectable eDNA. Therefore, we did not consider eDNA sources other than those from live fish here, but we suggest that further research is needed on the contribution of fish carcasses or predator feces as eDNA sources, in terms of their transportation in the ocean and how much DNA they produce.

Finally, there is another limitation when performing eDNA analysis on fish rather than on microorganisms. A suitable environment for a fish can vary with its growth and development (Fernández-Corredor et al., 2021), but its eDNA is unable to deliver information on its body size or life stages. Thus, the results of our study may combine the environmental preferences of larvae and adults of the same fish species. As mentioned in Section 4.2, we found that the temperature range preference of sardine appeared to shift to cooler as the depth increased (Figure 4A), whereas the warmer temperature preference of anchovy was not obvious in layers deeper than 100 m (Figure 4B). One possible explanation for this phenomenon is that eDNA signals on the surface mainly originated from larvae and juveniles, while those in deeper layers mainly originated from adult fish, and, in our case, the sardine and anchovy adults were better adapted to lower temperatures than their larvae and juveniles. Previous studies on related species have supported this assumption. For example, Boyra et al. (2016) found that juvenile anchovy (*E. encrasicolus*) in the French sector of the Bay of Biscay moved from above 50 m to 100 m depth or deeper (where it is also much cooler) as they grow. Similarly, as eDNA cannot tell us whether the mackerel were large enough to prey on the anchovy within the same area, we cannot deduce whether the prey-predator relationship actually existed. We can only deduce the relationship between prey fish and the distribution pattern of chub mackerel and blue mackerel based on eDNA data, like we have discussed in Section 4.3. Although the inability to distinguish fish sizes and life history stages limits the accuracy of the fish distribution pattern derived from eDNA data, researchers have not developed a solution for this problem in eDNA methods. Using a newly developed technology called environmental RNA (eRNA), which detects RNA released by organisms into the environment (Cristescu, 2019), it is possible to estimate the physiological status of target organisms (Tsuri et al., 2020). Therefore, combining eRNA with eDNA may be a potential way to distinguish the different life stages of fish. Conversely, as fish catches can provide direct information about their size and life history stages and acoustic sonar is also able to measure fish sizes (Rudstam et al., 1987), combining traditional and mature survey methods such as net sampling and acoustic sonar with eDNA methods may be another feasible solution to upgrade the accuracy of eDNA survey data. However, further efforts are needed to overcome the limitations of eDNA methods for fish surveys.

5 Conclusion

This study researched the environment-dependent distribution patterns of four small pelagic fishes, sardine, anchovy, chub mackerel, and blue mackerel, in the Kuroshio Current system based on eDNA data. The GAM revealed the diverse relationships of target fishes with the environment, which showed the influence of multiple environmental factors, such as sea water temperature, salinity, dissolved oxygen concentration, and chlorophyll-a

concentration. Among the four target fish species, the influence of sea water temperature was especially decisive for the distribution of sardine and anchovy, and the different temperature preferences of sardine and anchovy—that sardine prefers cooler water than anchovy—were supported by the results of this study. Our results suggest the distributions of chub and blue mackerel are highly dependent on anchovy and sardine quantities in the Kuroshio Current system, and we hypothesized that a prey-predator relationship between anchovy and mackerel influenced the mackerel distribution. We emphasized the necessity to consider prey fish effects when investigate piscivorous fish distribution. In addition, the comparison of target fish eDNA data between the two sides of the Kuroshio axis in this study showed the concentrated distribution of all target fishes in the inshore side and confirmed the "barrier effect" of the Kuroshio on the small pelagic fishes.

Data availability statement

The original contributions presented in the study are included in the article/Supplementary Material. Further inquiries can be directed to the corresponding author.

Ethics statement

Ethical review and approval was not required for the animal study because we investigated only enviromental DNA sampled from sea waters.

Author contributions

ZY and S-II contributed to the study conception and design. ZY, S-II, MW, JI, SI, KK, SA and TH curated data. ZY, MW, TH, and SH performed statistical analyses. ZY, S-II, JI, SI, KK, HS and SA participated in the study. S-II, SI, SH and HS administered the study. ZY wrote the first draft of the manuscript. All authors contributed to the manuscript revision and read and approved the submitted version.

Funding

S-II, JP21H04735, and JP22H05030. The Japan Society for the Promotion of Science (JSPS) KAKENHI, https://www.jsps.go.jp/english/. The funders had no role in the study design, data collection and analysis, decision to publish, or manuscript preparation. S-II and SH, The OceanDNA Project, The University of Tokyo Future Society Initiative, https://www.u-tokyo.ac.jp/adm/fsi/ja/projects/sdgs/projects_00103.html. The funders had no role in the study design, data collection and analysis, decision to publish, or manuscript preparation.

Acknowledgments

The OceanDNA survey was conducted by the research vessels Shinsei-Maru and Hakuho-Maru. We thank the captains and all members of the cruises KS-18-5, KS-21-8, KS-21-11, and KH-20-9. We also appreciate the assistance of Dr. Megumi Enomoto in sea water sampling. We express special thanks to Mr. Shinsuke Toyoda, Mr. Hironori Sato, Mr. Yo Watanabe, and Mr. Minoru Kamata of Marine Work Japan for their assistance with the CTD water sampling device. We deeply appreciate the contribution devoted to the observational and analytical support provided by Ms. Kiriko Ikeba.

Conflict of interest

The authors declare that the research was conducted in the absence of any commercial or financial relationships that could be construed as potential conflicts of interest.

Publisher's note

Supplementary material

The Supplementary Material for this article can be found online at: https://www.frontiersin.org/articles/10.3389/fmars.2023.1121088/full#supplementary-material

References

Alheit, J., Licandro, P., Coombs, S., Garcia, A., Giráldez, A., Santamaría, M. T. G., et al. (2014). Reprint of "Atlantic multidecadal oscillation (AMO) modulates dynamics of small pelagic fishes and ecosystem regime shifts in the eastern north and central atlantic". *J. Mar. Syst.* 133, 88–102. doi: 10.1016/j.jmarsys.2014.02.005

Ali, M. A., Gyulai, G., Hidvégi, N., Kerti, B., Al.Hemaid, F. M., Pandey, A. K., et al. (2014). The changing epitome of species identification – DNA barcoding. *Saudi. J. Biol. Sci.* 21, 204–231. doi: 10.1016/j.sjbs.2014.03.003

Allan, E. A., DiBenedetto, M. H., Lavery, A. C., Govindarajan, A. F., and Zhang, W. G. (2021). Modeling characterization of the vertical and temporal variability of environmental DNA in the mesopelagic ocean. *Sci. Rep.* 11. doi: 10.1038/s41598-021-00288-5

Ambe, D., Imawaki, S., Uchida, H., and Ichikawa, K. (2004). Estimating the kuroshio axis south of Japan using combination of satellite altimetry and drifting buoys. *J. Oceanogr.* 60, 375–382. doi: 10.1023/B:JOCE.0000038343.31468.fe

Barnes, M. A., and Turner, C. R. (2016). The ecology of environmental DNA and implications for conservation genetics. *Conserv* 17, 1–17. doi: 10.1007/s10592-015-0775-4

Boswell, K. M., Wilson, M. P., and Cowab, J. H. Jr. (2011). A semiautomated approach to estimating fish size, abundance, and behavior from dual-frequency

identification sonar (DIDSON) data. *N. Am. J. Fish. Manag.* 28, 799–807. doi: 10.1577/M07-116.1

Boyra, G., Peña, M., Cotano, U., Irigoien, X., Rubio, A., and Nogueira, E. (2016).). spatial dynamics of juvenile anchovy in the bay of Biscay. *Fish. Oceanogr.* 25, 529–543. doi: 10.1111/fog.12170

Brochier, T., Echevin, V., Tam, J., Chaigneau, A., Goubanova, K., and Bertrand, A. (2013). Climate change scenarios experiments predict a future reduction in small pelagic fish recruitment in the Humboldt current system. *Glob. Chang. Biol.* 19, 1841–1853. doi: 10.1111/gcb.12184

Brosset, P., Fromentin, J., Beveren, E. V., Lloret, J., Marques, V., and Basilone, G. (2017). Spatio-temporal patterns and environmental controls of small pelagic fish body condition from contrasted Mediterranean areas. *Prog. Oceanogr.* 151, 149–162. doi: 10.1016/j.pocean.2016.12.002

Bunce, M., Szulkin, M., Lerner, H. R., Barnes, I., Shapiro, B., Cooper, A., et al. (2005). Ancient DNA provides new insights into the evolutionary history of new zealand's extinct giant eagle. *PloS Biol.* 3, 14–23. doi: 10.1371/journal.pbio.0030009

Cabral, H. N., and Murta, A. G. (2002). The diet of blue whiting, hake, horse mackerel and mackerel off Portugal. *J. Appl. Ichthyol.* 18, 14–23. doi: 10.1046/j.1439-0426.2002.00297.x

Chen, X., Li, G., Bo, F., and Tian, S. (2009). Habitat suitability index of chub mackerel (Scomber japonicus) from July to September in the East China Sea. *J. Oceanogr.* 65, 93–102. doi: 10.1007/s10872-009-0009-9

Cristescu, M. E. (2019). Can environmental RNA revolutionize biodiversity science? *Trends Ecol. Evol.* 34, 694–697. doi: 10.1016/j.tree.2019.05.003

Curtis, A. N., and Larson, E. R. (2020). No evidence that crayfish carcasses produce detectable environmental DNA (eDNA) in a stream enclosure experiment. *PeerJ* 8, 603–618. doi: 10.7717/peerj.9333

Cury, P. M., Boyd, I. L., Bonhommeau, S., Anker-Nilssen, T., Crawford, R. J. M., Furness, R. W., et al. (2011). Global seabird response to forage fish depletion–One-Third for the birds. *Science* 334, 1703–1706. doi: 10.1126/science.1212928

Cury, P., Cury, A., Crawford, R., Jarre, A., Quinãones, R., Shannon, L., et al. (2000). Small pelagics in upwelling systems: patterns of interaction and structural changes in "wasp-waist" ecosystems. *ICES. J. Mar. Sci.* 57, 603–618. doi: 10.1006/jmsc.2000.0712

Deagle, B. E., Kirkwood, R., and Jarman, S. N. (2009). Analysis of Australian fur seal diet by pyrosequencing prey DNA in faeces. *Mol. Biol.* 18, 2022–2038. doi: 10.1111/j.1365-294X.2009.04158.x

Doi, H., Uchii, K., Takahara, T., Matsuhashi, S., Yamanaka, H., and Minamoto, T. (2015). Use of droplet digital PCR for estimation of fish abundance and biomass in environmental DNA surveys. *PloS One* 10. doi: 10.1371/journal.pone.0122763

Duarte, L. O., and García, C. B. (2004). Trophic role of small pelagic fishes in a tropical upwelling ecosystem. *Ecol. Modell.* 172, 323–338. doi: 10.1016/j.ecolmodel.2003.09.014

Emmett, R. L., and Krutzikowsky, G. K. (2011). Nocturnal feeding of pacific hake and jack mackerel off the mouth of the Columbia river 1998-2004: implications for juvenile salmon predation. *Trans. Am. Fish. Soc.* 137, 657–676. doi: 10.1577/T06-058.1

ESR (2009). *OSCAR third deg. ver. 1. PO.DAAC* (CA, USA). doi: 10.5067/OSCAR-03D01

Everts, T., Driessche, C. V., Neyrinck, S., Regge, N. D., Descamps, S., Vocht, A. D., et al. (2022). Using quantitative eDNA analyses to accurately estimate American bullfrog abundance and to evaluate management efficacy. *Environ. DNA*. 4, 1052–1064. doi: 10.1002/edn3.301

Fernández-Corredor, E., Albo-Puigserver, M., Pennino, M. G., Bellido, J. M., and Coll, M. (2021). Influence of environmental factors on different life stages of European anchovy (Engraulis encrasicolus) and European sardine (Sardina pilchardus) from the Mediterranean Sea: a literature review. *Reg. Stud. Mar. Sci.* 41. doi: 10.1016/j.rsma.2020.101606

Food and Agriculture Organization of the United Nations (2020). *FAO*. Available at: https://www.fao.org/publications/sofia/2022/en/ (Accessed May 15, 2022).

Food and Agriculture Organization of the United Nations (2022). *FAO*. Available at: https://www.fao.org/publications/sofia/2022/en/ (Accessed September 15, 2022).

Fuji, T., Nakayama, S., Hashimoto, M., Miyamoto, H., Kamimura, Y., Furuichi, S., et al. (2023). Biological interactions potentially alter the large-scale distribution pattern of the small pelagic fish, pacific saury cololabis saira. *Mar. Ecol. Prog. Ser.* 704, 99–117. doi: 10.3354/meps14230

Georgakarakos, S., and Kitsiou, D. (2008). Mapping abundance distribution of small pelagic species applying hydroacoustics and Co-kriging techniques. *Hydrobiologia* 612, 155–169. doi: 10.1007/s10750-008-9484-z

Guo, C., Ito, S., Kamimura, Y., and Xiu, P. (2022). Evaluating the influence of environmental factors on the early life history growth of chub mackerel (Scomber japonicus) using a growth and migration model. *Prog. Oceanogr.* 206. doi: 10.1016/j.pocean.2022.102821

Hattori, S. (1964). Studies on fish larvae in the kuroshio and adjacent waters. *Bull. Tokai. Reg. Fish. Res. Lab.* 40, 1–111.

Hayashi, S. (1990). Seasonal abundance and vertical distribution of fish eggs and larvae in toyama bay, the Japan Sea. *Bull. Toyama. Pre. Fish. Stn.* 2, 1–17.

Higuchi, T., Ito, S., Ishimura, T., Kamimura, Y., Shirai, K., Shindo, H., et al. (2019). Otolith oxygen isotope analysis and temperature history in early life stages of the chub mackerel scomber japonicus in the kuroshio–oyashio transition region. *Deep-Sea. Res. II.: Top. Stud. Oceanogr.* 169. doi: 10.1016/j.dsr2.2019.104660

Horiuchi, T., Masuda, R., Murakami, H., Yamamoto, S., and Minamoto, T. (2019). Biomass-dependent emission of environmental DNA in jack mackerel trachurus japonicus juveniles. *J. Fish. Biol.* 95, 979–981. doi: 10.1111/jfb.14095

Ichinokawa, M., Okamura, H., and Kurota, H. (2017). The status of Japanese fisheries relative to fisheries around the world. *ICES. J. Mar. Sci.* 74, 1277–1287. doi: 10.1093/icesjms/fsx002

Itoh, S., Yasuda, I., Nishikawa, H., Sasaki, H., and Sasai, Y. (2009). Transport and environmental temperature variability of eggs and larvae of the Japanese anchovy (Engraulis japonicus) and Japanese sardine (Sardinops melanostictus) in the western north pacific estimated *via* numerical particle-tracking experiments. *Fish. Oceanogr.* 18, 118–133. doi: 10.1111/j.1365-2419.2009.00501.x

Jeunen, G., Lamare, M. D., Knapp, M., Spencer, H. G., Taylor, H. R., Stat, M., et al. (2019). Water stratification in the marine biome restricts vertical environmental DNA (eDNA) signal dispersal. *Environ. DNA* 2, 99–111. doi: 10.1002/edn3.49

Kai, Y., and Motomura, H. (2022). "Origins and present distribution of fishes in Japan," in *Fish diversity of Japan*. Eds. Y. Kai, H. Motomura and K. Matsuura (Singapore: Springer). doi: 10.1007/978-981-16-7427-3_3

Kalchhauser, I. A., and Burkhardt-Holm, P. (2016). An eDNA assay to monitor a globally invasive fish species from flowing freshwater. *PloS One* 11. doi: 10.1371/journal.pone.0147558

Kamoroff, C., and Goldberg, C. S. (2018). An issue of life or death: using eDNA to detect viable individuals in wilderness restoration. *Freshw. Sci.* 37. doi: 10.1086/699203

Kanamori, Y., Nishijima, S., Okamura, H., Yukami, R., Watai, M., and Takasuka, A. (2021). Spatio-temporal model reduces species misidentification bias of spawning eggs in stock assessment of spotted mackerel in the western north pacific. *Fish. Res.* 236. doi: 10.1016/j.fishres.2020.105825

Kaneko, H. I., Okunishi, T., Seto, T., Kuroda, H., Itoh, S., Kouketsu, S., et al. (2018). Dual effects of reversed winter–spring temperatures on year-to-year variation in the recruitment of chub mackerel (Scomber japonicus). *Fish. Oceanogr.* 28, 212–227. doi: 10.1111/fog.12403

Kasai, A., Kimura, S., Nakata, H., and Okazaki, Y. (2002). Entrainment of coastal water into a frontal eddy of the kuroshio and its biological significance. *J. Mar. Syst.* 37, 185–198. doi: 10.1016/S0924-7963(02)00201-4

Kume, G., Shigemura, T., Okanishi, M., Hirai, J., Shiozaki, K., Ichinomiya, M., et al. (2021). Distribution, feeding habits, and growth of chub mackerel, scomber japonicus, larvae during a high-stock period in the northern satsunan area, southern Japan. *Front. Mar. Sci.* 8. doi: 10.3389/fmars.2021.725227

Lee, D., Son, S., Kim, W., Park, J. M., Joo, H., and Lee, S. H. (2018). Spatio-temporal variability of the habitat suitability index for chub mackerel (Scomber japonicus) in the East/Japan Sea and the south Sea of south Korea. *Remote Sens.* 10. doi: 10.3390/rs10060938

Lezama-Ochoa, A., Boyra, G., Goñi, N., Arrizabalaga, H., and Bertrand, A. (2010). Investigating relationships between albacore tuna (Thunnus alalunga) CPUE and prey distribution in the bay of Biscay. *Prog. Oceanogr.* 86, 105–114. doi: 10.1016/j.pocean.2010.04.006

Li, G., Chen, X., Lei, L., and Guan, W. (2014). Distribution of hotspots of chub mackerel based on remote-sensing data in coastal waters of China. *Int. J. Remote Sens.* 35, 4399–4421. doi: 10.1080/01431161.2014.916057

Littlefair, J. E., Hrenchuk, L. E., Blanchfield, P. J., Rennie, M. D., and Cristescu, M. E. (2020). Thermal stratification and fish thermal preference explain vertical eDNA distributions in lakes. *Mol. Ecol.* 30, 3083–3096. doi: 10.1111/mec.15623

Liu, S., Liu, Y., Alabia, I., Tian, Y., Ye, Z., Yu, H., et al. (2020). Impact of climate change on wintering ground of Japanese anchovy (Engraulis japonicus) using marine geospatial statistics. *Front. Mar. Sci.* 7. doi: 10.3389/fmars.2020.00604

Liu, S., Tian, Y., Liu, Y., Alabia, I. D., Cheng, J., and Ito, S. (2023). Development of a prey-predator species distribution model for a large piscivorous fish: a case study for Japanese Spanish mackerel scomberomorus niphonius and Japanese anchovy engraulis japonicus. *Deep. Sea. Res. Part II. Top. Stud. Oceanogr. DEEP-SEA. Res. PT. II.* 207. doi: 10.1016/j.dsr2.2022.105227

Lluch-Belda, D., Lluch-Cota, D. B., Hernández-Vázquez, S., Zavala, C. A. S., and Schwartzlose, R. A. (1991). Sardine and anchovy spawning as related to temperature and upwelling in the California current system. *CalCOFI. Rep.* 32, 105–111.

Lydolph, M. C., Jacobsen, J., Arctander, P., Gilbert, M. T. P., Gilichinsky, D. A., Hansen, A. J., et al. (2005). Beringian paleoecology inferred from permafrost-preserved fungal DNA. *Appl. Environ. Microbiol.* 71, 1012–1017. doi: 10.1128/AEM.71.2.1012-1017.2005

Mantua, N. J., Hare, S. R., Zhang, Y., Wallace, J. M., and Francis, R. C. (1997). A pacific interdecadal climate oscillation with impacts on salmon production. *Bull. Amer.* 78, 1069–1080. doi: 10.1175/1520-0477(1997)078<1069:APICOW>2.0.CO;2

Matsuo, Y., Sugisaki, H., and Yokouchi, K. (1997). *Observations over a 24 hours cycle of diurnal vertical migration of sardine [Sardinops melanostictus] larvae* (Japan: Bulletin of Tohoku National Fisheries Research Institute), 59.

Medwin, H., and Clay, C. (1998). *Fundamentals of acoustic oceanography* (Boston, Mass, USA: Academic Press).

Minamoto, T., Yamanaka, H., Takahara, T., Honjo, M. N., and Kawabata, Z. (2011). Surveillance of fish species composition using environmental DNA. *Limnology* 13, 193–197. doi: 10.1007/s10201-011-0362-4

Minegishi, Y., Wong, M. K., Kanbe, T., Araki, H., Kashiwabara, T., Ijichi, M., et al. (2019). Spatio-temporal distribution of juvenile chum salmon in otsuchi bay, iwate, Japan, inferred from environmental DNA. *PloS One* 14. doi: 10.1371/journal.pone.0222052

Minegishi, Y., Wong, M. K., Nakao, M., Nishibe, Y., Tachibana, A., Kim, Y., et al. (2023). Species-specific patterns in spatio-temporal dynamics of juvenile chum salmon and their zooplankton prey in otsuchi bay, Japan, revealed by simultaneous eDNA quantification of diverse taxa from the same water samples. *Fish. Oceanogr.* 32, 311–326. doi: 10.1111/fog.12631

Miya, M., Sato, Y., Fukunaga, T., Sado, T., Poulsen, J. Y., Sato, K., et al. (2015). MiFish, a set of universal PCR primers for metabarcoding environmental DNA from fishes: detection of more than 230 subtropical marine species. *R. Soc Open Sci.* 2, 99–117. doi: 10.1098/rsos.150088

Miyamoto, H., Itoh, H., and Okazaki, Y. (2017). Temporal and spatial changes in the copepod community during the 1974–1998 spring seasons in the kuroshio region; a time period of profound changes in pelagic fish populations. *Deep-Sea. Res. I.: Oceanogr. Res. Pap.* 128, 131–140. doi: 10.1016/j.dsr.2017.07.007

Muko, S., Ohshimo, S., Kurota, H., Yasuda, T., and Fukuwaka, M. (2018). Long-term change in the distribution of Japanese sardine in the Sea of Japan during population fluctuations. *Mar. Ecol. Prog. Ser.* 593, 141–154. doi: 10.3354/meps12491

Mullaney, T. J., and Suthers, I. M. (2013). Entrainment and retention of the coastal larval fish assemblage by a short-lived, submesoscale, frontal eddy of the East Australian current. *Limnol. Oceanogr.* 58, 1546–1556. doi: 10.4319/lo.2013.58.5.1546

Murakami, H., Yoon, S., Kasai, A., Minamoto, T., Yamamoto, S., Sakata, M. K., et al. (2019). Dispersion and degradation of environmental DNA from caged fish in a marine environment. *Fish. Sci.* 85, 327–337. doi: 10.1007/s12562-018-1282-6

Nagai, T., Tandon, A., Yamazaki, H., Doubell, M., and Gallager, S. (2012). Direct observations of microscale turbulence and thermohaline structure in the kuroshio. *Front. J. Geophys. Res. Oceans.* 117. doi: 10.1029/2011JC007228

Nakata, H., Funakoshi, S., and Nakamura, M. (2001). Alternating dominance of postlarval sardine and anchovy caught by coastal fishery in relation to the kuroshio meander in the enshu-nada Sea. *Fish. Oceanogr.* 9, 248–258. doi: 10.1046/j.1365-2419.2000.00140.x

Nakata, H., Kimura, S., Okazaki, Y., and Kasai, A. (2000). Implications of meso-scale eddies caused by frontal disturbances of the kuroshio current for anchovy recruitment. *ICES. J. Mar. Sci.* 57, 143–152. doi: 10.1006/jmsc.1999.0565

Nakatsuka, A., Kawabata, J., Takasuka, A., Kubota, H., Okamura, H., and Ozeki, Y. (2010). Estimating gastric evacuation rate and daily ration of chub mackerel and spotted mackerel in the kuroshio-oyashio transition and oyashio regions. *Bull. Jpn. Soc Fish. Oceanogr.* 74, 105–117.

Navarro, J., Louzao, M., Igual, J. M., Oro, D., Delgado, A., Arcos, J. M., et al. (2009). Seasonal changes in the diet of a critically endangered seabird and the importance of trawling discards. *Mar. Biol.* 156, 2571–2578. doi: 10.1007/s00227-009-1281-3

Navarro, J., Sáez-Liante, R., Albo-Puigserver, M., Coll, M., and Palomera, I. (2017). Feeding strategies and ecological roles of three predatory pelagic fish in the western Mediterranean Sea. *Deep. Sea. Res. Part II.* 140, 9–17. doi: 10.1016/j.dsr2.2016.06.009

Nevers, M. B., Przybyla-Kelly, K., Shively, D., Morris, C. C., Dickey, J., Byappanahalli, M., et al. (2020). Influence of sediment and stream transport on detecting a source of environmental DNA. *PloS One* 15. doi: 10.1371/journal.pone.0244086

Nishikawa, H. (2018). Relationship between recruitment of Japanese sardine (Sardinops melanostictus) and environment of larval habitat in the low-stock period, (1995–2010). *Fish. Oceanogr.* 28, 131–142. doi: 10.1111/fog.12397

Nishikawa, H., Itoh, S., Yasuda, I., and Komatsu, K. (2022). Overlap between suitable nursery grounds for Japanese anchovy (Engraulis japonicus) and Japanese sardine (Sardinops melanostictus) larvae. *Aquac. Fish.* 2, 179–188. doi: 10.1002/aff2.39

O'Donnell, J. L., Kelly, R. P., Shelton, A. O., Samhouri, J. F., Lowell, N. C., and Williams, G. D. (2017). Spatial distribution of environmental DNA in a nearshore marine habitat. *PeerJ* 5. doi: 10.7717/peerj.3044

Okazaki, Y., Nakata, H., and Kimura, S. (2002). Effects of frontal eddies on the distribution and food availability of anchovy larvae in the kuroshio extension. *Mar. Freshw. Res.* 53, 403–410. doi: 10.1071/MF01115

Okazaki, Y., Nakata, H., Kimura, S., and Kasai, A. (2003). Offshore entrainment of anchovy larvae and its implication for their survival in a frontal region of the kuroshio. *Mar. Ecol. Prog. Ser.* 248, 237–244. doi: 10.3354/meps248237

Parsons, K. M., Piertney, S. B., Middlemas, S. J., Hammond, P. S., and Armstrong, J. D. (2006). DNA-Based identification of salmonid prey species in seal faeces. *J. Zool.* 266, 275–281. doi: 10.1017/S0952836905006904

Pennino, M. G., Coll, M., Albo-Puigserver, M., Fernández-Corredor, E., Steenbeek, J., Giráldez, A., et al. (2020). Current and future influence of environmental factors on small pelagic fish distributions in the northwestern Mediterranean Sea. *Front. Mar. Sci.*, 7. doi: 10.3389/fmars.2020.00622

Pepin, P., Pearre jr., S., and Koslow, J. A. (1987). Predation on larval fish by Atlantic mackerel scomber scombrus, with a comparison of predation by zooplankton. *Can. J. Fish. Aquat. Sci.* 44, 2012–2018. doi: 10.1139/f87-247

Pine, III W. E., Kwak, T. J., Waters, D. S., and Rice, J. A. (2005). Diet selectivity of introduced Flathead catfish in coastal rivers. *Trans. Am. Fish. Soc* 134, 901–909. doi: 10.1577/T04-166.1

Plough, L. V., Ogburn, M. B., Fitzgerald, C. L., Geranio, R., Marafino, G. A., and Richie, K. D. (2018). Environmental DNA analysis of river herring in Chesapeake bay: a powerful tool for monitoring threatened keystone species. *PloS One* 13. doi: 10.1371/journal.pone.0205578

Poinar, H. N., Hofreiter, M., Spaulding, W. G., Martin, P. S., Stankiewicz, B. A., Helen, B., et al. (1998). Molecular coproscopy: dung and diet of the extinct ground sloth nothrotheriops shastensis. *Science* 281, 402–406. doi: 10.1126/science.281.5375.402

Pörtner, H. O., and Knust, R. (2007). Climate change affects marine fishes through the oxygen limitation of thermal tolerance. *Science* 315, 95–97. doi: 10.1126/science.1135471

Quattrocchi, F., and Maynou, F. (2017). Environmental drivers of sardine (Sardina pilchardus) in the Catalan Sea (NW Mediterranean Sea). *Mar. Biol. Res.* 13, 1003–1014. doi: 10.1080/17451000.2017.1331039

Robert, D., Takasuka, A., Nakatsuka, S., Kubota, H., Oozeki, Y., Nishida, H., et al. (2010). Predation dynamics of mackerel on larval and juvenile anchovy: is capture success linked to prey condition? *Fish. Sci.* 76, 183–188. doi: 10.1007/s12562-009-0205-y

Rourke, M. L., Fowler, A. M., Hughes, J. M., Broadhurst, M. K., DiBattista, J. D., Fielder, S., et al. (2021). Environmental DNA (eDNA) as a tool for assessing fish biomass: a review of approaches and future considerations for resource surveys. *Environ. DNA* 4, 9–33. doi: 10.1002/edn3.185

Rudstam, L. G., Clay, C. S., and Magnuson, J. J. (1987). Density and size estimates of cisco (Coregonus artedii) using analysis of echo peak PDF from a single-transducer sonar. *Can. J. Fish. Aquat.* 44, 811–821. doi: 10.1139/f87-099

Sabatés, A., Martín, P., Lloret, J., and Raya, V. (2006). Sea Warming and fish distribution: the case of the small pelagic fish, sardinella aurita, in the western Mediterranean. *Glob. Change Biol. Bioenergy* 12, 2209–2219. doi: 10.1111/j.1365-2486.2006.01246.x

Saito, T., and Doi, H. (2021). Degradation modeling of water environmental DNA: experiments on multiple DNA sources in pond and seawater. *Environ. DNA* 3, 850–860. doi: 10.1002/edn3.192

Salter, I., Joensen, M., Kristiansen, R., Steingrund, P., and Vestergaard, P. (2019). Environmental DNA concentrations are correlated with regional biomass of Atlantic cod in oceanic waters. *Commun. Biol.* 2. doi: 10.1038/s42003-019-0696-8

Saraux, C., Beveren, E. V., Brosset, P., Queiros, Q., Bourdeix, J., Dutto, G., et al. (2019). Small pelagic fish dynamics: a review of mechanisms in the gulf of lions. *Deep. Sea. Res. Part II.* 159, 52–61. doi: 10.1016/j.dsr2.2018.02.010

Sarr, O., Kindong, R., and Tian, S. (2021). Knowledge on the biological and fisheries aspects of the Japanese sardine, sardinops melanostictus (Schlegel 1846). *J. Mar. Sci. Eng.* 9. doi: 10.3390/jmse9121403

Sassa, C., Konishi, Y., and Mori, K. (2006). Distribution of jack mackerel (Trachurus japonicus) larvae and juveniles in the East China Sea, with special reference to the larval transport by the kuroshio current. *Fish. Oceanogr.* 15, 508–518. doi: 10.1111/j.1365-2419.2006.00417.x

Sassa, C., and Tsukamoto, Y. (2010). Distribution and growth of scomber japonicus and s. australasicus larvae in the southern East China Sea in response to oceanographic conditions. *Mar. Ecol. Prog. Ser.* 419, 185–199. doi: 10.3354/meps08832

Schick, R. S., and Lutcavage, M. E. (2009). Inclusion of prey data improves prediction of bluefin tuna (Thunnus thynnus) distribution. *Fish. Oceanogr.* 18, 77–81. doi: 10.1111/j.1365-2419.2008.00499.x

Sogawa, S., Hidaka, K., Kamimura, Y., Takahashi, M., Saito, H., Okazaki, Y., et al. (2019). Environmental characteristics of spawning and nursery grounds of Japanese sardine and mackerels in the kuroshio and kuroshio extension area. *Fish. Oceanogr.* 28, 454–467. doi: 10.1111/fog.12423

Stat, M., John, J., DiBattista, J. D., Newman, S. J., Bunce, M., and Harvey, E. S. (2019). Combined use of eDNA metabarcoding and video surveillance for the assessment of fish biodiversity. *Conserv. Biol.* 33, 196–205. doi: 10.1111/cobi.13183

Sumaila, U. R., Cheung, W. W. L., Lam, V. W. Y., Pauly, D., and Herrick, S. (2011). Climate change impacts on the biophysics and economics of world fisheries. *Nat. Clim. Change* 1, 449–456. doi: 10.1038/nclimate1301

Takahara, T., Minamoto, T., Yamanaka, H., Doi, H., and Kawabata, Z. (2012). Estimation of fish biomass using environmental DNA. *PloS One* 7. doi: 10.1371/journal.pone.0035868

Takahashi, M., Watanabe, Y., Yatsu, A., and Nishida, H. (2009). Contrasting responses in larval and juvenile growth to a climate–ocean regime shift between anchovy and sardine. *Can. J. Fish. Aquat. Sci. Can. J. Fish. Aquat. Sci.* 66, 972–982. doi: 10.1139/F09-051

Takasuka, A., Kubota, H., and Oozeki, Y. (2008a). Spawning overlap of anchovy and sardine in the western north pacific. *Mar. Ecol. Prog. Ser.* 366, 231–244. doi: 10.3354/meps07514

Takasuka, A., Kuroda, H., Okunishi, T., Shimizu, Y., Hirota, Y., Kubota, H., et al. (2014). Occurrence and density of pacific saury cololabis saira larvae and juveniles in relation to environmental factors during the winter spawning season in the kuroshio current system. *Fish. Oceanogr.* 23, 304–321. doi: 10.1111/fog.12065

Takasuka, A., Oozeki, Y., and Aoki, I. (2007). Optimal growth temperature hypothesis: why do anchovy flourish and sardine collapse or vice versa under the same ocean regime? can. *J. Fish. Aquat. Sci.* 64, 768–776. doi: 10.1139/f07-052

Takasuka, A., Oozeki, Y., Kubota, H., and Lluch-Cota, S. E. (2008b). Contrasting spawning temperature optima: why are anchovy and sardine regime shifts synchronous across the north pacific? *Prog. Oceanogr.* 77, 225–232. doi: 10.1016/j.pocean.2008.03.008

Thomsen, P. F., and Willerslev, E. (2015). Environmental DNA – an emerging tool in conservation for monitoring past and present biodiversity. *Biol. Conserv.* 183, 4–18. doi: 10.1016/j.biocon.2014.11.019

Tsuji, S., Ushio, M., Sakurai, S., Minamoto, T., and Yamanaka, H. (2017). Water temperature-dependent degradation of environmental DNA and its relation to bacterial abundance. *PloS One* 12, 14–21. doi: 10.1371/journal.pone.0176608

Tsuri, K., Ikeda, S., Hirohara, T., Shimada, Y., Minamoto, T., and Yamanaka, H. (2020). Messenger RNA typing of environmental RNA (eRNA): a case study on zebrafish tank water with perspectives for the future development of eRNA analysis on aquatic vertebrates. *Environ. DNA* 3, 14–21. doi: 10.1002/edn3.169

Watanabe, Y., Zenitani, H., Kimura, R., Sato, C., Okumura, Y., Sugisaki, H., et al. (2002). Naupliar copepod concentrations in the spawning grounds of Japanese sardine, sardinops melanostictus, along the kuroshio current. *Fish. Oceanogr.* 7, 101–109. doi: 10.1046/j.1365-2419.1998.00059.x

Webb, P. (2019). *Introduction to oceanography* (Roger Williams University, Bristol: Rebus Community). Available at: https://rwu.pressbooks.pub/webboceanography/.

Wei, Y., Duan, Y., and An, D. (2022). Monitoring fish using imaging sonar: capacity, challenges and future perspective. *Fish. Fish.* 23, 1347–1370. doi: 10.1111/faf.12693

Wolf, C., Rentsch, J., and Hübner, P. (1999). PCR–RFLP analysis of mitochondrial DNA: A reliable method for species identification. *J. Agric. Food Chem.* 47, 1350–1355. doi: 10.1021/jf9808426

Wong, M. K., Nakao, M., and Hyodo, S. (2020). Field application of an improved protocol for environmental DNA extraction, purification, and measurement using sterivex filter. *Sci. Rep.* 10. doi: 10.1038/s41598-020-77304-7

Wong, M. K., Nobata, S., Ito, S., and Hyodo, S. (2022). Development of species-specific multiplex real-time PCR assays for tracing the small pelagic fishes of north pacific with environmental DNA. *Environ. DNA* 4, 510–522. doi: 10.1002/edn3.275

Yamamoto, S., Minami, K., Fukaya, K., Takahashi, K., Sawada, H., Murakami, H., et al. (2016). Environmental DNA as a 'Snapshot' of fish distribution: a case study of Japanese jack mackerel in maizuru bay, Sea of Japan. *PloS One* 11. doi: 10.1371/journal.pone.0149786

Yatsu, A., Chiba, S., Yamanaka, Y., Ito, S., Shimizu, Y., Kaeriyama, M., et al. (2013). Climate forcing and the Kuroshio/Oyashio ecosystem. *ICES. J. Mar. Sci.* 70, 922–933. doi: 10.1093/icesjms/fst084

Yatsu, A., Sassa, C., Moku, M., and Kinoshita, T. (2005). Night-time vertical distribution and abundance of small epipelagic and mesopelagic fishes in the upper 100 m layer of the kuroshio–oyashio transition zone in spring. *Fish. Sci.* 71, 1280–1286. doi: 10.1111/j.1444-2906.2005.01094.x

Yoon, S., Kim, D., Baeck, G., and Kim, J. (2008). Feeding habits of chub mackerel (Scomber japonicus) in the south Sea of Korea. *Fish. Aquat. Sci.* 41, 26–31. doi: 10.5657/kfas.2008.41.1.026

Yu, W., Guo, A., Zhang, Y., Chen, X., Qian, W., and Li, Y. (2018). Climate-induced habitat suitability variations of chub mackerel scomber japonicus in the East China Sea. *Fish. Res.* 207, 63–73. doi: 10.1016/j.fishres.2018.06.007

Yu, Z., Ito, S., Wong, M. K., Yoshizawa, S., Inoue, J., Itoh, S., et al. (2022). Comparison of species-specific qPCR and metabarcoding methods to detect small pelagic fish distribution from open ocean environmental DNA. *PloS One* 17. doi: 10.1371/journal.pone.0273670

frontiers | Frontiers in Marine Science

TYPE Original Research
PUBLISHED 30 August 2023
DOI 10.3389/fmars.2023.1193083

OPEN ACCESS

EDITED BY
Yuki Minegishi,
The University of Tokyo, Japan

REVIEWED BY
Haakon Hop,
Norwegian Polar Institute, Norway
Hauke Flores,
Alfred Wegener Institute Helmholtz Centre for Polar and Marine Research (AWI), Germany

*CORRESPONDENCE
Tatsuya Kawakami
kawakami@fish.hokudai.ac.jp

RECEIVED 24 March 2023
ACCEPTED 07 August 2023
PUBLISHED 30 August 2023

CITATION
Kawakami T, Yamazaki A, Jiang H-C, Ueno H and Kasai A (2023) Distribution and habitat preference of polar cod (*Boreogadus saida*) in the Bering and Chukchi Seas inferred from species-specific detection of environmental DNA. *Front. Mar. Sci.* 10:1193083. doi: 10.3389/fmars.2023.1193083

Distribution and habitat preference of polar cod (*Boreogadus saida*) in the Bering and Chukchi Seas inferred from species-specific detection of environmental DNA

Tatsuya Kawakami[1]*, Aya Yamazaki[1,2], Hai-Chao Jiang[3], Hiromichi Ueno[1] and Akihide Kasai[1]

[1]Faculty of Fisheries Sciences, Hokkaido University, Hakodate, Japan, [2]Research Institute for Global Change, Marine Biodiversity and Environmental Assessment Research Center, Japan Agency for Marine-Earth Science and Technology, Yokosuka, Japan, [3]School of Fisheries Sciences, Hokkaido University, Hakodate, Japan

Ongoing warming and sea-ice reductions in the Arctic can seriously impact cold-water species, such as polar cod (*Boreogadus saida*), necessitating biomonitoring to reveal the ecological consequences. Recent methodological advancements in environmental DNA (eDNA) techniques have increased our ability to conduct ecological monitoring at various locations, including the Arctic. This study aimed to provide an overview of the distribution of polar cod across the Bering and Chukchi Seas by employing species-specific detection of eDNA. First, we successfully developed novel species-specific qPCR assay targeting the mitochondrial D-loop region, which exclusively amplifies eDNA derived from polar cod. Subsequently, polar cod eDNA was detected using the assay from the samples that we collected latitudinally across the study area during the open-water season. Polar cod eDNA was primarily detected in the surface water from the central Chukchi Sea shelf and the northernmost observation line (75°N), which was located on the shelf slope, off the Point Barrow, and in the marginal ice zone. In contrast, only trace amounts of eDNA were detected in the Bering Sea. This pattern corresponded well with the distribution of water masses classified based on environmental conditions. The detection of eDNA in surface water was clearly limited to cold (-1 to 5°C) and low salinity (25–32) water, whereas it was detected in a higher salinity range (32–34) in the middle and bottom layers. These findings are consistent with current knowledge about the distribution and habitat of the polar cod, suggesting that eDNA can be regarded as a reliable tool to replace or supplement conventional methods. Incorporating eDNA techniques into large-scale oceanographic surveys can improve the spatial and temporal resolution of fish species detection with a reasonable sampling effort and will facilitate the continuous monitoring of Arctic ecosystems.

KEYWORDS

Arctic, environmental DNA, logistic regression analysis, polar cod (*Boreogadus saida*), quantitative PCR, sea ice, species-specific assay, water mass classification

1 Introduction

Acquiring biological data at various spatiotemporal scales is a considerable challenge for understanding dynamic ecological changes, such as in the Arctic marine ecosystem, which is currently experiencing rapid changes in response to global warming (Huntington et al., 2020; Hirawake et al., 2021). The loss of Arctic sea ice has accelerated recently, and the combination of earlier sea ice melt and delayed freeze-up has expanded ice-free waters, altering the timing and magnitude of phytoplankton and zooplankton blooms (Ardyna and Arrigo, 2020). Increasing temperatures and sea ice reduction have also induced a poleward shift in the distribution of fish, leading to a borealization of fish communities in the Arctic (Fossheim et al., 2015). Such a poleward shift has consequently altered the Arctic marine food webs (Kortsch et al., 2015). Human activities such as commercial fishing, vessel traffic, and resource development have expanded in the Arctic Ocean, coupled with an increasing duration of ice-free periods (Alvarez et al., 2020; Fauchald et al., 2021), while local communities that rely on the presence of sea ice for traditional subsistence activities have also been critically affected (Carothers et al., 2019; Cooley et al., 2020). However, ecological data in the Arctic are rather sporadic, and several studies focusing on Arctic ecosystem changes have emphasized the importance of comprehensive monitoring (e.g., Eamer et al., 2013; Hirawake et al., 2021; Skjoldal, 2022).

Recently, advanced approaches have provided unique insights into the understudied Arctic environment, particularly focusing on sea-ice-associated ecosystems. The Surface and Under-Ice Trawl (SUIT), which can collect animals dwelling beneath sea ice, revealed a close association between polar cod (*Boreogadus saida*) and the sea ice habitat in the central Arctic Ocean (David et al., 2016). Continuous acoustic measurements via subsurface mooring in the Chukchi Sea revealed that biological variability occurs at multiple temporal scales (i.e., diel, seasonal, and annual) and is closely associated with temporal variability in environmental conditions (Gonzalez et al., 2021). The Multidisciplinary Drifting Observatory for the Study of Arctic Climate (MOSAiC), which moored an icebreaker inside the freezing sea-ice pack for continuous observation, provided a comprehensive suite of observations on the atmosphere, sea ice, ocean, ecosystem, and biogeochemistry over an annual cycle in the Central Arctic (Shupe et al., 2020). One of the most important outcomes of these studies was that overcoming the limitations inherent to conventional methods, such as net sampling, is clearly required to completely understand ecosystem structure and dynamics in the Arctic.

Methodological advances in environmental DNA (eDNA) techniques have improved our ability to conduct ecological monitoring in a variety of environments, including the Arctic (Lacoursière-Roussel et al., 2018; Leduc et al., 2019; Sevellec et al., 2021; Jensen et al., 2023; Merten et al., 2023). eDNA was originally defined as a complex mixture of genomic DNA from many different organisms found in environmental samples (Taberlet et al., 2012). Although the study of eDNA first drew attention in the 1980s by focusing on microbial DNA, pioneering works in the 2000s, which successfully detected eDNA originating from macroorganisms (e.g., Ficetola et al., 2008), stimulated the use of eDNA for ecological studies of aquatic animals such as amphibians, reptiles, fishes, and marine mammals (Taberlet et al., 2018). Fish are one of the most enthusiastically studied groups using eDNA, and an increasing number of studies have been conducted to reveal the ecology of eDNA (i.e., origin, state, fate, and transport; Barnes and Turner, 2016) and to reveal the fish biodiversity hidden beneath the water (Thomsen and Willerslev, 2015; Deiner et al., 2017). These studies have proven the usefulness of eDNA as an alternative or supplement to conventional methods for biodiversity monitoring, owing to its standardized sampling procedure, non-destructive nature, and sensitivity (Thomsen and Willerslev, 2015; Deiner et al., 2017).

Consequently, eDNA is a promising tool for studying the ecological changes in Arctic fish. Poleward shifts in fish associated with warming temperatures and sea-ice loss have been predicted and observed in recent years (Hollowed et al., 2013; Fossheim et al., 2015; Frainer et al., 2017). One of the clear advantages of the eDNA method is that it reduces laborious work in the field: eDNA can be retrieved by collection and filtration of water *in situ* (Thomsen and Willerslev, 2015), implying that eDNA reduces the limitations in the season, extent, and resolution of the study design, which are often encountered when using net sampling. Moreover, eDNA detection has been shown to have sufficient sensitivity to evaluate the horizontal and vertical distribution of target species in the open ocean, although estimation of their abundance based on eDNA concentration is often controversial (Knudsen et al., 2019; Canals et al., 2021; Shelton et al., 2022). Therefore, studies investigating distribution in Arctic fish would benefit from the application of eDNA techniques.

The polar cod is considered a key species in the Arctic ecosystem because of its circumpolar distribution (Mecklenburg et al., 2018), predominance in fish stocks (Hunt et al., 2013; Goddard et al., 2014), and major importance as a prey item for various predators, including seabirds and marine mammals, transmitting energy to higher trophic levels throughout the Arctic food web (Welch et al., 1992; Harter et al., 2013). Assuming that this species prefers cold water (probably about -1.5–5.0°C; Thorsteinson and Love, 2016) and is potentially dependent on sea ice as a habitat, spawning ground, and nursery ground (Gradinger and Bluhm, 2004; David et al., 2016), polar cod is considered very susceptible to sea ice reduction (Geoffroy et al., 2023). In attempts to prove this, recent model studies predicted the negative effect of warming events on polar cod ecology and suggested that changes are likely to have cascading effects on their predators (Huserbråten et al., 2019; Florko et al., 2021). Despite their prevalence in the Arctic ecosystem, there is a paucity of knowledge about their broad-scale abundance, as well as many ecological aspects regarding their life cycle, stock structures, and population movements with respect to important habitats (Pettitt-Wade et al., 2021; Geoffroy et al., 2023). In particular, mapping of polar cod distribution is essential for understanding the ecological importance of polar cod as a key component of the Arctic ecosystem (Forster et al., 2020).

In this study, we present the first application of species-specific eDNA detection to estimate the distribution of polar cod across the Bering Sea and Chukchi Sea. To illustrate the distribution of polar

cod eDNA, we developed a new species-specific quantitative real-time PCR (qPCR) TaqMan assay. We applied this assay to eDNA samples collected from the Bering Sea and Chukchi Sea to estimate the probable distribution of polar cod in the region. Subsequently, the habitat preference of polar cod was determined by combining the results of eDNA detection with environmental conditions.

2 Materials and methods

2.1 Study area

This study was conducted in the Bering Sea and the Chukchi Sea in the Arctic Ocean during a cruise (MR20-05C) conducted by the 'R/V Mirai' of the Japan Agency for Marine-Earth Science and Technology from September 19 to November 2, 2020 (Figure 1). The Bering Sea is surrounded by Alaska to the east, Siberia to the north-west, the Kamchatka Peninsula to the west, and Aleutian Islands to the south. The Bering Sea is divided into two regions: the southwestern part is an ocean basin with a depth of approximately 4,000 m, and the northeastern part is a continental shelf with a depth of less than 200 m. The Chukchi Sea, which connects to the Bering Sea via the Bering Strait, is composed of a continental shelf with a depth of approximately 50 m and is adjacent to the Canada Basin with a maximum depth of approximately 4,000 m.

Several distinct water masses have been found in the study area (Danielson et al., 2017). The Bering Slope Current, which flows northwestward along the continental slope, forms the boundary between the southwestern and northeastern parts of the Bering Sea. Three water masses have been recognized in the Bering Sea (Coachman et al., 1975): The Anadyr Water (AnW) is distinguished by its relatively saline, cold, and nutrient-rich water; The Alaska Coastal Water (ACW) is distinguished by its relatively warm and less saline water; The Bering Shelf Water (BeSW) having intermediate characteristics between AnW and ACW. These water masses flow into the Chukchi Sea through the Bering Strait and comprise the Bering-Chukchi Waters (BCSW; Bering-Chukchi Summer Water and BCWW; Bering-Chukchi Winter Water; Danielson et al., 2017). After entering the Chukchi Sea, these water masses flow northward along three major conduits: the Herald Canyon in the west, the Barrow Canyon in the east, and the Central Channel across the mid-shelf (Danielson et al., 2017). The Beaufort Gyre circumscribes the northern shelf slope of the Chukchi Sea shelf in a clockwise direction. The surface of the

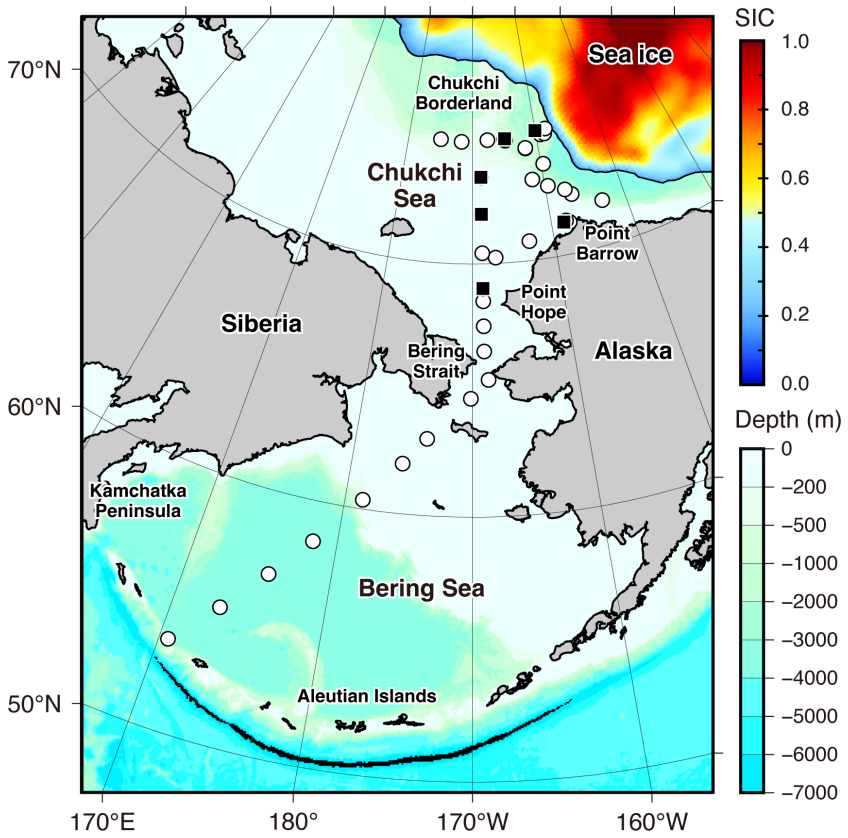

FIGURE 1
Map with bathymetric depth showing the study sites for eDNA collection. The white circles and black squares represent the locations where eDNA was collected from surface water and surface and middle or bottom layer water, respectively. The sea-ice concentration (SIC) on October 10, 2020, when eDNA sampling began in the Chukchi Sea, is indicated by color based on satellite-based data from Nimbus-7 SMMR and DMSP SSM/I-SSMIS Passive Microwave Data, Version 2, with a 25-km grid provided by the National Snow and Ice Data Center (NSIDC). Solid line enclosed sea ice area indicates the 0.15 concentration contour.

Canada Basin is covered by a polar mixed layer consisting of a low-salinity sea ice meltwater layer (MW) with near-freezing temperature (Danielson et al., 2017; Skjoldal, 2022).

The cruise was conducted during the open-water season. According to satellite-based sea ice concentration (SIC) data from Nimbus-7 SMMR and DMSP SSM/I-SSMIS Passive Microwave Data, Version 2, with a 25 km grid (provided by the National Snow and Ice Data Center (NSIDC); https://nsidc.org/data/data-access-tool/NSIDC-0051/versions/2), sea ice covered the Alaskan side of the Canada Basin. The northernmost edge of our study area, located around the Chukchi Borderland, was in the marginal ice zone (Figure 1).

The SIC data was also used to approximate the distance between the sampling sites and the sea ice edge. The daily SIC data corresponding to the study period were downloaded from the previously mentioned NSIDC website. The data were visualized using panoply version 5.2.3 (available online: https://www.giss.nasa.gov/tools/panoply/) and then exported as a KMZ file. These KMZ files were imported to Google Earth Pro 7.3.6.9345 (available online: https://www.google.co.jp/earth/about/versions/). The sea ice edge was defined as the contour of SIC = 0.15. The shortest distance between the sampling sites and the sea ice edge of the day was then calculated using the "Measure" function in Google Earth Pro. To avoid the path on a map intersecting land, the coordinates of Diomede, located in the middle of the Bering Strait (65° 45' 30" N, 168° 57' 06" W), and a sampling site located off Point Hope (68° 30' 1.31" N, 168° 49' 41.84" W), were used as waypoints when calculating the distance from the sampling sites in the Bering Sea.

2.2 eDNA sampling

eDNA samples were collected from 29 sites in the Chukchi Sea and nine sites in the Bering Sea from October 3 to October 24 (Figure 1). The geodesic distance from every sampling site to the nearest one ranged from 2 to 255 km (median [first quartile, third quartile] = 77 [24, 149] km). Based on the distance between our sampling sites and the current speed (m/s) that was obtained with a hull-mounted Acoustic Doppler Current Profiler (Teledyne RD Instruments, San Diego, CA, USA), it is estimated that eDNA shed at a particular site would take approximately 0.1–32 days (3.8 [1.6, 12.9] days) to drift from one sampling site to the nearest neighboring site.

As the surface water, seawater pumped from approximately 4.5 m depth was collected from the laboratory faucet of the ship. Because the seawater was used for continuous measurements of environmental conditions and water quality, it was filtered using a coarse metal scrub brush along the path of intake to remove large materials that could interfere with the measurements. We maintained a constant flow (approximately 5 L/min) of seawater throughout the cruise to ensure that the seawater in derivation pipes and tubes was always replaced with newly taken seawater. The insides of the pipes and tubes were considered to be constantly rinsed with fresh seawater. In addition to the surface water, water samples were collected from the middle or bottom layers using 12 L Niskin bottles mounted on a conductivity–temperature–depth (CTD)/Carousel Water Sampling System at six stations (Figure 1). The middle layer was defined as beneath the mixed layer or at the depth with the highest light attenuation rate, which is expected to be the most turbid layer (Supplementary Figure 1). The bottom layer was defined as being 5 m above the sea floor. For each water sample, a clean, foldable plastic bag was filled with 12 L of collected water.

Detailed sampling procedure for eDNA was described in Kawakami et al. (2023). Briefly, water samples were vacuum-filtered onto a Sterivex-HV filter unit (0.45 μm pore size, PVDF; Millipore, Burlington, MA, USA) using an aspirator (GAS-1N; AS ONE, Osaka, Japan) connected to a manifold (Multivac 310-MS; Rocker, Kaohsiung City, Taiwan) in the ship's laboratory, which was not used for processing organism samples. Filtration was halted when the filter became severely clogged. The filtration volume was calculated by subtracting the volume of unfiltered water from the initial volume (12L). Consequently, the filtration volume ranged from 1.6 to 12 L. The filtered sample was immersed in 1.6 mL of RNA*later* (Thermo Fisher Scientific, Waltham, MA, USA) and stored at −20°C until DNA extraction. For every 10–12 samples of seawater, negative controls were created by filtering 500 mL of Milli-Q water following the same procedure as seawater sampling.

To prevent cross-contaminations, all equipment used for water collection and filtration was decontaminated by soaking them in a 2% bleach solution (approximately 0.12% NaOCl) for at least 10 min. To remove any remaining bleach, the equipment was subsequently rinsed with tap and Milli-Q water. The workspace was decontaminated using bleach disinfectant spray (approximately 0.1% NaOCl). For each water collection and filtration, new gloves and masks were used.

Temperature (°C), salinity (psu), and chlorophyll *a* (chl *a*) fluorescence (RFU) of the surface water at the sampling sites were obtained from a Continuous Sea Surface Water Monitoring System (Marine Works Japan Co., Ltd., Kanagawa, Japan). Their vertical profiles were measured by the CTD at sampling sites where the middle and bottom waters were collected. The CTD data are available in the Arctic Data archive System (ADS) managed by the National Institute of Polar Research, Japan, under the ID of A20220803-010 (Nishino, 2020; Nishino, 2022).

2.3 eDNA extraction

DNA was extracted from each filter using the Qiagen DNeasy Blood and Tissue kit (Qiagen, Hilden, Germany), according to Wong et al. (2020), who modified the original extraction protocol to improve the extraction efficiency from the Sterivex filter. Extraction was performed using vacuum-driven liquid processing with a manifold (QiaVac; Qiagen) and vacuum pump (MAS-01; AS ONE). Throughout the process, a VacValve and VacConnector (Qiagen) were utilized in conjunction with the manifold to reduce the risk of contamination from backflow into the columns and direct contact with the manifold.

After removing the RNAlater, 2 mL of a lysis buffer mix containing PBS (990 L), Buffer AL (910 L), and Proteinase K (100

L) was introduced to the Sterivex through its outlet using a 2.5 mL syringe (Terumo Corporation, Tokyo, Japan). The filter was sealed with luer fittings and incubated at 56°C without rotation for 30 minutes. Subsequently, the filter was centrifuged at 2500 g for 10 minutes, and the lysate was retrieved in a 3 mL polypropylene tube. The lysate was filtered using a DNeasy Blood and Tissue kit column after being mixed with 1 mL of 99.5% ethanol (FUJIFILM Wako Pure Chemical Corporation, Osaka, Japan). The column was then washed sequentially with 0.8 mL of AW1 buffer and 0.8 mL of AW2 buffer, followed by 2 minutes of centrifugation at 21,300 *g* for drying. The adsorbed DNA was eluted from the column into a DNA LoBind Tube (Eppendorf, Hamburg, Germany) twice with 75 µL AE buffer to maximize recovery. A total of 150 µL DNA extract was collected from each filter and stored at –20°C.

2.4 Primer and probe design and specificity test

We designed novel primers and probes that exclusively amplify DNA derived from polar cod in samples collected from the Bering and Chukchi Seas. The mitochondrial D-loop region was chosen as a candidate region for designing a new specific marker because it is one of the major target regions adopted for species-specific eDNA detection owing to its high inter-specific variability (Tsuji et al., 2019).

Twelve gadid species are known to be distributed in the Arctic region (Mecklenburg et al., 2018). We searched and downloaded the D-loop sequences available for these species from GenBank (http://www.ncbi.nlm.nih.gov/), resulting in a set of D-loop sequences for polar cod and eight other species (saithe, *Pollachius virens*; Arctic cod, *Arctogadus glacialis*; saffron cod, *Eleginus gracilis*; Atlantic cod, *Gadus morhua*; walleye pollack, *G. chalcogrammus*; Pacific cod, *G. macrocephalus*; Haddock, *Melanogrammus aeglefinus*; and whiting, *Merlangius merlangus*).

Primer-BLAST (https://www.ncbi.nlm.nih.gov/tools/primer-blast/) was used to generate specific primer pairs for polar cod on the target region. For running Primer-BLAST, a sequence of the D-loop region of polar cod extracted from the reference sequence (NC_010121) was provided as a PCR template, and those of non-target species were set as a database for checking primer pair specificity. T_m of the candidate primers was calculated using the T_m calculator provided by ThermoFisher Scientific (https://www.thermofisher.com/jp/ja/home/brands/hermos-scientific/molecular-biology/molecular-biology-learning-center/molecular-biology-resource-library/hermos-scientific-web-tools/tm-calculator.html). Subsequently, primer pairs with an amplicon length of less than 180 bp and a T_m of 58-60°C were selected. Following that, an MGB probe was designed on the amplicon sequences using PrimerExpress 3.0 (Thermo Fisher Scientific, Waltham, MA, USA) using the default settings.

The specificity of the newly designed primers and probe for polar cod was confirmed *in silico* using Primer-BLAST (https://www.ncbi.nlm.nih.gov/tools/primer-blast/) against the nr database. Consequently, we selected the primer set and probe described in Table 1 and Supplementary Figure 2 for the polar cod eDNA assay.

TABLE 1 Primers and probe designed in this study for species-specific detection of polar cod, *Boreogadus saida*.

Primer (F and R) and Probe (Pr) name	Sequence (5′ -> 3′)
Bosa-Dlp-F	TAAGGCAATCTGTCCAATGAAGGTC
Bosa-Dlp-R	TGCAAATTATGAGCGATTGTCAGTC
Bosa-Dlp-Pr-FamMGB	FAM-CGAAGACCTACATCCCGTGAC-NFQ-MGB

All available sequences for these regions of polar cod were identical, except for one sequence containing one mismatch in the probe region.

The specificity of the assay was further confirmed *in vitro* using DNA samples extracted from the tissues of five gadid species (polar cod, Pacific cod, walleye pollock, Atlantic cod, and saffron cod), which may have co-occurred in the study area. Their DNA was extracted using the DNeasy Blood & Tissue kit (Qiagen) following manufacturer's protocol from the following tissues: the ethanol-preserved muscle of polar cod collected in the Chukchi Sea during the cruise of T/S *Oshoro-Maru* of Hokkaido University; the ethanol-preserved testis of pacific cod captured off Hokkaido, Japan; purchased dried fish for walleye pollock and saffron cod captured off Hokkaido, Japan; a dried dorsal fin of Atlantic cod, collected around Norway. In the specificity test, these extractions were diluted 10 pg/µL and 100 pg/µL after measuring the concentration using a Qubit dsDNA HS Assay Kit and Qubit 4 Fluorometer (ThermoFisher Scientific).

qPCR with a newly designed species-specific eDNA assay was performed in a StepOne plus real-time PCR system (Life Technologies) with a 15 µL reaction containing 1x Environmental Master Mix 2.0 (ThermoFisher Scientific), 900 nM of each primer, 125 nM of a probe, 0.075 µL of AmpErase™ Uracil N-Glycosylase (Thermo Fisher Scientific, Waltham, MA, USA), and 2 µL of DNA template. A no-template control (NTC) was included in the PCR run using 2.0 µL of nuclease-free water (UltraPure; Invitrogen, Waltham, MA, USA) in place of the DNA template. The thermal conditions were as follows: 50°C for 2 min, 95°C for 10 min, 55 cycles at 95°C for 15 s, and 60°C for 1 min.

2.5 Quantitative real-time PCR

A newly designed assay was applied to eDNA samples collected from the Bering and Chukchi Seas to estimate the distribution of polar cod. The assay was performed under the same PCR conditions as those described above. A 2 µL of eDNA extract was used as a template in each PCR. To evaluate cross-contamination, a no-template control (NTC) was included in each PCR run using 2 µL of nuclease-free water (UltraPure; Invitrogen, Waltham, MA, USA) instead of the DNA template. Three technical replicates were used for each sample.

To determine the quantity of target DNA in each sample, 10-fold serial dilutions ranging from 30 to 30,000 copies/reaction of the artificially-synthesized double-stranded DNA (gBlocks; Integrated

DNA Technologies, Inc., Coralville, IA, USA) containing the target sequence were included in triplicate for each qPCR run. The concentration of the stock standard solution was quantified using a Qubit dsDNA HS Assay Kit and a Qubit 4 Fluorometer (Thermo Fisher Scientific) and then diluted in TE buffer. To eliminate suspicious detection, reaction resulting in < 1 copies/reaction was converted to 0. After conversion, the mean of the triplicates was used to represent the number of eDNA copies in each sample. The eDNA concentration in seawater (copies/L) was calculated by converting the number of eDNA copies per reaction to the total number of eDNA copies present in the DNA extract, and then dividing this value by the filtration volume.

2.6 Contamination control during eDNA molecular work

For DNA extraction and PCR preparation, filter samples were processed in a laboratory dedicated to eDNA analysis, which was isolated from a room for PCR, ensuring neither tissue nor PCR products were handled. PCR amplification was performed in a separate room. During every step of the molecular work, researchers always wore new gloves and masks. The laboratory and all equipment (micropipettes, incubator, and centrifuge) were cleaned with DNA-OFF (Takara, Shiga, Japan) and distilled water. In addition, the extraction apparatus (manifold, valves, and tubes) was decontaminated with a bleach solution, as detailed previously.

2.7 Statistical analysis

All statistical analyses were performed using R v.4.1.2 (R Core Team, 2021) in combination with RStudio v.2022.02.3 (available online: https://www.rstudio.com/) and the packages implemented in it. Additionally, GMT 5.4.5 (Wessel et al., 2013) was used to visualize the results.

To explore the association between the study sites and water masses, the sampling sites were classified using clustering and ordination analyses based on water temperature, salinity, and chl *a*, which are potential indices of distinct water masses across the Bering and Chukchi Seas (Danielson et al., 2017). First, we performed a clustering analysis based on Euclidean distances using Ward's linkage. The similarity profile (SIMPROF) test (Clarke et al., 2008) using the "simprof" function of the "clustsig" package in R was subsequently applied to identify statistically significant clusters (the significance threshold was set at 0.05). The SIMPROF test examines the multivariate structure within groups of samples by comparing the similarity profile constructed from the results of the cluster analysis with that constructed from the original data using the iterative permutation procedure. The results of the cluster analysis were visualized by Principal Component Analysis (PCA) using the "prcomp" function of the "stats" package and "fviz_pca_biplot" function of the "factoextra" package in R. Chl *a* was included in these analyses after log transformation. Before these analyses were conducted, the environmental parameters were normalized.

The environmental conditions were compared between the sampling sites where polar cod eDNA was detected or not detected using the Wilcoxon rank-sum exact test after assuming homoscedasticity based on the results of the Bartlett test. The significance level was set at 0.05.

Multiple logistic regression analysis was used to relate the detection of polar cod eDNA to environmental conditions (water temperature, salinity, chl *a*, and topography). Prior to the logistic regression, the qPCR results were converted to presence/absence data. The distance from the sea ice edge was excluded from the analysis due to a significant and strong correlation with water temperature (Pearson's product moment correlation: $r = 0.906$, $t = 12.823$, $p < 0.001$). Chl *a* was incorporated into the model after log transformation. The topography was roughly determined based on the bottom depth as shelf (< 200 m) and slope or basin (≥ 200 m). The logistic model was fitted to the data with a binomial error distribution and a logit link using the "glm" function in the "stats" package in R. After constructing a full model, the best model was selected using the "stepAIC" function in the "MASS" package in R based on Akaike's information criterion (AIC).

3 Results

3.1 Specificity and validity of the newly designed assay

As a result of qPCR using DNA extracted from the tissues of five gadid species, including polar cod, our newly designed assay exclusively detected the DNA of polar cod at both concentrations (10 pg/μL and 100 pg/μL), except for one sample of walleye pollock containing 100 pg/μL of DNA (Supplementary Figure 3). Although nonspecific detection of walleye pollock DNA was observed, the DNA was not detected at lower concentration (10 pg/μL) and its Ct (45.98) was clearly higher than the intercept of standard curve (41.03, Supplementary Table 1), which corresponds to 1 copy/reaction. This suggested that the risk of false detection of walleye pollock can be negligible when using 1 copy/reaction as a cut-off value for quantity. Therefore, this assay was assumed to be sufficiently specific and was used in subsequent analyses.

The R^2, intercept, log-linear slope, and efficiency of the standard curve across four runs for eDNA samples were 0.998 ± 0.001, 41.03 ± 0.37, -3.50 ± 0.07, and 93.19 ± 2.47 (mean ± SD), respectively (Supplementary Table 1). None of the negative controls (field negative controls and NTC for PCR) yielded positive results for polar cod eDNA, indicating that cross-contamination during the experiment was negligible and that the qPCR results obtained in this study were reliable.

3.2 Classification of water masses

The sampling sites were classified into five significant clusters based on the SIMPROF results (Supplementary Figure 4). Overlaying the clustering results on the PCA ordination and a geographical map revealed that these clusters corresponded well with the known water

masses throughout the study area (Figure 2A, Table 2, Supplementary Figure 5). Cluster 1 consisted of sampling sites south of 62°N in the Bering Sea, where the water was saline, warm, and high in chl *a* concentration. The sampling sites across the Bering Strait and central Chukchi Sea shelf comprised two distinct clusters (clusters 2 and 3). Although salinity was comparable between these three clusters, both temperature and salinity decreased gradually with increasing latitude (Table 2, Supplementary Figure 5). The sites along the northernmost edge of our study area (approximately 75°N) were also classified as having subzero temperatures and low salinity (cluster 5). The sites near the Point Barrow were classified as another cluster (cluster 4) with intermediate temperature and salinity compared to those of clusters 3 and 5. In addition, both water temperature and salinity tended to decrease with increasing proximity to the sea ice edge. These clusters corresponded to the water masses identified by Danielson et al. (2017) based on temperature and salinity: ACW (cluster 1), BCSW (clusters 2 and 3), and MW (clusters 4 and 5), respectively.

3.3 Horizontal and vertical distribution of polar cod eDNA

Polar cod eDNA was detected primarily in the central part of the Chukchi Sea shelf and in the northernmost observation line, which was located on the shelf slope off the Point Barrow and marginal ice zone (Figure 2B). In contrast, polar cod eDNA was rarely found in the Bering Sea. Based on the classification of water masses, polar cod eDNA was most frequently and abundantly detected in the sites classified as clusters 4 and 5, which showed cold, less saline water (92% with 46 ± 69 copies/L in cluster 4, and 100% with 156 ± 289 copies/L in cluster 5; Table 2). In contrast, no polar cod eDNA was detected in the sites belonging to cluster 1, which showed warm, saline water. At sites belonging to clusters 2 and 3, polar cod eDNA was detected sporadically at moderate concentrations (50% with 7 ± 11 copies/L in cluster 4, and 40% with 95 ± 193 copies/L in cluster 5).

Polar cod eDNA was also detected in the middle and bottom layers of all six sites examined for vertical comparison, including sites where no polar cod eDNA was detected in surface samples (Figure 3). Despite the different environmental conditions of the site's surface water, polar cod eDNA was detected in the bottom layer across the Chukchi Sea shelf at depths of 50–120 m.

3.4 eDNA detection in relation to the environment

The juxtaposition of the concentration of polar cod eDNA on the temperature–salinity diagram showed that the distribution of polar cod eDNA in the surface water was clearly limited to < 5°C in temperature and < 32 psu in salinity (Figure 4). Maximum concentrations of eDNA in surface water occurred at approximately 0°C and 30 psu. There were significant differences in water temperature and salinity between sites where polar cod eDNA was detected and those where it was not (Supplementary Figure 6; Wilcoxon rank-sum exact test; $W = 35$, $p < 0.001$ for water temperature; $W = 32$, $p < 0.001$ for salinity). Depending on the depth, the relationship between eDNA distribution and environmental conditions varied; polar cod eDNA was detected in more saline water in the middle or bottom layers (> 32 psu) than in the surface water.

After developing a logistic regression model relating the presence or absence of polar cod eDNA to four environmental conditions (water temperature, salinity, log-transformed chl *a*, and topography), the model containing only water temperature as an independent variable was deemed the best (Supplementary Table 2).

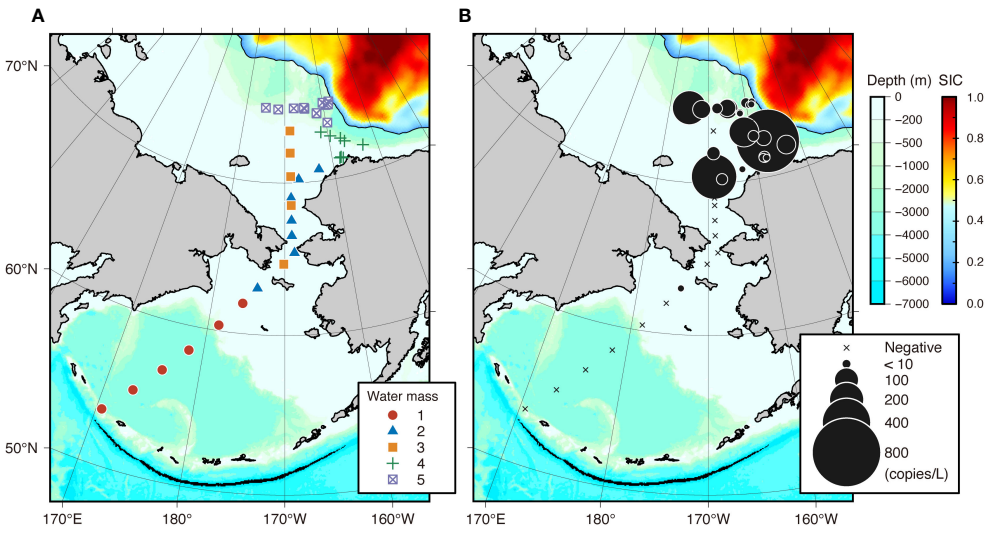

FIGURE 2
Water mass classification of eDNA sampling sites **(A)** and horizontal difference in polar cod *Boreogadus saida* eDNA concentrations (copies/L) across 38 sampling sites in the Bering and Chukchi Seas using a newly designed assay **(B)**. Sea-ice concentration (SIC) was overlaid on the map. Symbols indicating water masses in panel A correspond to the results of clustering analysis with the SIMPROF test shown in Table 2. The area of black circles in **(B)** indicates the eDNA concentration, while the crosses indicate locations where polar cod eDNA was not detected.

TABLE 2 Summary of detection results of Polar cod *Boreogadus saida* eDNA and environmental conditions (water temperature, salinity, chlorophyll *a* fluorescence, bottom depth, and distance from sea ice edge) in each water mass cluster identified by the SIMPROF test.

Water mass cluster	n	Frequency of eDNA detection (%)	eDNA concentration (copies/L)	Water temperature (°C)	Salinity (psu)	Chlorophyll *a* fluorescence (RFU)	Bottom depth (m)	Distance to sea ice edge (km)
1	6	0	0	7.8 ± 1.0	32.7 ± 0.2	7.7 ± 0.9	2036 ± 1956	2209 ± 442
2	7	42.9	6.3 ± 10.1	4.7 ± 1.0	31.3 ± 0.8	5.9 ± 3.9	54 ± 10	865 ± 339
3	5	40	95.3 ± 192.7	2.9 ± 0.7	31.9 ± 0.4	1.2 ± 0.7	61 ± 31	632 ± 334
4	8	100	155.7 ± 289.3	1.1 ± 0.6	30.1 ± 0.4	1.5 ± 0.3	229 ± 138	171 ± 64
5	12	91.7	46.0 ± 69.0	-0.6 ± 0.5	26.7 ± 1.3	1.2 ± 0.3	1163 ± 831	122 ± 57

The mean ± SD (standard deviation) of each parameter are indicated.

For each 1°C increase, the odds of detecting polar cod eDNA decreased by 50% (95% CI [24%, 67%]). The probability of detecting polar cod eDNA decreased with increasing water temperatures (Figure 5). The water temperature with a 50% detection probability was predicted to be 3.7°C.

4 Discussion

Using a newly designed species-specific assay, we successfully detected polar cod eDNA and described its horizontal distribution in surface water across the Bering and Chukchi Seas. The relationship between eDNA detection and environmental conditions indicated that polar cod eDNA is abundantly distributed in cold water, particularly in polar mixed layers with low salinity in the Arctic Ocean. Although eDNA analysis has been shown to be a promising method for estimating the distribution of a fish species in the ocean (e.g., Knudsen et al., 2019; Fraija-Fernández et al., 2020), only a few eDNA studies targeting marine fish have been conducted in the Arctic region (Lacoursière-Roussel et al., 2018; Leduc et al., 2019). A pilot study is recommended before applying the eDNA approach to a new field, such as the Arctic, because the persistence and detection probability of eDNA are influenced by site-specific environmental factors (Goldberg et al., 2016; Stoeckle et al., 2017). The success of eDNA detection in this study demonstrated that the common detection protocol was also effective without any special optimization in the Arctic environment, where the ecology of eDNA is poorly understood. The findings of this study can be translated into knowledge regarding the ecology of polar cod after addressing uncertainties regarding eDNA detection (Cristescu and Hebert, 2018).

4.1 Validity of the eDNA detection

As eDNA analysis in marine ecosystems detects DNA in water, which is a trace of individual organisms, it can only indirectly

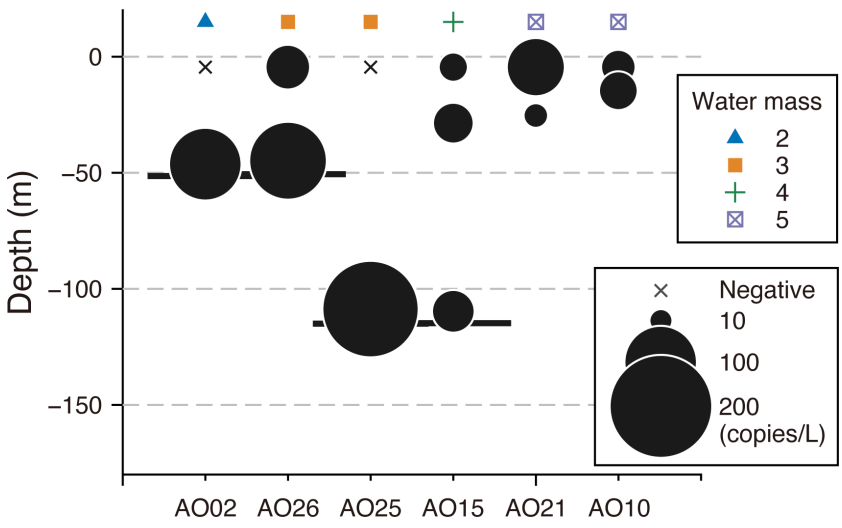

FIGURE 3
Vertical difference in polar cod *Boreogadus saida* eDNA concentrations (copies/L) at six sampling sites in the Chukchi Sea using a newly designed assay. The area of the black circles represents the concentration of eDNA (copies/L). Sampling sites were latitudinally arranged from the south (left) to the north (right). Crosses represent the sample in which no polar cod eDNA was detected. The sites along the x-axis were organized latitudinally. The bottom depths at each sampling site are indicated by thick horizontal lines, except for AO10 and AO21, where the bottom depths are 546 m and 1979 m, respectively. The symbols at the top of the panel correspond to the results of the clustering analysis using the SIMPROF test, as shown in Table 2.

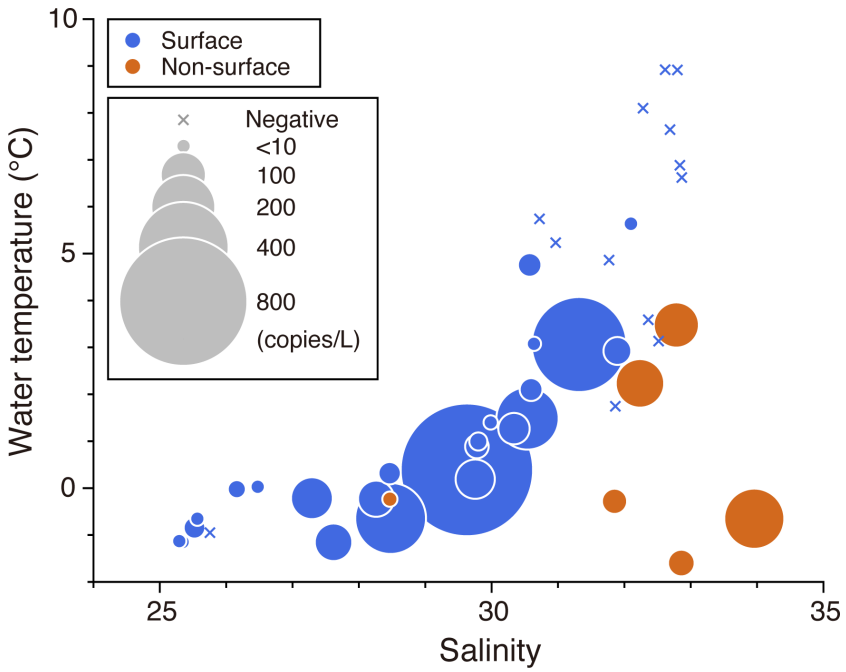

FIGURE 4
Polar cod *Boreogadus saida* eDNA concentrations (copies/L) across the Bering and Chukchi Seas plotted on a temperature-salinity diagram. The area of circles represents the concentration of eDNA. Crosses represent the sample in which no polar cod eDNA was detected. The colors blue and red represent the results from the surface water and middle or bottom layers, respectively.

suggest the presence of target species. Various biotic factors, such as species, physiological conditions, body size, and developmental stage, influence the amount and rate of eDNA shedding (e.g., Maruyama et al., 2014; Klymus et al., 2015; Takeuchi et al., 2019). The ecology of eDNA following its release is also affected by degradation, particle sinking, adsorption to sediments, and dispersion (Barnes and Turner, 2016; Stoeckle et al., 2017). False negatives (species not detected where they are present) and false positives (target species absent but DNA recovered) in eDNA detection can also arise from a variety of biological, physical, and chemical factors, and technical issues (Barnes and Turner, 2016; Cristescu and Hebert, 2018). Consequently, it is often difficult to

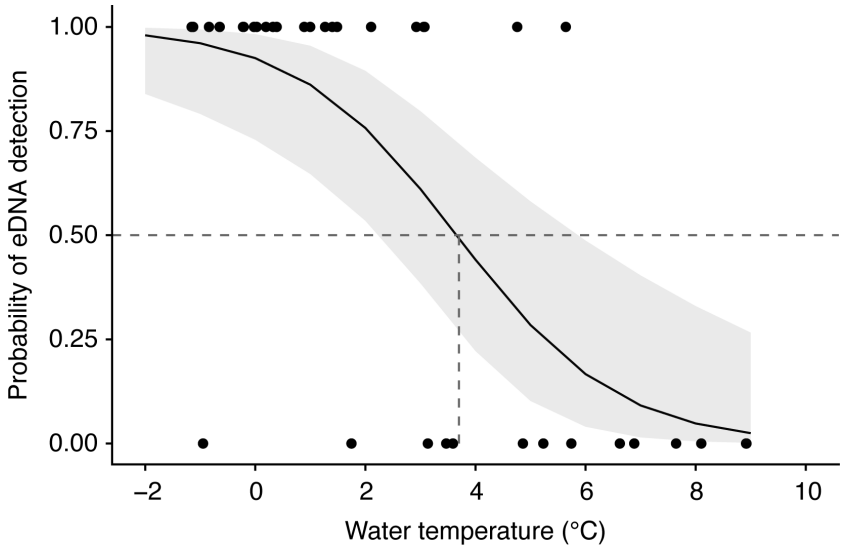

FIGURE 5
Logistic regression curve predicting the detection probability of polar cod *Boreogadus saida* eDNA as a function of water temperature. The logistic model was constructed with water temperature as the sole explanatory variable. The shaded area indicates the 95% confidence interval. A horizontal dotted line is drawn at 50% detection, and a vertical dotted line indicates the water temperature at 50% detection.

infer the distribution and abundance of the source organism based on the detection and quantification of eDNA. These obstacles could confound our inferences about the distribution and habitat preferences of polar cod in the present study, necessitating a careful inspection of the results.

A properly designed primer pair and probe are critical to avoid false results. Primers and probes that lack sufficient specificity can amplify unintended species, whereas high intraspecific variation in priming sites can result in failure to recover eDNA from the target species. Therefore, we rigorously tested the performance of the new assay to ensure its specificity for polar cod, employing publicly available sequences of polar cod and other related species, as well as PCR using DNA extracts of gadoids that may have co-occurred with polar cod in the study area. The results of *in silico* and *in vitro* specificity tests confirmed that the newly designed assay had the desired specificity, i.e., the assay was expected to amplify polar cod DNA exclusively. However, the risk of false results remains due to the uncertainty regarding unknown intraspecific diversity. A recent study on the genetic structure of polar cod populations using microsatellite loci found that polar cod in the North Bering, Chukchi, and Western Beaufort Seas formed a genetically distinct group from other regions, with very little genetic differentiation within the group (Nelson et al., 2020). A study that used mitochondrial DNA also suggested no significant structure from the northern Bering Sea to the western Beaufort Sea (Wilson et al., 2020). Although these results cannot directly imply negligible intraspecific diversity in our target region (mitochondrial D-loop), it is unlikely that the new assay produced false negative results due to intraspecific diversity.

As fish eDNA in the ocean is thought to represent only a small fraction of the DNA in seawater (Stat et al., 2017), the concentration of eDNA may be influenced by the dispersion and degradation processes critical for its detection. Therefore, insufficient sampling effort can lead to false-negative errors. However, the volume of water filtered in this study (mean ± SD, 7.4 ± 3.2 L per filter) exceeded that employed in previous fish eDNA surveys in the ocean to comprehensively detect the local diversity of fish fauna (0.5–2 L of seawater per sample, e.g., Thomsen et al., 2016; Sigsgaard et al., 2017; Afzali et al., 2021). Given the prevalence of polar cod in the Arctic and a large amount of water filtered in this study, we expected the occurrence of false negative errors to be negligible.

False positives caused by contamination of space and time should also be considered. Although dispersion lowers eDNA concentration, it can increase the probability of detecting non-local and non-temporal eDNA originating from spatially and temporally remote sources from a study site (Hansen et al., 2018). In the Antarctic, eDNA from the ocellated icefish, *Chionodraco rastrospinosus*, is expected to disperse up to 648 km from its source in a detectable state, assuming a current velocity and slow decay rate in subzero water temperature (Cowart et al., 2018). Bottom sediments and sea ice are other potential eDNA sources in the ocean, transporting allochthonous extracellular DNA (Collins and Deming, 2011; Kuwae et al., 2020). However, these cases likely represent extremes. Half-lives of marine fish eDNA have been estimated between approximately 7 and 60 h under 4–40°C and 71 h under -1°C (Collins et al., 2018). A field experiment in the temperate zone showed that eDNA shed by white trevally (*Pseudocaranx dentex*) was only detectable within a narrow range (<100 m) in a bay with a weak current (Murakami et al., 2019). These studies implied that eDNA detection is thought to represent a fish community on a short temporal and small spatial scale. In the present study, approximately 3.8 days (91 h) in the median were required for eDNA shed from a particular site to be transported to the nearest site, assuming the passive transportation of eDNA by the current. Although there is a possibility that the degradation of eDNA could be slower than expected under the Arctic environment, it could be presumed that our sampling sites did not share the same source for eDNA due to the temporal distance between sites.

4.2 Distribution and habitat preferences of polar cod inferred by eDNA analysis

The distribution of polar cod eDNA corresponded well with the putative water mass distribution, suggesting that the polar cod was heterogeneously distributed in the study area and was likely affected by site-specific environmental conditions. Although eDNA may reliably suggest the polar cod distribution as discussed above, when considering interactions with various environmental conditions, the complex relationship between eDNA concentrations, abundance, and body size of the source organism must be clarified to accurately convert the eDNA distribution into reliable data for conservation purposes (Collins et al., 2018; Jo et al., 2019; Jo and Minamoto, 2021). Across various taxonomic groups, rearing experiments have generally shown positive correlations between the amount of eDNA and the abundance, body weight, and developmental stage of source organisms (e.g., Takahara et al., 2012; Minegishi et al., 2019; Takeuchi et al., 2019). This relationship between eDNA concentration and the abundance of target species has also been supported in coastal environments (Thomsen et al., 2016; Yamamoto et al., 2016; Sato et al., 2021), with some exceptions in the open ocean (Knudsen et al., 2019; Shelton et al., 2022). Although uncertainty remains regarding obtaining comparable quantification from the eDNA results, we discuss what and how environmental conditions shape the polar cod distribution, carefully considering that limitation.

Although oceanographic conditions vary temporally and spatially, previous studies that intensively described polar cod distribution in the Chukchi Sea during the open-water period have shown their prevalence distribution across the shelf, but it was heterogeneous and linked to characteristics of the water mass. Polar cod occupy a remarkably wide range of habitats; they were collected from all parts of the water column, from the coast to offshore (Goddard et al., 2014; Logerwell et al., 2015). Gradual expansion in body size range, in which the maximum body length increased from 66 mm to 260 mm (corresponding to age-0/1 and age-3+, respectively) from the beach to the shelf surface, nearshore bottom, and benthic shelf, suggested a habitat shift linked to growth (Logerwell et al., 2015). Polar cod is the most abundant fish species in the region, except on the shelf surface, where capelin (*Mallotus villosus*) and saffron cod tend to represent a large proportion of the

fish stock (Norcross et al., 2010; Eisner et al., 2013; Goddard et al., 2014; Logerwell et al., 2015). Studies focusing on the early life stage distribution of polar cod suggested that their larvae and juveniles are abundant in cold water ranging between approximately -1.8–5° C (Norcross et al., 2010; Kono et al., 2016; Deary et al., 2021), while their occurrence in warmer water (2.6–11.2°C) was also reported (Eisner et al., 2013).

Hotspots of polar cod eDNA were observed in the central part of the Chukchi Sea shelf, off the Point Barrow, and in proximity to the Chukchi Borderland, while they were scarce in the northern Bering Sea, which corresponds to the southern limit of its distribution (Mecklenburg et al., 2018). These results are congruent with the synthesized distribution of the historical data described above and the recent acoustic-trawl survey targeting polar cod (De Robertis et al., 2017). Therefore, eDNA detection successfully inferred the distribution of the polar cod. In this study, we mainly collected surface seawater for eDNA detection, but eDNA was also detected in the water in the bottom or middle layers. A recent study showed that the distribution of eDNA is vertically different and can reflect the vertical distribution of marine fishes (Canals et al., 2021). Although the comparison between the different depth layers in this study is preliminary, eDNA can be expected to indicate the vertical distribution of polar cod.

The key finding of this study is that eDNA showed a clear linkage between the presence of polar cod and water temperature, implying that polar cod prefer cold water masses as a habitat. Polar cod eDNA was only found in water masses at lower temperatures (<5°C), and detection probability decreased with increasing temperature. This finding is consistent with the previously reported temperature range in which polar cod larvae and juveniles are abundant (Norcross et al., 2010; Kono et al., 2016; Deary et al., 2021). Thus, eDNA provides new empirical evidence that supports the general assumption that polar cod prefer cold water. Rearing experiments have also suggested that polar cod are most active and capable of growing at temperatures below 10°C (Laurel et al., 2016). However, salinity may not have been a decisive factor in polar cod habitat selection because we detected their eDNA in a wide salinity range (25–34 psu) in our study area. In addition to temperature and salinity, other environmental conditions, interactions with other species (predators, prey, and competitors), and internal factors (e.g., density, age, and fish condition) can influence fish distribution (Planque et al., 2011). Considering that polar cod inhabit abundantly in the cracks and crevices beneath the sea ice (Gradinger and Bluhm, 2004), the presence of sea ice itself could also influence the distribution of polar cod and, consequently, the probability of eDNA detection. However, due to the close relationship between the distribution of cold water masses and the presence of sea ice in our study area, it was difficult to determine whether the habitat preference of polar cod was for the water temperature or the habitat availability under sea ice. Although the habitat preferences of polar cod are extensively reviewed (Geoffroy et al., 2023), their details are still being discussed and warrant further investigation.

According to previous studies, the eDNA hotspot in the central Chukchi Sea shelf observed in this study could have captured an aggregation of larval or juvenile polar cods. It has generally been assumed that polar cod spawn in the winter (November to April) beneath the sea ice (Thorsteinson and Love, 2016). Pelagic eggs and larvae that hatch from spring to summer disperse over a broader geographical area (Aune et al., 2021; Deary et al., 2021). Assuming the Kotzebue Sound is a potential source of polar cod, as this area is unknown as a spawning ground in the Chukchi Sea, individual –based models in combination with particle tracking predicted that simulated polar cod hatching in the Kotzebue Sound was transported offshore to the north and to the west, concentrated in the central Chukchi Sea around 70°N (Deary et al., 2021). This estimated dispersal process was consistent with the eDNA distribution. However, the inability of eDNA to distinguish the biological parameters of the source organism (e.g., age, body size, and physiological condition) precludes further estimation of the factors controlling its observed distribution. Another limitation of eDNA is that it does not provide immediate information about target species, necessitating laboratory work after a field investigation. The combined use of the eDNA technique, and the reconstruction of life history traits using otolith microchemistry or tissue stable isotopes, and hydroacoustic surveys with high spatial coverage would expand our understanding of polar cod ecology considerably.

4.3 Perspectives

The application of eDNA techniques would likely benefit various studies on tracking the consequences of environmental change, ecological management and conservation, and policy-making decisions (Bohmann et al., 2014). This study demonstrated that species-specific detection of eDNA is an effective method to describe the distribution of polar cod, providing baseline data to reveal its environmental impact. However, uncertainties from eDNA must be overcome before its broad adoption (Bohmann et al., 2014; Cristescu and Hebert, 2018). For example, we were unable to conclusively generate informative relative abundance and population structure data, due to the unknown relationship between the abundance or biological condition of the source organisms and eDNA detection, as well as the unknown ecology of eDNA in the Arctic. Currently, the abundance data of polar cod in the Chukchi Sea are limited (De Robertis et al., 2017; Geoffroy et al., 2023), and if the eDNA technique can indicate its abundance and population structure, it could provide a basis for projecting shifts in distribution and abundance. Experimental studies regarding eDNA shedding from polar cod and its persistence in a subzero environment would facilitate future applications of the eDNA technique. Furthermore, due to the inability of eDNA to provide biological parameters of the source organism, which is invaluable information for conservation and management purposes, the eDNA method should be considered as a complementary tool for other individual-based methods, such as target fishing, otolith microchemistry (Andrade et al., 2020), stable isotopes (Kohlbach et al., 2017), and life history analysis (Bouchard et al., 2017), rather than replacing them. The eDNA method could also supplement hydroacoustic surveys and

observations using underwater optical camera by reducing ambiguity in species identification and enabling the production of distributional data at a large spatiotemporal scale with high taxonomic resolution.

Integrating eDNA techniques and oceanographic surveys will enhance our ability to detect predicted ecological changes in polar cod populations. eDNA samples can be collected concurrently with samples for biogeochemical, planktonic, and microbial studies, providing an additional layer for investigating biological interactions. A numerical hydrodynamic model incorporating oceanographical conditions (e.g., current, density, and temperature) and eDNA data (e.g., concentration and persistence) is a possible method for creating an accurate and quantified map of polar cod populations (Fukaya et al., 2020). In addition, recent advances in the application of eDNA, such as population genetic analysis (Sigsgaard et al., 2020; Tsuji et al., 2020) and analysis of eRNA associated with physiological conditions (Tsuri et al., 2021), may provide new insights into the population dynamics of polar cod. As this study may expand the applicability of eDNA techniques for Arctic studies, investigations targeting other species and accumulating basic knowledge of eDNA in the Arctic will facilitate the understanding of the processes and consequences of distributional shifts of fishes (Hollowed et al., 2013; Fossheim et al., 2015) predicted to occur under global warming in the future.

Data availability statement

The datasets presented in this study can be found in online repositories. The names of the repository/repositories and accession number(s) can be found below: The Arctic Data archive System (ADS), National Institute of Polar Research, Japan. No. A20230323-002 (https://ads.nipr.ac.jp/dataset/A20230323-002) and Zenodo (https://doi.org/10.5281/zenodo.8213184).

Author contributions

TK, AK, and HU conceived this study. TK collected and processed the eDNA samples. AY developed the species-specific assay. TK, AY, and H-CJ participated in molecular work. TK performed statistical analysis and visualization. TK wrote the first draft of the manuscript. All authors critically reviewed the manuscript and contributed to the final version.

Funding

This work was funded by the Arctic Challenge for Sustainability II (ArCS II), Program Grant Number JPMXD1420318865 from the Ministry of Education, Culture, Science and Technology of Japan. This study was partly supported by JSPS KAKENHI Grant Number 22H02415 from the Japan Society for the Promotion of Science (JSPS).

Acknowledgments

We express our sincere thanks to the captain and crew of the 'R/V Mirai' belonging to JAMSTEC for their assistance during the MR20-05C cruise. We thank Drs. Maud Alix and Olav Kjesbu (Institute of Marine Research, Norway), who kindly provided the tissue samples of the gadid species. We are grateful to Marty Kwok-Shing Wong (Atmosphere and Ocean Research Institute, University of Tokyo) for his help with the technical improvements in DNA extraction. We are also grateful to Qi-Fan Zhang (Graduate School of Fisheries Sciences, Hokkaido University) for assisting with the DNA analysis.

Conflict of interest

The authors declare that the research was conducted in the absence of any commercial or financial relationships that could be construed as a potential conflict of interest.

Publisher's note

All claims expressed in this article are solely those of the authors and do not necessarily represent those of their affiliated organizations, or those of the publisher, the editors and the reviewers. Any product that may be evaluated in this article, or claim that may be made by its manufacturer, is not guaranteed or endorsed by the publisher.

Supplementary material

The Supplementary Material for this article can be found online at: https://www.frontiersin.org/articles/10.3389/fmars.2023.1193083/full#supplementary-material

References

Afzali, S. F., Bourdages, H., Laporte, M., Mérot, C., Normandeau, E., Audet, C., et al. (2021). Comparing environmental metabarcoding and trawling survey of demersal fish communities in the Gulf of St. Lawrence, Canada. *Environ. DNA.* 3, 22–42. doi: 10.1002/edn3.111

Alvarez, J., Yumashev, D., and Whiteman, G. (2020). A framework for assessing the economic impacts of Arctic change. *Ambio.* 49, 407–418. doi: 10.1007/s13280-019-01211-z

Andrade, H., van der Sleen, P., Black, B. A., Godiksen, J. A., Locke, W. L., Carroll, M. L., et al. (2020). Ontogenetic movements of cod in Arctic fjords and the Barents Sea as revealed by otolith microchemistry. *Polar Biol.* 43, 409–421. doi: 10.1007/s00300-020-02642-1

Ardyna, M., and Arrigo, K. R. (2020). Phytoplankton dynamics in a changing Arctic Ocean. *Nat. Clim. Change.* 10, 892–903. doi: 10.1038/s41558-020-0905-y

Aune, M., Raskhozheva, E., Andrade, H., Augustine, S., Bambulyak, A., Camus, L., et al. (2021). Distribution and ecology of polar cod (*Boreogadus saida*) in the eastern Barents Sea: A review of historical literature. *Mar. Environ. Res.* 166, 105262. doi: 10.1016/j.marenvres.2021.105262

Barnes, M. A., and Turner, C. R. (2016). The ecology of environmental DNA and implications for conservation genetics. *Conserv. Genet.* 17, 1–17. doi: 10.1016/j.marenvres.2021.105262

Bohmann, K., Evans, A., Gilbert, M. T. P., Carvalho, G. R., Creer, S., Knapp, M., et al. (2014). Environmental DNA for wildlife biology and biodiversity monitoring. *Trends Ecol. Evol.* 29, 358–367. doi: 10.1016/j.tree.2014.05.012

Bouchard, C., Geoffroy, M., LeBlanc, M., Majewski, A., Gauthier, S., Walkusz, W., et al. (2017). Climate warming enhances polar cod recruitment, at least transiently. *Prog. Oceanogr.* 156, 121–129. doi: 10.1016/j.pocean.2017.06.008

Canals, O., Mendibil, I., Santos, M., Irigoien, X., and Rodríguez-Ezpeleta, N. (2021). Vertical stratification of environmental DNA in the open ocean captures ecological patterns and behavior of deep-sea fishes. *Limnol. Oceanogr. Lett.* 6, 339–347. doi: 10.1002/lol2.10213

Carothers, C., Sformo, T. L., Cotton, S., George, J. C., and Westley, P. A. H. (2019). Pacific salmon in the rapidly changing Arctic: Exploring local knowledge and emerging fisheries in Utqiaġvik and Nuiqsut, Alaska. *Arctic.* 72, 273–288. doi: 10.14430/arctic68876

Clarke, K. R., Somerfield, P. J., and Gorley, R. N. (2008). Testing of null hypotheses in exploratory community analyses: similarity profiles and biota-environment linkage. *J. Exp. Mar. Biol. Ecol.* 366, 56–69. doi: 10.1016/j.jembe.2008.07.009

Coachman, L. K., Aagaard, K., and Tripp, R. B. (1975). *Bering Strait: The Regional Physical Oceanography* (Seattle: University of Washington Press). 172 pp.

Collins, R. E., and Deming, J. W. (2011). Abundant dissolved genetic material in Arctic sea ice Part I: Extracellular DNA. *Polar Biol.* 34, 1819–1830. doi: 10.1007/s00300-011-1041-y

Collins, R. A., Wangensteen, O. S., O'Gorman, E. J., Mariani, S., Sims, D. W., and Genner, M. J. (2018). Persistence of environmental DNA in marine systems. *Commun. Biol.* 1, 185. doi: 10.1038/s42003-018-0192-6

Cooley, S. W., Ryan, J. C., Smith, L. C., Horvat, C., Pearson, B., Dale, B., et al. (2020). Coldest Canadian Arctic communities face greatest reductions in shorefast sea ice. *Nat. Clim. Change.* 10, 533–538. doi: 10.1038/s41558-020-0757-5

Cowart, D. A., Murphy, K. R., and Cheng, C.-H. C. (2018). Metagenomic sequencing of environmental DNA reveals marine faunal assemblages from the West Antarctic Peninsula. *Mar. Genomics* 37, 148–160. doi: 10.1016/j.margen.2017.11.003

Cristescu, M. E., and Hebert, P. D. N. (2018). Uses and misuses of environmental DNA in biodiversity science and conservation. *Annu. Rev. Ecol. Evol. Syst.* 49, 209–230. doi: 10.1146/annurev-ecolsys-110617-062306

Danielson, S. L., Eisner, L., Ladd, C., Mordy, C., Sousa, L., and Weingartner, T. J. (2017). A comparison between late summer 2012 and 2013 water masses, macronutrients, and phytoplankton standing crops in the northern Bering and Chukchi Seas. *Deep Sea Res. Part II.* 135, 7–26. doi: 10.1016/j.dsr2.2016.05.024

David, C., Lange, B., Krumpen, T., Schaafsma, F., van Franeker, J. A., and Flores, H. (2016). Under-ice distribution of polar cod *Boreogadus saida* in the central Arctic Ocean and their association with sea-ice habitat properties. *Polar Biol.* 39, 981–994. doi: 10.1007/s00300-015-1774-0

Deary, A. L., Vestfals, C. D., Mueter, F. J., Logerwell, E. A., Goldstein, E. D., Stabeno, P. J., et al. (2021). Seasonal abundance, distribution, and growth of the early life stages of polar cod (*Boreogadus saida*) and saffron cod (*Eleginus gracilis*) in the US Arctic. *Polar Biol.* 44, 2055–2076. doi: 10.1007/s00300-021-02940-2

Deiner, K., Bik, H. M., Mächler, E., Seymour, M., Lacoursière-Roussel, A., Altermatt, F., et al. (2017). Environmental DNA metabarcoding: Transforming how we survey animal and plant communities. *Mol. Ecol.* 26, 5872–5895. doi: 10.1111/mec.14350

De Robertis, A., Taylor, K., Wilson, C. D., and Farley, E. V. (2017). Abundance and distribution of Arctic cod (*Boreogadus saida*) and other pelagic fishes over the U.S. Continental Shelf of the Northern Bering and Chukchi Seas. *Deep Sea Res. Part II.* 135, 51–65. doi: 10.1016/j.dsr2.2016.03.002

Eamer, J., Donaldson, G. M., Gaston, A. J., Kosobokova, K. N., Lárusson, K. F., Melnikov, I. A., et al. (2013). *Life Linked to Ice: A guide to sea-ice-associated biodiversity in this time of rapid change. CAFF Assessment Series No. 10* (Iceland: Conservation of Arctic Flora and Fauna).

Eisner, L., Hillgruber, N., Martinson, E., and Maselko, J. (2013). Pelagic fish and zooplankton species assemblages in relation to water mass characteristics in the northern Bering and southeast Chukchi seas. *Polar Biol.* 36, 87–113. doi: 10.1007/s00300-012-1241-0

Fauchald, P., Arneberg, P., Debernard, J. B., Lind, S., Olsen, E., and Hausner, V. H. (2021). Poleward shifts in marine fisheries under Arctic warming. *Environ. Res. Lett.* 16, 074057. doi: 10.1088/1748-9326/ac1010

Ficetola, G. F., Miaud, C., Pompanon, F., and Taberlet, P. (2008). Species detection using environmental DNA from water samples. *Biol. Lett.* 4, 423–425. doi: 10.1098/rsbl.2008.0118

Florko, K. R. N., Tai, T. C., Cheung, W. W. L., Ferguson, S. H., Sumaila, U. R., Yurkowski, D. J., et al. (2021). Predicting how climate change threatens the prey base of Arctic marine predators. *Ecol. Lett.* 24, 2563–2575. doi: 10.1111/ele.13866

Forster, C. E., Norcross, B. L., Mueter, F. J., Logerwell, E. A., and Seitz, A. C. (2020). Spatial patterns, environmental correlates, and potential seasonal migration triangle of polar cod (*Boreogadus saida*) distribution in the Chukchi and Beaufort Seas. *Polar Biol.* 43, 1073–1094. doi: 10.1007/s00300-020-02631-4

Fossheim, M., Primicerio, R., Johannesen, E., Ingvaldsen, R. B., Aschan, M. M., and Dolgov, A. V. (2015). Recent warming leads to a rapid borealization of fish communities in the Arctic. *Nat. Clim. Change.* 5, 673–677. doi: 10.1038/nclimate2647

Fraija-Fernández, N., Bouquieaux, M., Rey, A., Mendibil, I., Cotano, U., Irigoien, X., et al. (2020). Marine water environmental DNA metabarcoding provides a comprehensive fish diversity assessment and reveals spatial patterns in a large oceanic area. *Ecol. Evol.* 10, 7560–7584. doi: 10.1002/ece3.6482

Frainer, A., Primicerio, R., Kortsch, S., Aune, M., Dolgov, A. V., Fossheim, M., et al. (2017). Climate-driven changes in functional biogeography of Arctic marine fish communities. *PNAS.* 114, 12202–12207. doi: 10.1073/pnas.1706080114

Fukaya, K., Murakami, H., Yoon, S., Minami, K., Osada, Y., Yamamoto, S., et al. (2020). Estimating fish population abundance by integrating quantitative data on environmental DNA and hydrodynamic modelling. *Mol. Ecol.* 30, 3057–3067. doi: 10.1111/mec.15530

Geoffroy, M., Bouchard, C., Flores, H., Robert, D., Gjosaeter, H., Hoover, C., et al. (2023). The circumpolar impacts of climate change and anthropogenic stressors on Arctic cod (*Boreogadus saida*) and its ecosystem. *Elementa-Sci. Anthrop.* 11, 00097. doi: 10.1525/elementa.2022.00097

Goddard, P., Lauth, R., and Armistead., C. (2014). *Results of the 2012 Chukchi Sea bottom trawl survey of bottomfishes, crabs, and other demersal macrofauna* Vol. 278 (U.S. Dep. Commer.: NOAA Tech. Memo. NMFS-AFSC-). 110 p.

Goldberg, C. S., Turner, C. R., Deiner, K., Klymus, K. E., Thomsen, P. F., Murphy, M. A., et al. (2016). Critical considerations for the application of environmental DNA methods to detect aquatic species. *Methods Ecol. Evol.* 7, 1299–1307. doi: 10.1111/2041-210x.12595

Gonzalez, S., Horne, J. K., and Danielson, S. L. (2021). Multi-scale temporal variability in biological-physical associations in the NE Chukchi Sea. *Polar Biol.* 44, 837–855. doi: 10.1007/s00300-021-02844-1

Gradinger, R. R., and Bluhm, B. A. (2004). *In-situ* observations on the distribution and behavior of amphipods and Arctic cod (*Boreogadus saida*) under the sea ice of the High Arctic Canada Basin. *Polar Biol.* 27, 595–603. doi: 10.1007/s00300-004-0630-4

Hansen, B. K., Bekkevold, D., Clausen, L. W., and Nielsen, E. E. (2018). The sceptical optimist: challenges and perspectives for the application of environmental DNA in marine fisheries. *Fish Fish.* 19, 751–768. doi: 10.1111/faf.12286

Harter, B. B., Elliott, K. H., Divoky, G. J., and Davoren, G. K. (2013). Arctic cod (*Boreogadus saida*) as prey: Fish length-energetics relationships in the Beaufort Sea and Hudson Bay. *Arctic.* 66, 191–196. doi: 10.14430/arctic4290

Hirawake, T., Oida, J., Yamashita, Y., Waga, H., Abe, H., Nishioka, J., et al. (2021). Water mass distribution in the northern Bering and southern Chukchi seas using light absorption of chromophoric dissolved organic matter. *Prog. Oceanogr.* 197, 102641. doi: 10.1016/j.pocean.2021.102641

Hollowed, A. B., Planque, B., and Loeng, H. (2013). Potential movement of fish and shellfish stocks from the sub-Arctic to the Arctic Ocean. *Fish. Oceanogr.* 22, 355–370. doi: 10.1111/fog.12027

Hunt, G. L., Blanchard, A. L., Boveng, P., Dalpadado, P., Drinkwater, K. F., Eisner, L., et al. (2013). The Barents and Chukchi Seas: comparison of two Arctic shelf ecosystems. *J. Mar. Syst.* 109–110, 43–68. doi: 10.1016/j.jmarsys.2012.08.003

Huntington, H. P., Danielson, S. L., Wiese, F. K., Baker, M., Boveng, P., Citta, J. J., et al. (2020). Evidence suggests potential transformation of the Pacific Arctic ecosystem is underway. *Nat. Clim. Change.* 10, 342–348. doi: 10.1038/s41558-020-0695-2

Huserbråten, M. B. O., Eriksen, E., Gjøsæter, H., and Vikebø, F. (2019). Polar cod in jeopardy under the retreating Arctic sea ice. *Commun. Biol.* 2, 407. doi: 10.1038/s42003-019-0649-2

Jensen, M. R., Høgslund, S., Knudsen, S. W., Nielsen, J., Møller, P. R., Rysgaard, S., et al. (2023). Distinct latitudinal community patterns of Arctic marine vertebrates along the East Greenlandic coast detected by environmental DNA. *Divers. Distrib.* 29, 316–334. doi: 10.1111/ddi.13665

Jo, T., and Minamoto, T. (2021). Complex interactions between environmental DNA (eDNA) state and water chemistries on eDNA persistence suggested by meta-analyses. *Mol. Ecol. Res.* 21, 1490–1503. doi: 10.1111/1755-0998.13354

Jo, T., Murakami, H., Yamamoto, S., Masuda, R., and Minamoto, T. (2019). Effect of water temperature and fish biomass on environmental DNA shedding, degradation, and size distribution. *Ecol. Evol.* 9, 1135–1146. doi: 10.1002/ece3.4802

Kawakami, T., Yamazaki, A., Asami, M., Goto, Y., Yamanaka, H., Hyodo, S., et al. (2023). Evaluating the sampling effort for the metabarcoding-based detection of fish environmental DNA in the open ocean. *Ecol. Evol.* 13, e9921. doi: 10.1002/ece3.9921

Klymus, K. E., Richter, C. A., Chapman, D. C., and Paukert, C. (2015). Quantification of eDNA shedding rates from invasive bighead carp *Hypophthalmichthys nobilis* and silver carp *Hypophthalmichthys molitrix*. *Biol. Conserv.* 183, 77–84. doi: 10.1016/j.biocon.2014.11.020

Knudsen, S. W., Ebert, R. B., Hesselsøe, M., Kuntke, F., Hassingboe, J., Mortensen, P. B., et al. (2019). Species-specific detection and quantification of environmental DNA from marine fishes in the Baltic Sea. *J. Exp. Mar. Biol. Ecol.* 510, 31–45. doi: 10.1016/j.jembe.2018.09.004

Kohlbach, D., Schaafsma, F. L., Graeve, M., Lebreton, B., Lange, B. A., David, C., et al. (2017). Strong linkage of polar cod (*Boreogadus saida*) to sea ice algae-produced carbon: Evidence from stomach content, fatty acid and stable isotope analyses. *Prog. Oceanogr.* 152, 62–74. doi: 10.1016/j.pocean.2017.02.003

Kono, Y., Sasaki, H., Kurihara, Y., Fujiwara, A., Yamamoto, J., and Sakurai, Y. (2016). Distribution pattern of Polar cod (*Boreogadus saida*) larvae and larval fish

assemblages in relation to oceanographic parameters in the northern Bering Sea and Chukchi Sea. *Polar Biol.* 39, 1039–1048. doi: 10.1007/s00300-016-1961-7

Kortsch, S., Primicerio, R., Fossheim, M., Dolgov, A. V., and Aschan, M. (2015). Climate change alters the structure of arctic marine food webs due to poleward shifts of boreal generalists. *Proc. Royal. Soc B.* 282, 20151546. doi: 10.1098/rspb.2015.1546

Kuwae, M., Tamai, H., Doi, H., Sakata, M. K., Minamoto, T., and Suzuki, Y. (2020). Sedimentary DNA tracks decadal-centennial changes in fish abundance. *Commun. Biol.* 3, 558. doi: 10.1038/s42003-020-01282-9

Lacoursière-Roussel, A., Howland, K., Normandeau, E., Grey, E. K., Archambault, P., Deiner, K., et al. (2018). eDNA metabarcoding as a new surveillance approach for coastal Arctic biodiversity. *Ecol. Evol.* 8, 7763–7777. doi: 10.1002/ece3.4213

Laurel, B. J., Spencer, M., Iseri, P., and Copeman, L. A. (2016). Temperature-dependent growth and behavior of juvenile Arctic cod (*Boreogadus saida*) and co-occurring North Pacific gadids. *Polar Biol.* 39, 1127–1135. doi: 10.1007/s00300-015-1761-5

Leduc, N., Lacoursière-Roussel, A., Howland, K. L., Archambault, P., Sevellec, M., Normandeau, E., et al. (2019). Comparing eDNA metabarcoding and species collection for documenting Arctic metazoan biodiversity. *Environ. DNA.* 1, 342–358. doi: 10.1002/edn3.35

Logerwell, E., Busby, M., Carothers, C., Cotton, S., Duffy-Anderson, J., Farley, E., et al. (2015). Fish communities across a spectrum of habitats in the western Beaufort Sea and Chukchi Sea. *Prog. Oceanogr.* 136, 115–132. doi: 10.1016/j.pocean.2015.05.013

Maruyama, A., Nakamura, K., Yamanaka, H., Kondoh, M., and Minamoto, T. (2014). The release rate of environmental DNA from juvenile and adult fish. *PLoS One* 9, e114639. doi: 10.1371/journal.pone.0114639

Mecklenburg, C. W., Lynghammar, A., Johannesen, E., Byrkjedal, I., Christiansen, J. S., Dolgov, A. V., et al. (2018). *Marine Fishes of the Arctic Region* (Akureyri, Iceland: Conservation of Arctic Flora and Fauna).

Merten, V., Puebla, O., Bayer, T., Reusch, T. B. H., Fuss, J., Stefanschitz, J., et al. (2023). Arctic nekton uncovered by eDNA metabarcoding: Diversity, potential range expansions, and benthic-pelagic coupling. *Environ. DNA.* 5, 503–518. doi: 10.1002/edn3.40326374943

Minegishi, Y., Wong, M. K.-S., Kanbe, T., Araki, H., Kashiwabara, T., Ijichi, M., et al. (2019). Spatiotemporal distribution of juvenile chum salmon in Otsuchi Bay, Iwate, Japan, inferred from environmental DNA. *PloS One* 14, e0222052. doi: 10.1371/journal.pone.0222052

Murakami, H., Yoon, S., Kasai, A., Minamoto, T., Yamamoto, S., Sakata, M. K., et al. (2019). Dispersion and degradation of environmental DNA from caged fish in a marine environment. *Fish. Sci.* 85, 327–337. doi: 10.1007/s12562-018-1282-6

Nelson, R. J., Bouchard, C., Fortier, L., Majewski, A. R., Reist, J. D., Præbel, K., et al. (2020). Circumpolar genetic population structure of polar cod, *Boreogadus saida*. *Polar Biol.* 43, 951–961. doi: 10.1007/s00300-020-02660-z

Nishino, S. (2020). *R/V Mirai Cruise Report MR20-05C* (Yokosuka, Japan: JAMSTEC).

Nishino, S. (2022). *CTD Data in MR20-05C, 1.00* (Japan: Arctic Data archive System (ADS). Available at: https://ads.nipr.ac.jp/dataset/A20220803-010.

Norcross, B. L., Holladay, B. A., Busby, M. S., and Mier, K. L. (2010). Demersal and larval fish assemblages in the Chukchi Sea. *Deep Sea Res. Part II.*, 57, 57–70. doi: 10.1016/j.dsr2.2009.08.006

Pettitt-Wade, H., Loseto, L. L., Majewski, A., and Hussey, N. E. (2021). Cod movement ecology in a warming world: Circumpolar arctic gadids. *Fish Fish.* 22, 562–591. doi: 10.1111/faf.12536

Planque, B., Loots, C., Petitgas, P., Lindstrøm, U., and Vaz, S. (2011). Understanding what controls the spatial distribution of fish populations using a multi-model approach. *Fish. Oceanogr.* 20, 1–17. doi: 10.1111/j.1365-2419.2010.00546.x

R Core Team (2021). *R: A Language and Environment for Statistical Computing* (Vienna, Austria: R Foundation for Statistical Computing). Available at: http://www.R-project.org/.

Sato, M., Inoue, N., Nambu, R., Furuichi, N., Imaizumi, T., and Ushio, M. (2021). Quantitative assessment of multiple fish species around artificial reefs combining environmental DNA metabarcoding and acoustic survey. *Sci. Rep.* 11, 19477. doi: 10.1038/s41598-021-98926-5

Sevellec, M., Lacoursière-Roussel, A., Bernatchez, L., Normandeau, E., Solomon, E., Arreak, A., et al. (2021). Detecting community change in Arctic marine ecosystems using the temporal dynamics of environmental DNA. *Environ. DNA.* 3, 575–590. doi: 10.1002/edn3.155

Shelton, A. O., Ramón-Laca, A., Wells, A., Clemons, J., Chu, D., Feist, B. E., et al. (2022). Environmental DNA provides quantitative estimates of Pacific hake abundance and distribution in the open ocean. *Proc. R. Soc B.* 289, 20212613. doi: 10.1098/rspb.2021.2613

Shupe, M. D., Rex, M., Dethloff, K., Damm, E., Fong, A. A., Gradinger, R., et al. (2020). Arctic report card 2020: The MOSAiC expedition: A year drifting with the Arctic sea ice. *Arctic Rep. Card.* doi: 10.25923/9g3v-xh92

Sigsgaard, E. E., Jensen, M. R., Winkelmann, I. E., Møller, P. R., Hansen, M. M., and Thomsen, P. F. (2020). Population-level inferences from environmental DNA—Current status and future perspectives. *Evol. Appl.* 13, 245–262. doi: 10.1111/eva.12882

Sigsgaard, E. E., Nielsen, I. B., Carl, H., Krag, M. A., Knudsen, S. W., Xing, Y., et al. (2017). Seawater environmental DNA reflects seasonality of a coastal fish community. *Mar. Biol.* 164, 128. doi: 10.1007/s00227-017-3147-4

H. R. Skjoldal (Ed.) (2022). *Ecosystem assessment of the Central Arctic Ocean: Description of the ecosystem. ICES Cooperative Research Reports*, (Copenhagen, Denmark: International Council for the Exploration of the Sea) Vol. 355, 341 pp. doi: 10.17895/ices.pub.20191787

Stat, M., Huggett, M. J., Bernasconi, R., DiBattista, J. D., Berry, T. E., Newman, S. J., et al. (2017). Ecosystem biomonitoring with eDNA: metabarcoding across the tree of life in a tropical marine environment. *Sci. Rep.* 7, 12240. doi: 10.1038/s41598-017-12501-5

Stoeckle, B. C., Beggel, S., Cerwenka, A. F., Motivans, E., Kuehn, R., and Geist, J. (2017). A systematic approach to evaluate the influence of environmental conditions on eDNA detection success in aquatic ecosystems. *PloS One* 12, e0189119. doi: 10.1371/journal.pone.0189119

Taberlet, P., Bonin, A., Zinger, L., and Coissac, E. (2018). *Environmental DNA* (New York: Oxford University Press). 268 pp.

Taberlet, P., Coissac, E., Hajibabaei, M., and Rieseberg, L. H. (2012). Environmental DNA. *Mol. Ecol.* 21, 1789–1793. doi: 10.1111/j.1365-294x.2012.05542.x

Takahara, T., Minamoto, T., Yamanaka, H., Doi, H., and Kawabata, Z. (2012). Estimation of fish biomass using environmental DNA. *PloS One* 7, e35868. doi: 10.1371/journal.pone.0035868

Takeuchi, A., Iijima, T., Kakuzen, W., Watanabe, S., Yamada, Y., Okamura, A., et al. (2019). Release of eDNA by different life history stages and during spawning activities of laboratory-reared Japanese eels for interpretation of oceanic survey data. *Sci. Rep.* 9, 6074. doi: 10.1038/s41598-019-42641-9

Thomsen, P. F., Møller, P. R., Sigsgaard, E. E., Knudsen, S. W., Jørgensen, O. A., and Willerslev, E. (2016). Environmental DNA from seawater samples correlate with trawl catches of subarctic, deepwater fishes. *PloS One* 11, e0165252. doi: 10.1371/journal.pone.0165252

Thomsen, P. F., and Willerslev, E. (2015). Environmental DNA – An emerging tool in conservation for monitoring past and present biodiversity. *Biol. Conserv.* 183, 4–18. doi: 10.1016/j.biocon.2014.11.019

Thorsteinson, L. K., and Love, M. S. (Eds.) (2016). *Alaska Arctic marine fish ecology catalog: U.S. Geological Survey Scientific Investigations Report 2016-5038 (OCS Study, BOEM 2016-048)* (Virginia: U.S. Geological Survey), 768. doi: 10.3133/sir20165038

Tsuji, S., Maruyama, A., Miya, M., Ushio, M., Sato, H., Minamoto, T., et al. (2020). Environmental DNA analysis shows high potential as a tool for estimating intraspecific genetic diversity in a wild fish population. *Mol. Ecol. Res.* 20, 1248–1258. doi: 10.1111/1755-0998.13165

Tsuji, S., Takahara, T., Doi, H., Shibata, N., and Yamanaka, H. (2019). The detection of aquatic macroorganisms using environmental DNA analysis—A review of methods for collection, extraction, and detection. *Environ. DNA.* 1, 99–108. doi: 10.1002/edn3.21

Tsuri, K., Ikeda, S., Hirohara, T., Shimada, Y., Minamoto, T., and Yamanaka, H. (2021). Messenger RNA typing of environmental RNA (eRNA): A case study on zebrafish tank water with perspectives for the future development of eRNA analysis on aquatic vertebrates. *Environ. DNA.* 3, 14–21. doi: 10.1002/edn3.169

Welch, H. E., Bergmann, M. A., Siferd, T. D., Martin, K. A., Curtis, M. F., Crawford, R. E., et al. (1992). Energy flow through the marine ecosystem of the lancaster sound region, Arctic Canada. *Arctic* 45, 343–357. doi: 10.14430/arctic1361

Wessel, P., Smith, W. H. F., Scharroo, R., Luis, J., and Wobbe, F. (2013). Generic mapping tools: Improved version released, EOS trans. *AGU* 94, 409–410. doi: 10.1002/2013EO450001

Wilson, R. E., Sonsthagen, S. A., Smé, N., Gharrett, A. J., Majewski, A. R., Wedemeyer, K., et al. (2020). Mitochondrial genome diversity and population mitogenomics of polar cod (*Boreogadus saida*) and Arctic dwelling gadoids. *Polar Biol.* 43, 979–994. doi: 10.1007/s00300-020-02703-5

Wong, M. K.-S., Nakao, M., and Hyodo, S. (2020). Field application of an improved protocol for environmental DNA extraction, purification, and measurement using Sterivex filter. *Sci. Rep.* 10, 21531. doi: 10.1038/s41598-020-77304-7

Yamamoto, S., Minami, K., Fukaya, K., Takahashi, K., Sawada, H., Murakami, H., et al. (2016). Environmental DNA as a 'Snapshot' of fish distribution: A case study of Japanese jack mackerel in Maizuru Bay, Sea of Japan. *PLoS One* 11, e0149786. doi: 10.1371/journal.pone.0149786

frontiers | Frontiers in Marine Science

TYPE Original Research
PUBLISHED 21 November 2023
DOI 10.3389/fmars.2023.1225923

OPEN ACCESS

EDITED BY
Ming-Tsung Chung,
National Taiwan University, Taiwan

REVIEWED BY
Joo Myun Park,
Korea Institute of Ocean Science and Technology (KIOST), Republic of Korea
Ching-Tsun Chang,
Council of Agriculture, Taiwan
Yiming Wang,
Max Planck Institute for the Science of Human History (MPI-SHH), Germany

*CORRESPONDENCE
Yu Umezawa
umezawa@me.tuat.ac.jp

RECEIVED 20 May 2023
ACCEPTED 26 October 2023
PUBLISHED 21 November 2023

CITATION
Ohno Y, Umezawa Y, Okunishi T, Yukami R, Kamimura Y, Yoshimizu C and Tayasu I (2023) Investigation of inter-annual variation in the feeding habits of Japanese sardine (*Sardinops melanostictus*) and mackerels (*Scomber* spp.) in the Western North Pacific based on bulk and amino acid stable isotopes.
Front. Mar. Sci. 10:1225923.
doi: 10.3389/fmars.2023.1225923

Investigation of inter-annual variation in the feeding habits of Japanese sardine (*Sardinops melanostictus*) and mackerels (*Scomber* spp.) in the Western North Pacific based on bulk and amino acid stable isotopes

Yosuke Ohno[1], Yu Umezawa[1]*, Takeshi Okunishi[2], Ryuji Yukami[3], Yasuhiro Kamimura[3], Chikage Yoshimizu[4] and Ichiro Tayasu[4]

[1]Department of Environmental Science on Biosphere, Tokyo University of Agriculture and Technology, Fuchu, Japan, [2]Fisheries Resources Institute, Japan Fisheries Research and Education Agency, Shiogama, Japan, [3]Fisheries Research Center, National Research Institute of Fisheries Science, Japan Fisheries Research and Education Agency, Yokohama, Japan, [4]Research Institute for Humanity and Nature, Kita-ku, Kyoto, Japan

Inter-annual variation in the feeding habits and food sources of Japanese sardine and mackerel at age-0 and age-1+ caught in the Kuroshio-Oyashio transition zone of the Western North Pacific were investigated based on analyses of bulk stable isotopes ($\delta^{13}C$, $\delta^{15}N$) and amino acid nitrogen isotopes ($\delta^{15}N_{AA}$). Differences in $\delta^{13}C$ and $\delta^{15}N$ between Japanese sardine and mackerel were small for age-0, and inter-annual variation trends were similar, suggesting they depend on similar food sources in the same food web at this age. In contrast, inter-annual variation in $\delta^{13}C$ and $\delta^{15}N$ were significantly different between both species at age-1+, and both $\delta^{15}N$ of phenylalanine ($\delta^{15}N_{Phe}$: an indicator of nitrogen source) and trophic position estimated from $\delta^{15}N_{AA}$ (TP_{AA}) were higher in mackerel, suggesting that the two species depend on distinct food webs as they age. Inter-annual variations in $\delta^{15}N_{Phe}$ were considered to have different causes for the two species; differences in food web structure due to the degree of southward intrusion of the Oyashio Current for Japanese sardine, compared to a shift in migration area and depth for mackerel. Furthermore, competition for food due to the recent increases in the population densities of both fishes appeared to be reflected in increased TP_{AA} of mackerel. Although they are caught in the same region, the mechanism of variation in food sources differs because of differences in migration area, depth, and feeding habits. Differences in the feeding habits of Japanese sardine and mackerel may affect trophic status and spawning characteristics, potentially leading to different shifts in stock abundances.

KEYWORDS

Kuroshio-Oyashio transition, amino acids, stable isotope, trophic position Japanese sardine, mackerels, feeding habit, inter-annual variation

1 Introduction

The western North Pacific is one of the largest fishing grounds in the world, with high productivity because of the mixing of the nutrient-rich cold Oyashio Current and warm Kuroshio Current (Longhurst, 2006; Yatsu, 2019; FAO, 2020). It is a major feeding ground for the important fishery resources such as Japanese sardine (*Sardinops melanostictus*) and mackerel (Chub mackerel: *Scomber japonicus*, Spotted mackerel: *Scomber australasicus*) (Yatsu et al., 2013). The spawning area of Japanese sardine and mackerel lies along the southern coast of the Japanese archipelago (Yatsu, 2019). Although the trophic level of mackerel is slightly higher than Japanese sardine based on the stomach contents analysis (i.e., copepods and diatoms for sardine, copepods, salps and anchovy for mackerel, Yatsu, 2019), both fishes are thought to migrate and grow in the same regions. Their abundance exhibits decadal-scale variability in response to climate change, known as "regime shifts" (Kawasaki, 1983; Mantua et al., 1997; Klyashtorin, 1998; Chavez et al., 2003). For juvenile Japanese sardine, the regime shift can be explained by increased survival rates of juvenile due to abundant plankton associated with higher nutrients supplied from bottom waters when the Aleutian Low develops in winter (Nishikawa and Yasuda, 2008). In the case of mackerel, it has also been suggested that a decrease in spawners due to large-scale fisheries also affects abundance fluctuations (Kawabata et al., 2012). However, the relationship between climate change and variability in abundance still needs to be clarified because both fish species, with similar spawning and feeding areas, show different fluctuations in abundance, and the survival mechanism of juveniles described above cannot fully explain the several-year scale abundance variability (Takasuka et al., 2007; Furuichi et al., 2022). Furthermore, recently the idea that the conditions of spawners (i.e., spawning experience, nutritional status, and experienced water temperature) have a significant effect on survival rates for the juveniles (i.e., maternal effect) has been proposed (Kurita, 2010; Yoneda et al., 2022). Since the nutritional status of fish depends on the amount of food resources, investigating the effects of changes in the marine environment (i.e., interaction between Oyashio and Kuroshio currents) and migration ecology on the feeding environment of adult Japanese sardine and mackerel is important for understanding the mechanisms behind the population dynamics of these fish species.

The cold Oyashio Current flows southward from the Kamchatka Peninsula along the Kuril Islands in subarctic region (Sakurai, 2007; Qiu, 2019) and its nutrient-rich water nourishes large diatoms (micro-autotrophs) and subsequently large zooplankton such as *Neocalanus* spp., which provides food resources for various marine organisms through the grazing food chain (Miyamoto et al., 2022). This area is an important feeding ground for sardine, mackerel, and squid in summer (Sakurai, 2007; Yatsu, 2019). On the other hand, the warm Kuroshio Current flows northward from the east of the Philippine Islands in subtropical region (Saito, 2019). Pico- to nano autotrophs, including nitrogen-fixing algae, are dominant due to low nutrient concentrations in the surface layer and are used by higher predators through various pathways, including the microbial food chain and the tunicate food chain (Kobari et al., 2019; Okazaki et al., 2019). Various fishes, such as chub mackerel and Japanese jack mackerel, use this current as a migration route and spawning ground (Sassa and Tsukamoto, 2010; Takahashi et al., 2019). These differences in nutrient dynamics and dominant organisms at lower trophic level in Oyashio and Kuroshio currents result in distinct differences in stable carbon and nitrogen isotopes values (δ^{13}C and δ^{15}N) for zooplankton and small fishes in each region (Ohshimo et al., 2019; Matsubayashi et al., 2020). In addition, water masses such as warm and cold anticyclonic eddies derived from the Kuroshio Extension and Oyashio form fronts between different water masses (Itoh and Yasuda, 2010) and produce dense schools of fish. Therefore, Japanese sardine and mackerel in the Kuroshio-Oyashio transition zone may be affected to different degrees by the dynamics of these cold and warm currents and show different inter-annual variations in their feeding habits.

δ^{13}C and δ^{15}N, mainly from whole tissue (bulk) samples of organisms, are widely used as a method to assess the diet of organisms (Sugisaki et al., 1991; Fry, 2006). Tissue δ^{13}C is an indicator of the carbon source of a food web because of the small alteration in isotope value between prey and predator (DeNiro and Epstein, 1978; Rau et al., 1983). In contrast, tissue δ^{15}N increases at a larger and more predictable rate, averaging around 3.4‰, compared to prey (DeNiro and Epstein, 1981; Minagawa and Wada, 1984; Post, 2002). This makes it suitable for estimating the trophic position (TP) of the organism based on the following equation, "TP = $[(\delta^{15}N_{consumer} - \delta^{15}N_{producer})/3.4] + 1$". Since δ^{13}C and δ^{15}N of phytoplankton are often characterized geographically by differences in biogeochemical processes such as nitrogen cycling and plankton productivity (Saino and Hattori, 1987; Minagawa et al., 2001; Houssard et al., 2017), these values in the muscle of pelagic fish have been successfully applied to trace migration routes and geographic distributions (Graham et al., 2010; Lorrain et al., 2015; Ohshimo et al., 2019). However, accurate estimation of TP by bulk isotope methods alone is difficult, because the δ^{15}N of primary producers varies greatly in space and time depending on the nitrogen forms supplied to the base of the food web (ex., NO_3^-, N_2 via nitrogen fixation) (Miyake and Wada, 1967) and the turnover time of phytoplankton is very short leading to large isotope variations (Yoshioka et al., 1994; Vander Zanden and Rasmussen, 2001; Jardine et al., 2006).

Recently, δ^{15}N of amino acids ($\delta^{15}N_{AA}$) has been used as a useful tool to estimate TP more accurately (McClelland and Montoya, 2002; Chikaraishi et al., 2009). This has the advantage over bulk isotopes in that the TP can be estimated solely on the basis of analyses of tissue amino acids (AAs) from the target organism by comparing "trophic AAs" (ex., Alanine, Glutamic acid), which exhibit high isotopic alteration between each trophic position, and "source AAs" (ex., Methionine. Phenylalanine), which exhibit low isotopic alteration through the food web (Popp et al., 2007; Houssard et al., 2017; Ishikawa et al., 2021). Furthermore, "source AAs" can be used as an indicator of the nitrogen source (e.g., δ^{15}N in phytoplankton) at the base of the food web (Hannides et al., 2009; Matsubayashi et al., 2020). Therefore, combining δ^{15}N of bulk and AAs is a useful method to elucidate the feeding and migratory ecology of marine organism (Hetherington et al., 2017; Xing et al., 2020; Kato et al., 2021).

In this study, we examined the differences in the food resources of Japanese sardine and mackerel species associated with growth stage and year and the factors that contribute to these differences, in the following procedure. First, inter-annual variation in the feeding habits of Japanese sardine and mackerel at age-0 and age-1+, which have the same spawning and migration area, was investigated based on bulk $\delta^{13}C$ and $\delta^{15}N$ analyses. Then, for fishes age-1+, $\delta^{15}N_{AA}$ was analyzed to reveal the causes of variation in bulk $\delta^{15}N$ (i.e., variation in nitrogen source vs. predation on food at different trophic position). These analyses and observations indicated that the factors influencing the feeding habits of Japanese sardine and mackerel were changes in the contribution of the Kuroshio and Oyashio Currents to food resources in the transition zone and the recent increase in recruitment and abundance of plankton feeders such as Japanese sardine and mackerel.

2 Materials and methods

2.1 Sample collection

Japanese sardine and mackerel were collected in the western North Pacific using a trawl net in the surface layer (0 to 30 m) during Pacific sardine and mackerel stock assessment research from May to July of each year from 2013 to 2018 aboard the research vessels: R/T/V *Hakuho-maru* (Hokkaido Government Board of Education) and *Soyo-maru* (Japan Fisheries Research and Education Agency) (Figure 1 in the Supplementary Material, hereafter Supplementary Figure 1). Fishes were flash-frozen on board and brought back to the laboratory. In comparison between chub mackerel and spotted mackerel, there was a slight difference in $\delta^{15}N$ only in age-1+ fish in some years (no significant difference in $\delta^{15}N$ in age-0 fish, and in $\delta^{13}C$ in both age-0 and age-1+ fishes, Table 1 in the Supplementary Material, hereafter Supplementary Table 1). However, the trends of annual variation in $\delta^{15}N$ were consistent in this study (Supplementary Figure 2). Furthermore, there are no significant differences in stomach contents, swimming depth, and other parameters between both fish species, at least in the 2000s, when the biomass of mackerel was low (Nakatsuka et al., 2010). Therefore, we decided to discuss these two mackerel species together as mackerel in this study. The mean body length of Japanese sardine and mackerel for each age shows large inter-annual changes influenced mainly by recruitment (Watanabe and Yatsu, 2004). In this study, following Aizawa and Takiguchi (1999), the body length ranges of age-0 and age-1+ fish in each year were first roughly estimated by dividing the length of frequency distribution at 5 mm intervals into several normal distributions, representing the same age-group. The estimated ranges at each age were finalized based on the length-at-age for that year in the stock assessments by Japan Fisheries Agency and Japan Fisheries Research and Education Agency (Furuichi et al., 2022; Yukami et al., 2022) (Table 1). Although "age-1+" might include some age-0 and age-2 individuals, most of them were age-1, so they are referred to as age-1+ in the following. The body length distribution of age-1+ used in this study is shown in Supplementary Figure 3. The inter-annual variations in the mean body length for age-1+ fishes were more observed in mackerel than Japanese sardine. The median body length of age-0 and age-1+ Japanese sardine in each year between 2014 and 2017 ranged from 84 mm to 109 mm and from 159 mm to 184 mm, respectively, while from 130 mm to 167 mm and 217 mm to 286 mm for mackerel, respectively (Table 1).

2.2 Bulk stable isotope analysis

After the bones were carefully removed by hand, the dorsal muscle tissue from each fish sample was freeze-dried for 3 days and powdered with a pestle and mortar. For delipidification, about 100 mg of powdered sub-samples were transferred into the glass test tube with a 5 ml chloroform/methanol (2:1, v/v) and left 24 hours. After removing supernatant liquid by centrifugation and drying for 24 hours, 0.3-0.5 mg sub-samples were transferred to silver capsules (SÄNTIS Analytical). The sample was acidified for 1 hour with a drop of 1 N HCl to remove inorganic carbon (i.e., HCO_3^- and $CaCO_3$), which may be contaminated from the skin and stomach contents during the sample processes. The fish samples used in this study did not contain inorganic carbon (i.e., no visible bubbles), and as in previous reports (Bosley and Wainright, 1999; Jacob et al., 2005), there was no difference in $\delta^{13}C$ and $\delta^{15}N$ values of the test samples with or without acid use beyond the analytical precision. The samples in silver capsules stored in Teflon well-plates were placed on the hotplates (60°C, 4 h) to remove water and HCl. Bulk carbon and nitrogen stable isotope value ($\delta^{13}C$ and $\delta^{15}N$: hereafter,

TABLE 1 Body length ranges of age-0 and age-1+ fish samples used in this study (mm).

	Sardinops melanostictus		*Scomber japonicus*		*Scomber australasicus*	
Year/Age	age-0	age-1+	age-0	age-1+	age-0	age-1+
2013	50-113 (76)	128-204 (171)	——	190-290 (257)	——	236-279 (246)
2014	36-131 (84)	160-209 (180)	121-178 (150)	196-293 (217)	141-174 (159)	203-255 (225)
2015	78-116 (101)	144-212 (159)	106-195 (130)	203-267 (231)	109-191 (151)	224-288 (254)
2016	79-119 (109)	144-189 (167)	116-177 (148)	195-339 (277)	117-197 (167)	210-326 (286)
2017	35-121 (95)	133-224 (184)	110-176 (146)	182-334 (242)	121-209 (165)	218-279 (256)
2018	61-91 (76)	——	83-151 (106)	——	88-164 (129)	——

The numbers in parentheses indicate the median value among the samples used in the analysis.
Age-0 mackerels in 2013 and age-1 mackerels in 2018 were removed from the analysis data because fish samples with sufficient quantities for the statistical analysis were not available.

unless otherwise noted, $\delta^{13}C$ and $\delta^{15}N$ denote bulk values) of fish samples were measured with an elemental analyzer and an isotope-ratio mass spectrometer (FLASH 2000-Conflo IV-Delta V Advantage; Thermo Fisher Scientific). The ratios of ^{13}C:^{12}C and ^{15}N:^{14}N were expressed relative to Vienna Pee-Dee Belemnite (VPDB) and atmospheric nitrogen, respectively, and were calculated as follows:

$$\delta^{13}\,C,\ \delta^{15}\,N = \{[R(\text{sample})/R(\text{standard})] - 1\} \times 1000\ (\text{‰})$$

where $R = {}^{13}C/{}^{12}C$ or $^{15}N/^{14}N$. L-alanine ($\delta^{13}C$ = -19.6‰, $\delta^{15}N$ = 8.7‰; Shoko Science) was measured every 5 samples as a calibration standard. Also, alanine ($\delta^{13}C$ = -19.6‰, $\delta^{15}N$ = 13.7‰: Shoko Science, Inc.) and glycine ($\delta^{13}C$ = -32.3‰, $\delta^{15}N$ = 1.12‰: Shoko Science, Inc.) with different isotopic ratios was measured several times to check the accuracy of the analysis. The instrumental precision was within 0.1‰ (standard deviation) for $\delta^{13}C$ and $\delta^{15}N$.

2.3 $\delta^{15}N$ of amino acids analysis

Analysis of nitrogen stable isotopes of amino acids ($\delta^{15}N_{AA}$) was conducted on age-1+ fish to reveal the factors of variation in $\delta^{15}N$. Each year, 2 to 3 samples were analyzed for Japanese sardine (i.e., 12 samples in total) and 2 to 4 samples for mackerel (i.e., 15 samples in total) (see Supplementary Table 2). Among these samples, the samples with similar body lengths close to the mean value were selected for each year because differences in body length can cause differences in trophic position (TP). Although there were differences in the body length of the samples in different years, body length-size dependent changes in TP were not observed.

For $\delta^{15}N_{AA}$ analysis, powder samples of fishes (3~4 mg) were hydrolyzed in 12 N HCl at 112°C for 12~24 h. The hydrolysate was washed with n-hexane/dichloromethane (3:2, v/v) to remove hydrophobic constituents, such as lipids, and then dried under an N_2 gas while adding 2-propanol as the solvent several times. After derivatization with thionyl chloride/2-propanol (1:4, v/v) at 112°C for 2 h and pivaloyl chloride/dichloromethane (1:4, v/v) at 112°C for 2 h, the Pv/iPr derivatives of amino acids were extracted with dichloromethane. Derivatization samples were stored under -30°C until measurement. The $\delta^{15}N_{AA}$ were measured using a gas chromatography/combustion/isotope ratio mass spectrometry system (GC/C/IRMS) consisting of an IRMS (Delta V advantage; Thermo Fisher Scientific) coupled to a GC (Trace GC Ultra; Thermo Fisher Scientific) via a modified GC-Isolink interface consisting of combustion and reduction furnaces. The programs on temperature, retention time, and carrier gas flow rate in each process followed the methods given in Ishikawa et al. (2014) (details are available in Supplementary Text 1). The CO_2 generated in the combustion furnace was removed using a liquid N trap. Standard mixtures of eight AAs (alanine, glycine, leucine, norleucine, aspartic acid, methionine, glutamic acid, and phenylalanine) with known $\delta^{15}N$ (range -25.9 to 45.6‰, Shoko Science, Inc.) was measured between every 2 to 3 samples to confirm the reproducibility of isotope value measurements. Standard deviations of the standards of glutamic acid and phenylalanine were better than 0.6 ‰ with a sample quantity of 60 ng N. TP of fishes based on the $\delta^{15}N$ values of glutamic acid ($\delta^{15}N_{Glu}$) and phenylalanine ($\delta^{15}N_{Phe}$) in the targeted fish sample were calculated using the following equation following to Chikaraishi et al. (2009),

$$TP_{AA} = (\delta^{15}N_{Glu} - \delta^{15}N_{Phe} - 3.4)/7.6 + 1$$

where 3.4 represents the mean difference between $\delta^{15}N_{Glu}$ and $\delta^{15}N_{Phe}$ in the primary producers (trophic level = 1.0), and 7.6 represents the mean difference of the trophic discrimination factors at each trophic level between glutamic acid and phenylalanine, respectively.

In addition, phenylalanine is one of the "source AAs" and has been used in several studies as an indicator of the nitrogen source at the base of the food web (Hannides et al., 2009; Matsubayashi et al., 2020). Here, $\delta^{15}N_{Phe}$ is taken to be an indicator of the inter-annual variation of nitrogen sources.

2.4 Statistical analysis

Since it is previously reported that the distribution of $\delta^{13}C$ and $\delta^{15}N$ in pelagic fishes having a wide migratory area vary according to their habitat (Miyachi et al., 2015; Ohshimo et al., 2019; Fuji et al., 2021), $\delta^{13}C$ and $\delta^{15}N$ in Japanese sardine and mackerel may potentially differ depending on the capture area. Therefore, considering the general migration route of these fish species, the fishes captured in the area bounded by N35-43°/E150-160° and N35-43°/E140-150° were analyzed for age-0 fishes and age-1+ fishes, respectively (Figure 1, age-0: n = 817, age-1+: n = 797). To examine the inter-annual variation of $\delta^{13}C$ and $\delta^{15}N$, the following statistical analysis were performed. First, a Shapiro-Wilk test was performed to examine whether the $\delta^{13}C$ and $\delta^{15}N$ values for each year followed a normal distribution, and the Bartlett test was performed to check the equality of variances. In this study, there was no normality for any fishes or age (Shapiro-Wilk test, $p<0.05$). Therefore, the data was examined to determine whether $\delta^{13}C$ and $\delta^{15}N$ differed for each year by the Kruskal-Wallis test. If there were significant differences, multiple comparisons were performed by the Steel-Dwass test to determine which years had significant differences. In addition, t-tests were used to check for significant differences between Japanese sardine and mackerel in each analysis item (Supplementary Table 3). All statistical analysis was performed with R (version 4.2.0) at the significant level of α = 0.05 and visualized using ggplot2 in R (Wickham, 2016).

2.5 The analyses of experienced temperature associated with fish migration

In the study area, the western North Pacific, both the cold Oyashio current and the warm Kuroshio current mix in the transitional zone and fluctuation in the strength of the two may cause changes in the feeding environment for fishes (Miyamoto et al., 2022), as noted in the Introduction section. The contribution of the currents (i.e., Oyashio vs. Kuroshio) to the water mass in the

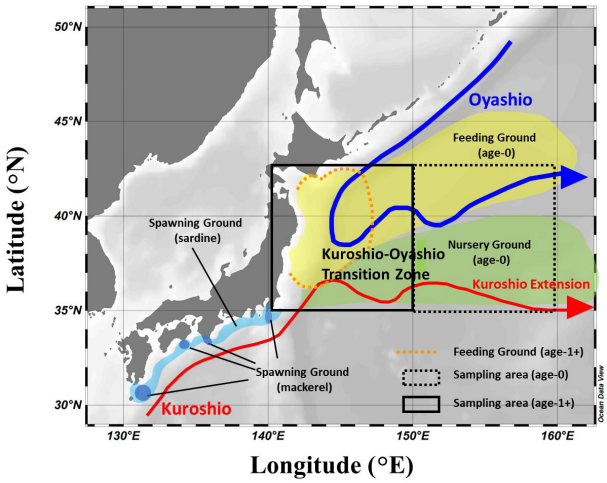

FIGURE 1
Schematic diagram of the ocean currents in the study area and the migration area along the life history of Japanese sardine and mackerel. The migration area of both fishes was referred to Furuichi et al. (2022) and Yukami et al. (2022). The squares indicate the main areas where fish samples were collected in this study.

transitional zone can be estimated from water temperature as a proxy, so we hypothesized that analysis of the experienced water temperature for fish during the migration could explain the factors that cause fluctuations in fish isotope values. Therefore, FRA-ROMS reanalysis data, an ocean forecast system based on the Regional Ocean Modeling System (Kuroda et al., 2017), was used to examine inter-annual changes in mean water temperature from February to June prior to the collection of age-1+ fishes in each year from 2013 to 2017. Actual observed data, such as water temperature and salinity obtained from satellite and shipboard observations, are incorporated into FRA-ROMS for reanalysis. Thereby, FRA-ROMS could reproduce seasonal and interannual variations of mesoscale oceanic features over the Kuroshio-Oyashio region, such as the position of the Kuroshio path, variability of the Kuroshio Extension, and southward intrusions of the Oyashio (Kuroda et al., 2017). The stable isotope values of fish are the integral of the isotope values of the food during the period corresponding to the turnover time. The turnover time (3 months) was estimated for Japanese sardine and mackerel using the relationship equation between weight and isotopic half-life given in Vander Zanden et al. (2015) to set the period for the water temperature analysis. The area for analysis was set at N35-40° and E140-150°, the general migration area of age-1+ Japanese sardine and mackerel during February-June (Yatsu, 2019). The analysis was conducted at 3 water depths (i.e., 100 m, 50 m and 30 m). In the Kuroshio-Oyashio transition zone, the Oyashio is submerged under the Kuroshio (Itoh and Yasuda, 2010; Ishikawa et al., 2021), so the effect of the Oyashio is expected to be stronger at 100 m depth. Depths between 30 m and 50 m correspond to the representative migration depths of Japanese sardine and mackerel, respectively (Inagake and Hirano, 1983; Ozawa, 2010; Kamimura et al., 2021), indicating the suitable depths to check the effect of water temperature on these fish species. Surface sea temperature (SST) was not included in this analysis because it is strongly affected by solar radiation.

3 Results

3.1 Inter-annual variation in bulk $\delta^{13}C$ and $\delta^{15}N$

In age-0 fish, the mean $\delta^{13}C$ values for all samples of Japanese sardine and mackerel were -20.2 ± 1.0‰ and -20.1 ± 1.0‰, respectively, while $\delta^{15}N$ values were 7.9 ± 1.6‰ and 7.8 ± 1.6‰, respectively, showing no differences between species (t-test, p=0.80, 0.44; Figures 2A, B; Supplementary Table 3). The annual mean $\delta^{13}C$ value for Japanese sardine and mackerel ranged from -21.2‰ to -19.1‰ and -21.3‰ to -18.6‰, respectively, while the annual mean $\delta^{15}N$ value ranged from 6.7‰ to 9.3‰ and 6.3‰ to 9.8‰, respectively (Table 2). Significant inter-annual variations in both $\delta^{13}C$ and $\delta^{15}N$ were observed for Japanese sardine and mackerel (Kruskal-Wallis test, $p<0.05$), with significant differences between years shown in Figure 2 (Steel-Dwass test, $p<0.05$). Comparing the mean values of Japanese sardine and mackerel by year, a significant difference was evident between Japanese sardine and mackerel for $\delta^{13}C$ in 2014 (t-test, $p<0.05$, Supplementary Table 3), but the trend in inter-annual variation was consistent for both fishes (Figure 2A). Similarly, for $\delta^{15}N$, significant differences were found in most of year between Japanese sardine and mackerel (t-test, $p<0.05$, Supplementary Table 3), but the trend in inter-annual variation was consistent for both fishes, with a significant decrease in the value of both in 2017 (Figure 2B).

In age-1+ fish, the mean $\delta^{13}C$ values for all samples of Japanese sardine and mackerel were -18.6 ± 0.7‰ and -19.1± 0.4‰, respectively, and $\delta^{15}N$ was 9.0 ± 0.8‰ and 10.5 ± 0.8‰, respectively (Table 2). A significant difference between species was confirmed (t-test, $p<0.05$; Figures 2C, D; Supplementary Table 3). The annual mean $\delta^{13}C$ value for Japanese sardine and mackerel ranged from -18.9‰ to -18.4‰ and -19.3‰ to -19.0‰, respectively, and the annual mean $\delta^{15}N$ value ranged from 8.8‰ to 9.3‰ and 9.8‰ to 10.8‰, respectively (Table 2). Significant inter-annual variation was observed, except for $\delta^{13}C$ for mackerel (Figures 2C, D; Kruskal-Wallis test, $p<0.05$). Larger inter-annual variation in the $\delta^{15}N$ was found for mackerel than Japanese sardine, with low $\delta^{15}N$ in 2014 and 2015, and high $\delta^{15}N$ in 2013, 2016, and 2017 (Steel-Dwass test, $p<0.05$). Comparing the mean values of Japanese sardine and mackerel by year, Japanese sardine had significantly higher $\delta^{13}C$ and lower $\delta^{15}N$ in all years (t-test, $p<0.05$; Figures 2C, D; Supplementary Table 3). As described above, at age-0, there was no significant difference in the mean $\delta^{13}C$ and $\delta^{15}N$ values of Japanese sardine and mackerel for the whole period of this study, and the trend of inter-annual variation was also consistent. In contrast at age-1+, the $\delta^{13}C$ and $\delta^{15}N$ values of these fish species were significantly different and the trend of inter-annual variation was inconsistent.

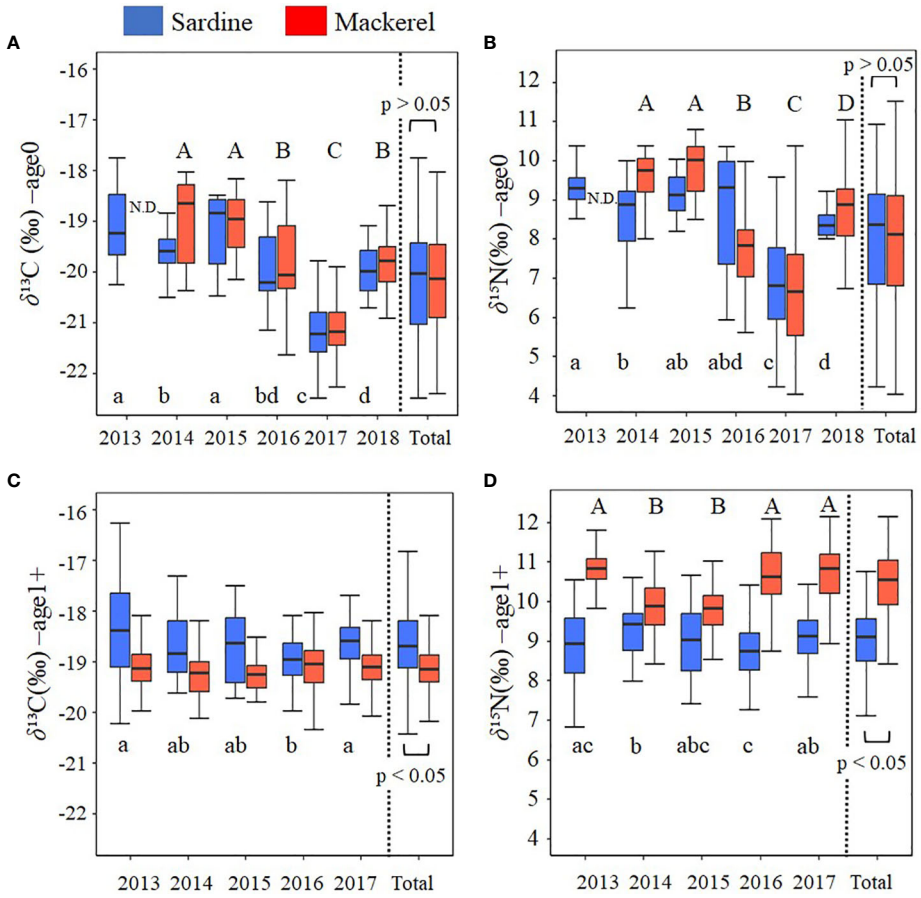

FIGURE 2
Inter-annual variation in **(A)** $\delta^{13}C$ at age-0, **(B)** $\delta^{15}N$ at age-0, **(C)** $\delta^{13}C$ at age-1+, and **(D)** $\delta^{15}N$ at age-1+ for Japanese sardine and mackerel. Boxplots show the median (middle line) and the interquartile range (box). The whiskers extend to the minimum and maximum observations. Different letters denote significant differences ($p<0.05$) among year (small letters: Japanese sardine, capital letters: mackerel). There was no significant difference in $\delta^{13}C$ for mackerel. at age-1+. Total is the value calculated by combining all samples from all years. N.D. means no data.

3.2 $\delta^{15}N$ of amino acids ($\delta^{15}N_{AA}$) variation for Japanese sardine and mackerel at age-1+

Analyses of $\delta^{15}N_{AA}$ were performed to examine the factors affecting inter-annual variation in bulk $\delta^{15}N$ for age-1+. The $\delta^{15}N$ of glutamic acid ($\delta^{15}N_{Glu}$) was 18.0 ± 0.8‰ (16.6 to 19.1‰) and 21.6 ± 1.0‰ (20.2 to 23.7‰) in Japanese sardine and mackerel, respectively, and the $\delta^{15}N$ of phenylalanine ($\delta^{15}N_{Phe}$) were 1.8 ± 1.2‰ (-0.7 to 3.4‰) and 3.1 ± 0.8‰ (1.8 to 4.1‰), respectively (Figures 3A, B; Supplementary Tables 2, 4). The $\delta^{15}N_{Phe}$, an indicator of nitrogen source, in mackerel showed higher values than Japanese sardine (t-test, $p<0.05$, Figure 3B), and trophic position estimated from $\delta^{15}N_{Glu}$ and $\delta^{15}N_{Phe}$ (TP_{AA}) was 2.7 ± 0.1 (2.4 to 2.9) for Japanese sardine compared to 3.0 ± 0.1 (2.8 to 3.3) for mackerel (Supplementary Tables 2, 4). As with $\delta^{15}N_{Phe}$, TP_{AA} for mackerel was significantly higher than for Japanese sardine (t-test, $p<0.05$, Figure 3C), consistent with the results from bulk $\delta^{15}N$ analysis (Figure 2D). Mean values of $\delta^{15}N_{Phe}$ for Japanese sardine were low in 2013 and high in 2015 and 2017 (Figure 3E; Supplementary Table 4). Correspondingly, TP_{AA} was higher in 2013 and lower in 2015 and 2017 (Figure 3F; Supplementary Table 4). Therefore, a significant negative correlation was found between $\delta^{15}N_{Phe}$ and TP_{AA} in Japanese sardine ($R^2 = 0.603$, $p< 0.05$, Figure 4B). In addition, there was a positive correlation between bulk $\delta^{15}N$ and $\delta^{15}N_{Phe}$ for Japanese sardine ($R^2 = 0.529$, slope = 0.355, $p< 0.05$, Figure 4A). $\delta^{15}N_{Glu}$ in Japanese sardine did not exhibit any noticeable annual fluctuations. On the other hand, mean values of $\delta^{15}N_{Phe}$ for mackerel were higher in 2013, 2016 and 2017 (Figure 3E; Supplementary Table 4), which was consistent with years with higher bulk $\delta^{15}N$ (Figure 2D). Therefore, a positive correlation was also observed between bulk $\delta^{15}N$ and $\delta^{15}N_{Phe}$ for mackerel ($R^2 = 0.710$, slope = 0.600, $p< 0.05$, Figure 4A). Although a slightly gradual increase in TP_{AA} was observed from 2013 to 2017 for mackerel (Figure 3F), there was no evidence of the relationship between $\delta^{15}N_{Phe}$ and TP_{AA} (Figure 4B) that was observed in Japanese sardine. $\delta^{15}N_{Glu}$ for mackerel showed a similar trend in inter-annual variation to $\delta^{15}N_{Phe}$ (Figures 3D, E).

10.3389/fmars.2023.1225923

TABLE 2 Bulk $\delta^{13}C$ and $\delta^{15}N$ values for Japanese sardine and mackerel (mean ± SD).

		mackerel		Sardine	
		age-0	age-1+	age-0	age-1+
$\delta^{13}C$ (‰)	2013	——	-19.0 ± 0.6 (n=55)	-19.1 ± 0.7 (n=82)	-18.4 ± 1.0 (n=90)
	2014	-18.6 ± 0.6 (n=21)[$]	-19.2 ± 0.4 (n=89)	-19.6 ± 0.4 (n=91)	-18.7 ± 0.6 (n=61)
	2015	-19.0 ± 0.5 (n=25)	-19.3 ± 0.3 (n=36)	-19.2 ± 0.7 (n=34)	-18.7 ± 0.7 (n=21)
	2016	-19.8 ± 0.8 (n=67)	-19.1 ± 0.5 (n=134)	-19.9 ± 0.7 (n=27)	-18.9 ± 0.5 (n=45)
	2017	-21.3 ± 0.2 (n=100)[$]	-19.1 ± 0.4 (n=152)	-21.2 ± 0.6 (n=181)	-18.7 ± 0.5 (n=114)
	2018	-19.8 ± 0.5 (n=118)	——	-20.0 ± 0.4 (n=56)	——
	total	-20.1 ± 1.0 (n=331)	-19.1 ± 0.4 (n=466)	-20.2 ± 1.0 (n=471)	-18.6 ± 0.7 (n=331)
$\delta^{15}N$ (‰)	2013	——	10.8 ± 0.6 (n=55)	9.3 ± 0.5 (n=82)	8.8 ± 0.6 (n=90)
	2014	9.8 ± 0.5 (n=21)[$]	9.8 ± 0.6 (n=89)	8.6 ± 1.0 (n=91)	9.3 ± 0.7 (n=61)
	2015	9.8 ± 0.6 (n=25)[$]	9.9 ± 0.7 (n=36)	8.9 ± 1.1 (n=34)	9.0 ± 0.9 (n=21)
	2016	8.1 ± 1.0 (n=67)[‡]	10.6 ± 0.8 (n=134)	8.7 ± 1.5 (n=27)	8.8 ± 0.7 (n=45)
	2017	6.3 ± 1.2 (n=100)[‡]	10.7 ± 0.7 (n=152)	6.7 ± 1.4 (n=181)	9.1 ± 0.6 (n=114)
	2018	8.5 ± 1.2 (n=118)[$]	——	7.9 ± 1.1 (n=56)	——
	total	7.8 ± 1.6 (n=331)	10.5 ± 0.8 (n=466)	7.9 ± 1.6 (n=471)	9.0 ± 0.8 (n=331)

Total is the value calculated by combining all samples from all years. Age-0 mackerels in 2013 and age-1 mackerels in 2018 were not used for the analysis, because fish samples with sufficient quantities for the statistical analysis were not available. [$]Significantly higher for mackerel than Japanese sardine. [‡]Significantly lower for mackerel than Japanese sardine. For age-1+ fish, $\delta^{13}C$ was significantly lower for mackerel and $\delta^{15}N$ was significantly higher for mackerel in all years.

3.3 Annual variation of water temperature experienced by the fishes compared to $\delta^{15}N_{Phe}$ and TP_{AA} in the fishes

Figure 5 shows the inter-annual variation of mean water temperature at N35-40°/E140-150° from February to June (Supplementary Table 5). The trend of inter-annual variation of water temperature at 100 m depth, which directly reflects the southward intrusion of the Oyashio Current into the study area, was also linked to those from 30 m to 50 m, which corresponds to the main migratory layer of Japanese sardine and mackerel. The water temperatures in 2015 and 2017 were lower than in other years (Figure 5). In order to investigate the effects of southward intrusion of the cold Oyashio at a depth of 100 m or deeper layer and the associated movement of the warm Kuroshio at the surface mixed layer on the feeding habits of both age-1+ fish species, the relationship between water temperature at 100m depth and $\delta^{15}N_{Phe}$ (reflecting $\delta^{15}N$ of phytoplankton, the base of the food web) and TP_{AA} of both fish species are plotted in Figures 6, 7, respectively. The mean water temperature at 100 m depth was negatively correlated with mean $\delta^{15}N_{Phe}$ for age-1+ Japanese sardine in each year (R^2 = 0.866, Figure 6A), but not with mean $\delta^{15}N_{Phe}$ for age-1+ mackerel (Figure 6B). On the other hand, the mean water temperature at 100 m depth was positively and negatively correlated with TP_{AA} for age-1+ Japanese anchovy (R^2 = 0.888, Figure 7A) and age-1+ mackerel (R^2 = 0.640, Figure 7B), respectively.

4 Discussion

4.1 Differences in feeding habits of Japanese sardine and mackerel according to growth stage

Both Japanese sardine and mackerel spawn along the central and southern coast of the Japanese archipelago from winter to spring (Kanamori et al., 2019; Yatsu, 2019). The juveniles are transported eastward by the Kuroshio Current, then northward from around June, and migrate in almost the same area every year (Figure 1, Sakamoto et al., 2018; Yatsu, 2019). Here, slight differences in $\delta^{13}C$ and $\delta^{15}N$ were observed at age-0 between Japanese sardine and mackerel in each year, but no significant differences were observed in the mean values for entire period of the study (Figures 2A, B). Therefore, although the trophic position (TP) of the fishes' diet may differ slightly, the finding is consistent with a previous study that suggested these species prey primarily on zooplankton (Yatsu, 2019). In addition, similar trends in inter-annual variation of $\delta^{13}C$ and $\delta^{15}N$ indicate that the two species may depend on the same food web. This is because even if $\delta^{15}N$ values differ between fishes due to differences in TP, when the dependent food web is the same, the $\delta^{15}N$ of the fishes shows the same inter-annual variation linked to the $\delta^{15}N$ of the basal nitrogen source (Bode et al., 2007; Hannides et al., 2009). By contrast, significant differences in $\delta^{13}C$ and $\delta^{15}N$ emerged at age-1+ between Japanese sardine and mackerel. This was particularly evident in $\delta^{15}N$ values,

10.3389/fmars.2023.1225923

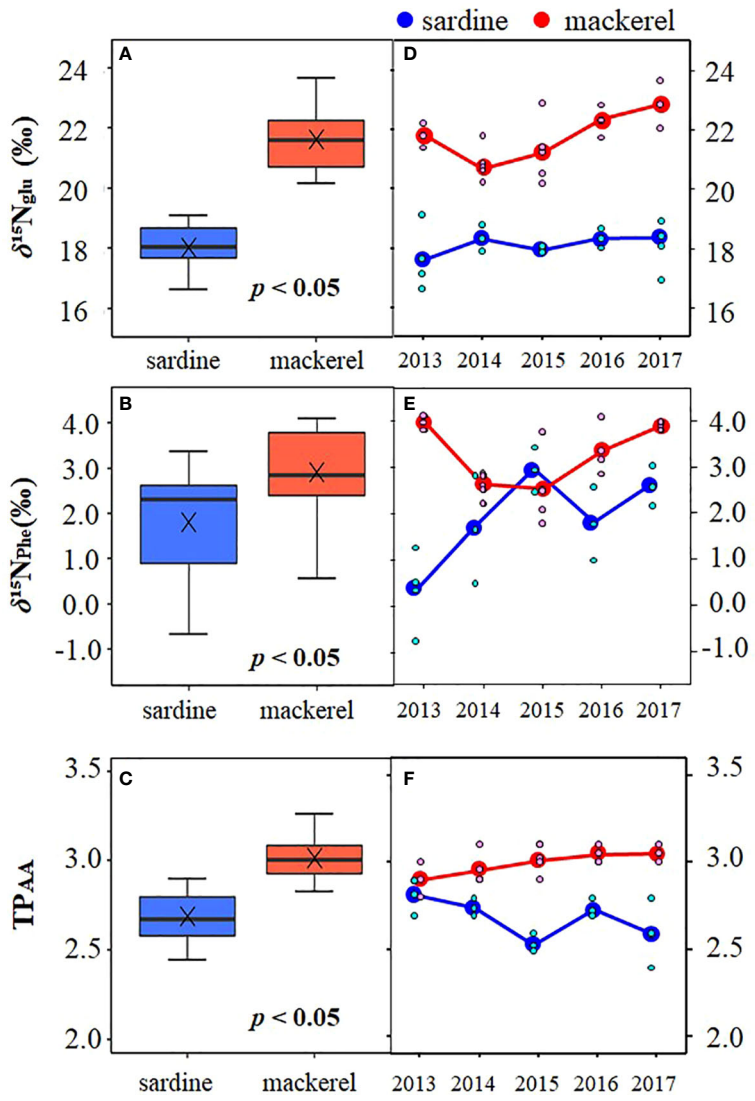

FIGURE 3
Comparison of **(A)** $\delta^{15}N_{Glu}$, **(B)** $\delta^{15}N_{Phe}$, and **(C)** TP_{AA} among Japanese sardine and mackerel at age-1+, and inter-annual variation of mean of **(D)** $\delta^{15}N_{Glu}$, **(E)** $\delta^{15}N_{Phe}$, and **(F)** TP_{AA} for these fishes. The symbol × in the panels **(A–C)** denotes mean value. The small symbols in the panels **(D–F)** indicate individual values.

often indicative of trophic position, where mackerel consistently higher values compared to Japanese sardine (Figure 2D). Indeed, mackerel are known to feed on small fishes in addition to zooplankton as they grow (Yatsu, 2019). Furthermore, the inconsistent trend of inter-annual variation in $\delta^{15}N$ between Japanese sardine and mackerel (Figure 2D) suggests that even in the same migration area, there may be differences in TP and/or the food web on which they depend.

In general, there are two possible reasons for variation in fish $\delta^{15}N$ values: changes in (1) TP and/or (2) the nitrogen sources supporting the food web. However, it was challenging to identify the reasons for $\delta^{15}N$ variation based only on bulk isotopes. So, $\delta^{15}N$ of amino acids ($\delta^{15}N_{AA}$) were measured to help clarify the reasons for variation in $\delta^{15}N$ for Japanese sardine and mackerel, and to obtain detailed insights into their feeding habits and food webs. The mean TP based on $\delta^{15}N_{AA}$ (TP_{AA}) of age-1+ was 3.0 (2.8 to 3.3) for mackerel and 2.7 (2.4 to 2.9) for Japanese sardine, with mackerel being significantly higher (Figure 3C). Therefore, part of the difference in $\delta^{15}N$ between both fish species can be explained by TP_{AA} (Supplementary Figure 4). This result for mackerel is consistent with the stomach content analysis, which has shown that zooplankton is the primary food resource (Yatsu, 2019). In contrast, for Japanese sardine, diatoms have frequently been found during stomach content analysis and are considered as a major food resource of the species (Kawasaki and Kumagai, 1984). However, $\delta^{15}N_{AA}$ analyses in this study suggest that zooplankton is more easily digested and contributes more to the diet of Japanese sardine than diatoms because TP_{AA} (2.7 ± 0.1) was close to the typical value of the first level carnivores (i.e., 3.0, Chikaraishi et al., 2014). Also, mackerel had significantly higher $\delta^{15}N$ of phenylalanine ($\delta^{15}N_{Phe}$) than Japanese sardine (Figure 3B), which reflects the $\delta^{15}N$ of nitrogen sources (e.g., primary producers), and the trends of

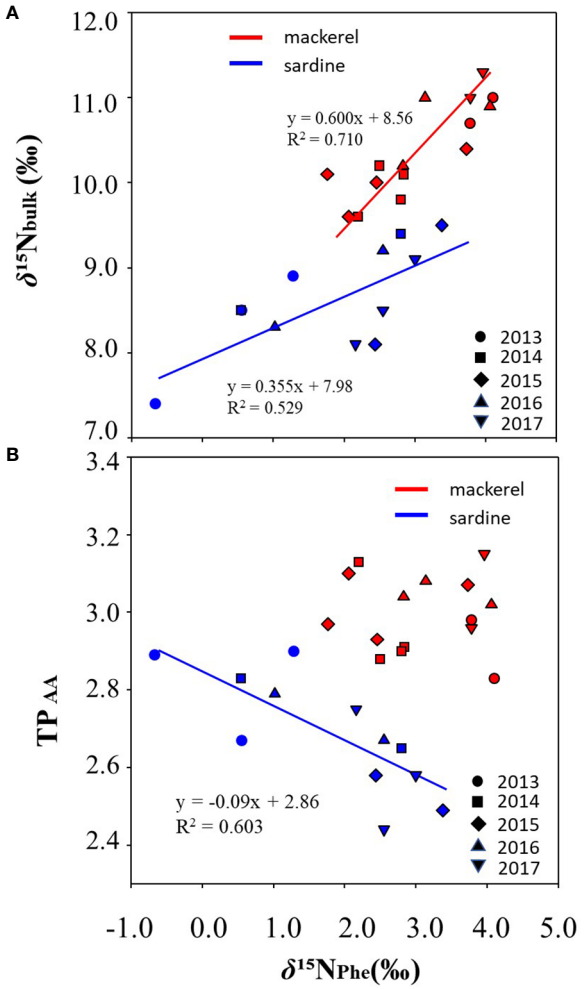

FIGURE 4
Correlations between **(A)** $\delta^{15}N_{bulk}$ and $\delta^{15}N_{Phe}$ and **(B)** TP_{AA} and $\delta^{15}N_{Phe}$, for individual fish samples of Japanese sardine and mackerel at age-1+ for each year during the targeted period. The solid lines are the regression line. No correlation was found between TP_{AA} and $\delta^{15}N_{Phe}$ in mackerel.

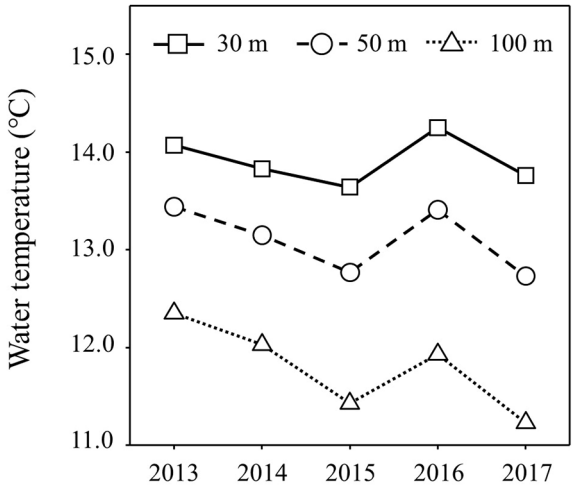

FIGURE 5
Inter-annual variation of water temperatures for each depth of 30 m, 50 m and 100 m at 35-40°N/140-150°E during February-June. Plots are the average of the mean values for each month during the targeted period.

inter-annual variation of $\delta^{15}N_{Phe}$ were different between Japanese sardine and mackerel (Figure 3E). Consequently, similarly to the results of the bulk method, $\delta^{15}N_{AA}$ analyses suggest that the food resources utilized by these fishes are different. It is assumed that differences in migration depth are related to changes in the food sources at age-1+. Generally, both Japanese sardine and mackerel at age-0 migrate shallower than 30 m, but as they grow, mackerel have been reported to migrate to depths of 50-80 m as a school of fish and up to 150 m as individuals in deeper water (Ozawa, 2010; Kamimura et al., 2021; Yasuda et al., 2023). In the Kuroshio-Oyashio transition zone, the Oyashio Current intrudes from a deeper layer below the Kuroshio Current (Itoh and Yasuda, 2010; Ishikawa et al., 2021), suggesting that mackerel are strongly influenced by the food supplied by the Oyashio Current. In fact, Matsubayashi et al. (2020) reported in their isoscape that the $\delta^{15}N$ of zooplankton (i.e., 6.7 ± 2.1‰ on average) found in the northern region of the Kuroshio-Oyashio transition zone, which is influenced by the Oyashio Current, was greater than that of zooplankton (i.e., 4.6 ± 2.2‰ on average) in the southern region of the zone. Furthermore, Miyamoto et al. (2022) reported that larger sized subarctic copepods (e.g., *Neocalanus* spp. And *Eucalanus bungii*) appear more frequently in the Kuroshio-Oyashio transition zone with southward intrusion of the Oyashio Current. In this way, the difference in food source associated with the migration depth may cause different inter-annual variations of $\delta^{13}C$ and $\delta^{15}N$ for Japanese sardine and mackerel at age-1+. In the following, the factors leading to variation in $\delta^{15}N$ in Japanese sardine and mackerel, respectively, are discussed in turn based on the results of $\delta^{15}N_{AA}$.

4.2 $\delta^{15}N$ and TP_{AA} variation of Japanese sardine at age-1+

There was a positive correlation between bulk $\delta^{15}N$ and $\delta^{15}N_{Phe}$ for Japanese sardine (Figure 4A). $\delta^{15}N_{Phe}$ is an indicator of the nitrogen source (e.g., $\delta^{15}N$ of phytoplankton) due to limited isotopic alterations between trophic positions (Hannides et al., 2009; Matsubayashi et al., 2020). Therefore, one of the reasons contributing to the variability of $\delta^{15}N$ in Japanese sardine (Figure 3E) may be the influence of differences in the $\delta^{15}N$ of phytoplankton, which is the basis of the food web. $\delta^{15}N$ of phytoplankton is known to fluctuate significantly with changes in nutrient supplies, and there are two possible mechanisms for lowering $\delta^{15}N$ values. First, in nutrient (nitrate)-rich waters, $\delta^{15}N$ of phytoplankton is decreased because of the substantial fractionation associated with nitrate utilization by phytoplankton (Yoshikawa et al., 2005; Yoshikawa et al., 2018). Second, in oligotrophic waters, $\delta^{15}N$ is decreased because of the increased contribution of N_2 fixation as a nitrogen source. Atmospheric N_2 by definition has a $\delta^{15}N$ of 0 ‰, which is lower than nitrate, so N_2-

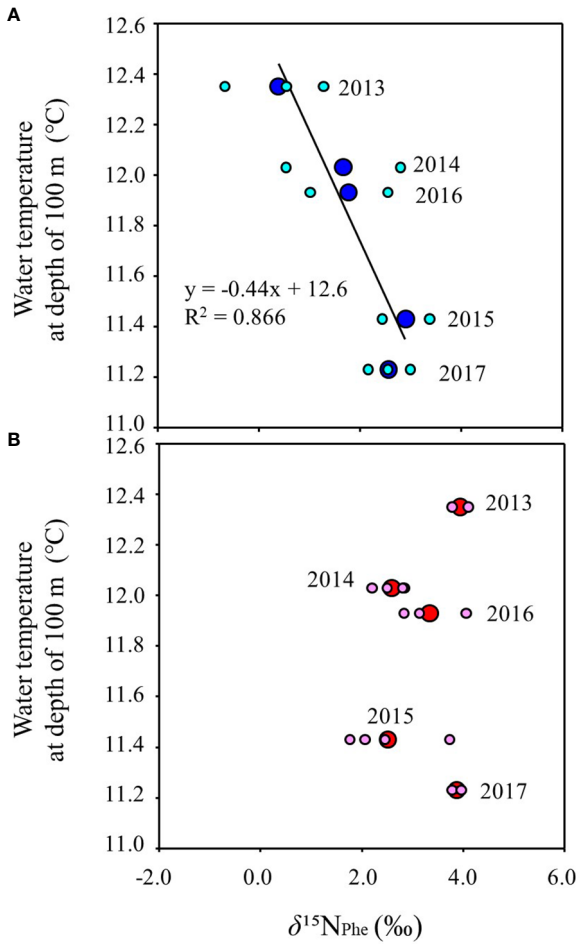

FIGURE 6
Relationships between the mean of $\delta^{15}N_{Phe}$ at age-1+ fishes and mean water temperature from February to June at a depth of 100 m in each year, for **(A)** Japanese sardine, and **(B)** mackerels. The large and small symbols indicate mean and individual values, respectively. The line in the figure is the regression line. The number in each plot indicates the year when the fish samples were collected (n=2 or 4 for each year).

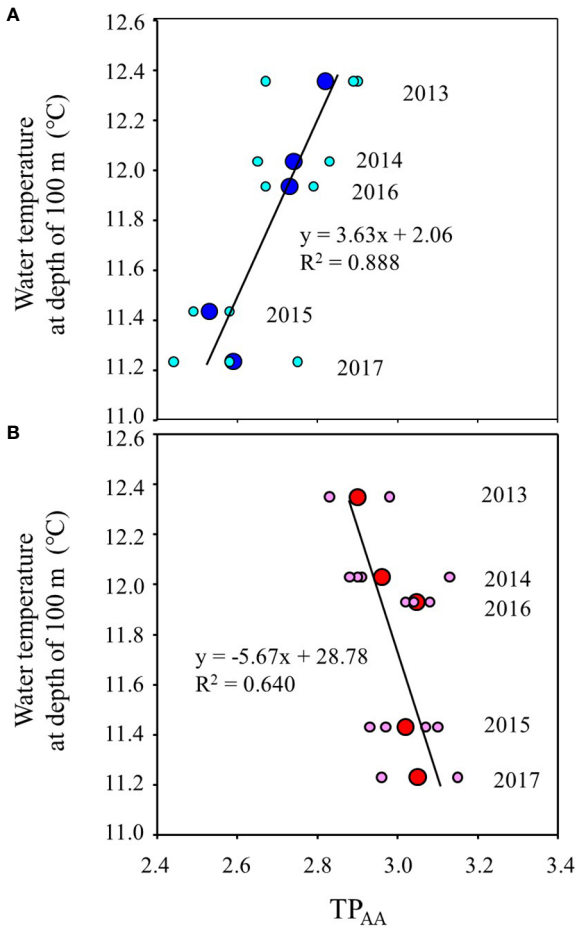

FIGURE 7
Relationships between the mean of TP_{AA} at age-1+ fishes and mean water temperature from February to June at a depth of 100 m in each year, for **(A)** Japanese sardine and **(B)** mackerels. The large and small symbols indicate mean and individual values. The line in each panel is the regression line. The number in each plot indicates the year when the fish samples were collected (n=2 or 4 for each year).

fixing algae have lower $\delta^{15}N$ than phytoplankton that use nitrate as a nitrogen source (Minagawa and Wada, 1984; Horii et al., 2018).

In the Oyashio-Kuroshio transition zone, the Oyashio Current, with low temperature and abundant nutrients, extends southward at depth deeper than 100 m with seasonal and inter-annual variations, potentially supplying nutrients from the bottom to the surface where nutrients are depleted in spring and summer (Komatsu and Hiroe, 2019; Nishikawa et al., 2020). A negative correlation was observed between the mean temperature at 100 m depth and $\delta^{15}N_{Phe}$ of Japanese sardine (i.e., $\delta^{15}N$ of phytoplankton, the base of the food web) in each year (Figure 6A). Therefore, lower $\delta^{15}N$ of phytoplankton during the year with relatively high-water temperature suggests that the degree of the southward flow of the Oyashio Current and associated variation of warm Kuroshio water contribution could be related to the variation in $\delta^{15}N$ of Japanese sardine. Thus, of the two mechanisms described above, the dominant N_2-fixing algae with low $\delta^{15}N$ in the transition zone (Shiozaki et al., 2015) during relatively oligotrophic and high temperatures surface water masses due to the increased contribution of the Kuroshio Current could cause low $\delta^{15}N$ in the Japanese sardine from year to year.

In addition, a significant negative correlation was found between $\delta^{15}N_{Phe}$ and TP_{AA} in Japanese sardine (Figure 4B), indicating that the species of phytoplankton at the base of the food web may be related to TP_{AA} for Japanese sardine. In oligotrophic regions, smaller phytoplankton tend to dominate, and food chain lengths are longer (Kobari et al., 2019). In fact, nanoplankton such as haptophytes are dominant in the Kuroshio Current (Endo and Suzuki, 2019; Kobari et al., 2019), and the energy of pico- and nanoplankton is transferred to fish through several sizes of tiny zooplankton (Hunt et al., 2015; Okazaki et al., 2019). Therefore, feeding in the warmer and relatively oligotrophic Kuroshio surface waters are expected to result in longer food chain

length and higher TP_{AA} for Japanese sardine. In fact, the positive correlation between water temperature and TP_{AA} of Japanese sardine in each year during the observation period may support this idea (Figure 7A). Thus, in the transition zone, the variation in the contribution of N_2-fixing algae and the change in the food web structure, depending on the degree of southward flow of the Oyashio Current (and associated change in the contribution of Kuroshio Current), are suggested to have a significant effect on the feeding characteristics and $\delta^{15}N$ of Japanese sardine. This can be because filter-feeding adult Japanese sardines have lower food selectivity (Nakai, 1962), and isotopic ratios of the fishes are likely to closely reflect changes in plankton species associated with changes in water masses.

4.3 $\delta^{15}N$ and TP_{AA} variation of mackerel at age-1+

Predation on prey from different TPs within the same ecosystem is one of the main factors causing variation in the $\delta^{15}N$ of organisms (Lindsay et al., 1998; MacKenzie et al., 2012). In the case of mackerel, which can prey on food across different TPs, the change in TP is often considered the main reason for $\delta^{15}N$ variation. However, no significant positive correlation was found between $\delta^{15}N$ and TP_{AA} in mackerel (Supplementary Figure 4), suggesting that there must be another factor explaining the variation in $\delta^{15}N$ for mackerel.

Like Japanese sardine, a positive correlation was observed between bulk $\delta^{15}N$ and $\delta^{15}N_{Phe}$ for mackerel (Figure 4A). Hannides et al. (2009) also showed a positive correlation between $\delta^{15}N$ and $\delta^{15}N_{Phe}$ for marine organisms in the subtropical North Pacific, similar to the results of this study: the difference in $\delta^{15}N$ between yellowfin tuna (*Thunnus albacares*) individuals was explained by the difference in $\delta^{15}N_{Phe}$, not TP_{AA}, although they utilize diet across different TPs as do mackerel species. This indicated that the variations of bulk $\delta^{15}N$ in the mackerel reflected variations in $\delta^{15}N$ in primary producers at the origin of the food web, rather than foraging the prey at different trophic levels. On the other hand, no correlation was found between $\delta^{15}N_{Phe}$ and TP_{AA} or $\delta^{15}N_{Phe}$ and water temperature in mackerel (Figures 4B, 6B), whereas negative correlations were found between these parameters in Japanese sardine (Figures 4B, 6A). Unlike Japanese sardine, which is a filter-feeder (Nakai, 1962; Checkley et al., 2017), mackerel is a predatory feeder (Nakatsuka et al., 2010; Robert et al., 2017) that is highly selective in their prey. Mackerel can consume a variety of trophic levels of food that may be less directly affected by water mass shifts than phytoplankton. Therefore, the effect of water mass shifts might not be easily reflected in the isotope value of mackerel. The body lengths of mackerel are larger than Japanese sardines and should have a longer turnover time (i.e., the time it takes for the isotopic components of the body to be replaced by the most recently consumed food) than Japanese sardines. This fact may be the other potential reason why the variation of $\delta^{15}N_{Phe}$ in response to annual changes in water temperature was different from that of Japanese sardines. In addition, the next paragraphs will discuss the possibility that the depths and areas where mackerel species temporarily migrate may be different from those of Japanese sardine, leading to different variation in the $\delta^{15}N_{Phe}$ of the two fish species.

The inter-annual variation of bulk $\delta^{15}N$ and $\delta^{15}N_{Phe}$ of age-1+ mackerel (Figures 2D, 3E) showed a similar trend to the mean body length for each year in the samples used in this study (Supplementary Figure 3B). That is, in years when mean body length was smaller (larger), the values of $\delta^{15}N$ and $\delta^{15}N_{Phe}$ seemed to be lower (higher). In a cluster analysis of the same samples used in this study, Nakamura (2022) showed that the cluster with large body length and good nutritional status was distributed at a relatively high latitude in the Kuroshio-Oyashio transition zone. The proportion of the mackerel categorized in this cluster was higher in 2013 and 2016 when the mackerels had relatively larger body lengths and higher $\delta^{15}N_{phe}$ values than in other years (Nakamura, 2022). Since the $\delta^{15}N$ of zooplankton is higher in the northern region of the transition zone, where the influence of the Oyashio is stronger (see section 4.1, Matsubayashi et al., 2020), the relative northward migration of the individuals to higher latitudes during the growing period may have contributed to the increase in $\delta^{15}N$ (Figure 8). Alternatively, mackerel may feed on prey resources derived from the Oyashio water mass by migrating deeper than Japanese sardine at the same latitude, since mackerel are known to occasionally migrate to depths of 100-150 m, which matches the intrusion depth of the Oyashio Current (Ozawa, 2010; Kamimura et al., 2021; Yasuda et al., 2023). The relatively high TP_{AA} of mackerel in this study in years when fishes experienced low water temperatures probably due to the Oyashio intrusion (Figure 7B) is consistent with a previous report that the TP of zooplankton is higher in the Oyashio region, where large zooplankton such as *Neocalanus* spp. are abundant, than in the transition zone (Ishikawa et al., 2023). Furthermore, the significantly lower bulk $\delta^{13}C$ values in age-1+ mackerel compared to Japanese sardine (Figure 2C) are consistent with the fact that mackerel is partially dependent on the food web of the Oyashio system, because $\delta^{13}C$ values of particulate organic matter (POM) and fishes in the cold Oyashio region are significantly lower compared with warm Kuroshio region (Ohshimo et al., 2019; Sakamoto et al., 2023). Although detailed data on migration history is not available for the samples in this study, the results indicate that changes in migration area or depth with growth may lead to inter-annual changes in food resources.

The mean TP_{AA} of mackerel slightly increased from 2013 to 2017 (Figure 3F), independent of $\delta^{15}N_{Phe}$ variations (Figure 4B), while inter-annual variation in TP_{AA} of Japanese sardine was linked to $\delta^{15}N_{Phe}$ and surface water temperature variations (Figures 4B, 6A). One factor in the annual increase in TP_{AA} may be the competition for food due to increased abundances of zooplankton feeders. Chub mackerel had an outstandingly high recruitment in 2013, and biomass continued to increase from 2012 (1.67 million tons) to 2018 (5.67 million tons) (Yukami et al., 2022). In addition, the biomass of Japanese sardine, which are competitors for the zooplankton feeder (Kishida and Matsuda, 1993; Yatsu et al., 2005), also increased significantly in recent years, rising from 0.51 million tons in 2012 to 2.86 million tons in 2018 (Furuichi et al., 2022). This

increase has resulted in food competition among mackerel populations (Kamimura et al., 2021). Therefore, the increase in the TP_{AA} of mackerel from 2013 to 2017 could be attributed to the relatively increased contribution of higher trophic position prey as a result of food competition due to increased population densities. As shown above, the variation in bulk $\delta^{15}N$ for mackerel was inferred to be caused by changes in $\delta^{15}N_{Phe}$ associated with changes in migration area and depth as individuals grow, and in some cases by an increase in TP_{AA} due to increased population densities.

5 Conclusion

In this study, the feeding habits of Japanese sardine and mackerel, which have the same spawning and migration area, and the factors contributing to inter-annual variations were investigated based on the analyses of bulk stable isotopes ($\delta^{13}C$ and $\delta^{15}N$), amino acid nitrogen isotopes ($\delta^{15}N_{Glu}$, $\delta^{15}N_{Phe}$, TP_{AA}), and mean water temperature (MWT) in the migration area. These fish species showed apparent differences in TP_{AA} and annual variation of stable isotopes at the age-1+ stage, indicating that they utilize different prey items partly supplied through different food webs, while they seemed to feed on a common plankton resource in the same food web at the age-0 stage. This suggests that the food source changed as a result of differences in feeding habits and migration depth with growth (Figure 8). For Japanese sardine at age-1+, negative correlations of $\delta^{15}N_{Phe}$ with TP_{AA} and MWT supported the idea that inter-annual variations in $\delta^{15}N$ and TP_{AA} were determined by the relative influence of warm water masses where small-size plankton including N_2-fixing algae dominate and food chain length is longer. In contrast, for mackerel at age-1+, there were no correlations of $\delta^{15}N_{Phe}$ with TP_{AA} and MWT, respectively, and relatively lower bulk $\delta^{13}C$ values than Japanese sardine and higher TP in the year when the lower water temperature was observed. These characteristics and an increase in $\delta^{15}N$ for mackerel seemed to be affected by some individuals that were highly dependent on the food web of the Oyashio water mass as a result of them migrating to relatively high latitudes or deeper areas in the transition zone compared to Japanese sardine. In addition, competition for food due to the recent increases in the population density of both fish species seemed to be reflected in the $\delta^{15}N$ of mackerel. Therefore, it is quite possible that differences in the

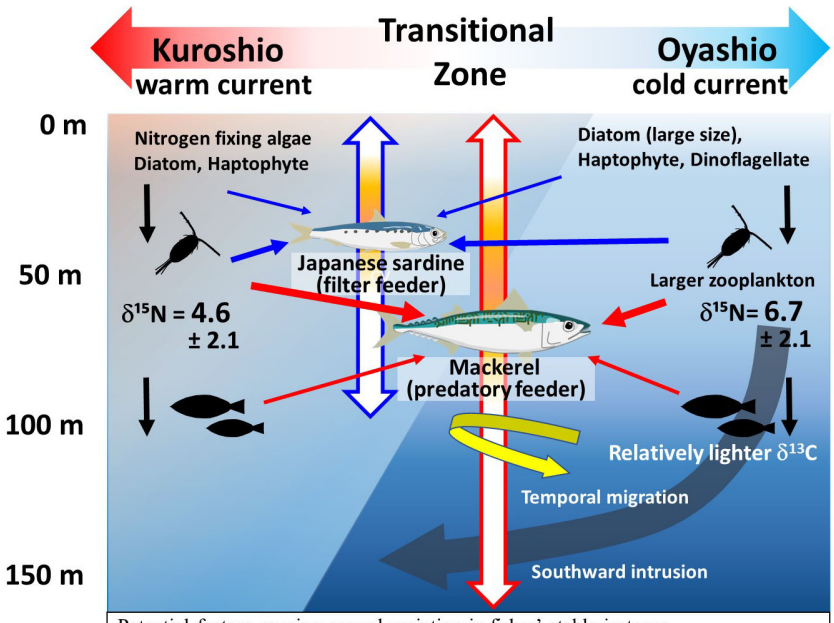

Potential factors causing annual variation in fishes' stable isotopes

Japanese sardine	Mackerels
Annual variability in the use of food resources	Annual variability in the use of food resources
1) originating from the Kuroshio region where smaller phytoplankton including nitrogen fixing algae contributes primary production.	1) originating from the Oyashio region due to migration into deeper depth or northern area
	2) at higher trophic levels due to competition for food associated with increase in the biomass.

FIGURE 8
Schematic diagram showing factors causing interannual variation in stable isotope ratios of Japanese sardines and mackerels. The blue and red arrows indicate the vertical migrating depths and predatory paths of Japanese sardine and mackerels, respectively. The colored portions of the vertical arrows indicate the depth of the center of the fish school (see discussion). Representative $\delta^{15}N$ values (mean ± S.D.) of zooplankton for the northern and southern parts of the Kuroshio-Oyashio Transitional Zone are those of the zooplankton in specific areas (i.e., 39-45°N, 143-155°E for the northern area: n=52, 35-38°N, 143-165°E for the southern area: n=9) reported in Supplementary Table 1 of Matsubayashi et al. (2020). The $\delta^{15}N$ of zooplankton species that are not representative of each region but commonly occur in both areas are as follows: 8.3 ± 2.2 (n=6) & 5.4 ± 1.9 (n=4) for *Paracalanus parvus*, and 6.5 ± 1.1 (n=6) & 4.2 ± 1.2 (n=3) for *Oncaea venusta*, in northern and southern areas, respectively.

factors causing fluctuations in food resources, which are reflected in $\delta^{13}C$ and $\delta^{15}N$ variations, could alter the nutritional status of parent fish from year to year. Japanese sardine and mackerel show different recruitment in a single year, as well as decadal-scale variability, and understanding the mechanisms for these fluctuations on abundance is a significant issue that could not be fully explained in this study. However, since it has been reported that the nutritional status of parent fish is related to fluctuations in abundance, more detailed information on feeding habits, nutritional status, and spawning will contribute to better elucidation of the mechanisms of abundance variability. Furthermore, the findings on the factors affecting the variation of isotope values for Japanese sardine and mackerel will greatly contribute to future interpretations of spatio-temporal variations in tissue isotopes for pelagic fishes.

Data availability statement

The raw data supporting the conclusions of this article will be made available by the authors, without undue reservation.

Ethics statement

The animal study was approved by Animal Experiment Regulations, Fisheries Research Education Agency Japan. The study was conducted in accordance with the local legislation and institutional requirements.

Author contributions

YU, TO, and YO contributed to conception and design of the study. RY and YK conducted field sampling. YU, YO, CY, and IT conducted chemical analyses. TO conducted water temperature analysis. YO wrote the first draft of the manuscript and performed the statistical analysis. YU, TO, and YK wrote sections of the manuscript. All authors contributed to the article and approved the submitted version.

Funding

The author(s) declare financial support was received for the research, authorship, and/or publication of this article. This research was partly supported by NIHU Research Projects "Object-based research of nature-human interactions up to the Anthropocene", and sample analyses were conducted by the support of Joint Research Grant for the Environmental Isotope Study of Research Institute for Humanity and Nature (RIHN). A part of sample analyses was also supported by the Cooperative Program (JURCAOSKAV20-09) of Atmosphere and Ocean Research Institute, the University of Tokyo. This study was also supported by Grant-in-Aid for Scientific Research (A) (KAKENHI No. 21H04737) and MacroCoast (Macro coastal oceanography: integrated simulation for the material dynamics from the land through the open ocean, KAKENHI No. 22A402) from the Japan Society for the Promotion of Science (JSPS). The entire study was conducted within the framework of the Study of Kuroshio Ecosystem Dynamics for Sustainable Fisheries (SKED) funded to FRA from the Ministry of Education, Culture, Sports, Science and Technology, Japan [grant number: JPMXD0511102330].

Acknowledgments

We thank the captains, officers and crews of R/T/V *Hokuo-maru* and *Soyo-maru* cruise for sample collection. We also thank T. Terado (Shimane Prefectural Fisheries Technology Center), R. Hashimoto and X. Wan (Nagasaki University), T. Nakamura (The University of Tokyo), and Y. Matsui (JAMSTEC) for sample analysis. We are grateful to Dr. A. Kawabata, Dr. C. Watanabe, Dr. S. Furuichi and Dr. H. Miyamoto (Fisheries Research and Education Agency) for valuable advices about the behavior of Japanese sardine, mackerel and zooplankton. We acknowledge Dr. H. Saito (The University of Tokyo) and Dr. M. Takahashi (Fisheries Research and Education Agency) who were the chief researchers of the project.

Conflict of interest

The authors declare that the research was conducted in the absence of any commercial or financial relationships that could be construed as a potential conflict of interest.

Publisher's note

Supplementary material

The Supplementary Material for this article can be found online at: https://www.frontiersin.org/articles/10.3389/fmars.2023.1225923/full#supplementary-material

References

Aizawa, Y., and Takiguchi, N. (1999). Consideration of the methods for estimation the Age-composition from the length frequency data with MS-Excel. *Bull. Jpn. Soc Fish. Oceanogr.* 63, 205–214. (in Japanese).

Bode, A., Alvarez-Ossorio, M. T., Cunha, M. E., Garrido, S., Peleteiro, J. B., Porteiro, C., et al. (2007). Stable nitrogen isotope studies of the pelagic food web on the Atlantic shelf of the Iberian Peninsula. *Prog. Oceanogr.* 74, 115–131. doi: 10.1016/j.pocean.2007.04.005

Bosley, K. L., and Wainright, S. C. (1999). Effects of preservatives and acidification on the stable isotope ratios (15N:14N, 13C:12C) of two species of marine animals. *Can. J. Fish Aquat. Sci.* 56, 2181–2185. doi: 10.1139/f99-153

Chavez, F. P., Ryan, J., Lluch-Cota, S. E., and Niquen, C. M. (2003). From anchovies to sardines and back multidecadal change in the Pacific Ocean. *Science* 299, 217–221. doi: 10.1126/science.1075880

Checkley, D. M.Jr, Asch, R. G., and Rykaczewski, R. R. (2017). Climate, anchovy, and sardine. *Annu. Rev. Mar. Sci.* 9, 469–493. doi: 10.1146/annurev-marine-122414-033819

Chikaraishi, Y., Ogawa, N. O., Kashiyama, Y., Takano, Y., Suga, H., Tomitani, A., et al. (2009). Determination of aquatic food-web structure based on compound-specific nitrogen isotopic composition of amino acids. *Limnol. Oceanogr-Meth* 7, 740–750. doi: 10.4319/lom.2009.7.740

Chikaraishi, Y., Steffan, S. A., Ogawa, N. O., Ishikawa, N. F., Sasaki, Y., Tsuchiya, M., et al. (2014). High-resolution food webs based on nitrogen isotopic composition of amino acids. *Ecol. Evol.* 4, 2423–2449. doi: 10.1002/ece3.1103

DeNiro, M. J., and Epstein, S. (1978). Influence of diet on the distribution on carbon isotopes in animals. *Geochim. Cosmochim. Acta* 42, 493–506. doi: 10.1016/0016-7037(78)90199-0

DeNiro, M. J., and Epstein, S. (1981). Influence of diet on the distribution on nitrogen isotopes in animals. *Geochim. Cosmochim. Acta* 45, 341–351. doi: 10.1016/0016-7037(81)90244-1

Endo, H., and Suzuki, K. (2019). "Spatial variations in community structure of haptophytes across the Kuroshio front in the Tokara Strait," in *Kuroshio Current: Physical, Biogeochemical, and Ecosystem Dynamics*. Eds. T. Nagai, H. Saito, K. Suzuki and M. Takahashi, (Geophys. Monogr.), Washington D.C-Hoboken NJ, AGU-Wiley. 207–221. doi: 10.1002/9781119428428.ch13

FAO (2020). *The State of World Fisheries and Aquaculture 2020. Sustainability in action* (Rome: FAO). Available at: https://www.fao.org/documents/card/en?details=ca9229en/.

Fry, B. (2006). *Stable isotope ecology* (Berlin: Springer Science + Business Media, LLC).

Fuji, T., Nakagami, M., Suyama, S., Miyamoto, H., and Kidokoro, H. (2021). Geographical differences in the stable isotope ratios of Pacific saury in the North Pacifc Ocean. *Fish Sci.* 87, 529–540. doi: 10.1007/s12562-021-01528-3

Furuichi, S., Yugami, R., Kamimura, Y., Nishijima, S., Isu, S., and Watanabe., R. (2022). *Stock assessment and evaluation for the Pacific stock of sardine (fiscal year 2021). Marine fisheries stock assessment for Japanese waters* (Tokyo: Japan Fisheries Agency and Japan Fisheries Research and Education Agency). (in Japanese).

Graham, B. S., Koch, P. L., Newsome, S. D., McMahon, K. W., and Aurioles, D. (2010). "Using isoscapes to trace the movements and foraging behavior of top predators in oceanic ecosystems," in *Isoscapes* (Dordrecht: Springer), 299–318. doi: 10.1007/978-90-481-3354-3_14

Hannides, C. C. S., Popp, B. N., Landry, M. R., and Graham, B. S. (2009). Quantification of zooplankton trophic position in the North Pacific Subtropical Gyre using stable nitrogen isotopes. *Limnol. Oceanogr.* 54, 50–61. doi: 10.4319/lo.2009.54.1.0050

Hetherington, E. D., Olson, R. J., Drazen, J. C., Lennert-Cody, C. E., Ballance, L. T., Kaufmann, R. S., et al. (2017). Spatial food-web structure in the eastern tropical Pacific Ocean based on compound-specific nitrogen isotope analysis of amino acids. *Limnol. Oceanogr.* 62, 541–560. doi: 10.1002/lno.10443

Horii, S., Takahashi, K., Shiozaki, T., Hashihama, F., and Furuya, K. (2018). Stable isotopic evidence for the differential contribution of diazotrophs to the epipelagic grazing food chain in the mid-Pacific Ocean. *Global Ecol. Biogeogr.* 27, 1467–1480. doi: 10.1111/geb.12823

Houssard, P., Lorrain, A., Tremblay-Boyer, L., Allain, V., Graham, B. S., Menkes, C. E., et al. (2017). Trophic position increase with thermocline depth in yellowfin and bigeye tuna across the Western and Central Ocean. *Prog. Oceanogr.* 154, 49–63. doi: 10.1016/j.pocean.2017.04.008

Hunt, B. P. V., Allain, V., Menkes, C. E., Lorrain, A., Graham, B., Rodier, M., et al. (2015). A coupled stable isotope-size spectrum approach to understanding pelagic food-web dynamics: a case study from the southwest sub-tropical Pacific. *Deep-Sea Res. PT II.* 113, 208–224. doi: 10.1016/j.dsr2.2014.10.023

Inagake, D., and Hirano, T. (1983). Vertical distribution of the Japanese sardine in relation to temperature and thermocline at the purse seine fishing ground east of Japan. *Bull. Japan. Soc. Sci. fisheries.* 49, 1533–1539. doi: 10.2331/suisan.49.1533

Ishikawa, N. F., Kato, Y., Togashi, H., Yoshimura, M., Yoshimizu, C., Okuda, N., et al. (2014). Stable nitrogen isotopic composition of amino acids reveals food web structure in stream ecosystems. *Oecologia* 175, 911–922. doi: 10.1007/s00442-014-2936-4

Ishikawa, N. F., Ogawa, N. O., Chikaraishi, Y., Yamaguchi, M., Fujikura, K., Miyairi, Y., et al. (2021). Influences of ocean currents on the diets of demersal fish communities in the Western North Pacific revealed by their muscle carbon and nitrogen isotopic compositions. *Front. Mar. Sci.* 8. doi: 10.3389/fmars.2021.641282

Ishikawa, N. F., Tadokoro, K., Matsubayashi, J., and Ohkouchi, N. (2023). Biomass pyramids of marine mesozooplankton communities as inferred from their integrated trophic positions. *Ecosystems* 26, 217–231. doi: 10.1007/s10021-022-00753-w

Itoh, S., and Yasuda, I. (2010). Water mass structure of warm and cold anticyclonic eddies in the western boundary region of the subarctic North Pacific. *J. Phys. Oceanogr.* 40, 2624–2642. doi: 10.1175/2010JPO4475.1

Jacob, U., Mintenbeck, K., Brey, T., Knust, R., and Beyer, K. (2005). Stable isotope food web studies: a case for standardized sample treatment. *Mar. Ecol. Prog. Ser.* 287, 251–253. doi: 10.3354/meps287251

Jardine, T. D., Kidd, K. A., and Fisk, A. T. (2006). Applications, considerations, and sources of uncertainty when using stable isotope analysis in ecotoxicology. *Environ. Sci. Technol.* 40, 7501–7511. doi: 10.1021/es061263h

Kamimura, Y., Taga, M., Yukami, R., Watanabe, C., and Furuichi, S. (2021). Intra- and inter specific density dependence of body condition, growth and habitat temperature in chub mackerel (*Scomber japonicus*). *ICES J. Mar.Sci.* 78, 3254–3264. doi: 10.1101/2021.03.25.436928

Kanamori, Y., Takasuka, A., Nishijima, S., and Okamura, H. (2019). Climate change shifts the spawning ground northward and extends the spawning period of chub mackerel in the western North Pacific. *Mar. Ecol. Prog. Ser.* 624, 155–166. doi: 10.3354/meps13037

Kato, Y., Togashi, H., Kurita, Y., Osada, Y., Amano, Y., Yoshimizu, C., et al. (2021). Segmental isotope analysis of the vertebral centrum reveals the spatiotemporal population structure of adult Japanese flounder *Paralichthys olivaceus* in Sendai Bay, Japan. *Mar. Biol.* 168, 57. doi: 10.1007/s00227-021-03868-1

Kawabata, A., Watanabe, C., and Takahashi, M. (2012). Population dynamics of chub mackerel in the Pacific waters around Japan in 1970-2010. *Fish. Biol. oceanogr. Kuroshio.* 13, 33–36. (in Japanese).

Kawasaki, T. (1983). "Why do some pelagic fishes have wide fluctuations in their numbers? Biological basis of fluctuation from the viewpoint of evolutionary ecology," in *Proceedings of the Expert Consultation to Examine Changes in Abundance and Species Composition of Neritic Fish Resources*, vol. 291 . Eds. G. D. Sharp and J. Csirke, FAO Fisheries Report, Rome, FAO, 1065–1080. Available at: https://www.fao.org/3/x6851b/x6851b.pdf.

Kawasaki, T., and Kumagai, A. (1984). Food habits of the Far Eastern sardine and their implication in the fluctuation pattern of the sardine stocks. *Bull. Japan. Soc. Sci. Fish.* 50 (10), 1657–1663.

Kishida, T., and Matsuda, H. (1993). Statistical analyses of intra and interspecific density effects on recruitment of chub mackerel and sardine in Japan. *Fish. Oceanogr.* 2, 278–287. doi: 10.1111/j.1365-2419.1993.tb00142.x

Klyashtorin, L. B. (1998). Long-term climate change and main commercial fish production in the Atlantic and. *Pacific. Fish. Res.* 37, 115–125. doi: 10.1016/S0165-7836(98)00131-3

Kobari, T., Kobari, Y., Miyamoto, H., Okazaki, Y., Kume, G., Kondo, R., et al. (2019). "Variability in taxonomic composition, standing stock, and productivity of the plankton community in the Kuroshio and its neighboring waters.," in *Kuroshio Current: Physical, Biogeochemical, and Ecosystem Dynamics*. Eds. T. Nagai, H. Saito, K. Suzuki and M. Takahashi (Geophys. Monogr.), Washington D.C-Hoboken NJ, AGU-Wiley. 223–243. doi: 10.1002/9781119428428.ch14

Komatsu, K., and Hiroe, Y. (2019). "Structure and impact of the Kuroshio nutrient stream.," in *Kuroshio Current: Physical, Biogeochemical, and Ecosystem Dynamics*. Eds. T. Nagai, H. Saito, K. Suzuki and M. Takahashi (Geophys. Monogr), Washington D.C-Hoboken NJ, AGU-Wiley. 83–104. doi: 10.1002/9781119428428.ch5

Kurita, Y. (2010). Influence of spatio-temporal changes in stock reproductive potential on the recruitment level of fish. *Bull. Jpn. Soc Fish. Oceanogr.* 74, 4–18. (in Japanese with English abstract).

Kuroda, H., Setou, T., Kakehi, S., Ito, S., Taneda, T., Azumaya, T., et al. (2017). Recent advances in Japanese fisheries science in the Kuroshio-Oyashio region through development of the FRA-ROMS ocean forecast system. Overview of the reproducibility of reanalysis products. *Open J. Mar. Sci.* 7, 62–90. doi: 10.4236/ojms.2017.71006

Lindsay, D. J., Minagawa, M., Mitani, I., and Kawaguchi, K. (1998). Trophic shift in the Japanese anchovy Engraulis japonicus in its early life history stages as detected by stable isotope ratios in Sagami Bay, Central Japan. *Fish. Sci.* 34, 403–410. doi: 10.2331/fishsci.64.403

Longhurst, A. R. (2006). *Ecological geography of the sea. 2nd edition* (London: Academic Press).

Lorrain, A., Graham, B. S., Popp, B. N., Allain, V., Olson, R. J., Hunt, B. P. V., et al. (2015). Nitrogen isotopic baselines and implications for estimating foraging habitat and trophic position of yellowfin tuna in the Indian and Pacific Oceans. *Deep-Sea Res. PT II.* 113, 188–198. doi: 10.1016/j.dsr2.2014.02.003

MacKenzie, K. M., Trueman, C. N., Palmer, M. R., Moore, A., Ibbotson, A. T., Beaumont, W. R., et al. (2012). Stable isotopes reveal age-dependent trophic level and spatial segregation during adult marine feeding in populations of salmon. *ICES J. Mar. Sci.* 69, 1637–1645. doi: 10.1093/icesjms/fss074

Mantua, N. J., Hare, S. R., Zhang, Y., Wallance, J. M., and Francis, R. C. (1997). A Pacific interdecadal climate oscillation with impact on salmon production. *B. Am. Meteorol. Soc* 78, 1069–1079. doi: 10.1175/1520-0477(1997)078%3C1069:APICOW%3E2.0.CO;2

Matsubayashi, J., Osada, Y., Tadokoro, K., Abe, Y., Yamaguchi, A., Shirai, K., et al. (2020). Tracking long-distance migration of marine fishes using compound-specific stable isotope analysis of amino acids. *Ecol. Lett.* 23, 881–890. doi: 10.1111/ele.13496

McClelland, J. W., and Montoya, J. P. (2002). Trophic relationships and the nitrogen isotopic composition of amino acids in plankton. *Ecology* 83, 2173–2180. doi: 10.1890/0012-9658(2002)083[2173:TRATNI]2.0.CO;2

Minagawa, M., Ohashi, M., Kuramoto, T., and Noda, N. (2001). δ^{15}N of PON and nitrate as a clue to the origin and transformation of nitrogen in the subarctic North Pacific and its marginal sea. *J. Oceanogr.* 57, 285–300. doi: 10.1023/A:1012430512137

Minagawa, M., and Wada, E. (1984). Stepwise enrichment of ^{15}N along food chains: Further evidence and the relation between δ^{15}N and animal age. *Geochim. Cosmochim. Acta* 48, 1135–1140. doi: 10.1016/0016-7037(84)90204-7

Miyachi, S., Mayahara, T., Tsushima, K., Sasada, K., Kohno, E., Ogawa, N., et al. (2015). Approach to determine individual trophic level and the difference in food source of Japanese anchovy *Engraulis japonicus* in Sagami Bay, based on compound-specific nitrogen stable isotope analysis of amino acids. *Fish. Sci.* 81, 1053–1062. doi: 10.1007/s12562-015-0923-2

Miyake, Y., and Wada., E. (1967). The abundance ratio of ^{15}N/^{14}N in marine environments. *Rec. Oceanogr. Works Japan* 9, 37–53.

Miyamoto, H., Takahashi, K., Kuroda, H., Watanabe, T., Taniuchi, Y., Kuwata, A., et al. (2022). Copepod community structure in the transition region of the North Pacific Ocean: Water mixing as a key driver of secondary production enhancement in subarctic and subtropical waters. *Prog. Oceanogr.* 207, 102865. doi: 10.1016/j.pocean.2022.102865

Nakai, Z. (1962). Studies relevant to mechanisms underlying the fluctuation in the catch of the Japanese sardine, *Sardinops melanosticta* (Temminck & Schlegel). *Japan. J. Ichthyol.* 9, 1–115.

Nakamura, T. (2022). "Comparative study of interannual variation of δ^{13}C and δ^{15}N in Japanese sardine and mackerels," in *Master thesis at Graduate School of Frontier Sciences* (The University of Tokyo, Chiba). 91pp. (in Japanese).

Nakatsuka, S., Kawabata, A., Takasuka, A., Kubota, H., and Okamura, H. (2010). Estimating gastric evacuation rate and daily ration of chub mackerel and spotted mackerel in the Kuroshio-Oyashio transition and Oyashio regions. *Bull. Japan. Soc. Fish. Oceanogr.* 74, 105–117. (in Japanese with English abstract).

Nishikawa, H., Nishikawa, S., Ishizaki, H., Wakamatsu, T., and Ishikawa, Y. (2020). Detection of the Oyashio and Kuroshio fronts under the projected climate change in the 21st century. *Prog. Earth Planet. Sci.* 7, 1–12. doi: 10.1186/s40645-020-00342-2

Nishikawa, H., and Yasuda, I. (2008). Japanese sardine (*Sardinops melanostictus*) Mortality in relation to the winter mixed layer depth in the Kuroshio Extension region. *Fish. Oceanogr.* 17, 411–420. doi: 10.1111/j.1365-2419.2008.00487.x

Ohshimo, S., Madigan, D. J., Komada, T., Tanaka, H., Komoto, K., Suyama, S., et al. (2019). Isoscapes reveal patterns of δ^{13}C and δ^{15}N of pelagic forage fish and squid in the Northwest Pacific Ocean. *Prog. Oceanogr.* 175, 124–138. doi: 10.1016/j.pocean.2019.04.003

Okazaki, Y., Miyamoto, H., Suzuki, K., Saito, H., Hidaka, K., and Ichikawa, T. (2019). ""Diverse trophic pathways from zooplankton to larval and juvenile fishes in the Kuroshio ecosystem."," in *Kuroshio Current: Physical, Biogeochemical, and Ecosystem Dynamics*, vol. 243 . Eds. T. Nagai, H. Saito, K. Suzuki and M. Takahashi, (Geophys. Monogr.), Washington D.C-Hoboken NJ, AGU-Wiley. 245–256. doi: 10.1002/9781119428428.ch15

Ozawa, R. (2010). Surveys of pelagic fish with a quantitative echo sounder in the sea off Joban ~ Boso. *Bull. Ibaraki Prefect. Fish. Experiment Station* 41, 35–49. (in Japanese with English abstract).

Popp, B. N., Graham, B. S., Olson, R. J., Hannides, C. C., Lott, M. J., López-Ibarra, G. A., et al. (2007). Insight into the trophic ecology of yellowfin tuna, *Thunnus albacares*, from compound-specific nitrogen isotope analysis of proteinaceous amino acids. *Terr. Ecol.* 1, 173–190. doi: 10.1016/S1936-7961(07)01012-3

Post, D. M. (2002). Using stable isotopes to estimate trophic position. models, methods, and assumptions. *Ecology* 83, 703. doi: 10.1890/0012-9658(2002)083[0703:USITET]2.0.CO;2

Qiu, B. (2019). Kuroshio and Oyashio currents. *Encycl. Ocean Sci.* 3, 384–394. doi: 10.1016/B978-0-12-409548-9.11295-3

Rau, G. H., Mearns, A. J., Young, D. R., Olson, R. J., Schafer, H. A., and Kaplan, I. R. (1983). Animal ^{13}C/^{12}C correlates with trophic level in pelagic food webs. *Ecology* 64, 1314–1318. doi: 10.2307/1937843

Robert, D., Takasuka, A., Nakatsuka, S., Kubota, H., Ozeki, Y., Nishida, H., et al. (2017). Predation dynamics of mackerel on larval and juvenile anchovy: is capture success linked to prey condition? *Fish. Sci.* 76, 183–188. doi: 10.1007/s12562-009-0205-y

Saino, T., and Hattori, A. (1987). Geographical variation of the water column distribution of suspended particulate organic nitrogen and its 15N natural abundance in the Pacific and its marginal seas. *Deep Sea Res.* 34, 807–827. doi: 10.1016/0198-0149(87)90038-0

Saito, H. (2019). "The Kuroshio. its recognition, scientific activities and emerging issues," in *Kuroshio current. Physical, biogeochemical, and ecosystem dynamics*, 1–11. doi: 10.1002/9781119428428.ch1

Sakamoto, T., Horii, S., Kodama, T., Takahashi, K., Tawa, A., Tanaka, Y., et al. (2023). Stable isotopes in eye lenses reveal migration and mixing patterns of diamond squid in the western North Pacific and its marginal seas. *ICES J. Mar. Sci.*, fsad145. doi: 10.1093/icesjms/fsad145

Sakamoto, T., Komatsu, K., Shirai, K., Higuchi, T., Ishimura, T., Setou, T., et al. (2018). Combining microvolume isotope analysis and numerical simulation to reproduce fish migration history. *Methods Ecol. Evol.* 10, 59–69. doi: 10.1111/2041-210X.13098

Sakurai, Y. (2007). An overview of the Oyashio ecosystem. *Deep Sea Res. II* 54, 2526–2542. doi: 10.1016/j.dsr2.2007.02.007

Sassa, C., and Tsukamoto, Y. (2010). Distribution and growth of *Scomber japonicus* and *S. australasicus* larvae in the southern East China Sea in response to oceanographic conditions. *Mar. Ecol. Prog. Ser.* 419, 185–199. doi: 10.3354/meps08832

Shiozaki, T., Nagata, T., Ijichi, M., and Furuya, K. (2015). Nitrogen fixation and the diazotroph community in the temperate coastal region of the northwestern North Pacific. *Biogeosciences* 12, 4751–4764. doi: 10.1029/2020JC017071

Sugisaki, H., Terazaki, M., Wada, E., and Nemoto, T. (1991). Feeding habits of a pelagic amphipod, Themisto japonica. *Mar. Biol.* 109, 241–244. doi: 10.1007/BF01319392

Takahashi, M., Sassa, C., Nishiuchi, K., and Tsukamoto, Y. (2019). ""Variability in growth rates of Japanese jack mackerel *Trachurus japonicus* larvae and juveniles in the East China Sea–effects of temperature and prey abundance"," in *Kuroshio Current: Physical, Biogeochemical, and Ecosystem Dynamics*. Eds. T. Nagai, H. Saito, K. Suzuki and M. Takahashi, (Geophys. Monogr.), Washington D.C-Hoboken NJ, AGU-Wiley. 295–308. doi: 10.1002/9781119428428.ch18

Takasuka, A., Oozeki, Y., and Aoki, I. (2007). Optimal growth temperature hypothesis. Why do anchovy flourish and sardine collapse or vice versa under the same ocean regime? *Can. J. Fish. Aquat Sci.* 64, 768–776. doi: 10.1139/F07-052

Vander Zanden, M. J., Clayton, M. K., Moody, E. K., Solomon, C. T., and Weidel, B. C. (2015). Stable isotope turnover and half-life in animal tissues. A literature synthesis. *PloS One* 10, e0116182. doi: 10.1371/journal.pone.0116182

Vander Zanden, M. J., and Rasmussen, J. B. (2001). Variation in δ^{15}N and δ^{13}C trophic fractionation. implications for aquatic food web studies. *Limnol. Oceanogr.* 46, 2061–2066. doi: 10.4319/lo.2001.46.8.2061

Watanabe, C., and Yatsu, A. (2004). Effects of density-dependence and sea surface temperature on inter-annual variation in length-at-age of chub mackerel (*Scomber japonicus*) in the Kuroshio-Oyashio area during 1970–1997. *Fish. Bull.* 102, 196–206.

Wickham, H. (2016). *ggplot2, Elegant Graphics for Data Analysis* (Cham: Springer), 203–220. doi: 10.1007/978-3-319-24277-4_10

Xing, D., Choi, B., Takizawa, Y., Fan, R., Sugaya, S., Tsuchiya, M., et al. (2020). Trophic hierarchy of coastal marine fish communities viewed via compound-specific isotope analysis of amino acids. *Mar. Ecol. Prog. Ser.* 652, 137–144. doi: 10.3354/meps13475

Yasuda, T., Kinoshita, J., Niino, Y., and Okuyama, J. (2023). Vertical migration patterns linked to body and environmental temperatures in chub mackerel. *Prog. Oceanogr.* 213, 10317. doi: 10.1016/j.pocean.2023.103017

Yatsu, A. (2019). Review of population dynamics and management of small pelagic fishes around the Japanese Archipelago. *Fish. Sci.* 85, 611–639. doi: 10.1007/s12562-019-01305-3

Yatsu, A., Chiba, S., Yamanaka, Y., Ito, S. I., Shimizu, Y., Kaeriyama, M., et al. (2013). Climate forcing and the Kuroshio/Oyashio ecosystem. *ICES J. Mar. Sci.* 70, 922–933. doi: 10.1093/icesjms/fst084

Yatsu, A., Watanabe, T., Ishida, M., Sugisaki, H., and Jacobson, L. D. (2005). Environmental effects on recruitment and productivity of the Japanese sardine, *Sardinops melanostictus*, and chub mackerel, *Scomber japonicus*, with recommendations for management. *Fish Oceanogr.* 14, 263–278. doi: 10.1111/j.1365-2419.2005.00335.x

Yoneda, M., Kitano, H., Nyuji, M., Nakamura, M., Takahashi, M., Kawabata, A., et al. (2022). Maternal spawning experience and thermal effects on offspring viability of chub mackerel and their influence on reproductive success. *Front. Mar. Sci.* 9. doi: 10.3389/fmars.2022.1063468

Yoshikawa, C., Makabe, A., Matsui, Y., Nunoura, T., and Ohkouchi, N. (2018). Nitrate isotope distribution in the subarctic and subtropical North Pacific. *Geochem. Geophys.* 19, 2212–2224. doi: 10.1029/2018GC007528

Yoshikawa, C., Yamanaka, Y., and Nakatsuka, T. (2005). An ecosystem model including nitrogen isotopes: perspectives on a study of the marine nitrogen cycle. *J. Oceanogr.* 61, 921–942. doi: 10.1007/s10872-006-0010-5

Yoshioka, T., Wada, E., and Hayashi, H. (1994). A stable isotope study on seasonal food web dynamics in a lake. *Ecology* 75, 835–846. doi: 10.2307/1941739

Yukami, R., Nishijima, S., Kamimura, Y., Furuichi, S., Isu, S., and Watanabe, R. (2022). "Stock assessment and evaluation for Pacific stock of chub mackerel (fiscal year 2021)," in *Marine fisheries stock assessment for Japanese waters* (Tokyo: Japan Fisheries Agency and Japan Fisheries Research and Education Agency). (in Japanese).

frontiers | Frontiers in Marine Science

TYPE Original Research
PUBLISHED 27 November 2023
DOI 10.3389/fmars.2023.1254461

OPEN ACCESS

EDITED BY
Tomihiko Higuchi,
The University of Tokyo, Bunkyo, Japan

REVIEWED BY
Kat Bolstad,
Auckland University of Technology, Auckland, New Zealand
Carlos Rosas,
National Autonomous University of Mexico, Mexico

*CORRESPONDENCE
Bethany Jackel
Bethany.jackel@flinders.edu.au

RECEIVED 07 July 2023
ACCEPTED 19 October 2023
PUBLISHED 27 November 2023

CITATION
Jackel B, Baring R, Doane MP, Henkens J, Martin B, Rough K and Meyer L (2023) Towards unlocking the trophic roles of rarely encountered squid: Opportunistic samples of *Taningia danae* and a *Chiroteuthis* aff. *veranii* reveal that the Southern Ocean top predators are nutrient links connecting deep-sea and shelf-slope environments.
Front. Mar. Sci. 10:1254461.
doi: 10.3389/fmars.2023.1254461

Towards unlocking the trophic roles of rarely encountered squid: Opportunistic samples of *Taningia danae* and a *Chiroteuthis* aff. *veranii* reveal that the Southern Ocean top predators are nutrient links connecting deep-sea and shelf-slope environments

Bethany Jackel[1]*, Ryan Baring[1], Michael P. Doane[1], Jessica Henkens[1], Belinda Martin[1], Kirsten Rough[2] and Lauren Meyer[1,3]

[1]College of Science and Engineering, Flinders University, Adelaide, SA, Australia, [2]Australian Southern Bluefin Tuna Industry Association, Port Lincoln, SA, Australia, [3]The Georgia Aquarium, Atlanta, GA, United States

Deep-sea squids are presumably vital components of largely undescribed marine ecosystems, yet limited access to specimens has hampered efforts to detail their ecological roles as predators and preys. Biochemical techniques such as stable isotope analyses, fatty acid analyses, and bomb calorimetry are increasingly recognized for their ability to infer trophic ecology and dietary information from small quantities of tissue. This study used five opportunistically collected *Taningia danae* specimens and one *Chiroteuthis* aff. *veranii* specimen retrieved from the Great Australian Bight, South Australia, to detail the trophic ecology of these poorly understood squids. Four body tissue types (i.e., arm, buccal mass, mantle, and digestive gland) were assessed for their utility in stable isotope (SI) and fatty acid (FA) analyses, and we found that the arm, buccal mass, and mantle tissues had similar SI and FA profiles, suggesting that they can be used interchangeably when the entire specimen is unavailable. $\delta^{13}C$, $\delta^{15}N$, and fatty acid data suggests that the *T. danae* and *C.* aff. *veranii* specimens lived in the Southern Ocean and were high-trophic-level predators, feeding on deep-sea fishes and small squids, while also taking advantage of the summer upwelling region of the Great Australian Bight. The fatty acid analysis and bomb calorimetry results indicate that these squids might be important reservoirs of essential FAs (EPA and DHA) for Southern Ocean predators and that the whole-body energy content of *T. danae* individuals can reach up to 362,250 kJ. Our findings indicate that these squids may be contributing greatly to the transport of nutrients and energy between the Southern Ocean deep-sea and the Great Australian Bight shelf–slope environments. In addition to building our understanding of the

trophic ecology of two poorly understood deep-sea squids, these findings also highlight the utility of partial specimens and demonstrate the important ecological information that can be obtained from few samples that may be opportunistically collected.

KEYWORDS

deep-sea squid, trophic ecology, stable isotope analysis, fatty acid analysis, energy content, *Taningia danae*, *Chiroteuthis* aff. *veranii*

1 Introduction

Squids are vital components of marine ecosystems globally, occupying a broad range of ecological roles owing to their diverse morphology, habitat, behavior, and diet (Jereb and Roper, 2010; Coll et al., 2013). The 300 known species of squid range from low-trophic-level species in nearshore reefs to top predators in deep-sea and pelagic ecosystems (Navarro et al., 2013). Most squids are mesopredators feeding on small fishes and crustaceans and shunting key nutrients to large fishes, cetaceans, sharks, pinnipeds, and seabirds (De La Chesnais et al., 2019). Thus, squids are vital ecosystem members that facilitate energy and nutrient transfer in food webs (Merten et al., 2021) and can exert both top-down (i.e., predator influencing prey) and bottom-up (i.e., prey influencing predator) controls on a multitude of important marine species (De La Chesnais et al., 2019). The Southern Ocean alone is home to 42 different squid species, ranging in size from 5.7 cm (*Abraliopsis gilchristi*) to greater than 2 m (*Mesonychoteuthis hamiltoni* and *Architeuthis dux*) (Cherel, 2020). Furthermore, there is evidence to suggest that 12–24 million tonnes of cephalopods (primarily squids) might be consumed in the Southern Ocean annually (Santos et al., 2001) by at least 45 diverse predator species, showcasing the importance of squid as energy and nutrient resources in pelagic environments (Rodhouse, 2013). Additionally, global squid catches and abundances have both increased in recent decades (Doubleday et al., 2016), and their rapid growth and ability to adapt to environmental changes may make squid an especially ecologically and economically important taxa in changing ecosystems (Xavier et al., 2015).

Despite a global distribution and their increasingly important ecological roles, little is known about many squid species, with substantial knowledge gaps regarding diet, behavior, reproduction, distribution, physiology, and genetics (Albertin et al., 2012; Xavier et al., 2015; Xavier et al., 2018; Cherel, 2020; Ibáñez et al., 2021; Sato, 2021). The most researched are species that are commercially important, such as Humboldt squid (*Dosidicus gigas*) in the eastern Pacific Ocean or those that are easy to keep in aquaria (Roper and Shea, 2013). Comparatively little research effort has been applied to deep-sea and large-bodied squid species (Roper and Shea, 2013), owing to the myriad of difficulties associated with sampling animals occupying these mysterious habitats (Cherel et al., 2009b). Trawling often yields mixed and unreliable capture success (Roper and Shea, 2013), as large and fast squid are able to avoid trawl capture (Judkins et al., 2017), while trawls are known to damage delicate deep-sea specimens (Braid et al., 2014). Direct sightings of elusive species are becoming more common as camera technology becomes more affordable and accessible (O'Brien et al., 2018), but rarely do these provide information other than distribution, external morphology, and a snapshot of behavior (Kubodera et al., 2007; Gomes-Pereira and Tojeira, 2014; Hoving et al., 2014; Robinson et al., 2021). Much of the current genetic, physiological, and ecological data available on deep-sea and large squids has come from opportunistically retrieved carcasses, and beaks recovered from squid predators (Bolstad and O'Shea, 2004; Cherel and Hobson, 2005; Rosa et al., 2005). Research of large, deep-sea, or rarely sighted squids must be conducted whenever opportunities arise, and as they are abundant predators and preys, understanding their trophic interactions may be key for understanding food webs, nutrient dynamics, and ecosystems that are otherwise difficult to research and monitor.

Trophic ecology research aims to understand predator–prey interactions using methods such as direct observations, images or video recordings of predation events, gut content analyses, or molecular analyses of fatty acids (FAs) and stable isotopes (SIs) (Guerreiro et al., 2015; Da Silveira et al., 2020). Unfortunately, many of these methods are difficult to apply to inconspicuous marine species, especially large and deep-sea squids. Direct observation or image evidence of feeding events is difficult to attain due to the high cost and low success of these sampling methods (Robinson et al., 2021). Much of our understanding of large-bodied and deep-sea squids has instead come from investigations of deceased, opportunistically obtained specimens (see González et al., 2003; Rosa et al., 2005). In these cases, gut content analysis has varied success, typically requiring large sample sizes due to the frequency of empty stomachs, and the results are limited to identifiable prey items, which only represent the most recent feeding events (Braley et al., 2010; Rodhouse, 2013). Squids also have fast rates of digestion and a narrow esophagus that travels directly through the center of the brain, meaning that preys are thoroughly macerated with the beak and radula, reducing the incidence of identifiable stomach contents (Ibáñez et al., 2021).

Stable isotope analysis for trophic ecology primarily uses ratios of carbon-13 to carbon-12, and nitrogen-15 to nitrogen-14 isotopes in biological tissues (referred to as $\delta^{13}C$ and $\delta^{15}N$) to infer foraging area and trophic level, respectively. $\delta^{13}C$ varies predictably with latitude and is depleted in pelagic food webs *vs.* coastal and benthic

zones (Cherel et al., 2000), while $\delta^{15}N$ enriches as it travels up food webs with each successive link from prey to predator (Kelly, 2000). The use of these isotopes has been applied to studying the trophic ecology of squids and has also more recently been expanded into studies of ontogenic shifts in diet and species migrations (Merten et al., 2017; Golikov et al., 2019; Queirós et al., 2019). Stable isotope analysis is commonly used on cephalopod beaks, as these are undigestible hard parts readily found in the stomachs of their predators, including sperm whales (Cherel and Hobson, 2005). However, as SI analysis can be applied to any body tissue, it is an ideal tool for detailing the trophic ecology of opportunistically sampled animals, where only limited tissue types might be available (Jackson et al., 2007). Similar to $\delta^{13}C$, FAs differ at the base of the food web, as primary producers synthesize and retain unique FAs (Dalsgaard et al., 2003; Parrish, 2013). These FAs are assimilated in predators with minimal modification from prey items and thus can be used to infer a predator's diet and trace nutrient pathways to basal food webs (e.g., pelagic zooplankton vs. diatoms vs. coastal macroalgae) (Desforges et al., 2022). Additionally, FAs can be used to explore the availability of key nutrients within an ecosystem and can indicate the potential role or importance of species as prey items (Parzanini et al., 2018). As with SIs, FAs can be measured from most body tissues, although the different physiological roles of varying tissues mean that they preferentially retain different FAs (Phillips et al., 2002), eliminating the possibility of cross-tissue comparisons. Regardless, FA analyses are an ideal tool for trophic ecologists working with rare and opportunistically collected samples, and multiple tissues should be collected to fully capitalize on these occasions.

The Great Australian Bight (GAB), located off the southern coast of Australia, is a site of high productivity, driven by the convergence of the warm eastward flowing Leeuwin current and the cold westward flowing Flinders current as well as annual summer upwelling events (Van Ruth et al., 2018). The GAB includes the shallow continental shelf area around the southern coast, including Kangaroo Island, as well as the continental slope and the abyssal plains, which exceed 5,000-m depth (Rogers et al., 2013). Over the past decade, efforts to improve our understanding of the deep-sea ecosystem of the GAB have increased substantially (e.g., the GAB Research Program and GAB Deepwater Survey by CSIRO). From 2013 to 2017, 304 survey operations were conducted from 200- to 5,000-m depths in the GAB. Of the 1,267 invertebrate species recorded, almost one quarter (401 species) of these were previously undescribed (MacIntosh et al., 2018), indicating how poorly understood the diversity of the benthic and abyssal depths are in this region.

The present study was developed from the opportunistic recovery of five large squid carcasses from the ocean surface in the eastern GAB in March of 2019. The largest of these specimens measured approximately 120 cm in mantle length, and all five of these specimens were identified as *Taningia danae*. *Taningia danae* is a globally distributed and abundant, but rarely seen or researched, species of deep-sea squid, with no tentacles (i.e., only has arms present) and two large photophores on the tips of two arms (Quetglas et al., 2006). In December of 2021, an additional smaller squid specimen, identified as *Chiroteuthis* aff. *veranii*, was retrieved from a similar location and included in the study due to its rarity and unknown diet and trophic role. The aim of this study was to use $\delta^{13}C$ and $\delta^{15}N$ SIs, FAs, and energy content to determine the ecological role of these elusive deep-sea squids in the GAB with reference to other cephalopod species encompassing global, southern temperate, and polar squid distributions. Two libraries of published SI and FA data were compiled for comparison with the data collected from the squids in this study. One dataset consisted of global squid data and was a source of comparison to other squid species that may have similar diets, trophic roles, and physiology. The second dataset included multi-taxa marine species (e.g., cetaceans, fishes, crustaceans, etc.) from the GAB and southeast Australia, the Southern Ocean, New Zealand, and the Antarctic (Supplementary Figure S1) and was used to assess potential trophic interactions between the squids and other local species. The specific objectives of this study were to (a) assess the utility of different body sections for trophic ecology by comparing SI, FA, and energy density data from four different body parts (arms, buccal mass, mantle, and digestive gland); (b) determine the foraging habitat and trophic role of *Taningia danae* and *Chiroteuthis* aff. *veranii* with comparison to published data from squid globally; and (c) describe the roles of these squids and potential trophic interactions within their identified food webs with comparison of published data collected from multi-taxa marine species across the southern hemisphere.

2 Materials and methods

2.1 Specimen collection and identification

The six squid specimens analyzed in this study ("GAB squids"; five *Taningia danae* and one *Chiroteuthis* aff. *veranii*) were opportunistically collected from the eastern GAB, from 34-39°S and 135-139°E (Supplementary Figure S1) between 2019 and 2021 by Australian Fishing Enterprises. The deceased squids were initially spotted floating on the ocean surface by commercial tuna fishery spotter planes and subsequently collected by tuna fishing vessels. The squids were generally in good condition, with evidence of only minor post-mortem scavenging (eyes missing from seabird predation) and decomposition only on specimen Td3 (Supplementary Figure S2). The specimens were frozen onboard the vessels and transported to the Australian Fishing Enterprises facility in Port Lincoln, South Australia, where they were stored at –20°C until transport to Flinders University for subsampling. The specimens were thawed only sufficiently to be measured (e.g., mantle length, and arm length), described (i.e., noting distinguishing features such as arm and tentacle morphology and mantle and fin shape), and subsampled (Supplementary Table S1). Approximately 5 g of tissue from the mantle, arms, buccal mass, and digestive gland was sampled from each individual, cutting from the central portions of the tissues to avoid contamination, and immediately refrozen at –20°C for subsequent analyses. Approximately 3 g of each tissue type for each specimen was freeze-dried at –88°C for 72 h and then manually homogenized into a fine powder using a mortar and pestle.

2.2 Stable isotope analysis

Although squid mantle and arms have low lipid content (<2% wet weight, Phillips et al., 2002), making lipid removal not explicitly necessary for these tissues, the digestive gland has a high lipid content, which is variable both between and within squid species (6–55% wet weight; Phillips et al., 2002; Phillips et al., 2003; Pethybridge et al., 2012; Moovendhan et al., 2019). Therefore, lipid extraction was performed on all samples to ensure consistency across the study and to allow for comparisons with SI data available in the scientific literature, most of which have been chemically lipid extracted. Following a modified Bligh and Dyer (1959) protocol, lipids were removed by soaking the samples in 10 mL of 2:1 dichloromethane/methanol solution for 24 h. The delipidated samples were filtered and oven-dried at 60°C for 48 h to remove the remaining solvent. For each tissue type in each individual squid, one sample of approximately 1.50 mg (± 10%) of homogenized, delipidated tissue was weighed and placed into a tin capsule. The samples were analyzed in triplicate to confirm analytical precision.

Stable carbon and nitrogen isotope ratios were measured using an Isoprime GC5 continuous flow isotope ratio mass spectrometer with a vario ISOTOPE cube elemental analyzer (Elementar Australia Pty Ltd) at Flinders University Chemical Analysis Services. Blank tin capsules and standards were run throughout the analysis to measure analytical precision and correct for isotopic drift. The standards used were L-glutamic acid enriched in light C and N isotopes (^{12}C and ^{14}N) (USGS40) and heavy C and N isotopes (^{13}C and ^{15}N) (USGS41) (Sercon Ltd., UK). Stable isotope results were exported using the IonVantage software from Elementar and expressed in a standard notation as follows:

$$\delta X = [\frac{R\text{sample}}{R\text{standard}} - 1] * 1000$$

where X is ^{15}N or ^{13}C and R is the ratio of ^{15}N to ^{14}N or ^{13}C to ^{12}C in the sample, following the international standards of Pee Dee Belemnite for CO_2, and atmospheric nitrogen for N_2.

2.3 Fatty acid analysis

Three replicates of approximately 0.025 g per tissue type per individual squid specimen were weighed into 20-mL glass test tubes for FA extraction by direct transmethylation (Parrish et al., 2015). To separate the FAs from their glycerol backbones, tissue was soaked in 3 mL of 10:1:1 methanol/dichloromethane/hydrochloric acid solution at 80°C for 2 h. At the completion of the 2-h solvent soak, the samples were removed from heat and cooled to ambient temperature before the addition of 1 mL of milli-Q water and 1.8 mL of 2:1 hexane/dichloromethane solution, followed by vortex mixing and centrifuging at 2,000 rpm for 5 min. The upper layer containing the FA methyl esters (FAMEs) was removed and placed into 2-mL glass vials. The vials were placed under nitrogen gas streams to evaporate the solvent, leaving only pure FAMEs. The addition of 1.8 mL of hexane/dichloromethane solution and dehydration with nitrogen gas was repeated three times, maximizing the FA retention. The FAMEs were suspended in 1 mL of dichloromethane for subsequent quantification. Fatty acid methyl esters were identified and quantified using gas chromatography mass spectrophotometry (GCMS) analysis with Agilent Technologies 5975C Series GC/MSD (Agilent Technologies, Inc., USA) equipped with Triple-Axis HED-EM Detector, SGE Analytical Science (Ringwood, Victoria, Australia) BP21 capillary column (15 m length, 0.25 mm internal diameter, and 0.25 µm film thickness), Agilent 7683B Series Injector, and Agilent/HP 7683 automatic liquid sampler. Quality checks were performed throughout the analysis with a blank sample containing 1 mL dichloromethane at the start of each run, plus an internal FA standard (C4–C24) (Sigma-Aldrich, USA). The output was analyzed and processed using MassHunter Qualitative Analysis software and the National Institute of Standards and Technology (https://www.nist.gov) database of FA compounds. Individual FA values were reported as percentage of the total FAs per sample analyzed so that contributions to FA profiles could be established. Fatty acids contributing<0.1% across the 45 samples were removed, leaving 21 FAs for tissue and species comparisons within the GAB squids (Supplementary Table S2).

2.4 Energy content (GAB *Taningia danae*)

One sample of each *T. danae* tissue type was combusted in a bomb calorimeter (Parr 6200 Isoperibol with semi-micro bomb) to obtain the energy content of the tissues. Before measuring the samples, a standard of benzoic acid was run. For each *T. danae* sample, approximately 0.025 g of freeze-dried, homogenized tissue was pressed into a pellet, packed into a crucible, and ignited in the bomb calorimeter. The heat released was measured and converted to kilojoules per gram wet weight.

2.5 Data analysis (GAB squids)

The isotopic compositions and FA profiles of the GAB squids alone were analyzed using PRIMER 7 + PERMANOVA (Anderson et al., 2008; Clarke and Gorley, 2015). To visually compare the isotopic composition across tissue types and species, a $\delta^{13}C$ and $\delta^{15}N$ biplot was created. Multivariate data visualization was used to assess if and how FA profiles differed across tissue type and species. Fatty acid data was square-root-transformed, and a resemblance matrix was generated using a Bray–Curtis measure of similarity. The data was visualized using a principal coordinates ordination (PCO) plot, and vectors were overlaid showing FAs with Pearson correlations >0.8 to indicate the direction and magnitude of the correlation with individual FAs. Similarity of Percentages (SIMPER) analyses were conducted using the previously generated resemblance matrices on factors of tissue type and species to determine the percentage dissimilarities between groups and the FAs contributing to the between-group differences.

The whole-body energy density of *T. danae* was roughly estimated using the energy density results for the mantle, arm, and digestive gland tissues. These were multiplied by the body

weight proportions of *T. danae* given in Kelly (2019), wherein fins comprised 61% of body mass, mantle 14%, head and arms 23%, and viscera 4% (the digestive gland being 0.88%). Mantle energy density was multiplied by the fins + mantle proportions (0.75), arm energy density was multiplied by head and arms proportions (0.23), and digestive gland energy density was multiplied by the digestive gland proportion (0.0088). These were summed to provide an estimate of the whole animal energy density of *T. danae* tissues.

2.6 Collection, filtering, and refinement of published data

Additional SI and FA data were collected from published literature and legacy datasets (Nichols et al., 2023), enabling for the determination of the feeding ecology and trophic role of the GAB squids (available in Supplementary Tables S8–S12). Data were collected for (a) any squid species globally and (b) any marine species found in the southeast Australia, New Zealand, the Southern Ocean, and the Antarctica marine regions (henceforth referred to as southern marine species; Supplementary Figure S1).

Stable isotope data as mean $\delta^{13}C$ and $\delta^{15}N$ and associated metadata including species, location (sea or ocean sampled), and tissue type were collated from published literature. In total, 155 SI datapoints were used from the muscle and beak analyses of squid globally, and 293 data points were used from any tissue of multi-taxa southern marine species, including groups such as crustaceans, fishes, seabirds, and marine mammals. Beaks are commonly used for SI research of cephalopods but are comprised of chitin, which is known to be enriched in in 14-nitrogen, resulting in $\delta^{15}N$ values lower than that of muscle tissues from the same animal. In previous works, the $\delta^{15}N$ values of beaks have been adjusted for comparison to muscle samples by adding between 3.5‰ and 4.8‰ (Cherel and Hobson, 2005; Navarro et al., 2013; Guerreiro et al., 2015). Thus, we adjusted all beak $\delta^{15}N$ data that were not already corrected in the source publication by + 3.5‰ to allow more reliable comparisons with our GAB squids. The triplicate SI ratios generated for each tissue type across the GAB squids were condensed to the mean muscle-specific isotope ratio per specimen. The isotope ratios in the digestive gland were depleted in both $\delta^{13}C$ and $\delta^{15}N$ and so were excluded from the muscle-specific mean. A $\delta^{13}C$ and $\delta^{15}N$ biplot was created to qualitatively compare the trophic ecology of the six specimens in this study with squid globally and to assess the role that these squids play within local food webs.

Fatty acid profiles were recorded as the percent contribution of each FA to the total FA quantity. For each profile, metadata including the species, taxon type (cephalopod, fish, chondrichthyan, etc.), location (sea or ocean sampled), and tissue type were recorded, as well as other information such as sex and maturity status, if available. If multiple FA profiles were reported within a single source for the same species, location, and tissue type, the mean FA profile across all samples was calculated for use. In total, 116 and 298 FA profiles were used from tissues of squids globally and tissues of multi-taxa southern marine species, respectively (metadata and citations can be found in the Supplementary Material).

Fatty acid data are reported differently throughout the literature. Up to 60 different FAs are often measurable on the GCMS; however, only those exceeding 2%, 1%, 0.2%, or 0.1% or simply those deemed "of interest" by the authors tend to be reported in the literature. Thus, depending on the author, the means of analysis, and tissue types, FA profiles may not be directly comparable. As this study combined FA data from a wide range of sources, many FAs needed to be grouped together to minimize the effects of differing sources. Firstly, FA profiles were standardized to sum up to 100%, eliminating the influence of minor FAs that were not measured or reported in many profiles. Secondly, FAs were filtered to further minimize any confounding effects of data source. For the global squid dataset, FAs reported in fewer than 50 samples and those with a mean of less than 0.5% across all samples were removed. For the southern marine species dataset, the mean percentage of each FA was calculated across each separate taxa group (cephalopods, fishes, chondrichthyes, etc.), and FAs with a mean of less than 2% within all taxa groups were removed. This ensured that any FAs important to only one taxon group were retained for analysis rather than be removed due to their lack of contribution in other taxon groups. This standardization process followed Meyer et al. (2019) and resulted in a 15 FA global squid dataset and a 12 FA southern marine, multi-taxon species dataset (Supplementary Table S2).

The triplicate FA profiles generated for each tissue type across the GAB squids were averaged to one profile per tissue type, per specimen, and included in the final FA datasets. The comparison of the six specimens within this study to squid globally was divided into two datasets: muscular tissue profiles (unspecified soft tissues, mantle, buccal mass, arm, and fin) and digestive tissue profiles (digestive gland, stomach, stomach fluid, cecum oil, and whole homogenized individuals). These datasets warranted a separate analysis, as the two tissue types have distinct FA profiles that are not directly comparable. Bray–Curtis similarity matrices were generated from the square-root-transformed data. The data were visualized using a PCO plot, and vectors were overlaid showing FAs with Pearson correlations >0.5. Similarity of Percentages (SIMPER) analyses were conducted using the previously generated resemblance matrices on factors of tissue type and location to determine the percentage dissimilarities between groups and the FAs contributing to the between-group differences.

Energy density data, as kilojoules per gram wet weight, were collected and analyzed for southern mid-trophic marine species (squids and fishes). In instances wherein one species had several differing energy densities available, the greatest kilojoules per gram value was retained for analysis. Additionally, body mass data were collected of all species included in the energy density analyses so that the approximate energy content per individual could be calculated. "As reported body masses can vary greatly; the greatest published body masses were used for analysis. This was so that the energy contents calculated per individual were more likely overestimations than underestimations, and thus comparisons made to *T. danae* energy content would be viable. *Taningia danae* whole-body energy density was multiplied by both the greatest individual body mass recorded, 161 kg, and a more conservative body mass, 60 kg (Roper and Jereb, 2010), to

provide two points of comparison with the other southern marine species.

3 Results

3.1 GAB squids

Stable isotope ratios differed between individual specimen, species, and tissue type (Table 1; Figure 1), with the highest $\delta^{15}N$ found in the mantle and the lowest in the buccal mass. Digestive gland tissues were depleted in $\delta^{13}C$ and $\delta^{15}N$ *versus* the muscle tissues (mantle, arm, and buccal mass) (Figure 1). The carbon-to-nitrogen (C:N) ratio of all muscle tissues in all squid specimens ranged from 2.83 to 3.14, and the C:N ratio of the digestive gland was higher than that of the muscle tissues (Table 1).

In *T. danae* and *C.* aff. *veranii*, saturated fatty acids (SFAs) and polyunsaturated fatty acids (PUFAs) were most abundant in the muscle tissues, while monounsaturated fatty acids (MUFAs) were most abundant in the digestive gland (Table 2). In muscles, the most abundant individual FAs were 16:0, 22:6ω3, and 20:5ω3, whereas in the digestive glands the most abundant were 16:0, 18:0, and 20:1ω9 (Table 2). The fatty acid profiles were differentiated primarily by tissue type (digestive gland or muscle tissue), followed by species (Figure 2), as the digestive gland FA profiles of *T. danae* were 19.09–20.10% dissimilar from the muscle FA profiles (Supplementary Table S3). This dissimilarity was influenced by higher proportions of 18:1ω9, 20:1ω9, and 24:1ω9 and lower proportions of 22:6ω3, 20:5ω3, and 16:0 in the digestive gland (Figure 2). The muscle tissues were all<10% dissimilar within each species (Supplementary Table S4). The muscle tissues of the *T. danae* specimens were 9.92–11.80% dissimilar to the muscles of the *C.* aff. *veranii* specimen (Supplementary Table S5). In total, 59% of this dissimilarity was influenced by the *C.* aff. *veranii* tissues having higher proportions of 16:1ω7*t*, 18:2ω6, and 20:5ω3 and lower proportions of 22:6ω3, 20:3ω3, and 24:0 *versus* the *T. danae* tissues.

The digestive gland of *T. danae* had a greater energy content (5.94 kJ/g) than the muscular tissues which ranged from 2.53 kJ/g for the mantle tissue to only 0.50 kJ/g for the buccal mass (Table 3). Using the body part proportions given for *T. danae* in Kelly (2019), the whole-body energy density of *T. danae* is estimated at approximately 2.25 kJ/g.

3.2 GAB squids vs. global squids

Globally, squids had a $\delta^{13}C$ range from -25.80‰ to -15.10‰ and a $\delta^{15}N$ range from 6.30‰ to 17.90‰ (Figure 3). The GAB squids were comparatively depleted in $\delta^{13}C$, and most aligned with squid species collected from the Southern Ocean (Figure 3; Supplementary Figure S3). The GAB squids were also enriched in $\delta^{15}N$, with few squids from the Southern Ocean, southeast Australia, and New Zealand areas having higher $\delta^{15}N$ in comparison (Figure 3; Supplementary Figure S4). Four specimens of *T. danae* (Td) from the Southern Ocean and southeast Australia had similarly enriched $\delta^{15}N$ values compared to the GAB *T. danae* specimens (Figure 3). In contrast, one *T. danae* specimen from the Southern Ocean was considerably enriched in $\delta^{15}N$ than the GAB specimens, at 15.30‰ (Figure 3). *Chiroteuthis* sp. and *C. veranii* specimens (two and three samples, respectively) had $\delta^{15}N$ values ranging from 11.50‰ to 12.90‰ and $\delta^{13}C$ values ranging from -20.00‰ to -16.50‰ (Figure 3).

The SIMPER analysis revealed a 23.30% dissimilarity between the FA profiles of digestive gland and mantle muscle tissues from squids sampled globally. In total, 47% of this dissimilarity between tissue types was due to higher proportions of MUFAs (18:1, 20:1, 22:1, 16:1, and 24:1) in the digestive gland tissue, and 27.00% was attributed to higher proportions of 22:6ω3, 20:5ω3, and 16:0 in mantle tissue.

TABLE 1 $\delta^{13}C$ and $\delta^{15}N$ (‰) composition and carbon-to-nitrogen ratio (C:N) of arm (A), buccal mass (B), mantle (M), and digestive gland (DG) from *Taningia danae* (Td) and *Chiroteuthis* aff. *veranii* (Cav) specimens collected from the eastern Great Australian Bight.

		Td1	Td2	Td3	Td4	Td5	Cav1
$\delta^{13}C$	A	-21.29 ± 0.14	-20.94 ± 0.18	-20.59 ± 0.31			-21.71 ± 0.29
	B	-22.37 ± 0.18	-20.70 ± 0.35	-20.04 ± 0.12			-21.35 ± 0.34
	M	-21.41 ± 0.03		-20.76 ± 0.14	-21.51 ± 0.19	-21.78 ± 0.15	-22.37 ± 0.40
	DG	-23.80 ± 0.22		-22.15 ± 0.17			
$\delta^{15}N$	A	10.37 ± 0.16	10.48 ± 0.15	11.49 ± 0.21			10.10 ± 0.08
	B	11.01 ± 0.10		12.80 ± 0.08	12.03 ± 0.10	12.23 ± 0.06	11.23 ± 0.05
	M	10.77 ± 0.21	10.98 ± 0.16	12.08 ± 0.47			9.94 ± 0.11
	DG	9.57 ± 0.29		10.78 ± 0.13			
C:N	A	2.96 ± 0.02	2.87 ± 0.05	2.95 ± 0.06			2.91 ± 0.27
	B	3.08 ± 0.03	2.98 ± 0.01	2.83 ± 0.03			2.83 ± 0.04
	M	2.99 ± 0.03		2.99 ± 0.03	3.11 ± 0.02	3.14 ± 0.04	3.03 ± 0.06
	DG	3.98 ± 0.02		3.37 ± 0.05			

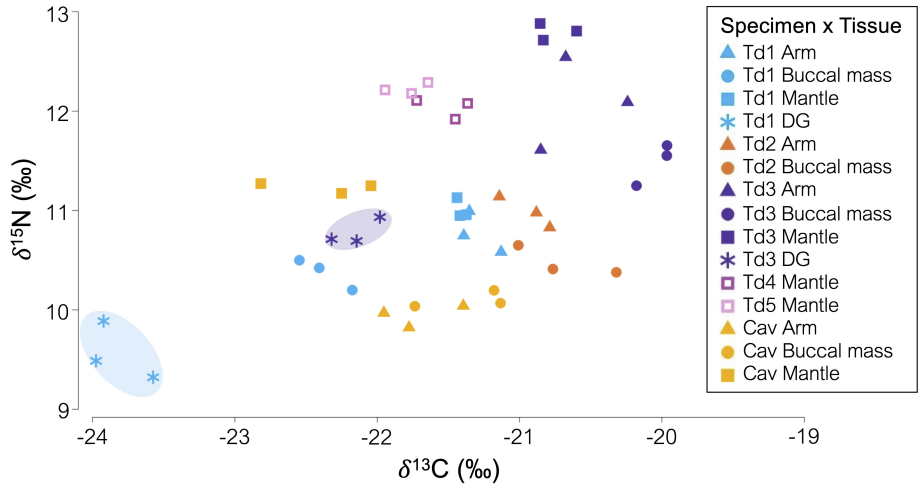

FIGURE 1
$\delta^{13}C$ and $\delta^{15}N$ (‰) composition of mantle, arm, buccal mass, and digestive gland from *Taningia danae* and *Chiroteuthis* aff. *veranii* collected from the eastern Great Australian Bight. Ellipses are drawn to illustrate the separation between muscle tissues and the digestive gland.

Globally, squid muscle tissue FA profiles were well separated by sampling area (Figure 4A), with GAB *T. danae* and GAB *C.* aff. *veranii* being least dissimilar to the squid samples taken from the northeast Atlantic (12.26% and 13.52% dissimilar, respectively) and southeast Australia (12.25% and 13.57% dissimilar, respectively; Supplementary Table S6). The GAB squid samples grouped closely with southeast Australian samples including *Todarodes filippovae* (Tf), *Idioteuthis cordiformis* (Ics), and *Ommastrephes brevimanus* (Omb) (Figure 4A). Two *Architeuthis dux* (Ad) samples were also similar in FAs, with one from eastern Australia and the other from the northeast Atlantic Ocean. The southeast Australia and Southern Ocean samples were differentiated from other areas by higher proportions of FAs 16:0, 20:1, 22:1, and 24:1. The Southern Ocean samples were differentiated from southeast Australia samples by higher proportions of FAs 16:1, 18:1, and 22:5ω3, while the southeast Australian samples, including the samples from this study, had higher 18:0. There were two samples taken from chiroteuthids, a *C. veranii* (Cv) sample from the northwestern Atlantic and a *Chiroteuthis* sp. (Cx) from southeast Australia. Both samples had lower proportions of FA 18:0 and higher proportions of 18:1 in the mantle *versus* the GAB *C.* aff. *veranii*. Zero *Taningia* spp. were found for comparison.

The fatty acid profiles from the digestive parts of squids (including whole squids, digestive glands, stomachs, stomach fluid, or cecum oil) showed less grouping by sampling area than was evident in the muscle tissues (Figure 4B). The Southern Ocean squid species remain characterized by MUFAs including 16:1, 18:1, and 24:1, as with the muscle FA profiles of Southern Ocean squid. The GAB *T. danae* was least dissimilar (19.30%) to the southeast Australian samples (Supplementary Table S7) and clustered close to several whole squid samples of *Octopoteuthis megaptera* (Ome), *Lycoteuthis lorigera* (Ll), *Histioteuthis atlantica* (Ha), *Mastigoteuthis* sp. (Max), *Ancistrocheirus lesueurii* (Ale), and *O. bartramii* (Omb), plus a digestive gland sample of *Nototodarus gouldi* (Ng). These samples were characterized by lower proportions of 14:0, 16:1, and 18:1 and higher proportions of 18:0 and 20:1. When filtering the dataset to include only the digestive gland samples and re-generating the PCO plot, the digestive gland samples of the GAB *T. danae* were distinct from all but one sample; *Nototodarus gouldi* (Ng) from southeast Australia (Supplementary Figure S5). No *Taningia* spp. FA samples were available for comparison.

3.3 GAB squids vs. southern marine species

The isotopic ratios of the marine species from southeast Australia, New Zealand, the Southern Ocean and Antarctica were well grouped by sample area along the $\delta^{13}C$ axis, with samples with $\delta^{13}C$ lower than -20‰ almost entirely Southern Ocean and Antarctic species (Figure 5). The GAB squids' $\delta^{13}C$ values (from -20.59‰ through -21.71‰) were most similar to taxa from the Southern Ocean. Overall, the southeast Australian samples were more enriched in $\delta^{15}N$ over the Southern Ocean species but had a slightly smaller range, from 6.00‰ to 16.10‰ in the southeast Australian samples, versus 5.00‰ to 17.80‰ in Southern Ocean samples (Figure 5). The GAB squids had $\delta^{15}N$ values similar to intermediate trophic level species such as fishes among the samples from southeast Australian taxa or similar to high-trophic-level species, such as seabirds, among the samples from Southern Ocean taxa.

The fatty acid profiles of the multi-taxon species sampled in this study were best grouped by taxon, with most variation occurring along the PCO1 axis (Figure 6). Squid FA profiles had higher proportions of 22:6ω3, 20:5ω3, 18:0, and 16:0 than other southeast Australia, New Zealand, Southern Ocean, and Antarctic taxa. The GAB squids were closely grouped and characterized by these same FAs, although they had relatively higher proportions of these FAs than most published squid samples (Supplementary Figure S6). The digestive gland profiles from GAB *T. danae* specimens Td1 and Td3 had higher proportions of MUFA and lower 22:6ω3 and 20:5ω3

TABLE 2 Percentage contribution of specific fatty acids to total FAs as mean ± standard deviation in the mantle, arm, buccal mass, and digestive gland tissues of *Taningia danae* and *Chiroteuthis* aff. *veranii* collected from the eastern Great Australian Bight.

	Taningia danae				*Chiroteuthis* aff. *veranii*		
	Arm	Buccal mass	Mantle	Digestive gland	Arm	Buccal mass	Mantle
	n = 3	*n* = 3	*n* = 4	*n* = 2	*n* = 1	*n* = 1	*n* = 1
12:0	0.00 ± 0.0	0.06 ± 0.2	0.27 ± 0.8	0.00 ± 0.0	0.05 ± 0.1	0.58 ± 1.0	0.00 ± 0.0
14:0	1.60 ± 0.3	1.22 ± 0.4	1.80 ± 0.3	2.12 ± 0.4	2.97 ± 0.9	1.78 ± 0.4	1.28 ± 0.1
15:0	0.26 ± 0.1	0.24 ± 0.1	0.27 ± 0.1	0.41 ± 0.1	0.44 ± 0.2	0.32 ± 0.1	0.43 ± 0.2
16:0	25.58 ± 1.0	25.95 ± 1.8	26.71 ± 2.0	21.52 ± 3.9	26.7 ± 3.0	27.62 ± 0.7	28.67 ± 1.4
17:0	1.07 ± 0.0	1.19 ± 0.1	1.12 ± 0.1	1.76 ± 0.6	1.02 ± 0.1	1.20 ± 0.0	1.09 ± 0.0
18:0	11.91 ± 1.6	12.69 ± 1.5	11.06 ± 2.8	18.04 ± 3.9	10.65 ± 1.8	12.29 ± 0.6	11.95 ± 0.8
20:0	0.42 ± 0.0	0.49 ± 0.2	0.31 ± 0.1	0.61 ± 0.1	0.26 ± 0.1	0.30 ± 0.1	0.25 ± 0.0
24:0	0.72 ± 0.3	0.50 ± 0.4	0.51 ± 0.3	0.06 ± 0.1	0.35 ± 0.3	0.11 ± 0.2	0.30 ± 0.3
ai-17:0	0.06 ± 0.1	0.06 ± 0.1	0.04 ± 0.1	0.61 ± 0.1	0.33 ± 0.1	0.26 ± 0.0	0.27 ± 0.0
Σ SFA	41.64 ± 2.1	42.41 ± 2.5	42.09 ± 4.3	45.12 ± 8.9	42.79 ± 4.4	44.47 ± 0.5	44.24 ± 2.2
16:1ω7c	0.22 ± 0.1	0.19 ± 0.1	0.29 ± 0.0	0.61 ± 0.2	0.65 ± 0.2	0.32 ± 0. 0	0.35 ± 0.0
16:1ω7t	0.02 ± 0.1	0.00 ± 0.0	0.05 ± 0.1	0.23 ± 0.1	0.81 ± 0.3	0.82 ± 0.0	1.01 ± 0.0
18:1ω9c	2.14 ± 0.3	2.47 ± 0.8	2.39 ± 0.6	11.54 ± 5.8	2.55 ± 0.5	1.35 ± 1.0	2.21 ± 0.1
20:1ω9c	7.97 ± 0.3	8.85 ± 0.5	7.76 ± 1.6	16.35 ± 0.9	6.95 ± 0.4	8.41 ± 1.5	7.36 ± 0.1
22:1ω9c	3.04 ± 0.4	3.01 ± 0.9	2.90 ± 0.4	4.11 ± 0.9	3.21 ± 0.0	2.40 ± 0.4	3.79 ± 0.3
24:1ω9c	0.72 ± 0.1	0.81 ± 0.3	0.67 ± 0.2	2.23 ± 0.2	0.78 ± 0.2	0.72 ± 0.1	0.54 ± 0.5
Σ MUFA	14.11 ± 0.9	15.34 ± 2.1	14.06 ± 2.7	35.06 ± 6	14.95 ± 0.4	14.04 ± 0.1	15.26 ± 0.2
18:2ω6t	0.00 ± 0.0	0.00 ± 0.0	0.00 ± 0.0	0.26 ± 0.0	0.94 ± 0.5	0.30 ± 0.0	0.38 ± 0.0
20:2ω6c	0.36 ± 0.1	0.26 ± 0.0	0.33 ± 0.1	0.97 ± 0.2	0.41 ± 0.1	0.46 ± 0.3	0.33 ± 0.0
20:3ω3c	0.93 ± 0.3	0.39 ± 0.4	0.50 ± 0.4	0.28 ± 0.1	0.28 ± 0.1	1.27 ± 0.9	0.00 ± 0.0
20:4ω6c	1.46 ± 0.2	2.09 ± 1.0	1.34 ± 0.4	2.35 ± 0.2	1.81 ± 0.1	1.66 ± 0.4	2.20 ± 0.1
20:5ω3c	13.47 ± 1.1	13.86 ± 1.5	13.77 ± 1.4	9.01 ± 1.3	16.51 ± 0.7	19.16 ± 0.6	16.86 ± 0.6
22:6ω3c	28.03 ± 1.2	25.65 ± 2.8	27.91 ± 4.4	6.94 ± 2.1	22.31 ± 3.1	18.65 ± 0.8	20.74 ± 1.6
Σ PUFA	44.25 ± 1.8	42.25 ± 3.8	43.86 ± 5.3	19.81 ± 3.6	42.26 ± 4.0	41.50 ± 0.5	40.50 ± 2.3

FAs<0.1% were excluded.
SFA, saturated fatty acids; MUFA, monounsaturated fatty acids; PUFA, polyunsaturated fatty acids.

than the other GAB squid muscle samples and were clustered closely to FA profiles from four fish species; *Epigonus lenimen* (Ele), *E. carlsbergi* (Ec), *Lepidorhynchus denticulatus* (Ld), and *Nemichthys* sp. (Nmx) (Figure 6).

The whole-animal energy density per gram of *T. danae* is lower than all other southern marine squid and fish species that could be found in published literature (Figure 7; Supplementary Table S8). However, as *T. danae* is a large-bodied squid species, the whole-animal energy content of even the moderately sized individuals can surpass 130,000 kJ, which is higher than all species analyzed except for the toothfishes (*Dissostichus* spp.). The largest *T. danae* individual reliably measured, weighing 161 kg (Roper and Jereb, 2010), might contain an energy content of up to 362,250 kJ (Figure 7), greater than all other squids and fishes analyzed except for Antarctic toothfish, *Dissostichus mawsoni*.

4 Discussion

Deep-sea squids are presumably vital components of these largely undescribed marine ecosystems, yet limited access to specimens has hampered efforts to detail their ecological roles as predators and prey. The opportunistic collection of five *Taningia danae* specimens and one *Chiroteuthis* aff. *veranii* specimen from the GAB enabled the comparison of FAs and SIs across four body tissue types showcasing that muscular tissues can be used interchangeably in the absence of entire specimens. It also suggested that the digestive gland offers insights into the foraging habitats of squids as predators while also being the key site of nutrient storage and indicating which nutrients are gained by the predators feeding on them. The SIs and FAs suggested that the *T. danae* and *C.* aff. *veranii* specimens probably lived in the Southern

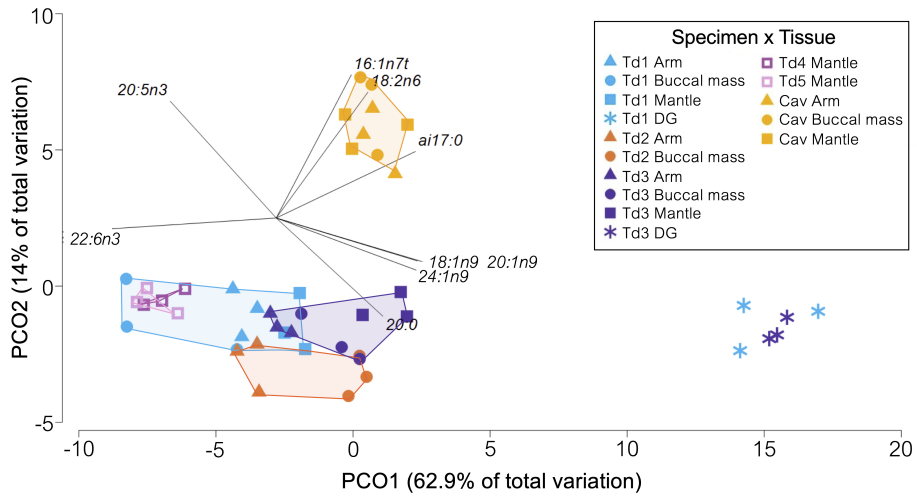

FIGURE 2
Principal coordinates ordination plot of fatty acid (FA) profiles from *Taningia danae* and *Chiroteuthis* aff. *veranii* collected from the eastern Great Australian Bight. A vector showing Pearson correlations >0.8 is overlaid, indicating the FAs contributing to differences between samples, and polygons are drawn to show the grouping of muscle tissue profiles by specimen.

Ocean and were high-trophic-level predators likely consuming deep-sea fishes and small squids and are sources of essential FAs (EPA and DHA) and calories for Southern Ocean predators.

4.1 Limitations

As this study was entirely opportunistic with regard to the GAB squid specimens, there are several limitations. These limitations may cause variation in both the stable isotope values recorded and the fatty acid results as well as affect the reliability of the results due to the small sample size. This should be considered when reading the hypotheses and conclusions presented here. In SI analysis, squid beaks are a commonly sampled tissue as they are retrieved frequently in predator stomachs (Hoving et al., 2014). Beaks contain chitin, which causes depletion in $\delta^{15}N$ values, and there is tissue accumulation, rather than turnover, across an organism's lifetime (Cherel and Hobson, 2005). Newly synthesized areas of the beak, such as the lower wing, have less chitin and can more reliably show recent dietary signatures, while the rostrum and whole homogenized beaks compress an entire lifetime of ecological information into a single isotopic ratio (Cherel and Hobson, 2005). There is some uncertainty when comparing beaks to muscle tissues, and therefore comparing the GAB squids data to published squid beak data may impact the comparison with squid globally. Correction values of +3.5‰ (Navarro et al., 2013) and +4.8‰ $\delta^{15}N$ (Guerreiro et al., 2015) have been applied to beak isotopic ratios to make them more comparable to muscle tissues. However, different correction factors would be required for beak samples taken from the wing, rostrum, or whole beak, which has not, to the best of our knowledge, been developed yet. In this study, we applied a single, conservative correction factor of +3.5‰ to any beak samples taken from the literature that were not already corrected in the source publication. We did this so that these samples could be more reliably compared with the muscle samples taken from the GAB squids, but we are aware that applying a single-correction factor may have caused over- or under-corrections of particular samples, potentially impacting conclusions made here.

Additionally, *Taningia danae* is an ammoniacal squid, which means that their tissues contain elevated levels of ammonia, which helps the animal achieve neutral buoyancy and reduce energy costs (Clarke et al., 1979). Ammonia in the muscle tissues of elasmobranchs can have effects on SI values, and studies have suggested that rinsing samples in deionized water can remove the urea (Li et al., 2016). When comparing shark muscle samples with lipids extracted *versus* samples that were both lipid-extracted and deionized-water-rinsed, the urea extracted samples had $\delta^{15}N$ values increased by just under 1.0‰ and $\delta^{13}C$ values decreased by just under 1.0‰ (Martin and Jaquemet, 2019). To our knowledge, this method has not been tested in ammoniacal squid tissues and is not currently standard among SIA of squid muscle.

Comparisons among beak data, lipid extracted muscle data, and urea removed muscle data will likely require the development of a set of correction factors that could be applied to allow for better use of published data, which is a convenient way of utilizing opportunistic sampling events, regardless of how small sample sizes are.

TABLE 3 Energy density of *Taningia danae* (n = 1) tissues as measured through bomb calorimetry.

Tissue type	Energy content (kJ/g wet weight)
Arm	1.31
Buccal mass	0.50
Mantle	2.53
Digestive gland	5.94
Whole[a]	2.25

[a]Whole-body energy density estimated using body part proportions given in Kelly (2019).

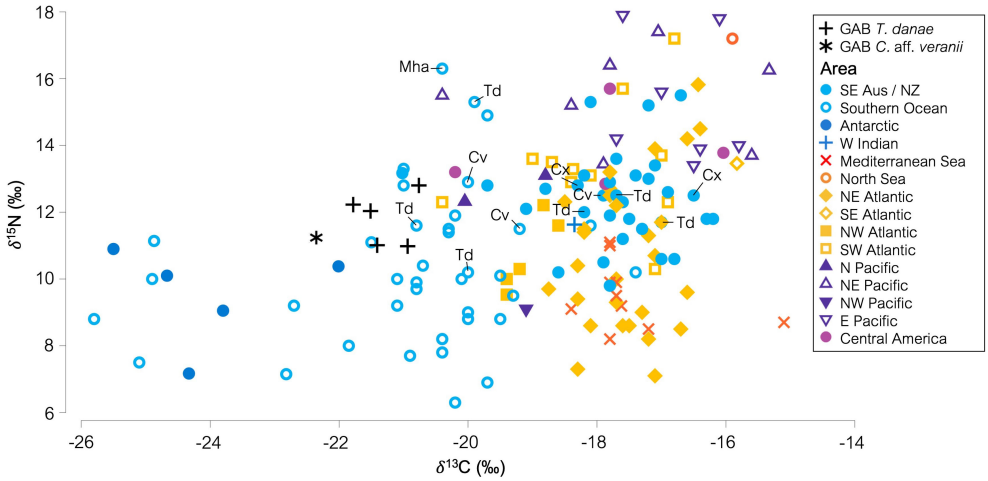

FIGURE 3
Biplot of $\delta^{13}C$ and $\delta^{15}N$ (‰) from global squid studies. Great Australian Bight squid data used is mean muscle $\delta^{13}C$ and $\delta^{15}N$. The data points referred to in the text are labeled with species abbreviation. GAB Td, *Taningia danae* from the eastern Great Australian Bight; GAB Cav, *Chiroteuthis* aff. *veranii* from the eastern Great Australian Bight; Mha, *Mesonychoteuthis hamiltoni*; Td, *Taningia danae*; Ln, *Loliolus noctiluca*; Cv, *Chiroteuthis veranii*; Cx, *Chiroteuthis* sp.

In FA analysis, both decomposition and frozen storage are known to cause the degradation of PUFAs over time (Budge et al., 2006; Atayeter and Ercoşkun, 2011; Meyer et al., 2017). The GAB squid specimens were potentially decomposing in the environment for an unknown amount of time before retrieval and then were frozen for at least 3 years before samples were taken and processed for SI analysis and FA analysis. In another study, squid mantle frozen for 12 months at -20°C had proportions of PUFAs (especially 22:6ω3) decrease by approximately 10% and SFAs (especially 16:0 and 18:0) increase by approximately 10% *versus* fresh tissue (Atayeter and Ercoşkun, 2011). The GAB squids in this study were found to have relatively high 16:0 and 18:0 and low PUFAs in their tissues *versus* other squid samples, which may be an artefact of extended frozen storage or decomposition. Additionally, with the collection and use of published data, the storage period of many of those samples or levels of decomposition by the time of retrieval is unknown. Thus, we suggest that detailed tissue information is provided in future studies that use opportunistically collected specimens.

4.2 Body part utility

The clustering of the GAB squid muscle tissues (arm, buccal mass, and mantle) and the distinctiveness of the digestive glands

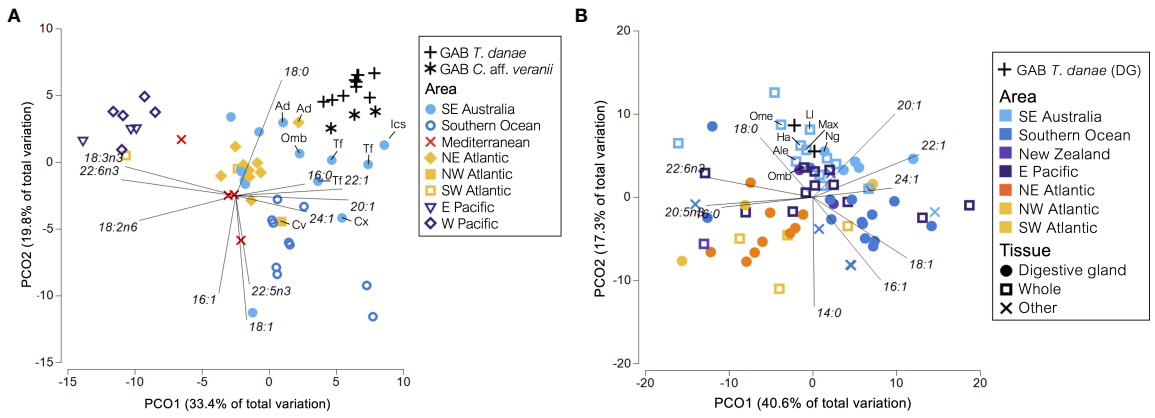

FIGURE 4
Principal coordinates ordination plots of fatty acid (FA) profiles of **(A)** squid muscle tissues (unspecified muscle, mantle, arms, fins, and buccal mass) and **(B)** squid digestive parts (digestive gland, whole squid, stomach, stomach fluid, and cecum oil) in studies conducted globally. Only FAs with a mean proportion of >0.5% across the global squid dataset and present in >50 of the samples were retained. A vector overlay showing Pearson correlations >0.5 indicates the individual FAs contributing to differences between samples. GAB, Great Australian Bight. Only samples referred to in the text are labeled with species abbreviation. Ad, *Architeuthis dux*; Omb, *Ommastrephes bartramii*; Tf, *Todarodes filippovae*; Cv, *Chiroteuthis veranii*; Cx, *Chiroteuthis* sp.; Ics, *Idioteuthis cordiformis*; Ome, *Octopoteuthis megaptera*; Ale, *Ancistrocheirus lesueurii*; Ha, *Histioteuthis atlantica*; Ll, *Lycoteuthis lorigera*; Max, *Mastigoteuthis* sp.; Ng, *Nototodarus gouldi*.

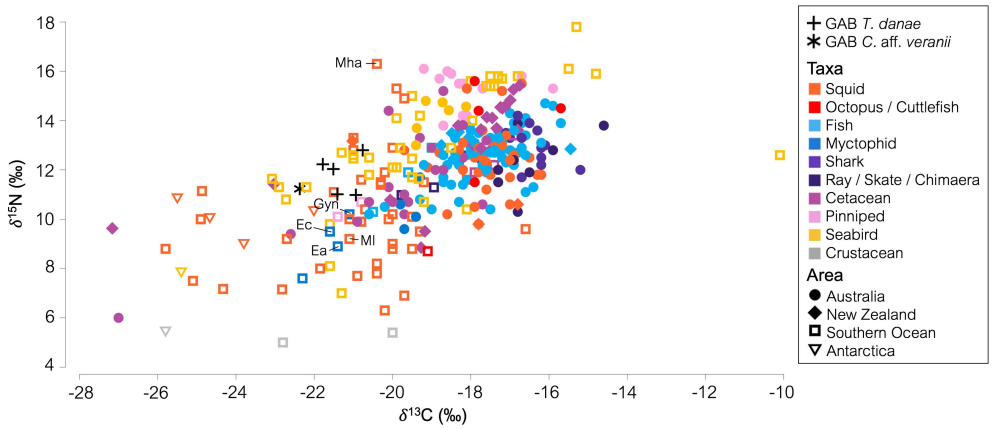

FIGURE 5
Biplot of $\delta^{13}C$ and $\delta^{15}N$ (‰) from marine species sampled from southeast Australia, New Zealand, the Southern Ocean, and Antarctica. GAB squid data used is mean muscle $\delta^{13}C$ and $\delta^{15}N$. GAB, Great Australian Bight. The data points referred to in the text are labeled with species abbreviation. Ec, *Electrona carlsbergi*; Ea, *Electrona antarctica*; Gyn, *Gymnoscopelus nicholsi*; Ml, *Moroteuthopsis longimana*; Mha, *Mesonychoteuthis hamiltoni*; Ln, *Loliolus noctiluca*.

suggest that the three muscle tissues could be used mostly equivalently, with similar SI and FA profiles. Often in opportunistic sampling of squid only a portion of the animal is retrieved, so being able to sample any of these muscle tissues and gain similar, useable results is vital for describing deep-sea and continental shelf food webs.

There are minor and variable isotopic differences among muscle tissue types, such as mantle being the most enriched in $\delta^{15}N$ and buccal mass the least enriched, but these are likely due to the minor differences in protein content between the three tissue types (Shulman et al., 2002; Hobson and Cherel, 2006). Due to the limited number of squids with all three muscle tissue types available (three individuals across the two species), this could not be explored further within this study. However, these relatively minor isotopic differences should not preclude the interchangeable use of muscle tissues when equivalent tissues are unavailable across specimens, as the differences among these tissues do not exceed the differences among individuals of the same species. The digestive gland samples were relatively depleted in both $\delta^{13}C$ and $\delta^{15}N$ and increased in C:N ratio compared to the other tissues analyzed, which is likely due to the high oil content (Cherel et al., 2009a; Ruiz-Cooley et al., 2011; Svensson et al., 2016). Studies using SIs to

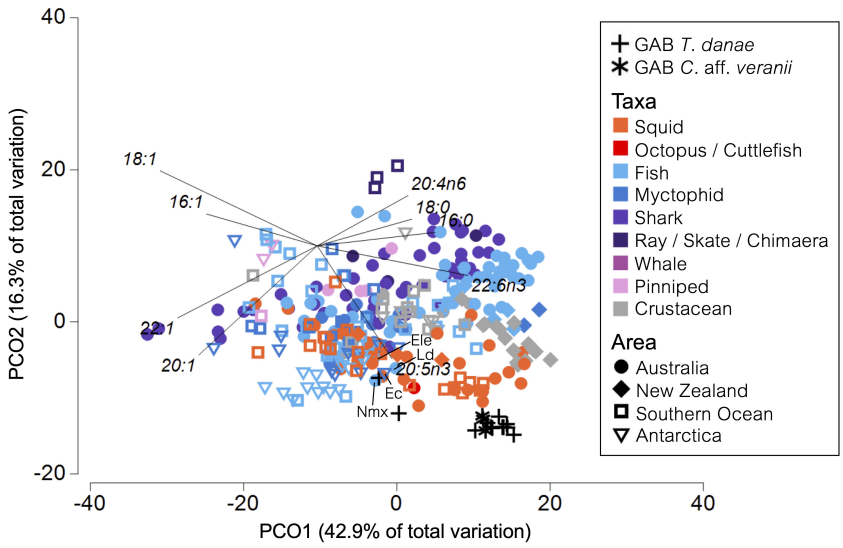

FIGURE 6
Principal coordinates ordination plot of published fatty acid (FA) profiles of marine species collected in southeast Australia, New Zealand, the Southern Ocean, and Antarctica. Only FAs with a mean proportion >2% in all taxa groups were retained. A vector showing Pearson correlations >0.5 has been overlaid, indicating the individual FAs contributing to differences between samples. GAB: Great Australian Bight. The data points referred to in the text are labeled with species abbreviation. Nmx, *Nemichthys* sp.; Ele, *Epigonus lenimen*; Ec, *Electrona carlsbergi*; Ld, *Lepidorhynchus denticulatus*.

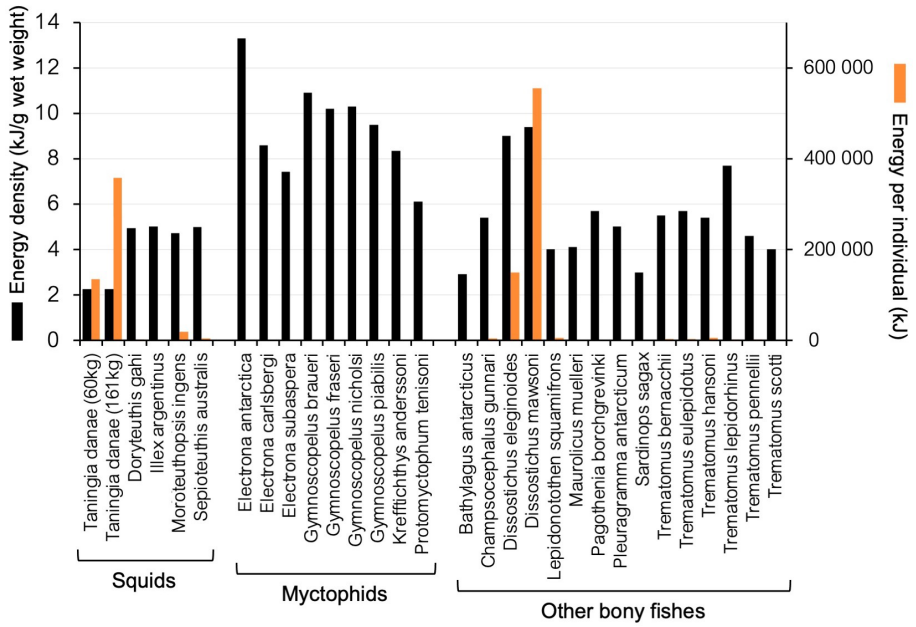

FIGURE 7
Energy content of Southern Ocean fishes and squids as found in published literature. Whole-body energy densities, as kilojoules per gram wet weight, are shown with black columns. An estimate of the whole-animal energy content is shown with orange columns and was determined by multiplying the greatest recorded whole-body energy density by the greatest recorded whole-animal body mass.

examine the trophic ecology of squids will either need to limit comparisons to within digestive glands or develop mathematical correction factors as has been done with beaks and other tissues.

The digestive gland of squid has been the preferred source tissue for diet determination using FAs, as it is the primary lipid storage organ, incorporating FAs from the diet across the previous 10 days with minimal biomodification (Phillips et al., 2001; Stowasser et al., 2006). Additionally, the digestive gland has greater lipid content (13–54% wet weight) compared to muscle tissues (<2% wet weight) (Phillips et al., 2002; Shulman et al., 2002; Phillips et al., 2003) with phospholipids, which are involved in tissue structure, comprising much of this observed differences (20:5ω3, 22:6ω3, 16:0; Rosa et al., 2005). Squid digestive glands typically contain lower proportions of these phospholipid PUFAs and higher levels of key MUFAs (Phillips et al., 2001; Zhukova, 2019). The GAB squid results were consistent with data from previous Australian and Southern Ocean oegopsid studies, where the proportion of PUFA in the muscles was 42.40–58.10% *versus* 17.30–32.40% in the digestive gland, and the proportion of MUFA in the muscles was 13.60–21.80% *versus* 47.00–66.10% in the digestive gland (Phillips et al., 2001; Phillips et al., 2002; Pethybridge et al., 2013). However, the suite of FAs contributing to clustering of FA data by area appeared to be similar between muscle and digestive tissues—for example, the southeast Australian squid samples including the GAB squids were differentiated from the rest of the samples by higher proportions of 16:0, 18:0, and 22:1 in both plots, while the Southern Ocean samples were differentiated by higher proportions of 16:1, 18:1, and 24:1. Digestive gland tissue is not often available from opportunistically collected squid, but these results indicate that similar dietary information and ecological inferences may instead be attainable from muscle tissues.

In the future, multi-species comparisons of squid tissues through controlled feeding studies should aim to determine how SIs and dietary FAs incorporate into squid muscle and digestive gland tissues to understand the molecular processes unique to squids. The differences across tissue types observed in this study indicate that this is an important area of future work that should be undertaken on more easily accessible squid species, such as southern calamari *Sepioteuthis australis*.

4.3 Foraging grounds

$\delta^{13}C$ from squid muscle tissues between -22.90‰ and -19.50‰ are classified as "subantarctic" (Guerreiro et al., 2015), a finding that fits well with both the global squids and southern multi-taxa SI data compiled here. The GAB squids, retrieved from latitudes of approximately 39-34°S, had $\delta^{13}C$ ranging from -23.80‰ to -20.04‰, similar to SI ratios recorded in samples from the Kerguelen Plateau (49°S), Marion Island (47°S), Macquarie Island (55°S), and South Georgia (55°S). Therefore, the GAB squids having "subantarctic" carbon ratios might indicate that they lived further south than where they were collected and may have been moved to the GAB post-mortem, perhaps by a predator such as a sperm whale.

Alternatively, the GAB squids might have migrated from their subantarctic range north toward the GAB to feed in the high-productivity, cold-water upwelling food web that exists along the

continental slope each austral summer (Van Ruth et al., 2018). The copepod FA biomarkers 20:1ω9 and 22:1ω9 (Parrish et al., 2005; Stowasser et al., 2009) are referenced frequently in FA studies of deep-sea and Southern Ocean squids, with several authors suggesting the presence of a copepod–myctophid–squid higher-order predator food chain within the Southern Ocean (Rodhouse et al., 1992; Phillips et al., 2001; Pethybridge et al., 2013). The GAB squids had high proportions of these FAs within their digestive glands and muscles, suggesting that the GAB squids likely feed within this food chain. The GAB *T. danae* and southeast Australian squids also had higher proportions of these two FAs in their digestive glands *versus* other Southern Ocean squids. Copepods are abundant in the eastern GAB (Van Ruth and Ward, 2009) and can significantly increase in population size in times of upwelling (Weikert, 1977; Jemi and Hatha, 2019), so it is possible that the GAB squids may have moved north to the continental slope to opportunistically forage upon fish schools that follow copepods around these upwelling regions. The rate of FA incorporation and isotopic turnover of squid muscle has yet to be determined, although studies on fishes have suggested a FA incorporation time of a few days or weeks, while the isotopes turnover was at a rate of several months (Young et al., 2010). This might further explain why the FA profiles of the GAB squids reflect more recent GAB feeding, while $\delta^{13}C$ reflects a long-term subantarctic range.

If movements between the Southern Ocean and the GAB are regular for these squid species, whether for foraging or some other cause such as spawning, they may be previously unrecognized vectors of nutrient and energy transport between these environments. The role these squids play in linking the nutrient-rich shelf–slope environment of the GAB to the nutrient-poor Southern Ocean deep-sea may be important to the trophic functioning of both environments.

4.4 Trophic role and diet

Squids in the Southern Ocean and southeast Australia occupy a broad range of trophic levels, with $\delta^{15}N$ values ranging from 5.00‰ to 17.80‰—equating to four or five trophic levels (assuming an average trophic enrichment factor of approximately 2.75‰ $\delta^{15}N$ per trophic level; Caut et al., 2009). The GAB squids with high $\delta^{15}N$ values were at the second highest trophic level, just below the colossal squid *Mesonychoteuthis hamiltoni* from the Southern Ocean. *Mesonychoteuthis hamiltoni* is the heaviest known invertebrate (Rosa et al., 2017) and is thought to consume Antarctic toothfish (*Dissostichus mawsoni*, Remeslo et al., 2015), which, in turn, are high-trophic-level predators of mid- to large-sized cephalopods and fishes (Queirós et al., 2021). Additionally, the similarities between the GAB squid FAs and FA profiles from other large, actively predatory squid species including giant squid *Architeuthis dux*, Antarctic flying squid *Todarodes filippovae*, flying squid *Ommastrephes bartramii*, whiplash squid *Idioteuthis cordiformis*, and arrow squid *Nototodarus gouldi* suggest roles as active pelagic predators. When comparing the GAB squids' $\delta^{15}N$ to other taxa from the southern ecosystems, it appears that the GAB squids occupied a similar trophic level to a broader range of Southern Ocean top predators including seabirds, cetaceans, and other large squids. Thus, it is suggested that the GAB *T. danae* and *C.* aff. *veranii* were high-trophic-level predators within the Southern Ocean ecosystem.

Little is known of the diet of most deep-sea animals in general, and only a few opportunistic records of identifiable prey items have been recorded from the stomachs of large-bodied squids. Fortunately, some items have been identified from the stomach contents of two *T. danae* retrieved off the coast of Spain, consisting of a few blue whiting (*Micromesistius poutassou*) vertebrae, *Gonatus* sp. tentacle hooks, and integuments from crustaceans (González et al., 2003). These results are far from a comprehensive analysis of *T. danae* diet but do provide some evidence that *T. danae* is capable of feeding on active, pelagic fish and squid species as well as crustaceans. *Chiroteuthis* aff. *veranii* diet has not been described, although other chiroteuthids are known to feed on crustaceans, molluscs, and fish (Kubota et al., 1981). However, the *C.* aff. *veranii* specimen from this study is substantially larger than most previously studied *Chiroteuthis veranii* specimens [approximately 400 mm mantle length *versus* 50–297 mm in Rodhouse and Lu (1998); Mensch (2010), and Guerra et al. (2011)]. Therefore, the diet and general trophic ecology of the GAB *C.* aff. *veranii* specimen may be very different from what has previously been described for *C. veranii* globally.

Using the global mean trophic enrichment factors (2.75‰ for $\delta^{15}N$ and 0.75‰ for $\delta^{13}C$; Caut et al., 2009), the predicted prey items of the GAB squids include *Gymnoscopelus nicholsi*, *Electrona carlsbergi*, and *Electrona antarctica*, three deep-sea myctophids abundant in the Southern Ocean (Kozlov, 1995), and *Moroteuthopsis longimana*, an Antarctic deep-sea squid. The maximum prey length suggested for squid are prey that measure between half to two thirds of the squid's mantle length (Bidder, 1966), which would be 50–80 and 20–30 cm for *T. danae* and *C* aff. *veranii*, respectively. The myctophid species are small in length, with total length less than 20 cm (Collins et al., 2012), placing them within the GAB squids' prey size range, but *M. longimana* can attain mantle lengths of up to 1 m (Laptikhovsky et al., 2013), which is out of this range.

The *T. danae* digestive gland FA profiles in this study further suggest deep-sea fish and squid predation. The *T. danae* digestive gland samples were similar in FA profile to whole homogenized fish samples and whole homogenized squid samples (Figure 6). The whole deep-sea fishes that were similar to the GAB *T. danae* digestive gland samples (and might represent potential prey species) were *E. carlsbergi*, *Epigonus lenimen*, *Lepidorhynchus denticulatus*, and *Nemichthys* sp. With the exception of *Nemichthys* sp., these species are within the size range of *T. danae* prey (<50 cm, Meynier et al., 2008; Pethybridge et al., 2013; Froese and Pauly, 2022) and are abundant in the deep-sea and continental slope communities of the Southern Ocean and southeast Australia (May and Blaber, 1989; Kozlov, 1995). The whole squid profiles and therefore possible squid prey species grouped closely to *T. danae* digestive glands were *Octopoteuthis megaptera*, *Lycoteuthis lorigera*, *Histioteuthis atlantica*, *Mastigoteuthis* sp., and *Ancistrocheirus lesueurii*. Comparatively less is known about the abundance of these species *versus* the potential fish prey, but they are all deep-sea

and pelagic ones (SeaLifeBase 2022). In addition, apart from *A. lesueurii* which grows to 54 cm in mantle length (Hoving and Lipinski, 2015), these squid species are all classified as small with mantle lengths less than 25 cm (Lipiński, 1993; Hoving et al., 2007; Pethybridge et al., 2010; Kelly, 2019), again fitting within the suggested maximum prey size of *T. danae*.

The GAB squid had high proportions of EPA 20:5ω3 and DHA 22:6ω3 within their muscle tissues, even compared to other squids. This could be due to these FAs being taken in by the GAB squids through their diet and may be further evidence for a diet consisting of squid, as EPA and DHA are common in squid muscle tissues (Ozogul et al., 2008), and research has shown that fish that are fed squid diets have increased levels of these FAs in their tissues (Turner and Rooker, 2005; Sun et al., 2018). Additionally, dietary EPA and DHA have been linked to higher growth rates in fish (Lutfi et al., 2022), and therefore a diet rich in these two FAs may be necessary for the maintenance of muscle tissue synthesis in large squids such as the GAB squids in this study.

EPA and DHA are physiologically important for all omnivorous organisms, including humans (Gladyshev et al., 2013), and have been linked with a variety of important processes including anti-inflammatory processes, stress resistance, neural development, and behavior (Parrish, 2013; Zhukova, 2019). The high levels of these FAs in the tissues of the GAB squids may mean that these are important sources of dietary EPA and DHA for their known predator species including sperm whales (*Physeter macrocephalus*), northern elephant seals (*Mirounga angustirostris*), and seabirds (Cherel et al., 2009b; Guerreiro et al., 2015; Yoshino et al., 2020). *Chiroteuthis* aff. *veranii* could be especially important, as its similar proportions of EPA and DHA, but smaller body size, may make it an important source of these FAs for smaller predators such as swordfishes (e.g., *Xiphias gladius*), toothfishes (*Dissostichus* spp.) (Cherel and Hobson, 2005; Young et al., 2010), and deep-sea-foraging Southern Ocean cetaceans such as the pygmy sperm whale (*Kogia breviceps*) (Dos Santos and Haimovici, 2001).

4.5 Energy content

Squids are generally less energy-dense than fishes, primarily due to lower levels of lipid and protein in their tissues (Croxall and Prince, 1982). This is reflected in the energy content of *T. danae* tissues, which was lower than the calorie content of all other deep-sea fishes and squids. The digestive gland, with a higher lipid content than the other tissues, also had a greater energy density. Many deep-sea squids, including *T. danae*, are considered ammoniacal. This results in a reduced energy density of muscle tissues, and a previous study estimates that ammoniacal squids have a whole-body energy density of 2.3 kJ/g (Clarke et al., 1985), which supports the *T. danae* whole-body energy density estimate made in this study.

Taningia danae has been noted in the diets of many marine predators globally, forming minor components of the diets of seabirds (Clarke et al., 1981; Guerreiro et al., 2015), marine mammals (Condit and Le Boeuf, 1984; MacLeod et al., 2003; Cherel et al., 2009b; Yoshino et al., 2020), sharks (Smale and Cliff, 1998; Mendonça, 2009; Ménard et al., 2013), and predatory fishes (Tsuchiya et al., 1998; Cherel et al., 2004; Potier et al., 2007; Ménard et al., 2013) and significant components of the diets of both sperm whales and sleeper sharks (identified in source as *Somnoisus cf.* microcephalus, likely *Somniosus antarcticus*) in the Southern Ocean (Cherel et al., 2004, Evans and Hindell, 2004). While *T. danae* is not densely calorific when compared to smaller Southern Ocean fish and squid species, their large body size means that, per individual, they are the second most calorie-rich mid-trophic species in the Southern Ocean. One *T. danae* individual might provide as many calories as several dozens of smaller prey items, with the added benefit of reducing the foraging costs for the predator (Evans and Hindell, 2004; Goldbogen et al., 2019). A previous study by Aoki et al. (2012) suggested that foraging on large squids may provide sperm whales with a high caloric intake for reduced energetic expenditure, especially given that the bursts of speed required to catch these squids can be highly costly (Aoki et al., 2012).

4.6 Conclusions

In the biodiverse and economically important areas of the Southern Ocean and the GAB, there is a need to fully understand the trophic interactions of higher-order predators such as large squids. The use of opportunistic sampling events is critical for studying elusive species in deep-sea areas, and this study has shown that even remnants of large squid muscle tissues floating on the sea surface can provide useful ecological information. Squid digestive glands are widely acknowledged to be effective in FA analysis to provide additional evidence of diet, but in this study, we found that muscle tissues can also be used. Researchers who intend to use opportunistic samples of squid in trophic ecology studies should collect any biological tissues that they have access to (e.g., arm, mantle, and buccal mass) for both SI analysis and FA analysis to gain information regarding potential diet, food chains, geographic origin, and trophic role. For the GAB squids, the comparison of multiple tissue types helped us determine that they were most likely living in the Southern Ocean and had a broad diet of deep-sea fishes and other squids. We also found that the GAB squids might play a role in providing important nutrients to other higher-order predators and could have an additional role in facilitating nutrient and energy transport between the Southern Ocean deep-sea and the GAB shelf–slope environments. Despite the small sample sizes, the lower quality of the GAB squids due to opportunistic sampling, and the other discussed limitations, this study has highlighted the types of ecological information that can be obtained from small and degraded biological samples, which can be important in building knowledge of trophic ecology in deep-sea squid research.

Data availability statement

The raw data supporting the conclusions of this article will be made available by the authors without undue reservation.

Ethics statement

Ethical approval was not required for the study involving animals in accordance with the local legislation and institutional requirements because the samples used were already deceased naturally upon collection.

Author contributions

BJ: Conceptualization, Data curation, Formal analysis, Visualization, Writing - original draft, Writing - review & editing. RB: Conceptualization, Funding acquisition, Supervision, Writing - original draft, Writing - review & editing. MD: Conceptualization, Funding acquisition, Supervision, Writing - review & editing. JH: Formal Analysis, Methodology, Supervision, Writing - review & editing. BM: Formal analysis, Investigation, Resources, Validation, Writing – review & editing. KR: Conceptualization, Resources, Writing – review & editing. LM: Conceptualization, Formal analysis, Funding acquisition, Methodology, Supervision, Writing - original draft, Writing - review & editing.

Funding

The author(s) declare financial support was received for the research, authorship, and/or publication of this article. Funding for this study was acquired by the Ecosystem Resilience Research Group (ERRG), the Southern Shark Ecology Group (SSEG), and Flinders Accelerator for Microbiome Exploration (FAME) at Flinders University, South Australia, as well as Australian Research Council DE220101409.

Acknowledgments

The authors would like to acknowledge that this study was made possible by samples obtained from the Australian Southern Bluefin Tuna Industry Association (ASBTIA), crew of Australian Fishing Enterprises, and Kim Mundy, who provided the squids. We would like to acknowledge the work of the Auckland University of Technology Lab for Cephalopod Ecology and Systematics (ALCES) in identifying the species of the squids sampled, the South Australian Museum (Shirley Sorokin, Andrea Crowther and Rachael King) for housing the squid specimens. We acknowledge funding for genetic identification from the Flinders Accelerator for Microbiome Exploration under project #010. The authors would like to acknowledge and thank those involved in dissections, lab work, and sample analysis including Zöe Doubleday, Erica Durante, Taryn-Lee Perrior, Chloe Roberts, Russel Fuller, the Marine Ecology class of 2021, and all others who attended the dissection at Flinders University.

Conflict of interest

Author KR is employed by Australian Southern Bluefin Tuna Industry Association.

The remaining authors declare that the research was conducted in the absence of any commercial or financial relationships that could be construed as a potential conflict of interest.

Publisher's note

Supplementary material

The Supplementary Material for this article can be found online at: https://www.frontiersin.org/articles/10.3389/fmars.2023.1254461/full#supplementary-material

References

Albertin, C. B., Bonnaud, L., Brown, C. T., Crookes-Goodson, W. J., Da Fonseca, R. R., Di Cristo, C., et al. (2012). Cephalopod genomics: A plan of strategies and organization. *Stand. Genomic Sci.* 7, 175–188. doi: 10.4056/sigs.3136559

Anderson, M. J., Gorley, R. N., and Clarke, K. R. (2008). *PERMANOVA+ for PRIMER: Guide to Software and Statistical Methods* (Plymouth, UK: PRIMER-E).

Aoki, K., Amano, M., Mori, K., Kourogi, A., Kubodera, T., and Miyazaki, N. (2012). Active hunting by deep-diving sperm whales: 3D dive profiles and maneuvers during bursts of speed. *Mar. Ecol. Prog. Ser.* 444, 289–301. doi: 10.3354/meps09371

Atayeter, S., and Ercoşkun, H. (2011). Chemical composition of European squid and effects of different frozen storage temperatures on oxidative stability and fatty acid composition. *J. Food Sci. Technol.* 48, 83–89. doi: 10.1007/s13197-010-0139-5

Bidder, A. M. (1966). "Feeding and digestion in cephalopods," in *Physiology of the mollusca*, vol. 2 . Eds. K. Wilbur and C. Yonge (New York, NY: Academic Press Inc), 97–124.

Bligh, E. G., and Dyer, W. J. (1959). A rapid method of total lipid extraction and purification. *N. Can. J. Biochem. Physiol.* 37, 911–917. doi: 10.1139/o59-099

Bolstad, K. S., and O'Shea, S. (2004). Gut contents of a giant squid *Architeuthis dux* (Cephalopoda: Oegopsida) from New Zealand waters. *N.Z. J. Zool.* 31, 15–21. doi: 10.1080/03014223.2004.9518354

Braid, H. E., McBride, P. D., and Bolstad, K. S. R. (2014). Molecular phylogenetic analysis of the squid family Mastigoteuthidae (Mollusca, Cephalopoda) based on three mitochondrial genes. *Hydrobiologia* 725, 145–164. doi: 10.3354/meps11008

Braley, M., Goldsworthy, S. D., Page, B., Steer, M., and Austin, J. J. (2010). Assessing morphological and DNA-based diet analysis techniques in a generalist predator, the arrow squid *Nototodarus gouldi*. *Mol. Ecol. Resour.* 10, 466–474. doi: 10.1111/j.1755-0998.2009.02767.x

Budge, S. M., Iverson, S. J., and Koopman, H. N. (2006). Studying trophic ecology in marine ecosystems using fatty acids: A primer on analysis and interpretation. *Mar. Mamm. Sci.* 22, 759–801. doi: 10.1111/j.1748-7692.2006.00079.x

Caut, S., Angulo, E., and Courchamp, F. (2009). Variation in discrimination factors ($\delta^{15}N$ and $\delta^{13}C$): the effect of diet isotopic values and applications for diet reconstruction. *J. Appl. Ecol.* 46, 443–453. doi: 10.1111/j.1365-2664.2009.01620.x

Cherel, Y. (2020). A review of Southern Ocean squids using nets and beaks. *Mar. Biodivers.* 50, 98. doi: 10.1007/s12526-020-01113-4

Cherel, Y., Duhamel, G., and Gasco, N. (2004). Cephalopod fauna of subantarctic islands: new information from predators. *Mar. Ecol. Prog. Ser.* 266, 143–156. doi: 10.3354/meps266143

Cherel, Y., Fontaine, C., Jackson, G., Jackson, C., and Richard, P. (2009a). Tissue, ontogenic and sex-related differences in $\delta^{13}C$ and $\delta^{15}N$ values of the oceanic squid *Todarodes filippovae* (Cephalopoda: Ommastrephidae). *Mar. Biol.* 156, 699–708. doi: 10.1007/s00227-008-1121-x

Cherel, Y., and Hobson, K. A. (2005). Stable isotopes, beaks and predators: a new tool to study the trophic ecology of cephalopods, including giant and colossal squids. *Proc. R. Soc B.* 272, 1601–1607. doi: 10.1098/rspb.2005.3115

Cherel, Y., Hobson, K. A., and Weimerskirch, H. (2000). Using stable-isotope analysis of feathers to distinguish moulting and breeding origins of seabirds. *Oecologia* 122, 155–162. doi: 10.1007/pl00008843

Cherel, Y., Ridoux, V., Spitz, J., and Richard, P. (2009b). Stable isotopes document the trophic structure of a deep-sea cephalopod assemblage including giant octopod and giant squid. *Biol. Lett.* 5, 364–367. doi: 10.1098/rsbl.2009.0024

Clarke, A., Clarke, M. R., Holmes, L. J., and Waters, T. D. (1985). Calorific values and elemental analysis of eleven species of oceanic squids (Mollusca : Cephalopoda). *J. Mar. Biolog. Assoc. U.K.* 65, 983–986. doi: 10.1017/S0025315400019457

Clarke, M. R., Croxall, J. P., and Prince, P. A. (1981). Cephalopod remains in the regurgitations of the wandering albatross *Diomedea exulans* L. at South Georgia. *Sci. Rep. Br. Antarct. Surv.* 54, 9–21.

Clarke, M. R., Denton, E. J., and Gilpin-Brown, J. B. (1979). On the use of ammonium for buoyancy in squids. *J. Mar. Biolog. Assoc. U.K.* 59, 259–276. doi: 10.1017/S0025315400042570

Clarke, K. R., and Gorley, R. N. (2015). *Getting started with PRIMER v7* (Plymouth, UK: PRIMER-E).

Coll, M., Navarro, J., Olson, R. J., and Christensen, V. (2013). Assessing the trophic position and ecological role of squids in marine ecosystems by means of food-web models. *Deep-Sea Res. II: Top. Stud. Oceanogr.* 95, 21–36. doi: 10.1016/j.dsr2.2012.08.020

Collins, M. A., Stowasser, G., Fielding, S., Shreeve, R., Xavier, J. C., Venables, H. J., et al. (2012). Latitudinal and bathymetric patterns in the distribution and abundance of mesopelagic fish in the Scotia Sea. *Deep-Sea Res. II: Top. Stud. Oceanogr.* 59-60, 189–198. doi: 10.1016/j.dsr2.2011.07.003

Condit, R., and Le Boeuf, B. J. (1984). Feeding habits and feeding grounds of the northern elephant seal. *J. Mammal.* 65, 281–290. doi: 10.2307/1381167

Croxall, J. P., and Prince, P. A. (1982). Calorific content of squid (Mollusca: Cephalopoda). *Br. Antarct. Surv. Bull.* 55, 27–31.

Dalsgaard, J., St John, M., Kattner, G., Müller-Navarra, D., and Hagen, W. (2003). Fatty acid trophic markers in the pelagic marine environment. *Adv. Mar. Biol.* 46, 225–340. doi: 10.1016/s0065-2881(03)46005-7

Da Silveira, E. L., Semmar, N., Cartes, J. E., Tuset, V. M., Lombarte, A., Ballester, E. L. C., et al. (2020). Methods for trophic ecology assessment in fishes: A critical review of stomach analyses. *Rev. Fish. Sci. Aquac.* 28, 71–106. doi: 10.1080/23308249.2019.1678013

De La Chesnais, T., Fulton, E. A., Tracey, S. R., and Pecl, G. T. (2019). The ecological role of cephalopods and their representation in ecosystem models. *Rev. Fish. Biol. Fish.* 29, 313–334. doi: 10.1007/s11160-019-09554-2

Desforges, J.-P., Kohlbach, D., Carlyle, C. G., Michel, C., Loseto, L. L., Rosenberg, B., et al. (2022). Multi-dietary tracer approach reveals little overlap in foraging ecology between seasonally sympatric ringed and harp seals in the high Arctic. *Front. Mar. Sci.* 9. doi: 10.3389/fmars.2022.969327

Dos Santos, R. A., and Haimovici, M. (2001). Cephalopods in the diet of marine mammals stranded or incidentally caught along southeastern and southern Brazil (21–34°S). *Fish. Res.* 52, 99–112. doi: 10.1016/S0165-7836(01)00234-X

Doubleday, Z. A., Prowse, T. A. A., Arkhipkin, A., Pierce, G. J., Semmens, J., Steer, M., et al. (2016). Global proliferation of cephalopods. *Curr. Biol.* 26, R406–R407. doi: 10.1016/j.cub.2016.04.002

Evans, K., and Hindell, M. A. (2004). The diet of sperm whales (*Physeter macrocephalus*) in southern Australian waters. *ICES J. Mar. Sci.* 61, 1313–1329. doi: 10.1016/S1095-6433(03)00045-X

Froese, R., and Pauly, D. (2022) *FishBase*. Available at: www.fishbase.org (Accessed 29 November, 2022).

Gladyshev, M. I., Sushchik, N. N., and Makhutova, O. N. (2013). Production of EPA and DHA in aquatic ecosystems and their transfer to the land. *Prostaglandins Other Lipid Mediat.* 107, 117–126. doi: 10.1016/j.prostaglandins.2013.03.002

Goldbogen, J. A., Cade, D. E., Wisniewska, D. M., Potvin, J., Segre, P. S., Savoca, M. S., et al. (2019). Why whales are big but not bigger: Physiological drivers and ecological limits in the age of ocean giants. *Science* 366, 1367–1372. doi: 10.1126/science.aax9044

Golikov, A. V., Ceia, F. R., Sabirov, R. M., Ablett, J. D., Gleadall, I. G., Gudmundsson, G., et al. (2019). The first global deep-sea stable isotope assessment reveals the unique trophic ecology of Vampire Squid *Vampyroteuthis infernalis* (Cephalopoda). *Sci. Rep.* 9, 19099. doi: 10.1038/s41598-019-55719-1

Gomes-Pereira, J. N., and Tojeira, I. (2014). The cephalopod Taningia danae Joubin 1931 observed near bottom at over 2,000 m depth on Seine seamount. *Mar. Biodivers.* 44, 151–155. doi: 10.1007/s12526-013-0197-9

González, Á., Guerra, A., and Rocha, F. (2003). New data on the life history and ecology of the deep-sea hooked squid *Taningia danae*. *Sarsia N. Atlantic Mar. Sci.* 88, 297–301. doi: 10.1080/00364820310002524

Guerra, Á., Portela, J. M., and Río, J. L. D. (2011). Cephalopods caught in the outer Patagonian shelf and its upper and medium slope in relation to the main oceanographic features. *Fish. Res.* 109, 179–186. doi: 10.1016/j.fishres.2011.02.003

Guerreiro, M., Phillips, R., Cherel, Y., Ceia, F., Alvito, P., Rosa, R., et al. (2015). Habitat and trophic ecology of Southern Ocean cephalopods from stable isotope analyses. *Mar. Ecol. Prog. Ser.* 530, 119–134. doi: 10.3354/meps11266

Hobson, K., and Cherel, Y. (2006). Isotopic reconstruction of marine food webs using cephalopod beaks: New insight from captively raised *Sepia officinalis*. *Can. J. Zool.* 84, 766–770. doi: 10.1139/Z06-049

Hoving, H. J. T., and Lipinski, M. R. (2015). Observations on age and reproduction of the oceanic squid *Ancistrocheirus lesueurii* (d'Orbigny 1842) (Cephalopoda: ancistrocheiridae). *J. Nat. Hist.* 49, 1319–1325. doi: 10.1080/00222933.2013.840748

Hoving, H. J. T., Lipinski, M. R., Roeleveld, M. A. C., and Durholtz, M. D. (2007). Growth and mating of southern African *Lycoteuthis lorigera* (Steenstrup 1875) (Cephalopoda; lycoteuthidae). *Rev. Fish. Biol. Fish.* 17, 259–270. doi: 10.1007/s11160-006-9031-9

Hoving, H. J. T., Perez, J. A. A., Bolstad, K. S. R., Braid, H. E., Evans, A. B., Fuchs, D., et al. (2014). The study of deep-sea cephalopods. *Adv. Mar. Biol.* 67, 235–359. doi: 10.1016/B978-0-12-800287-2.00003-2

Ibáñez, C. M., Riera, R., Leite, T., Díaz-Santana-Iturrios, M., Rosa, R., and Pardo-Gandarillas, M. C. (2021). Stomach content analysis in cephalopods: past research, current challenges, and future directions. *Rev. Fish. Biol. Fish.* 31, 505–522. doi: 10.1007/s11160-021-09653-z

Jackson, G. D., Bustamante, P., Cherel, Y., Fulton, E. A., Grist, E. P. M., Jackson, C. H., et al. (2007). Applying new tools to cephalopod trophic dynamics and ecology: perspectives from the Southern Ocean Cephalopod Workshop, February 2–3, 2006. *Rev. Fish. Biol. Fish.* 17, 79–99. doi: 10.1007/s11160-007-9055-9

Jemi, J. N., and Hatha, A. A. M. (2019). Copepod community structure during upwelling and non-upwelling seasons in coastal waters off Cochin, southwest coast of India. *Acta Oceanol. Sin.* 38, 111–117. doi: 10.1007/s13131-019-1491-6

Jereb, P., and Roper, C. F. E. (2010). "Cephalopods of the world. An annotated and illustrated catalogue of cephalopod species known to date," in *Myopsid and Oegopsid Squids*, vol. 2. (Italy: FAO).

Judkins, H., Vecchione, M., Cook, A., and Sutton, T. (2017). Diversity of midwater cephalopods in the northern Gulf of Mexico: comparison of two collecting methods. *Mar. Biodivers.* 47, 647–657. doi: 10.1007/s12526-016-0597-8

Kelly, J. (2000). Stable isotopes of carbon and nitrogen in the study of avian and mammalian trophic ecology. *Can. J. Zool.* 78, 1–27. doi: 10.1139/z99-165

Kelly, J. T. (2019). *Systematics of the Octopoteuthidae Berry 1912 (Cephalopoda: Oegopsida). [PhD dissertation]* (Auckland, New Zealand: Auckland University of Technology).

Kozlov, A. N. (1995). A review of the trophic role of mesopelagic fish of the Family Myctophidae in the Southern Ocean ecosystem. *CCAMLR Sci.* 2, 71–77.

Kubodera, T., Koyama, Y., and Mori, K. (2007). Observations of wild hunting behaviour and bioluminescence of a large deep-sea, eight-armed squid, *Taningia danae*. *Proc. R. Soc B.* 274, 1029–1034. doi: 10.1098/rspb.2006.0236

Kubota, T., Koshiga, M., and Okutani, T. (1981). Rare and interesting squid from Japan—VII. Some biological data on *Chiroteuthis imperator* from Suroga Bay, Japan (Cephalopoda: Chiroteuthidae). *Venus Jap. J. Malacol.* 40, 150–159.

Laptikhovsky, V., Collins, M. A., and Arkhipkin, A. (2013). First case of possible iteroparity among coleoid cephalopods: the giant warty squid *Kondakovia longimana*. *J. Molluscan Stud.* 79, 270–272. doi: 10.1093/mollus/eyt014

Li, Y., Zhang, Y., Hussey, N. E., and Dai, X. (2016). Urea and lipid extraction treatment effects on $\delta^{15}N$ and $\delta^{13}C$ values in pelagic sharks. *Rapid Commun. Mass Spectrom.* 30, 1–8. doi: 10.1002/rcm.7396

Lipiński, M. R. (1993). Description of mature males of the histioteuthid cephalopod *Histioteuthis atlantica* (Hoyle 1885) (Cephalopoda: oegopsida) from the South Atlantic Ocean. *S. Afr. J. Mar. Sci.* 13, 51–62. doi: 10.2989/025776193784287383

Lutfi, E., Berge, G., Baeverfjord, G., Sigholt, T., Bou, M., Larsson, T., et al. (2022). Increasing dietary levels of the omega-3 long-chain polyunsaturated fatty acids, EPA and DHA, improves the growth, welfare, robustness, and fillet quality of Atlantic salmon in sea cages. *Br. J. Nutr.* 129, 1–48. doi: 10.1017/s0007114522000642

MacIntosh, H., Althaus, F., Williams, A., Tanner, J. E., Alderslade, P., Ahyong, S. T., et al. (2018). Invertebrate diversity in the deep Great Australian Bight (200–5000 m). *Mar. Biodivers. Rec.* 11, 23. doi: 10.1186/s41200-018-0158-x

MacLeod, C. D., Santos, M. B., and Pierce, G. J. (2003). Review of data on diets of beaked whales: Evidence of niche separation and geographic segregation. *J. Mar. Biolog. Assoc. U.K.* 83, 651–665. doi: 10.1017/S0025315403007616h

Martin, U., and Jaquemet, S. (2019). Effects of urea and lipid removal from *Carcharhinus leucas* and *Galeocerdo cuvier* white muscle on carbon and nitrogen stable isotope ratios. *West. Indian Ocean J. Mar. Sci.* 18, 47–56. doi: 10.4314/wiojms.v18i1.5

May, J. L., and Blaber, S. J. M. (1989). Benthic and pelagic fish biomass of the upper continental slope off eastern Tasmania. *Mar. Biol.* 101, 11–25. doi: 10.1007/BF00393474

Ménard, F., Potier, M., Jaquemet, S., Romanov, E., Sabatié, R., and Cherel, Y. (2013). Pelagic cephalopods in the western Indian Ocean: New information from diets of top predators. *Deep-Sea Res. II: Top. Stud. Oceanogr.* 95, 83–92. doi: 10.1016/j.dsr2.2012.08.022

Mendonça, A. (2009). *Diet of the blue shark, Prionace glauca, in the Northeast Atlantic. [master's thesis]* (Portugal: University of Porto).

Mensch, R. (2010). *A systematic review of the squid genus Chiroteuthis (Mollusca: Cephalopoda) in New Zealand waters. [master's thesis]* (Auckland, New Zealand: Auckland University of Technology).

Merten, V., Bayer, T., Reusch, T. B. H., Puebla, O., Fuss, J., Stefanschitz, J., et al. (2021). An integrative assessment combining deep-sea net sampling, in *situ* observations and environmental DNA analysis identifies Cabo Verde as a cephalopod biodiversity hotspot in the Atlantic Ocean. *Front. Mar. Sci.* 8, 760108. doi: 10.3389/fmars.2021.760108

Merten, V., Christiansen, B., Javidpour, J., Piatkowski, U., Puebla, O., Gasca, R., et al. (2017). Diet and stable isotope analyses reveal the feeding ecology of the orangeback squid *Sthenoteuthis pteropus* (Steenstrup 1855) (Mollusca, Ommastrephidae) in the eastern tropical Atlantic. *PloS One* 12, e0189691. doi: 10.1371/journal.pone.0189691

Meyer, L., Pethybridge, H., Nichols, P. D., Beckmann, C., Bruce, B. D., Werry, J. M., et al. (2017). Assessing the functional limitations of lipids and fatty acids for diet determination: the importance of tissue type, quantity, and quality. *Front. Mar. Sci.* 4, 369. doi: 10.3389/fmars.2017.00369

Meyer, L., Pethybridge, H., Nichols, P. D., Beckmann, C., and Huveneers, C. (2019). Abiotic and biotic drivers of fatty acid tracers in ecology: A global analysis of chondrichthyan profiles. *Funct. Ecol.* 33, 1243–1255. doi: 10.1111/1365-2435.13328

Meynier, L., Morel, P. C. H., MacKenzie, D. D. S., MacGibbon, A., Chilvers, B. L., and Duignan, P. J. (2008). Proximate composition, energy content, and fatty acid composition of marine species from Campbell Plateau, New Zealand. *N.Z. J. Mar. Freshw. Res.* 42, 425–437. doi: 10.1080/00288330809509971

Moovendhan, M., Shanmugam, A., and Shanmugam, V. (2019). Nutritional composition of liver (Digestive gland) from thondi squid (*Sepioteuthis lessoniana*). *Indian J. Mar. Sci.* 48, 1398–1403.

Navarro, J., Coll, M., Somes, C. J., and Olson, R. J. (2013). Trophic niche of squids: Insights from isotopic data in marine systems worldwide. *Deep-Sea Res. II: Top. Stud. Oceanogr.* 95, 93–102. doi: 10.1007/s00227-009-1281-3

Nichols, P. D., Pethybridge, H. R., Zhang, B., Virtue, P., Meyer, L., Dhurmeea, Z., et al. (2023). Fatty acid profiles of more than 470 marine species from the Southern Hemisphere. *Ecology* 104, e3888. doi: 10.1002/ecy.3888

O'Brien, C. E., Roumbedakis, K., and Winkelmann, I. E. (2018). The current state of cephalopod science and perspectives on the most critical challenges ahead from three early-career researchers. *Front. Physiol.* 9. doi: 10.3389/fphys.2018.00700

Ozogul, Y., Duysak, O., Ozogul, F., Ozkutuk, A. S., and Tuereli, C. (2008). Seasonal effects in the nutritional quality of the body structural tissue of cephalopods. *Food Chem.* 108, 847–852. doi: 10.1016/j.foodchem.2007.11.048

Parrish, C. C. (2013). Lipids in marine ecosystems. *ISRN Oceanography* 2013, 604045. doi: 10.5402/2013/604045

Parrish, C. C., Nichols, P. D., Pethybridge, H., and Young, J. W. (2015). Direct determination of fatty acids in fish tissues: quantifying top predator trophic connections. *Oecologia* 177, 85–95. doi: 10.1007/s00442-014-3131-3

Parrish, C. C., Thompson, R. J., and Deibel, D. (2005). Lipid classes and fatty acids in plankton and settling matter during the spring bloom in a cold ocean coastal environment. *Mar. Ecol. Prog. Ser.* 286, 57–68. doi: 10.3354/meps286057

Parzanini, C., Parrish, C. C., Hamel, J. F., and Mercier, A. (2018). Functional diversity and nutritional content in a deep-sea faunal assemblage through total lipid, lipid class, and fatty acid analyses. *PloS One* 13, e0207395. doi: 10.1371/journal.pone.0207395

Pethybridge, H., Daley, R., Virtue, P., Butler, E. C. V., Cossa, D., and Nichols, P. D. (2010). Lipid and mercury profiles of 61 midtrophic species collected off southeastern Australia. *Mar. Freshw. Res.* 61, 1092–1108. doi: 10.1071/MF09237

Pethybridge, H. R., Nichols, P. D., Virtue, P., and Jackson, G. D. (2013). The foraging ecology of an oceanic squid, *Todarodes filippovae*: The use of signature lipid profiling to monitor ecosystem change. *Deep-Sea Res. II: Top. Stud. Oceanogr.* 95, 119–128. doi: 10.1016/j.dsr2.2012.07.025

Pethybridge, H., Virtue, P., Casper, R., Yoshida, T., Green, C. P., Jackson, G., et al. (2012). Seasonal variations in diet of arrow squid (*Nototodarus gouldi*): stomach content and signature fatty acid analysis. *J. Mar. Biol. Assoc. U.K.* 92, 187–196. doi: 10.1017/S0025315411000841

Phillips, K. L., Nichols, P. D., and Jackson, G. D. (2001). Predation on myctophids by the squid *Moroteuthis ingens* around Macquarie and Heard Islands: stomach contents and fatty acid analyses. *Mar. Ecol. Prog. Ser.* 215, 179–189. doi: 10.3354/meps215179

Phillips, K. L., Nichols, P. D., and Jackson, G. D. (2002). Lipid and fatty acid composition of the mantle and digestive gland of four Southern Ocean squid species: implications for food-web studies. *Antarct. Sci.* 14, 212–220. doi: 10.1017/s0954102002000044

Phillips, K. L., Nichols, P. D., and Jackson, G. D. (2003). Dietary variation of the squid *Moroteuthis ingens* at four sites in the Southern Ocean: stomach contents, lipid and fatty acid profiles. *J. Mar. Biolog. Assoc.* 83, 523–534. doi: 10.1017/S0025315403007446h

Potier, M., Marsac, F., Cherel, Y., Lucas, V., Sabatié, R., Maury, O., et al. (2007). Forage fauna in the diet of three large pelagic fishes (lancetfish, swordfish and yellowfin tuna) in the western equatorial Indian Ocean. *Fish. Res.* 83, 60–72. doi: 10.1016/j.fishres.2006.08.020

Queirós, J. P., Phillips, R. A., Baeta, A., Abreu, J., and Xavier, J. C. (2019). Habitat, trophic levels and migration patterns of the short-finned squid *Illex argentinus* from stable isotope analysis of beak regions. *Polar Biol.* 42, 2299–2304. doi: 10.1007/s00300-019-02598-x

Queirós, J. P., Ramos, J. A., Cherel, Y., Franzitta, M., Duarte, B., Rosa, R., et al. (2021). Cephalopod fauna of the Pacific Southern Ocean using Antarctic toothfish (*Dissostichus mawsoni*) as biological samplers and fisheries bycatch specimens. *Deep-Sea Res. I: Oceanogr. Res. Papers* 174, 103571. doi: 10.1016/j.dsr.2021.103571

Quetglas, A., Fliti, K., Massuti, E., Refes, W., Guijarro, B., and Zaghdoudi, S. (2006). First record of *Taningia danae* (Cephalopoda: Octopoteuthidae) in the Mediterranean Sea. *Sci. Mar.* 70, 153–155. doi: 10.3989/scimar.2006.70n1153

Remeslo, A. V., Yakushev, M. R., and Laptikhovsky, V. (2015). Alien vs. Predator: interactions between the colossal squid (*Mesonychoteuthis hamiltoni*) and the Antarctic toothfish (*Dissostichus mawsoni*). *J. Nat. Hist.* 49, 2483–2491. doi: 10.1080/00222933.2015.1040477

Robinson, N. J., Johnsen, S., Brooks, A., Frey, L., Judkins, H., Vecchione, M., et al. (2021). Studying the swift, smart, and shy: Unobtrusive camera-platforms for observing large deep-sea squid. *Deep-Sea Res. I: Oceanogr. Res. Papers* 172, 103538. doi: 10.1016/j.dsr.2021.103538

Rodhouse, P. G. K. (2013). Role of squid in the Southern Ocean pelagic ecosystem and the possible consequences of climate change. *Deep-Sea Res. II: Top. Stud. Oceanogr.* 95, 129–138. doi: 10.1016/j.dsr2.2012.07.001

Rodhouse, P. G. K., and Lu, C. C. (1998). *Chiroteuthis veranyi* from the Atlantic sector of the Southern Ocean (Cephalopoda: Chiroteuthidae). *S. Afr. J. Mar. Sci.* 20, 311–322. doi: 10.2989/025776198784126593

Rodhouse, P. G. K., White, M. G., and Jones, M. R. R. (1992). Trophic relations of the cephalopod *Martialia hyadesi* (Teuthoidea: Ommastrephidae) at the Antarctic Polar Front, Scotia Sea. *Mar. Biol.* 114, 415–421. doi: 10.1007/BF0035003

Rogers, P., Ward, T., van Ruth, P., Williams, A., Bruce, B. D., Connell, S., et al. (2013). *Physical processes, biodiversity and ecology of the Great Australian Bight region: a literature review* (Australia: CSIRO).

Roper, C. F. E., and Jereb, P. (2010). "Family octopoteuthidae," in *Cephalopods of the world. An annotated and illustrated catalogue of species known to date. Volume 2. Myopsid and Oegopsid Squids. FAO Species Catalogue for Fishery Purposes*, vol. 4 . Eds. P. Jereb and C. F. E. Roper (Rome: FAO), 262–268.

Roper, C. F. E., and Shea, E. K. (2013). Unanswered questions about the giant squid *Architeuthis* (Architeuthidae) illustrate our incomplete knowledge of coleoid cephalopods. *Am. Malacol. Bull.* 31, 109–122. doi: 10.4003/006.031.0104

Rosa, R., Lopes, V. M., Guerreiro, M., Bolstad, K., and Xavier, J. C. (2017). Biology and ecology of the world's largest invertebrate, the colossal squid (*Mesonychoteuthis hamiltoni*): a short review. *Polar Biol.* 40, 1871–1883. doi: 10.1007/s00300-017-2104-5

Rosa, R., Pereira, J., and Nunes, M. L. (2005). Biochemical composition of cephalopods with different life strategies, with special reference to a giant squid, *Architeuthis* sp. *Mar. Biol.* 146, 739–751. doi: 10.2307/3593118

Ruiz-Cooley, R. I., Garcia, K. Y., and Hetherington, E. D. (2011). Effects of lipid removal and preservatives on carbon and nitrogen stable isotope ratios of squid tissues: Implications for ecological studies. *J. Exp. Mar. Biol. Ecol.* 407, 101–107. doi: 10.1016/j.jembe.2011.07.002

Santos, M. B., Clarke, M. R., and Pierce, G. J. (2001). Assessing the importance of cephalopods in the diets of marine mammals and other top predators: problems and solutions. *Fish. Res.* 52, 121–139. doi: 10.1016/S0165-7836(01)00236-3

Sato, N. (2021). A review of sperm storage methods and post-copulatory sexual selection in the Cephalopoda. *Biol. J. Linn. Soc* 134, 285–302. doi: 10.1093/biolinnean/blab096

Shulman, G. E., Chesalin, M. V., Abolmasova, G. I., Yuneva, T. V., and Kideys, A. (2002). Metabolic strategy in pelagic squid of genus *Sthenoteuthis* (Ommastrephidae) as the basis of high abundance and productivity. An overview of the Soviet investigations. *Bull. Mar. Sci.* 71, 815–836.

Smale, M. J., and Cliff, G. (1998). Cephalopods in the diets of four shark species (*Galeocerdo cuvier*, *Sphyrna lewini*, *S. zygaena* and *S. mokarran*) from KwaZulu-Natal, South Africa. *S. Afr. J. Mar. Sci.* 20, 241–253. doi: 10.2989/025776198784126610

Stowasser, G., McAllen, R., Pierce, G. J., Collins, M. A., Moffat, C. F., Priede, I. G., et al. (2009). Trophic position of deep-sea fish—Assessment through fatty acid and stable isotope analyses. *Deep-Sea Res. I: Oceanogr. Res. Papers* 56, 812–826. doi: 10.1016/j.dsr.2008.12.016

Stowasser, G., Pierce, G. J., Moffat, C. F., Collins, M. A., and Forsythe, J. W. (2006). Experimental study on the effect of diet on fatty acid and stable isotope profiles of the squid *Lolliguncula brevis*. *J. Exp. Mar. Biol. Ecol.* 333, 97–114. doi: 10.1016/j.jembe.2005.12.008

Sun, X., Guo, H., Zhu, K., Zhang, N., Yu, W., Wu, N., et al. (2018). Feed type regulates the fatty acid profiles of golden pompano *Trachinotus ovatus* (Linnaeus 1758). *J. Appl. Anim. Res.* 46, 60–63. doi: 10.1080/09712119.2016.1259110

Svensson, E., Schouten, S., Hopmans, E. C., Middelburg, J. J., and Sinninghe Damsté, J. S. (2016). Factors controlling the stable nitrogen isotopic composition ($\delta^{15}N$) of lipids in marine animals. *PloS One* 11, e0146321. doi: 10.1371/journal.pone.0146321

Tsuchiya, K., Okamoto, H., and Uozumi, Y. (1998). Cephalopods eaten by pelagic fishes in the tropical East Pacific, with special reference to the feeding habitat of pelagic fish. *La Mer* 36, 57–66.

Turner, J. P., and Rooker, J. R. (2005). Effect of diet on fatty acid compositions in *Sciaenops ocellatus*. *J. Fish Biol.* 67, 1119–1138. doi: 10.1111/j.0022-1112.2005.00816.x

Van Ruth, P. D., Patten, N. L., Doubell, M. J., Chapman, P., Rodriguez, A. R., and Middleton, J. F. (2018). Seasonal- and event-scale variations in upwelling, enrichment and primary productivity in the eastern Great Australian Bight. *Deep-Sea Res. II: Top. Stud. Oceanogr.* 157-158, 36–45. doi: 10.1016/j.dsr2.2018.09.008

Van Ruth, P. D., and Ward, T. M. (2009). Meso-zooplankton abundance, distribution and community composition in the Eastern Great Australian Bight. *Trans. R. Soc S. Aust.* 133, 274–283. doi: 10.1080/03721426.2009.10887124

Weikert, H. (1977). Copepod carcasses in the upwelling region south of Cap Blanc, N.W. Africa. *Mar. Biol.* 42, 351–355. doi: 10.1007/BF00402197

Xavier, J. C., Allcock, A. L., Cherel, Y., Lipinski, M. R., Pierce, G. J., Rodhouse, P. G. K., et al. (2015). Future challenges in cephalopod research. *J. Mar. Biol. Assoc. U.K.* 95, 999–1015. doi: 10.1017/s0025315414000782

Xavier, J. C., Cherel, Y., Allcock, L., Rosa, R., Sabirov, R. M., Blicher, M. E., et al. (2018). A review on the biodiversity, distribution and trophic role of cephalopods in the Arctic and Antarctic marine ecosystems under a changing ocean. *Mar. Biol.* 165, 93. doi: 10.1007/s00227-018-3352-9

Yoshino, K., Takahashi, A., Adachi, T., Costa, D. P., Robinson, P. W., Peterson, S. H., et al. (2020). Acceleration-triggered animal-borne videos show a dominance of fish in the diet of female northern elephant seals. *J. Exp. Biol.* 223, 9. doi: 10.1242/jeb.212936

Young, J. W., Guest, M. A., Lansdell, M., Phleger, C. F., and Nichols, P. D. (2010). Discrimination of prey species of juvenile swordfish *Xiphias gladius* (Linnaeus 1758) using signature fatty acid analyses. *Prog. Oceanogr.* 86, 139–151. doi: 10.1016/j.pocean.2010.04.028

Zhukova, N. V. (2019). Fatty acids of marine mollusks: Impact of diet, bacterial symbiosis and biosynthetic potential. *Biomolecules* 9, 857. doi: 10.3390/biom9120857

frontiers | Frontiers in Marine Science

TYPE Original Research
PUBLISHED 22 January 2024
DOI 10.3389/fmars.2024.1294608

OPEN ACCESS

EDITED BY
Paulo Sergio Salomon,
Federal University of Rio de Janeiro, Brazil

REVIEWED BY
Hyun Je Park,
Gangneung-Wonju National University, Republic of Korea
Patrick Rafter,
University of California, Irvine, United States

*CORRESPONDENCE
Chisato Yoshikawa
yoshikawac@jamstec.go.jp

RECEIVED 15 September 2023
ACCEPTED 03 January 2024
PUBLISHED 22 January 2024

CITATION
Yoshikawa C, Shigemitsu M, Yamamoto A, Oka A and Ohkouchi N (2024) A nitrogen isoscape of phytoplankton in the western North Pacific created with a marine nitrogen isotope model.
Front. Mar. Sci. 11:1294608.
doi: 10.3389/fmars.2024.1294608

A nitrogen isoscape of phytoplankton in the western North Pacific created with a marine nitrogen isotope model

Chisato Yoshikawa[1]*, Masahito Shigemitsu[2], Akitomo Yamamoto[2], Akira Oka[3] and Naohiko Ohkouchi[1]

[1]Biogeochemistry Research Center, Research Institute for Marine Resources Utilization, Japan Agency of Marine-Earth Science and Technology (JAMSTEC), Yokosuka, Japan, [2]Research Institute for Global Change (RIGC), JAMSTEC, Yokosuka, Japan, [3]Atmosphere and Ocean Research Institute, The University of Tokyo, Kashiwa, Chiba, Japan

The nitrogen isotopic composition ($\delta^{15}N$) of phytoplankton varies substantially in the ocean reflecting biogeochemical processes such as N_2 fixation, denitrification, and nitrate assimilation by phytoplankton. The $\delta^{15}N$ values of zooplankton or fish inherit the values of the phytoplankton on which they feed. Combining $\delta^{15}N$ values of marine organisms with a map of $\delta^{15}N$ values (i.e., a nitrogen isoscape) of phytoplankton can reveal the habitat of marine organisms. Remarkable progress has been made in reconstructing time-series of $\delta^{15}N$ values of migratory fish from various tissues, such as otoliths, fish scales, vertebrae, and eye lenses. However, there are no accurate nitrogen isoscapes of phytoplankton due to observational heterogeneity, preventing improvement in the accuracy of estimating migratory routes using the fish $\delta^{15}N$ values. Here we present a nitrogen isoscape of phytoplankton in the western North Pacific created with a nitrogen isotope model. The simulated phytoplankton is relatively depleted in ^{15}N at the subtropical site (annual average $\delta^{15}N$ value of phytoplankton of 0.6‰), where N_2 fixation occurs, and at the subarctic site (2.1‰), where nitrate assimilation by phytoplankton is low due to iron limitation. The simulated phytoplankton is enriched in ^{15}N at the Kuroshio–Oyashio transition site (3.9‰), where nitrate utilization is high, and in the region around the Bering Strait site (6.7‰), where partial nitrification and benthic denitrification occur. The simulated $\delta^{15}N$ distributions of nitrate, phytoplankton, and particulate organic nitrogen are consistent with $\delta^{15}N$ observations in the western North Pacific. The seamless nitrogen isoscapes created in this study can be used to improve our understanding of the habitat of marine organisms or fish migration in the western North Pacific.

KEYWORDS

isoscape, nitrogen isotopes, marine nitrogen cycle, nitrogen isotope model, western North Pacific

1 Introduction

Identifying the migration routes of marine animals is crucial for sustainable fisheries management and biodiversity conservation. Many methods, such as catch per unit effort with location (e.g., Thorson et al., 2016), dart tag/capture studies (e.g., Hanselman et al., 2015), and bio-logging (e.g., Hays et al., 2016), are used to study the migration routes. Although tracking technologies have advanced greatly, the migration routes over the entire life cycle of marine animals, including the spawning sites or the larval and juvenile habitats, are often unknown due to body size limitations (Lowerre-Barbieri et al., 2019). Chemical signatures in otoliths and other body parts have become a promising tool for tracing these migration routes (Tzadik et al., 2017).

The isotopic composition of animal tissues and local environments can be used as a natural tag to track an animal's movements through isotopically distinct habitats, called iso-logging (Matsubayashi et al., 2022). Nitrogen isotope ($\delta^{15}N$) analysis of incremental growth tissues, such as eye lenses and vertebral bones, has proven promising for reconstructing migration routes and feeding environments over the animal's life (Matsubayashi et al., 2017; Matsubayashi et al., 2020; Vecchio and Peebles, 2020; Harada et al., 2022). It is essential to understand the spatial variations in $\delta^{15}N$ values (nitrogen isoscapes) across the habitat for using the $\delta^{15}N$ values for iso-logging of marine animals. However, seamless nitrogen isoscapes are generally difficult to obtain through field sampling (McMahon et al., 2013; Matsubayashi et al., 2020; Fripiat et al., 2021) because there are wide spatial and temporal variations in $\delta^{15}N$ values.

The variations in $\delta^{15}N$ values reflect biogeochemical processes. When phytoplankton assimilates nitrate, nitrogen isotopes are fractionated (Wada and Hattori, 1978; Montoya and McCarthy, 1995). The $\delta^{15}N$ value of nitrate ($\delta^{15}N_{Nitrate}$) increases as nitrate consumption increases due to an isotopic effect ranging from 5‰ to 8‰ during nitrate assimilation by phytoplankton (Granger et al., 2010). When denitrification occurs in the water column, the $\delta^{15}N_{Nitrate}$ value increases dramatically due to a strong isotopic effect of ~15‰ (Granger et al., 2008). N_2-fixation produces fixed nitrogen with a $\delta^{15}N$ value of ~0‰, because nitrogen fixers take up N_2 with little isotopic effect (Minagawa and Wada, 1986). This fixed nitrogen with a low $\delta^{15}N$ value is eventually converted into nitrate with a low $\delta^{15}N$ value through the degradation of nitrogenous organic compounds via remineralization and subsequent nitrification. The spatial patterns of $\delta^{15}N_{Nitrate}$ values in the euphotic zone are conserved in phytoplankton and are subsequently transferred to organisms with higher trophic positions (zooplankton and fish) with ^{15}N enrichment of ~3‰ per trophic position (Minagawa and Wada, 1984).

In this study, we developed a marine nitrogen isotope model that includes biogeochemical processes, and we generated a seamless nitrogen isoscape of phytoplankton as the base of the food web ($\delta^{15}N_{Base}$) in the western North Pacific for iso-logging studies. The western North Pacific, the focus of this article, is one of the most biologically diverse and productive fishery regions (FAO, 2022). Identifying fish movements in the western North Pacific is commercially important for pelagic fish in countries in the Asia–Pacific region.

2 Model description

2.1 Nitrogen isotope model

The marine nitrogen isotope model used in this study has seven compartments: phytoplankton (PHY), diazotrophs (DIA), zooplankton (ZOO), particulate organic nitrogen (PON), dissolved organic nitrogen (DON), nitrate (NO_3^-), ammonium (NH_4^+), and dinitrogen (N_2) (Figure 1). The prognostic variables are the N and ^{15}N concentrations of these compartments, except N_2. The concentration of N_2 is set to always be sufficient for DIA and the $\delta^{15}N$ value is set as 0‰. The equations for the N and ^{15}N cycles are essentially the same as those used by previous modeling studies in the western North Pacific (Yoshikawa et al., 2005; Yoshikawa et al., 2016; Yoshikawa et al., 2022). The parameters and isotopic fractionation factors used here are shown in Tables 1, 2, respectively. The N_2 fixation and denitrification schemes are introduced in this study.

2.2 N_2 fixation and denitrification

The N_2 fixation scheme is a modified version of the model developed by Hood et al. (2001) (see also Coles et al., 2004; Hood et al., 2004; Coles and Hood, 2007; Yoshikawa et al., 2013). The prognostic variable of DIA is calculated as a function of time, t, and each grid using the following governing equations.

$$d[\mathrm{DIA}]/dt = (\mathrm{Growth}_{\mathrm{DIA}}) - (\mathrm{Mortality}_{\mathrm{DIA}}) - (\mathrm{Grazing}_{\mathrm{DIA}}) - (\mathrm{Extracellular\ Excretion}_{\mathrm{DIA}}) \quad (1)$$

Growth $_{\mathrm{DIA}}$ in Equation 1 is modeled by:

$$(\mathrm{Growth}_{\mathrm{DIA}}) = \mu_T\left(1 - e^{-I/I_T}\right)(\min([\mathrm{DIP}]/([\mathrm{DIP}] + K_{PT}), [\mathrm{Fe}]/([\mathrm{Fe}] + K_{FeT}))[\mathrm{DIA}] \quad (2)$$

which describes light-, dissolved inorganic phosphorous (DIP)-, and Fe-dependent variations in diazotroph growth. In Equation 2, μ_T is the maximum growth rate. Variable I is the irradiance, and I_T is the light saturation parameter. In addition, K_{PT} and K_{FeT} are half-saturation constants for diazotroph DIP and Fe uptake. Diazotrophs fix N_2 with 0‰ and no isotopic fractionation (ϵ_9). The diazotroph nitrate uptake is modeled by:

$$(\mathrm{Nitrate\ assimilation}_{\mathrm{DIA}}) = \mu_T\left(1 - e^{-I/I_T}\right)(\min([NO_3^-]/[NO_3^-] + K_{NT}), [\mathrm{DIP}]/([\mathrm{DIP}] + K_{PT}), [\mathrm{Fe}]/([\mathrm{Fe}] + K_{FeT}))[\mathrm{DIA}] \quad (3)$$

where K_{NT} is the half-saturation constant for nitrate. Although diazotrophs take up nitrate, their growth rate is not limited by nitrate availability. Thus, when nitrate concentrations are very low, diazotroph growth is supported almost entirely by N_2 fixation.

10.3389/fmars.2024.1294608

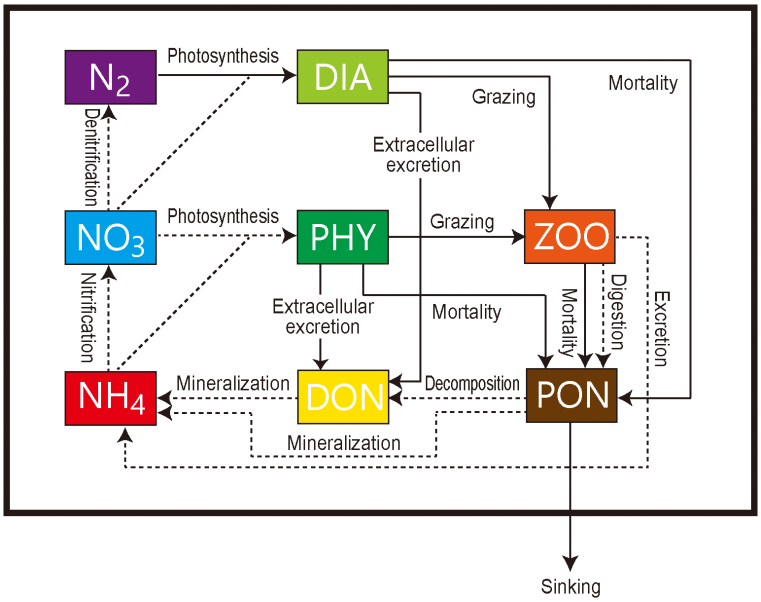

FIGURE 1
Schematic of the marine ecosystem isotope model. NO_3^-, nitrate concentration; NH_4^+, ammonium; N_2, dinitrogen; PHY, phytoplankton; DIA, diazotrophs; ZOO, zooplankton; PON, particulate organic nitrogen; DON, dissolved organic nitrogen. Dashed and solid arrows indicate nitrogen flows with and without isotopic fractionation, respectively.

TABLE 1 Biological parameters in the nitrogen isotope model.

Symbol	Parameter	Value		Citation
V_{max}	Phytoplankton maximum photosynthetic rate at 0 °C	0.25	/day	Yoshikawa et al. (2022)
K_{NO3}	Phytoplankton half saturation constant for nitrate	2.0	μmolN/L	Yoshikawa et al. (2022)
K_{NH4}	Phytoplankton half saturation constant for ammonium	0.2	μmolN/L	Yoshikawa et al. (2022)
ψ	Phytoplankton ammonium inhibition coefficient	1.5	L/μmolN	Yoshikawa et al. (2022)
k	Phytoplankton temperature coefficient for photosynthesis	0.0693	/°C	Yoshikawa et al. (2022)
I_{opt}	Phytoplankton optimum light intensity	100.0	W/m^2	Yoshikawa et al. (2022)
M_{p0}	Phytoplankton mortality rate at 0 °C	0.04375	L/μmolN/day	Yoshikawa et al. (2022)
k_{Mp}	Phytoplankton temperature coefficient for mortality	0.0693	/°C	Yoshikawa et al. (2022)
μ_T	Diazotroph maximum growth rate	0.23	/day	Yoshikawa et al. (2013)
K_{NT}	Diazotroph half saturation constant for nitrate	0.5	μmolN/L	Yoshikawa et al. (2013)
K_{PT}	Diazotroph half saturation constant for phosphate	0.0077	μmolN/L	Yoshikawa et al. (2013)
K_{FeT}	Diazotroph half saturation constant for iron	0.0001	μmolN/L	Yoshikawa et al. (2013)
I_T	Diazotroph light saturation	70.0	W/m^2	Yoshikawa et al. (2013)
S_T	Diazotroph mortality rate	0.005	/day	Yoshikawa et al. (2013)
γ	Ratio of extracellular excretion to photosynthesis	0.135	(nodim.)	Yoshikawa et al. (2022)
G_{Rmax}	Zooplankton maximum grazing rate of phytoplankton at 0 °C	0.3	/day	Yoshikawa et al. (2022)
G_{RmaxT}	Zooplankton maximum grazing rate of diazotrophs at 0 °C	0.1	/day	*
k_G	Zooplankton temperature coefficient for grazing	0.0693	/°C	Yoshikawa et al. (2022)
λ	Zooplankton ivlev constant	1.4	L/μmolN	Yoshikawa et al. (2022)
P^*_Z	Zooplankton threshold value for grazing	0.04	μmolN/L	Yoshikawa et al. (2022)

(Continued)

TABLE 1 Continued

Symbol	Parameter	Value		Citation
α	Zooplankton assimilation efficiency	0.7	(nodim.)	Yoshikawa et al. (2022)
β	Zooplankton growth efficiency	0.3	(nodim.)	Yoshikawa et al. (2022)
M_{z0}	Zooplankton mortality rate at 0 °C	0.0585	L/μmolN/day	Yoshikawa et al. (2022)
k_{Mz}	Zooplankton temperature coefficient for mortality	0.0693	/°C	Yoshikawa et al. (2022)
α_1	Light dissipation coefficient of sea water	0.04	/m	Yoshikawa et al. (2022)
α_2	Self shading coefficient	0.054	L/μmolN/m	Yoshikawa et al. (2022)
α_3	Self shading coefficient	0.6667	(nodim.)	Yoshikawa et al. (2022)
α_4	Self shading coefficient	0.0088	L/μmolN/m	Yoshikawa et al. (2022)
R_{chla}	Chlorophyll to nitrogen ratio	1.59	(nodim.)	Yoshikawa et al. (2022)
S_{PON}	PON sinking velocity at the surface layer	7.00	m/day	Schmittner et al. (2008)
m_w	Increase of sinking speed with depth	0.04	/day	Schmittner et al. (2008)
N_{Nit0}	Nitrification rate at 0 °C	0.6	/day	Yoshikawa et al. (2022)
k_{Nit}	Temperature coefficient for nitrification	0.0693	/°C	Yoshikawa et al. (2022)
I_1	Light inhibition coefficient for nitrification	0.0364	W/m^2	Yoshikawa et al. (2022)
I_2	Light inhibition coefficient for nitrification	0.074	W/m^2	Yoshikawa et al. (2022)
V_{PA0}	Remineralization rate of PON to ammonium at 0 °C	0.1	/day	Yoshikawa et al. (2022)
k_{PA}	Temperature coefficient for PON remineralization to ammonium	0.0693	/°C	Yoshikawa et al. (2022)
V_{PD0}	Decomposition rate of PON to DON at 0 °C	0.1	/day	Yoshikawa et al. (2022)
k_{PD}	Temperature coefficient for POM decomposition to DON	0.0693	/°C	Yoshikawa et al. (2022)
V_{DA0}	Remineralization rate of DON to ammonium at 0 °C	0.01	/day	**
k_{DA}	Temperature coefficient for DON remineralization to ammonium	0.0693	/°C	Yoshikawa et al. (2022)
$R_{O:N}$	Atomic ratio of O to N	8.652	(nodim.)	Hajima et al. (2020)
D_{min}	Nitrate threshold for water column denitrification	50.0	μmolN/L	***
α_{BD}	Benthic denitrification coefficient	0.3	(nodim.)	***

* The G_{Rmax} of diazotrophs is reduced from 0.3 to 0.1 /day to reproduce the observed abundance of diazotrophs compiled by Yoshikawa et al. (2013).
** The V_{DA0} is reduced from 0.1 /day (Yoshikawa et al., 2022) to 0.01 /day to reproduce the surface DON concentrations observed by Letscher et al. (2013).
*** The D_{min} and α_{BD} are tuned to set the global fluxes of water column denitrification and benthic denitrification in the model to the previous estimates (see the main text).

Mortality $_{DIA}$ in Equation 1 is modeled using:

$$(\text{Mortality}_{\text{DIA}}) = S_T[\text{DIA}] \quad (4)$$

where S_T is the mortality rate of DIA.

Grazing $_{DIA}$ in Equation 1 is modeled using:

$$(\text{Grazing}_{\text{DIA}}) = G_{RmaxT}(\max(0, 1 - \exp(\lambda(P_\star z - [\text{DIA}])))\exp(K_G T)[\text{ZOO}] \quad (5)$$

where G_{RmaxT}, λ, and P^*z are the zooplankton maximum grazing rate for DIA, zooplankton Ivlev constant, and zooplankton threshold value for grazing, respectively. Variable T is the temperature, and K_G is the zooplankton temperature coefficient for mortality.

Extracellular Excretion $_{DIA}$ in Equation 1 is modeled by:

$$(\text{Extracellular Excretion}_{\text{DIA}}) = \gamma(\text{Growth}_{\text{DIA}}) \quad (6)$$

where γ is the ratio of extracellular excretion of DIA to growth.

The water-column denitrification scheme is essentially the same as that reported by Schmittner et al. (2008). Oxygen consumption in suboxic waters (<3 μM) is inhibited and replaced by the oxygen-equivalent oxidation of nitrate:

$$r_{NO3} = 0.5(1 - \tanh([O_2] - 3.0)) \quad (7)$$

Denitrification consumes nitrate at a rate of 80% of the oxygen equivalent rate, according to:

$$(\text{Denitrification}) = ((\text{Decomposition}) + (\text{Excretion}) + (\text{Remineralization}) - (\text{Growth}_{\text{PHY}}) - (\text{Growth}_{\text{DIA}}))(-0.8D_{flag}R_{O:N}r_{NO3}) \quad (8)$$

where $R_{O:N}$ is the ratio of O to N. D_{flag} limits the rate of water column N-loss at a given nitrate threshold of D_{min}:

$$D_{flag} = 0.5 + \text{sign}(0.5, [NO_3^-] - D_{min}) \quad (9)$$

TABLE 2 Isotope fractionation factors in the nitrogen isotope model.

Process	ϵ (‰)	Citation
NO_3^- assimilation by phytoplankton or diazotroph	$\epsilon_1 = 5$	Yoshikawa et al. (2005)
NH_4^+ assimilation by phytoplankton	$\epsilon_2 = 0$	*
Excretion by zooplankton	$\epsilon_3 = 5$	Yoshikawa et al. (2022)
Egestion by zooplankton	$\epsilon_4 = 2$	Yoshikawa et al. (2022)
Nitrification	$\epsilon_5 = 14$	Yoshikawa et al. (2022)
Remineralization from PON to DON	$\epsilon_6 = 1$	Yoshikawa et al. (2022)
Remineralization from DON to NH_4^+	$\epsilon_7 = 1$	Yoshikawa et al. (2022)
Remineralization from PON to NH_4^+	$\epsilon_8 = 1$	Yoshikawa et al. (2022)
N_2 fixation by diazotroph	$\epsilon_9 = 0$	**
Water column denitrification	$\epsilon_{10} = 25$	**
Benthic denitrification	$\epsilon_{11} = 1$	**

* There are no previous estimates at ammonium concentrations < 4 μM. However, Liu et al. (2013) implied that the isotope effect in the surface water of the open ocean (<1 μM) may be much smaller than previous estimates of 5‰–18‰. Therefore, the isotope fractionation factor (ϵ_2) is reduced from 10 ‰ (Yoshikawa et al., 2022) to 0‰ in this study.
** The isotope fractionation factors (ϵ_9, ϵ_{10}, and ϵ_{11}) are introduced in this study and are set within field estimates (0‰–2‰, 22‰–30‰, and 0‰–4‰, respectively) compiled by Somes et al. (2010).

The isotopic fractionation factor for water-column denitrification (ϵ_{10}) is set to 25‰.

The benthic denitrification scheme is essentially the same as that reported by Shigemitsu et al. (2016). The benthic denitrification flux is parameterized based on the organic carbon flux to the seafloor (F_{POC_bot}) and bottom water O_2 and NO_3^- concentrations ($[O_2]_{bottom}$ and $[NO_3^-]_{bottom}$) as:

$$F_{BD} = \alpha_{BD} \cdot F_{POC\_bot}\left(0.06 + 0.19 \times 0.99^{[O_2]_{bottom}-[NO_3^-]_{bottom}}\right) \quad (10)$$

where α_{BD} is tuned to set the globally integrated rates of benthic denitrification in the model to the rates within the range of previous estimates (80–140 Tg N yr^{-1}; Bianchi et al., 2012; Bohlen et al., 2012; DeVries et al., 2013; Somes et al., 2013; Shigemitsu et al., 2016; Somes et al., 2017). The isotopic fractionation factor for benthic denitrification (ϵ_{11}) is set to 1‰.

2.3 Offline biogeochemical model

The nitrogen isotope model was incorporated into the ocean general circulation model (COCO) with an offline method (Oka et al., 2008; Shigemitsu et al., 2016). The model has 256 × 198 grid points in the horizontal direction and 44 vertical layers. The horizontal resolution is about 1°, and the vertical spacing varies from 5 m at the top to 250 m at the bottom. The concentration of biogeochemical tracers is calculated by the following tracer equation:

$$\frac{\partial C}{\partial t} = -\nabla \cdot (vC) + K_H \nabla_H^2 C + \frac{\partial}{\partial z}\left(K_V \frac{\partial C}{\partial z}\right) + S_C \quad (11)$$

where C is the tracer concentration, v is the velocity, K_H and K_V are the horizontal and vertical diffusivity, and S_C is the source/sink term for the tracer due to biogeochemical processes. The model was driven by climatological monthly mean physical fields (horizontal ocean velocities, vertical diffusivity, temperature, salinity, sea surface height, sea surface wind speed, sea ice fraction, and sea surface solar radiation) obtained from the outputs of a pre-industrial control simulation performed with an Earth system model (MIROC-ESM) (Watanabe et al., 2011) as in Shigemitsu et al. (2017). The climatological monthly mean concentration of dissolved iron was obtained from the output of a pre-industrial control simulation performed with an ocean biogeochemical model including an iron cycle (Yamamoto et al., 2019). In order to rapidly reach steady state, the initial conditions were set to values that have already reached steady state and were within the range of observations. The initial conditions of the nitrogen, phosphate, and oxygen concentrations were obtained from the outputs of a pre-industrial control simulation with MIROC-ESM (Watanabe et al., 2011). The initial conditions of $\delta^{15}N$ of PHY, DIA, ZOO, PON, DON, NO_3^-, and NH_4^+ were set to constant values of 3‰, 0‰, 6‰, 6‰, 6‰, 5‰, and 6‰, respectively. The results of the simulations presented here are shown after 3000 years of time integration.

3 Results

3.1 Horizontal distributions of nitrate and chlorophyll *a* concentrations

The simulated distributions of annual mean nitrate and chlorophyll *a* concentrations in the surface layer are generally consistent with the climatological annual mean concentrations of the World Ocean Atlas 2018 (Garcia et al., 2019) and the SeaWiFS satellite data (O'Reilly et al., 1998), respectively (Figure 2). The model represents the high nitrate concentrations exceeding 5 μM observed in the subarctic region and the low concentrations below 2 μM observed in the subtropical region (Figures 2A, C). Because of the nitrate availability, the simulated chlorophyll *a* concentrations are also high in the subarctic region and low in the subtropical region (Figures 2B, D). The root-mean-square error (RMSE), which is an estimate of the absolute magnitude of the difference between the observed and modeled values, is relatively high in the northwestern North Pacific for both nitrate and chlorophyll *a* concentrations (Figures 2E, F). This is because of the lack of terrestrial inputs of nitrogenous nutrients in the model and its coarse resolution. The extremely high RMSE in the coastal region for the chlorophyll *a* concentration may also be attributed to the

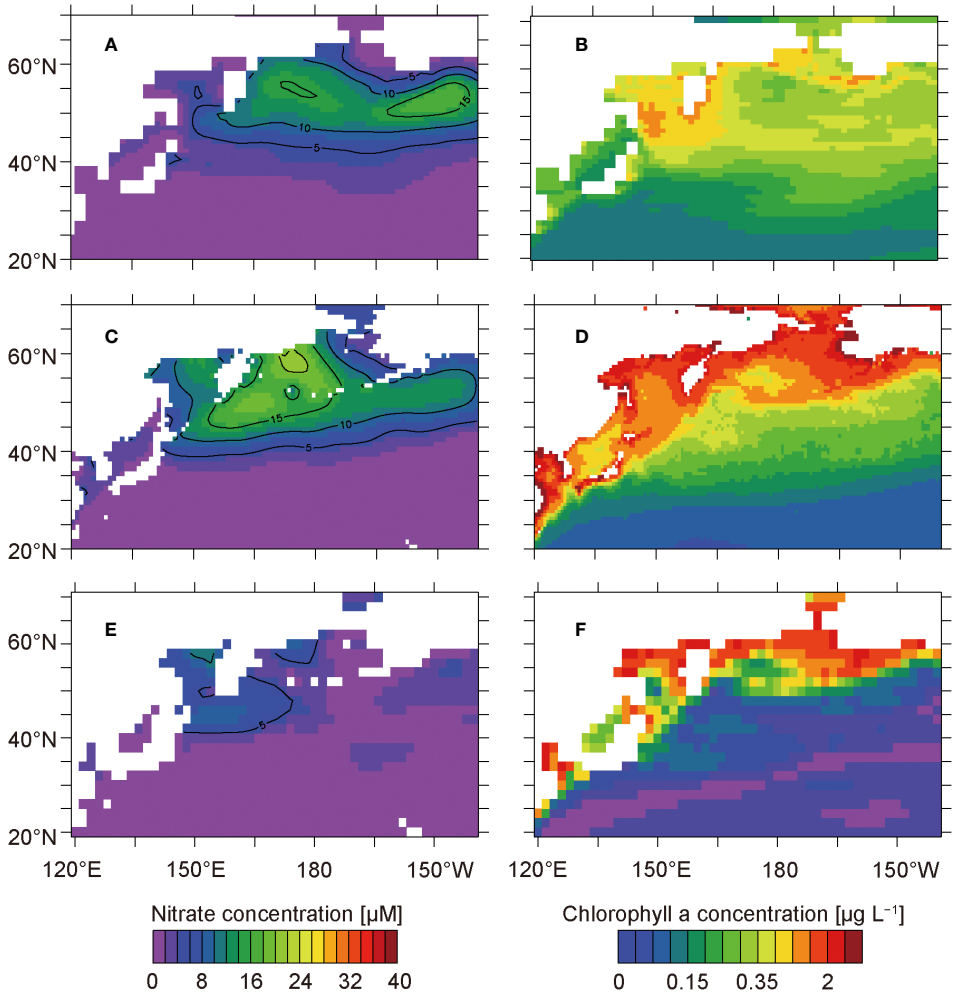

FIGURE 2
Concentrations of annual mean nitrate and chlorophyll *a* at the surface from the model simulations **(A, B)** and observations **(C, D)**. Panels **(C, D)** show the climatological annual mean nitrate concentrations in the surface waters of the World Ocean Atlas 2018 (Garcia et al., 2019) and the climatological annual mean chlorophyll *a* concentrations based on the SeaWiFS satellite data from 1997 to 2006 (O'Reilly et al., 1998), respectively. Panels **(E, F)** show the root-mean-square error of the model simulations of nitrate and chlorophyll *a* concentrations, respectively.

difficulty of satellite-based chlorophyll *a* estimation caused by terrestrial inputs of colored dissolved organic matter or suspended particles.

3.2 Horizontal distributions of $\delta^{15}N_{Nitrate}$, $\delta^{15}N_{Phytoplankton}$, and $\delta^{15}N_{PON}$ values

The simulated annual mean $\delta^{15}N$ values of nitrate in the surface layer and phytoplankton and PON in the euphotic layers have similar high–low distributions, except in the Bering Strait (Figure 3). The model represents the ^{15}N depletion observed in the subtropical and subarctic regions and the ^{15}N enrichment observed in the Oyashio–Kuroshio transition region. The model also represents the overall observed ^{15}N enrichment of nitrate and ^{15}N depletion of phytoplankton.

The simulated values are not precisely consistent with the observed values shown in Figure 3 for the following reasons. The simulated $\delta^{15}N_{Nitrate}$ values (Figure 3A) are annual mean surface values, whereas the observed values (Figure 3D) are the shallowest data that were measured in a single expedition compiled by Rafter et al. (2019) and Fripiat et al. (2021). The simulated $\delta^{15}N_{Phytplankton}$ values (Figure 3B) are the weighted averages of the euphotic layer throughout the year, whereas the observed values (Figure 3E) are the $\delta^{15}N_{Base}$ values estimated from the $\delta^{15}N$ measurements of bulk nitrogen and amino acids of zooplankton obtained from various depths and seasons (Matsubayashi et al., 2022). The simulated $\delta^{15}N_{PON}$ values (Figure 3C) are the weighted averages of the euphotic layer throughout the year, whereas the observed values (Figure 3F) are the $\delta^{15}N_{Bulk}$ values of surface sediments obtained from various depths and redox conditions compiled by NICOPP (Tesdal et al., 2013), which could be affected by digenesis.

For the discussion, we selected four representative sites in the western subtropical North Pacific (ST: 145°E, 22°N), the Kuroshio–Oyashio transition zone (TR: 155°E, 44°N), the western subarctic North Pacific (SA: 170°E, 55°N), and the Bering Strait region (BS: 190°E, 60°N) (Figure 3). The simulated $\delta^{15}N_{Nitrate}$ values in the surface layer are 1.1‰ at ST, 7.3‰ at TR, 6.8‰ at SA, and 6.6‰ at

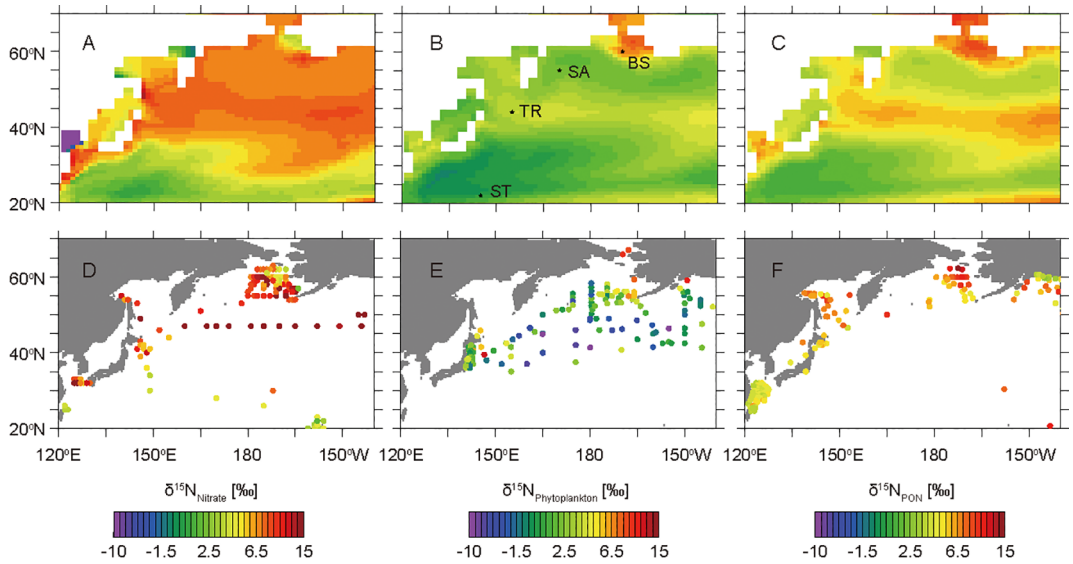

FIGURE 3
Horizontal $\delta^{15}N$ distributions of annual mean nitrate, phytoplankton, and PON from the model simulations **(A–C)** and observations **(D–F)**. Panels **(A-C)** show the $\delta^{15}N_{Nitrate}$ values at the surface layer, the weighted average of $\delta^{15}N_{Phytoplankton}$ values in the layers at 0–200 m, and the weighted average of $\delta^{15}N_{PON}$ values in the layers at 0–200 m, respectively. Panels **(D-F)** show the shallowest $\delta^{15}N_{Nitrate}$ values compiled by Rafter et al. (2019) and Fripiat et al. (2021), the $\delta^{15}N_{Base}$ values estimated from the $\delta^{15}N$ measurements of bulk nitrogen and amino acids of zooplankton (Matsubayashi et al., 2022), and the $\delta^{15}N$ values of surface sediments compiled by NICOPP (Tesdal et al., 2013), respectively. Locations of the western subtropical North Pacific site (ST: 145°E, 22°N), the Kuroshio–Oyashio transition zone site (TR: 155°E, 44°N), the western subarctic North Pacific site (SA: 170°E, 55°N), and the Bering Strait region site (BS: 190°E, 60°N) selected for this study are shown.

BS (Figure 3A). In the uppermost 200 m layers, the simulated weighted averages of $\delta^{15}N_{Phytoplankton}$ are 0.6‰ at ST, 3.9‰ at TR, 2.1‰ at SA, and 6.7‰ at BS (Figure 3B), whereas those of $\delta^{15}N_{PON}$ are 1.8‰ at ST, 5.9‰ at TR, 3.7‰ at SA, and 7.3‰ at BS (Figure 3C).

3.3 Seasonal cycles of nitrate, ammonium and phytoplankton concentrations

At ST, the simulated nitrate in the surface layer is depleted to<0.2 μM throughout the year and shows a slight increase from February to March (Figure 4A). The simulated ammonium accumulates slightly up to 0.02 μM in the layers at depths of 40–80 m from April to November (Figure 4B). The simulated phytoplankton concentration is low (<0.1 μM), equivalent to 0.2 μg Chl L^{-1}, throughout the year and has a small bloom in April (Figure 4C).

At TR, the simulated nitrate in the surface layer reaches a maximum concentration of 8.5 μM in March and is depleted to 0.3 μM in August (Figure 4D). Then, until March, the nitrate concentration increases as the surface mixed layer deepens. The simulated ammonium accumulates to >0.3 μM in the layers at 30–60 m from May to November, and the maximum concentration is 0.9 μM at a depth of 40 m in August (Figure 4E). The simulated phytoplankton has high concentrations of >0.1 μM throughout the year and has a bloom in June (Figure 4F).

At SA, the simulated nitrate in the surface layer reaches a maximum concentration of 17.0 μM in April and decreases to 10.4 μM in August (Figure 4G). The simulated ammonium accumulates to >0.3 μM in the layers at 30–60 m from July to October, and the maximum concentration is 0.6 μM at a depth of 40 m in August (Figure 4H). The simulated phytoplankton has high concentrations of >0.1 μM from April to October and has a bloom in June (Figure 4I).

At BS, the simulated nitrate in the surface layer reaches a maximum concentration of 3.8 μM in March and decreases to 1.9 μM in September (Figure 4J). The nitrate concentration in the bottom layer is<1.0 μM in July and August. The simulated ammonium accumulates to >2.0 μM in the bottom layer in July and August (Figure 4K), and then spreads to the upper layers as the surface mixed layer deepens from September to December. Then, until April, the ammonium concentration drops to 0.3 μM. The simulated phytoplankton has a high concentration of >0.1 μM from February to October and has blooms in June and August (Figure 4L).

3.4 Seasonal cycles of $\delta^{15}N$ values of nitrate, ammonium and phytoplankton

At ST, the simulated $\delta^{15}N_{Nitrate}$ value in the surface layer is 0.6‰ in February, and increases to 10.7‰ in May (Figure 5A). Subsequently, the $\delta^{15}N_{Nitrate}$ value decreases to −2.1‰ in August. The simulated ammonium in the surface layer is depleted in ^{15}N from May to September, and the minimum value is −1.1‰ in July (Figure 5B). The ammonium is enriched in ^{15}N from October to February, and reaches a maximum value of 6.0‰ in February. The

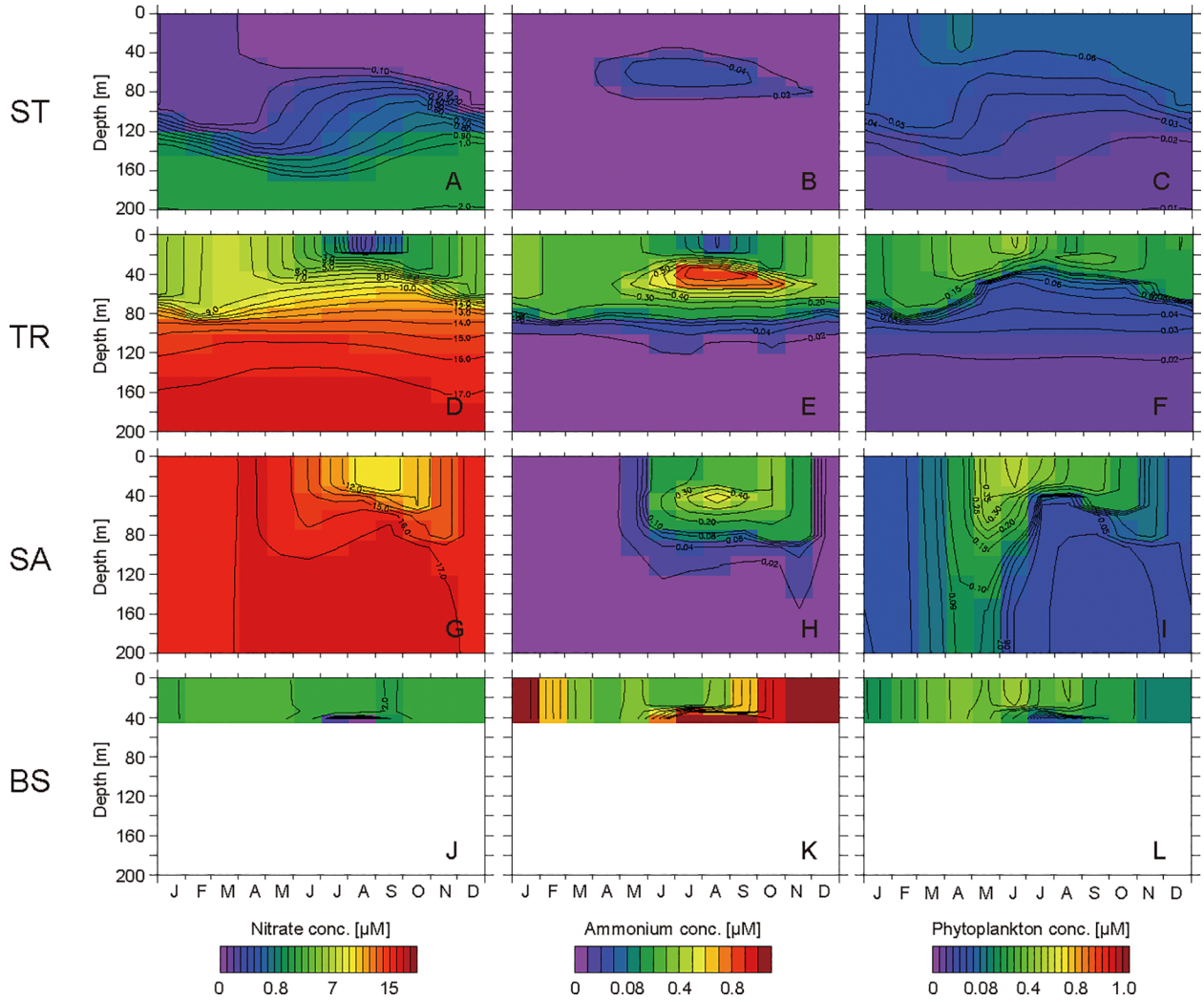

FIGURE 4
Seasonal cycles of simulated concentrations of nitrate, ammonium, and phytoplankton in the layers at 0–200 m at the western subtropical North Pacific site ST **(A–C)**, the Kuroshio–Oyashio transition zone site TR **(D–F)**, the western subarctic North Pacific site SA **(G–I)**, and the Bering Strait region site BS **(J–L)**.

simulated $\delta^{15}N_{Phytoplankton}$ value is 0.5‰ in the surface layer during a small bloom period in April, and is<0.0‰ from June to November (Figure 5C). The phytoplankton is enriched in ^{15}N and >2.0‰ in the layers at depths of 60–100 m from June to October.

At TR, the simulated $\delta^{15}N_{Nitrate}$ value in the surface layer is 6.2‰ in February (Figure 5D). The value increases to 17.0‰ in August, and then decreases gradually as the surface mixed layer deepens. The nitrate is slightly depleted in ^{15}N in the layers at depths of 40–140 m. The simulated ammonium in the surface layer is more depleted in ^{15}N than the nitrate from March to November, and the minimum value is 0.8‰ in May (Figure 5E). The ammonium is enriched in ^{15}N from September to February, and the maximum value is 7.8‰ in February. The simulated $\delta^{15}N_{Phytoplankton}$ value is 3.6‰ in the surface layer during the bloom period in June (Figure 5F). The phytoplankton in the surface layer has a minimum $\delta^{15}N$ value of 1.9‰ in May, and is subsequently enriched in ^{15}N to July and is depleted in ^{15}N to February as with the seasonal nitrate cycle. The phytoplankton is enriched in ^{15}N and >5.0‰ in the layers at depths of 30–90 m from July to January.

At SA, the simulated $\delta^{15}N_{Nitrate}$ value in the surface layer is 6.3‰ in February (Figure 5G), increases to 8.5‰ in August, and then decreases gradually as the surface mixed layer deepens. The seasonal variation in SA is similar to that in TR, although the amplitude is smaller. The simulated ammonium in the surface layer is more depleted in ^{15}N than nitrate from May to October, and the minimum value is −0.4‰ in July (Figure 5H). Subsequently, the ammonium is enriched in ^{15}N with a maximum value of 16.8‰ in December. The simulated $\delta^{15}N_{Phytoplankton}$ value is 1.4‰ in the surface layer during the bloom period in June and increases gradually to 4.2‰ in November (Figure 5I).

At BS, the simulated $\delta^{15}N_{Nitrate}$ value in the surface layer is 3.7‰ in January (Figure 5J). The value increases to 10.8‰ in August, and then decreases gradually as the surface mixed layer deepens. The simulated ammonium in the surface layer is more depleted in ^{15}N than nitrate from May to October, and the

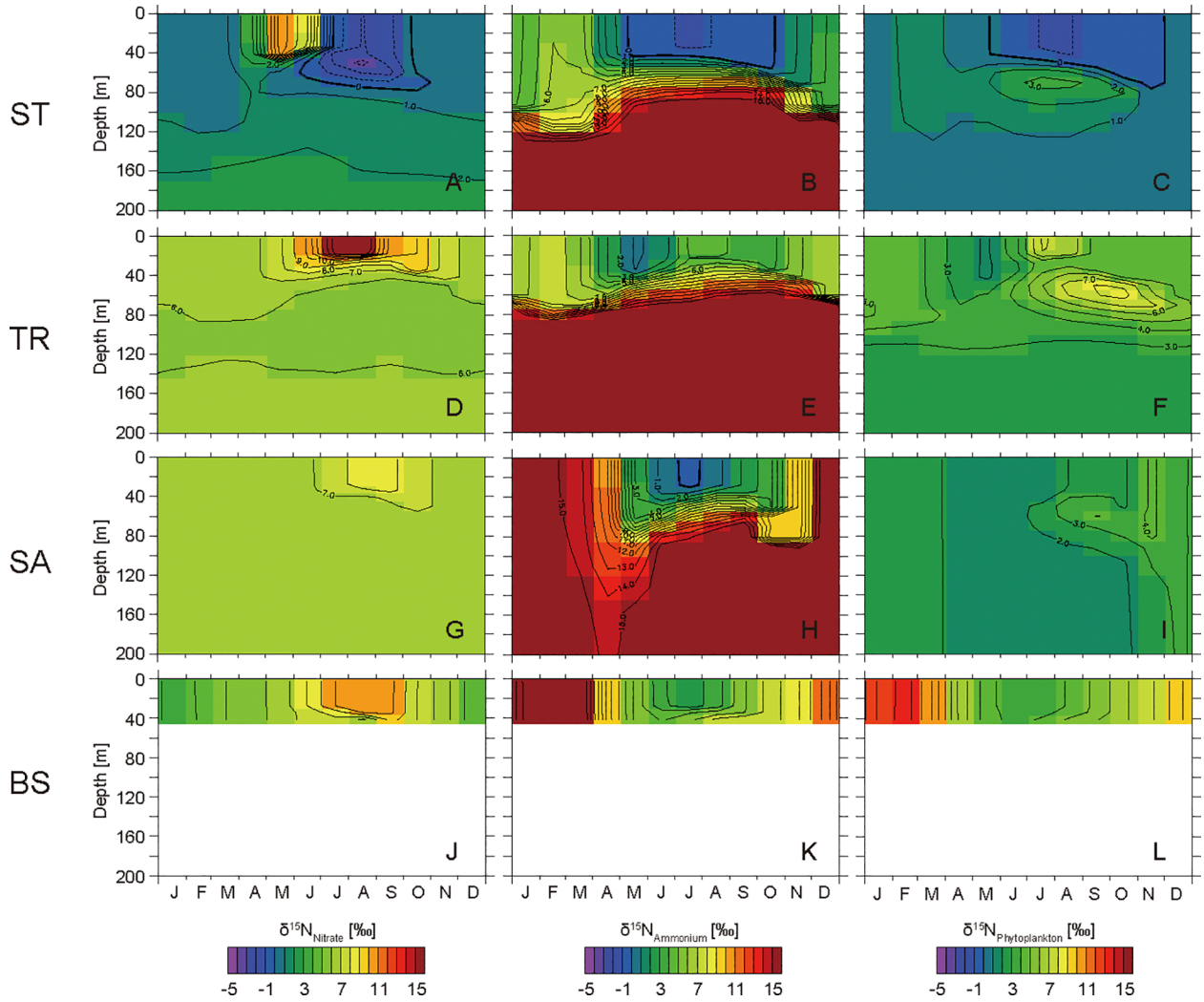

FIGURE 5
Seasonal cycles of simulated $\delta^{15}N$ values of nitrate, ammonium, and phytoplankton in the layers at 0–200 m at the western subtropical North Pacific site ST **(A–C)**, the Kuroshio–Oyashio transition zone site TR **(D–F)**, the western subarctic North Pacific site SA **(G–I)**, and the Bering Strait region site BS **(J–L)**.

minimum value is 2.4‰ in July (Figure 5K). Subsequently, the ammonium is enriched in ^{15}N with a maximum value of 17.9‰ in February. The simulated $\delta^{15}N_{Phytoplankton}$ values are 3.2‰ and 4.2‰ in the surface layer during bloom periods in June and August, respectively, and the value increases gradually to 13.6‰ in February (Figure 5L).

4 Discussion

4.1 Western subtropical North Pacific

The western subtropical North Pacific is characterized as an oligotrophic, low-productivity ocean (Figure 2). Active N_2 fixation occurs in the model due to nitrate depletion in the surface water throughout the year (Figure 6). The simulated annual mean $\delta^{15}N_{Phytoplankton}$ value in the euphotic layer at ST is 0.6‰, which is the lowest value among the selected sites. The diazotrophs take up N_2 gas, the $\delta^{15}N$ value of which is 0.0‰, and are remineralized to ammonium and nitrate. The phytoplankton takes up the ^{15}N-depleted ammonium and nitrate, and consequently is depleted in ^{15}N.

In winter, a small amount of nitrate is present in the surface water (Figure 4A). In early spring, the phytoplankton consumes the nitrate with an isotopic fractionation of 5‰ (Table 2). Therefore, the nitrate in the surface water is enriched in ^{15}N at the end of the small bloom (Figure 5A). In summer, the nitrate is completely consumed in the surface water, and the diazotrophs begin to take up N_2 actively (Figure 6B). N_2 fixation depletes ^{15}N in ammonium, nitrate, and phytoplankton in the surface water (Figures 5A–C).

Ammonium is produced by remineralization of PON, and is consumed by phytoplankton assimilation in the euphotic layer and by nitrification below the euphotic layer. As such, ammonium is accumulated at the bottom of the euphotic layer from spring to autumn (Figure 4B). The isotopic fractionation effect of ammonium assimilation by phytoplankton is as small as 0‰, and that of nitrification is as large as 14‰ (Table 2). As such, the ^{15}N enrichment of ammonium increases with depth (Figure 5B). The

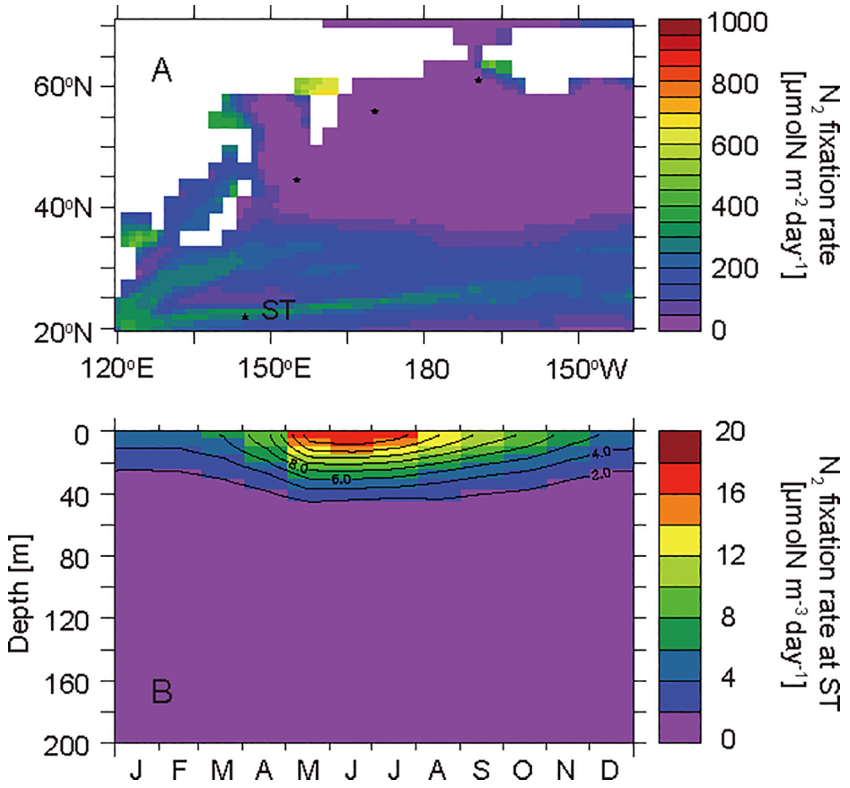

FIGURE 6
Horizontal distribution of annual mean N_2 fixation rates that were depth-integrated throughout the water column **(A)** and seasonal cycle of N_2 fixation rates in the layers at 0–200 m at the western subtropical North Pacific site ST **(B)**.

^{15}N-enriched ammonium in the subsurface water is supplied to the surface layer by the deepening of the mixed layer from autumn to winter.

4.2 Oyashio–Kuroshio transition zone

The Oyashio–Kuroshio transition zone in the western North Pacific is characterized as high-productivity ocean (Figure 2). The annual nitrate supply to the surface water is much higher than that at ST (Figures 4A, D), and the phytoplankton growth is limited only by nitrogen in the surface water (Figure 7A). Therefore, primary productivity is relatively high and phytoplankton exhausts nitrate in the surface water in summer. The simulated annual mean $\delta^{15}N_{Phytoplankton}$ value in the euphotic layer at TR is 3.9‰, which is a high value among the selected sites.

In winter, the nitrate in the surface water reaches its maximum concentration during the year due to winter convective mixing (Figure 4D). In spring, phytoplankton starts to consume the nitrate with an associated isotopic fractionation. Therefore,^{15}N enrichment of nitrate in the surface water proceeds toward summer (Figure 5D). In summer, nitrate is exhausted in the surface water and the maximum $\delta^{15}N_{Nitrate}$ value during the year is reached. Because phytoplankton actively assimilates nitrate, the seasonal variation in $\delta^{15}N_{Phytoplankton}$ is synchronized with that in $\delta^{15}N_{Nitrate}$ in the surface water (Figures 5D, F).

Ammonium accumulation is high in the subsurface water from spring to autumn due to active remineralization of PON (Figure 4E). The large isotopic fractionation of nitrification causes ^{15}N enrichment in ammonium and ^{15}N depletion in nitrate in the subsurface water (Figures 5D, E). The ^{15}N enrichment in phytoplankton in the subsurface water from summer to autumn is attributed to the phytoplankton assimilating ^{15}N-enriched ammonium (Figure 5F).

4.3 Western subarctic North Pacific

The western subarctic North Pacific is characterized as a high-nutrient low-chlorophyll ocean (Figure 2; e.g., Nishioka et al., 2020). Phytoplankton is affected by iron limitation and cannot assimilate all nitrate in the surface water in summer (Figure 7). The simulated annual mean $\delta^{15}N_{Phytoplankton}$ value in the euphotic layer at SA is 2.2‰, which is a low value among the selected sites. The low utilization of the surface nitrate pool by phytoplankton causes ^{15}N depletion in phytoplankton at SA, as suggested by Yoshikawa et al. (2018).

In winter, nitrate in the surface water reaches its maximum concentration during the year due to winter convective mixing (Figure 4G). In spring, phytoplankton starts to consume the nitrate with an associated isotopic fractionation, and thus the nitrate in the surface water is gradually enriched in ^{15}N toward summer

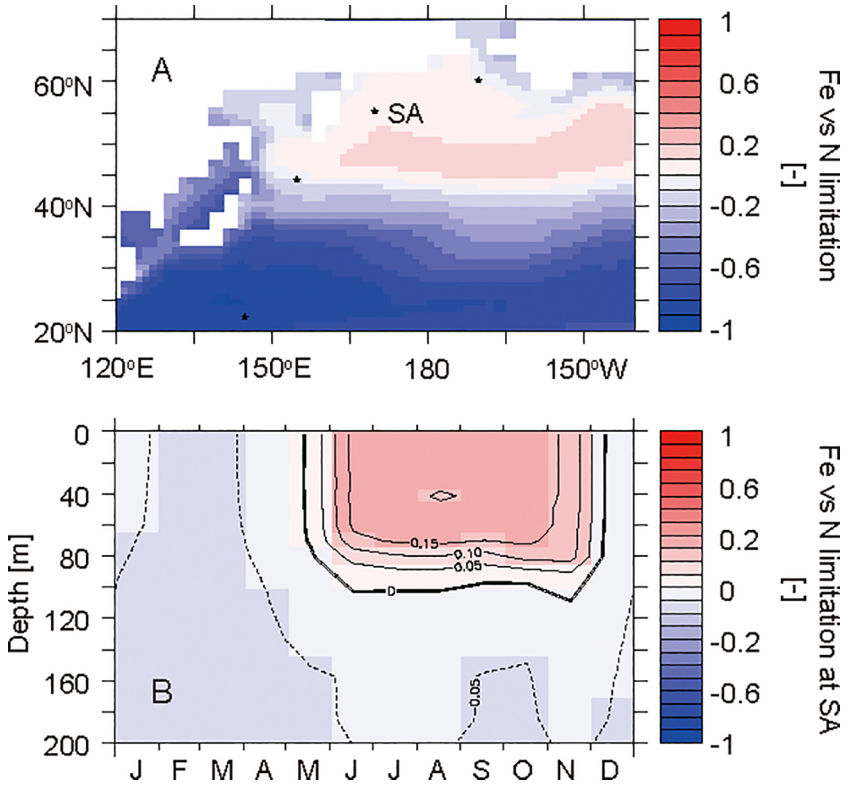

FIGURE 7
Horizontal distribution of the annual mean nutrient limitation (iron versus nitrogen) for phytoplankton in the surface layer **(A)** and the seasonal cycle in the layers at 0–200 m at the western subarctic North Pacific site SA **(B)**. The values were calculated from a nutrient-dependent term in the phytoplankton growth rate equation. Red shows the area where phytoplankton growth is limited by iron concentrations. Blue shows the area where phytoplankton growth is limited by nitrate and ammonium concentrations.

(Figure 5G). Because the nitrate assimilation by phytoplankton is limited by iron from May to December (Figure 7B), the minimum nitrate concentration and the maximum $\delta^{15}N_{Nitrate}$ value at SA are much higher and much lower than those at TR, respectively.

The ammonium is accumulated in the subsurface water from spring to autumn due to remineralization of PON (Figure 4H). As found at ST and TR, the ammonium is enriched in ^{15}N with depth at SA (Figure 5H). The ^{15}N-enriched ammonium in the subsurface water is supplied to the surface layer by the deepening of the mixed layer. From autumn to winter, the ammonium at SA is much more enriched in ^{15}N than that at TR. Because the phytoplankton assimilates the extremely ^{15}N-enriched ammonium (Figure 5I), the phytoplankton in the surface water from autumn to winter is the most enriched in ^{15}N during the year.

4.4 Bering Strait region

The Bering Strait region is characterized by a highly productive coastal ocean (Figure 2). The high sinking PON flux reaching the seafloor causes active benthic denitrification (Figure 8A). The depth of the ocean floor is only 41 m, and thus nitrification is inhibited by light in most of the water column (Figure 8B), and ammonium is not completely oxidized to nitrate throughout the year. The simulated annual mean $\delta^{15}N_{Phytoplankton}$ value in the euphotic layer at BS is 6.7‰, which is the highest value among the selected sites. The ^{15}N enrichment in phytoplankton is attributed to the uptake of highly-concentrated ^{15}N-enriched ammonium caused by partial nitrification and the removal of ^{15}N-depleted nitrate by benthic denitrification, as suggested by Granger et al. (2011).

In winter, nitrate in the surface water reaches its maximum concentration during the year (Figure 4J). In spring, phytoplankton starts to consume nitrate with an associated isotopic fractionation, and consequently the nitrate in the surface water is enriched in ^{15}N toward summer (Figure 5J). The $\delta^{15}N_{Nitrate}$ value in winter at BS is much lower than that at TR and SA due to incomplete nitrification with a large isotopic fractionation. The ^{15}N-depleted nitrate is removed from the benthic water by benthic denitrification after the bloom in June. The $\delta^{15}N_{Nitrate}$ value in the benthic water increases slightly with the decrease in nitrate concentration (Figures 4J and 5J) because the isotope fractionation during the benthic denitrification is small as 1‰ (Table 2).

Ammonium is not completely consumed by nitrification due to photo-inhibition throughout the water column, and thus ammonium accumulation is high in the benthic layer (Figures 4K and 8B). The ammonium is enriched in ^{15}N due to partial nitrification with a large isotopic fractionation. ^{15}N-enriched ammonium in the benthic water is supplied to the surface layer by the deepening of the mixed layer from autumn to winter and is gradually consumed by nitrification. As such, the $\delta^{15}N_{Ammonium}$ value in the surface water is high and varies drastically. As the phytoplankton takes up the ammonium throughout the year, the

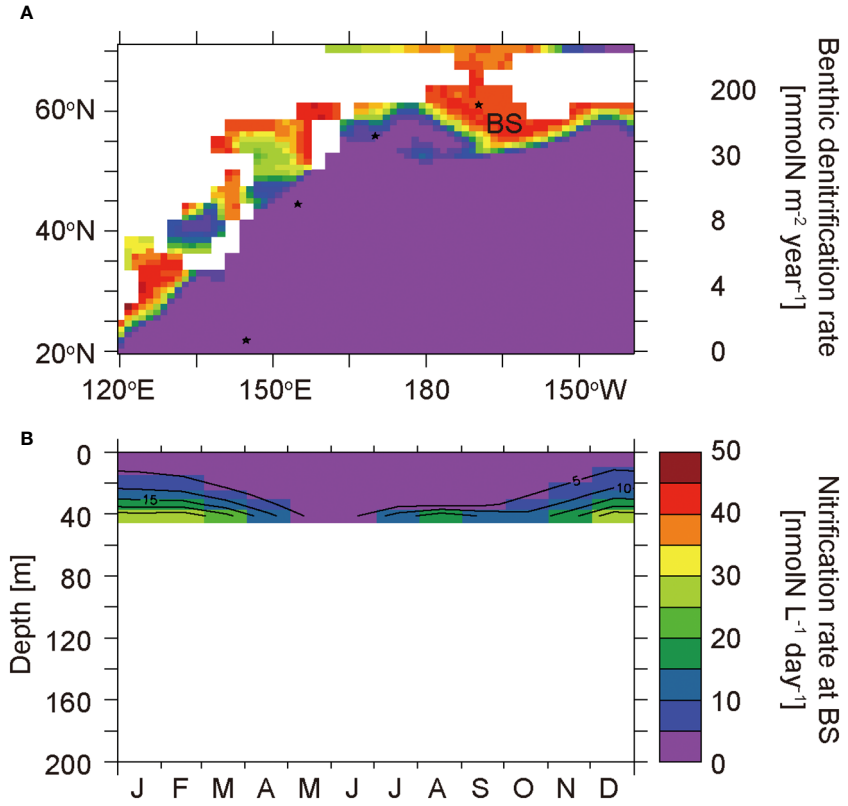

FIGURE 8
Horizontal distribution of benthic denitrification rates **(A)** and the seasonal cycle of nitrification rates in the layers at 0–41 m at the Bering Strait region site BS **(B)**.

$\delta^{15}N_{Phytoplankton}$ value at BS is high and is synchronized with the cycle of the $\delta^{15}N_{Ammonium}$ value (Figures 5K, L).

5 Summary

A seamless nitrogen isoscape of phytoplankton in the western North Pacific was created by using a marine nitrogen isotope model. The simulated annual average of $\delta^{15}N_{Phytoplankton}$ values in the euphotic layer ranged between −2.9‰ and 17.2‰ in the western North Pacific. Four distinctive sites were selected for discussion. At ST in the western subtropical North Pacific, the $\delta^{15}N_{Phytoplankton}$ value was as low as 0.6‰. The depletion in ^{15}N of phytoplankton was attributed to N_2 fixation. At TR in the Oyashio–Kuroshio transition zone, the $\delta^{15}N_{Phytoplankton}$ value was as high as 3.9‰. The ^{15}N enrichment of phytoplankton was attributed to the high utilization of the surface nitrate pool by phytoplankton. At SA in the western subarctic North Pacific, the $\delta^{15}N_{Phytoplankton}$ value was as low as 2.1‰. The depletion of ^{15}N in phytoplankton was attributed to the low utilization of the surface nitrate pool by phytoplankton due to iron limitation. At BS, the $\delta^{15}N_{Phytoplankton}$ value was as high as 6.7‰. The enrichment of ^{15}N in phytoplankton was attributed to partial nitrification with benthic denitrification.

The $\delta^{15}N_{Phytoplankton}$ value showed a characteristic seasonal variation at each site. At ST, the $\delta^{15}N_{Phytoplankton}$ value varied from −1.1‰ to 1.3‰. The nitrate and ammonium were exhausted and N_2 fixation occurred throughout the year. Because the N_2 and recycled ammonium supported most of the production, the seasonal variation in $\delta^{15}N_{Phytoplankton}$ at ST was as small as 2.4‰. At TR, the $\delta^{15}N_{Phytoplankton}$ values varied from 1.9‰ to 7.1‰. Convective mixing supplied nitrate from the subsurface to the surface in winter. Because phytoplankton consumes nitrate almost completely with an associated isotopic fractionation, nitrate was enriched greatly in ^{15}N from 6.2‰ to 17.0‰, and subsequently phytoplankton was also enriched greatly in ^{15}N. The high utilization of nitrate by phytoplankton caused the large seasonal variation in $\delta^{15}N_{Phytoplankton}$ values of 5.2‰. At SA, the $\delta^{15}N_{Phytoplankton}$ values varied from 1.3‰ and 4.2‰. The phytoplankton was affected by iron limitation and could not consume nitrate completely. The low utilization of nitrate by phytoplankton causes the relatively small seasonal variation in $\delta^{15}N_{Phytoplankton}$ values of 2.9‰. At BS, the $\delta^{15}N_{Phytoplankton}$ values varied from 3.2‰ and 13.6‰. The ammonium concentration was extremely high throughout the year due to partial nitrification. As nitrification proceeded gradually from autumn to winter with a large isotopic fractionation, ammonium was greatly enriched in ^{15}N from 2.5‰ to 17.9‰. Because phytoplankton assimilates the ammonium, the seasonal variation in $\delta^{15}N_{Phytoplankton}$ values at BS was as large as 10.4‰.

The annual mean $\delta^{15}N_{Phytoplankton}$ value had sufficient spatial variations (e.g., 0.6‰ at ST, 3.9‰ at TR, 2.1‰ at SA, and 6.7‰ at BS) for iso-logging studies in the western North Pacific compared with the analytical errors of the $\delta^{15}N_{Base}$ values of fish ($1\sigma < \pm$ 0.8‰) (Matsubayashi et al., 2017; Matsubayashi et al., 2020; Harada et al.,

2022). The seasonal variability of $\delta^{15}N_{Phytoplankton}$ reached 5.2‰ at TR and 10.4‰ at BS, which were greater than the spatial variability in the western North Pacific. To trace the movement of fish whose habitat is expected to include those areas, the seasonal variations of the nitrogen isoscape should be considered carefully.

Both $\delta^{15}N_{Base}$ values of fish and a nitrogen isoscape of phytoplankton are needed for iso-logging studies. The estimation of $\delta^{15}N_{Base}$ values requires the $\delta^{15}N$ measurement of amino acids to correct for ^{15}N-enrichment of ~3‰ per trophic position of the $\delta^{15}N$ values of bulk nitrogen of fish (Matsubayashi et al., 2017; Matsubayashi et al., 2020; Harada et al., 2022). However, because the $\delta^{15}N$ measurement of amino acids still takes much time and effort, there have been a few previous studies of the $\delta^{15}N$ values of amino acids. Nitrogen isoscapes of diet (zooplankton or small fish) using a nitrogen isotope model, including higher-trophic-level organisms, will advance iso-logging studies.

Data availability statement

The raw data supporting the conclusions of this article will be made available by the authors, without undue reservation.

Author contributions

CY: Conceptualization, Data curation, Formal Analysis, Funding acquisition, Methodology, Project administration, Software, Validation, Visualization, Writing – original draft, Writing – review & editing. MS: Conceptualization, Methodology, Software, Writing – review & editing. AY: Conceptualization, Methodology, Software, Writing – review & editing. AO: Conceptualization, Methodology, Software, Writing – review & editing. NO: Conceptualization, Funding acquisition, Project administration, Supervision, Writing – review & editing.

Funding

The author(s) declare financial support was received for the research, authorship, and/or publication of this article. We acknowledge support from JSPS KAKENHI Grants 19H04247, 19KK0293, 19K22917 20KK0165, and 21H03579. MS acknowledges support from JSPS KAKENHI Grants 18H04129 and 19H04246.

Acknowledgments

We thank D.M. Sigman, P.A. Rafter, an reviewer, and the editor for their valuable comments, and D. Marconi for suggestions about compiling the $D_{15}N_{Nitrate}$ data. The simulations with a nitrogen isotope model were performed using the Earth Simulator (ES4) at JAMSTEC. This study is partially supported by the Cooperative Research Activities of Collaborative Use of Computing Facility of the Atmosphere and Ocean Research Institute, the University of Tokyo. The analysis and graphics in this paper employed the Ferret program of NOAA's Pacific Marine Environmental Laboratory.

Conflict of interest

The authors declare that the research was conducted in the absence of any commercial or financial relationships that could be construed as a potential conflict of interest.

Publisher's note

Supplementary material

The Supplementary Material for this article can be found online at: https://www.frontiersin.org/articles/10.3389/fmars.2024.1294608/full#supplementary-material

References

Bianchi, D., Dunne, J. P., Sarmiento, J. L., and Galbraith, E. D. (2012). Data-based estimates of suboxia, denitrification, and N_2O production in the ocean and their sensitivities to dissolved O_2. *Global Biogeochem. Cycles* 26, GB2009. doi: 10.1029/2011GB004209

Bohlen, L., Dale, A. W., and Wallmann, K. (2012). Simple transfer functions for calculating benthic fixed nitrogen losses and C:N:P regeneration ratios in global biogeochemical models. *Global Biogeochem. Cycles* 26, GB3029. doi: 10.1029/2011GB004198

Coles, V. J., and Hood, R. R. (2007). Modeling the impact of iron and phosphorus limitations on nitrogen fixation in the Atlantic Ocean. *Biogeoscienced* 4, 455–497. doi: 10.5194/bg-4-455-2007

Coles, V. J., Hood, R. R., Pascual, M., and Capone, D. G. (2004). Modeling the effects of Trichodesmium and nitrogen fixation in the Atlantic Ocean. *J. Geophys. Res.* 109, C06007. doi: 10.01029/02002JC001754

DeVries, T., Deutsch, C., Rafter, P. A., and Primeau, F. (2013). Marine denitrification rates determined from a global 3-D inverse model. *Biogeosciences* 10, 2481–2496. doi: 10.5194/bg-10-2481-2013

FAO (2022). "The state of world fisheries and aquaculture 2022," in *Towards Blue Transformation* (Rome, Italy: Food and Agriculture Organization of the United Nations (FAO)). doi: 10.4060/cc0461en

Fripiat, F., Marconi, D., Rafter, P. A., Sigman, D. M., Altabet, M. A., Bourbonnais, A., et al. (2021). Compilation of nitrate δ^{15}N in the ocean. *PANGAEA*. doi: 10.1594/PANGAEA.936484

Garcia, H. E., Weathers, K., Paver, C. R., Smolyar, I., Boyer, T. P., Locarnini, R. A., et al. (2019). World Ocean Atlas 2018, Volume 4: Dissolved Inorganic Nutrients (phosphate, nitrate and nitrate+nitrite, silicate). *A. Mishonov Tech. Ed.; NOAA Atlas NESDIS* 84, 35.

Granger, J., Prokopenko, M. G., Sigman, D. M., Mordy, C. W., Morse, Z. M., Morales, L. V., et al. (2011). Coupled nitrification-denitrification in sediment of the eastern Bering Sea shelf leads to ^{15}N enrichment of fixed N in shelf waters. *J. Geophys. Res.* 116, C11006. doi: 10.1029/2010JC006751

Granger, J., Sigman, D. M., Lehmann, M. F., and Tortell, P. D. (2008). Nitrogen and oxygen isotope fractionation during dissimilatory nitrate reduction by denitrifying bacteria. *Limnol. Oceanogr.* 53 (6), 2533–2545. doi: 10.4319/lo.2008.53.6.2533

Granger, J., Sigman, D. M., Rohde, M. M., Maldonado, M. T., and Tortell, P. D. (2010). N and O isotope effects during nitrate assimilation by unicellular prokaryotic and eukaryotic plankton cultures. *Geochim. Cosmochim. Acta* 74, 1030–1040. doi: 10.1016/j.gca.2009.10.044

Hajima, T., Watanabe, M., Yamamoto, A., Tatebe, H., Noguchi, M. A., Abe, M., et al. (2020). Development of the MIROC-ES2L Earth system model and the evaluation of biogeochemical processes and feedbacks. *Geosci. Model. Dev.* 13, 2197–2244. doi: 10.5194/gmd-13-2197-2020

Hanselman, D. H., Heifetz, J., Echave, K. B., and Dressel, S. C. (2015). Move it or lose it: movement and mortality of sablefish tagged in Alaska. *Can. J. Fisheries Aquat. Sci.* 72, 238–251. doi: 10.1139/cjfas-2014-0251

Harada, Y., Ito, S., Ogawa, N. O., Yoshikawa, C., Ishikawa, N. F., Yoneda, M., et al. (2022). Compound-specific nitrogen isotope analysis of amino acids in eye lenses as a new tool to reconstruct the geographic and trophic histories of fish. *Front. Mar. Sci.* 8. doi: 10.3389/fmars.2021.796532

Hays, G. C., Ferreira, L. C., Sequeira, A. M., Meekan, M. G., Duarte, C. M., Bailey, H., et al. (2016). Key questions in marine megafauna movement ecology. *Trends Ecol. Evol.* 31, 463–475. doi: 10.1016/j.tree.2016.02.015

Hood, R. R., Bates, N. R., Capone, D. G., and Olson, D. B. (2001). Modeling the effect of nitrogen fixation on carbon and nitrogen fluxes at BATS. *Deep-Sea Res. II* 48, 1609–1648. doi: 10.1016/S0967-0645(00)00160-0

Hood, R. R., Coles, V. J., and Capone, D. G. (2004). Modeling the distribution of Trichodesmium and nitrogen fixation in the Atlantic Ocean. *J. Geophys. Res.* 109, C06006. doi: 10.1029/2002JC001753

Letscher, R. T., Hansell, D. A., Carlson, C. A., Lumpkin, R., and Knapp, A. N. (2013). Dissolved organic nitrogen in the global surface ocean: Distribution and fate, Global Biogeochem. *Cycles* 27, 141–153. doi: 10.1029/2012GB004449

Liu, K.-K., Kao, S.-J., Chiang, K.-P., Gong, G.-C., Chang, J., Cheng, J.-S., et al. (2013). Concentration dependent nitrogen isotope fractionation during ammonium uptake by phytoplankton under an algal bloom condition in the Danshuei estuary, northern Taiwan. *Mar. Chem.* 157, 242–252. doi: 10.1016/j.marchem.2013.10.005

Lowerre-Barbieri, S. K., Kays, R., Thorson, J. T., and Wikelski, M. (2019). The ocean's movescape: fisheries management in the bio-logging decade, (2018–2028). *ICES J. Mar. Sci.* 76, 477–488. doi: 10.1093/icesjms/fsy211

Matsubayashi, J., Kimura, K., Ohkouchi, N., Ogawa, N. O., Ishikawa, N. F., Chikaraishi, Y., et al. (2022). Using geostatistical analysis for simultaneous estimation of isoscapes and ontogenetic shifts in isotope ratios of highly migratory marine fish. *Front. Mar. Sci.* 9. doi: 10.3389/fmars.2022.1049056

Matsubayashi, J., Osada, Y., Tadokoro, K., Abe, Y., Yamaguchi, A., Shirai, K., et al. (2020). Tracking long-distance migration of marine fishes using compound-specific stable isotope analysis of amino acids. *Ecol. Lett.* 23, 881–890. doi: 10.1111/ele.13496

Matsubayashi, J., Saitoh, Y., Osada, Y., Uehara, Y., Habu, J., Sasaki, T., et al. (2017). Incremental analysis of vertebral centra can reconstruct the stable isotope chronology of teleost fishes. *Methods Ecol. Evol.* 8, 1755–1763. doi: 10.1111/2041-210X.12834

McMahon, K. W., Hamady, L., and Thorrold, S. R. (2013). A review of ecogeochemistry approaches to estimating movements of marine animals. *Limnol. Oceanogr.* 58, 697–714. doi: 10.4319/lo.2013.58.2.0697

Minagawa, M., and Wada, E. (1984). Stepwise enrichment of 15N along food chains: Further evidence and the relation between d15N and animal age. *Geochim. Cosmochim. Acta* 48, 1135–1140. doi: 10.1016/0016-7037(84)90204-7

Minagawa, M., and Wada, E. (1986). Nitrogen isotope ratio of red tide organisms in the East China Sea: A characterization of biological nitrogen fixation. *Mar. Chem.* 19, 245–259. doi: 10.1016/0304-4203(86)90026-5

Montoya, J. P., and McCarthy, J. J. (1995). Isotopic fractionation during nitrate uptake by phytoplankton grown in continuous culture. *J. Plankton Res.* 17, 439–464. doi: 10.1093/plankt/17.3.439

Nishioka, J., Obata, H., Ogawa, H., Ono, K., Yamashita, Y., Lee, K., et al. (2020). Subpolar marginal seas fuel the North Pacific through the intermediate water at the termination of the global ocean circulation. *Proc. Natl. Acad. Sci.* 117 (23), 202000658–202000658. doi: 10.1073/pnas.2000658117

Oka, A., Kato, S., and Hasumi, H. (2008). Evaluating effect of ballast mineral on deep-ocean nutrient concentration by using an ocean general circulation model. Global Biogeochem. *Cycles* 22, GB3004. doi: 10.1029/2007GB003067

O'Reilly, J. E., Maritorena, S., Mitchell, B. G., Siegal, D. A., Carder, K. L., Garver, S. A., et al. (1998). Ocean color chlorophyll algorithms for SeaWiFS. *J. Geophys. Res.* 103, 24937–24953. doi: 10.1029/98JC02160

Rafter, P., Bagnell, A., DeVries, T., and Marconi, D. (2019). Compiled dataset consisting of published and unpublished global nitrate d15N measurements from from 1975-2018. *Biol. Chem. Oceanogr. Data Manage. Office*. doi: 10.1575/1912/bco-dmo.768627.1

Schmittner, A., Oschlies, A., Matthews, H. D., and Galbraith, E. D. (2008). Future changes in climate, ocean circulation, ecosystems and biogeochemical cycling simulated for a business-as-usual CO2 emission scenario until year 4000 AD. *Global Biogeochem. Cycles* 22, GB1013. doi: 10.1029/2007GB002953

Shigemitsu, M., Gruber, N., Oka, A., and Yamanaka, Y. (2016). Potential use of the N_2/Ar ratio as a constraint on the oceanic fixed nitrogen loss. *Global Biogeochem. Cycles* 30, 576–594. doi: 10.1002/2015GB005297

Shigemitsu, M., Yamamoto, A., Oka, A., and Yamanaka, Y. (2017). One possible uncertainty in CMIP5 projections of low-oxygen water volume in the Eastern Tropical Pacific. *Global Biogeochem. Cycles* 31, 804–820. doi: 10.1002/2016GB005447

Somes, C., Oschlies, J. A., and Schmittner, A. (2013). Isotopic constraints on the pre-industrial oceanic nitrogen budget. *Biogeosciences* 10, 5889–5910. doi: 10.5194/bg-10-5889-2013

Somes, C. J., Schmittner, A., Galbraith, E. D., Lehmann, M. F., Altabet, M. A., Montoya, J. P., et al. (2010). Simulating the global distribution of nitrogen isotopes in the ocean. Global Biogeochem. *Cycles* 24, GB4019. doi: 10.1029/2009GB003767

Somes, C. J., Schmittner, A., Muglia, J., and Oschlies, A. (2017). A three-dimensional model of the marine nitrogen cycle during the last glacial maximum constrained by sedimentary isotopes. *Front. Mar. Sci.* 4. doi: 10.3389/fmars.2017.00108

Tesdal, J. E., Galbraith, E. D., and Kienast, M. (2013). Nitrogen isotopes in bulk marine sediment: linking seafloor observations with subseafloor records. *Biogeosciences* 10, 101–118. doi: 10.5194/bg-10-101-2013

Thorson, J. T., Jannot, J., Somers, K., and Punt, A. (2016). Using spatio-temporal models of population growth and movement to monitor overlap between human impacts and fish populations. *J. Appl. Ecol.* 54, 577–587. doi: 10.1111/1365-2664.12664

Tzadik, O. E., Curtis, J. S., Granneman, J. E., Kurth, B. N., Pusack, T. J., Wallace, A. A., et al. (2017). Chemical archives in fishes beyond otoliths: a review on the use of other body parts as chronological recorders of microchemical constituents for expanding interpretations of environmental, ecological, and life-history changes. *Limnol. Oceanogr.: Methods* 15, 238–263. doi: 10.1002/lom3.10153

Vecchio, J. L., and Peebles, E. B. (2020). Spawning origins and ontogenetic movements for demersal fishes: An approach using eye-lens stable isotopes. *Estuar. Coast. Shelf. Sci.* 246, 107047. doi: 10.1016/j.ecss.2020.107047

Wada, E., and Hattori, A. (1978). Nitrogen isotope effects in the assimilation of inorganic nitrogenous compounds by marine diatoms. *Geomicrobiol. J.* 1, 85–101. doi: 10.1080/01490457809377725

Watanabe, S., Hajima, T., Sudo, K., Nagashima, T., Takemura, T., Okajima, H., et al. (2011). MIROC-ESM 2010: Model description and basic results of CMIP5-20c3m experiments, Geosci. *Model. Dev.* 4, 845–872. doi: 10.5194/gmd-4-845-2011

Yamamoto, A., Abe-Ouchi, A., Ohgaito, R., Ito, A., and Oka, A. (2019). Glacial CO_2 decrease and deep-water deoxygenation by iron fertilization from glaciogenic dust. *Climate Past* 15 (3), 981–996. doi: 10.5194/cp-15-981-2019

Yoshikawa, C., Abe, H., Aita, M. N., Breider, F., Kuzunuki, K., Toyoda, S., et al. (2016). Insight into nitrous oxide production processes in the western North Pacific based on a marine ecosystem isotopomer model. *J. Oceanogr.* 72 (3), 491–508. doi: 10.1007/s10872-015-0308-2

Yoshikawa, C., Coles, V. J., Hood, R. R., Capone, D. G., and Yoshida, N. (2013). Modeling how surface nitrogen fixation influences subsurface nutrient patterns in the North Atlantic. *J. Geophys. Res. Oceans* 118, 2520–2534. doi: 10.1002/jgrc.20165

Yoshikawa, C., Makabe, A., Matsui, Y., Nunoura, T., and Ohkouchi, N. (2018). Nitrate isotope distribution in the subarctic and subtropical North Pacific. *Geochem. Geophys. Geosystems* 19, 2212–2224. doi: 10.1029/2018GC007528

Yoshikawa, C., Ogawa, N. O., Chikaraishi, Y., Makabe, A., Matsui, Y., Sasai, Y., et al. (2022). Nitrogen isotopes of sinking particles reveal the seasonal transition of the nitrogen source for phytoplankton. *Geophys. Res. Lett.* 49, e2022GL098670. doi: 10.1029/2022GL098670

Yoshikawa, C., Yamanaka, Y., and Nakatsuka, T. (2005). An ecosystem model including nitrogen isotopes: Perspectives on a study of the marine nitrogen cycle. *J. Oceanogr.* 61 (5), 921–942. doi: 10.1007/s10872-006-0010-5

Frontiers in Marine Science

Explores ocean-based solutions for emerging global challenges

The third most-cited marine and freshwater biology journal, advancing our understanding of marine systems and addressing global challenges including overfishing, pollution, and climate change.

Discover the latest Research Topics

See more →

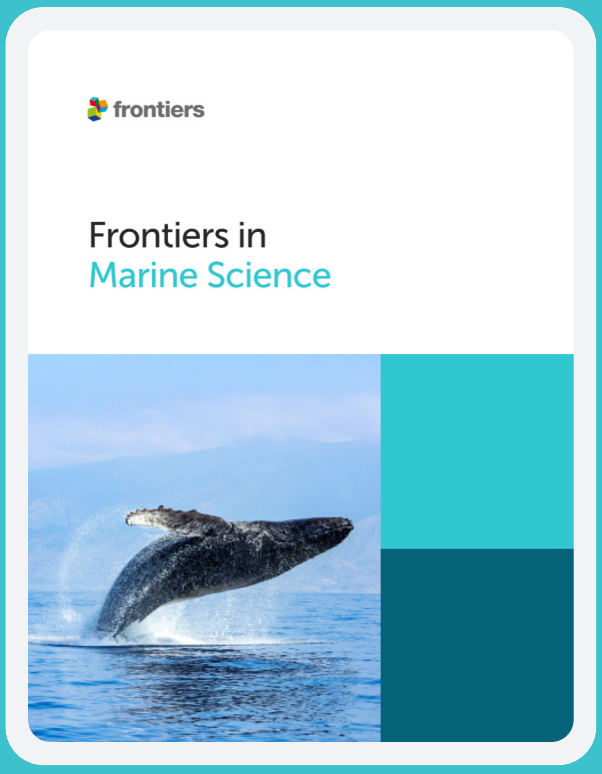

Frontiers

Avenue du Tribunal-Fédéral 34
1005 Lausanne, Switzerland
frontiersin.org

Contact us

+41 (0)21 510 17 00
frontiersin.org/about/contact